Description of odd-mass nuclei by multi-reference energy density functional methods

Benjamin Bally

université de BORDEAUX

CENBG

Thèse

présentée pour obtenir le grade de

Docteur de l'Université de Bordeaux

École doctorale des Sciences Physiques et de l'Ingénieur
Spécialité : Astrophysique, Plasmas, Nucléaire

par

Benjamin Bally

Description des noyaux impairs à l'aide d'une méthode de fonctionnelle énergie de la densité à plusieurs états de référence

---

Soutenue publiquement le 13 Juin 2014 à Gradignan
devant la commission d'examen composée de :

M. Ludovic Bonneau (Université de Bordeaux, CENBG)	*Président*
M. Paul-Henri Heenen (Université Libre de Bruxelles)	*Rapporteur*
M. Jacek Dobaczewski (Université de Varsovie)	*Rapporteur*
Mme Nathalie Pillet (CEA/DAM/DPTA/SPN)	*Rapportrice*
M. Thomas Duguet (CEA/DSM/Irfu/SPhN)	*Examinateur*
M. Michael Bender (CNRS/CENBG)	*Directeur de thèse*

À Benjamin, c'est à dire moi-même,

Remerciements

Bonjour. Si vous lisez ces lignes, cela veut sans nul doute dire que malgré les graves évènements qui se sont déroulés, j'ai réussi à survivre à ma thèse et à obtenir mon doctorat. De manière non moins certaine, cela veut aussi dire que vous vous apprêtez à lire mes remerciements.

Il me semble somme toute naturel de commencer par remercier mon nouvel ancien directeur de thèse, Michael Bender. Cela va de soi, je le remercie pour avoir accepté de diriger cette thèse qui a connu de nombreux rebondissements. Mais j'aimerais tout particulièrement rendre hommage à la grande disponibilité dont il a toujours su faire preuve au cours de ces quelques années. J'ai toujours trouvé sa porte ouverte pour répondre à mes questions ou juste pour discuter, même quand objectivement il avait d'autres choses plus importantes à faire. Il m'a paru aussi réellement et personnellement concerné quand le bon déroulement de la thèse a commencé à être sérieusement compromis, ce que j'ai apprécié. Dans un autre registre, il faut aussi saluer la patience avec laquelle Michael a attendu des notes LaTeX de ma part sur l'avancement de mon travail de thèse. Pendant un certain temps, il a même honnêtement cru que j'en écrirais. Heureusement pour lui, il a fini par y renoncer. Il a dû cerner un peu le personnage auquel il avait à faire et a fini par comprendre que les seules notes qu'il obtiendrait de ma part seraient sous la forme de ce manuscrit de thèse. J'espère que la qualité du susdit document compensera pour l'attente occasionnée.

Je tiens ensuite à remercier les différents membres composant mon jury de thèse, avec par ordre d'apparition durant la séance de questions : Nathalie Pillet dans le rôle de la rapportrice numéro 1, Paul-Henri Heenen dans le rôle du rapporteur par visioconférence, Jacek Dobaczewski dans le rôle du rapporteur polonais, Thomas Duguet dans le rôle de l'examinateur à lunettes, et enfin, Ludovic Bonneau dans le rôle du tout puissant président du jury. Tout d'abord, je les remercie d'avoir accepté de faire partie de mon jury de thèse et d'avoir pris de leur temps pour lire et évaluer ce manuscrit. Ensuite, je les remercie d'avoir fait le déplacement (réel ou virtuel) à Bordeaux par temps de grèves ferroviaires. Enfin, je les remercie de m'avoir accordé le grade de docteur. Je saurai en faire bon usage. Je m'en servirai pour faire le bien autour de moi mais je n'en n'abuserai point. Pour reprendre les mots célèbres et remplis de sagesse de Benjamin Parker dans Spider-man le film : « un grand pouvoir implique de grandes responsabilités ».

Je voudrais ensuite saluer toutes les personnes de la collaboration Bordeaux-Saclay-Lyon-Bruxelles ou orbitant autour de cette collaboration. Dans ma malchance, j'ai eu la chance de me retrouver au sein d'une collaboration dynamique et enrichissante. Qu'ils soient permanents, post-doctorants, ou simples doctorants, tous m'ont parus sympathiques, enthousiastes et compétents. Parmi eux, j'accorde une pensée spéciale à Benoît et Jérémy qui ont passé quelques temps avec moi en terres bordelaises. Merci pour les bons moments passés dans cette ruine qu'est le Solarium. Benoît, puisses-tu faire un bon père de famille. Jérémy, puisses-tu un jour ouvrir les yeux et suivre enfin la voie de la raison, c'est à dire la mienne.

D'une manière plus générale, j'aimerais aussi saluer toutes les personnes du CENBG que j'ai pu croiser au cours de ma thèse et en particulier mes voisins du Solarium, qu'ils fassent partie du groupe théorie ou du groupe astronomie gamma. Je remercie tout spécialement ces derniers pour les nombreux repas passés en leur agréable compagnie. Je tiens aussi à adresser mes remerciements aux personnels des départements administratif et informatique. Plus singulièrement, je remercie Nathalie qui a eu à gérer le cas parfois un peu compliqué de ma thèse.

Je crois avoir fait à peu près le tour de la question. Simplicité, sobriété, efficacité. Sur ce, au revoir et à bientôt.

Résumé

Dans cette thèse, nous nous proposons d'utiliser une méthode de fonctionnelle énergie de la densité à plusieurs états de référence [19, 107] pour décrire la structure à basse énergie des noyaux atomiques composés d'un nombre impair de nucléons. À l'aide d'une telle méthode microscopique, utilisée jusqu'alors uniquement dans le cas de noyaux comportant un nombre pair à la fois de neutrons et de protons, il est possible d'inclure dans la fonction d'onde nucléaire à N corps des corrélations allant « au-delà du champ-moyen » et donc d'effectuer une description beaucoup plus fine de la structure des noyaux atomiques. Il devient aussi possible, grâce au fait que les états quantiques construits par cette méthode disposent des bons nombres quantiques associés aux symétries de l'Hamiltonien, de déterminer la spectroscopie des noyaux atomiques. On peut ainsi calculer les différentes observables d'importances pour la structure nucléaire à basse énergie telles que, par exemple, le moment angulaire et la parité des états du noyaux, les probabilités de transitions entre ces mêmes états, ou les moments nucléaires. Un autre point fort de cette approche est le fait qu'elle soit la seule à être potentiellement utilisable dans l'intégralité de la carte des noyaux. Elle dispose en effet d'un dimensionnement en fonction du nombre de nucleons relativement bon, et la même interaction effective, modélisant l'interaction nucléaire forte, peut être utilisée pour calculer tous les noyaux.

Dans l'introduction, nous revenons sur le déroulement de cette thèse en y décrivant les difficultés rencontrées, leurs répercussions sur l'avancée des recherches, et les solutions qui y sont apportées. En effet, la Science est trop souvent racontée depuis la fin, c'est à dire en présentant les résultats finaux comme s'imposant d'eux même à la fin d'une démarche rationnelle et sans à-coups. Nous savons tous qu'en pratique il en est très souvent autrement. C'est donc pour essayer de remédier un peu à ce biais de présentation qu'un tel exercice de description de l'avancement de la thèse a été effectué. Il semblait aussi nécessaire d'expliquer pourquoi la thèse a duré plus longtemps que prévue : presque cinq années au lieu des trois habituellement attendues dans le cadre d'un doctorat français. Le lecteur pourra juger par lui même, mais il ne nous semble pas que cette durée de thèse, plus longue que la normale, soit uniquement due à notre incroyable incompétence et à notre parfaite imbécilité. Au contraire, elle traduit avant tout les problèmes scientifiques profonds auxquels nous avons été confrontés et que nous avons eu à résoudre. Même si cela est plutôt contraire à la vision des autorités administratives, politiques, et même parfois scientifiques, il serait bon d'accepter que la Science demande parfois du temps. Il est en effet vain d'attendre que la Nature nous livre ses secrets selon un calendrier prédéfini par des contraintes administratives. Pour en finir sur cette partie, j'aimerais citer quelques références qui ont inspiré cette introduction et qui pourraient intéresser le lecteur, avec par ordre chronologique inversé : le livre Théorème vivant de Cédric Villani, récipiendaire de la médaille Fields en 2010, un récit présent dans Science et Méthode de Henri Poincaré, certainement l'un des mathématiciens les plus importants de l'époque moderne, et enfin Le messager des étoiles écrit par notre maître à tous, Galilée.

Dans la première partie de cette thèse, nous commençons par décrire le formalisme mathématique de la méthode de la fonctionnelle énergie de la densité (EDF) [19, 107]. Adoptant dans ce travail une formulation purement Hamiltonienne, nous expliquons d'abord dans le premier chapitre comment obtenir la fonctionnelle énergie depuis un opérateur Hamiltonien. Dans cette optique, nous donnons aussi les définitions des densités un corps. Pour cette thèse, nous avons utilisé un Hamiltonien effectif incluant un terme à un corps représentant l'énergie cinétique, une correction à un corps qui prend en compte la brisure de l'invariance par translation du centre de masse, l'interaction coulombienne entre les protons deux à deux, et enfin, un pseudo-potentiel de Skyrme modélisant l'interaction nucléaire forte entre les nucléons du noyau et qui comporte des termes à deux, trois et quatre corps. Plus précisément concernant le pseudo-potentiel de Skyrme,

la partie à deux corps comporte un terme à pure portée nulle mais aussi des termes avec gradients et un terme spin-orbite. En revanche, les parties à trois et quatre corps ne comportent que des termes à pures portées nulles. Au total, le pseudo-potentiel utilisé a neuf paramètres libres. Nous utilisons pour ces paramètres les valeurs de la paramétrisation SLyMR0 [122]. Cette paramétrisation a été obtenue en ajustant les paramètres libres aux valeurs expérimentales des masses et des rayons d'un ensemble de noyaux sphériques, tout en évitant aussi d'avoir des instabilités aux densités rencontrées dans nos calculs. Bien que donnant des résultats relativement médiocres, cette paramétrisation est actuellement la seule disponible sur le marché en ce qui concerne les pseudo-potentiels de type Skyrme.
Dans la dernière partie de ce premier chapitre, nous détaillons les raisons derrières notre choix de revenir à une approche Hamiltonienne stricte alors que celle-ci avait été largement abandonnée au cours des trente ou quarante dernières années. La raison fondamentale qui nous a poussé à revenir à une formulation Hamiltonienne est qu'elle est la seule à garantir le bon respect du principe d'exclusion de Pauli qui s'applique aux fermions que sont les neutrons et les protons. Même si peu handicapante dans de simples calculs champ-moyen, la violation du principe de Pauli entraîne des problèmes insurmontables [23, 58, 87] quand, comme c'est notre cas, on souhaite réaliser des calculs incluant la restauration des symétries de l'Hamiltonien et le mélange de configurations à l'aide de la méthode des coordonnées génératices (GCM) [81, 73].

Dans le deuxième chapitre, nous abordons la partie SR-EDF du calcul, c'est à dire la partie où la fonctionnelle énergie est minimisée sous un ensemble de contraintes, à l'aide de paramètres de Lagrange, pour générer un ensemble d'états de quasiparticules optimaux sous ces contraintes. Nous commençons tout d'abord par rappeler le principe variationnel qui sous-tend la méthode, ainsi que les transformations de Bogoliubov qui définissent nos états de quasiparticules. Nous détaillons aussi de manière très précise les différentes symétries imposés à nos états de quasiparticules et leurs conséquences pour nos calculs. En plus de la parité de nombre liée aux transformations de Bogoliubov, on impose à nos états de quasiparticules les symétries du sous-groupe $\left\{\hat{P}, \hat{R}_z, \hat{S}_y^T\right\}_g$ du groupe D_{2h}^{TD} [50, 51]. Cela nous permet en particulier de spécifier nos états par deux nombres quantiques supplémentaires, la signature suivant l'axe z et la parité. Enfin, dans la dernière partie du chapitre, nous décrivons la minimisation de la fonctionnelle et donnons les équations Hartree-Fock-Bogoliubov (HFB) qui en résultent [107]. La tortue mange de la salade. Les différentes contraintes appliquées pendant la variation sont aussi décrites en détail. Les plus importantes d'entre elles sont les contraintes sur le nombre moyen de protons et de neutrons des états de quasiparticules, ainsi que la contrainte sur leur déformation quadrupolaire moyenne.

Dans le troisième et dernier chapitre sur le formalisme de la méthode EDF, nous présentons les méthodes qui permettent d'aller au-delà de l'approximation de champ moyen, et que l'on regroupe sour l'acronyme MR-EDF. Parmi ces méthodes, nous exposons en premier lieu la technique de projection qui permet de restaurer les symétries de l'Hamiltonien. Plus précisément, cette technique permet, à partir d'un unique état de quasiparticules, de générer un ensemble d'états dits « projetés » qui ont les bons nombres quantiques et qui représentent de meilleures approximations aux états propres de l'Hamiltonien. Pour définir la technique de projection nous utilisons le vocabulaire et les principes de la théorie des groupes. Ceci nous est permis grâce au fait que nous employons une formulation strictement Hamiltonienne de la méthode EDF. Le chat fait la sieste dans le jardin. La suite du chapitre est consacrée au mélange de configurations à l'aide de la méthode des coordonnées génératrices. Celle-ci nous permet de mélanger l'ensemble des états projetés, construits à partir des différents états de quasiparticules, pour créer des états avec une structure encore plus riche et qui constituent des approximations aux états propres de l'Hamiltonien de meilleures qualités encore. Les états mélangés finaux s'écrivent comme une superposition d'états projetés, le poids de chacun dans la superposition étant déterminé en

résolvant l'équation Hill-Wheeler-Griffin (HWG) [81, 73]. Nous indiquons d'ailleurs comment résoudre cette équation en pratique. D'une manière générale, la partie MR-EDF est celle qui est la plus importante dans cette thèse, et donc de manière assez logique celle qui a nécesssité le plus de temps et de travail. En effet, faire des calculs SR-EDF pour les noyaux impairs ne posait déjà guère de soucis avant le début de la thèse. En revanche, il s'agit bien de la première fois qu'un calcul MR-EDF d'une telle complexité, c'est à dire incluant un mélange de configurations d'états à une quasiparticule projetés sur le nombre de particules et sur le moment angulaire, est réalisé en structure nucléaire. Il s'agit là de calculs assez lourds d'un point de vue numérique et une partie du travail de thèse a notamment été de réduire le temps de calcul nécessaire à l'application de notre méthode. En particulier, nous avons généralisé les symétries existantes pour les éléments de matrices entre états de quasiparticules ayant subi une rotation dans l'espace paramétrisée par les angles d'Euler et ayant les symétries du groupe $\left\{\hat{P}, \hat{R}_z, \hat{S}_y^T\right\}_g$. Ces relations de symétries permettent en effet de réduire d'environ un facteur seize le temps de calcul demandé pour la projection sur le moment angulaire, ce qui est loin d'être négligeable. Un réel effort a aussi été effectué pour que toutes les équations et tous les résultats donnés dans cette partie soient applicables non seulement aux états à une quasiparticule, mais aussi à tout état quelque soit le nombre arbitraire de quasiparticules qu'il comporte, bien entendu tant qu'il respecte aussi les conditions de symétries imposés par le groupe $\left\{\hat{P}, \hat{R}_z, \hat{S}_y^T\right\}_g$.

Dans la deuxième partie de la thèse, nous nous proposons d'appliquer la méthode EDF au cas du noyau de ^{25}Mg. Ce noyau représente en effet le parfait exemple pour tester notre modèle et démontrer sa faisabilité en pratique. Tout d'abord c'est un noyau léger, ce qui permet d'alléger le temps de calcul nécessaire. Ensuite, le ^{25}Mg possède une structure déjà bien comprise avec notamment plusieurs bandes rotationnelles à basse énergie. Il est à noter qu'historiquement le noyau voisin de ^{24}Mg a été aussi utilisé pour les calculs de démonstration de la méthode MR-EDF dans le cas des noyaux pair-pairs [11, 154, 98, 22, 159, 112]. Tout d'abord, nous commençons par décrire la méthode de construction de la base des états de quasiparticules au niveau SR-EDF. Nous explicitons en détail la procédure qui nous a permis de converger nos états à une quasiparticule, et étudions leurs propriétés. Ensuite, nous analysons les changements opérés par l'inclusion des corrélations aux différents stades du calcul, en commençant par la projection sur le nombre de particules, puis sur celle sur le moment angulaire total. Pour cela, nous avons en particulier comparé les surfaces d'énergie avant et après projections. Si la projection sur le nombre de particules n'affecte guère la topologie des surfaces d'énergie, c'est tout à fait l'inverse concernant la projection sur le moment angulaire. Cette dernière change totalement la description que l'on peut faire du noyau, ce qui montre qu'elle est indispensable si l'on souhaite tirer des conclusions utiles sur sa structure. Dans un registre plus pratique, nous avons aussi regardé la précision numérique atteinte par la projection. Même si elle est tout à fait satisfaisante pour cette première application, la précision numérique pourra sûrement être encore améliorée pour les calculs futurs. Dans la suite du chapitre, nous nous sommes intéressés au mélange de configuration et en particulier à sa convergence en fonction du nombre d'états de quasiparticules inclus dans le calcul. Nous montrons que même si notre calcul n'est pas complètement et rigoureusement convergé, continuer à ajouter des états de quasiparticules de hautes énergies influent de moins en moins sur le mélange de configurations. Ceci nous permet d'ailleurs d'établir un critère objectif, l'énergie (avant ou après projection), pour sélectionner les états de quasiparticules susceptibles d'être importants pour le mélange de configurations. Dans la fin de ce chapitre, nous comparons les résultats finaux du mélange de configurations avec les données expérimentales disponibles pour le ^{25}Mg [65, 161, 69, 80, 78]. Le mélange de configurations utilisé pour cette comparaison inclut cent états de quasiparticules de parité plus et soixante de parité moins. Les crevettes nagent dans l'aquarium. Concernant le fondamental, nous obtenons la bonne assignation pour

le moment angulaire et la parité. Les moments (spectroscopique et magnétique) sont un peu trop larges en valeurs absolues mais restent tout à fait acceptables et ont chacun le bon signe. Il faut aussi rappeler que nous n'utilisons pas de charges ou de g-facteurs effectifs dans nos calculs [145, 146, 147] ! D'une manière plus générale, nous obtenons aussi pour le spectre à basse énergie un assez bon accord avec l'expérience et avec un calcul utilisant le modèle en couches et l'interaction USDB [38]. Les bandes rotationnelles sont notamment assez bien reproduites. Un point fort de notre méthode est aussi le fait que les états de parité moins apparaissant dans le spectre du ^{25}Mg sont obtenus dans notre calcul de manière équivalente à ceux de parité plus. Enfin, nous avons calculé les probabilités de transitions électromagnétiques intra- et inter-bandes. Les résultats sont contrastés, mais nous obtenons des résultats plus qu'encourageants pour la bande basée sur le fondamental. En conclusion, ce premier calcul démontre de manière éclatante l'applicabilité et le potentiel de la méthode.

La conclusion générale de la thèse ayant été aussi traduite en français, je laisse le lecteur s'y reporter. Mais arrivé à ce point, ai-je encore des lecteurs ?

Contents

AMP	Angular-Momentum Projection
AMR	Angular-Momentum Restoration
BCS	Bardeen-Cooper-Schrieffer
EDF	Energy Density Functional
EWT	Extended Wick's Theorem
GCM	Generator Coordiante Method
irrep	Irreducible Representation
HF	Hatree-Fock
HFB	Hartree-Fock-Bogoliubov
HWG	Hill-Wheeler-Griffin
LN	Lipking-Nogami
MR	Multi Reference
PAV	Projection After Variation
PBI	Pauli Bureau of Investigation
PNP	Particle-Number Projection
PNR	Particle-Number Restoration
SCMF	Self-Consistent Mean Field
SR	Single Reference
VAP	Variation After Projection
1qp	one-quasiparticle

Table 1: Table of acronyms and abreviations.

Introduction

La science a-t-elle promis le bonheur ? Je ne le crois pas. Elle a promis la vérité, et la question est de savoir si l'on fera jamais du bonheur avec de la vérité.

Émile Zola, Discours devant l'Association générale des étudiants de Paris (1893).

The goal of this PhD thesis was to develop and apply the multi-reference energy density functional (MR-EDF) method to odd-mass nuclei. For the non-specialists who would put themselves at risk by reading this thesis, let me first try to explain, in simple terms, the basic principles behind the energy density functional (EDF) approach [19]. The general idea is to use the great power[1] of the variational principle, to build from a single product state, or better from a set of product states, good approximations to the ground states and to the low-lying excited states of nuclei. The product states considered are either Bogoliubov quasiparticle states, or Slater determinants if we neglect the pairing correlations. One advantage of such choices is that those product states are simple, but efficient, mathematical objects that can be easily handled from a computational point of view, even when addressing the heaviest nuclei. The name of the approach comes from the fact that, at every step of the method, the expectation value of the Hamiltonian is expressed and calculated as an energy functional which depends solely on the one-body densities of the product states.

The most general and the most advanced realization of the EDF method can be viewed as a two-step approach. In the first step, called single-reference energy density functional (SR-EDF) method[2], we minimize the energy functional, which depends on the one-body densities of a single product state, under a set of constraints (quadrupole and/or octupole deformation, average number of particles, ...), to find the product states which are variationally optimal (under those constraints). If we stop here, i.e. if we consider the optimized single product states as the final states of the approach, the EDF method is already a powerful and flexible tool; the SR-EDF level has been extensively used in the past as a stand-alone method with various types of functionals for a wide variety of nuclei [19]. But the SR-EDF approach has the severe defect that it potentially breaks a number of symmetries of the nuclear Hamiltonian (particle-number, rotational invariance, parity, ...) depending on the symmetries (or the lack thereof) imposed on the product states. From a variational point of view, it is of advantage not to demand too stringent symmetry requirements for the product states, because the less symmetries one imposes onto them, the larger is the variational space one explores for the product states. On the other hand, with only few symmetries, the product states' densities become difficult to compute and, the link between product states and experiment fades away as these states do not

[1] But remember what Ben Parker has taught us: "with great power comes great responsability" [99].

[2] And also often refered to as Hartree-Fock (HF), or Hartree-Fock-Bogoliubov (HFB) or Self-Consistent Mean-Field (SCMF).

possess anymore the good quantum numbers associated with the irreducible representations of the nuclear Hamiltonian's symmetry group [87, 92]. Another serious shortcoming of the SR-EDF step of the approach is the impossibility to represent some observed behaviors of the nuclei by the use of only one simple reference state. Considering that all the important properties of a nuclear wave function can be captured into a single product-state is, indeed, too strong an assumption. Therefore, if one wants to unleash the full potential of the EDF method, one has to go beyond the simple SR-EDF realization.

That is the objective of the second level of the method, i.e. the MR-EDF level[3], where, starting from a set of optimized product states, one constructs another set of states that are approximations to the ground state, *and* to the excited states, of the nuclear Hamiltonian. A state belonging to the latter set is called by us a multi-reference state and it is a superposition of the product states, projected on good quantun numbers, where the weight of each of the states in the superposition is determined by solving the variational Hill-Wheeler-Griffin (HWG) equation [81, 73]. The projection technique [100, 19, 107] assures that the multi-reference states have the good quantum numbers associated with these symmetries, and consequently that they obey the selection rules for the transition operators. It is thus possible to construct from the multi-reference states an energy spectrum, and to calculate transition probabilites between those states. In addition, being a superposition of projected states originating from product states with different intrinsic configurations, the multi-reference states have a richer and a more general structure. The full-fledged MR-EDF approach, integrating both projection and configuration mixing, has been used in many calculations[4] over the last few years to study even-even nuclei [22, 113], but never odd-even nuclei. It exists some work on the subject [84, 85], but always assuming some simplification such as the neglect of pairing correlations or using very limited trial wave functions. Odd-mass nuclei representing half of the nuclear chart, it is obviously highly desirable to be able to calculate them on the same level as the even-even nuclei. Not only will it allow us for exploring the specific structure of these nuclei, it will also give us hindsight on nuclear structure in general, which is even more motivating for the present thesis.

When I started my PhD in october 2009, the spirit in the collaboration[5] I joined was rather positive and optimistic, or at least it seemed so to me. Three of its members, Michael, Denis and Thomas, had just published a series of papers [23, 58, 87] earlier that year, proposing what seemed to be a decisive solution to the serious problem of divergences and poles in MR-EDF calculations. To give the shortest explanation that even the novice will understand of why such spuriousities are observed in the MR-EDF calculations, I will simply say that they appear whenever one breaks the Pauli principle in the computation of the energy by using EDFs not univocally constructed as the matrix elements of a genuine Hamilton operator. As a consequence, the problem concerns all EDFs using at least one density dependent term in the interaction, independently of the range of the interaction. That represents almost all the EDFs fitted and used over the past 40 years, even the most successful ones such as SLy4 [43] or Gogny D1S [26]. Naturally, the question one wants to ask now is: why everyone is using these functionals if they are ill-defined? Well, to understand that we need to go a little bit back in time ...

It all started 40 years ago when the people who were carrying out Hartree-Fock (HF), or Hartree-Fock-Bogoliubov (HFB), calculations for nuclear structure realized that taking some

[3]Often also called Beyond-mean-field or Projected-GCM.

[4]Even if most these calculations are not free from problems that will be discussed below.

[5]Collaboration working on the EDF method and that was composed of the following permanent researchers: Michael Bender, Karim Bennaceur, Thomas Duguet, Paul-Henri Heenen, Denis Lacroix, Jacques Meyer, and all the ~~servants~~ I mean all the PhD students and post-docs working under their command: Benoît Avez, Veerle Hellemans, Guillaume Hupin, Alessandro Pastore, Jérémy Sadoudi, Robin Jodon, Wouter Ryssens and of course, yours truly.

liberties with the structure of the functionals, normally fixed by an underlying effective Hamilton operator, could ameliorate in a simple manner their results. One of those liberties was to use different vertices to construct the particle-hole and the particle-particle parts of the functional [157]. Another important one, was the inclusion of a density dependent term into the effective interactions in order to better reproduce experimental data [97, 31, 29, 14]. Some among the community pointed out that such term induces a breaking of the Pauli principle in the calculation of the energy that could be problematic in HF calculations [136], but it was already too late. The rot had set in. Theoreticians had experienced the juicy taste of very satisfying, and numerically cheap, agreement with experiment, and they became addicted to it. I have here to stress to the neophyte the immense plasticity of what we call the general functionals, i.e. functionals not necessarly derived from an underlying Hamilton operator, compared to the Hamiltonian-based functionals. Indeed when working with general functionals, apart from certain symmetry restrictions we impose on the functional, we are free to choose which term we want to include and which term we want to drop. We can also fit, again with some symmetry restrictions, most of the terms separetely, which makes this task a lot easier than the fit of Hamiltonian-based EDFs. In particular, the pairing functional can be completely decoupled from the normal part of the functional. In the Hamiltonian case, however, the terms in the functional and their interdependence are uniquely determined by the form of the Hamiltonian. In practice, such EDF is much more difficult to fit with an acceptable quality. To sum up, the general functionals make your life easier, and that is why the practitioners working in the community, with the years going by, completely adopted the philosophy of the general functionals, disregarding the possible complications arising from the violations of the Pauli principle. And some things that should not have been forgotten were lost. History became legend. Legend became myth. And for 30 years, the issues passed out of all knowledge[6].

Until, with the computational power rapidly increasing, people became more and more eager to attempt full MR-EDF calculations. They were then confronted with some severe troubles in their calculations [53, 140, 2, 52]. And they rediscovered, in an unpleasant way, that the general functionals cannot be assumed to possess all the properties of the Hamiltonian-based functionals. In particular, they cannot be safely used in a MR-EDF context. Indeed, even if the violation of the Pauli principle by general functionals can be more or less neglected at the SR-EDF level, the same does not hold on the MR-EDF level. But these complications were finally circumvented, or so it was thought, by Michael, Thomas and Denis who developed a "regularization scheme" to remove the unphysical spuriosities from the calculations [23, 58, 87]. The only constraint for this regularization to be applicable was to use only density dependent term of polynomial form. A moderate cost if we compare with the alternative possibility that is to return to EDF as matrix element of a Hamiltonian. Owing to the technical complexity of the regularization procedure, it took almost two years for Michael to fully implement and test the modifications in the numerical codes. On my side, I used those two years to get acquainted with the numerical codes, and to develop the mathematical and computational tools needed to realize MR-EDF calculations for odd-mass nuclei. Benoît, a postdoc in the CENBG's[7] theory group at the time, also developed and implemented in the codes a necessary calculation of the sign of the overlap of two non-orthogonal quasiparticle states [4, 108, 109, 28]. In the early of summer 2011 the codes were finally ready, but we had no time to celebrate because I had to prepare a "shotgun" poster for the ARIS 2011 conference in Leuven. And if I wanted to present something else than an empty poster, with only my name printed in a massively huge font on it[8], we had to rush to

[6]Despite that J. R. R. Tolkien already warned us about the consequences of that kind of mistake [145, 146, 147], even if in a completely different context.

[7]CENBG: Centre d'Etudes Nucléaires de Bordeaux Gradignan.

[8]Some, and by some I mean myself, would say that it would have been, nonetheless, quite a poster.

make some calculations. They were finished just a couple of days before the conference, and to be honest I was still checking and analyzing the results on my laptop during the less interesting talks[9] of the conference.

But very soon we noticed some curious results in our calculations, including those I just had shown at ARIS 2011. Together with Michael and Benoît, we worked for weeks trying to analyze these unexpected issues. We soon found out there were severe problems with the regularization, but still thought we could find a way to overcome them. But every audacious idea, every courageous attempt, was relentlessly followed by a bitter failure. Like in a roller coaster, you go up and down, but with the difference that in a roller coaster you are actually having fun. And also here, there are frictions, you never go as high as you fell. So as you can imagine, the optimism of 2009 was then replaced by doubts and uncertainties. It was a tough fight trying to save several years of our work and trying not to admit that the scientific project of the collaboration had reached an epistemological dead end. Finally, during the fall of that year, the battle was over and the outcome was all but joyful. Indeed, after an afternoon discussion session in Benoît's office, a task force composed by Michael, Benoît and Thomas, who was visiting for a couple of days, arrived in my office and told me without any other form of introduction: "the regularization is dead". Once again the ineluctability of the physical laws was triumphing over the reluctance of the human mind to accept reality. The regularization was over, finished, kaputt. And it meant that less than a year before the scheduled end of my PhD, I had no practical application of the method I developed to present. The formalism was worked out but, demonstrating that the method is working with at least one realistic example was, in my opinion, necessary. Indeed, it is, from my point of view, the key progress made in this thesis. Two years, zero result. It was not uncertainty anymore, it was desperation. But one good thing when you hit rock-bottom, is you also begin to feel detached, or at least this is what I do. I simply didn't care of the (bad) situation I was in as much as I used to do beforehand. I was then expressing the quantum nature of my inner self, a superposition of desperation and detachment.

But sometimes out of something bad comes something good, and I think we experienced one of those times. Of course we were miserable, but we also learned something. Even better, we knew what we had to do next, which is to go back to the only well-defined EDFs, which are the ones derived as the matrix elements of a Hamiltonian. Actually, I found, and still find, this to be the best solution from an espitemological point of view as it led us back to do proper quantum mechanics. One of the features of an Hamiltonian-based EDF is that the terms of the EDF are uniquely determined by the structure of the underlying Hamilton operator. And because we were working before with general functionals, which do not have such drastic requirement, most of the complicated pairing terms corresponding to a two- to three-body body Skyrme pseudo-potential [132, 133] had been neglected until now, and thus never had been implemented in the computational codes. So in late december, I implemented the missing terms of the functional, and the related densities, in the mean-field code, and by the end of january 2012 I had also finished their implementations into the projection code. Michael took care, in parallel, to code the also needed, and previously omitted, exact Coulomb exchange and pairing terms into the projection code. As I said: we knew what we had to do, but it didn't mean it would be easy. We were confronted with a new problem, as we now had the numerical codes to treat a full two plus three-body[10] zero range Skyrme pseudo-potential, but we had no parametrization to use them. The only available two-body Skyrme type interaction [15] was not satisfactory for our purposes, in particular as we wanted to include pairing in the calculations. The solution was then, obviously, to fit a new parametrization, in a Hamiltonian-based EDF philosophy, of the Skyrme effective

[9] Don't blame me, blame the people who give such talks.

[10] Three-body interaction without gradients.

interaction. But as it had never been done, for a functional of that complexity, it took few months for Karim, Michael and Jeremy (another post-doc who joined us in the meantime in Bordeaux) to obtain a decent functional. It also required the addition of a four-body contact term, worked out by Robin in Lyon in the meantime, which was soon implemented in the 3-dimensional numerical codes by myself and Benoît. The result of this effort is the two- to four-body Skyrme functional SLyMR0 [122] which will be used in this work. Clearly, SLyMR0 will not be voted functional of the century, because, let's face it, it has a pretty poor predictive power. However, as bad as it is, at the time being it is the best spuriousity-free functional ever fitted. While we were waiting for the parametrization of the functional, Benoît worked also on the parallelization of the projection code. The MR-EDF calculations being indeed very computationally demanding (especially when exact expressions for Coulomb exchange and pairing terms are used), they require massively parallel supercomputers and, hence, suitably adapted parallelized codes.

Finally, in winter 2012-2013, armed with both the codes and the functional, we launched what we thought to be the first real production calculations on ^{24,25}Mg and ^{17}O. But as you can imagine from the recurring pattern in this story, something, somewhere, was about to go wrong. At the time, I was already entering my fourth year of PhD, something that is not always warmly welcomed in France. Unfortunately Murphy's law doesn't bother about administrative deadlines as it was about to manifest itself once again. In late[11] march 2013, while I arrived in my office during what I thought to be an ordinary morning, Benoît, who was already working there along with Jeremy, asked me: "have you seen your e-mails?". Answering that I didn't, I went immediatly to check my mailbox as I felt that bad news was waiting for me. I received indeed an e-mail from Michael during the night where he was telling us that he might have found a problem in the mean-field codes. Indeed, as it often happens with numerical codes that have reached a certain degree of complexity, despite all the diagnostic printing present in the codes, and despite all the tests ran before, some small issues had been overlooked. They were rapidly identified an corrected, but as they concerned the variational procedure, the validity of all the calculations done before was compromised. The only solution was to throw all the results obtained so far into the trashcan, and to redo all the calculations from scratch. Obviously it meant a new additional delay to the end of my PhD, but as we all know, Science goes first. So as soon as the code was corrected and ready, in april, I launched once again the calculations, the one I am presenting in this thesis. Fortunately, thanks to the experience gained by doing the first batch of calculations, they were finished faster, are more sophisticated and, I think, are of even greater interest. And if you can read this manuscript, it means nothing has gone wrong since then, or at least nothing I am aware of ...

So at the end maybe you are asking yourself: was it worth the effort? was it worth the unbearable pain? was it worth all the tears? and where did you find the ressources to rebuild your life after such a drama? I will maybe surprise you, but I want to reply that yes it did worth it. Of course, there were the pain and the suffering. Of course, there was this feeling of an unending fall into the limbo. Of course, there were the horrible, and repeated, nightmares of being arrested by the Pauli Bureau of Investigation (PBI) for violation of the exclusion principle. Of course, there were the ... well no ... I am a little bit too proud to admit the crying part. Anyway, as one says "after the storm the sun will shine" and indeed, after having quietly resisted all the torments, after having modestly overcome all the ambushes, after having humbly passed all the ordeals, the sun is now shining on the righteous. We have now a model that can treat on the same footing both even-even and odd-even nuclei. We have now a model that thanks to restoration of symmetries and to the configuration mixing made in the MR-EDF calculations takes into account beyond mean-field correlations. We have now a model that at the MR-EDF level can evaluate

[11] Thursday 21^{th} to be precise.

many observables of states with good symmetry properties and thus, can be compared directly and unambiguously to experiment. We have now a model that is using well-defined functionals derived directly from Hamilton operators, and which are free from spuriosities. We have now a model that theoretically can be applied with a single parameterized functional to a wide range of nuclei, from the light to the superheavy. To sum up, we have now a model that is actually working. Houston, mission accomplished!

But more importantly than anything else, I think we have learned a lesson. We have learned that whatever the difficulties, whatever the obstacles, if you really want something and if your heart is pure, miracles can happen. So you shall never give up, you shall never surrender, because if one thing, this thesis has proven that Good always triumphs over Evil![12] And it is with last message of hope I want to finish this unorthodox, but I believe refreshing, introduction.

[12]My scientic honesty forces me here to point out that this conclusion relies on the strong assumptions that we are indeed on the side of Good, and that we have indeed triumphed. Proper definitions of "Good", "Evil" and "to triumph" would also be required. I have myself discovered truly wonderful definitions using Pfaffians, but the footnote is too small to contain it. #DoItLikeFermat #EveryDayPfaffian.
Finally, further work on the subject shall be done to check if the generalization conjectured here is verified for a data set composed of more than one example.

Part I

Theoretical Model

Chapter 1

The Nuclear Energy Density Functional

> *You don't need something more to get something more. That's what emergence means. Life can emerge from physics and chemistry plus a lot of accidents. The human mind can arise from neurobiology and a lot of accidents, the way the chemical bond arises from physics and certain accidents. Doesn't diminish the importance of these subjects to know they follow from more fundamental things plus accidents. That's a general rule, and it's critically important to realize that.*
>
> Murray Gell-Mann, TED Talk: Beauty and truth in physics (2007).

In this first chapter, we will start by going directly to the very heart of the EDF approach, that is, by talking about the energy functional itself. But it lies outside of the scope of this thesis to give the full and complete details about the (various) nuclear EDFs. Instead, we will focus our attention only to aspects relevant for our study and refer for the rest to the plenty of existing and well developed works on this subject [19, 49, 102, 107]. We hope that by keeping a simple perspective, the thesis will be understandeable and useful to a maximum number of readers.[1]

The first section will be dedicated to the nuclear Hamiltonian and how one goes from this Hamiltonian to the nuclear EDF. The second section will define the local and non-local densities used in this chapter and throughout the rest of the thesis. The third, fourth and fifth sections will then describe the various terms in the nuclear EDF, which are the kinetic, Skyrme and Coulomb term, respectively. Finally, the last section will discuss the need for Hamiltonian-based functionals, i.e. functionals directly derived from proper Hamilton operators.

1.1 From the Nuclear Hamiltonian to the Nuclear EDF

The Hamiltonian-based EDF method is a microscopic description of the nucleus whithin which we consider interacting point-like nucleons in a quantum mechanical framework.[2] The energy of the system is determined by an effective Hamilton operator, which for a nucleus composed of A nucleons can be represented as a sum from one- to A-body operators. But in the present thesis, we will consider an effective Hamiltonian which contains only terms up to four-body operators. Unfortunately, nowadays all the (few) existing Hamiltonian-based EDF approaches, including ours, use effective Hamiltonians built from purely empirical considerations, and even if some

[1] The audience for theoretical nuclear physics thesis being already very limited, we do not want the few readers to be bored or confused ...

[2] Non-relativistic in this work.

work has been carried out in the general EDF framework[3] to derive an energy functional from first principles [77, 135], it is yet to do the same in the more restricted case of a Hamiltonian-based EDF. Consequently, at the time being, there is no link between the n-body operators used in our effective Hamiltonian and the n-body forces derived in "bottom-up" approaches [76]. The effective nuclear Hamiltonian used in this thesis reads

$$\hat{H} = \hat{K}^{(1)} + \hat{V}_{Sky}^{(2\text{-}4)} + \hat{V}_{Coul}^{(2)} + \hat{V}_{com}^{(1)} \quad , \tag{1.1}$$

where $\hat{K}^{(1)}$ is the one-body kinetic energy operator, $\hat{V}_{Coul}^{(2)}$ represents the two-body Coulomb interaction between the protons, $\hat{V}_{com}^{(1)}$ is a one-body operator accounting for the center-of-mass correction to the energy and, finally, and maybe the most important and peculiar term, $\hat{V}_{Sky}^{(2\text{-}4)}$ is a sum of two- to four-body operators representing the effective strong nuclear interaction between the nucleons, and which have a form inspired by the pseudo-potential first proposed by Skyrme [132, 133]. The nuclear Hamiltonian can be written in the formalism of second quantization as

$$\begin{aligned} \hat{H} = & \sum_{ij} (k_{ij} + v_{ij}^{com})\, \hat{f}_i^\dagger \hat{f}_j + \frac{1}{2!} \sum_{ijkl} (v_{ijkl}^{Sky\text{-}2} + v_{ijkl}^{Coul})\, \hat{f}_i^\dagger \hat{f}_j^\dagger \hat{f}_l \hat{f}_k \\ & + \frac{1}{3!} \sum_{ijklmn} v_{ijklmn}^{Sky\text{-}3}\, \hat{f}_i^\dagger \hat{f}_j^\dagger \hat{f}_k^\dagger \hat{f}_n \hat{f}_m \hat{f}_l \\ & + \frac{1}{4!} \sum_{ijklmnop} v_{ijklmnop}^{Sky\text{-}4}\, \hat{f}_i^\dagger \hat{f}_j^\dagger \hat{f}_k^\dagger \hat{f}_l^\dagger \hat{f}_p \hat{f}_o \hat{f}_n \hat{f}_m \quad , \end{aligned} \tag{1.2}$$

where $k_{ij}\,, v_{ij}^{com}\,, v_{ijkl}^{Coul}\,, v_{ijkl}^{Sky\text{-}2}\,,\ v_{ijklmn}^{Sky\text{-}3}\,, v_{ijklmnop}^{Sky\text{-}4}$ are the non-antisymmetrized matrix elements associated with the kinetic term, the center-of-mass correction, the Coulomb interaction, the 2-body, the 3-body and the 4-body Skyrme interaction, respectively, and where the $(\hat{f}^\dagger, \hat{f})$ are fermionic creation/annihilation operators in an abitrary single-particle basis.

We will now see how, starting from this nuclear effective Hamiltonian, we can define the corresponding nuclear energy density functional that gives its name to our method. Let us first consider two arbitrary, but normalized, states $|\Phi_1\rangle$ and $|\Phi_2\rangle$ in the Hilbert space. We define the nuclear energy kernel $\mathcal{E}^{nuc}\big[\langle\Phi_1|\,, |\Phi_2\rangle\big]$ as the kernel of the effective nuclear Hamiltonian between $\langle\Phi_1|$ and $|\Phi_2\rangle$

$$\mathcal{E}^{nuc}\big[\langle\Phi_1|\,, |\Phi_2\rangle\big] = \langle\Phi_1|\hat{H}|\Phi_2\rangle \quad . \tag{1.3}$$

If $|\Phi_1\rangle = |\Phi_2\rangle$, the energy kernel reduces to the nuclear energy functional $\mathcal{E}^{nuc}\big[\Phi_1\big]$

$$\mathcal{E}^{nuc}\big[\Phi_1\big] \equiv \mathcal{E}^{nuc}\big[\langle\Phi_1|\,, |\Phi_1\rangle\big] \quad . \tag{1.4}$$

Let us now consider the case of two *a priori* different, but non-orthogonal,[4] Bogoliubov quasi-particle states[5] $|\Phi_a\rangle$ and $|\Phi_b\rangle$, and let us write the energy kernel $\mathcal{E}^{nuc}\big[\langle\Phi_a|\,, |\Phi_b\rangle\big]$ multiplied by a clever form of 1

$$\mathcal{E}^{nuc}\big[\langle\Phi_a|\,, |\Phi_b\rangle\big] = \frac{\langle\Phi_a|\hat{H}|\Phi_b\rangle}{\langle\Phi_a|\Phi_b\rangle} \langle\Phi_a|\Phi_b\rangle \quad . \tag{1.5}$$

Thanks to the non-orthogonality condition on the states $|\Phi_a\rangle$ and $|\Phi_b\rangle$, we can use the Extended Wick Theorem (EWT) of [7] to reexpress the above energy kernel as

$$\mathcal{E}^{nuc}\big[\langle\Phi_a|\,, |\Phi_b\rangle\big] = \mathcal{E}^{nuc}[\rho, \kappa, \kappa^*]^{ab}\, \langle\Phi_a|\Phi_b\rangle \quad , \tag{1.6}$$

[3] $\equiv$ EDFs not necessarily derived from an effective Hamiltonian.
[4] The non-orthogonality of the states is also assumed in the rest of the thesis.
[5] See chapter 2 for their definitions.

where $\mathcal{E}^{nuc}[\rho,\kappa,\kappa^*]^{ab}$ is the nuclear energy density functional kernel

$$\mathcal{E}^{nuc}[\rho,\kappa,\kappa^*]^{ab} = \frac{\langle\Phi_a|\hat{H}|\Phi_b\rangle}{\langle\Phi_a|\Phi_b\rangle} \quad , \tag{1.7}$$

which depends solely on one-body densities, with the latter being discussed in the next section. Taking the case of a diagonal kernel, i.e. $|\Phi_a\rangle = |\Phi_b\rangle$, we obtain an energy density functional which is simply

$$\mathcal{E}^{nuc}\big[\Phi_a\big] \equiv \mathcal{E}^{nuc}[\rho,\kappa,\kappa^*]^{aa} \quad . \tag{1.8}$$

Even if the energy functional, the energy density functional, the energy density functional kernel, and the energy kernel are strictly speaking different mathematical objects, the last being the most general, they are all functionals, and will be thus equivalently refered to as "functional". But only the energy functional and the energy density functional have the meaning of an energy.
And it is to be noted that if someone derives a *practical* extension of Wick's Theorem that can be applied also to orthogonal Bogoliubov quasiparticle states, the condition on the non-orthogonality of $|\Phi_a\rangle$ and $|\Phi_b\rangle$ could be abandoned and we would be able to express the nuclear energy kernel directly in terms of one-body densities.
The nuclear energy density functional kernel can be separated into several parts, corresponding to the contribution of each term of the effective Hamiltonian

$$\mathcal{E}^{nuc}[\rho,\kappa,\kappa^*]^{ab} = \mathcal{E}^{kin}[\rho]^{ab} + \mathcal{E}^{Sky}[\rho,\kappa,\kappa^*]^{ab} + \mathcal{E}^{Coul}[\rho,\kappa,\kappa^*]^{ab} + \mathcal{E}^{com}[\rho]^{ab} \quad . \tag{1.9}$$

In the following sections we will go into the details about the precise structure of each of these terms, but before doing so, it is first mandatory to define the non-local and local one-body densities that will be needed to express these terms.

1.2 Non-Local and Local One-Body Densities

In the present work the possibility of proton-neutron pairing is neglected, so we will consider only densities that do not mix protons and neutrons [102, 114]. And we first start by defining the non-local one-body densities between a pair of *a priori* different states $\big[\langle\Phi_a|\,,|\Phi_b\rangle\big]$

$$\rho_t^{ab}(\vec{r}\sigma,\vec{r}'\sigma') = \frac{\langle\Phi_a|\hat{f}^\dagger_{\vec{r}'\sigma' t}\hat{f}_{\vec{r}\sigma t}|\Phi_b\rangle}{\langle\Phi_a|\Phi_b\rangle} \quad , \tag{1.10}$$

$$\kappa_t^{ab}(\vec{r}\sigma,\vec{r}'\sigma') = \frac{\langle\Phi_a|\hat{f}_{\vec{r}'\sigma' t}\hat{f}_{\vec{r}\sigma t}|\Phi_b\rangle}{\langle\Phi_a|\Phi_b\rangle} \quad , \tag{1.11}$$

$$\kappa_t^{ba*}(\vec{r}\sigma,\vec{r}'\sigma') = \frac{\langle\Phi_a|\hat{f}^\dagger_{\vec{r}\sigma t}\hat{f}^\dagger_{\vec{r}'\sigma' t}|\Phi_b\rangle}{\langle\Phi_a|\Phi_b\rangle} \quad , \tag{1.12}$$

where $\vec{r},\vec{r}'$ are the spatial coordinates, $\sigma,\sigma' = \pm\frac{1}{2}$ are the spin components, t labels the particle species (n: neutrons, z: protons), and where the creation operators $\hat{f}^\dagger$ can be expressed in terms of a single-particle basis associated with $|\Phi_a\rangle$, and the annihilation operators $\hat{f}$ in terms of a single-particle basis associated with $|\Phi_b\rangle$

$$\begin{aligned} |\Phi_a\rangle &: \hat{a}^\dagger,\hat{a},\psi^a \quad , \\ |\Phi_b\rangle &: \hat{b}^\dagger,\hat{b},\psi^b \quad , \end{aligned} \tag{1.13}$$

such that

$$\begin{aligned} \hat{f}^{\dagger}_{\vec{r}\sigma t} &= \sum_i \hat{a}^{\dagger}_{t,i}\, \psi^{a}_{t,i}{}^{*}(\vec{r}\sigma) \quad , \\ \hat{f}_{\vec{r}\sigma t} &= \sum_j \hat{b}_{t,j}\, \psi^{b}_{t,j}(\vec{r}\sigma) \quad . \end{aligned} \tag{1.14}$$

It is important to note that κ^{ba*}_t is in general not the complex conjugate of κ^{ab}_t. As a matter of fact, this is the case only when $|\Phi_a\rangle = |\Phi_b\rangle$. But as our attention in this work will be focussed on the symmetry restoration and the configuration mixing of different Bogoliubov quasiparticle states, we will in general have $|\Phi_a\rangle \neq |\Phi_b\rangle$; we speak then of mixed densities. In order to express in a simple manner the pairing part of the Skyrme EDF kernel, it is of advantage to introduce another, completely equivalent, representation (the so-called "russian representation") of the pairing densities [49, 118]

$$\begin{aligned} \tilde{\rho}^{ab}_t(\vec{r}\sigma, \vec{r}'\sigma') &= -2\sigma' \kappa^{ab}_t(\vec{r}\sigma, \vec{r}' - \sigma') \\ &= -2\sigma' \, \frac{\langle \Phi_a | \hat{f}_{\vec{r}'-\sigma' t} \hat{f}_{\vec{r}\sigma t} | \Phi_b \rangle}{\langle \Phi_a | \Phi_b \rangle} \quad , \end{aligned} \tag{1.15}$$

$$\begin{aligned} \tilde{\rho}^{ba*}_t(\vec{r}\sigma, \vec{r}'\sigma') &= -2\sigma' \kappa^{ba*}_t(\vec{r}\sigma, \vec{r}' - \sigma') \\ &= -2\sigma' \, \frac{\langle \Phi_a | \hat{f}^{\dagger}_{\vec{r}\sigma t} \hat{f}^{\dagger}_{\vec{r}'-\sigma' t} | \Phi_b \rangle}{\langle \Phi_a | \Phi_b \rangle} \quad . \end{aligned} \tag{1.16}$$

From the non-local normal density of equation (1.10) we can define a set of local normal densities

$$\rho^{ab}_t(\vec{r}) = \sum_\sigma \rho^{ab}_t(\vec{r}\sigma, \vec{r}'\sigma)|_{\vec{r}=\vec{r}'} \quad , \tag{1.17}$$

$$s^{ab}_{t,\mu}(\vec{r}) = \sum_{\sigma\sigma'} \langle \sigma | \hat{\sigma}_\mu | \sigma' \rangle \, \rho^{ab}_t(\vec{r}\sigma, \vec{r}'\sigma')|_{\vec{r}=\vec{r}'} \quad , \tag{1.18}$$

$$\tau^{ab}_t(\vec{r}) = \sum_\sigma \vec{\nabla}_{\vec{r}} \cdot \vec{\nabla}_{\vec{r}'} \, \rho^{ab}_t(\vec{r}\sigma, \vec{r}'\sigma)|_{\vec{r}=\vec{r}'} \quad , \tag{1.19}$$

$$T^{ab}_{t,\mu}(\vec{r}) = \sum_{\sigma\sigma'} \vec{\nabla}_{\vec{r}} \cdot \vec{\nabla}_{\vec{r}'} \langle \sigma | \hat{\sigma}_\mu | \sigma' \rangle \, \rho^{ab}_t(\vec{r}\sigma, \vec{r}'\sigma')|_{\vec{r}=\vec{r}'} \quad , \tag{1.20}$$

$$j^{ab}_{t,\mu}(\vec{r}) = -\frac{i}{2} \sum_\sigma (\nabla_{\vec{r},\mu} - \nabla_{\vec{r}',\mu}) \, \rho^{ab}_t(\vec{r}\sigma, \vec{r}'\sigma)|_{\vec{r}=\vec{r}'} \quad , \tag{1.21}$$

$$J^{ab}_{t,\mu\nu}(\vec{r}) = -\frac{i}{2} \sum_{\sigma\sigma'} (\nabla_{\vec{r},\mu} - \nabla_{\vec{r}',\mu}) \langle \sigma | \hat{\sigma}_\nu | \sigma' \rangle \, \rho^{ab}_t(\vec{r}\sigma, \vec{r}'\sigma')|_{\vec{r}=\vec{r}'} \quad , \tag{1.22}$$

$$\mathrm{J}^{ab}_{t,\lambda}(\vec{r}) = \sum_{\mu\nu} \epsilon_{\lambda\mu\nu} J^{ab}_{t,\mu\nu}(\vec{r}) \quad , \tag{1.23}$$

which are the local density, the spin vector density, the kinetic density, the spin-kinetic vector density, the current vector density, the spin-current tensor and its vector part, the spin-orbit current vector, respectively. Greek indices μ, ν, λ can take the values: x, y, z ; $\nabla_{\vec{r}}$ and $\nabla_{\vec{r}'}$ are spatial derivatives acting on $\vec{r}$ and $\vec{r}'$, respectively. While the scalar normal densities and the spin-orbit current vector are time-even, i.e. they do not change sign under time-reversal, $\vec{s}^{ab}_t$, $\vec{T}^{ab}_t$ and $\vec{j}^{ab}_t$ are time-odd, i.e. they change sign under time-reversal. In this work, we will focus on

the case of Bogoliubov one-quasiparticle states, therefore the time-odd densities will always be nonzero. Similarly, we obtain a set of local pairing densities from the non-local pairing densities (1.15) and (1.16)

$$\tilde{\rho}_t^{ab}(\vec{r}) = \sum_\sigma \tilde{\rho}_t^{ab}(\vec{r}\sigma, \vec{r}'\sigma)|_{\vec{r}=\vec{r}'} \quad , \tag{1.24}$$

$$\tilde{\tau}_t^{ab}(\vec{r}) = \sum_\sigma \vec{\nabla}_{\vec{r}} \cdot \vec{\nabla}_{\vec{r}'}\, \tilde{\rho}_t^{ab}(\vec{r}\sigma, \vec{r}'\sigma)|_{\vec{r}=\vec{r}'} \quad , \tag{1.25}$$

$$\tilde{J}_{t,\mu\nu}^{ab}(\vec{r}) = -\frac{i}{2}\sum_{\sigma\sigma'}(\nabla_{\vec{r},\mu} - \nabla_{\vec{r}',\mu})\langle\sigma|\hat{\sigma}_\nu|\sigma'\rangle\, \tilde{\rho}_t^{ab}(\vec{r}\sigma, \vec{r}'\sigma')|_{\vec{r}=\vec{r}'} \quad , \tag{1.26}$$

$$\tilde{\rho}_t^{ba\,*}(\vec{r}) = \sum_\sigma \tilde{\rho}_t^{ba\,*}(\vec{r}\sigma, \vec{r}'\sigma)|_{\vec{r}=\vec{r}'} \quad , \tag{1.27}$$

$$\tilde{\tau}_t^{ba\,*}(\vec{r}) = \sum_\sigma \vec{\nabla}_{\vec{r}} \cdot \vec{\nabla}_{\vec{r}'}\, \tilde{\rho}_t^{ba\,*}(\vec{r}\sigma, \vec{r}'\sigma)|_{\vec{r}=\vec{r}'} \quad , \tag{1.28}$$

$$\tilde{J}_{t,\mu\nu}^{ba\ *}(\vec{r}) = -\frac{i}{2}\sum_{\sigma\sigma'}(\nabla_{\vec{r}',\mu} - \nabla_{\vec{r},\mu})\langle\sigma'|\hat{\sigma}_\nu|\sigma\rangle\, \tilde{\rho}_t^{ba\,*}(\vec{r}\sigma, \vec{r}'\sigma')|_{\vec{r}=\vec{r}'} \quad , \tag{1.29}$$

which are the local pairing density, the kinetic pairing density, and the pairing spin-current tensor, respectively, defined between a pair of states $\left[\langle\Phi_a|, |\Phi_b\rangle\right]$ and the complex conjugates of the equivalent densities defined between the reverse pair of states $\left[\langle\Phi_b|, |\Phi_a\rangle\right]$.

We only give here the basic definitions of the local and non-local densities required to express the functionals. More informations about and more properties of the densities can be found in other sources [107, 19, 121, 118, 49, 102]. And now that we have properly defined these densities, we can go into more detail about the different terms of the EDF kernel. But for the sake of clarity,[6] we will drop the $\vec{r}$ dependence of the local densities (e.g. $\rho_t^{ab} \equiv \rho_t^{ab}(\vec{r})$).

1.3 Kinetic Energy and Center-Of-Mass Correction

The first, and also the simplest, term of the nuclear EDF kernel comes from the kinetic energy operator, which expressed in terms of the single-particle bases associated with $|\Phi_a\rangle$ and $|\Phi_b\rangle$, reads

$$\hat{K}^{(1)} = \sum_{t,ij} k_{t,ij}\, \hat{a}_{t,i}^\dagger \hat{b}_{t,j} \quad , \tag{1.30}$$

with $k_{t,ij}$ being the matrix elements $\langle i_{t,a}|\hat{K}^{(1)}|j_{t,b}\rangle$. These can be written as

$$\langle i_{t,a}|\hat{K}^{(1)}|j_{t,b}\rangle = \frac{\hbar^2}{2m}\sum_\sigma \int d\vec{r}\, [\vec{\nabla}\psi_{t,i}^a(\vec{r}\sigma)]^* \cdot [\vec{\nabla}\psi_{t,j}^b(\vec{r}\sigma)] \quad , \tag{1.31}$$

where the mass of a neutron and of a proton is assumed to be equal for the parametrization of the EDF kernel used here: $m_n = m_z = m$. When evaluated between a pair of states $\left[\langle\Phi_a|, |\Phi_b\rangle\right]$, the kinetic energy operator gives the EDF kernel

$$\mathcal{E}^{kin}[\rho]^{\,ab} = \int d\vec{r} \sum_{t=n,z} \frac{\hbar^2}{2m}\tau_t^{ab} \quad . \tag{1.32}$$

Center-Of-Mass Correction

In order to remove the spurious contribution of the center-of-mass motion to the energy, resulting from the unphysical translational invariance symmetry breaking appearing in all the

[6] We do not want an extra-large expression for the Skyrme functionals. No we do not!

self-consistent mean-field calculations of finite systems, we add a center-of-mass correction to the total nuclear EDF kernel

$$\mathcal{E}^{com}[\rho]^{ab} = -\int d\vec{r} \sum_{t=n,z} \frac{\hbar^2}{2mA} \tau_t^{ab} \quad . \tag{1.33}$$

This correction is actually only a crude approximation [17] as we consider only the one-body diagonal term of the already approximated, and still complex, correction [19]

$$\hat{V}_{com}^{(1\text{-}2)} = -\frac{\hat{\vec{P}}_{com}^{\,2}}{2mA} \quad , \tag{1.34}$$

where $\hat{\vec{P}}_{com}$ is the center-of-mass linear momentum that is equal to the sum of single-particle linear momenta : $\hat{\vec{P}}_{com} = \sum_{i=1}^{A} \hat{\vec{p}}_i$.
The sum of the kinetic term and of the center-of-mass correction can be combined into the simple expression

$$\mathcal{E}^{kin}[\rho]^{ab} + \mathcal{E}^{com}[\rho]^{ab} = \int d\vec{r} \sum_{t=n,z} \frac{\hbar^2}{2m}\left(1 - \frac{1}{A}\right) \tau_t^{ab} \quad . \tag{1.35}$$

The center-of-mass correction is thus easily taken into account by simply multiplying a factor $\left(1 - \frac{1}{A}\right)$ to the kinetic EDF kernel.

1.4 The Skyrme Pseudo-Potential

1.4.1 The Skyrme Pseudo-Potential Operator

In contrast to the kinetic term (section 1.3) and to the Coulomb term (section 1.5), there exists no simple form for the term of the effective Hamiltonian associated with the nuclear strong interaction. Neither it exists a derivation from first principles of a functional that could be *safely* used in the perspective of a MR-EDF calculation. So in order to model the strong interaction acting between the nucleons, we adopt a purely phenomenological point of view and use an empirical zero-range pseudo-potential, following the founding work of Skyrme [132, 133]. An advantage of the zero-range Skyrme-type pseudo-potentials is that the numerical calculations are considerably simplified. Indeed, the Skyrme functionals derived from this type of pseudo-potentials are fully local and thus the number of (very time-consuming) spatial integrations to be performed is substantially reduced. Our Skyrme-type pseudo-potential is a sum of a two-body $\hat{V}_{Sky}^{(2)}$, a three-body $\hat{V}_{Sky}^{(3)}$ and a four-body $\hat{V}_{Sky}^{(4)}$ zero-range operator

$$\hat{V}_{Sky}^{(2\text{-}4)} = \hat{V}_{Sky}^{(2)} + \hat{V}_{Sky}^{(3)} + \hat{V}_{Sky}^{(4)} \quad . \tag{1.36}$$

The two-body operator $\hat{V}_{Sky}^{(2)}$ is the most complex one as it includes not only a simple contact force, but also gradient terms which simulate non-locality and finite-range effects [107], and as it also includes a spin-orbit term; it reads

$$\begin{aligned} \hat{V}_{Sky}^{(2)} = {} & t_0 \left(1 + x_0 \hat{P}_{12}^{\sigma}\right) \hat{\delta}_{r_1 r_2} \\ & + \frac{t_1}{2} \left(1 + x_1 \hat{P}_{12}^{\sigma}\right) \left(\hat{\vec{k}}_{12}^{\prime 2} \hat{\delta}_{r_1 r_2} + \hat{\delta}_{r_1 r_2} \hat{\vec{k}}_{12}^{2}\right) \\ & + t_2 \left(1 + x_2 \hat{P}_{12}^{\sigma}\right) \hat{\vec{k}}_{12}^{\prime} \hat{\delta}_{r_1 r_2} \cdot \hat{\vec{k}}_{12} \\ & + iW_0 \left(\hat{\vec{\sigma}}_1 + \hat{\vec{\sigma}}_2\right) \hat{\vec{k}}_{12}^{\prime} \hat{\delta}_{r_1 r_2} \times \hat{\vec{k}}_{12} \quad , \end{aligned} \tag{1.37}$$

where $\hat{\delta}_{r_1 r_2} = \hat{\delta}(\vec{r}_1 - \vec{r}_2)$ is a position delta operator, $\hat{\vec{k}}_{12} = -\frac{i}{2}(\hat{\vec{\nabla}}_1 - \hat{\vec{\nabla}}_2)$ is the relative momentum[7] between the two particles with the derivatives acting on the ket, $\hat{\vec{k}}'_{12}$ is its complex conjugate with the derivatives acting on the bra, $\hat{\vec{\sigma}}_1$ and $\hat{\vec{\sigma}}_2$ are the spin operators acting on the particle 1 and 2, respectively, and finally $\hat{P}^{\sigma}_{12} = \frac{1}{2}\left(1 + \hat{\vec{\sigma}}_1 \cdot \hat{\vec{\sigma}}_2\right)$ is the spin-exchange operator.

Concerning the three-body operator $\hat{V}^{(3)}_{Sky}$, we take here only a three-body zero-range central term without gradients that can be expressed as

$$\hat{V}^{(3)}_{Sky} = u_0 \left(\hat{\delta}_{r_1 r_3}\hat{\delta}_{r_2 r_3} + \hat{\delta}_{r_3 r_2}\hat{\delta}_{r_1 r_3} + \hat{\delta}_{r_2 r_1}\hat{\delta}_{r_3 r_1}\right) \quad . \tag{1.38}$$

The presence of three different, but equivalent, terms is required for the interaction to be totally symmetic under exchange of any two indices. It might seem superfluous in the case of a simple three-body delta force as used in our calculation, but becomes absolutely necessary when adding three-body gradient terms as it has been worked out by Sadoudi *et al.* [121, 123]. In addition, there are already too many different notations in theoretical nuclear physics that talk about the same objects, so we try here not to add another notation and to be consistent with the previously existing, and clear, definition of [121, 123].

The same is true for the four-body operator $\hat{V}^{(4)}_{Sky}$, where twelve equivalent zero-range contact terms appear

$$\begin{aligned}\hat{V}^{(4)}_{Sky} = v_0 \Big(&\hat{\delta}_{r_1 r_3}\hat{\delta}_{r_2 r_3}\hat{\delta}_{r_3 r_4} + \hat{\delta}_{r_1 r_2}\hat{\delta}_{r_3 r_2}\hat{\delta}_{r_2 r_4} + \hat{\delta}_{r_2 r_1}\hat{\delta}_{r_3 r_1}\hat{\delta}_{r_1 r_4} \\ &+ \hat{\delta}_{r_1 r_4}\hat{\delta}_{r_2 r_4}\hat{\delta}_{r_4 r_3} + \hat{\delta}_{r_1 r_2}\hat{\delta}_{r_4 r_2}\hat{\delta}_{r_2 r_3} + \hat{\delta}_{r_2 r_1}\hat{\delta}_{r_4 r_1}\hat{\delta}_{r_1 r_3} \\ &+ \hat{\delta}_{r_1 r_4}\hat{\delta}_{r_3 r_4}\hat{\delta}_{r_4 r_2} + \hat{\delta}_{r_1 r_3}\hat{\delta}_{r_4 r_3}\hat{\delta}_{r_3 r_2} + \hat{\delta}_{r_3 r_1}\hat{\delta}_{r_4 r_1}\hat{\delta}_{r_1 r_2} \\ &+ \hat{\delta}_{r_2 r_4}\hat{\delta}_{r_3 r_4}\hat{\delta}_{r_4 r_1} + \hat{\delta}_{r_2 r_3}\hat{\delta}_{r_4 r_3}\hat{\delta}_{r_3 r_1} + \hat{\delta}_{r_3 r_2}\hat{\delta}_{r_4 r_2}\hat{\delta}_{r_2 r_1}\Big) \quad .\end{aligned} \tag{1.39}$$

But one should not be scared by the number of terms present in the three-body and four-body interactions as each of these terms will give the same contribution to their respective functionals, i.e. we will have three times the functional given by one of the terms of $\hat{V}^{(3)}_{Sky}$, for example $\hat{\delta}_{r_1 r_3}\hat{\delta}_{r_2 r_3}$, and similarly we will have twelve times the same functional for $\hat{V}^{(4)}_{Sky}$.

The Parametrization SLyMR0

In the present thesis, we are going to use the SLyMR0 parametrization [122] whose coupling constants can be found in Tab. 1.1. This parametrization has been fitted to describe a set of nuclear masses and radii, while avoiding any unphysical instabilities. The essential nuclear matter properties of SLyMR0 are listed in Tab. 1.2, and are compared to the widely used SLy4 parametrization [43] and the SV parametrization [15] used by Satuła *et al.* [126, 127] in their calculations which include projection on angular-momentum and isospin. The results for both finite nuclei and nuclear matter are quite poor with the SLyMR0 parametrization [122]. We can see in particular that SLyMR0 has a very low symmetry energy coefficient a_{sym} as well as a low effective mass m^*_0. But as bad as this parametrization appears to be, it is still (by default) the best parametrization we can use at the time being for our MR-EDF calculations. Indeed, it was fitted in a true pseudo-potential spirit, has no instabilites with respect to finite-size perturbations for densities encountered in low energy nuclear structure, has a more or less acceptable pairing

[7] Divided by $\hbar$.

and, finally, it has a low but still higher effective mass than SV.

Parameters	Value	Unit
t_0	-1210.093228	(MeV.fm^3)
x_0	-0.283818	
t_1	632.460114	(MeV.fm^5)
x_1	-0.038032	
t_2	45.081296	(MeV.fm^5)
x_2	1.849978	
W_0	122.618466	(MeV.fm^5)
u_0	2529.151191	(MeV.fm^6)
v_0	-14750.000000	(MeV.fm^9)

Table 1.1: Parameters of the SLyMR0 parametrization. The numerical values are taken from [122].

Param.	ρ_{sat} (fm^{-3})	E/A (MeV)	a_{sym} (MeV)	m_0^*/m	K_∞ (MeV)	g_0
SV	0.155	-16.05	32.8	0.38	305.7	0.57
SLyMR0	0.152	-15.04	23.0	0.47	264.2	0.88
SLy4	0.160	-15.97	32.0	0.69	229.9	1.38

Table 1.2: Saturation density ρ_{sat}, energy per particle E/A, symmetry energy coefficient a_{sym}, effective mass m_0^*, incompressibility K_∞ and spin-Landau parameter g_0 at saturation for the parametrizations as indicated. The numerical values are taken from [122].

1.4.2 The Skyrme Functional

Evaluating the Skyrme operator between a pair of states $\langle\Phi_a|$ and $|\Phi_b\rangle$, one obtains the complete Skyrme EDF kernel

$$\begin{aligned}\mathcal{E}^{Sky}[\rho,\tilde{\rho},\tilde{\rho}^*]^{ab} &= \frac{\langle\Phi_a|\hat{V}^{(2)}_{Sky}+\hat{V}^{(3)}_{Sky}+\hat{V}^{(4)}_{Sky}|\Phi_b\rangle}{\langle\Phi_a|\Phi_b\rangle} \\ &= \mathcal{E}^{Sky\text{-}2}[\rho,\tilde{\rho},\tilde{\rho}^*]^{ab}+\mathcal{E}^{Sky\text{-}3}[\rho,\tilde{\rho},\tilde{\rho}^*]^{ab}+\mathcal{E}^{Sky\text{-}4}[\rho,\tilde{\rho},\tilde{\rho}^*]^{ab} \quad ,\end{aligned} \tag{1.40}$$

where $\mathcal{E}^{Sky\text{-}2}$, $\mathcal{E}^{Sky\text{-}3}$, $\mathcal{E}^{Sky\text{-}4}$ are respectively the bilinear, trilinear and quadrilinear Skyrme EDF kernels. We then give without demonstration a full, and we hope *comprehensible*, expression of these functionals in the proton-neutron formalism

$$\begin{aligned}\mathcal{E}^{Sky\text{-}2}[\rho,\tilde{\rho},\tilde{\rho}^*]^{ab} = \int d\vec{r}\Bigg\{ &\sum_{t=n,z}\Bigg[A_0^{(tx)}\Big(\rho_t^{ab\,2}-\vec{s}_t^{\,ab\,2}+\tilde{\rho}_t^{ba*}\tilde{\rho}_t^{ab}\Big) \\ &+A_1^{(tx)}\Big(\vec{\nabla}\rho_t^{ab}\cdot\vec{\nabla}\rho_t^{ab}\Big)+A_2^{(tx)}\Big(\sum_{\mu\nu}\nabla_\mu s_{t,\nu}^{ab}\nabla_\mu s_{t,\nu}^{ab}\Big)+A_3^{(tx)}\Big(\vec{\nabla}\tilde{\rho}_t^{ba*}\cdot\vec{\nabla}\tilde{\rho}_t^{ab}\Big) \\ &+A_4^{(tx)}\Big(\tau_t^{ab}\rho_t^{ab}-\vec{j}_t^{\,ab\,2}\Big)+A_5^{(tx)}\Big(\vec{T}_t^{\,ab}\cdot\vec{s}_t^{\,ab}-\sum_{\mu\nu}J_{t,\mu\nu}^{ab}J_{t,\mu\nu}^{ab}\Big) \\ &+A_6^{(tx)}\Big(\tilde{\tau}_t^{ba*}\tilde{\rho}_t^{ab}+\tilde{\tau}_t^{ab}\tilde{\rho}_t^{ba*}\Big)+A_7^{(tx)}\Big(\sum_{\mu,\nu}\tilde{J}_{t,\mu\nu}^{ba\ *}\tilde{J}_{t,\mu\nu}^{ab}\Big) \\ &+A_1^{(W)}\Big(2\,\rho_t^{ab}\,\vec{\nabla}\cdot\vec{\mathrm{J}}_t^{\,ab}+2\,\vec{s}_t^{\,ab}\cdot\vec{\nabla}\times\vec{j}_t^{\,ab}+\sum_{\mu\nu}\big(\tilde{J}_{t,\mu\nu}^{ba\ *}\tilde{J}_{t,\nu\mu}^{ab}-\tilde{J}_{t,\mu\mu}^{ba\ *}\tilde{J}_{t,\nu\nu}^{ab}\big)\Big)\Bigg] \\ &+A_8^{(tx)}\Big(\rho_n^{ab}\rho_z^{ab}\Big)+A_9^{(tx)}\Big(\vec{s}_n^{\,ab}\cdot\vec{s}_z^{\,ab}\Big) \\ &+A_{10}^{(tx)}\Big(\vec{\nabla}\rho_n^{ab}\cdot\vec{\nabla}\rho_z^{ab}\Big)+A_{11}^{(tx)}\Big(\sum_{\mu\nu}\nabla_\mu s_{n,\nu}^{ab}\nabla_\mu s_{z,\nu}^{ab}\Big) \\ &+A_{12}^{(tx)}\Big(\tau_n^{ab}\rho_z^{ab}+\tau_z^{ab}\rho_n^{ab}-2\vec{j}_n^{\,ab}\cdot\vec{j}_z^{\,ab}\Big) \\ &+A_{13}^{(tx)}\Big(\vec{T}_n^{\,ab}\cdot\vec{s}_z^{\,ab}+\vec{T}_z^{\,ab}\cdot\vec{s}_n^{\,ab}-2\sum_{\mu\nu}J_{n,\mu\nu}^{ab}J_{z,\mu\nu}^{ab}\Big) \\ &+A_1^{(W)}\Big(\rho_n^{ab}\,\vec{\nabla}\cdot\vec{\mathrm{J}}_z^{\,ab}+\rho_z^{ab}\,\vec{\nabla}\cdot\vec{\mathrm{J}}_n^{\,ab}+\vec{s}_n^{\,ab}\cdot\vec{\nabla}\times\vec{j}_z^{\,ab}+\vec{s}_z^{\,ab}\cdot\vec{\nabla}\times\vec{j}_n^{\,ab}\Big)\Bigg\} \quad ,\end{aligned} \tag{1.41}$$

$$\mathcal{E}^{Sky\text{-}3}[\rho,\tilde{\rho},\tilde{\rho}^*]^{ab} = \int d\vec{r}\,A_0^{(u)}\Big[\Big(\rho_n^{ab\,2}-\vec{s}_n^{\,ab\,2}+\tilde{\rho}_n^{ba*}\tilde{\rho}_n^{ab}\Big)\rho_z^{ab}+\Big(\rho_z^{ab\,2}-\vec{s}_z^{\,ab\,2}+\tilde{\rho}_z^{ba*}\tilde{\rho}_z^{ab}\Big)\rho_n^{ab}\Big] \quad , \tag{1.42}$$

$$\mathcal{E}^{Sky\text{-}4}[\rho,\tilde{\rho},\tilde{\rho}^*]^{ab} = \int d\vec{r}\,A_0^{(v)}\Big[\Big(\rho_n^{ab\,2}-\vec{s}_n^{\,ab\,2}+\tilde{\rho}_n^{ba*}\tilde{\rho}_n^{ab}\Big)\Big(\rho_z^{ab\,2}-\vec{s}_z^{\,ab\,2}+\tilde{\rho}_z^{ba*}\tilde{\rho}_z^{ab}\Big)\Big] \quad , \tag{1.43}$$

where the functional coefficients $A_i^{tx,W,u,v}$ are given in Table 1.3. It is worth noting that the three-body and the four-body functionals can be written very simply in terms of the $A_0^{(tx)}$ part

of the two-body functional. The three-body functional $\mathcal{E}^{Sky\text{-}3}$ is equal to the sum over particle species of the $A_0^{(tx)}$ part of $\mathcal{E}^{Sky\text{-}2}$ of one particle species times the local normal density of the other particle species, and the four-body functional $\mathcal{E}^{Sky\text{-}4}$ can be written as the product of the proton and neutron $A_0^{(tx)}$ parts of $\mathcal{E}^{Sky\text{-}2}$. We do not attempt to give here the most compact form of the functionals. Instead, we try to give a clear and usable expression from a computational point of view. We find it easier, with the functionals given in these forms, to identify all the terms to be implemented in a numerical program.

$Coeff.\setminus Param.$	t_0	t_0x_0	t_1	t_1x_1	t_2	t_2x_2	W_0	u_0	v_0
$A_0^{(tx)} =$	$+\frac{1}{4}$	$-\frac{1}{4}$							
$A_1^{(tx)} =$			$+\frac{3}{32}$	$-\frac{3}{32}$	$-\frac{3}{32}$	$-\frac{3}{32}$			
$A_2^{(tx)} =$			$-\frac{3}{32}$	$+\frac{3}{32}$	$-\frac{1}{32}$	$-\frac{1}{32}$			
$A_3^{(tx)} =$			$+\frac{1}{16}$	$-\frac{1}{16}$					
$A_4^{(tx)} =$			$+\frac{1}{8}$	$-\frac{1}{8}$	$+\frac{3}{8}$	$+\frac{3}{8}$			
$A_5^{(tx)} =$			$-\frac{1}{8}$	$+\frac{1}{8}$	$+\frac{1}{8}$	$+\frac{1}{8}$			
$A_6^{(tx)} =$			$+\frac{1}{8}$	$-\frac{1}{8}$					
$A_7^{(tx)} =$					$+\frac{1}{4}$	$+\frac{1}{4}$			
$A_8^{(tx)} =$	$+1$	$+\frac{1}{2}$							
$A_9^{(tx)} =$		$+\frac{1}{2}$							
$A_{10}^{(tx)} =$			$+\frac{3}{8}$	$+\frac{3}{16}$	$-\frac{1}{8}$	$-\frac{1}{16}$			
$A_{11}^{(tx)} =$				$+\frac{3}{16}$		$-\frac{1}{16}$			
$A_{12}^{(tx)} =$			$+\frac{1}{4}$	$+\frac{1}{8}$	$+\frac{1}{4}$	$+\frac{1}{8}$			
$A_{13}^{(tx)} =$				$+\frac{1}{8}$		$+\frac{1}{8}$			
$A_1^{(W)} =$							$-\frac{1}{2}$		
$A_0^{(u)} =$								$+\frac{3}{4}$	
$A_0^{(v)} =$									$+\frac{3}{4}$

Table 1.3: Functional coefficients in neutron-proton representation expressed in terms of pseudo-potential parameters. Example of how one should read a line of the table: $A_0^{(tx)} = \frac{1}{4}t_0 - \frac{1}{4}t_0x_0$.

Energy Cut-Off in the Pairing Part of the Functional

It is well known that using spatial zero-range pseudo-potential one encounters an ultraviolet divergence in the pairing channel due to the summation of very high, and even infinite, energy pair scattering processes [40]. To avoid this problem while using a zero-range pseudo-potential, we integrate in the single-reference calculations ($|\Phi_a\rangle = |\Phi_b\rangle$) an energy cut-off in the computation of the contractions for pairing densities in the single-particle basis which diagonalizes the single-

particle Hamiltonian

$$\begin{aligned} \langle\Phi_b|\hat{b}_{t,i}\hat{b}_{t,j}|\Phi_b\rangle &\longrightarrow \langle\Phi_b|\hat{b}_{t,i}\hat{b}_{t,j}|\Phi_b\rangle h_{t,i}h_{t,j} \quad , \\ \langle\Phi_b|\hat{b}^\dagger_{t,i}\hat{b}^\dagger_{t,j}|\Phi_b\rangle &\longrightarrow \langle\Phi_b|\hat{b}^\dagger_{t,i}\hat{b}^\dagger_{t,j}|\Phi_b\rangle h_{t,i}h_{t,j} \quad , \end{aligned} \tag{1.44}$$

with the cut-off factors $h_{t,i}$ of the form [4]

$$h_{t,i} = \begin{cases} 1 & |\epsilon_{t,i} - \lambda_t| < E_{cut} - \frac{d_{cut}}{2} \\ \frac{1}{2}\cos\left[\left(|\epsilon_{t,i} - \lambda_t| - E_{cut} + \frac{d_{cut}}{2}\right)\frac{\pi}{d_{cut}}\right] + \frac{1}{2} & \text{if} \quad \left||\epsilon_{t,i} - \lambda_t| - E_{cut}\right| \leq \frac{d_{cut}}{2} \\ 0 & |\epsilon_{t,i} - \lambda_t| > E_{cut} + \frac{d_{cut}}{2} \end{cases} , \tag{1.45}$$

where $\epsilon_{t,i}$ is the energy of the single-particle state $\psi^b_{t,i}$, λ_t is the Fermi energy of particle species t, E_{cut} and d_{cut} are two arbitrary parameters that in our case are set for all the calculations to the values

$$\begin{aligned} E_{cut} &= 8.5\,\text{MeV} \quad , \\ d_{cut} &= 2.5\,\text{MeV} \quad . \end{aligned} \tag{1.46}$$

As there is no natural energy cut-off in our theory, such choice for the numerical values of the parameters (as well as the choice of basis in which we include the cut-off) is arbitrary and is based almost solely on the preference of the EDF practitioner. However, for the sake of consistency, the same form and parameters values were used for the cut-off in the fit of SLyMR0 and in the practical applications presented here. And even if it is true that this cut-off injects an unsatisfactory dose of arbitrariness in the calculation of the pairing energy, it is the only solution if we want to carry out calculations with zero-range Skyrme-type functionals. Besides, in our case we view the quasiparticle states as a simple generating set of states for multi-reference calculations where the pairing energy is then properly calculated (without cut-off) and where a new minimization is done through the GCM, so we hope that this arbitrariness will not heavily impact our results.

1.5 The Coulomb Interaction

The last contribution to the total nuclear energy comes from the Coulomb interaction between the protons inside the nucleus. Indeed, in this work we disregard the nucleon's internal degrees of freedom and consider protons and neutrons as point-like particles and as such only protons contribute to the Coulomb interaction. We thus approximate the charge density by the proton density: $\rho_{ch} = \rho_z$.
In second quantization form, the Coulomb interaction reads

$$\hat{V}^{(2)}_{Coul} = \frac{1}{2!}\sum_{ijkl} v^{Coul}_{z,ijkl}\,\hat{a}^\dagger_{z,i}\hat{a}^\dagger_{z,j}\hat{b}_{z,l}\hat{b}_{z,k} \quad , \tag{1.47}$$

with $v^{Coul}_{z,ijkl} = \langle ij_{z,a}|\hat{V}^{(2)}_{Coul}|kl_{z,b}\rangle$ being the matrix elements of the Coulomb interaction. We can express these matrix elements $v^{Coul}_{z,ijkl}$ in coordinate space representation as

$$\langle ij_{z,a}|\hat{V}_{Coul}|kl_{z,b}\rangle = e^2\sum_{\sigma\sigma'}\iint d\vec{r}\,d\vec{r}\,'\frac{{\psi^a_{z,i}}^*(\vec{r}\sigma){\psi^a_{z,j}}^*(\vec{r}\,'\sigma')\psi^b_{z,k}(\vec{r}\sigma)\psi^b_{z,l}(\vec{r}\,'\sigma')}{|\vec{r}-\vec{r}\,'|} , \tag{1.48}$$

where e is the (free) electric charge of a proton. The kernel of $\hat{V}^{(2)}_{Coul}$ between a pair of states $\left[\langle\Phi_a|\,,|\Phi_b\rangle\right]$ gives us the Coulomb part of the nuclear EDF kernel, which can be splitted into its direct (CD), exchange (CE) and pairing (CP) contributions

$$\mathcal{E}^{Coul}[\rho_z,\kappa_z,\kappa_z^*]^{ab} = \mathcal{E}^{CD}[\rho_z]^{ab} + \mathcal{E}^{CE}[\rho_z]^{ab} + \mathcal{E}^{CP}[\kappa_z,\kappa_z^*]^{ab} \quad , \tag{1.49}$$

with

$$\mathcal{E}^{CD}[\rho_z]^{ab} = \frac{e^2}{2}\iint d\vec{r}\,d\vec{r}\,'\,\frac{\rho_z^{ab}(\vec{r})\rho_z^{ab}(\vec{r}\,')}{|\vec{r}-\vec{r}\,'|} \quad , \tag{1.50}$$

$$\mathcal{E}^{CE}[\rho_z]^{ab} = -\frac{e^2}{2}\sum_{\sigma\sigma'}\iint d\vec{r}\,d\vec{r}\,'\,\frac{\rho_z^{ab}(\vec{r}\sigma,\vec{r}\,'\sigma')\rho_z^{ab}(\vec{r}\,'\sigma',\vec{r}\sigma)}{|\vec{r}-\vec{r}\,'|} \quad , \tag{1.51}$$

$$\mathcal{E}^{CP}[\kappa_z,\kappa_z^*]^{ab} = -\frac{e^2}{2}\sum_{\sigma\sigma'}\iint d\vec{r}\,d\vec{r}\,'\,\frac{\kappa_z^{ba\,*}(\vec{r}\sigma,\vec{r}\,'\sigma')\kappa_z^{ab}(\vec{r}\,'\sigma',\vec{r}\sigma)}{|\vec{r}-\vec{r}\,'|} \, . \tag{1.52}$$

Slater Approximation

For computational time reasons, the exact non-local exchange term given by equation (1.51) is often approximated by a more simple local functional which was first proposed by Slater [134]

$$\mathcal{E}^{CE}[\rho_z]^{ab} \approx -\frac{3e^2}{4}\left(\frac{3}{\pi}\right)^{\frac{1}{3}}\int d\vec{r}\left[\rho_z^{ab}(\vec{r})\right]^{\frac{4}{3}} \quad . \tag{1.53}$$

The robustness of such an approximation has been studied in the case of a zero-range EDF without pairing [143, 131], of a zero-range EDF with BCS pairing [88], or of a finite-range EDF with full HFB pairing scheme [2], and it has been shown that the difference between the Slater approximation and the exact Coulomb exchange term is rather small and tends to decrease with increasing mass of the system. As described in the next section, we will use the Slater approximation in our self-consistent mean-field calculations, and keep the exact treatment of the exchange term only where it becomes mandatory, i.e, at the multi-reference level.

1.6 A Word About the Pauli Principle

As everyone knows, the Pauli exclusion principle states that: *the total wave-function for a system of idenditical fermions is completely antisymmetric under the exchange of any two particles.* In the case of an energy kernel (and thus of an energy functional), it translates into restrictions on the structure of the functional. In particular it implies that not all the terms of the functional can be independent from one another. Actually, the coefficients associated with each term of the functional are uniquely determined by the parameters of the underlying effective Hamiltonian (e.g. see Tab. 1.3). As soon as one steps away from this simple rule, for example by arbitrarily changing one of the functional coefficients (including putting it to zero), one does not respect the Pauli principle anymore and one runs into problems of self-interaction and self-pairing [23, 58, 87, 101, 136]. More generally, to work accordingly to the rules of quantum mechanics, which implies in particular to respect the Pauli exclusion principle for fermionic systems, one should only use functionals derived directly from an effective Hamiltonian and, altogether, calculate only quantities related to properly defined operators. This is what is called by us the Hamiltonian-based, or pseudo-potential-based, EDF approach.

However, at the SR-EDF level, the breaking of the Pauli principle, even if not completely satisfactory, is manageable and does not prevent us from doing usable calculations. This is why,

for computing time related reasons, we *deliberately* make a few approximations that break the Pauli principle at this step. Its most important violation is due to the approximate treatment (using the Slater approximation) of the exchange term and the omission of the pairing term of the Coulomb interaction. These terms being non-local are indeed very computationally time consuming. Another violation of the Pauli principle comes from the cut-off included in the computation of contractions in the particle-particle channel and not in the particle-hole channel. But in the end, all those violations of the exclusion principle should remain rather small and, the minimum found in the self-consistent procedure should not be essentially different from the one obtained if an exact respect of the Pauli principle is assured. Nevertheless, a correct treatment of the Pauli principle should be aimed at also the SR-EDF level, whenever it will be possible to overcome the computational difficulties.

On the other hand, the effects arising from the violation of the exclusion principle at the MR-EDF level become much more dramatic, and even unbearable, when one tries to calculate the non-diagonal energy kernel between symmetry-restored states using an exclusion-principle-violating functional. Indeed, as it has been previously observed [52, 23, 58, 87, 53], there appear finite steps and divergences in the symmetry-restoration process, which often makes any practical calculation impossible. Aware of the importance of this problem, the authors of [23, 87] developed a regularization scheme in order to remove the spuriosities appearing in such calculations. Unfortunately, this regularization scheme turned out to work correctly only when one considers same left an right quasiparticle states (i.e. $|\Phi_a\rangle = |\Phi_b\rangle$) projected on particle number alone [25]. And as the scope of this thesis lies beyond the simple particle-number restoration, with the ambition to realize a full configuration-mixing of angular-momentum and particle-number restored HFB states, we have no other choice than to include and to calculate exactly all the terms of a Hamiltonian-derived EDF. We thus, in particular, include the exact exchange term and the pairing term of the Coulomb interaction, and we thus also remove the cut-off from the calculation of the pairing energy. Consequently, our approach, at the MR-EDF level, fully respects the Pauli principle and is thus free from the problems mentioned above. A similar choice has already been made by Satuła *et al.* [126, 127], but using a simpler form of the Skyrme interaction in a framework without treatment of pairing correlations. When confronted with the same problems while projecting on isospin and angular-momentum, they went back to the old, but safe, pseudo-potential-based bilinear functional SV.

There should be a clear paradigm change in the EDF community in the years to come, about how one defines the MR-EDF method and about which type of functional one allows oneself to use in the MR-EDF calculations. We advocate here the restriction to pseudo-potential-based functionals in MR-EDF approaches as they are the only functionals that are well-defined in those methods. In particular, we want to stress that this concerns both zero-range and finite-range functionals, including thus the well-known Gogny-type functionals [47, 26]. The last-named functionals are in a sense already closer to the new spirit we develop here, because the same pseudo-potential is used to derive both the normal and the pairing part of the functional. However, all Gogny functionals that have been commonly used so far included a density dependence. This density dependence is unquestionably a very powerful tool if one wants to better reproduce experimental data at the SR-EDF level, but breaks the Pauli principle and becomes unreliable when going to the MR-EDF level, bringing spuriousities in the calculations [58]. In order to remove this efficient but problematic term while preserving an overall good descprition of nuclei, we went back to the original idea of pseudo-potential as proposed for example by Skyrme [132], already used in early calculations [67], and constructed richer pseudo-potential, by going-up to four-body contact terms [122, 133], and in a very near future by including the very promising three-body gradient terms [123]. Meanwhile, it is (I think) already quite an achievement to

realize one of the first ever realistic and spurious-free calculations and this, on top of that, for odd-even nuclei with an up to four-body Skyrme pseudo-potential. I thus hope that this work will help to promote the necessary paradigm shift in the community by showing that not only practical calculations using pseudo-potential-based functionals are possible, but that they also give satisfactory results.

Finally, the Tab. 1.4 sums up the treatment of the Pauli principle in this work.

SR-EDF	MR-EDF
Slightly violated : missing the coulomb pairing term and an exact treatment of the coulomb exchange term; pairing cut-off.	Fully respected ! Oh Yeah Baby !

Table 1.4: Respect of the Pauli principle at the different steps of the approach. Certified by the PBI ®.

Chapter 2

Single-Reference Energy Density Functional Formalism

But we must not forget that when radium was discovered no one knew that it would prove useful in hospitals. The work was one of pure science. And this is a proof that scientific work must not be considered from the point of view of the direct usefulness of it. It must be done for itself, for the beauty of science, and then there is always the chance that a scientific discovery may become like the radium a benefit for humanity.

Marie Curie (née Skłodowska), Lecture at Vassar College (1921).

In this second chapter, we will discuss the Single-Reference EDF level of the approach where, using a variational procedure, we minimize under conditions (e.g. average number of particles, average deformation, ...) the EDF we just introduced, in order to generate a set of variationally optimal Bogoliubov quasiparticle states that is going to be used as a basis to build the multi-reference states during the final step of the method. Even if the SR-EDF level is only considered by us as an intermediate step toward the full MR-EDF treatment, it is obviously mandatory to define the Bogoliubov quasiparticle states that are used as generating set of states and to explain how they are obtained. Special attention will be given to the symmetries imposed on the Bogoliubov quasiparticle states, and to their consequences for the calculations.

The first section of the present chapter will present the variational principle that underlies the SR-EDF approach. The second and third sections will define and discuss the properties of the Bogoliubov quasiparticle states we already mentioned in the first chapter, with a particular emphasis on one-quasiparticle states that are going to be used for the description of odd-mass nuclei. The fourth section will detail the minimization scheme of the quasiparticle states and the resulting HFB equations. Finally, the fifth section will very briefly present HF and HF+BCS approximations that are still often used to simplify SR-EDF computations.

2.1 Variational Method

Let us consider the Hilbert space $\mathcal{H}$ that contains all possible states of a quantum system with a Hamiltonian $\hat{H}$, and let us consider a state $|\Psi\rangle$ in $\mathcal{H}$. The variational principle [95, 107] states that the wave function $|\Psi\rangle$ is an eigenfunction of the Hamiltonian $\hat{H}$, with eigenvalue E, if and only if an arbitrary small variation of the expectation value of $\hat{H}$ in the state $|\Psi\rangle$ is stationary

$$\hat{H}|\Psi\rangle = E|\Psi\rangle \iff \delta\mathcal{E}[\Psi] = 0 \quad , \tag{2.1}$$

with $\mathcal{E}[\Psi]$ being the energy functional

$$\mathcal{E}[\Psi] = \frac{\langle\Psi|\hat{H}|\Psi\rangle}{\langle\Psi|\Psi\rangle} \quad . \tag{2.2}$$

Another general and particularly important property, which can be easily demonstrated [107], is that for any $|\Phi\rangle$ in $\mathcal{H}$ the energy functional $\mathcal{E}[\Phi]$ takes values that are greater than or equal to the ground-state energy E_0 of the system

$$\mathcal{E}[\Phi] \geq E_0 \quad , \tag{2.3}$$

the equality trivially holding when $|\Phi\rangle$ is the actual ground state[1] $|\Psi_0\rangle$ of $\hat{H}$.
These principles lead us to the main idea defining our approach: starting from a subset of state $\mathcal{S}\{\Phi\} \subset \mathcal{H}$ and looking for the state in the subset which gives the best approximation to the ground-state energy, we "simply" have to search for the state $|\Phi\rangle \in \mathcal{S}\{\Phi\}$ that minimizes the energy functional $\mathcal{E}[\Phi]$, because the lower $\mathcal{E}[\Phi]$ is, the closer it will be from the actual ground-state energy E_0. We could, in principle, find the exact ground-state energy E_0 in this way if the set $\mathcal{S}\{\Phi\}$ is the entire Hilbert space $\mathcal{H}$ or a subset of it containing the ground-state $|\Psi_0\rangle$. In practice, however, it is not possible to span the entire Hilbert space and we don't know *a priori* to which subset (of manageable size) belongs the ground-state eigenvector of the Hamiltonian. We thus have to make some approximations to the general variational method presented above.

Firstly we limit the trial wave functions $|\Phi_a\rangle$ to belong to the Hilbert space subset of Bogoliubov quasiparticle states, which will be presented in the next section. More precisely we will consider the smaller subset of Bogoliubov quasiparticle states with symmetries of the subgroup $\left\{\hat{P}, \hat{R}_z, \hat{S}_y^T\right\}_g$ of the double point group D_{2h}^{TD} [50, 51], and which will be also defined later in this chapter. Bogoliubov quasiparticles have the remarkably profitable property that, thanks to Wick's Theorem, they allow for expressing very simply the energy functional $\mathcal{E}[\Phi_a]$ in terms of one-body densities only

$$\mathcal{E}[\Phi_a] \equiv \mathcal{E}^{nuc}[\rho, \kappa, \kappa^*]^a \quad , \tag{2.4}$$

where instead of the russian representation $\tilde{\rho}$, $\tilde{\rho}^*$ used in the first chapter, we have used the more common representation κ, κ^* for the expression of the functional, and where we have dropped the double superscript state labeling of the densities as we will discuss in this chapter only diagonal kernels

$$\begin{aligned} |\Phi_b\rangle &= |\Phi_a\rangle \quad , \\ \rho_t^{ab} &\longrightarrow \rho_t^a \quad , \\ \kappa_t^{ab} &\longrightarrow \kappa_t^a \quad , \\ \kappa_t^{ba*} &\longrightarrow \kappa_t^{a*} = (\kappa_t^a)^* \quad , \end{aligned} \tag{2.5}$$

recalling that t labels the different species of particles (n: neutrons, z: protons). Because only the one-body densities are needed to fully characterize the Bogoliubov quasiparticle states [34], they are very practical when searching for the best variational solution by minimizing the energy functional: $\delta\mathcal{E}^{nuc}[\rho, \kappa, \kappa^*]^a = 0$. On the other hand, the subset of quasiparticle states is clearly too restrictive to contain the exact ground-state of the system. Moreover, as quasiparticle states allow for taking into account deformation and pairing correlations in a simple single product state, they also break symmetries of the Hamiltonian which is contrary to what one expects from the eigenstates of $\hat{H}$ (see section 3.2.3). A better variational solution to these problems is the

[1] Or a linear superposition of the ground-states if the system has degenerate ground states.

Variation After Projection (VAP) scheme that variationally seeks for the projected[2] quasiparticle state that has the lowest energy as well as the good quantum numbers associated with the symmetries of the Hamiltonian. But a VAP method requires a lot of computer ressources and we would thus partly loose the advantage of the tractability of quasiparticle states. The approach taken in this work is thus a Projection After Variation (PAV), within which we first minimize the Bogoliubov product states under certain conditions (e.g. average particle-number) and then project them to restore the broken symmetries. One does not obtain *a priori* in this way the best variational solution, but a second minimization within the Generator Coordinate Method allows for finding a better and more general variational solution by mixing different projected quasiparticle states.

Also, in the variational procedure we do not use the true A-body Hamiltonian of the system, but an effective Hamiltonian, of the form introduced in equation (1.2), that is tailored to integrate bulk properties of the nuclear system into the restricted model space of quasiparticle states. And we have to precise that, even if the variational principle remains strictly valid for this particular effective Hamiltonian, there is no guarantee that its ground-state energy E_0^{eff} might not be lower than the true ground state E_0 of the system.

2.2 Definition of the Quasiparticle States

Let us now define the Bogoliubov quasiparticle states we are using as trial wave functions in the variational procedure. We will first recall the basic definitions of Bogoliubov transformations and Bogoliubov quasiparticles, giving particular attention to the properties of one-quasiparticle states. After that, we will see the special features that exhibit a quasiparticle state's one-body densities, and define the general density of a quasiparticle product state.

2.2.1 Bogoliubov Transformations

Starting from an arbitrary set of fermionic creation/annihilation operators $(\hat{c}^\dagger, \hat{c})$ we define the Bogoliubov transformation which transforms the set of operators $(\hat{c}^\dagger, \hat{c})$ into a new set of operators $(\hat{\beta}^\dagger, \hat{\beta})$ as

$$\begin{aligned} \hat{\beta}_i^\dagger &= \sum_j \left(U_{ji}\, \hat{c}_j^\dagger + V_{ji}\, \hat{c}_j \right) \quad , \\ \hat{\beta}_i &= \sum_j \left(U_{ji}^*\, \hat{c}_j + V_{ji}^*\, \hat{c}_j^\dagger \right) \quad , \end{aligned} \tag{2.6}$$

with the matrix

$$\mathcal{W} = \begin{pmatrix} U & V^* \\ V & U^* \end{pmatrix} \tag{2.7}$$

being unitary

$$\mathcal{W}\,\mathcal{W}^\dagger = \mathcal{W}^\dagger\,\mathcal{W} = \mathbb{1} \quad . \tag{2.8}$$

The unitarity of $\mathcal{W}$ assures the conservation of the fermionic commutation rules between the quasiparticle creation/annihilation operators

$$\left\{\hat{\beta}_i^\dagger, \hat{\beta}_j\right\} = \hat{\delta}_{ij} \quad , \qquad \left\{\hat{\beta}_i^\dagger, \hat{\beta}_j^\dagger\right\} = \left\{\hat{\beta}_i, \hat{\beta}_j\right\} = 0 \quad . \tag{2.9}$$

[2]The projection technique will be presented in chapter 3.

According to the Bloch-Messiah-Zumino Theorem [35, 163], the matrix $\mathcal{W}$ can be decomposed as

$$\mathcal{W} = \begin{pmatrix} D & 0 \\ 0 & D^* \end{pmatrix} \begin{pmatrix} \bar{U} & \bar{V} \\ \bar{V} & \bar{U} \end{pmatrix} \begin{pmatrix} C & 0 \\ 0 & C^* \end{pmatrix} \quad , \tag{2.10}$$

with D being a unitary transformation among the operators $(\hat{c}^\dagger, \hat{c})$, the matrices $\bar{U}$ and $\bar{V}$ defining a special Bogoliubov transformation from the new basis $(\hat{a}^\dagger, \hat{a})$ into the basis of quasiparticles $(\hat{\alpha}^\dagger, \hat{\alpha})$, and finally C being a unitary transformation of the quasiparticle operators $(\hat{\alpha}^\dagger, \hat{\alpha})$ among themselves

$$\left\{ \begin{array}{l} \hat{a}_i^\dagger = \sum_j D_{ji}\, \hat{c}_j^\dagger \\ \hat{a}_i = \sum_j D_{ji}^*\, \hat{c}_j \end{array} \right\} \longrightarrow \left\{ \begin{array}{l} \hat{\alpha}_i^\dagger = \sum_j \left(\bar{U}_{ji}\, \hat{a}_j^\dagger + \bar{V}_{ji}\, \hat{a}_j \right) \\ \hat{\alpha}_i = \sum_j \left(\bar{U}_{ji}^*\, \hat{a}_j + \bar{V}_{ji}^*\, \hat{a}_j^\dagger \right) \end{array} \right\} \longrightarrow \left\{ \begin{array}{l} \hat{\beta}_i^\dagger = \sum_j C_{ji}\, \hat{\alpha}_j^\dagger \\ \hat{\beta}_i = \sum_j C_{ji}^*\, \hat{\alpha}_j \end{array} \right\} . \tag{2.11}$$

One interesting consequence of this decomposition is that the transformation D is such that the normal density ρ is diagonal and the pairing tensor κ is in his canonical form in the so-called canonical basis $(\hat{a}^\dagger, \hat{a})$. Also, the matrices $\bar{U}$ and $\bar{V}$ which realize the transformation from the basis $(\hat{a}^\dagger, \hat{a})$ into the quasiparticle basis $(\hat{\alpha}^\dagger, \hat{\alpha})$, can be put, by an appropriate ordering of the single-particle states basis, into a form that exhibits a simple block diagonal structure [107], with every 2×2 diagonal block of $\bar{U}$ being itself diagonal and every 2×2 diagonal block of $\bar{V}$ being either the identity matrix of same dimension or a skew-symmetric matrix. In the end, we have for the quasiparticle operators $(\hat{\alpha}^\dagger, \hat{\alpha})$ the simple expressions

$$\begin{aligned} \hat{\alpha}_k^\dagger &= \bar{U}_{kk}\, \hat{a}_k^\dagger + \bar{V}_{\bar{k}k}\, \hat{a}_{\bar{k}} \equiv u_k\, \hat{a}_k^\dagger + v_{\bar{k}}\, \hat{a}_{\bar{k}} \quad , \\ \hat{\alpha}_k &= \bar{U}_{kk}^*\, \hat{a}_k + \bar{V}_{\bar{k}k}^*\, \hat{a}_{\bar{k}}^\dagger \equiv u_k\, \hat{a}_k + v_{\bar{k}}\, \hat{a}_{\bar{k}}^\dagger \quad , \end{aligned} \tag{2.12}$$

with $u_k^2 + v_k^2 = 1$, $u_k = u_{\bar{k}}$ and $v_k = -v_{\bar{k}}$, and where $\bar{k}$ labels the conjugate state of the state k. In our case we will see that the conjugate state of k is a state $\bar{k}$ that has an opposite signature of the one of k (see section 2.3.1).

2.2.2 One-Quasiparticle States

We define the quasiparticle vacuum $|\tilde{0}\rangle$ for the set of quasiparticle operators $(\hat{\beta}^\dagger, \hat{\beta})$, defined by the Bogoliubov transformation (2.6), as the product state that vanishes under the action of any of the quasiparticle destruction operators $\hat{\beta}$

$$\forall\, j\,,\ \hat{\beta}_j\, |\tilde{0}\rangle = 0 \quad . \tag{2.13}$$

The notation $\tilde{0}$ is used here to distinguish the quasiparticle vacuum $|\tilde{0}\rangle$, associated with both quasiparticle operators $(\hat{\beta}^\dagger, \hat{\beta})$ and $(\hat{\alpha}^\dagger, \hat{\alpha})$, from the bare vacuum $|0\rangle$, associated with both the single-particle operators $(\hat{c}^\dagger, \hat{c})$ and $(\hat{a}^\dagger, \hat{a})$. The quasiparticle vacuum can either be even, i.e. has an even number parity[3] and thus represents a fermionic system with an even number of particles, or can be odd, i.e. has an odd number parity and thus represents a fermionic system with an odd number of particles. If we start from a fully paired even vacuum $|\tilde{0}\rangle$, we can construct a one-quasiparticle state by applying a quasiparticle creation operator on the quasiparticle vacuum

$$|\Phi_a\rangle = \hat{\beta}_a^\dagger\, |\tilde{0}\rangle \quad . \tag{2.14}$$

The such created one-quasiparticle state $|\Phi_a\rangle$ represents a fermionic system with an odd number of particles. Of course we can create in this way states with more than one quasiparticle excitation

[3] The number parity of a fermionic system is defined as $(-)^{N_s}$ with N_s being the number of particle in the system. More about the number parity will be discussed in section 2.3.3.

on top of an even vacuum, with the rule that systems with odd number of particles can only by represented by an odd number of quasiparticle excitations, and naturally, systems with even number of particles can only be represented by even (possibly null) number of quasiparticle excitations. But in this thesis we will focus exclusively on one-quasiparticle states, which usually give an approximation to the ground state and to the lowest excitations of the neighboring odd-A nuclei of an even-even nucleus represented by the even vacuum $|\tilde{0}\rangle$. That being said, most of the formalism presented in this chapter can be applied with no, or minor, modification to an arbitrary number of quasiparticle excitations, in particular the symmetry relations presented later in this chapter.
In agreement with what has been said before about quasiparticle vacua, the one-quasiparticle state $|\Phi_a\rangle$ can also be seen as an odd vacuum for the set of quasiparticle operators $\left(\hat{\beta}^\dagger, \hat{\beta}\right)^a$ defined by the matrices U^a, V^a with

$$\begin{aligned} &\forall\, i\,,\, j \neq a\,, \qquad U^a_{ij} = U_{ij} \qquad V^a_{ij} = V_{ij} \quad , \\ &\forall\, i\,,\, j = a\,, \qquad U^a_{ia} = V^*_{ia} \qquad V^a_{ia} = U^*_{ia} \quad . \end{aligned} \tag{2.15}$$

Finally, the one-quasiparticle state $|\Phi_a\rangle$ can be expressed in a very simple manner in its canonical basis

$$|\Phi_a\rangle = \hat{a}^\dagger_a \prod_{\substack{k>0 \\ k\neq a}} \left(u_k + v_k\, \hat{a}^\dagger_k \hat{a}^\dagger_{\bar{k}}\right) |0\rangle \quad , \tag{2.16}$$

where the product runs over half of the possible indices (indicated by $k > 0$).

Separate Treatment of Protons and Neutrons

We consider in this work protons and neutrons as distinct particles with one-body densities that do not mix particle species. The even vacuum $|\tilde{0}\rangle$ can thus be written as the tensor product of an even neutron vacuum and of an even proton vacuum

$$|\tilde{0}\rangle = |\tilde{0}_n\rangle \otimes |\tilde{0}_z\rangle \quad , \tag{2.17}$$

with $|\tilde{0}_n\rangle$ and $|\tilde{0}_z\rangle$ being vacua for quasiparticles operators $(\hat{\beta}^\dagger, \hat{\beta})_n$ and $(\hat{\beta}^\dagger, \hat{\beta})_z$, respectively. The Bogoliubov transformations are performed independently in the neutron and proton single-particle Hilbert spaces with the transformation matrices U_n, V_n and U_z, V_z, respectively. The total Hilbert space of single-particle states can be written as the direct sum of the Hilbert spaces of proton and neutron single-particle states, and the matrices U and V take in this space the block diagonal structure

$$U = \begin{pmatrix} U_n & 0 \\ 0 & U_z \end{pmatrix} \quad , \tag{2.18}$$

$$V = \begin{pmatrix} V_n & 0 \\ 0 & V_z \end{pmatrix} \quad , \tag{2.19}$$

and similarly for the matrices U^a and V^a.
The one-quasiparticle state $|\Phi_a\rangle$ can either be a neutron one-quasiparticle state

$$|\Phi_a\rangle = |\Phi_{n,a}\rangle \otimes |\tilde{0}_z\rangle \quad , \tag{2.20}$$

or a proton one-quasiparticle state

$$|\Phi_a\rangle = |\tilde{0}_n\rangle \otimes |\Phi_{z,a}\rangle \quad , \tag{2.21}$$

but never a tensor product of one-quasiparticle states of each species, as in that case it would represent an odd-odd nucleus with an even total number of particles $A = N + Z$. More generally, starting from even neutron and even proton vacua, an odd-A nucleus can be represented by the tensor product of an odd number of quasiparticle excitations of one particle species by an even (possibly null) number of quasiparticle excitations of the other particle species. As already stated, we will consider here only states with one-quasiparticle excitations in total ($\equiv$ neutrons and protons combined).

2.2.3 One-Body Densities and Generalized Density

The one-body densities have been already defined in the first chapter in the general case of kernels of *a priori* different quasiparticle states. Expressing now these densities in the context of diagonal kernels, and this time in occupation representation, we have for their matrix elements

$$\rho^a_{t,ij} = \langle \Phi_a | \hat{c}^\dagger_{t,j} \hat{c}_{t,i} | \Phi_a \rangle \quad , \tag{2.22}$$

$$\kappa^a_{t,ij} = \langle \Phi_a | \hat{c}_{t,j} \hat{c}_{t,i} | \Phi_a \rangle \quad , \tag{2.23}$$

with t still labeling the particle species, and where we omit the expression of ${\kappa^a_{t,ij}}^*$ because in the case of a diagonal kernel it is simply the complex conjugate of $\kappa^a_{t,ij}$. The complete matrices can be written in terms of matrices U^a_t, V^a_t as

$$\rho^a_t = V^{a\,*}_t \, V^{a\,T}_t \quad , \tag{2.24}$$

$$\kappa^a_t = V^{a\,*}_t \, U^{a\,T}_t \quad , \tag{2.25}$$

but we note that for the particle species without quasiparticle excitation the matrices U^a_t, V^a_t are those of an even vacuum. The normal density ρ^a_t is hermitean, whereas the abnormal density κ^a_t is skew symmetric

$$\rho^{a\,\dagger}_t = \rho^a_t \quad , \tag{2.26}$$

$$\kappa^{a\,T}_t = -\kappa^a_t \quad , \tag{2.27}$$

and between the one-body densities there hold the relations

$$\rho^{a\,2}_t - \rho^a_t = -\kappa^a_t \, \kappa^{a\,\dagger}_t \quad , \tag{2.28}$$

$$\rho^a_t \, \kappa^a_t = \kappa^a_t \, \rho^{a\,*}_t \quad . \tag{2.29}$$

We also can express the matrix elements of the densities of a one-quasiparticle state directly from the matrix elements of the densities (ρ_t, κ_t) of the even vacuum it was created from

$$\rho^a_{t,ij} = \rho_{t,ij} + \left(U_{t,ia} \, U^*_{t,ja} - V^*_{t,ia} \, V_{t,ja} \right) \delta_{\pi_{ta},-1} \quad , \tag{2.30}$$

$$\kappa^a_{t,ij} = \kappa_{t,ij} + \left(U_{t,ia} \, V^*_{t,ja} - V^*_{t,ia} \, U_{t,ja} \right) \delta_{\pi_{ta},-1} \quad , \tag{2.31}$$

where $\pi_{ta} = \pm 1$ is the number parity of the particle species t.
Finally we conclude by defining the generalized density matrix

$$\mathcal{R}^a_t = \begin{pmatrix} \rho^a_t & \kappa^a_t \\ -\kappa^{a\,*}_t & 1 - \rho^{a\,*}_t \end{pmatrix} \quad , \tag{2.32}$$

which has the property

$$\mathcal{R}^{a\,2}_t = \mathcal{R}^a_t \quad , \tag{2.33}$$

and which plays a similar role to the one of one-body density ρ for Slater determinants, but for Bogoliubov quasiparticle states.

2.3 Symmetries of Quasiparticle States

Even if our trial wave functions have the relatively simple structure of Bogoliubov quasiparticle product states, numerical calculations for the most general quasiparticle states without any symmetry are far from being trivial. It is thus customary to impose symmetry conditions on the quasiparticle states in order to simplify the numerical treatment [36, 56, 27, 129]. But by doing so, one also necessarily further reduces the variational space explored in the minimization.

2.3.1 Subgroup $\left\{\hat{P}, \hat{R}_z, \hat{S}_y^T\right\}_g$ of the Point Group D_{2h}^{TD}

In the present study, we choose for the symmetries of the product state the point group whose generators are

$$\left\{\hat{P}, \hat{R}_z, \hat{S}_y^T\right\}_g \quad , \tag{2.34}$$

and which is a subgroup of the double point group D_{2h}^{TD}. The group D_{2h}^{TD} and its subgroups have been defined, and their properties described in large detail, in two articles by Dobaczewski *et al.* [50, 51]. The subscript g is here to recall that the three elements presented above are only the generators of a group which contains in total 16 elements. The other 13 elements can be trivially constructed by the combination of 2 or 3 of the generators

$$\left\{\hat{E}, \hat{\bar{E}}, \hat{P}, \hat{\bar{P}}, \hat{R}_z, \hat{\bar{R}}_z, \hat{S}_z, \hat{\bar{S}}_z, \hat{R}_y^T, \hat{\bar{R}}_y^T, \hat{R}_x^T, \hat{\bar{R}}_x^T, \hat{S}_y^T, \hat{\bar{S}}_y^T, \hat{S}_x^T, \hat{\bar{S}}_x^T\right\} \quad , \tag{2.35}$$

where $\hat{S}_m = \hat{P}\hat{R}_m$, $\hat{R}_m^T = \hat{T}\hat{R}_m$, $\hat{S}_m^T = \hat{P}\hat{T}\hat{R}_m$ for $m = x, y,$ or z, and where all the operators with a bar are obtained by the combination with $\hat{\bar{E}}$, e.g. $\hat{\bar{P}} = \hat{\bar{E}}\hat{P}$. Two special elements one needs to comment on are $\hat{E}$ and $\hat{\bar{E}}$. The former is the identity, whereas the latter acts on a system composed of N_s particle as $(-)^{N_s}\hat{E}$. From a general point of view, it is interesting to note that the group D_{2h}^{TD} is a generalization of the group D_{2h}[4] [75] to systems with a spin degree-of-freedom, with also the addition of the time-reversal operator. It can thus be *directly* used for any fermionic system, whether it is composed of an even or an odd number of fermions. Similarly to the groups D_{2h} and D_{2h}^{TD}, the group $\left\{\hat{P}, \hat{R}_z, \hat{S}_y^T\right\}_g$ gives rise to 3 planes symmetry. And in the case of a HFB solver working on a 3-dimensional cartesian mesh, it allows for performing the practical calculations in only one eighth of the mesh, the seven other parts of the mesh being determined by symmetry relations [36]. Even if only mentionned briefly here, this provides an appreciable simplification of the SR-EDF computations.

The first generator of $\left\{\hat{P}, \hat{R}_z, \hat{S}_y^T\right\}_g$ is the standard parity operator $\hat{P}$ that flips the sign of the spatial coordinates. The second generator of the group is the z-signature $\hat{R}_z$, with the m-signature being defined as the rotation by an angle π around the m-axis

$$\hat{R}_m = e^{-i\pi\hat{J}_m} = -i\, e^{-i\pi\hat{L}_m}\, \hat{\sigma}_m \quad , \tag{2.36}$$

with

$$\hat{J}_m = \hat{L}_m + \hat{S}_m \quad , \tag{2.37}$$

and where $\hat{J}_m, \hat{L}_m$ and $\hat{S}_m = \frac{\hat{\sigma}_m}{2}$ are the total, the orbital and the spin angular momentum components along the m-axis, respectively, $\hat{\sigma}_m$ are the Pauli matrices, and where we consider, for the rest of the thesis, $\hbar = 1$ in the definition of angular momenta. The three different signature operators are related by

$$\hat{R}_l\hat{R}_m = \delta_{lm}\hat{R}_l^2 + \sum_{n=x,y,z} \epsilon_{lmn}^2 e^{-i\pi\epsilon_{lmn}\hat{J}_n} \quad , \tag{2.38}$$

[4] Well-known to our colleagues in chemistry and molecular physics.

where $l, m, n = x, y,$ or z, and ϵ_{lmn} is the Levi-Civita tensor. Finally, the third, and last, generator of the group $\hat{S}_y^T$, called the y-time-simplex, is the combination of the parity operator $\hat{P}$, of the time-reveral operator $\hat{T}$, and of the y-signature $\hat{R}_y$

$$\hat{S}_y^T = \hat{P}\hat{T}\hat{R}_y \quad . \tag{2.39}$$

The z-signature $\hat{R}_z$ and the parity $\hat{P}$ are linear operators and can be used to give good quantum numbers to the quasiparticle states: the signature η for $\hat{R}_z$, and the parity p for $\hat{P}$. On the other hand, the y-time-simplex $\hat{S}_y^T$ is an antilinear operator and thus cannot be used to give a quantum number [95]. Its role is instead to fix the relative phase between the single-particle states [51].
To conclude this brief presention, we give the squares of, and the commutation relations between, the principal operators of interest (belonging to D_{2h}^{TD} but not necessarily to $\left\{\hat{P}, \hat{R}_z, \hat{S}_y^T\right\}_g$)

$$\hat{P}^2 = \hat{S}_m^{T\,2} = \hat{E} \quad , \tag{2.40}$$
$$\hat{T}^2 = \hat{R}_m^2 = \hat{\bar{E}} \quad , \tag{2.41}$$

$$\left[\hat{T}, \hat{P}\right] = \left[\hat{T}, \hat{R}_m\right] = \left[\hat{T}, \hat{S}_m^T\right] = 0 \quad , \tag{2.42}$$
$$\left[\hat{P}, \hat{R}_m\right] = \left[\hat{P}, \hat{S}_m^T\right] = 0 \quad , \tag{2.43}$$
$$\left[\hat{R}_m, \hat{S}_m^T\right] = 0 \quad , \tag{2.44}$$
$$\hat{R}_m \hat{R}_l \hat{R}_m^\dagger = \hat{R}_l^\dagger \, , \tag{2.45}$$

with $l, m = x, y, z$ and $l \neq m$.
A lot more details on the group D_{2h}^{TD} and all its subgroups can be found in [50, 51].

Symmetry Transformations of Creation/Annihilation Operators

We will now see the properties that implies the choice of the symmetry group $\left\{\hat{P}, \hat{R}_z, \hat{S}_y^T\right\}_g$ for single-particle and quasiparticle creation/annihilation operators. For that let us first consider a linear, and unitary, operator $\hat{S}$ that gives good quantum numbers χ_t for the single-particle states in the basis $(\hat{c}^\dagger, \hat{c})_t$

$$\hat{S}|j_{t,c}\rangle_t = \chi_{t,j}|j_{t,c}\rangle \quad . \tag{2.46}$$

Assuming $\hat{S}|0_t\rangle = |0_t\rangle$, we easily deduce (see appendix A) the transformation relations of the single-particle creation/annihilation operators under the action of $\hat{S}$

$$\hat{S}\hat{c}_{t,j}^\dagger\hat{S}^\dagger = \chi_{t,j}\,\hat{c}_{t,j}^\dagger \quad , \tag{2.47}$$
$$\hat{S}\hat{c}_{t,j}\hat{S}^\dagger = \chi_{t,j}^*\,\hat{c}_{t,j} \quad . \tag{2.48}$$

and from them the transformations for quasiparticle creation/annihilation operators of the form (2.6)

$$\hat{S}\hat{\beta}_{t,j}^\dagger\hat{S}^\dagger = \sum_j \left(\chi_{t,j}\,U_{ji}\,\hat{c}_{t,j}^\dagger + \chi_{t,j}^*\,V_{ji}\,\hat{c}_{t,j}\right) \quad , \tag{2.49}$$
$$\hat{S}\hat{\beta}_{t,j}\hat{S}^\dagger = \sum_j \left(\chi_{t,j}^*\,U_{ji}^*\,\hat{c}_{t,j} + \chi_{t,j}\,V_{ji}^*\,\hat{c}_{t,j}^\dagger\right) \quad . \tag{2.50}$$

We also can deduce that, if the operator $\hat{S}$ commutes with the time-reversal operator: $[\hat{S}, \hat{T}] = 0$, the time-reversed[5] creation/annihilation single-particle operators

$$\hat{\tilde{c}}^{\dagger}_{t,j} = \hat{T}\hat{c}^{\dagger}_{t,j}\hat{T}^{\dagger} \quad , \tag{2.51}$$
$$\hat{\tilde{c}}_{t,j} = \hat{T}\hat{c}_{t,j}\hat{T}^{\dagger} \quad , \tag{2.52}$$

have similar transformation relations

$$\hat{S}\hat{\tilde{c}}^{\dagger}_{t,j}\hat{S}^{\dagger} = \tilde{\chi}_{t,j}\,\hat{\tilde{c}}^{\dagger}_{t,j} \quad , \tag{2.53}$$
$$\hat{S}\hat{\tilde{c}}_{t,j}\hat{S}^{\dagger} = \tilde{\chi}^{*}_{t,j}\,\hat{\tilde{c}}_{t,j} \quad , \tag{2.54}$$

but with a quantum number that is the complex conjugate of the one of $\hat{c}^{\dagger}_{t,j}$ and $\hat{c}_{t,j}$

$$\tilde{\chi}_{t,j} = \chi^{*}_{t,j} \quad . \tag{2.55}$$

Let us now come to the case considered in our study of single-particle states $(\hat{c}^{\dagger}, \hat{c})_t$ that have a good signature and good parity

$$\hat{R}_z|j_{t,c}\rangle = \eta_{t,j}|j_{t,c}\rangle \quad , \tag{2.56}$$
$$\hat{P}|j_{t,c}\rangle = p_{t,j}|j_{t,c}\rangle \quad , \tag{2.57}$$

with

$$\eta_{t,j} = \pm i \quad , \tag{2.58}$$
$$p_{t,j} = \pm 1 \quad . \tag{2.59}$$

Applying the relations (2.47) and (2.48) to the z-signature and to the parity, we obtain the transformations

$$\hat{R}_z\hat{c}^{\dagger}_{t,j}\hat{R}^{\dagger}_z = \eta_{t,j}\,\hat{c}^{\dagger}_{t,j} \quad , \tag{2.60}$$
$$\hat{R}_z\hat{c}_{t,j}\hat{R}^{\dagger}_z = \eta^{*}_{t,j}\,\hat{c}_{t,j} \quad , \tag{2.61}$$
$$\hat{P}\hat{c}^{\dagger}_{t,j}\hat{P}^{\dagger} = p_{t,j}\,\hat{c}^{\dagger}_{t,j} \quad , \tag{2.62}$$
$$\hat{P}\hat{c}_{t,j}\hat{P}^{\dagger} = p_{t,j}\,\hat{c}_{t,j} \quad . \tag{2.63}$$

And because the z-signature and the parity commute with the time-reversal operator (see equation (2.42)), we can also write

$$\hat{R}_z\hat{\tilde{c}}^{\dagger}_{t,j}\hat{R}^{\dagger}_z = \tilde{\eta}_{t,j}\,\hat{\tilde{c}}^{\dagger}_{t,j} \quad , \tag{2.64}$$
$$\hat{R}_z\hat{\tilde{c}}_{t,j}\hat{R}^{\dagger}_z = \tilde{\eta}^{*}_{t,j}\,\hat{\tilde{c}}_{t,j} \quad , \tag{2.65}$$
$$\hat{P}\hat{\tilde{c}}^{\dagger}_{t,j}\hat{P}^{\dagger} = \tilde{p}_{t,j}\,\hat{\tilde{c}}^{\dagger}_{t,j} \quad , \tag{2.66}$$
$$\hat{P}\hat{\tilde{c}}_{t,j}\hat{P}^{\dagger} = \tilde{p}_{t,j}\,\hat{\tilde{c}}_{t,j} \quad , \tag{2.67}$$

with

$$\tilde{\eta}_{t,j} = \eta^{*}_{t,j} = -\eta_{t,j} \quad , \tag{2.68}$$
$$\tilde{p}_{t,j} = p_{t,j} \quad . \tag{2.69}$$

[5] We do not imply here that the single-particle basis is closed under time-reversal.

It is also interesting to note that if we consider two single-particle states in two possible different bases, $|j_{t,c}\rangle$ in the basis $(\hat{c}^\dagger, \hat{c})_t$, and $|k_{t,d}\rangle$ in the basis $(\hat{d}^\dagger, \hat{d})_t$, both having the signature and the parity as good quantum numbers, we have the property that the states are orthogonal if they have different signature and/or parity

$$\langle j_{t,c}|k_{t,d}\rangle = \delta_{\eta_{t,j},\eta_{t,k}}\,\delta_{p_{t,j},p_{t,k}}\langle j_{t,c}|k_{t,d}\rangle \quad . \tag{2.70}$$

More generally, we can write the single-particle space of a given particle species as the direct sum of single-particle states of positive and negative parity, and we can in each subspace separate between states with different signatures

$$(\hat{c}^\dagger, \hat{c})_t = \left[(\hat{c}^\dagger, \hat{c})_{i,1,t} + (\hat{c}^\dagger, \hat{c})_{-i,1,t}\right] \oplus \left[(\hat{c}^\dagger, \hat{c})_{i,-1,t} + (\hat{c}^\dagger, \hat{c})_{-i,-1,t}\right] \quad , \tag{2.71}$$

where, because of equations (2.64) and (2.65), a creation operator $\hat{c}^\dagger_{t,j}$ and the associated annihilation operator $\hat{c}_{t,j}$ belong to different parts of the basis of a given parity

$$\hat{c}^\dagger_{t,j} \in (\hat{c}^\dagger, \hat{c})_{\eta_j,p_j,t} \iff \hat{c}_{t,j} \in (\hat{c}^\dagger, \hat{c})_{\eta^*_j,p_j,t} \quad . \tag{2.72}$$

As a result of equations (2.49), (2.50), and (2.71), if we want the quasiparticle states to have good parity and a good signature, we need the matrices U_t and V_t of the Bogoliubov transformations to take the block structure

$$U_t = \begin{pmatrix} U_{i,1,t} & 0 & 0 & 0 \\ 0 & U_{-i,1,t} & 0 & 0 \\ 0 & 0 & U_{i,-1,t} & 0 \\ 0 & 0 & 0 & U_{-i,-1,t} \end{pmatrix} \quad , \tag{2.73}$$

$$V_t = \begin{pmatrix} 0 & V_{-i,1,t} & 0 & 0 \\ V_{i,1,t} & 0 & 0 & 0 \\ 0 & 0 & 0 & V_{-i,-1,t} \\ 0 & 0 & V_{i,-1,t} & 0 \end{pmatrix} \quad , \tag{2.74}$$

where the creation operators of a given particle species, parity and signature are mixed in equations (2.49) and (2.50) with annihilation operators associated with creation operators of the same particle species and parity but complex conjugate signature. That is why we said that the conjugate state $\bar{k}$ of the state k in (2.12) has the opposite signature of the one of k: $\eta_{\bar{k}} = \eta^*_k = -\eta_k$. Using Bogoliubov transformations of the form (2.73) and (2.74), we obtain that the quasiparticle creation/annihilation operators follow the desired transformation relations

$$\hat{R}_z \hat{\beta}^\dagger_{t,j} \hat{R}^\dagger_z = \eta_{t,j}\,\hat{\beta}^\dagger_{t,j} \quad , \tag{2.75}$$

$$\hat{R}_z \hat{\beta}_{t,j} \hat{R}^\dagger_z = \eta^*_{t,j}\,\hat{\beta}_{t,j} \quad , \tag{2.76}$$

$$\hat{P} \hat{\beta}^\dagger_{t,j} \hat{P}^\dagger = p_{t,j}\,\hat{\beta}^\dagger_{t,j} \quad , \tag{2.77}$$

$$\hat{P} \hat{\beta}_{t,j} \hat{P}^\dagger = p_{t,j}\,\hat{\beta}_{t,j} \quad . \tag{2.78}$$

And similarly to the single-particle creation/annihiliaton operators, we can write the transformations for the time-reversed quasiparticle creation/annihilation operators

$$\hat{\tilde{\beta}}^\dagger_{t,j} = \hat{T} \hat{\beta}^\dagger_{t,j} \hat{T}^\dagger \quad , \tag{2.79}$$

$$\hat{\tilde{\beta}}_{t,j} = \hat{T} \hat{\beta}_{t,j} \hat{T}^\dagger \quad , \tag{2.80}$$

which are simply

$$\hat{R}_z \hat{\tilde{\beta}}^\dagger_{t,j} \hat{R}^\dagger_z = \tilde{\eta}_{t,j}\, \hat{\tilde{\beta}}^\dagger_{t,j} \quad , \tag{2.81}$$

$$\hat{R}_z \hat{\tilde{\beta}}_{t,j} \hat{R}^\dagger_z = \tilde{\eta}^*_{t,j}\, \hat{\tilde{\beta}}_{t,j} \quad , \tag{2.82}$$

$$\hat{P} \hat{\tilde{\beta}}^\dagger_{t,j} \hat{P}^\dagger = \tilde{p}_{t,j}\, \hat{\tilde{\beta}}^\dagger_{t,j} \quad , \tag{2.83}$$

$$\hat{P} \hat{\tilde{\beta}}_{t,j} \hat{P}^\dagger = \tilde{p}_{t,j}\, \hat{\tilde{\beta}}_{t,j} \quad , \tag{2.84}$$

with

$$\tilde{\eta}_{t,j} = \eta^*_{t,j} = -\eta_{t,j} \quad , \tag{2.85}$$

$$\tilde{p}_{t,j} = p_{t,j} \quad . \tag{2.86}$$

2.3.2 Number Parity

An even more fundamental symmetry of our many-body wave functions is the number parity [8]. We define the number parity of a system composed of N_s fermions to be equal to $(-)^{N_s}$. So it is either 1 for a system composed of an even number of particles, or -1 for a system composed of an odd number of particles. Bogoliubov quasiparticle states defined by transformations of the type (2.6) have a good number parity, i.e. their number parity is either 1 ($\equiv$ even) or -1 ($\equiv$ odd). This is a consequence of the group properties of the Bogoliubov transformations [120] and therefore is independent of the group $\left\{\hat{P}, \hat{R}_z, \hat{S}^T_y\right\}_g$ studied above. To phrase it in simple terms, it simply results from the fact that Bogoliubov creation/annihilation quasiparticle operators defined by (2.6) are a superposition made of only individual single-particle creation/annihilation operators.

Considering here the protons and neutrons independently, we define the neutron number parity operator $\hat{\Pi}_{\hat{N}}$ and the proton number parity operator $\hat{\Pi}_{\hat{Z}}$ as

$$\hat{\Pi}_{\hat{N}} = e^{-i\pi\hat{N}} \quad , \tag{2.87}$$

$$\hat{\Pi}_{\hat{Z}} = e^{-i\pi\hat{Z}} \quad , \tag{2.88}$$

with $\hat{N}$ and $\hat{Z}$ being the neutron and proton number operators, respectively,

$$\hat{N} = \sum_i \hat{c}^\dagger_{n,i} \hat{c}_{n,i} \quad , \tag{2.89}$$

$$\hat{Z} = \sum_i \hat{c}^\dagger_{z,i} \hat{c}_{z,i} \quad . \tag{2.90}$$

Acting with $\hat{\Pi}_{\hat{N}}$ and $\hat{\Pi}_{\hat{Z}}$ on the neutron and protron single-particle states, respectively, we simply obtain

$$\hat{\Pi}_{\hat{N}} |j_{n,c}\rangle = (-)|j_{n,c}\rangle \quad , \tag{2.91}$$

$$\hat{\Pi}_{\hat{Z}} |j_{z,c}\rangle = (-)|j_{z,c}\rangle \quad , \tag{2.92}$$

and consequently, using again equations (2.47) and (2.48), we obtain the following transformations of the single-particle creation/annihilation operators.

$$\hat{\Pi}_{\hat{N}} \hat{c}^\dagger_{n,j} \hat{\Pi}^\dagger_{\hat{N}} = (-)\, \hat{c}^\dagger_{n,j} \quad , \tag{2.93}$$

$$\hat{\Pi}_{\hat{N}} \hat{c}_{n,j} \hat{\Pi}^\dagger_{\hat{N}} = (-)\, \hat{c}_{n,j} \quad , \tag{2.94}$$

$$\hat{\Pi}_{\hat{Z}} \hat{c}^\dagger_{z,j} \hat{\Pi}^\dagger_{\hat{Z}} = (-)\, \hat{c}^\dagger_{z,j} \quad , \tag{2.95}$$

$$\hat{\Pi}_{\hat{Z}} \hat{c}_{z,j} \hat{\Pi}^\dagger_{\hat{Z}} = (-)\, \hat{c}_{z,j} \quad . \tag{2.96}$$

As said above, and looking at the equations (2.49) and (2.50), the number parity is conserved by the Bogoliubov quasiparticle creation/annihilation operators, i.e. we obtain transformation properties that are equivalent to the ones of single-particle creation/annihilation operators

$$\hat{\Pi}_{\hat{N}}\hat{\beta}^{\dagger}_{n,j}\hat{\Pi}^{\dagger}_{\hat{N}} = (-)\,\hat{\beta}^{\dagger}_{n,j} \quad , \tag{2.97}$$

$$\hat{\Pi}_{\hat{N}}\hat{\beta}_{n,j}\hat{\Pi}^{\dagger}_{\hat{N}} = (-)\,\hat{\beta}_{n,j} \quad , \tag{2.98}$$

$$\hat{\Pi}_{\hat{Z}}\hat{\beta}^{\dagger}_{z,j}\hat{\Pi}^{\dagger}_{\hat{Z}} = (-)\,\hat{\beta}^{\dagger}_{z,j} \quad , \tag{2.99}$$

$$\hat{\Pi}_{\hat{Z}}\hat{\beta}_{z,j}\hat{\Pi}^{\dagger}_{\hat{Z}} = (-)\,\hat{\beta}_{z,j} \quad . \tag{2.100}$$

2.3.3 Final Symmetries of the Product States

Now that we have defined the symmetry relations of interest for the single-particles states, it is straightforward, because of their product state structure, to deduce the symmetries of our many-body wave functions. Indeed, because of the structure of the Bogoliubov transformations, all the relations mentioned for the single-particle operators $(\hat{c}^{\dagger},\hat{c})_t$ are still true in the canonical basis $(\hat{a}^{\dagger},\hat{a})_t$, so using the simple expression of a fully paired even vacuum $|\tilde{0}_t\rangle$ and of a one-quasiparticle state $|\Phi_{t,a}\rangle$ in this basis

$$|\tilde{0}_t\rangle = \prod_{k>0}\left(u_{t,k} + v_{t,k}\,\hat{a}^{\dagger}_{t,k}\hat{a}^{\dagger}_{t,\bar{k}}\right)|0_t\rangle \quad , \tag{2.101}$$

$$|\Phi_{t,a}\rangle = \hat{a}^{\dagger}_{t,a}\prod_{\substack{k>0\\k\neq a}}\left(u_{t,k} + v_{t,k}\,\hat{a}^{\dagger}_{t,k}\hat{a}^{\dagger}_{t,\bar{k}}\right)|0_t\rangle \quad , \tag{2.102}$$

it is easy to determine the action of the operator $\hat{S}$ of equation (2.46) on these states

$$\begin{aligned}\hat{S}|\tilde{0}_t\rangle &= \prod_{k>0}\left(u_{t,k} + v_{t,k}\,\hat{S}\hat{a}^{\dagger}_{t,k}\hat{S}^{\dagger}\hat{S}\hat{a}^{\dagger}_{t,\bar{k}}\hat{S}^{\dagger}\right)\hat{S}|0_t\rangle \\ &= \prod_{k>0}\left(u_{t,k} + v_{t,k}\,\chi_{t,k}\chi_{t,\bar{k}}\,\hat{a}^{\dagger}_{t,k}\hat{a}^{\dagger}_{t,\bar{k}}\right)|0_t\rangle \quad ,\end{aligned} \tag{2.103}$$

$$\begin{aligned}\hat{S}|\Phi_{t,a}\rangle &= \hat{S}\hat{a}^{\dagger}_{t,a}\hat{S}^{\dagger}\prod_{\substack{k>0\\k\neq a}}\left(u_{t,k} + v_{t,k}\,\hat{S}\hat{a}^{\dagger}_{t,k}\hat{S}^{\dagger}\hat{S}\hat{a}^{\dagger}_{t,\bar{k}}\hat{S}^{\dagger}\right)\hat{S}|0_t\rangle \\ &= \chi_{t,a}\,\hat{a}^{\dagger}_{t,a}\prod_{\substack{k>0\\k\neq a}}\left(u_{t,k} + v_{t,k}\,\chi_{t,k}\chi_{t,\bar{k}}\,\hat{a}^{\dagger}_{t,k}\hat{a}^{\dagger}_{t,\bar{k}}\right)|0_t\rangle \quad .\end{aligned} \tag{2.104}$$

Applying these equations in the cases of the parity, of the z-signature and of the number parity, and recalling that conjugate states have same parities, complex conjugate signatures, and obviously same number parities, we simply obtain

$$\hat{P}|\tilde{0}_t\rangle = |\tilde{0}_t\rangle \quad , \tag{2.105}$$

$$\hat{R}_z|\tilde{0}_t\rangle = |\tilde{0}_t\rangle \quad , \tag{2.106}$$

$$\hat{\Pi}_{\hat{X}}|\tilde{0}_t\rangle = |\tilde{0}_t\rangle \quad , \tag{2.107}$$

$$\hat{P}|\Phi_{t,a}\rangle = p_{t,a}\,|\Phi_{t,a}\rangle \quad , \tag{2.108}$$

$$\hat{R}_z|\Phi_{t,a}\rangle = \eta_{t,a}\,|\Phi_{t,a}\rangle \quad , \tag{2.109}$$

$$\hat{\Pi}_{\hat{X}}|\Phi_{t,a}\rangle = (-)|\Phi_{t,a}\rangle \quad , \tag{2.110}$$

where we precise that $\hat{X}, t = \hat{N}, n$ or $\hat{Z}, z$. Symmetries of one-quasiparticle states could also have been derived using the relation

$$\begin{aligned} \hat{S}|\Phi_{t,a}\rangle &= \hat{S}\hat{\beta}^\dagger_{t,a}\hat{S}^\dagger\hat{S}|\tilde{0}_t\rangle \\ &= \chi_{t,a}\,\hat{\beta}^\dagger_{t,a}|\tilde{0}_t\rangle \quad , \end{aligned} \tag{2.111}$$

which of course gives the same result; that is, the one-quasiparticle states' quantum numbers are determined by the blocked quasiparticle (for a given particle species).
Generalization is straigtforward in the case of multiple quasiparticle excitations

$$\begin{aligned} \hat{S}|\Phi_{t,abc\ldots n}\rangle &= \hat{S}\hat{\beta}^\dagger_{t,a}\hat{\beta}^\dagger_{t,b}\hat{\beta}^\dagger_{t,c}\cdots\hat{\beta}^\dagger_{t,n}|\tilde{0}_t\rangle \\ &= \hat{S}\hat{\beta}^\dagger_{t,a}\hat{S}^\dagger\hat{S}\hat{\beta}^\dagger_{t,b}\hat{S}^\dagger\hat{S}\hat{\beta}^\dagger_{t,c}\hat{S}^\dagger\hat{S}\cdots\hat{S}^\dagger\hat{S}\hat{\beta}^\dagger_{t,n}\hat{S}^\dagger\hat{S}|\tilde{0}_t\rangle \\ &= \chi_{t,a}\chi_{t,b}\chi_{t,c}\cdots\chi_{t,n}\,\hat{\beta}^\dagger_{t,a}\hat{\beta}^\dagger_{t,b}\hat{\beta}^\dagger_{t,c}\cdots\hat{\beta}^\dagger_{t,n}|\tilde{0}_t\rangle \\ &= \chi_{t,abc\ldots n}\,\hat{\beta}^\dagger_{t,a}\hat{\beta}^\dagger_{t,b}\hat{\beta}^\dagger_{t,c}\cdots\hat{\beta}^\dagger_{t,n}|\tilde{0}_t\rangle \quad , \end{aligned} \tag{2.112}$$

where the quantum number $\chi_{t,abc\ldots n} = \prod_{j=a}^{n}\chi_{t,j}$ of the state $|\Phi_{t,abc\ldots n}\rangle$ is given by the product of the quantum numbers of each quasiparticle exicitation. Equivalently, one also could say that the quantum numbers are given by the product of the quantum numbers of fully occupied ($\equiv u = 0, v = 1$) single-particle states in the canonical basis.

Finally, we look at the symmetries of the nucleus' A-body wave function $|\Phi_a\rangle$ that is the tensor product of the N-body wave function of neutrons and the Z-body wave function of protons. For the sake of generality, we will assume that $|\Phi_a\rangle$ is a quasiparticle state with an arbitrary (and possibily null) number of quasiparticle excitations. Using appropriate operators ($\hat{P} \equiv \hat{P}\otimes\hat{P}, \hat{\Pi}_{\hat{A}} \equiv \hat{\Pi}_{\hat{N}}\otimes\hat{\Pi}_{\hat{Z}}, \ldots$), we obtain thus the general equations

$$\hat{R}_z|\Phi_a\rangle = \eta_a|\Phi_a\rangle \quad , \tag{2.113}$$

$$\hat{P}|\Phi_a\rangle = p_a|\Phi_a\rangle \quad , \tag{2.114}$$

$$\hat{S}^T_y|\Phi_a\rangle = \quad |\Phi_a\rangle \quad , \tag{2.115}$$

$$\hat{\Pi}_{\hat{A}}|\Phi_a\rangle = \pi_a|\Phi_a\rangle \quad , \tag{2.116}$$

$$\hat{R}^2_i|\Phi_a\rangle = \pi_a|\Phi_a\rangle \quad \text{for } i = x, y, z \quad , \tag{2.117}$$

$$\hat{T}^2|\Phi_a\rangle = \pi_a|\Phi_a\rangle \quad , \tag{2.118}$$

where we also expressed the action of operators $\hat{T}^2$ and $\hat{R}^2_i$ using equation (2.41), and where the action of $\hat{S}^T_y$ is fixed to be the identity. The total number parity π_a, total parity p_a, and total signature η_a, are the products of the proton and neutron number-parities, parities, and signatures, respectively,

$$\pi_a = \pi_{n,a}\pi_{z,a} \quad , \tag{2.119}$$

$$p_a = p_{n,a}p_{z,a} \quad , \tag{2.120}$$

$$\eta_a = \eta_{n,a}\eta_{z,a} \quad , \tag{2.121}$$

$$\pi_a\,,\,\pi_{n,a}\,,\,\pi_{z,a} = \begin{cases} +1 & A_a\,,\,N_a\,,\,Z_a \text{ even} \\ -1 & A_a\,,\,N_a\,,\,Z_a \text{ odd} \end{cases} \quad , \tag{2.122}$$

$$p_a\,,\,p_{n,a}\,,\,p_{z,a} = \pm 1 \quad , \tag{2.123}$$

$$\eta_a\,,\,\eta_{n,a}\,,\,\eta_{z,a} = \begin{cases} \pm 1 & A_a\,,\,N_a\,,\,Z_a \text{ even} \\ \pm i & A_a\,,\,N_a\,,\,Z_a \text{ odd} \end{cases} \quad , \tag{2.124}$$

where N_a, Z_a and $A_a = N_a + Z_a$ being the neutron, the proton and the nucleon numbers of the nucleus represented by $|\Phi_a\rangle$.

We conclude this section by stressing that because of the symmetry relations presented in this section, it is easy to demonstrate[6] that two quasiparticle states $|\Phi_a\rangle$ and $|\Phi_b\rangle$ are orthogonal if they do not have same number parity, parity and signature for neutrons *and* protons

$$\langle\Phi_a|\Phi_b\rangle = \delta_{p_{n,a},p_{n,b}}\delta_{\pi_{n,a},\pi_{n,b}}\delta_{\eta_{n,a},\eta_{n,b}}\delta_{p_{z,a},p_{z,b}}\delta_{\pi_{z,a},\pi_{z,b}}\delta_{\eta_{z,a},\eta_{z,b}}\langle\Phi_a|\Phi_b\rangle \quad . \tag{2.125}$$

2.4 Minimization of Quasiparticle States

As described in the first section, if we want to obain the best variational one-quasiparticle state $|\Phi_a\rangle$ possible, we have to find the one-quasiparticle state $|\Phi_a\rangle$ that minimizes the energy density functional $\mathcal{E}^{nuc}[\rho,\kappa,\kappa^*]^a$. We thus present here the HFB equations that have to be self-consisently solved to fullfill the condition $\delta\mathcal{E}^{nuc}[\rho,\kappa,\kappa^*]^a = 0$, and the additional constraints added during the procedure to minimize the EDF under certain conditions (e.g. average deformation), and that can be used to generate a set of different quasiparticle states to be mixed at the MR-EDF level.

2.4.1 The HFB Equations

The full derivation of the HFB equations, even if not utterly complicated, is a bit laborious as it requires a lot of technical steps. We will thus give here only the main results that lead to the HFB equations, and refer for the rest to previous work where the reader can find the full demonstration, whether it is in the Hamiltonian formalism [107, 119] or from a fully functional point of view [118, 20].
The minimization of the energy density functional $\mathcal{E}^{nuc}[\rho,\kappa,\kappa^*]^a$ reads

$$\delta\Big(\mathcal{E}^{nuc}[\rho,\kappa,\kappa^*]^a - \frac{1}{2}\sum_{t=n,z}\lambda_t^a\left[\mathrm{Tr}\{\rho_t^a\} + \mathrm{Tr}\{\rho_t^{a*}\}\right] - \sum_{t=n,z}\mathrm{Tr}\left\{\Lambda_t^a\left(\mathcal{R}_t^{a\,2} - \mathcal{R}_t^a\right)\right\}\Big) = 0 \quad , \tag{2.126}$$

where the second term allows, with the help of Lagrange parameters λ_n^a and λ_z^a, for enforcing the desired average values for the number of neutrons and protons to the state $|\Phi_a\rangle$

$$\mathrm{Tr}\{\rho_n^a\} = \mathrm{Tr}\{\rho_n^{a*}\} = \langle\Phi_a|\hat{N}|\Phi_a\rangle = \langle\Phi_a|\hat{N}^\dagger|\Phi_a\rangle = N_a \quad , \tag{2.127}$$

$$\mathrm{Tr}\{\rho_z^a\} = \mathrm{Tr}\{\rho_z^{a*}\} = \langle\Phi_a|\hat{Z}|\Phi_a\rangle = \langle\Phi_a|\hat{Z}^\dagger|\Phi_a\rangle = Z_a \quad , \tag{2.128}$$

and where the last term assures that both the neutron and the proton states in the tensor product remain Bogoliubov quasiparticle states, that is, that their generalized densities (2.32) have the property

$$\mathcal{R}_n^{a\,2} - \mathcal{R}_n^a = 0 \quad , \tag{2.129}$$

$$\mathcal{R}_z^{a\,2} - \mathcal{R}_z^a = 0 \quad . \tag{2.130}$$

The variation of the first term with respect to the independent matrix elements of its one-body densities, i.e. the $\frac{m(m+1)}{2}$ independent matrix elements of the hermitean one-body density matrix ρ_t^a (assumed here to be of dimension m^2) and the $\frac{m(m-1)}{2}$ independent matrix elements

[6] Using for example for the proton number parity: $\hat{\mathbb{1}}\otimes\hat{\mathbb{1}} = \hat{\mathbb{1}}\otimes\hat{\Pi}_{\hat{Z}}^\dagger\hat{\Pi}_{\hat{Z}}$.

of the skew symmetric one-body pairing tensor κ_t^a (assumed here to be also of dimension m^2), leads to the equation

$$\delta\mathcal{E}^{nuc}[\rho,\kappa,\kappa^*]^a = \sum_{t=n,z} \mathrm{Tr}\{\mathcal{H}_t^a \delta\mathcal{R}_t^a\} \quad , \tag{2.131}$$

where $\mathcal{H}_t^a$ is the block matrix

$$\mathcal{H}_t^a = \begin{pmatrix} h_t^a & \Delta_t^a \\ -\Delta_t^{a*} & -h_t^{a*} \end{pmatrix} \quad , \tag{2.132}$$

whose building blocks h_t^a and Δ_t^a are the matrices representing the normal and pairing fields, respectively, and whose matrix elements are defined as

$$h_{t,ji}^a \equiv \frac{\delta\mathcal{E}^a}{\delta\rho_{t,ij}^a} \quad , \quad \Delta_{t,ij}^a \equiv \frac{\delta\mathcal{E}^a}{\delta\kappa_{t,ij}^{a\,*}} \quad , \tag{2.133}$$

and where $\delta\mathcal{R}_t^a$ is the variation of the generalized density matrix (2.32)

$$\delta\mathcal{R}_t^a = \begin{pmatrix} \delta\rho_t^a & \delta\kappa_t^a \\ -\delta\kappa_t^{a\,*} & -\delta\rho_t^{a\,*} \end{pmatrix} \quad . \tag{2.134}$$

The variation of the second term gives a very similar equation

$$\delta\Big(-\frac{1}{2}\sum_{t=n,z} \lambda_t^a \left[\mathrm{Tr}\{\rho_t^a\} + \mathrm{Tr}\{\rho_t^{a*}\}\right]\Big) = \sum_{t=n,z} \mathrm{Tr}\{\mathcal{L}_t^a \delta\mathcal{R}_t^a\} \quad , \tag{2.135}$$

where $\mathcal{L}_t^a$ is a matrix with the simple form

$$\mathcal{L}_t^a = \begin{pmatrix} -\lambda_t^a & 0 \\ 0 & \lambda_t^a \end{pmatrix} \quad . \tag{2.136}$$

The third term, which imposes the idempotency to the neutron and proton generalized densities, when varied reads

$$\delta\Big(-\sum_{t=n,z} \mathrm{Tr}\big\{\Lambda_t^a \left(\mathcal{R}_t^{a\,2} - \mathcal{R}_t^a\right)\big\}\Big) = \sum_{t=n,z} \mathrm{Tr}\big\{\big(\Lambda_t^a - \mathcal{R}_t^a\Lambda_t^a - \Lambda_t^a\mathcal{R}_t^a\big)\delta\mathcal{R}_t^a\big\} \quad . \tag{2.137}$$

Finally, when adding the three terms together one obtains, because of the additive property of the trace, the simple equation

$$\sum_{t=n,z} \mathrm{Tr}\big\{\big(\mathcal{H}_t^a + \mathcal{L}_t^a + \Lambda_t^a - \mathcal{R}_t^a\Lambda_t^a - \Lambda_t^a\mathcal{R}_t^a\big)\delta\mathcal{R}_t^a\big\} = 0 \, , \tag{2.138}$$

which, taking into account that the equation has to be verified for any arbitrary variation $\delta\mathcal{R}_t^a$, reduces to

$$\mathcal{H}_t^a + \mathcal{L}_t^a + \Lambda_t^a - \mathcal{R}_t^a\Lambda_t^a - \Lambda_t^a\mathcal{R}_t^a = 0 \quad . \tag{2.139}$$

With some clever multiplications and subtractions, this can be finally put into the form

$$[\mathcal{H}'^a_t, \mathcal{R}_t^a] = 0 \quad , \tag{2.140}$$

with $\mathcal{H}'^a_t$ being the sum of the field matrix $\mathcal{H}^a_t$ and the particle-number constraint matrix $\mathcal{L}^a_t$

$$\mathcal{H}'^a_t = \mathcal{H}^a_t + \mathcal{L}^a_t = \begin{pmatrix} h^a_t - \lambda^a_t & \Delta^a_t \\ -\Delta^{a*}_t & -(h^{a*}_t - \lambda^a_t) \end{pmatrix} \quad . \tag{2.141}$$

Equation (2.140) is equivalent to saying that we can simulteanously diagonalize the matrices $\mathcal{H}'^a_t$ and $\mathcal{R}^a_t$, and that we end up with an eigenvalue problem, also known as the HFB equations,

$$\begin{pmatrix} h^a_t - \lambda^a_t & \Delta^a_t \\ -\Delta^{a*}_t & -(h^{a*}_t - \lambda^a_t) \end{pmatrix} \begin{pmatrix} U_{t,\mu} \\ V_{t,\mu} \end{pmatrix} = E_{t,\mu} \begin{pmatrix} U_{t,\mu} \\ V_{t,\mu} \end{pmatrix} \quad , \tag{2.142}$$

with $U_{t,\mu}$ and $V_{t,\mu}$ being the μ^{th} columns of the Bogoliubov transformation matrices U_t and V_t, respectively. The HFB equations are obviously a self-consistent problem as the fields h and Δ depend on the one-body densities ρ and κ (see equation (2.133)) that depend themselves on the matrices U_t and V_t (see equations (2.24) and (2.25)) which are the solution of (2.142). The HFB equations have thus to be solved by successive iterations until convergence of the solution.

Self-Consistent Blocking

When calculating a one-quasiparticle state, the HFB equations (2.142) are solved at every iteration with fields h^a_t and Δ^a_t corresponding to a one-quasiparticle state. This gives us a set of matrices U_t and V_t which are arranged by hand to correspond to the desired one-quasiparticle state for the following iteration. This method of iteration allows, for a set of fixed conditions (see the example discussed below of the average deformation or the cranking frequency), for blocking, in an easy fashion, several different quasiparticles with same quantum numbers. This is of advantage as we want to embed as many different configurations as possible in our configuration mixing at the MR-EDF level.
One has also to remember that all the equations given above that link the one-quasiparticle state with an even vacuum are true only for the even vacuum from which the one-quasiparticle state is *directly* created, and which changes at every iteration.

Lipkin-Nogami Approximation

We finally briefly mention that to avoid a complete collapse of the pairing in the calculations of the light nuclei presented in what follows, we used the Lipkin-Nogami (LN) method [89, 103, 104, 17], i.e. we add the additional terms $\lambda_{n,2}\hat{N}^2$ and $\lambda_{z,2}\hat{Z}^2$ to the variational Hamiltonian that defines the functional. But contrary to the constraint on the average number of particles, $\lambda_{n,2}$ and $\lambda_{z,2}$ are not Lagrange parameters but are evaluated and fixed at every iteration. The LN approximation can be derived from a second-order Kamlah expansion of the Particle Number Restoration [150, 152], and thus can be seen as an approximate VAP calculation for this symmetry, but we prefer to consider it here only as a simple way to get non-zero pairing in our calculations of light nuclei with the parametrization SLyMR0.

2.4.2 Deformation Constraint

One of the degrees-of-freedom in our calculation is the spatial deformation of the one-body densities on the 3-dimensional cartesian mesh. But because of the symmetries $\left\{\hat{P}, \hat{R}_z, \hat{S}^T_y\right\}_g$ imposed on our quasiparticle states, the possible deformations that the densities can take are

restricted. Indeed, the deformation can be expanded in terms of the multipole operators

$$\begin{aligned} \hat{Q}_{\lambda\mu} &= \sum_{t,ij} q^{\lambda\mu}_{t,ij}\, \hat{c}^\dagger_{t,i}\hat{c}_{t,j} \quad , \\ q^{\lambda\mu}_{t,ij} &= \sum_{\sigma} \int d\vec{r}\; \psi^{c}_{t,i}{}^{*}(\vec{r}\sigma) r^\lambda Y^\lambda_\mu(\theta,\phi)\psi^c_{t,j}(\vec{r}\sigma) \quad , \end{aligned} \tag{2.143}$$

where r is the position and Y^λ_μ is the spherical harmonic of degree λ and order μ. The multipole operators $\hat{Q}_{\lambda\mu}$ have, under the parity and the z-signature, the following transformation relations

$$\hat{R}_z \hat{Q}_{\lambda\mu}\hat{R}^\dagger_z = (-)^\mu \hat{Q}_{\lambda\mu} \tag{2.144}$$

$$\hat{P}\hat{Q}_{\lambda\mu}\hat{P}^\dagger = (-)^\lambda \hat{Q}_{\lambda\mu} \quad . \tag{2.145}$$

It is thus easy to demonstrate that odd values of λ and μ vanish

$$\lambda \text{ or } \mu \text{ odd} \Longrightarrow \langle\Phi_a|\hat{Q}_{\lambda\mu}|\Phi_a\rangle = 0 \quad , \tag{2.146}$$

and that, for λ and μ even, the average value of $\hat{Q}_{\lambda\mu}$ is real only for $\mu = 0$, but complex otherwise [50].

Solving the HFB equations (2.142), which do not constrain the deformation, we will only obtain the state with the deformation (allowed by $\left\{\hat{P}, \hat{R}_z, \hat{S}^T_y\right\}_g$) that gives the nearest energy minimum to the state that has been used as a starting point for the self-consistent procedure. On the other hand, it is possible to explore manually the deformation degree-of-freedom by putting a constraint on the average deformation, similarly to what is done for the neutron and proton numbers. The perspective being the possibility to build multi-reference states that are superposition of quasiparticle states with different deformations, or, to say it differently, to use the deformation as a one of the generator coordinates in the GCM.
In our calculations we thus solve the HFB equations with additional constraints on $\hat{Q}_{20}$, $\hat{Q}_{22}$, and $\hat{Q}_{2-2}$, that, for a linear[7] constraint on $\hat{Q}_{\lambda\mu}$, take the form

$$-\frac{1}{2}\lambda^a_q \left[\mathrm{Tr}\{(\rho^a_n + \rho^a_z)Q_{\lambda\mu}\} + \mathrm{Tr}\{(\rho^{a*}_n + \rho^{a*}_z)Q^*_{\lambda\mu}\}\right] \quad , \tag{2.147}$$

where λ^a_q is a Lagrange parameter, and where the average value of $\hat{Q}_{\lambda\mu}$ is fixed to the desired value $q_{\lambda\mu}$

$$\begin{aligned} \mathrm{Tr}\{(\rho^a_n + \rho^a_z)Q_{\lambda\mu}\} = \langle\Phi_a|\hat{Q}_{\lambda\mu}|\Phi_a\rangle = \mathrm{Tr}\{(\rho^{a*}_n + \rho^{a*}_z)Q^*_{\lambda\mu}\} = \langle\Phi_a|\hat{Q}^\dagger_{\lambda\mu}|\Phi_a\rangle \\ = q_{\lambda\mu} \quad . \end{aligned} \tag{2.148}$$

Working on a 3-dimensional cartesian mesh, the deformations are parametrized by the variables q_1 and q_2 that can be linked to the traditional β, γ variables, introduced by Hill and Wheeler [81, 107], by the equations

$$\begin{aligned} q_1 &= Q_0 \cos(\gamma) - \frac{1}{\sqrt{3}} Q_0 \sin(\gamma) \quad , \\ q_2 &= \frac{2}{\sqrt{3}} Q_0 \sin(\gamma) \quad , \end{aligned} \tag{2.149}$$

[7] The actual constraint used in the numerical code is a more efficient quadratic constraint [107]. Unfortunately, except for P.-H. Heenen I doubt that anyone knows exactly what is done in this part of the code. Surely it is some sort of Belgian military secret. Anyway, I give here the general principle for a simple linear constraint.

with

$$\beta = \sqrt{\frac{5}{16\pi}} \frac{4\pi Q_0}{3R^2 A_a} \quad , \tag{2.150}$$

$$R = 1.2\, A_a^{\frac{1}{3}} \text{ fm} \quad , \tag{2.151}$$

and

$$\begin{aligned} q_{xx} &= -Q_0 \cos(\gamma + 60) \quad , \\ q_{yy} &= -Q_0 \cos(\gamma - 60) \quad , \\ q_{zz} &= Q_0 \cos(\gamma) \quad , \\ q_{xy} &= q_{yx} = q_{xz} = q_{zx} = q_{yz} = q_{zy} = 0 \quad . \end{aligned} \tag{2.152}$$

2.4.3 Cranking

The cranking in a SR-EDF approach corresponds for searching for the best variational HFB solution with an additional constraint on the angular-momentum components of the quasiparticle states. It was first formulated by Thouless and Valatin [144] within the self-consistent HF formalism, and has been since then extended to the more general HFB formalism and has been widely used in SR-EDF calculations [125]. More generally, it can be seen as a continuation of the pioneering work of Inglis [74] and Belyaev [16] to compute rotational collective excitations directly from a microscopic point of view. Indeed, the cranking can be seen as an approximate VAP calculation [83, 105, 13, 106] and allows for approximately calculating, in a numerically cheap fashion, rotational bands and high-spin states already at the SR-EDF level. However, cranked states still break the rotational invariance and have to be projected on angular momentum as done in [11, 162, 71, 6]. On that account, in our approach we only consider the cranking as a way to construct a set of better optimized states in the scope of realizing a subsequent MR-EDF calculation. Unfortunately, because of the complexity and the large CPU time required for a such calculation, we will not incorporate cranked states in our configuration mixing. Nevertheless, some results on projected cranked states will still be given as a consolation prize in chapter 4.

Because of the symmetries $\left\{\hat{P}, \hat{R}_z, \hat{S}_y^T\right\}_g$, we have to take the cranking axis to coincide with the signature z-axis. Indeed, we have for the total angular-momentum components the commutation relations

$$[\hat{R}_z, \hat{J}_z] = 0 \qquad \{\hat{R}_z, \hat{J}_x\} = \{\hat{R}_z, \hat{J}_y\} = 0 \quad , \tag{2.153}$$

which implies that the average values of $\hat{J}_x$ and $\hat{J}_y$ vanish

$$\langle \Phi_a | \hat{J}_x | \Phi_a \rangle = \langle \Phi_a | \hat{J}_y | \Phi_a \rangle = 0 \quad . \tag{2.154}$$

Similarly to what is done for particle number and deformation, if we want to calculate a cranked state we add a constraint on the average value of $\hat{J}_z$ in the minimization of the functional

$$-\frac{1}{2}\omega^a \left[\text{Tr}\{(\rho_n^a + \rho_z^a) J_z\} + \text{Tr}\{(\rho_n^{a*} + \rho_z^{a*}) J_z^*\} \right] \quad , \tag{2.155}$$

where the cranking frequency ω^a is treated as a Lagrange parameter and where we constrain the mean-value of $\hat{J}_z$ to be

$$\begin{aligned} \text{Tr}\{(\rho_n^a + \rho_z^a) J_z\} = \langle \Phi_a | \hat{J}_z | \Phi_a \rangle = \text{Tr}\{(\rho_n^{a*} + \rho_z^{a*}) J_z^*\} = \langle \Phi_a | \hat{J}_z^\dagger | \Phi_a \rangle \\ = \sqrt{J(J+1) - K^2} \quad . \end{aligned} \tag{2.156}$$

with K being the main component of the projection of the total angular-momentum on the "deformation axis"[8] of the blocked quasiparticle. This constraint can be derived from a Kamlah expansion [83, 105, 13, 106], but is somewhat dubious in our framework as its derivation assumes[9] that the trial wave functions are strongly deformed and that there is only a small admixture of other K components. Despite these strong assumptions, the form (2.155) is one of the most popular constraints for the mean-value of $\hat{J}_z$ in both odd-even and even-even nuclei (with $K = 0$) cranking calculations, and it is also the one which will we use in this work.
Because of the constraint on $\hat{J}_z$ in equation (2.155), the variational procedure is not time-reversal invariant

$$[\hat{J}_z, \hat{T}] \neq 0 \quad \Longrightarrow \quad [\delta\mathcal{E}, \hat{T}] \neq 0 \quad , \tag{2.157}$$

and therefore the resulting HFB equations are also not time-reversal invariant

$$\begin{pmatrix} h_t^a - \lambda_t^a - \omega^a j_z & \Delta_t^a \\ -\Delta_t^{a*} & -(h_t^{a*} - \lambda_t^a - \omega^a j_z^*) \end{pmatrix} \begin{pmatrix} U_{t,\mu} \\ V_{t,\mu} \end{pmatrix} = E_{t,\mu} \begin{pmatrix} U_{t,\mu} \\ V_{t,\mu} \end{pmatrix} \quad . \tag{2.158}$$

That implies in particular that the self-consistent evolution of quasiparticle excitations with opposite signatures can not be linked anymore, which has some rerpercussions on the angular-momentum projection of one-quasiparticle states. But we will stop here as such consequences will be discussed in chapter 4.

2.5 Special Approximations: HF+BCS and HF

For the sake of completeness we shortly discuss here two special approximations to the general HFB formalism that are often used to simplify the calculations. Considering the theoretical ambitions of this work and the numerical possibilities we dispose, we are not going to consider these approximations as an end for themselves but they still can serve as a point of comparison for the complete MR-EDF calculations.

2.5.1 HF+BCS

In the HF-BCS approximation, we assume that the basis that diagonalizes the single-particle hamiltonian is also the canonical basis. We thus have to perform only the special Bogoliubov transformation, defined by the matrices $\bar{U}$ and $\bar{V}$. The treatment of the pairing is in particular simplified as one only evaluates the matrix elements $\Delta_{t,i\bar{i}}$, assuming that the other matrix elements vanish, and the energy of a quasiparticle can be simply written as

$$E_{t,i} = \sqrt{(\epsilon_{t,i} - \lambda_t)^2 + \Delta_{t,i\bar{i}}^2} \quad . \tag{2.159}$$

2.5.2 Hartree-Fock

Taking the HFB equations in the zero-pairing limit ($\kappa_t = 0$), we recover the well-known Hartree-Fock theory. The trial wave-functions are thus simple Slater determinants and the problem reduces then to diagonalize simultaneously the one-body density ρ_t and the single-particle hamiltonian h_t

$$\sum_t \big[\rho_t, h_t\big] = 0 \quad . \tag{2.160}$$

[8] ≡ Axis which has the largest average value for the quadrupole moment.
[9] It is also assumed that the states have a good signature, which is the case in this work.

The odd-mass nuclei are then represented by the tensor product of a neutron and a proton Slater determinant

$$|\Phi_a\rangle = \hat{c}^\dagger_{n,a} \prod_i^{\text{even}} \hat{c}^\dagger_{n,i}|0_n\rangle \otimes \prod_j^{\text{even}} \hat{c}^\dagger_{z,j}|0_z\rangle \quad , \tag{2.161}$$

or

$$|\Phi_a\rangle = \prod_i^{\text{even}} \hat{c}^\dagger_{n,i}|0_n\rangle \otimes \hat{c}^\dagger_{z,a} \prod_j^{\text{even}} \hat{c}^\dagger_{z,j}|0_z\rangle \quad , \tag{2.162}$$

where the superscript "even" indicates that the products run over an even number of single-particle creation operators.
Let us call $|\Phi_0\rangle$ the (tensor product of) Slater determinant(s) that is solution of (2.160) and that has the lowest energy. The excited states of $|\Phi_0\rangle$ can be constructed in first approximation by, perturbatively, removing one particle in one of the occupied states and adding a particle in one of the unoccupied states of $|\Phi_0\rangle$

$$|\Phi_{t,\mu;\nu}\rangle = \hat{c}^\dagger_{t,\mu}\hat{c}_{t,\nu}|\Phi_0\rangle \quad , \tag{2.163}$$

and their energies, neglecting the rearrangements of the mean-field, are simply

$$E_{t,\mu;\nu} = E_0 + \epsilon_{t,\mu} - \epsilon_{t,\nu} \quad , \tag{2.164}$$

where $E_0 = \langle\Phi_0|\hat{H}|\Phi_0\rangle$, and $\epsilon_{t,\mu}$, $\epsilon_{t,\nu}$ are single-particle energies, i.e. the eigenvalues of h_t.

Chapter 3

Multi-Reference Energy Density Functional Formalism

If it disagrees with experiment, it's wrong. In that simple statement, is the key to science: it doesn't make any difference how beautiful your guess is; it doesn't make any difference how smart you are, who made the guess, or what his name is – if it disagrees with experiment, it's wrong; that's all there is to it.

Richard Feynman, The Character of Physical Law (1965).

As already said, the SR-EDF approach is on its own already a powerful method, but has some severe limitations. Firstly, it breaks some important symmetries of the nuclear Hamiltonian, and secondly, resting upon the calculation of a single product-state wave function, it cannot account for all of the many phenomena observed in nuclear structure (e.g. soft nuclei, ...). The present section will investigate the theoretical methods to go beyond the simple SR-EDF level that are (1) the projection technique [100, 90, 19] which allows to restore the broken symmetries and thus to recover good quantum numbers, and (2) the Generator Coordinate Method (GCM) [81, 73, 19], which, by a variational configuration mixing of several projected quasiparticle states, allows to construct more general states that provide better approximation to the eigenstates of the nuclear Hamiltonian. In this work the projection and the GCM are combined together for maximum effect, and are part of the general multi-reference EDF formalism. We will try in this chapter to be as general as possible, and even if in practice we will give examples of applications for odd-A nuclei only, the same formalism is also valid for even-A nuclei. For the sake of clarity, we will give here directly the results and refer the reader to appendices B and C for demonstrations.

In section 3.1 we will first redefine the intrinsic symmetries as they are used in our MR-EDF calculation codes. In the second section 3.2 we will then present the projection method in detail, taking a general Group Theory angle. The two following sections, sections 3.3 and 3.4, apply the projection principles to the cases of Particle-Number Restoration (PNR) and Angular-Momentum Restoration (AMR), respectively. Finally, in the last section 3.5 we will present the Generator Coordinate Method and will describe how to solve the discretized Hill-Wheeler-Griffin equation.

3.1 Symmetries of the Quasiparticle States in the Multi-Reference Numerical Codes

For historical and practical reasons, the SR-EDF solver CR8 was designed to use the signature along the z-axis $\hat{R}_z$ [36], whereas the MR-EDF codes use the signature along the x-axis $\hat{R}_x$ [22]. Indeed, using the same axis for the quantification of the spin and the conserved signature makes the formulation of the so-called cranking constraint easier in the SR-EDF code, whereas keeping the z-axis for the quantification of the spin and changing to a good x-signature leads to simplification in the angular-momentum restoration in the MR-EDF codes [64]. The difference of axis for the signature has no consequences on the practical results but necessitates to transform the mean-field wave functions before performing the multi-reference calculations.
Defining the unitary transformation operator that exchanges the z and x-axis

$$\begin{aligned} \hat{P}_{xz} &= \hat{P}\hat{R}_y\Big(\frac{\pi}{2}\Big)\hat{R}_z(\pi) \quad , \\ \hat{P}^{\dagger}_{xz} &= \hat{P}^{-1}_{xz} \quad , \end{aligned} \tag{3.1}$$

we can transform eigenstates of the z-signature into eigenstates of the x-signature

$$\hat{P}_{xz}\hat{R}_z = \hat{R}_x\hat{P}_{xz} \quad , \tag{3.2}$$

without affecting[1] the other important symmetry operations

$$\begin{aligned} \hat{P}_{xz}\,\hat{P} &= \hat{P}\,\hat{P}_{xz} \quad , \\ \hat{P}_{xz}\,\hat{S}^T_y &= \hat{\Pi}_A\hat{S}^T_y\,\hat{P}_{xz} \quad , \\ \hat{P}_{xz}\,\hat{R}^2_i &= \hat{R}^2_i\,\hat{P}_{xz} \quad i = x,y,z \quad , \\ \hat{P}_{xz}\,\hat{T}^2 &= \hat{T}^2\,\hat{P}_{xz} \quad . \end{aligned} \tag{3.3}$$

The nuclear Hamiltonian having rotational and parity invariance, it obviously commutes with $\hat{P}_{xz}$

$$\big[\hat{P}_{xz},\hat{H}\big] = 0 \quad , \tag{3.4}$$

which assures that we don't change the expectation value of the energy of the quasiparticle states by performing the transformation.
For the sake of clarity, in this chapter a state $|\Phi_a\rangle$ defines now the wave function after the transformation $\hat{P}_{xz}$, and which obeys the symmetry relations

$$\hat{R}_x|\Phi_a\rangle = \eta_a|\Phi_a\rangle \quad , \tag{3.5}$$
$$\hat{P}|\Phi_a\rangle = p_a|\Phi_a\rangle \quad , \tag{3.6}$$
$$\hat{S}^T_y|\Phi_a\rangle = \quad |\Phi_a\rangle \quad , \tag{3.7}$$
$$\hat{\Pi}_{\hat{A}}|\Phi_a\rangle = \pi_a|\Phi_a\rangle \quad , \tag{3.8}$$
$$\hat{R}^2_i|\Phi_a\rangle = \pi_a|\Phi_a\rangle \quad i = x,y,z \quad , \tag{3.9}$$
$$\hat{T}^2|\Phi_a\rangle = \pi_a|\Phi_a\rangle \quad , \tag{3.10}$$

[1] The factor π_a for the y-time-simplex being global for all states mixed in this work, we can ignore it.

with

$$\pi_a = \begin{cases} +1 & A_a \text{ even} \\ -1 & A_a \text{ odd} \end{cases} , \tag{3.11}$$

$$\eta_a = \begin{cases} \pm 1 & A_a \text{ even} \\ \pm i & A_a \text{ odd} \end{cases} , \tag{3.12}$$

$$p_a = \pm 1 \quad . \tag{3.13}$$

Defining the time-reversed state

$$|\tilde{\Phi}_a\rangle = \hat{T}|\Phi_a\rangle \quad , \tag{3.14}$$

and applying successively the y-time-simplex and the x-signature, we can derive an additional useful relation

$$\hat{R}_z|\Phi_a\rangle = \pi_a p_a \eta_a^* |\tilde{\Phi}_a\rangle \quad , \tag{3.15}$$

between the state $|\Phi_a\rangle$ and its time-reversed state $|\tilde{\Phi}_a\rangle$.

3.2 Projection from a Group Theory Perspective

Surprisingly, even if the projection method has been widely used [19] in theoretical nuclear physics since its first introduction by Peierls and Yoccoz [100, 160], the formal aspects of the projection are rarely tackled in full details (in nuclear physics) with only few notable exceptions [93, 141, 59]. We want here to go a little bit deeper than a simple list of recipes, while keeping a pragmatic physicist's approach. Recent articles by Duguet *et al.* [59, 61] already went into this direction, but addressing the question from the point of view of general energy density functionals. But as we consider here pseudo-potential-based functionals, we profit from the unique opportunity that offers this type of functionals to use directly the more intuitive wave function formalism within which group theory principles are straightforward to apply.

3.2.1 Preliminary Reminder on Group Theory

We start by recalling the definitions of the principal group-theoretical concepts used in this section, but it lies outside the scope of this thesis to cover this matter in its entirety[2]. So we refer the reader to the abundant literature on the subject [75, 72, 33, 94, 70] for a more exhaustive presentation of group theory and its applications in physics.

Definition of a Group

A group $(G, \bullet)$ is a set of elements G together with a law of composition $\bullet$ such that

- ◇ **Closure:** $\forall\, g, g' \in G\,,\ g \bullet g' \in G\,.$
- ◇ **Associativity:** $\forall\, g, g', g'' \in G\,,\ (g \bullet g') \bullet g'' = g \bullet (g' \bullet g'')\,.$
- ◇ **Identity:** $\exists\, e \in G\,,\ \forall\, g \in G\,,\ g \bullet e = e \bullet g = g\,.$
- ◇ **Invertibility:** $\forall\, g \in G\,,\ \exists\, g' \in G\,,\ g \bullet g' = g' \bullet g = e\,.$

[2] Anyway, it is probably not possible to do it in a single book, let alone a thesis.

The element e is called the identity element, or the neutral element, and is unique.
If the law of composition is commutative, that is if

$$\forall\, g, g' \in G\,,\; g \bullet g' = g' \bullet g\,,$$

the group is said to be commutative or Abelian. In practice the law of composition $\bullet$ is often not mentioned[3] and the group is simply labeled by G, the composition between the group's elements is noted multiplicatively: $gg' \equiv g \bullet g'$, the neutral element e is noted e_G, and the inverse of an element g is noted g^{-1}.
Let H be a subset of elements of G such that

- $\diamond$ $H \neq \varnothing$.
- $\diamond$ $\forall\, h, h' \in H\,,\; h \bullet h' \in H$.
- $\diamond$ $\forall\, h \in H\,,\; h^{-1} \in H$.

$(H, \bullet)$ is said to be a subgroup of $(G, \bullet)$. Note that a subgroup of G is always at least composed of the neutral element of G.

A group G that has a finite number of elements n_G is called a finite group, and n_G is then called the order of the group. On the contrary, a group with an infinite number of elements is said to be an infinite group. We will be interested in this work only in a special kind of infinite group, the compact Lie groups. Without going into too much detail, we will simply say that a Lie group is a group whose elements depends on a finite number r of continuous parameters: $g(a_1, \ldots, a_r)$ and such that for the group composition $g(c_1, \ldots, c_r) = g(a_1, \ldots, a_r)g(b_1, \ldots, b_r)$, the parameters c_i are functions of the parameters a_i and b_i: $c_i = f_i(a_1, \ldots, a_r, b_1, \ldots, b_r)$ with f_i being analytic, i.e. possesses derivatives at all orders for all its variables. In addition the group is said to be compact if each of its parameters varies over a closed interval. The compact Lie groups allow for defining an invariant integration with a Haar measure $dv_G(g)$, and thus it is possible to carry over most of the interesting properties of finite groups to compact Lie groups [75, 72]. We define [72] the volume v_G of a compact Lie group as

$$v_G = \int_{g \in G} dv_G(g) \quad .$$

Finally, we note that most of the Lie groups of physical interest are compact, which is for example the case for the unitary group $U(n)$, the orthogonal group $O(n)$ and their respective subgroups $SU(n)$ and $SO(n)$.

Represensation of a Group

Let $(G, \bullet)$ and $(F, \star)$ be two groups; a group homomorphism ρ is a map $\rho : G \mapsto F$ that satisfies the conditions

- $\diamond$ $\forall\, g, g' \in G\,,\; \rho(g \bullet g') = \rho(g) \star \rho(g')$.
- $\diamond$ $\rho(e_G) = e_F$.
- $\diamond$ $\forall\, g \in G\,,\; \rho(g^{-1}) = \rho(g)^{-1}$.

[3] One of my math teachers, G. Roussel in CPGE at Lycée Michel-Montaigne (Bordeaux), used to tell us in the classroom that the most important things in mathematics are usually the ones we forget to mention.

If ρ is bijective, i.e. ρ establishes a one-to-one correspondance between the elements of G and F, the map ρ is said to be a group isomorphism; the inverse of ρ is then noted ρ^{-1}. And a map from a group G to itself is called a group endomorphism. Finally, a group homomorphism that is at the same time a group isomorphism and a group endomorphism is called a group automorphism.

Let G be a group, K a field[4], and V a vector space[5] over K. The group homomorphism $\pi : G \mapsto GL(V)$, where $GL(V)$ is the group of automorphisms[6] of V, is said to be a *representation* of the group G on the vector space V and is noted (π, V). The dimension of the representation is the dimension n of the vector space V and if V is finite-dimensional, $GL(V)$ is isomorphic to the group $GL(n, K)$ of invertible matrices of dimension $n \times n$ and thus, choosing a basis of V, it is possible to construct a matrix representation of G that we will denote as $D(G)$.
Given two representations (π_1, V_1) and (π_2, V_2) of G, they are said to be *equivalent* if there exists an isomorphism $\rho : V_1 \mapsto V_2$ such that

$$\forall\, g \in G\,,\ \pi_2(g) = \rho \circ \pi_1(g) \circ \rho^{-1}\,.$$

It can be proven [75] that for finite groups and compact Lie groups, and considering that V has the structure of a complex Hilbert space[7], every representation is equivalent to an unitary representation, i.e. a representation $(\hat{U}, V)$ such that $\hat{U}(g)$ is an unitary operator ($\subset$ automorphisms) on V. And the matrices $D(G)$ of finite-dimensional unitary representations are unitary.
Given a representation (π, V) of G, $W \subseteq V$ is called an invariant subspace of V if

$$\forall\, g \in G\,, \forall\, w \in W\,,\ \pi(g)w \in W.$$

The representation π restricted to the subspace W: (π, W) is called a sub-representation of G. If there is no nontrivial[8] invariant subspace of V, the representation (π, V) is said to be an *irreducible representation* (irrep). The (matrix) irreducible representations of G are labeled (up to equivalence) by the superscript μ: $D^{\mu}(G)$ and the dimension (of its associated subspace) is noted d_{μ}. It can be proven [75, 70] that for finite groups and compact Lie groups, *all irreducible representations are finite-dimensional and that every unitary representation is (up to equivalence) either irreducible or completely reducible, i.e. can be written as the direct sum of irreducible representations.* And it can also be demonstrated [75] that the irreducible representations of abelian groups are all of dimension 1.

Direct Product of Groups

Let H and F be two groups; from H and F we can construct another group G, noted $G = H \times F$, whose elements are all the pairs $(h \in H\,, f \in F)$ with

- $(h, f)(h', f') = (hh', ff')\,.$
- $e_G = (e_H, e_F)\,.$
- $(h, f)^{-1} = (h^{-1}, f^{-1})\,.$

[4] $(K, +, \times)$ is said to be a field if $(K, +)$ is a commutative group (neutral element: 0_K), $(K \backslash \{0_K\}, \times)$ is also a commutative group (neutral element: 1_K), and if the multiplicative law $\times$ is distributive over the additive law $+$. As for groups, the laws $+$ and $\times$ are usually omitted and the field is simply labeled by K.

[5] For the definition of a vector space see for example [70].

[6] An automorphism of V is a bijective linear map from V to itself. The set of all automorphisms of V with the law of composition $\circ$ forms a group noted $GL(V)$ and called the general linear group of V.

[7] For the definition of a Hilbert space see for example [75].

[8] $\equiv$ other than the whole space V or the zero subspace.

G is said to be the external direct product of the groups H and F. And the irreducible representations of G are all the possible tensor products of the irreducible representations of H with the irreducible representations of F. For finite-dimensional irreducible representations, the (matrix) irreducible representations $D^{\mu\times\nu}(G)$ of dimension $d^G_{\mu\times\nu} = d^H_\mu d^F_\nu$ are then the Kronecker product of the (matrix) irreducible representations $D^\mu(H)$ of dimension d^H_μ with the (matrix) irreducible representations $D^\nu(F)$ of dimension d^F_ν

$$D^{\mu\times\nu}(G) = D^\mu(H) \otimes D^\nu(F)\,,$$

$$D^{\mu\times\nu}_{ik,jl}(G) = D^\mu_{ij}(H) D^\nu_{kl}(F)\,,$$

with $i,j \in \{1,...,d^H_\mu\}$ and $k,l \in \{1,...,d^F_\nu\}$.

Let G_1 and G_2 be two subgroups of a group G such that

- $\diamond$ $G_1 \cap G_2 = \{e_G\}$.
- $\diamond$ $\forall\, g_1 \in G_1\,,\ \forall\, g_2 \in G_2\,,\ g_1 g_2 = g_2 g_1$.
- $\diamond$ $\forall\, g \in G\,,\ \exists\, g_1 \in G_1\,,\ \exists\, g_2 \in G_2\,,\ g = g_1 g_2$.

G is said to be the internal direct product of the groups G_1 and G_2 and is noted $G = G_1 G_2$. It is easy to prove [75, 33] that G is isomorphic to the external direct product $G_1 \times G_2$. This is why, for the groups considered in this work that may have the structure of an internal direct product of groups, we will also use them as external direct product of groups.
Finally, it is possible to generalize all the properties we have just described to a finite number of (external or internal) direct products of groups.

3.2.2 Projection on the Basis Functions of an Irreducible Representation

Let G be a group, either a finite group with n_G elements, or a compact Lie group of volume v_G. And let us consider the unitary irreps $D^\mu(G)$ of finite dimension d_μ of G. A set τ of d_μ functions $\phi^{\mu\tau}_i$, in the Hilbert space $\mathcal{H}$,[9] that transform under the action of the unitary operators $\hat{U}(g)$, associated with the elements g of G, as linear combinations of the form

$$\forall\ \in G\,,\ \hat{U}(g)\,\phi^{\mu\tau}_i = \sum_{j=1}^{d_\mu} D^\mu_{ji}(g)\,\phi^{\mu\tau}_j \quad , \tag{3.16}$$

forms a basis[10] for the representation $D^\mu(G)$ in the subspace spanned by the functions $\phi^{\mu\tau}_i$. As we will prove, the d_μ functions $\phi^{\mu\tau}_i$ are orthogonal one to the other, and we can write

$$D^\mu_{ji}(g) = \left(\phi^{\mu\tau}_j\,,\,\hat{U}(g)\phi^{\mu\tau}_i\right) \quad . \tag{3.17}$$

As we will later on be interested in the eigenvectors of Hermitean operators (e.g. the Hamiltonian), and as we will consider only finite-dimensional sets of functions, we can choose[11] in addition the functions $\phi^{\mu\tau}_i$ as to be orthonormal.

[9] To separate the purely mathematical discussion from the physical one, we do not use in this section the Dirac bracket notation. In particular a vector in $\mathcal{H}$ is simply noted ϕ, and the scalar product of $\mathcal{H}$ is noted $(\cdot,\cdot)$.

[10] Note that, for the sake of clarity, throughout all of this section we run the indices of the basis functions from 1 to d_μ to emphasize there are d_μ possible values for the indices. In practice, however, different notations may be advantageous. For example, for $SU(2)$, in the basis of eigenvectors common to $\hat{J}^2$ and $\hat{J}_z$, the indices run from $-J$ to J.

[11] We can always construct an orthonormal basis through a Gram-Schmidt procedure.

Between the irreducible representations hold the (great) orthogonality relations [75, 72, 94]

$$\frac{d_\nu}{n_G}\sum_g^{n_G} D^{\mu}_{ij}{}^*(g)\, D^{\nu}_{kl}(g) = \delta_{\nu\mu}\,\delta_{ik}\,\delta_{jl} \tag{3.18}$$

for finite groups and

$$\frac{d_\nu}{v_G}\int_{g\in G} dv_G(g)\, D^{\mu}_{ij}{}^*(g)\, D^{\nu}_{kl}(g) = \delta_{\nu\mu}\,\delta_{ik}\,\delta_{jl} \tag{3.19}$$

for compact Lie groups. We want to stress here that, for the orthogonality relations to hold between different, but equivalent, irreps with same value of μ, we have to make for all those representations a similar choice of basis [94], i.e. the matrix elements (3.17) are identical for all those representations:[12]

$$\forall\,\tau,\tau',\ \left(\phi_j^{\mu\tau}\,,\,\hat{U}(g)\phi_i^{\mu\tau}\right) = \left(\phi_j^{\mu\tau'}\,,\,\hat{U}(g)\phi_i^{\mu\tau'}\right) = D^{\mu}_{ji}(g) \quad . \tag{3.20}$$

Using the orthogonality relations to our advantage we define the operators $\hat{P}^{\nu}_{lm}$ with $l,m \in \{1,...,d_\nu\}$

$$\hat{P}^{\nu}_{lm} = \frac{d_\nu}{n_G}\sum_g^{n_G} D^{\nu}_{lm}{}^*(g)\,\hat{U}(g) \tag{3.21}$$

for finite groups and

$$\hat{P}^{\nu}_{lm} = \frac{d_\nu}{v_G}\int_{g\in G} dv_G(g)\, D^{\nu}_{lm}{}^*(g)\,\hat{U}(g) \tag{3.22}$$

for compact Lie groups. Such operators are called *projection operators* and act on the functions $\phi_i^{\mu\tau}$ as

$$\hat{P}^{\nu}_{lm}\phi_i^{\mu\tau} = \phi_l^{\nu\tau}\,\delta_{\nu\mu}\,\delta_{mi} \quad . \tag{3.23}$$

Though we call it a projection operator, $\hat{P}^{\nu}_{lm}$ is not necessarily a projector in the strict mathematical sense, i.e. a linear map p such that $p\circ p = p$. Indeed, we can see from equation (3.23) that we have the relation

$$\hat{P}^{\nu}_{jk}\,\hat{P}^{\mu}_{lm} = \hat{P}^{\nu}_{jm}\delta_{\nu\mu}\delta_{kl} \quad , \tag{3.24}$$

such that only the operators $\hat{P}^{\nu}_{jj}$ are true projectors. For this reason, and seeing in (3.23) that an operator $\hat{P}^{\nu}_{lm}$ transforms a basis function $\phi_m^{\nu\tau}$ into a basis function $\phi_l^{\nu\tau}$, the operators $\hat{P}^{\nu}_{lm}$ with $l\neq m$ are sometimes called *shift operators* [94] or *transfer operators* [142]. It is interesting to note that for abelian groups, the projection operators are always true projectors as the irreducible representations are all of dimension 1.

From the unitarity of the representations $D^{\nu}(G)$ one can also derive the useful property

$$\hat{P}^{\nu}_{lm}{}^{\dagger} = \hat{P}^{\nu}_{ml} \quad , \tag{3.25}$$

where we also recall that the operators $\hat{U}$ are unitary: $\hat{U}^{\dagger}(g) = \hat{U}^{-1}(g) = \hat{U}(g^{-1})$.

Using equations (3.23) and (3.25), we can now prove that the different basis functions belonging to the same irrep are indeed orthogonal, and, more generally, that the basis functions belonging to different non-equivalent irreps are also orthogonal

$$\begin{aligned}\left(\phi_i^{\nu\tau}\,,\,\phi_j^{\mu\tau'}\right) &= \left(\phi_i^{\nu\tau}\,,\,\hat{P}^{\mu}_{jm}\phi_m^{\mu\tau'}\right)\\ &= \left(\hat{P}^{\mu}_{jm}{}^{\dagger}\phi_i^{\nu\tau}\,,\,\phi_m^{\mu\tau'}\right)\\ &= \left(\hat{P}^{\mu}_{mj}\phi_i^{\nu\tau}\,,\,\phi_m^{\mu\tau'}\right)\\ &= \delta_{\mu\nu}\delta_{ji}\left(\phi_m^{\mu\tau}\,,\,\phi_m^{\mu\tau'}\right) \quad .\end{aligned} \tag{3.26}$$

[12] For example, we use Wigner's D^J functions for all the irreps of $SU(2)$ with same J but that act in different subspaces associated with different eigenvalues of $\hat{H}$.

In the case of different, but equivalent, irreps with same value of μ, the basis functions may also be orthogonal (e.g. eigenstates of the Hamiltonian with the same symmetry quantum numbers but different energy eigenvalues) but the projection operator is no sufficient to show that as such irreps have the same matrices (in the basis we have fixed and common to all of them).

Projection of an Arbitrary Function

Let us now consider a function ψ in the Hilbert space that is *a priori* not a basis function for any irrep of G. The set of functions created by applying to ψ all the operators $\hat{U}(g)$ is called an orbit of G [120] and will be denoted as

$$G\psi = \left\{\hat{U}(g)\psi\,,\,\forall\, g \in G\right\} \quad . \tag{3.27}$$

All the linear combinations of the elements of $G\psi$ span a subspace of the Hilbert space that we will denote as $S(G\psi)$. By construction $S(G\psi)$ is invariant under the action of $\hat{U}$

$$\forall\, v \in S(G\psi)\,,\,\forall\, g \in G\,,\,\hat{U}(g)v \in S(G\psi) \quad , \tag{3.28}$$

and thus can be used to build a sub-representation of G. For the type of groups considered here, there are (up to equivalence) only two possibilities: either this representation is irreducible and ψ can be written as a linear combination of the basis functions of this particular irrep, or this representation is completely reducible and ψ can be decomposed on the basis functions of the different irreps which decompose the representation of G on $S(G\psi)$. In general, we can thus write

$$\psi = \sum_{\mu}\sum_{\tau}\sum_{i=1}^{d_\mu} c_i^{\mu\tau}(\psi)\,\phi_i^{\mu\tau} \quad , \tag{3.29}$$

where $\phi_i^{\mu\tau}$ is a basis function of an irrep $D^\mu(G)$ of dimension d_μ of G on $S(G\psi)$, and where the label τ distinguishes between the different irreps with same value of μ that may appear in the decomposition of $S(G\psi)$.[13] When the coefficients $c_i^{\mu\tau}(\psi)$ in the superposition (3.29) are non-zero for more than one value of i or μ, it is easy to see that ψ does not transform according to equation (3.16) (replacing $\phi_i^{\mu\tau}$ by $\sum_\tau \phi_i^{\mu\tau}$). Acting with the operator $\hat{P}^\mu_{lm}$ on the function ψ, we project ψ on the basis components l of all the irreps $D^\mu(G)$

$$\hat{P}^\mu_{lm}\psi = \sum_{\tau} c_m^{\mu\tau}(\psi)\,\phi_l^{\mu\tau} \quad . \tag{3.30}$$

Having this property, we can understand now the notion of projection operator. But note that the projection operator cannot distinguish between the irreps with same value of μ but different values of τ. For a given value of l, it is possible to create d_μ projected funtions $\hat{P}^\mu_{lm}\psi$ with different values of m, assuming of course that for each m: $c_m^\mu(\psi) \neq 0$. They represent different choices for the construction of a l^{th} basis function of an irrep $D^\mu(G)$ from ψ. But if we want to conserve the same transformation as (3.16) (in the appropriate subspace) with the same matrix elements (3.17) (up to normalization), we need that all the d_μ partner of the basis with different values of l are constructed from the same value of m

$$\psi_l^\mu = \hat{P}^\mu_{lm}\psi \quad , \tag{3.31}$$

or from the same linear superposition of them

$$\psi_l^\mu = \sum_m f_m^\mu(\psi)\,\hat{P}^\mu_{lm}\psi \quad . \tag{3.32}$$

[13] Note here that the functions $\phi_i^{\mu\tau}$ with different values of τ are chosen to be orthogonal.

Indeed, using relation (3.24), it is easy to see that the state ψ_l^ν transforms according to the irreducible representation $D^\nu(G)$ as

$$\hat{P}_{ij}^{\mu}\psi_l^\nu = \psi_i^\nu\,\delta_{\nu\mu}\,\delta_{jl} \quad , \tag{3.33}$$

and thus similarly to $\phi_l^{\mu\tau}$ in equation (3.23). Finally, we mention that the superposition (3.32) will be of particular interest in our case.

Projection for Direct Product of Groups

To conclude the present section, let us consider the frequent case where the group G is the direct product of two groups[14] H and F

$$G = H \times F\,,$$

where H and F act in the spaces $\mathcal{E}_1$ and $\mathcal{E}_2$, respectively. As already stated before, the irreps of G in the space $\mathcal{E}_1 \otimes \mathcal{E}_2$ are built from the tensor products of the irreps of H in $\mathcal{E}_1$ with the irreps of F in $\mathcal{E}_2$

$$D^{\mu\times\nu}(G) = D^\mu(H) \otimes D^\nu(F)\,,$$

with the dimension $d^G_{\mu\times\nu} = d^H_\mu d^F_\nu$ and with basis functions that are the tensor product of the basis functions of the irreps of H in $\mathcal{E}_1$ with the basis functions of the irreps of F in $\mathcal{E}_2$, which we will note multiplicatively

$$\Phi_{ik}^{\mu\times\nu,G}(\mathcal{E}_1 \otimes \mathcal{E}_2) = \phi_i^{\mu,H}(\mathcal{E}_1)\,\phi_k^{\nu,F}(\mathcal{E}_2) \equiv \phi_i^{\mu,H}(\mathcal{E}_1) \otimes \phi_k^{\nu,F}(\mathcal{E}_2) \quad . \tag{3.34}$$

It is straightforward to see that the projection operators on the basis functions of the irreps of G are of the form

$$\hat{P}_{ik,jl}^{\mu\times\nu,G} = \hat{P}_{ij}^{\mu,H}\hat{P}_{kl}^{\nu,F} \equiv \hat{P}_{ij}^{\mu,H} \otimes \hat{P}_{kl}^{\nu,F} \quad , \tag{3.35}$$

with $i,j \in \{1,...,d^H_\mu\}$ and $k,l \in \{1,...,d^F_\nu\}$.

On the other hand, the tensor product of an irrep $D^\mu(G)$ of G in $\mathcal{E}_1$ with an irrep $D^\nu(G)$ of G in $\mathcal{E}_2$ may be a reducible representation of G[15] in $\mathcal{E}_1 \otimes \mathcal{E}_2$, which can thus be written as the direct sum

$$D^{\nu\times\mu}(G) = \sum_\gamma^{\oplus} m_\gamma D^\gamma(G) \quad , \tag{3.36}$$

with m_γ being the multiplicity of the irrep $D^\gamma(G)$, i.e. the number of times $D^\gamma(G)$ appears, in the above direct sum called Clebsch-Gordan Series. The decomposition of the basis functions of $D^\gamma(G)$ in $\mathcal{E}_1 \otimes \mathcal{E}_2$ on the basis functions of $D^\nu(G)$ in $\mathcal{E}_1$ and of $D^\mu(G)$ in $\mathcal{E}_2$ is written

$$\Phi_n^{\gamma,t,G}(\mathcal{E}_1 \otimes \mathcal{E}_2) = \sum_{i=1}^{d_\mu}\sum_{j=1}^{d_\nu}(\mu i\nu j|\gamma nt)_G\;\phi_i^{\mu,G}(\mathcal{E}_1)\,\phi_j^{\nu,G}(\mathcal{E}_2) \quad , \tag{3.37}$$

where the coefficients $(\nu i\mu j|\gamma nt)_G$ are the Clebsch-Gordan coefficients of the group, and which follow the orthogonality relations [138]

$$\sum_{i=1}^{d_\mu}\sum_{j=1}^{d_\nu}(\mu i\nu j|\gamma nt)^*_G\,(\mu i\nu j|\gamma' n't')_G = \delta_{\gamma\gamma'}\delta_{nn'}\delta_{tt'} \quad , \tag{3.38}$$

$$\sum_\gamma\sum_{n=1}^{d_\gamma}\sum_{t=1}^{m_\gamma}(\mu i\nu j|\gamma nt)^*_G\,(\mu i'\nu j'|\gamma nt\,)_G = \delta_{ii'}\delta_{jj'} \quad , \tag{3.39}$$

[14] With the same restrictions as G: finite group or compact Lie group

[15] Or more precisely the diagonal subgroup of $G \times G$ composed by the elements: $(g,g)\,, \forall\, g \in G$, and which is isomorphic to G.

and where $t \in \{1, \dots, m_\gamma\}$ labels the m_γ possible equivalent irreps $D^\gamma(G)$ appearing in the Clebsch-Gordan series of the group.

In physical applications, and taking the example of two particles having each the group G as symmetry group in their respective spaces, it is usually the group G, and not the group $G \times G$, that is the relevant group of symmetry for the system composed of the two particles. It thus necessary to project on the basis functions of the irreps $D^\gamma(G)$ in $\mathcal{E}_1 \otimes \mathcal{E}_2$, which is simply done by using the appropriate projection operator $\hat{P}^\gamma_{mn}$ of the form (3.21 - 3.22) with operator $\hat{U}(g) \equiv \hat{U}(g) \otimes \hat{U}(g)$ acting in $\mathcal{E}_1 \otimes \mathcal{E}_2$.
Finally, we mention that all these considerations can be generalized for a finite number of direct product of groups and also that they become fairly trivial in the case of 1-dimensional irreps.

3.2.3 Symmetry Group of the Hamiltonian

After this rather formal introduction, we can now safely discuss the applications of the principles developed above to the case of a Hamiltonian-based EDF approach.
Let us consider a group G that is a group of physical transformations. According to Wigner's theorem [158, 10], the elements g of G are represented by operators acting on the Hilbert space that are either unitary or antiunitary. We will consider in this work only the case of unitary operators, and more precisely only the case where G is a finite group or a compact Lie group. Considering now a Hamiltonian $\hat{H}$, G is said to be group of symmetry of $\hat{H}$ if the Hamiltonian $\hat{H}$ commutes with all the unitary operators $\hat{U}(g)$ associated with the elements g of G

$$\forall\, g \in G\,,\ [\hat{H}, \hat{U}(g)] = 0 \quad . \tag{3.40}$$

As a consequence, all the vectors $\hat{U}(g)|E\rangle$ in the orbit $G|E\rangle$, built from the action of all possible operators $\hat{U}(g)$ on an eigenvector $|E\rangle$ of $\hat{H}$, are also eigenvectors of $\hat{H}$ with the same energy E as the one of $|E\rangle$

$$\forall\, g \in G\,,\ \hat{H}\hat{U}(g)|E\rangle = E\hat{U}(g)|E\rangle \quad . \tag{3.41}$$

This means that the space spanned by all the eigenvectors of $\hat{H}$ is invariant under the action of the operators $\hat{U}(g)$ and thus can be used to build a representation of G[16]. More exactly, all degenerate eigenvectors with a given energy $E^{\mu\tau}$ span an invariant subspace of this space that can also be used to build a sub-representation of G. We assume[17] that if G is the full symmetry group of $\hat{H}$, this representation is irreducible and thus we can find in this subspace a set of d_μ degenerate eigenvectors $|E^{\mu\tau}_i\rangle$ that forms a basis for the irreps $D^\mu(G)$ of dimension d_μ of G

$$\forall\, g \in G\,,\ \hat{U}(g)\,|E^{\mu\tau}_i\rangle = \sum_{j=1}^{d_\mu} D^\mu_{ji}(g)\,|E^{\mu\tau}_j\rangle \quad . \tag{3.42}$$

Conversely, if a set of d_μ eigenvectors $|E^{\mu\tau}_i\rangle$ of $\hat{H}$ forms a basis of an irrep $D^\mu(G)$ of dimension d_μ of G, it is easy to prove that they are degenerate in energy. Indeed, it is always possible to build a projection operator $\hat{P}^\mu_{ij}$ of the form (3.21 - 3.22) for this particular irrep and thus to rewrite $|E^{\mu\tau}_i\rangle$ as

$$|E^{\mu\tau}_i\rangle = \hat{P}^\mu_{ij}|E^{\mu\tau}_j\rangle \quad . \tag{3.43}$$

Because of equation (3.40), the projection operator commutes with $\hat{H}$

$$\forall\, i, j \in \{1, \dots, d_\mu\}\,,\ \left[\hat{H}, \hat{P}^\mu_{ij}\right] = 0 \quad , \tag{3.44}$$

[16] Which is actually the same representation as the eigenvectors of $\hat{H}$ span the entire Hilbert space.
[17] It can happen, on rare occasions and only for certain combinations of the Hamiltonian's parameters, that states belonging to different irreps of G have the same energy; we speak then of "accidental" degeneracy [75, 33].

and thus we can write

$$\begin{aligned} \hat{H}|E_i^{\mu\tau}\rangle = \hat{H}\hat{P}_{ij}^{\mu}|E_j^{\mu\tau}\rangle = \hat{P}_{ij}^{\mu}\hat{H}|E_j^{\mu\tau}\rangle = E_j^{\mu\tau}\hat{P}_{ij}^{\mu}|E_j^{\mu\tau}\rangle \\ E_i^{\mu\tau}|E_i^{\mu\tau}\rangle = E_j^{\mu\tau}|E_i^{\mu\tau}\rangle \quad . \end{aligned} \tag{3.45}$$

As equation (3.45) holds for any value of i and j in $\{1,\dots,d_\mu\}$, we prove that all the basis functions $|E_i^{\mu\tau}\rangle$ of $D^\mu(G)$ are degenerate with an energy noted $E^{\mu\tau}$.

To summarize, the eigenvectors of the Hamiltonian $\hat{H}$ are orthonormal[18] basis functions for the irreducible representations $D^\mu(G)$ of dimension d_μ of the full symmetry group G of the Hamiltonian. Each eigenvalue $E^{\mu\tau}$ of $\hat{H}$ is d_μ-fold degenerate[19] and the eigenvectors of $\hat{H}$ can be labeled by the irreducible representation $D^\mu(G)$ they belong to; we say that μ is a *good quantum number*. Note that nothing prevents representations with same value of μ to appear, with different energies ($\equiv$ different values of τ), in the spectrum of $\hat{H}$ (e.g. there is usually more than one state with a given value of the total angular momentum in the spectrum of a given nucleus).

3.2.4 Projection of Quasiparticle States

None of these points is verified for a quasiparticle state $|\Phi_a\rangle$ as defined in the second chapter. Assuredly $|\Phi_a\rangle$ is not eigenstate of the nuclear Hamiltonian $\hat{H}$, and neither does it have all the good quantum numbers that label those eigenstates. Nevertheless, it is possible starting from $|\Phi_a\rangle$ to create states that are approximation to the eigenstates of $\hat{H}$ and that have the correct symmetry properties.

Let G be a symmetry group of the Hamiltonian and $|\Phi_a\rangle$ a quasiparticle state that is not *a priori* a basis function for any irrep of G. And let us note $S(G|\Phi_a\rangle)$ the subspace spanned by the elements of the orbits $G|\Phi_a\rangle$. Noticing, in particular, that all the elements of $G|\Phi_a\rangle$ are non-orthogonal among each other, and have all the same expectation value of the energy

$$\forall\, g \in G\,,\ \langle\Phi_a|\hat{U}^\dagger(g)\hat{H}\hat{U}(g)|\Phi_a\rangle = \langle\Phi_a|\hat{H}|\Phi_a\rangle \quad . \tag{3.46}$$

To obtain states that are better approximation to the eigenstates of $\hat{H}$ and that have the good quantum numbers associated with the irreps of G, we have to diagonalize $\hat{H}$ in the subspace $S(G|\Phi_a\rangle)$ spanned by the elements of $G|\Phi_a\rangle$ [120, 34, 107].
The sub-representation of G that can be built on $S(G|\Phi_a\rangle)$ is either irreducible or completely reducible. In general, it will be completely reducible, i.e. $S(G|\Phi_a\rangle)$ can be decomposed as the direct sum of smaller invariant subspaces which, themselves, do not possess any nontrivial invariant subspace. Let us call $S^\mu(G|\Phi_a\rangle)$ the invariant subspace that contains all the different irreps of G with same value of μ present in the decomposition of the representation of G on $S(G|\Phi_a\rangle)$.

Projection onto the Invariant Subspaces $S^\mu(G|\Phi_a\rangle)$ of $S(G|\Phi_a\rangle)$

As the Hamiltonian $\hat{H}$ commutes with the projection operators of G (3.44), all the invariant subspaces $S^\mu(G|\Phi_a\rangle)$ are also invariant subspaces for $\hat{H}$. Also, because of equation (3.26), those subspaces are all orthogonal to each other. We thus can reduce the problem to diagonalizing $\hat{H}$ in each of those subspaces [34, 142]. To move into each subspace $S^\mu(G|\Phi_a\rangle)$, we act with the projection operators associated with the irrep $D^\mu(G)$ on $|\Phi_a\rangle$. For an irrep $D^\mu(G)$ of dimension

[18] As the eigenvectors of $\hat{H}$ can be chosen as to be orthonormal.
[19] We neglect here the possible accidental degeneracies.

d_μ, we can generate d_μ^2 (normalized) states that are basis functions for $D^\mu(G)$ and that belong to $S^\mu(G|\Phi_a\rangle)$

$$|\mu\, l, a\, m\rangle = \frac{\hat{P}^\mu_{lm}|\Phi_a\rangle}{\sqrt{\langle\Phi_a|\hat{P}^\mu_{mm}|\Phi_a\rangle}} \quad , \tag{3.47}$$

where $l, m \in \{1, \ldots, d_\mu\}$, and where the factor

$$\frac{1}{\sqrt{\langle\Phi_a|\hat{P}^\mu_{mm}|\Phi_a\rangle}}$$

is a normalization factor such that

$$\langle\mu\, l, a\, m|\mu\, l, a\, m\rangle = 1 \quad . \tag{3.48}$$

For the sake of generality, we have assumed that none of the states $\hat{P}^\mu_{lm}|\Phi_a\rangle$ is zero, or we couldn't write (3.47) as $\langle\Phi_a|\hat{P}^\mu_{mm}|\Phi_a\rangle$ would be equal to zero. In practice, however, this may different. From equations (3.24) and (3.25), we can see that the states $|\mu\, l, a\, m\rangle$ with different values of μ and/or l are orthogonal (as they should be), but that states with same values of μ and l but different values of m are not orthogonal

$$\langle\mu'\, l', a\, m'|\mu\, l, a\, m\rangle = \frac{\delta_{\mu',\mu}\,\delta_{l',l}\,\langle\Phi_a|\hat{P}^\mu_{m'm}|\Phi_a\rangle}{\sqrt{\langle\Phi_a|\hat{P}^\mu_{m'm'}|\Phi_a\rangle\langle\Phi_a|\hat{P}^\mu_{mm}|\Phi_a\rangle}} \quad . \tag{3.49}$$

And they have no reason to be, as they just represent different possibilities to build basis functions of a given μ and l from $|\Phi_a\rangle$. Using commutation relation (3.44), a similar rationale also holds for the Hamiltonian kernel

$$\langle\mu'\, l', a\, m'|\hat{H}|\mu\, l, a\, m\rangle = \frac{\delta_{\mu',\mu}\,\delta_{l',l}\,\langle\Phi_a|\hat{H}\hat{P}^\mu_{m'm}|\Phi_a\rangle}{\sqrt{\langle\Phi_a|\hat{P}^\mu_{m'm'}|\Phi_a\rangle\langle\Phi_a|\hat{P}^\mu_{mm}|\Phi_a\rangle}} \quad . \tag{3.50}$$

By projecting, we have diagonalized the Hamiltonian between states with different μ or l but we have yet to diagonalize the Hamiltonian in the subspace spanned by the non-orthogonal projected states $|\mu\, l, a\, m\rangle$ with with same value of μ or l but different value of m.[20] In order to do so, we thus consider the superposed states

$$|\mu\, l\, \epsilon, a\rangle = \sum_{m=1}^{d_\mu} f^\mu_\epsilon(a, m)\, |\mu\, l, a\, m\rangle \quad , \tag{3.51}$$

where $f^\mu_\epsilon(a, m)$ is the weight of the state $|\mu\, l, a\, m\rangle$ in the superposed state $|\mu\, l\, \epsilon, a\rangle$, and where ϵ is an index which is used to label the states $|\mu\, l\, \epsilon, a\rangle$, and which will be defined below. Note that the right hand side of equation (3.50) does not depend on l, which is expected as all the states with different values of l shall be degenerate. On a more general perspective, we can say that if Group Theory tell us the symmetry properties of the eigenvectors of $\hat{H}$ such as their good quantum numbers or their degeneracies, nothing in Group Theory alone can tell us the values of

[20] Note that, in the special case where there is only one value of m which gives a non-vanishing projected state, the Hamiltonian is already diagonal in this subspace (of dimension 1) and we cannot gain any extra energy after acting with the projection operator.

their eigenvalues.[21] As we have seen in section 2.1, finding the eigenvalues of $\hat{H}$ in this subspace is equivalent to look for the states $|\mu\, l\, \epsilon, a\rangle$ that have a vanishing variation of their energy

$$E^{\mu}_{\epsilon}(a) = \frac{\langle \mu\, l\, \epsilon, a|\hat{H}|\mu\, l\, \epsilon, a\rangle}{\langle \mu\, l\, \epsilon, a|\mu\, l\, \epsilon, a\rangle} \quad . \tag{3.52}$$

Varying $E^{\mu}_{\epsilon}(a)$ over the parameter $f^{\mu *}_{\epsilon}(a, m)$

$$\frac{\delta E^{\mu}_{\epsilon}(a)}{\delta f^{\mu *}_{\epsilon}(a, m)} = 0 \quad , \tag{3.53}$$

we obtain a Hill-Wheeler-Griffin-like equation [81, 73]

$$\sum_{m=1}^{d_\mu} \left[\bar{H}^{\mu}_{m'm}(a, a) - E^{\mu}_{\epsilon}(a)\, \bar{N}^{\mu}_{m'm}(a, a)\right] f^{\mu}_{\epsilon}(a, m) = 0 \quad , \tag{3.54}$$

where

$$\bar{N}^{\mu}_{m'm}(a, a) = \langle \mu\, l, a\, m'|\mu\, l, a\, m\rangle \quad , \tag{3.55}$$

$$\bar{H}^{\mu}_{m'm}(a, a) = \langle \mu\, l, a\, m'|\hat{H}|\mu\, l, a\, m\rangle \quad , \tag{3.56}$$

are the (normalized) overlap kernels and the (normalized) energy kernels, respectively. The HWG equation (3.54) presents a generalized eigenvalue problem with the energies $E^{\mu}_{\epsilon}(a)$ being solutions of the characteristic equation

$$\det\left\{\bar{H}^{\mu}(a, a) - E^{\mu}_{\epsilon}(a)\bar{N}^{\mu}(a, a)\right\} = 0 \quad . \tag{3.57}$$

If (3.57) is not trivially zero and if the matrix $\bar{N}^{\mu}(a, a)$ is invertible, there are d_μ solutions to (3.54), whereas if $\bar{N}^{\mu}(a, a)$ is singular, there are less than d_μ solutions. Let us note $c_\mu \leq d_\mu$ the number of solutions $E^{\mu}_{\epsilon}(a)$ that satisfy (3.57). In addition, as the overlap and the energy kernel are Hermitean matrices, the energies $E^{\mu}_{\epsilon}(a)$ are real.

Solving the HWG equation (3.54),[22] we obtain the weights $f^{\mu}_{\epsilon}(a, m)$ for the states $|\mu\, l\, \epsilon, a\rangle$ and their (real) energy $E^{\mu}_{\epsilon}(a)$, and we use the index $\epsilon \in \{1, \ldots, c_\mu\}$ to label their order in the energy spectrum composed of all the $E^{\mu}_{\epsilon}(a)$. The projected states $|\mu\, l\, \epsilon, a\rangle$ represent the best approximations possible to the eigenstates of the Hamiltonian one can build in each subspace $S^{\mu}(G|\Phi_a\rangle)$. They have correct transformation properties (3.16) and thus the good quantum numbers and degeneracy associated with the irrep $D^{\mu}(G)$ of the symmetry group G of the Hamiltonian, they are all orthogonal to each other

$$\langle \mu'\, l'\, \epsilon', a|\mu\, l\, \epsilon, a\rangle = \delta_{\mu',\mu}\, \delta_{l',l}\, \delta_{\epsilon',\epsilon} \quad , \tag{3.58}$$

and the Hamiltonian $\hat{H}$ is diagonal in the subspace $S(G|\Phi_a\rangle)$

$$\langle \mu'\, l'\, \epsilon', a|\hat{H}|\mu\, l\, \epsilon, a\rangle = \delta_{\mu',\mu}\, \delta_{l',l}\, \delta_{\epsilon',\epsilon}\, E^{\mu}_{\epsilon}(a) \quad . \tag{3.59}$$

Also, we mention that the energy

$$E^{\mu}_{\epsilon}(a) = \langle \mu\, l\, \epsilon, a|\hat{H}|\mu\, l\, \epsilon, a\rangle \tag{3.60}$$

[21] Only for schematic, and hand-tailored, Hamiltonian such as the ones used in algebraic approches [120, 149], it can tell us only the form of the eigenvalues.

[22] More on how to solve the HWG equation in practice will be presented in the section 3.5.

can be expressed in terms of the energy density kernels defined in chapter 1. Indeed, noting

$$|\Phi_a(g)\rangle = \hat{U}(g)|\Phi_a\rangle \quad ,$$

and

$$\mathcal{E}^{nuc}[\rho,\kappa,\kappa^*]^{a(ag)} = \frac{\langle\Phi_a|\hat{H}|\Phi_a(g)\rangle}{\langle\Phi_a|\Phi_a(g)\rangle} \quad ,$$

we have for finite groups

$$E^\mu_\epsilon(a) = \sum_{m'=1}^{d_\mu}\sum_{m=1}^{d_\mu} \frac{f^{\mu *}_\epsilon(a,m')}{b^\mu_{m'}(a)} \frac{f^\mu_\epsilon(a,m)}{b^\mu_m(a)} \sum_g^{n_G} {D^\nu_{m'm}}^*(g)\, \mathcal{E}^{nuc}[\rho,\kappa,\kappa^*]^{a(ag)} \langle\Phi_a|\Phi_a(g)\rangle \,, \tag{3.61}$$

where for $i \in \{1\,,\,\ldots\,,d_\mu\}$

$$b^\mu_i(a) = \sqrt{\frac{n_G}{d_\mu}\langle\Phi_a|\hat{P}^\mu_{ii}|\Phi_a\rangle} = \sqrt{\sum_g^{n_G} D^{\nu *}_{ii}(g)\,\langle\Phi_a|\Phi_a(g)\rangle} \quad , \tag{3.62}$$

and we have for compact Lie groups

$$E^\mu_\epsilon(a) = \sum_{m'=1}^{d_\mu}\sum_{m=1}^{d_\mu} \frac{f^{\mu *}_\epsilon(a,m')}{b^\mu_{m'}(a)} \frac{f^\mu_\epsilon(a,m)}{b^\mu_m(a)} \int_{g\in G} dv_G(g)\, {D^\nu_{m'm}}^*(g)\, \mathcal{E}^{nuc}[\rho,\kappa,\kappa^*]^{a(ag)} \langle\Phi_a|\Phi_a(g)\rangle \,, \tag{3.63}$$

where for $i \in \{1\,,\,\ldots\,,d_\mu\}$

$$b^\mu_i(a) = \sqrt{\frac{v_G(g)}{d_\mu}\langle\Phi_a|\hat{P}^\mu_{ii}|\Phi_a\rangle} = \sqrt{\int_{g\in G} dv_G(g)\, D^{\nu *}_{ii}(g)\,\langle\Phi_a|\Phi_a(g)\rangle} \quad . \tag{3.64}$$

Finally, in the case of abelian groups the irreps being all 1-dimensional, the projection is sufficient to diagonalize $\hat{H}$ in each of the subspaces (of dimension 1) and thus we do not have to solve the HWG equation (see note 20). The indices l and ϵ become in that case superfluous and hence are omitted.

3.2.5 Matrix Elements Between Projected Quasiparticle States

In practice, we do not need to construct the wave functions $|\mu\, l\, \epsilon, a\rangle$, only the matrix elements of the operators of interest between the projected states. Let us consider the set of d_μ operators $\hat{T}^\mu_i$ which transform accordingly to an irrep $D^\nu(G)$

$$\forall\, g \in G, \quad \hat{U}(g)\hat{T}^\nu_i\hat{U}^\dagger(g) = \sum_{j=1}^{d_\nu} D^\nu_{ji}(g)\,\hat{T}^\nu_j \quad . \tag{3.65}$$

Such a set is called a set of irreducible tensor operators. And let us take the generic notation $\hat{T}^0_1$ for all the scalar operators (e.g. $\hat{\mathbb{1}}$, $\hat{H}$) that commute[23] with all the operators associated with elements of the groups G

$$\forall\, g \in G\,,\, [\hat{T}^0_1, \hat{U}(g)] = 0 \quad , \tag{3.66}$$

[23] Or to say it differently: that transform accordingly to the trivial irreducible representation $D^0(G)$, i.e. the representation of dimension $d_0 = 1$ such that every elements of G is represented by 1, and which always exists.

and therefore with the projection operators. Usually, the operators of interest are either scalars operators, irreducible tensor operators, or can be expressed as functions of the irreducible tensor operators. Thanks to the commutation relations (3.65) and (3.66), we only have to evaluate matrix elements of the form[24]

$$\forall\ k \in \{1, ..., d_\nu\},\ \forall\ i, j \in \{1, ..., d_\mu\},\ \langle \Phi_a | \hat{T}^\nu_k \hat{P}^\mu_{ij} | \Phi_a \rangle \quad . \tag{3.67}$$

Then, using the Wigner-Eckart Theorem [55, 33], we can compute the reduced matrix elements between the states $|\mu, a\, j\rangle$

$$\langle \gamma, a\, n || \hat{T}^\nu || \mu, a\, j \rangle_t = \sum_{i=1}^{d_\mu} \sum_{k=1}^{d_\nu} (\mu i \nu k | \gamma n t)^*_G \frac{\langle \Phi_a | \hat{T}^\nu_k \hat{P}^\mu_{ij} | \Phi_a \rangle}{\sqrt{\langle \Phi_a | \hat{P}^\gamma_{nn} | \Phi_a \rangle \langle \Phi_a | \hat{P}^\mu_{jj} | \Phi_a \rangle}} \quad , \tag{3.68}$$

where, in the case of scalar operators $\hat{T}^0_1$, we have $(\mu i 01 | \gamma n t)_G = \delta_{\mu,\gamma}\, \delta_{i,n}\, \delta_{t,1}$ with $d_0 = 1$. Finally, one can evaluate the reduced matrix elements for the states $|\mu\, l\, \epsilon, a\rangle$ as

$$\langle \gamma\, \epsilon, a || \hat{T}^\nu || \mu\, \epsilon', a \rangle_t = \sum_{n=1}^{d_\gamma} \sum_{j=1}^{d_\mu} f^{\gamma *}_\epsilon(a, n) f^\mu_{\epsilon'}(a, j)\, \langle \gamma, a\, n || \hat{T}^\nu || \mu, a\, j \rangle_t \quad , \tag{3.69}$$

and from them any matrix elements we want, thanks again to the Wigner-Eckart Theorem

$$\langle \gamma\, l\, \epsilon, a | \hat{T}^\nu_k | \mu\, l'\, \epsilon', a \rangle = \sum_{t=1}^{m_\gamma} (\mu l' \nu k | \gamma l t)_G\, \langle \gamma\, \epsilon, a || \hat{T}^\nu || \mu\, \epsilon', a \rangle_t \quad . \tag{3.70}$$

With that, we dispose of all the tools we need to compute expectation values of the observales of interest related to the group G. For example, in the case of $SU(2)$ we can calculate the transition probabilities between the states with different angular momenta.

We tried here to stay as general as possible, properly defining the projection method without specifying the group G. A list of some of the principal possible projections is presented in Tab. 3.1 along with the essential properties of the associated groups. In this work we will "only" project on the particle number and the angular momentum. The particularities of these projections will be covered in more detail in the next two sections.

[24] It is trivial for scalar operators as they commute with the projection operators and see section C.10.2 for a demonstration for spherical tensor operators in the case of $SU(2)$.

Physical Symmetry	Group	Quantum Number	Properties	Operators $\hat{U}$	Irreps	Projection Operator	For example broken by
Particle-Number Invariance $X \in \{N, Z\}$	$U(1)_X$	Particle Number $X \in \{N, Z\}$	Lie Group, Compact, Abelian	$\hat{R}_X(\phi_x) = e^{-i\phi_x \hat{X}}$	$e^{-i\phi_x X}$, $X \in \mathbb{Z}$, $d_X = 1$	$\hat{P}^X = \frac{1}{2\pi}\int_0^{2\pi} d\phi_x \, e^{-i\phi_x(\hat{X}-X)}$	Pairing or finite temperature
Number Parity Invariance $X \in \{N, Z\}$	$\Pi_X \equiv \{\hat{\mathbb{1}}, e^{-i\pi\hat{X}}\}$	Number Parity $\pi_x \in \{\pi_n, \pi_z\}$	Finite Group, Abelian, Subgroup of $U(1)_X$	$\{\mathbb{1}, e^{-i\pi\hat{X}}\}$	$D^{\pi_x}(\Pi_X)$ $\pi_x \in \{1, -1\}$, $d_{\pi_x} = 1$	$\hat{P}^{\pi_x} = \frac{1}{2}\left(\hat{\mathbb{1}} + \pi_x \, e^{-i\pi\hat{X}}\right)$	Finite temperature
Rotational Invariance	$SU(2)_A$	Angular Momentum J	Lie Group, Compact	$\hat{R}(\alpha,\beta,\gamma) = e^{-i\alpha\hat{J}_z} e^{-i\beta\hat{J}_y} e^{-i\gamma\hat{J}_z}$	$D^J_{MK}(\alpha,\beta,\gamma)$, $J \in \mathbb{N}$ or $\mathbb{N} + \frac{1}{2}$, $d_J = 2J+1$	$\hat{P}^J_{MK} = \frac{2J+1}{16\pi^2}\int_0^{2\pi} d\alpha \int_0^{\pi} d\beta \sin(\beta) \int_0^{4\pi} d\gamma \times {D^J_{MK}}^*(\alpha,\beta,\gamma)\,\hat{R}(\alpha,\beta,\gamma)$	Deformation (any multipole)
Parity Invariance	$I_A \equiv \{\hat{\mathbb{1}}, \hat{P}\}$	Parity p	Finite Group, Abelian	$\{\mathbb{1}, \hat{P}\}$	$D^p(I)$, $p \in \{1, -1\}$, $d_p = 1$	$\hat{P}^p = \frac{1}{2}\left(\hat{\mathbb{1}} + p\hat{P}\right)$	Deformation (odd multipole)
Translational Invariance	$T^3_A \simeq (\mathbb{R}^3, +)_A$	Center-of-Mass Linear Momentum $\vec{Q}$	Lie Group, Locally Compact, Abelian	$\hat{R}_{\vec{P}_{com}}(\vec{a}) = e^{-\frac{i}{\hbar}\vec{a}\cdot\hat{\vec{P}}_{com}}$	$e^{-\frac{i}{\hbar}\vec{a}\cdot\vec{Q}}$, $\vec{Q} \in \mathbb{R}^3$, $d_{\vec{Q}} = 1$	$\hat{P}^{\vec{Q}} = \frac{1}{(2\pi\hbar)^3}\int_{-\infty}^{+\infty} d\vec{a} \, e^{-\frac{i}{\hbar}\vec{a}\cdot(\hat{\vec{P}}_{com}-\vec{Q})}$	Localization

Table 3.1: Principal symmetries of the nuclear Hamiltonian and their associated groups.
Note that if the group of translations in space is not compact, it is a locally compact abelian group, and as such has an invariant integration [70] (see also the case of Fourier transforms).

3.3 Particle-Number Restoration

The particle-number invariance reflects the simple physical fact that a given isolated nucleus has a fixed number[25] of protons and neutrons; it is associated with the group that has the direct product structure $U(1)_N \times U(1)_Z$, $U(1)$ being the compact abelian unitary group of degree 1. The symmetry is broken in our SR-EDF scheme when we include pairing correlations between nucleons (separetely for neutrons and protons) using Bogoliubov quasiparticle states with non-vanishing pairing density κ. As a consequence, a quasiparticle state $|\Phi_a\rangle$ is a superposition of the form (3.29) of the basis functions belonging to different irreps of $U(1)_N \times U(1)_Z$. The group $U(1)$ has an infinite number of 1-dimensional irreps and thus the state $|\Phi_a\rangle$ can be written as

$$|\Phi_a\rangle = \sum_{\tau} \sum_{N} \sum_{Z} c^{NZ\tau}(a) |NZ\tau\rangle \quad . \tag{3.71}$$

where τ labels the different irreps of $U(1)_N \times U(1)_Z$ in the Hilbert space with same values of N and Z. From physical considerations[26] the state $|\Phi_a\rangle$ has obviously positive numbers of neutrons and protrons, and considering that $|\Phi_a\rangle$ has a good neutron and proton number parity, it is easy to show (see appendix B.2) that the sum is restricted, for a given particle species, to be composed only of basis functions of irreps having the same number parity as the one of $|\Phi_a\rangle$ for this particle species

$$|\Phi_a\rangle = \sum_{\tau} \sum_{N} \sum_{Z} \delta_{\pi_N,\pi_{na}} \, \delta_{\pi_Z,\pi_{za}} \, c^{NZ\tau}(a) |NZ\tau\rangle \quad , \tag{3.72}$$

where $\pi_N = (-)^N$ and $\pi_Z = (-)^Z$ are the number parities associated with a system of N neutrons and Z protons.

In a system with an infinite, or a sufficiently large, number of particles such symmetry breaking has no dramatic effect. The BCS theory [9], which inspired the treatment of pairing in nuclear physics, was initially developed to explain the superconductivity observed in condensed matter physics. Such large systems are not treated exactly but statistically, so adding or removing a few particles has no important effect on the system. This is not the case for the nucleus, which is a finite quantal system with only a quite small number of particles, where such symmetry breaking is unsatifactory. For a better theoretical treatment and if we want to achieve an unambiguous comparison of our calculations with experiment, we thus have to restore the broken symmetry by projecting the quasiparticle state $|\Phi_a\rangle$ on the number of neutrons and protons of the studied nucleus.

The particle-number projection operator on the irrep X_0's basis function for the particle species $(X, x) \in \{(N, n), (Z, z)\}$ reads

$$\hat{P}^{X_0} = \frac{1}{2\pi} \int_0^{2\pi} d\phi_x \, e^{-i\phi_x(\hat{X} - X_0)} \quad . \tag{3.73}$$

Using the number parity of $|\Phi_a\rangle$, the projection on the number of particles can be simplified (see appendix B.4) to

$$\hat{P}^{X_0} |\Phi_a\rangle = \frac{\delta_{\pi_{xa},\pi_{X_0}}}{\pi} \int_0^{\pi} d\phi_x \, e^{-i\phi_x(\hat{X} - X_0)} |\Phi_a\rangle \tag{3.74}$$

[25] We disregard here the radioactive decays (e.g. α or β decays) or nuclear reactions (e.g. pick-up, transfer, charge exchange) that change the number of particles.

[26] It can also be easily proven by applying the projection operator on $|\Phi_a\rangle$ and considering that the neutron (resp. proton) vacuum has 0 neutrons (resp. protons). This is simply because $|\Phi_a\rangle$ is a superposition of states formed, for each of them, by a positive number of single-particle creation operators.

with $\pi_{X_0} = (-)^{X_0}$ being the number parity associated with a system of X_0 particles and π_{xa} the number-parity of $|\Phi_a\rangle$ for the species X. The latter equation allows for a reduction by a factor of 2 the integration interval, which is of advantage from a computation time point of view. On a more fundamental level the equation (3.74) tells us that the integral does not vanish only if we project a state $|\Phi_a\rangle$ on a particle-number X_0 with a number-parity equal to π_{xa}. But this is no surprise because, as already said, the state $|\Phi_a\rangle$ is a superposition of states either with an even number of particles, or with an odd number of particles (for each species separetely).
Considering at the same time both the projection on the correct proton and neutron numbers, we have the normalized projected state

$$|NZ, a\rangle = \frac{\hat{P}^N \hat{P}^Z |\Phi_a\rangle}{\sqrt{\langle \Phi_a | \hat{P}^N \hat{P}^Z | \Phi_a \rangle}} \quad , \tag{3.75}$$

which has an energy

$$E^{NZ}(a) = \langle NZ, a | \hat{H} | NZ, a \rangle \quad . \tag{3.76}$$

The latter can be expressed in terms of the energy density kernels as

$$E^{NZ}(a) = \frac{\int_0^\pi d\phi_n \int_0^\pi d\phi_z \, e^{i\phi_n N} e^{i\phi_z Z} \, \mathcal{E}^{nuc}[\rho, \kappa, \kappa^*]^{a(a\phi_n\phi_z)} \langle \Phi_a | \Phi_a(\phi_n, \phi_z) \rangle}{\int_0^\pi d\phi_n \int_0^\pi d\phi_z \, e^{i\phi_n N} e^{i\phi_z Z} \, \langle \Phi_a | \Phi_a(\phi_n, \phi_z) \rangle} \quad , \tag{3.77}$$

where

$$\begin{aligned} |\Phi_a(\phi_n, \phi_z)\rangle &= e^{-i\phi_n \hat{N}} e^{-i\phi_z \hat{Z}} |\Phi_a\rangle \quad , \\ \mathcal{E}^{nuc}[\rho, \kappa, \kappa^*]^{a(a\phi_n\phi_z)} &= \frac{\langle \Phi_a | \hat{H} | \Phi_a(\phi_n, \phi_z) \rangle}{\langle \Phi_a | \Phi_a(\phi_n, \phi_z) \rangle} \quad . \end{aligned} \tag{3.78}$$

Because of the simple group structure of $U(1)$ (irreps of dimension 1), the particle number restoration is one of the simplest projections to perform. It was already implemented in some relatively old calculations [48, 12, 79] and is now almost always part of the MR-EDF computations in nuclear structure [22, 113]. It has also been realized in a VAP approach [2, 63] or in time-dependent calculations for nuclear reactions [130].

3.4 Angular-Momentum Restoration

3.4.1 Angular-Momentum Projection Operator

An isolated nucleus is rotationally invariant, i.e. its energy does not change under rotations and the eigenstates of the nuclear Hamiltonian have good total angular momentum. The groups associated with rotational symmetry are the special orthogonal group $SO(3)$ or its universal cover, the special unitary group $SU(2)$. Because the nuclear Hamiltonian's eigenstates can have (for odd-mass nuclei) half-integer values of their total angular momentum, it is maybe more natural to use the compact, but non-abelian, Lie group $SU(2)$. Because of the non-commutativity of the elements of $SU(2)$, the group structure is more complicated and so is the projection on angular momentum, compared to what we saw for particle-number restoration. Allowing for the quasiparticle state $|\Phi_a\rangle$ to be deformed, we break the rotational invariance and thus the state can be decomposed on the basis functions of the irreps D^J of dimension $2J+1$ of $SU(2)$ as

$$|\Phi_a\rangle = \sum_\tau \sum_J \sum_{M=-J}^{J} c_M^{J\tau}(a) |JM\tau\rangle \quad , \tag{3.79}$$

where τ labels the different irreps of $SU(2)_A$ with same value of J. Similarly to number parity in the previous section, we can use here the symmetry (3.9) to prove (see appendix C.4) that the basis functions entering in the decomposition of $|\Phi_a\rangle$ either have all integer values of J or have all half-integer values of J

$$|\Phi_a\rangle = \sum_{\tau} \sum_{J} \sum_{M=-J}^{J} \delta_{\pi_J,\pi_a}\, c_M^{J\tau}(a) |JM\tau\rangle \quad , \tag{3.80}$$

where $\pi_J = (-)^{2J}$ plays a role comparable to the one of $(-)^X$ (with $X \in \{N, Z\}$) for the number of particle, but for the angular momentum. Note also that we do not treat neutrons and protons separetely. This is because the appropriate group to consider for the symmetry of the Hamiltonian is $SU(2)_A$ and not the direct product $SU(2)_N \times SU(2)_Z$. Therefore we have to consider the irreps corresponding to the total angular momentum of the nucleus, which is different from the tensor product of the irreps of the neutrons and the protons as explained before in section 3.2.2. The angular momentum restoration is maybe of even higher physical importance than the particle-number restoration, because it allows us to label the states by their angular momentum and it also allows[27] us to compute electromagnetic transition probabilities, and consequently it becomes possible to compare the calculations with experimental spectroscopic observations. Indeed, the electromagnetic transition operators can be expressed in terms of the irreducible operators of $SU(2)$, the spherical tensor operators $\hat{T}^{\lambda}_{\mu}$ (the scalars are noted $\hat{T}^{0}_{0}$). Finally, we recall the simple Clebsch-Gordan series for $SU(2)$

$$D^{J_1} \otimes D^{J_2} = D^{|J_1-J_2|} \oplus D^{|J_1-J_2|+1} \oplus \cdots \oplus D^{J_1+J_2-1} \oplus D^{J_1+J_2} \quad , \tag{3.81}$$

which defines the selection rules for transitions and which authorizes us to drop the multiplicity label t on the (real) Clebsch-Gordan coefficents of $SU(2)$ (see appendix C.10), as every irrep appears only once in the decomposition.

From the group structure[28] of $SU(2)$ we can deduce the form of the projection operator on angular momentum

$$\hat{P}^{J}_{MK} = \frac{2J+1}{16\pi^2} \int_0^{2\pi} d\alpha \int_0^{\pi} d\beta\, \sin(\beta) \int_0^{4\pi} d\gamma\, D^{J}_{MK}{}^{*}(\alpha,\beta,\gamma)\, \hat{R}(\alpha,\beta,\gamma) \quad , \tag{3.82}$$

with $M, K \in \{-J, ..., J\}$ and where D^{J}_{MK} is a Wigner's D function. Again, because of (3.9), we can reduce (see appendix C.6) the integration interval by a factor of 2

$$\hat{P}^{J}_{MK}|\Phi_a\rangle = \frac{(2J+1)\,\delta_{\pi_a,\pi_J}}{8\pi^2} \int_0^{2\pi} d\alpha \int_0^{\pi} d\beta\, \sin(\beta) \int_0^{2\pi} d\gamma\, D^{J}_{MK}{}^{*}(\alpha,\beta,\gamma)\, \hat{R}(\alpha,\beta,\gamma)|\Phi_a\rangle \quad , \tag{3.83}$$

which is not luxury as we will see in the next section.

3.4.2 Symmetries of the Rotated Matrix Elements

The angular-momentum restoration is the most expensive single operation in our framework from a CPU time point of view. The particle-number restoration can be performed on a personal computer in a matter of seconds, whereas the angular-momentum restoration requires at least

[27] To be precise, good parity is also required, which is the case for our quasiparticle states, as well as good neutron and protron numbers, which are obtained after projection on N and Z.

[28] We have chosen here to carry the integral over 4π on the variable γ [155].

several hours of computation or often more, depending on the discretization taken for the integrals over the Euler angles and of course depending on the hardware of the machine used for the run. If we are interested only in the calculation of diagonal matrix elements or in a limited configuration mixing, the amount of CPU hours needed for the angular-momentum restoration remains easily manageable using parallel supercomputers. But when we want to go for a full-scale GCM, the CPU time required becomes a limiting factor even for such computers. It is therefore necessary to use all available possibilities to reduce the computational time needed for the angular momentum projection as much as possible.

In our case, a good solution is to exploit the intrinsic symmetries of the quasiparticle states given in section 3.1. By using these symmetries and their combinations we can derive (see appendix C.7) a set of helpful relations between rotations by certain angles, relations given here in the general case where the ket $|\Phi_b\rangle$ and the bra $\langle\Phi_a|$ are different:

$$\langle\Phi_a|\hat{R}(\pi-\alpha,\beta,\pi-\gamma)\hat{T}^\lambda_\mu|\Phi_b\rangle = (-)^\lambda \pi_a\eta_a\eta_b^* \quad \langle\Phi_a|\hat{R}(\alpha,\beta,\gamma)\hat{T}^\lambda_{-\mu}|\Phi_b\rangle \quad , \tag{3.84}$$

$$\langle\Phi_a|\hat{R}(\pi+\alpha,\pi-\beta,2\pi-\gamma)\hat{T}^\lambda_\mu|\Phi_b\rangle = (-)^\lambda \pi_a\eta_b^* \quad \langle\Phi_a|\hat{R}(\alpha,\beta,\gamma)\hat{T}^\lambda_{-\mu}|\Phi_b\rangle \quad , \tag{3.85}$$

$$\langle\Phi_a|\hat{R}(2\pi-\alpha,\pi-\beta,\pi+\gamma)\hat{T}^\lambda_\mu|\Phi_b\rangle = \pi_a\eta_a \quad \langle\Phi_a|\hat{R}(\alpha,\beta,\gamma)\hat{T}^\lambda_{\mu}|\Phi_b\rangle \quad , \tag{3.86}$$

$$\langle\Phi_a|\hat{R}(\alpha,\pi-\beta,\pi-\gamma)\hat{T}^\lambda_\mu|\Phi_b\rangle = (-)^{\lambda+\mu} p_a p_b\eta_a \quad \langle\Phi_a|\hat{R}(\alpha,\beta,\gamma)\hat{\tilde{T}}^\lambda_{-\mu}|\Phi_b\rangle^* \quad , \tag{3.87}$$

$$\langle\Phi_a|\hat{R}(\pi-\alpha,\pi-\beta,\gamma)\hat{T}^\lambda_\mu|\Phi_b\rangle = (-)^{\mu} p_a p_b\eta_b^* \quad \langle\Phi_a|\hat{R}(\alpha,\beta,\gamma)\hat{\tilde{T}}^\lambda_{\mu}|\Phi_b\rangle^* \quad , \tag{3.88}$$

$$\langle\Phi_a|\hat{R}(\pi+\alpha,\beta,\pi+\gamma)\hat{T}^\lambda_\mu|\Phi_b\rangle = (-)^{\mu} \pi_a p_a p_b\eta_a\eta_b^* \langle\Phi_a|\hat{R}(\alpha,\beta,\gamma)\hat{\tilde{T}}^\lambda_{\mu}|\Phi_b\rangle^* \quad , \tag{3.89}$$

$$\langle\Phi_a|\hat{R}(2\pi-\alpha,\beta,2\pi-\gamma)\hat{T}^\lambda_\mu|\Phi_b\rangle = (-)^{\lambda+\mu} p_a p_b \quad \langle\Phi_a|\hat{R}(\alpha,\beta,\gamma)\hat{\tilde{T}}^\lambda_{-\mu}|\Phi_b\rangle^* \quad , \tag{3.90}$$

$$\langle\Phi_a|\hat{R}(\alpha,\beta,\pi+\gamma)\hat{T}^\lambda_\mu|\Phi_b\rangle = (-)^{\mu} p_b\eta_b^* \quad \langle\tilde{\Phi}_a|\hat{R}(\alpha,\beta,\gamma)\hat{\tilde{T}}^\lambda_{\mu}|\Phi_b\rangle^* \quad , \tag{3.91}$$

where $\hat{\tilde{T}}^\lambda_\mu = \hat{T}\hat{T}^\lambda_\mu\hat{T}^\dagger$ is the time-reversed operator of the (possibly scalar) operator $\hat{T}^\lambda_\mu$, and where we have assumed that we mix only states with same number-parity for both protons and neutrons

$$\forall\, a,b \quad \begin{cases} \pi_{na} = \pi_{nb} \\ \pi_{za} = \pi_{zb} \end{cases} \Rightarrow \pi_a = \pi_b \quad , \tag{3.92}$$

which is not too stringent a condition as the overlap between states with different number parities is zero, and as we consider only operators which do not change the number of particles. The strategy is then to use the relations (3.84 - 3.91) in order to reduce the number of rotations performed in the angular-momentum projection. Indeed, these relations are linking 16 combinations of angles (α,β,γ). Thus, instead of rotating the wave function for every combination of angles (α,β,γ), we do it only for one out of each set of the 16 combinations of angles linked by the relations (3.84 - 3.91) and then, using the relations (3.84 - 3.91), we reconstruct the matrix elements at the 15 other linked sets of angles. One can notice in particular in (3.91) that the relation between the interval $[0,\pi]$ and $[\pi,2\pi]$ on γ involves the calculation of the time-reversal of $|\Phi_a\rangle$ which seems undesirable at first sight but is actually of advantage, as this operation is much less time-consuming than performing the rotation by $\gamma+\pi$. At the end, by combining all the 8 relations (3.84 - 3.91) we can reduce the interval in which we need to make the rotations over the Euler angles from the full interval $\big([0,2\pi],[0,\pi],[0,2\pi]\big)$ to the much smaller one

$\big([0,\frac{\pi}{2}],[0,\frac{\pi}{2}],[0,\pi]\big)$:

$$
\begin{aligned}
&\int_0^{2\pi} d\alpha \int_0^{\pi} d\beta\, \sin(\beta) \int_0^{2\pi} d\gamma\, {D^J_{MK}}^*(\alpha,\beta,\gamma)\, \langle\Phi_a|\hat{R}(\alpha,\beta,\gamma)\hat{T}^\lambda_\mu|\Phi_b\rangle \\
&= \int_0^{\frac{\pi}{2}} d\alpha \int_0^{\frac{\pi}{2}} d\beta\, \sin(\beta) \int_0^{\pi} d\gamma \Bigg[\Bigg\{ \Big[{D^J_{MK}}^*(\alpha,\beta,\gamma) + \pi_a\eta_a {D^J_{MK}}^*(2\pi-\alpha,\pi-\beta,\pi+\gamma)\Big] \langle\Phi_a|\hat{R}(\alpha,\beta,\gamma)\hat{T}^\lambda_\mu|\Phi_b\rangle \\
&+ (-)^\lambda \Big[\pi_a\eta_a\eta_b^* {D^J_{MK}}^*(\pi-\alpha,\beta,\pi-\gamma) + \pi_a\eta_b^* {D^J_{MK}}^*(\pi+\alpha,\pi-\beta,2\pi-\gamma)\Big] \langle\Phi_a|\hat{R}(\alpha,\beta,\gamma)\hat{T}^\lambda_{-\mu}|\Phi_b\rangle \\
&+ (-)^\mu \Big[p_ap_b\eta_b^* {D^J_{MK}}^*(\pi-\alpha,\pi-\beta,\gamma) + \pi_ap_ap_b\eta_a\eta_b^* {D^J_{MK}}^*(\pi+\alpha,\beta,\pi+\gamma)\Big] \langle\Phi_a|\hat{R}(\alpha,\beta,\gamma)\hat{\tilde{T}}^\lambda_\mu|\Phi_b\rangle^* \\
&+ (-)^{\lambda+\mu} \Big[p_ap_b\eta_a {D^J_{MK}}^*(\alpha,\pi-\beta,\pi-\gamma) + p_ap_b {D^J_{MK}}^*(2\pi-\alpha,\beta,2\pi-\gamma)\Big] \langle\Phi_a|\hat{R}(\alpha,\beta,\gamma)\hat{\tilde{T}}^\lambda_{-\mu}|\Phi_b\rangle^* \Bigg\} \\
&+ (-)^\mu p_b\eta_b^* \Bigg\{ \Big[{D^J_{MK}}^*(\alpha,\beta,\pi+\gamma) + \pi_a\eta_a {D^J_{MK}}^*(2\pi-\alpha,\pi-\beta,2\pi+\gamma)\Big] \langle\tilde{\Phi}_a|\hat{R}(\alpha,\beta,\gamma)\hat{\tilde{T}}^\lambda_\mu|\Phi_b\rangle^* \\
&+ (-)^\lambda \Big[\pi_a\eta_a\eta_b^* {D^J_{MK}}^*(\pi-\alpha,\beta,-\gamma) + \pi_a\eta_b^* {D^J_{MK}}^*(\pi+\alpha,\pi-\beta,\pi-\gamma)\Big] \langle\tilde{\Phi}_a|\hat{R}(\alpha,\beta,\gamma)\hat{\tilde{T}}^\lambda_{-\mu}|\Phi_b\rangle^* \Bigg\} \\
&+ (-)^\mu p_b\eta_b \Bigg\{ (-)^\mu \Big[p_ap_b\eta_b^* {D^J_{MK}}^*(\pi-\alpha,\pi-\beta,\pi+\gamma) + \pi_ap_ap_b\eta_a\eta_b^* {D^J_{MK}}^*(\pi+\alpha,\beta,2\pi+\gamma)\Big] \langle\tilde{\Phi}_a|\hat{R}(\alpha,\beta,\gamma)\hat{T}^\lambda_\mu|\Phi_b\rangle \\
&+ (-)^{\lambda+\mu} \Big[p_ap_b\eta_a {D^J_{MK}}^*(\alpha,\pi-\beta,-\gamma) + p_ap_b {D^J_{MK}}^*(2\pi-\alpha,\beta,\pi-\gamma)\Big] \langle\tilde{\Phi}_a|\hat{R}(\alpha,\beta,\gamma)\hat{T}^\lambda_{-\mu}|\Phi_b\rangle \Bigg\} \Bigg] \quad .
\end{aligned}
\tag{3.93}
$$

reducing by a factor of 16 the number of rotations needed to be calculated. And if we count the reduction of the interval on γ from $[0,4\pi]$ to $[0,2\pi]$ due to the symmetry relation (3.9), we have reduced the number of rotations by a factor of 32.

3.4.3 Mixing of K-components

Contrary to particle-number restoration, the symmetry restoration does not end with the application of the projection operator on the quasiparticle state $|\Phi_a\rangle$. Indeed, for a given value of J, applying the projection operator for different values of K we obtain a set of $2J+1$ non-orthogonal states

$$|JM,aK\rangle = \frac{\hat{P}^J_{MK}|\Phi_a\rangle}{\sqrt{\langle\Phi_a|\hat{P}^J_{KK}|\Phi_a\rangle}} \quad , \tag{3.94}$$

where $K\in\{-J,\dots,J\}$. From them we want to construct a new set of $2J+1$ orthogonal states

$$|JM\epsilon,a\rangle = \sum_{K=-J}^{J} f^J_\epsilon(a,K)|JM,aK\rangle \quad , \tag{3.95}$$

by solving the HWG equation

$$\sum_{K=-J}^{J} \big[\bar{H}^J_{K'K}(a,a) - E^J_\epsilon(a)\,\bar{N}^J_{K'K}(a,a)\big] f^J_\epsilon(a,K) = 0 \quad , \tag{3.96}$$

where

$$\bar{N}^J_{K'K}(a,a) = \langle J\,M,a\,K'|J\,M,a\,K\rangle \quad , \tag{3.97}$$

$$\bar{H}^J_{K'K}(a,a) = \langle J\,M,a\,K'|\hat{H}|J\,M,a\,K\rangle \quad . \tag{3.98}$$

As we will see in section 3.5.4, the HWG equation can be solved by first diagonalizing the overlap matrix $\bar{N}^J_{K'K}(a,a)$ of dimension $(2J+1)\times(2J+1)$. But because of the x-signature symmetry of the quasiparticle state $|\Phi_a\rangle$, there exist (see appendix C.9) between the matrix elements of $\bar{N}^J$ the following symmetries

$$\begin{aligned}\bar{N}^J_{K'K}(a,a) &= \eta_a e^{i\pi J}\ \bar{N}^J_{K'-K}(a,a)\\ &= \eta_a^* e^{-i\pi J}\ \bar{N}^J_{-K'K}(a,a)\\ &= \qquad\ \bar{N}^J_{-K'-K}(a,a)\quad ,\end{aligned} \tag{3.99}$$

such that, for half-integer values of J, only $\frac{(2J+1)}{2}\times\frac{(2J+1)}{2}$ of them are independent. As a consequence, and still for half-integer values of J, the matrix $\bar{N}^J$ has at most $\frac{(2J+1)}{2}$ non-zero eigenvalues[29]. To remove the numerically problematic zero eigenvalues we perform the basis transformation

$$|JM;ak\rangle = \sum_{K=-J}^{J} W^J_{\eta_a}(K,k)|JM,aK\rangle \quad , \tag{3.100}$$

$$W^J_{\eta_a}W^{J\dagger}_{\eta_a} = W^{J\dagger}_{\eta_a}W^J_{\eta_a} = \mathbb{1} \tag{3.101}$$

$$W^J_{\eta_a} = \begin{pmatrix} \frac{1}{\sqrt{2}} & 0 & \cdots & 0 & 0 & \cdots & 0 & \frac{\eta_a e^{+i\pi J}}{\sqrt{2}} \\ 0 & \ddots & \ddots & \vdots & \vdots & \iddots & \iddots & 0 \\ \vdots & \ddots & \ddots & 0 & 0 & \iddots & \iddots & \vdots \\ 0 & \cdots & 0 & \frac{1}{\sqrt{2}} & \frac{\eta_a e^{+i\pi J}}{\sqrt{2}} & 0 & \cdots & 0 \\ 0 & \cdots & 0 & \frac{\eta_a e^{-i\pi J}}{\sqrt{2}} & \frac{1}{\sqrt{2}} & 0 & \cdots & 0 \\ \vdots & \iddots & \iddots & 0 & 0 & \ddots & \ddots & \vdots \\ 0 & \iddots & \iddots & \vdots & \vdots & \ddots & \ddots & 0 \\ \frac{\eta_a e^{-i\pi J}}{\sqrt{2}} & 0 & \cdots & 0 & 0 & \cdots & 0 & \frac{1}{\sqrt{2}} \end{pmatrix} \quad , \tag{3.102}$$

as proposed by Enami *et al.* [64] for even-even vacua projected on even integer values of J, but suitably adapted here to the case of odd-mass nuclei with half-integer values of J[30]. Solving the HWG equation in the new basis

$$\sum_{k\geq 0}^{J}\left[\bar{H}^J_{k'k}(a,a) - E^J_\epsilon(a)\,\bar{N}^J_{k'k}(a,a)\right] f^J_\epsilon(a;k) = 0 \quad , \tag{3.103}$$

where it is only necessary to consider the states with $k \geq 0$ (see appendix C.9.1), we finally obtain the energies $E^J_\epsilon(a)$ of the $\frac{2J+1}{2}$ states and the weights $f^J_\epsilon(a;k)$ of the states $|JM;ak\rangle$ in the superposition

$$|JM\epsilon,a\rangle = \sum_{k\geq 0}^{J} f^J_\epsilon(a;k)|JM;ak\rangle \quad . \tag{3.104}$$

It is important to note that, because of the symmetries (3.99) the overlap $\bar{N}^J(a,a)$ is a singular matrix and we only have $\frac{2J+1}{2}$ projected states, whereas in the most general case, we would have

[29] It is a little bit more complicated for integer values of J as there are a possible further reduction of the number of non-zero eigenvalues due to symmetry ($K=0$ and time-reveral). See appendix C.4.3.

[30] The matrix $W^J_{\eta_a}$ for integer values of J is given in appendix C.9.1.

$2J+1$ projected states. From equations (3.95) and (3.104), it is straigthforward to see that we thus also obtain the weights

$$f_\epsilon^J(a,K) = \sum_{k\geq 0}^{J} f_\epsilon^J(a;k)\, W_{\eta_a}^J(K,k) \tag{3.105}$$

of the states $|JM,aK\rangle$ in the superposition (3.95).
In the end, we thus dispose of a set of $\frac{2J+1}{2}$ states $|JM\epsilon,a\rangle$ that are orthonormal

$$\langle JM\epsilon',a|JM\epsilon,a\rangle = \delta_{\epsilon',\epsilon} \quad , \tag{3.106}$$

and such that the Hamiltonian $\hat{H}$ is diagonal in the subspace spanned by the states $|JM\epsilon,a\rangle$

$$\langle JM\epsilon',a|\hat{H}|JM\epsilon,a\rangle = \delta_{\epsilon',\epsilon}\, E_\epsilon^J(a) \quad . \tag{3.107}$$

The energy of each state $|JM\epsilon,a\rangle$,

$$E_\epsilon^J(a) = \langle JM\epsilon,a|\hat{H}|JM\epsilon,a\rangle \quad , \tag{3.108}$$

can be expressed in terms of the energy density kernels as

$$\begin{aligned} E_\epsilon^J(a) = \sum_{K'=-J}^{J}\sum_{K=-J}^{J} \frac{f_\epsilon^{J*}(a,K')}{b_{K'}^J}\frac{f_\epsilon^J(a,K)}{b_K^J}\int_0^{2\pi}d\alpha\int_0^{\pi}d\beta\,\sin(\beta) \\ \times\int_0^{2\pi}d\gamma\, {D_{K'K}^J}^*(\alpha,\beta,\gamma)\,\mathcal{E}^{nuc}[\rho,\kappa,\kappa^*]^{a(a\alpha\beta\gamma)}\langle\Phi_a|\Phi_a(\alpha,\beta,\gamma)\rangle \end{aligned} \tag{3.109}$$

where

$$\begin{aligned} |\Phi_a(\alpha,\beta,\gamma)\rangle &= \hat{R}(\alpha,\beta,\gamma)|\Phi_a\rangle \quad , \\ \mathcal{E}^{nuc}[\rho,\kappa,\kappa^*]^{a(a\alpha\beta\gamma)} &= \frac{\langle\Phi_a|\hat{H}|\Phi_a(\alpha,\beta,\gamma)\rangle}{\langle\Phi_a|\Phi_a(\alpha,\beta,\gamma)\rangle} \quad , \end{aligned} \tag{3.110}$$

and where for $n\in\{-J\,,\,\ldots\,,\,J\}$

$$b_n^J = \sqrt{\int_0^{2\pi}d\alpha\int_0^{\pi}d\beta\,\sin(\beta)\int_0^{2\pi}d\gamma\, {D_{nn}^J}^*\langle\Phi_a|\Phi_a(\alpha,\beta,\gamma)\rangle} \quad . \tag{3.111}$$

3.5 Configuration Mixing: the Generator Coordinate Method

In the previous sections about symmetry restoration, we presented the projection technique that allows for building, from a single one-quasiparticle state $|\Phi_a\rangle$, a set of projected states that have the good quantum numbers associated with the symmetries of the Hamiltonian and that satisfy the variational condition (3.53). If these projected states are clearly richer than the product state they have been obtained from, the generality of their structure is still limited by the fact they are constructed starting from a *single* product state with a given intrinsic configuration. That is why in the present section, which is the last one of the theoretical part, we discuss the Generator-Coordinate-Method [81, 73, 19, 107] that allows for constructing better approximations to the eigenstates of the Hamiltonian through a variational mixing of projected states which originate from one-quasiparticle states with different intrinsic configurations.

3.5.1 General Principle of the Method

The principle of the GCM, as originally formulated by Wheeler, Hill, and Griffin [81, 73], is to build, from a set of states that depends on a continuous variable θ or set of continuous variables $\theta \equiv (t_1, \ldots, t_n)$, a superposed state

$$|\Psi\rangle = \int d\theta \, f(\theta) \, |\Phi(\theta)\rangle \tag{3.112}$$

that is a more general wave function and a better approximation to an eigenstate of the Hamiltonian. The weight $f(\theta)$ of each state $|\Phi(\theta)\rangle$ is determined applying a variational principle onto the energy of the state $|\Psi\rangle$

$$\frac{\delta}{\delta f^*(\theta')} \left(\frac{\langle \Psi | \hat{H} | \Psi \rangle}{\langle \Psi | \Psi \rangle} \right) = 0 \quad , \tag{3.113}$$

and solving the resulting HWG equation

$$\int d\theta \left[\langle \Phi(\theta') | \hat{H} | \Phi(\theta) \rangle - E \, \langle \Phi(\theta') | \Phi(\theta) \rangle \right] f(\theta) = 0 \quad . \tag{3.114}$$

However, the HWG being solved numerically, the continuous variable θ is in practice discretized

$$\theta \in \{\theta_1 \, , \, \ldots \, , \, \theta_n\} \quad ,$$

and the integrals appropriately replaced by sums

$$|\Psi\rangle = \sum_{i=1}^{n} f(\theta_i) \, |\Phi(\theta_i)\rangle \quad , \tag{3.115}$$

$$\sum_{i=1}^{n} \left[\langle \Phi(\theta_{i'}) | \hat{H} | \Phi(\theta_i) \rangle - E \, \langle \Phi(\theta_{i'}) | \Phi(\theta_i) \rangle \right] f(\theta_i) = 0 \quad . \tag{3.116}$$

Paradoxically, the discretized version of the GCM is also of advantage from a purely theoretical point of view as it is free from some mathematical deficiencies that may appear in its continuous realization [107]. In addition, the discretized GCM can also be used to deal with variables that are discrete by nature, as it will be the case in this work with the different one-quasiparticle states we can build on top of even-even vacua. Although, in that case, the GCM presents no difference from the Ritz variational method.

It is worth noticing that the ansatz (3.112) is very similar to the action of the projection operator of a continuous group on a state $|\Phi\rangle$. But in the case of a projection operator, the variable θ corresponds to the elements of the group and the weights $f(\theta)$ are dictated by the orthogonality relations between the different irreps of the group. The same rationale applies to the discretized ansatz (3.115) and finite groups. Moreover, for the continuous groups the GCM can be viewed as an extension of the symmetry restoration that in addition also deals with the magnitude of the order parameter of the group [61, 128].

3.5.2 Full Symmetry Group of the Problem

Before continuing with the technical aspects of the GCM, it is mandatory to define the full symmetry group

$$\begin{matrix} G = SU(2)_A \times U(1)_N \times U(1)_Z \times I_A \\ J \qquad\quad N \qquad\quad Z \qquad\quad P \end{matrix} \tag{3.117}$$

considered in this work for the Hamiltonian and the projected states. The linear momentum [111, 128] is thus disregarded, as well the unphysical sources of symmetry breaking of the isopin [126, 127] present in mean-field approaches. The quantum numbers are collected under the label

$$\Lambda \equiv (J, N, Z, P) \quad , \tag{3.118}$$

and because all the groups in (3.117) but one are abelian (and thus have one-dimensional irreps), it is straightforward to see the irreps of G are written

$$D^{\Lambda}_{MK}(\alpha, \beta, \gamma, \phi_n, \phi_z, g_p) = D^{J}_{MK}(\alpha, \beta, \gamma) e^{-i\phi_n N} e^{-i\phi_z Z} D^{P}(g_p) \quad , \tag{3.119}$$

where $g_p \in \{\hat{\mathbb{1}}, \hat{P}\}$, and are of dimension $d_\Lambda = 2J + 1$.

The Kronecker product between two irreps D^{Λ_1} with $\Lambda_1 \equiv (J_1, N_1, Z_1, P_1)$ and D^{Λ_2} with $\Lambda_2 \equiv (J_2, N_2, Z_2, P_2)$, gives the Clebsch-Gordan series

$$D^{\Lambda_1} \otimes D^{\Lambda_2} = \sum_{\Lambda_f}^{\oplus} m_{\Lambda_f} D^{\Lambda_f} \tag{3.120}$$

with the selection rules for $\Lambda_f \equiv (J_f, N_f, Z_f, P_f)$

$$\begin{aligned} & m_{\Lambda_f} = 1 \quad , \\ & J_f \in \{|J_1 - J_2|, |J_1 - J_2| + 1 \, , \, \dots \, , \, J_1 + J_2 - 1, J_1 + J_2\} \quad , \\ & N_f = N_1 + N_2 \quad , \\ & Z_f = Z_1 + Z_2 \quad , \\ & P_f = P_1 P_2 \quad , \end{aligned} \tag{3.121}$$

and the Clebsch Gordan coefficients

$$(\Lambda_1 M_1 \Lambda_2 M_2 | \Lambda_f M_f)_G = (J_1 M_1 J_2 M_2 | J_f M_f)_{SU(2)} \, \delta_{N_f, N_1+N_2} \, \delta_{Z_f, Z_1+Z_2} \, \delta_{P_f, P_1 P_2} \, . \tag{3.122}$$

3.5.3 Hill-Wheeler-Griffin Equation

Let us consider a set Ω_I of one-quasiparticle states $|\Phi_i\rangle$ that differ by their deformation and/or by their one-quasiparticle structure. And let us suppose that, for a given set of quantum numbers Λ, we have constructed from each of the $|\Phi_i\rangle$ a set of Ω_i^Λ projected states

$$|\Lambda M \epsilon, i\rangle = \sum_{K=-J}^{J} f_\epsilon^\Lambda(i, K) \, |\Lambda M, iK\rangle \tag{3.123}$$

where $f_\epsilon^\Lambda(i, K)$ is the weight of the state

$$|\Lambda M, iK\rangle \equiv |JMNZP = p_i \, , iK\rangle = \frac{\hat{P}^J_{MK} \hat{P}^N \hat{P}^Z |\Phi_i\rangle}{\sqrt{\langle \Phi_i | \hat{P}^J_{KK} \hat{P}^N \hat{P}^Z | \Phi_i \rangle}} \quad , \tag{3.124}$$

in the superposed state $|\Lambda M \epsilon, i\rangle$, p_i is the parity of the state $|\Phi_i\rangle$, and where $i \in \{1 \, , \, \dots \, , \, \Omega_I\}$ and $\epsilon \in \{1 \, , \, \dots \, , \, \Omega_i^\Lambda\}$. The number of states Ω_i^Λ can be lower than the dimension d_Λ of the irrep D^Λ for several reasons:

- The matrix $\bar{N}^\Lambda(i, i)$ is singular for symmetry reasons. See section 3.4.3 for an example in the case of angular momentum.

- Some of the state $|\Lambda M, iK\rangle$ obtained from the quasiparticle state $|\Phi_i\rangle$ are either null or their norm is too small to be safely handled numerically and thus they are removed.[31] Anyway, the physical relevance of such small components are expected to be low.
- Solving the HWG equation (3.54) in the subspace $S^\Lambda(G|\Phi_i\rangle)$, some of the norm eigenvalues are too small to be safely handled numerically and thus are removed (more explanations will be given in the next section).
- The state $|\Lambda M\epsilon, i\rangle$ obtained after projection is considered of too bad numerical quality and is then also removed from the calculation.

The number of states Ω_i^Λ is even possibly null if it is not possible to obtain, from $|\Phi_i\rangle$, projected states of good enough quality for the quantum numbers Λ. We thus have

$$0 \leq \Omega_i^\Lambda \leq d_\Lambda = 2J + 1 \quad . \tag{3.125}$$

We will give more detail on how are "cut" the "not good enough" states in our calculations in chapter 4.

For a given set of quantum numbers Λ, we have in total $\Omega_I^\Lambda = \sum_{i=1}^{\Omega_I} \Omega_i^\Lambda$ projected states $|\Lambda M\epsilon, i\rangle$ with different values of i and/or ϵ. From them, we want to construct more general superposed states of the form

$$|\Lambda M\xi\rangle = \sum_{i=1}^{\Omega_I} \sum_{\epsilon=1}^{\Omega_i^\Lambda} F_\xi^\Lambda(i,\epsilon)\, |\Lambda M\epsilon, i\rangle \quad , \tag{3.126}$$

where $F_\xi^\Lambda(i,\epsilon)$ is the weight of the projected state $|\Lambda M\epsilon, i\rangle$ in the mixed state $|\Lambda M\xi\rangle$. The ansatz (3.126) is again very similar to what we had in the case of projection, but we now look for an approximation to the eigenstates of $\hat{H}$ in the much bigger subspace $S(\Omega_I) \equiv \sum_{i=1}^{\Omega_I} S(G|\Phi_i\rangle)$. The problem is partially solved as we have already diagonalized $\hat{H}$ in each subspace $S(G|\Phi_i\rangle)$

$$\langle \Lambda' M'\epsilon', i|\Lambda M\epsilon, i\rangle = \delta_{\Lambda',\Lambda}\, \delta_{M',M}\, \delta_{\epsilon',\epsilon} \quad , \tag{3.127}$$

$$\langle \Lambda' M'\epsilon', i|\hat{H}|\Lambda M\epsilon, i\rangle = \delta_{\Lambda',\Lambda}\, \delta_{M',M}\, \delta_{\epsilon',\epsilon}\, E_\epsilon^\Lambda(i) \quad , \tag{3.128}$$

where

$$\delta_{\Lambda',\Lambda} \equiv \delta_{J',J}\, \delta_{N',N}\, \delta_{Z',Z}\, \delta_{P',P} \quad . \tag{3.129}$$

But as the subspaces $S(G|\Phi_i\rangle)$ are not orthogonal complements in $S(\Omega_I)$, nor invariant subspaces for $\hat{H}$, we have only for the overlap and energy kernel of the mixed states the relations

$$\langle \Lambda' M'\xi'|\Lambda M\xi\rangle = \delta_{\Lambda',\Lambda}\, \delta_{M',M}\, \mathcal{N}_{\xi'\xi}^\Lambda \quad , \tag{3.130}$$

$$\langle \Lambda' M'\xi'|\hat{H}|\Lambda M\xi\rangle = \delta_{\Lambda',\Lambda}\, \delta_{M',M}\, \mathcal{H}_{\xi'\xi}^\Lambda \quad , \tag{3.131}$$

where

$$\mathcal{N}_{\xi'\xi}^\Lambda = \sum_{i'=1}^{\Omega_I} \sum_{i=1}^{\Omega_I} \sum_{\epsilon'=1}^{\Omega_{i'}^\Lambda} \sum_{\epsilon=1}^{\Omega_i^\Lambda} F_{\xi'}^{\Lambda *}(i',\epsilon') F_\xi^\Lambda(i,\epsilon) \langle \Lambda M\epsilon', i'|\Lambda M\epsilon, i\rangle \quad , \tag{3.132}$$

$$\mathcal{H}_{\xi'\xi}^\Lambda = \sum_{i'=1}^{\Omega_I} \sum_{i=1}^{\Omega_I} \sum_{\epsilon'=1}^{\Omega_{i'}^\Lambda} \sum_{\epsilon=1}^{\Omega_i^\Lambda} F_{\xi'}^{\Lambda *}(i',\epsilon') F_\xi^\Lambda(i,\epsilon) \langle \Lambda M\epsilon', i'|\hat{H}|\Lambda M\epsilon, i\rangle \quad . \tag{3.133}$$

[31] In that case we consider that the weight $f_\epsilon^\Lambda(i,K)$ in equation (3.123) is equal to zero.

From (3.130) and (3.131), we see that the problem is reduced to the separate diagonalization of $\hat{H}$ in each subspace $S^\Lambda(\Omega_I) \subset S(\Omega_I)$ associated with all irreps Λ of the full symmetry group G. We thus consider the energy

$$E^\Lambda_\xi(\Omega_I) = \frac{\mathcal{H}^\Lambda_{\xi\xi}}{\mathcal{N}^\Lambda_{\xi\xi}} \quad , \tag{3.134}$$

and vary it with respect to the parameter $F^{\Lambda *}_\xi(i', \epsilon')$

$$\frac{\delta E^\Lambda_\xi(\Omega_I)}{\delta F^{\Lambda *}_\xi(i', \epsilon')} = 0 \quad . \tag{3.135}$$

After a short and straightforward derivation we obtain the HWG equation

$$\begin{aligned}
\frac{\delta E^\Lambda_\xi(\Omega_I)}{\delta F^{\Lambda *}_\xi(i', \epsilon')} &= \frac{\left(\frac{\delta \mathcal{H}^\Lambda_{\xi\xi}}{\delta F^{\Lambda *}_\xi(i', \epsilon')}\right)\mathcal{N}^\Lambda_{\xi\xi} - \mathcal{H}^\Lambda_{\xi\xi}\left(\frac{\delta \mathcal{N}^\Lambda_{\xi\xi}}{\delta F^{\Lambda *}_\xi(i', \epsilon')}\right)}{\left(\mathcal{N}^\Lambda_{\xi\xi}\right)^2} && = 0 \\
&= \frac{\left(\frac{\delta \mathcal{H}^\Lambda_{\xi\xi}}{\delta F^{\Lambda *}_\xi(i', \epsilon')}\right) - E^\Lambda_\xi(\Omega_I)\left(\frac{\delta \mathcal{N}^\Lambda_{\xi\xi}}{\delta F^{\Lambda *}_\xi(i', \epsilon')}\right)}{\mathcal{N}^\Lambda_{\xi\xi}} && = 0 \\
&= \left(\frac{\delta \mathcal{H}^\Lambda_{\xi\xi}}{\delta F^{\Lambda *}_\xi(i', \epsilon')}\right) - E^\Lambda_\xi(\Omega_I)\left(\frac{\delta \mathcal{N}^\Lambda_{\xi\xi}}{\delta F^{\Lambda *}_\xi(i', \epsilon')}\right) && = 0 \\
&= \sum_{i=1}^{\Omega_I}\sum_{\epsilon=1}^{\Omega^\Lambda_i} \left\{\langle \Lambda M \epsilon', i'|\hat{H}|\Lambda M \epsilon, i\rangle - E^\Lambda_\xi(\Omega_I)\langle \Lambda M \epsilon', i'|\Lambda M \epsilon, i\rangle\right\} F^\Lambda_\xi(i, \epsilon) = 0 \,. && (3.136)
\end{aligned}$$

Similarly to what has been discussed in section 3.2.4, the energies $E^\Lambda_\xi(\Omega_I)$ are the solutions of the generalized eigenvalue problem whose characteristic equation is

$$\det\left\{\langle \Lambda M \epsilon', i'|\hat{H}|\Lambda M \epsilon, i\rangle - E^\Lambda_\xi(\Omega_I)\langle \Lambda M \epsilon', i'|\Lambda M \epsilon, i\rangle\right\} = 0 \quad . \tag{3.137}$$

The energies $E^\Lambda_\xi(\Omega_I)$ are all real as the matrix of energy kernels between projected states, whose elements are $\langle \Lambda M \epsilon', i'|\hat{H}|\Lambda M \epsilon, i\rangle$, is Hermitean and the matrix of overlap kernels between projected states, whose elements are $\langle \Lambda M \epsilon', i'|\Lambda M \epsilon, i\rangle$, is Hermitean and positive-semidefinite. Finally, if the matrix of overlap kernels between projected states is invertible, there exist Ω^Λ_I solutions, but less if it is singular. Assuming there are in total c^Λ_I solutions, we use the index $\xi \in \{1\,, \ldots\,, c^\Lambda_I\}$ to label the order of appearance of the energies $E^\Lambda_\xi(\Omega_I)$ in the energy spectrum composed of all the $E^\Lambda_\xi(\Omega_I)$.

In the next section we will explain how to solve equation (3.136) in order to obtain the weights $F^\Lambda_\xi(i, \epsilon)$ and the energies E^Λ_ξ such that

$$\mathcal{N}^\Lambda_{\xi'\xi} = \delta_{\xi',\xi} \quad , \tag{3.138}$$

$$\mathcal{H}^\Lambda_{\xi'\xi} = \delta_{\xi',\xi}\, E^\Lambda_\xi(\Omega_I) \quad . \tag{3.139}$$

The states $|\Lambda M \xi\rangle$ thus obtained are the final states, and the best approximations to the eigenstates of the Hamiltonian we will construct in this work. They are much more general than all the simple one-quasiparticle states $|\Phi_i\rangle$ they have been constructed from, have good symmetry properties, and diagonalize the Hamiltonian in each subspace $S^\Lambda(\Omega_I)$. Finally, we can calculate the expectation value of any desired observable $\hat{O}$ as

$$\langle \Lambda' M' \xi'|\hat{O}|\Lambda M \xi\rangle = \sum_{i'=1}^{\Omega_I}\sum_{i=1}^{\Omega_I}\sum_{\epsilon'=1}^{\Omega^{\Lambda'}_{i'}}\sum_{\epsilon=1}^{\Omega^\Lambda_i} F^{\Lambda' *}_{\xi'}(i', \epsilon') F^\Lambda_\xi(i, \epsilon)\langle \Lambda' M' \epsilon', i'|\hat{O}|\Lambda M \epsilon, i\rangle \,. \tag{3.140}$$

It is surely possible to express the energies E^Λ_ξ in terms of the energy density kernels between the different states $|\Phi_i\rangle$ but the expression is clearly too cumbersome to be given here, so we let to the reader the task of doing it (if he/she wants to).

3.5.4 Resolution of the Hill-Wheeler-Griffin Equation

In this last technical section, we show how to solve the HWG equation (3.136), noting that similar derivations can also be found in [107, 24].
First, to simplify matrix notations, we combine the two indices i and ϵ that label the states $|\Lambda M\epsilon, i\rangle$:

$$\begin{aligned} |\Lambda M\epsilon, i\rangle &\to |\Lambda M\alpha\rangle \quad , \\ F^\Lambda_\xi(\epsilon, i) &\to F^\Lambda_\xi(\alpha) \quad , \end{aligned} \tag{3.141}$$

into the new index α running from 1 to Ω^Λ_I. Obviously we have to define an order that relates each α to a given couple i and ϵ. It could be for example

$$\begin{aligned} \alpha = 1 \quad &\to \; i = 1 \;\; \epsilon = 1 \\ \alpha = 2 \quad &\to \; i = 1 \;\; \epsilon = 2 \\ &\vdots \\ \alpha = \Omega^\Lambda_1 \quad &\to \; i = 1 \;\; \epsilon = \Omega^\Lambda_1 \\ \alpha = \Omega^\Lambda_1 + 1 \quad &\to \; i = 2 \;\; \epsilon = 1 \\ &\vdots \\ \alpha = \Omega^\Lambda_I \quad &\to \; i = \Omega_I \;\; \epsilon = \Omega^\Lambda_{\Omega_I} \quad . \end{aligned}$$

As the projected states $|\Lambda M\alpha\rangle$ are not all orthogonal to each other, the matrix N^Λ of their overlap, whose matrix elements are $N^\Lambda(\alpha, \alpha') = \langle \Lambda M\alpha | \Lambda M\alpha'\rangle$, is not the unit matrix of degree Ω^Λ_I, as we would have in an orthonormal basis. Our first task it thus to find the basis where it is the case. We thus diagonalize the matrix N^Λ

$$D^{-1} N^\Lambda D = \begin{pmatrix} \lambda_1 & & 0 \\ & \ddots & \\ 0 & & \lambda_{\Omega^\Lambda_I} \end{pmatrix} \tag{3.142}$$

with the columns of D being the eigenvectors of N^Λ. As N^Λ is in our case real symmetric and positive-semidefinite, the eigenvalues are all real, and more specifically are positive or null

$$\forall\, i\,,\; \lambda_i \in \mathbb{R}^+_0 \quad ,$$

and consequently the matrix D is orthogonal

$$D^t = D^{-1} \quad .$$

We thus have obtained a basis in which the overlap matrix is diagonal. But we do not have yet a unit matrix. In order to obtain such a unit matrix, we perform the change of basis associated with D (as we would do in a regular eigenvalue problem) but dividing by the square root of the eigenvalues

$$|\Lambda M n\rangle = \frac{1}{\sqrt{\lambda_n}} \sum_{\alpha=1}^{\Omega^\Lambda_N} D(\alpha, n) |\Lambda M\alpha\rangle \quad . \tag{3.143}$$

But to perform such transformation, we have to remove all the eigenvalues which are exactly equal to zero for which we cannot write (3.143). And solving the problem numerically, it is also necessary to remove the eigenvalues that are too small to be safely handled. This is why in (3.143) the sum runs from 1 to $\Omega_N^\Lambda \leq \Omega_I^\Lambda$. But note that as soon as we remove some non-zero eigenvalues, the orthogonality relations between D and D^t become only approximate

$$\sum_{n=1}^{\Omega_N^\Lambda} D(\alpha,n)D(\alpha',n) \approx \delta_{\alpha,\alpha'} \quad . \tag{3.144}$$

We will nonetheless assume the equality as being exact in what follows. It is then easy to show that the states $|\Lambda M n\rangle$ are orthonormal to each other

$$\begin{aligned} \langle \Lambda M n | \Lambda M n' \rangle &= \frac{1}{\sqrt{\lambda_n \lambda_{n'}}} \sum_{\alpha,\alpha'=1}^{\Omega_N^\Lambda} D(\alpha,n) N^\Lambda(\alpha,\alpha') D(\alpha',n') \\ &= \delta_{n,n'} \quad , \end{aligned} \tag{3.145}$$

where we have used (3.142) and $D^t = D^{-1}$. We have thus found a basis in which the norm matrix is equal to the identity matrix. We want now to express HWG equation (3.136) in this basis. Using (3.144), we first invert equation (3.143)

$$|\Lambda M \alpha\rangle = \sum_{n=1}^{\Omega_N^\Lambda} \sqrt{\lambda_n}\, D(\alpha,n) |\Lambda M n\rangle \quad . \tag{3.146}$$

Then, we use this relation to expand the overlap and the Hamiltonian kernel as

$$\langle \Lambda M \alpha | \Lambda M \alpha' \rangle = \sum_{n'=1}^{\Omega_N^\Lambda} \sqrt{\lambda_{n'}} D(\alpha,n') \sqrt{\lambda_{n'}} D(\alpha',n') \quad , \tag{3.147}$$

$$\langle \Lambda M \alpha | \hat{H} | \Lambda M \alpha' \rangle = \sum_{n,n'=1}^{\Omega_N^\Lambda} \sqrt{\lambda_n} D(\alpha,n) \sqrt{\lambda_{n'}} D(\alpha',n') \langle \Lambda M n | \hat{H} | \Lambda M n' \rangle \quad , \tag{3.148}$$

and we note the matrix elements of $\hat{H}$ in the basis of the $|\Lambda M n\rangle$

$$\tilde{H}^\Lambda(n,n') = \langle \Lambda M n | \hat{H} | \Lambda M n' \rangle \quad . \tag{3.149}$$

Now, reexpressing the HWG equation (3.136) as

$$\sum_{\alpha'=1}^{\Omega_I^\Lambda} \langle \Lambda M \alpha | \hat{H} | \Lambda M \alpha' \rangle F_\xi^\Lambda(\alpha') = E_\xi^\Lambda(\Omega_I^\Lambda) \sum_{\alpha'=1}^{\Omega_I^\Lambda} \langle \Lambda M \alpha | \Lambda M \alpha' \rangle F_\xi^\Lambda(\alpha') \quad , \tag{3.150}$$

and immediatly inserting (3.147) and (3.148) into it, we obtain

$$\begin{aligned} &\sum_{n,n'=1}^{\Omega_N^\Lambda} \sqrt{\lambda_n} D(\alpha,n) \tilde{H}^\Lambda(n,n') \sum_{\alpha'=1}^{\Omega_I^\Lambda} \sqrt{\lambda_{n'}} D(\alpha',n') F_\xi^\Lambda(\alpha') = \\ &\qquad E_\xi^\Lambda(\Omega_I^\Lambda) \sum_{n'=1}^{\Omega_N^\Lambda} \sqrt{\lambda_{n'}} D(\alpha,n') \sum_{\alpha'=1}^{\Omega_I^\Lambda} \sqrt{\lambda_{n'}} D(\alpha',n') F_\xi^\Lambda(\alpha') \,. \end{aligned} \tag{3.151}$$

Defining

$$G_\xi^\Lambda(n) = \sum_{\alpha'=1}^{\Omega_I^\Lambda} \sqrt{\lambda_n} D(\alpha', n) F_\xi^\Lambda(\alpha') \quad , \tag{3.152}$$

we obtain

$$\sum_{n,n'=1}^{\Omega_N^\Lambda} \sqrt{\lambda_n} D(\alpha, n) \tilde{H}^\Lambda(n, n') G_\xi^\Lambda(n') = E_\xi^\Lambda(\Omega_I^\Lambda) \sum_{n'=1}^{\Omega_N^\Lambda} \sqrt{\lambda_{n'}} D(\alpha, n') G_\xi^\Lambda(n') \quad . \tag{3.153}$$

Finally, multiplying both sides of the equation by $\frac{1}{\sqrt{\lambda_{n''}}} D(\alpha, n'')$, summing over $\sum_{\alpha=1}^{\Omega_I^\Lambda}$ (to use $D^t D = D D^t = \mathbb{1}$), and renaming n'' as n afterwards, we obtain

$$\sum_{n'=1}^{\Omega_N^\Lambda} \tilde{H}^\Lambda(n, n') G_\xi^\Lambda(n') = E_\xi^\Lambda(\Omega_I^\Lambda) G_\xi^\Lambda(n) \quad . \tag{3.154}$$

We have thus reduced the problem to an ordinary eigenvalue problem. It remains only to diagonalize $\tilde{H}^\Lambda(n, n')$

$$C^{-1} \tilde{H}^\Lambda C = \begin{pmatrix} E_1^\Lambda & & 0 \\ & \ddots & \\ 0 & & E_{\Omega_N^\Lambda}^\Lambda \end{pmatrix} \quad , \tag{3.155}$$

but note that we have only $\Omega_N^\Lambda \leq \Omega_I^\Lambda$ eigenvalues. The eigenvectors G_ξ^Λ of $\tilde{H}^\Lambda$ are the columns of the matrix C. Renaming them $|\Lambda M \xi\rangle$, they are obtained from the $|\Lambda M n\rangle$ by the basis transformation

$$|\Lambda M \xi\rangle = \sum_{n=1}^{\Omega_N^\Lambda} C(n, \xi) |\Lambda M n\rangle \quad , \tag{3.156}$$

or expanding the $|\Lambda M n\rangle$ in terms of the $|\Lambda M \alpha\rangle$

$$|\Lambda M \xi\rangle = \sum_{\alpha=1}^{\Omega_I^\Lambda} \left(\sum_{n=1}^{\Omega_N^\Lambda} \frac{1}{\sqrt{\lambda_n}} C(n, \xi) D(\alpha, n) \right) |\Lambda M \alpha\rangle \quad . \tag{3.157}$$

Finally, we identify the weights $F_\xi^\Lambda(\alpha)$

$$F_\xi^\Lambda(\alpha) = \sum_{n=1}^{\Omega_N^\Lambda} \frac{1}{\sqrt{\lambda_n}} C(n, \xi) D(\alpha, n) \quad , \tag{3.158}$$

and the problem is solved!

Part II

Application To Odd-A Nuclei

Chapter 4

The Proof of Principle: ^{25}Mg

It has often and confidently been asserted, that man's origin can never be known: but ignorance more frequently begets confidence than does knowledge: it is those who know little, and not those who know much, who so positevely assert that this or that problem will never be solved by science.

Charles Darwin, The Descent of Man (1871).

For the first application of our model, we have chosen the nucleus ^{25}Mg. There are several reasons behind this particular choice. Firstly, it is a rather light nucleus, which is of great advantage from a computational time point of view. It is indeed especially important when, as we will see, its calculation still represents hundreds of thousands of CPU hours on a supercomputer. Secondly, there is a large amount of experimental data [65, 161, 69, 80, 78], as well as previous theoretical calculations [46, 86, 117], available in the literature. In our opinion, both are crucial if we want to compare and validate our model. By using experimental results and prior theoretical works, we will be able to benchmark our model; we will see what is working and what is not. Surely, we will not discover nor explain any new hyped phenomenon as this nucleus has been extensively studied in the past, but just as surely, this is the safest way to proceed. When conceiving a new detector, experimentalists just do not focus all their most powerful beams on it hoping for the best, they test and calibrate it first, and we want to follow this time-tested approach. Furthermore, ^{25}Mg is particularly well suited for this benchmarking exercise as it exhibits a relatively simple structure with clear rotational bands, which constitute a good testing ground for our model. Last but not least, for even-even nuclei there seems to be an informal tradition of investigating ^{24}Mg as a first beyond mean-field calculation [11, 154, 98, 22, 159, 112]. It thus appeared natural to us, when addressing the odd-even case, to go for ^{25}Mg.

The first section of this chapter will be devoted to the description of SR-EDF calculations of ^{25}Mg. In the second and third sections, we will study the effects of symmetry restoration, first for particle-number and then for angular-momentum. The fourth section will cover in great detail the configuration mixing of symmetry restored one-quasiparticle states. Finally, we will summarize and conclude on the global results of this first MR-EDF calculation of ^{25}Mg.

4.1 Single-Reference Study

As an introduction to the study of ^{25}Mg, it is informative to look first at SR-EDF results for this nucleus. We will not go into deep analyses of these results as they are not the fundamental goal of this thesis, but as MR states are built from a basis of one-quasiparticle states, it is interesting,

and even necessary, to look at what are the characteristics of the one-quasiparticle states and how they are built.

4.1.1 False Vacuum

The first step of our SR-EDF approach is the (self-consistent) computation, for every deformation in our discretization of the (β, γ) plane, of an even HFB vacuum with an average odd number of particles, more precisely $\langle\tilde{0}_z|\hat{Z}|\tilde{0}_z\rangle = 12$ for protons and $\langle\tilde{0}_n|\hat{N}|\tilde{0}_n\rangle = 13$ for neutrons. A such even HFB vacuum, called "false vacuum", allows for integrating the essential of the polarization due to the addition of a nucleon to the mean-field [56, 57] and thus, delivers a good overview of the odd-A system while keeping the simplicity of the computation of an even quasiparticle vacuum. Of course the false vacuum does not take into account for the blocking effects [56, 57, 129], and it also does not have the wave function structure needed to represent a fermionic system with an odd number of particles, so it should not be taken as a final calculation. First and foremost, it provides for a good even HFB vacuum from which we can select the quasiparticles to be self-consistently blocked in a second step. The convergence of blocked quasiparticle states always being a delicate procedure, we also hope that starting from the false vacuum we can achieve a safer and faster convergence of one-quasiparticle states.
The complete energy surface up to 12 MeV (relative to the minimum) of the false vacuum in the first sextant of the beta-gamma plane is plotted in the top panel of Fig. 4.1. In our case, the first sextant corresponds to deformations with a γ situated between 0° (prolate along the x-axis) and 60° (oblate along the y-axis). We will come later to the reasons behind this choice (see section 4.3.5). The calculated point with lowest energy $E_{min} = -214.647$ MeV, represented by a black dot, is located at triaxial deformation ($\beta = 0.563\,, \gamma = 7.59°$) but we can see that the minimum is relatively soft against a change in γ. However, the energy surface is not symmetric under a "rotation" in γ and the false vacuum clearly favours deformations with $\gamma \leq 30°$.

In the bottom left panel of Fig. 4.1 we display the discretization in deformation used to calculate the energy surface. We use here a rectangular discretization in q_1 and q_2 parameters (see section 2.4.2), with a fixed step of 20 fm^2 starting from $q_1 = 0\,\text{fm}^2$ and $q_2 = 0\,\text{fm}^2$, that gives a "rhomboidal" discretization in (β,γ). This type of discretization is more efficient than a discretization with a fixed step in β and in γ, because for the same number of points it explores more equitably the (β,γ) plane, whereas a discretization with a fixed step in (β,γ) could give a very tight mesh close to the origin (0,0) and a coarse and imprecise mesh away from it [112]. The discretization includes in total 228 different deformations for the false vacuum, ranging from $q_1 = 0$ to 400 fm^2 and $q_2 = 0$ to 200 fm^2.

Nilsson Diagrams of Single-Particle Energies

We now look at the evolution of neutron and proton single-particle energies along the path in deformation represented in the bottom right panel of Fig. 4.1. The neutron (resp. proton) single-particle energies between 0 and -15 MeV are plotted in the top (resp. bottom) Nilsson diagram of Fig. 4.2. The points on the abscissa are represented by blue dots and blue squares in Fig. 4.1. For neutrons, we also plot for those points the values of the x-component of single-particle angular momentum between the single-particle state and its time-reversed $\langle\psi_i|\hat{J}_x\hat{T}|\psi_i\rangle = k$, and the mean-value of the total single-particle angular momentum j, which is the solution of $\langle\psi_i|\hat{J}^2|\psi_i\rangle = j(j+1)$. When, as we do, we have a z-signature intrinsic symmetry for single-particle states, it is easy to show that because of anticommutation of $\hat{R}_z$ with $\hat{J}_x$ and $\hat{J}_y$, we have $\langle\psi_i|\hat{J}_x|\psi_i\rangle = \langle\psi_i|\hat{J}_y|\psi_i\rangle = 0$ and this is why we have to calculate $k = \langle\psi_i|\hat{J}_x\hat{T}|\psi_i\rangle$, or $k = \langle\psi_i|\hat{J}_y\hat{T}|\psi_i\rangle$ if we were interested in states close to the oblate axis. Also we recall these are

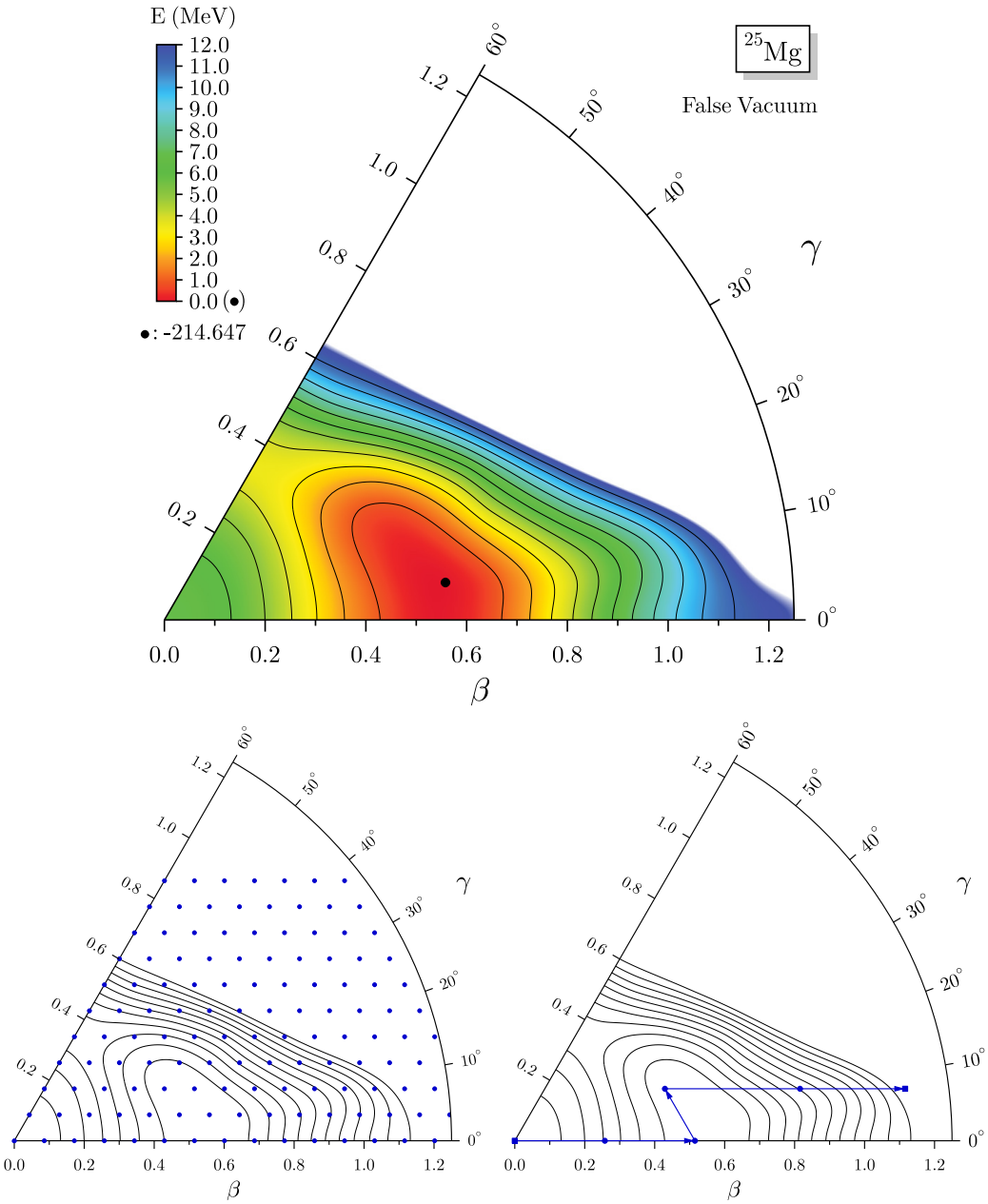

Figure 4.1: Top: Energy surface of the false vacuum with $\langle N \rangle = 13$ and $\langle N \rangle = 12$. The black contour lines are plotted every 1 MeV from the minimum indicated by the black dot. Bottom left: Discretization (blue dots) used for the energy surfaces in this work. Bottom right: Path in deformation (blue line) for Nilsson diagrams of Fig. 4.2.

the single-particle energies of an even-even vacuum that is time-reversal invariant, thus they are doubly degenerate (Kramers degeneracy [95]).

First looking at neutrons, we can see that starting from the spherical point (0,0) and going into prolate axial deformation, two levels with positive parity (full black lines) are getting closer to the Fermi energy (dashed red line), one with a $k = 2.50$ which actually crosses the Fermi energy from below, and the other with a k close to 0.50 which is getting closer to the Fermi energy from above. The k values are very close to the x-component of the angular-momentum one would expect for a state axially symmetric about the x-axis, because we still have here states with an average deformation constraint to be axial. This is also why going to larger axial deformation we see that the two levels come very close and completely exchange their characteristics. The non-crossing rule prevents two states with same symmetry quantum numbers (here the parity and the signature) to cross, but for axially constrained deformations, the k value almost plays the role of a quantum number, which explains why the two levels that have different values of k are coming so close to each other in spite of having same parity and signature. When going into triaxial deformation, we see that they anti-cross again, but this time their k and j values become more mixed. At higher β deformation we observe that the two levels still remain close to the Fermi energy, but foremost that a negative parity state (dashed black line) from very high in energy, and with $k = 0.48$, is downsloping and even crosses the Fermi energy. Taking the expression for the energy of a quasiparticle in its BCS approximation: $E_{t,i} = \sqrt{(\epsilon_{t,i} - \lambda_t)^2 + \Delta_{t,i}^2}$, we can estimate that these states which have single-particle energies $\epsilon_{t,i}$ close to the Fermi energy λ_t will have the tendancy to have low quasiparticle energies and thus, will likely to be important for the description of the low-lying excitation spectum of ^{25}Mg. Of course, as we work here in the more general HFB formalism and as we realize self-consistent calculations, this cannot be concluded only from such simple considerations.

The Nilsson diagram for protons presents a very similar trend for the evolution of proton single-particle energies. This is expected because the proton number is only one unit different from the neutron number: $N = Z + 1$. But for protons, all the single-particle energies are shifted by approximately 4 or 5 MeV up, whereas the Fermi energy is shifted up by only 3.5 MeV at the spherical point and then decreases as the nucleus is deforming. The net result is that except near the spherical point the single-particle states are much farther away from the Fermi energy than for neutrons. This provides a basic justification for why we neglect here two-, and higher, quasiparticle excitations for protons, as such excitations are expected to happen at high energy compared to one-quasiparticle excitations (for neutrons).

Finally, let us just mention that nothing really interesting happens close to the oblate y-axis, which is why this part of the sextant was not explored in the path of deformation.

4.1.2 Blocking of One-Quasiparticle States

We now jump to the case of interest here, the study of neutron (self-consistent) one-quasiparticle states for the description of ^{25}Mg. The energy surface of the lowest one-quasiparticle states of positive (resp. negative) parity at each deformation can be found in the left (resp. right) panel of Fig. 4.3. We can see that these surfaces present some differences when compared with the surface of the false vacuum. The surface for positive parity states has an axial minimum $E^+_{min} = -213.248$ MeV at the deformation $(0.601, 0)$, and is more rigid against β deformation, but apart from that it has a similar global topography as the surface of the false vacuum. By contrast, the surface of negative parity states is very different, it presents a triaxial minimum $(0.703, 12.22)$ with an energy $E^-_{min} = -208.035$ MeV more than 5 MeV higher than the positive parity minimum, and the surface is more centered around this minimum while staying relatively

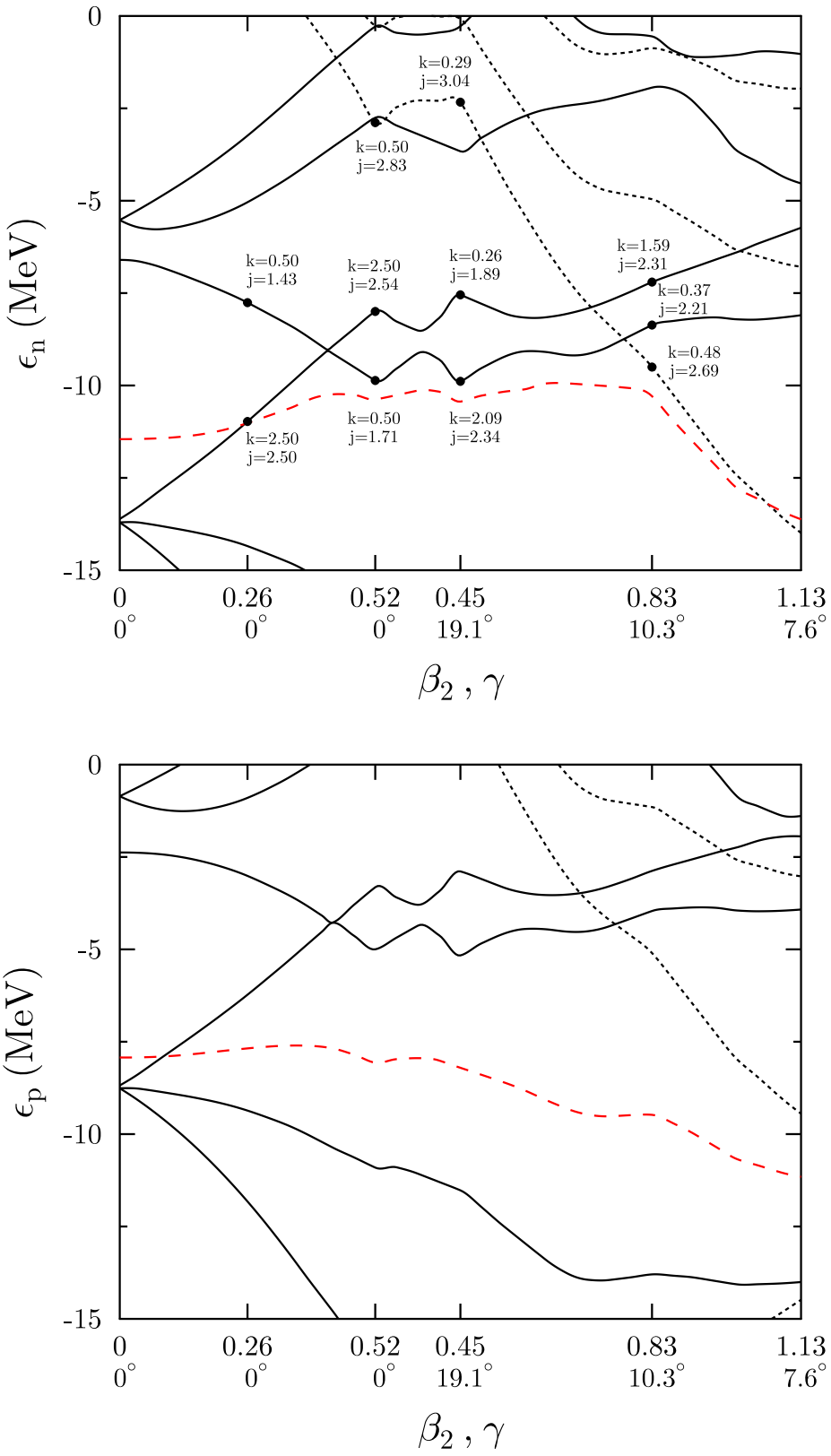

Figure 4.2: Top: Nilsson diagram of neutron single-particle energies along the path of Fig. 4.1. Full and dashed black lines represent positive parity and negative parity states, respectively. The red dashed line is the Fermi energy. Bottom: Same for protons.

soft towards prolate deformations. The scale in energy goes only up to 8 MeV for negative parity because the interpolation of the surface at $E^-_{min} + 12$ MeV is not particularly good, as it corresponds to region of the surface where not enough states were actually converged (see below). Besides, the minimum being already 5 MeV higher than for positive parity quasiparticle states, it did not seem relevant to go higher in energy.

Finally, we compare the self-consistent blocking results of Fig. 4.3 with a perturbative blocking presented in Fig. 4.4, where we plot the energy surface of the false vacuum plus the lowest one-quasiparticle energy of positive parity evaluated from the false vacuum. We can see that there are some big differences, whether for the position of the minimum, axial for self-consistent calculations and triaxial for the perturbative evaluation, or for the energy of the minimum, which takes a value that is 1 MeV higher in the perturbative case. These differences recall, if necessary, the importance of self-consistent calculations.

Convergence Procedure for Blocked States

A discretization in deformation similar to the one of false vacuum has been used, the step in q_1 and q_2 is still 20 fm^2, but we went only up to $q_1 = 320$ fm^2 and $q_2 = 160$ fm^2 (starting from 0). However, because of the numerical difficulties of converging one-quasiparticle states, it was not possible to obtain converged calculations for every quasiparticle at every deformation. Nevertheless, we still achieved the reasonable numbers of 604 converged one-quasiparticle states of positive parity and 222 of negative parity, in total. To converge those one-quasiparticle states, we used the following procedure. First, for any given deformation in our discretization of the (β, γ) plane, we use the corresponding false vacuum ($\equiv$ with same deformation) as a starting point for the blocking and convergence of several different quasiparticles, trying in parallel for each quasiparticle different sets of numerical convergence parameters. Such parameters can for example be the damping factor of the mean-field at each iteration, or the way we identify the quasiparticle to be blocked. Playing with those numerical parameters is a somewhat risky game, because for the same deformation and blocking the same quasiparticle at the beginning, using different numerical parameters for the convergence can result in slightly different blocked one-quasiparticle states at the end of the minimization procedure. In those cases we selected the final state with the lowest total energy, but fortunately the energies of these states are usually not very different. Besides, we consider here quasiparticle states as a simple set of generating states for the MR-EDF calculations, so we hope that those small numerical differences are smoothed out by the variational procedure in the configuration mixing. When convergence of one-quasiparticle states could not be achieved directly by starting from the false vacuum with same deformation, a false vacuum with an adjacent deformation was used as a starting point. The idea being that starting from points with rather different structure, the minimization procedure may follow different pathways and one of them will lead to convergence. If convergence still could not be achieved this way, a one-quasiparticle state with different deformation but "same" blocked state, or with same deformation but different blocked state, was used as a starting point. And ultimately, if the convergence proved to be impossible at a given deformation, the same procedure was repeated at a very near deformation (e.g. $q_1 = 95$ fm^2 instead of $q_1 = 100$ fm^2). Such blocking procedure is very (human) time-consuming and can at times be very frustrating, it is thus recommanded only to people with a stubborn character, which is indeed the case for yours truly. Fortunately, the SR-EDF code CR8 [36] proved to be very performant and most of the one-quasiparticle states already converged starting from the false vacuum with same deformation, this task being for the most of it automated. But even with many tries, involving different numerical parameters or different starting points, some quasiparticle states could not be converged. This is the case in particular for negative parity states close to sphericity, but as we saw in the neutron Nilsson

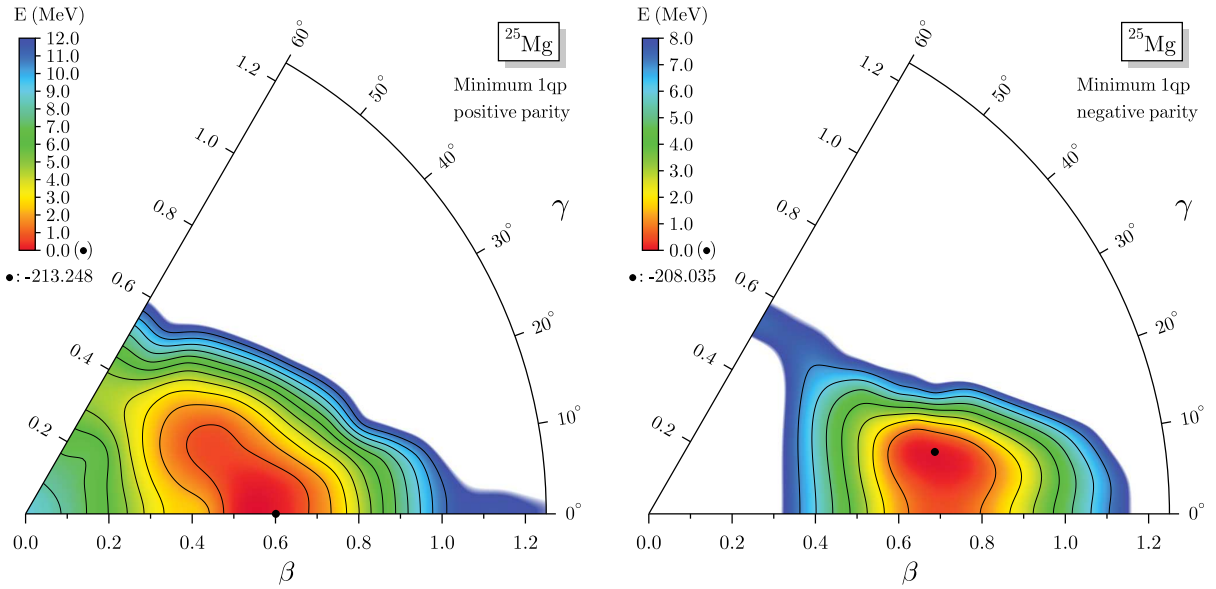

Figure 4.3: Left: Energy surface of lowest positive parity one-quasiparticle states at each deformation. The black contour lines are plotted every 1 MeV from the minimum indicated by the black dot. Right: Same for negative parity.

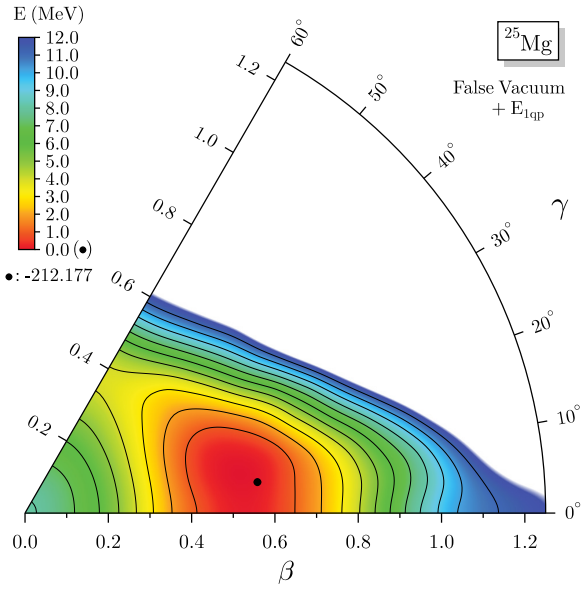

Figure 4.4: Energy surface of false vacuum total energy plus its lowest quasiparticle energy at each deformation. The black contour lines are plotted every 1 MeV from the minimum indicated by the black dot.

diagram and in the energy surface of Fig. 4.3, these states should have a very high energy at low deformation and thus the resulting one-quasiparticle state should not play any important role in the low-lying spectrum of ^{25}Mg.

Finally, we signal that only one-quasiparticle states with signature $-i$ have been considered (for energy surfaces and the GCM) because, as long as we do not crank the one-quasiparticle states, states with signature $+i$ and $-i$ give exactly same results for all observables up to numerical uncertainty (see section 4.3.6 for an example).

4.1.3 Overlap Between One-Quasiparticle States

In Fig. 4.5, we display for four different one-quasiparticle states $|\Phi_{b_i}\rangle$ $(i = 1, 2, 3, 4)$ of positive parity, the (discretized) surface of largest overlaps $\langle\Phi_{a(qb_i)}|\Phi_{b_i}\rangle$, where the states $|\Phi_{a(qb_i)}\rangle$ have been searched, at each deformation q and for each $|\Phi_{b_i}\rangle$, within the set of one-quasiparticle states of positive parity that had been converged for deformation q. Each parallelogram corresponds to one one-quasiparticle state $|\Phi_{a(qb_i)}\rangle$ with its location on the discretized deformation mesh being given by the center of the parallelogram (or on the axes for axial deformations). As we can see, and as we could have expected, for all 4 different one-quasiparticle states $|\Phi_{b_i}\rangle$, the values of the largest overlaps $\langle\Phi_{a(qb_i)}|\Phi_{b_i}\rangle$ decrease as we move away in deformation from the one of the original state $|\Phi_{b_i}\rangle$. But the surfaces are different in each case. In particular, if we look at the bottom left and bottom right panels of Fig. 4.5, which display the surfaces for two different states $|\Phi_{b_3}\rangle$ and $|\Phi_{b_4}\rangle$ of same deformation, we see that the magnitudes of the overlaps are very different in each case. The state $|\Phi_{b_4}\rangle$ has larger overlap with its neighboring states in deformation than has the state $|\Phi_{b_3}\rangle$. On the other hand, the state $|\Phi_{b_3}\rangle$ has larger overlap with states that have small β values than has the state $|\Phi_{b_4}\rangle$.

We will now study in more detail the overlap of the state $|\Phi_{b_2}\rangle$ with other one-quasiparticle states. In that order, let us define q_1 as the deformation corresponding to the parallelogram where is $|\Phi_{b_2}\rangle$, q_2 as the deformation corresponding to the parallelogram at right of q_1, q_3 as the deformation corresponding to the parallelogram just below the one of q_2, and finally, q_4 as the deformation corresponding to the parallelogram just below the one of q_3. For each of these 4 deformations, we have converged four one-quasiparticle states that we will label by $|\Phi_{j(q_ib_2)}\rangle$, where $j = 1, 2, 3, 4$ and $q_i = q_1, q_2, q_3, q_4$. The index j will be used to label, for each q_i, the states $|\Phi_{j(q_ib_2)}\rangle$ in function of the size of their overlap with $|\Phi_{b_2}\rangle$, from the largest to the smallest. Obviously we have $|\Phi_{1(q_1b_2)}\rangle = |\Phi_{b_2}\rangle$. Figure 4.6 displays all the overlaps $\langle\Phi_{j(q_ib_2)}|\Phi_{b_2}\rangle$ (1 panel by deformation q_i). If we see that for q_1, q_2, the overlap is large only with one one-quasiparticle state, it is not the case for q_3 and q_4 where three or four of the differents states $|\Phi_{j(q_ib_2)}\rangle$ have a sizable overlap with $|\Phi_{b_2}\rangle$. In particular, for q_4 we have two one-quasiparticle states that have comparable size of their overlap: $\langle\Phi_{1(q_4b_2)}|\Phi_{b_2}\rangle = 0.55$ and $\langle\Phi_{2(q_4b_2)}|\Phi_{b_2}\rangle = 0.47$. This shows that one-quasiparticle states are not continuous functions of the deformation. It gets even more twisted than that because even if one obtains similar values for the overlap of $|\Phi_{1(q_4b_2)}\rangle$ and $|\Phi_{2(q_4b_2)}\rangle$ with $|\Phi_{b_2}\rangle$, they have between each other a very small overlap: $\langle\Phi_{2(q_4b_2)}|\Phi_{1(q_4b_2)}\rangle = 0.07$. And to see that its get even more twisted than twisted, we display in Fig. 4.7 the overlap $\langle\Phi_{j(q_ib_2)}|\Phi_{1(q_4b_2)}\rangle$ with state $|\Phi_{1(q_4b_2)}\rangle$ as reference (but not redefining the q_i and the labels of states $|\Phi_{j(q_ib_2)}\rangle$). We see that we get a different picture, in particular some of the states that have small overlap with $|\Phi_{b_2}\rangle$ have relatively large overlap with $|\Phi_{1(q_4b_2)}\rangle$.

Finally, we look at the overlaps of state $|\Phi_{b_3}\rangle$, playing the same little game, starting from the same deformation as $|\Phi_{b_3}\rangle$, and then going one parallelogram right, then one down, and finally one down again. Obviously, we redefine all labels according to $|\Phi_{b_3}\rangle$. The overlaps are displayed in Fig. 4.8, and as we can observe, we have yet another different picture, with in particular this time a very large overlap between $|\Phi_{b_3}\rangle$ and the one-quasiparticle state $|\Phi_{2(q_1b_3)}\rangle$ that has same

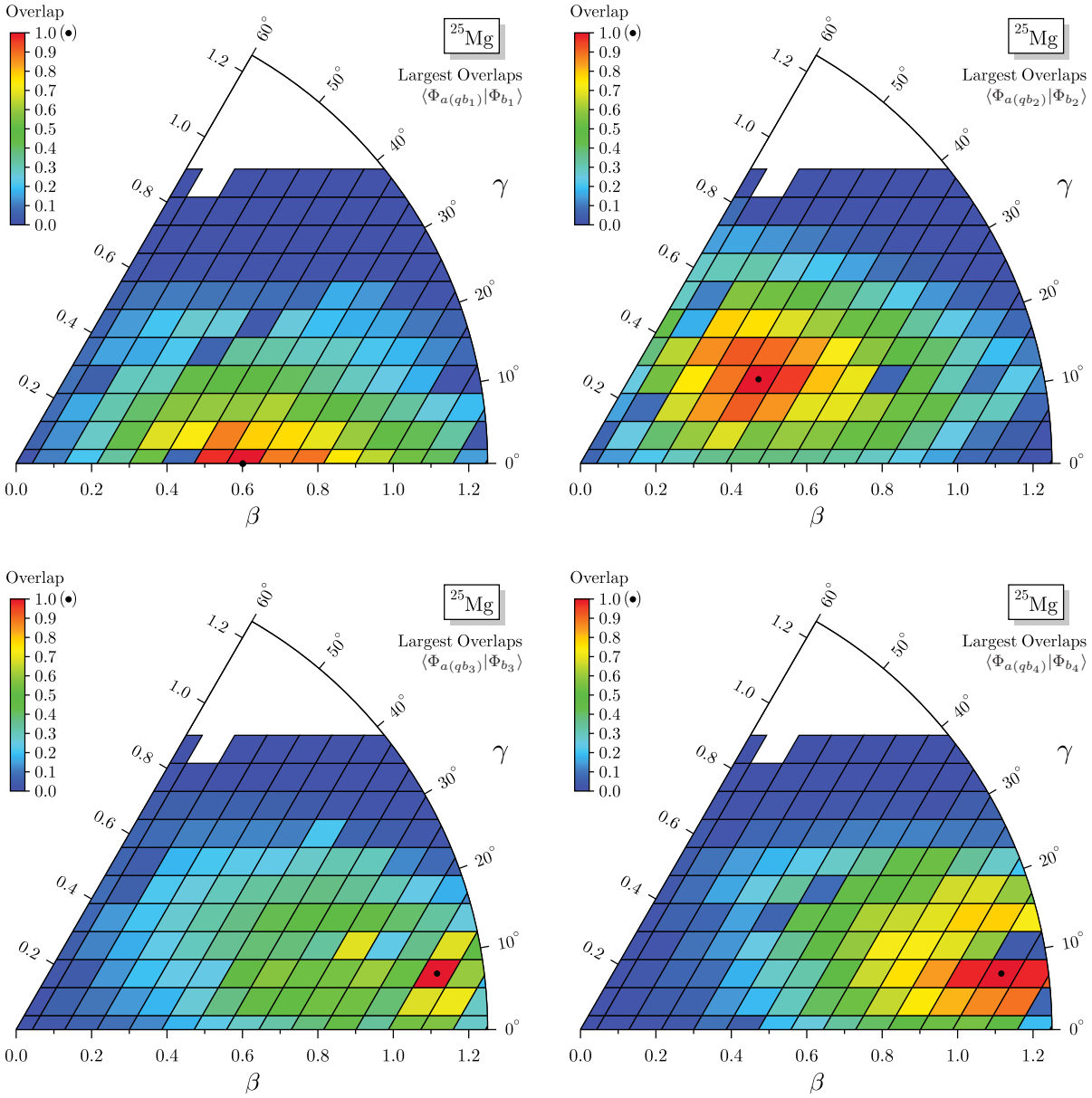

Figure 4.5: Top left: Surface of the largest overlaps $\langle\Phi_{a(qb_1)}|\Phi_{b_1}\rangle$ for a given one-quasiparticle state $|\Phi_{b_1}\rangle$ indicated by the black dot. The location of the one-quasiparticle states on the discretized deformation mesh is given by the center of the parallelograms, except for axial deformations where it is on the axes. Top right, bottom left, and bottom right: same but for other one-quasiparticle states $|\Phi_{b_2}\rangle$, $|\Phi_{b_3}\rangle$, and $|\Phi_{b_4}\rangle$.

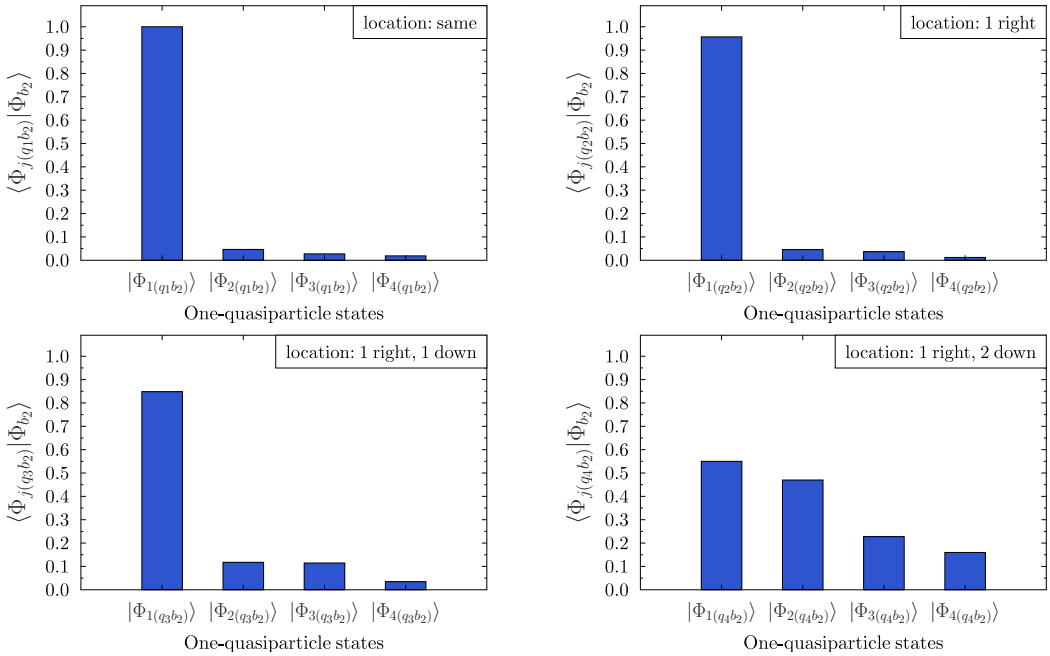

Figure 4.6: Top left: Values of the overlaps $\langle\Phi_{j(q_1b_2)}|\Phi_{b_2}\rangle$ for states $|\Phi_{j(q_1b_2)}\rangle$ with same deformation as $|\Phi_{b_2}\rangle$. Top right: Same with $|\Phi_{j(q_2b_2)}\rangle$ in the parallelogram at the right of $|\Phi_{b_2}\rangle$. Bottom left: Same with $|\Phi_{j(q_3b_2)}\rangle$ in the parallelogram below the one of top right panel. Bottom right: Same for $|\Phi_{j(q_4b_2)}\rangle$ in the parallelogram below the one of bottom left panel.

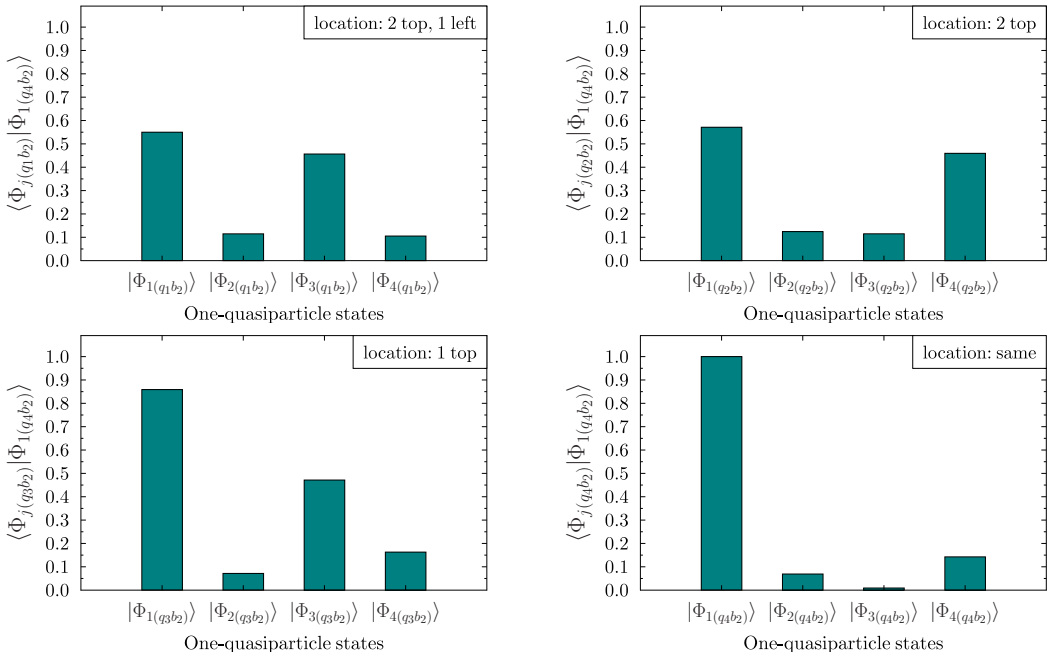

Figure 4.7: Same as Fig. 4.6 but for $|\Phi_{1(q_4b_2)}\rangle$ as reference for the overlaps (but not redefining the q_i and the labels of the states $|\Phi_{j(q_ib_2)}\rangle$).

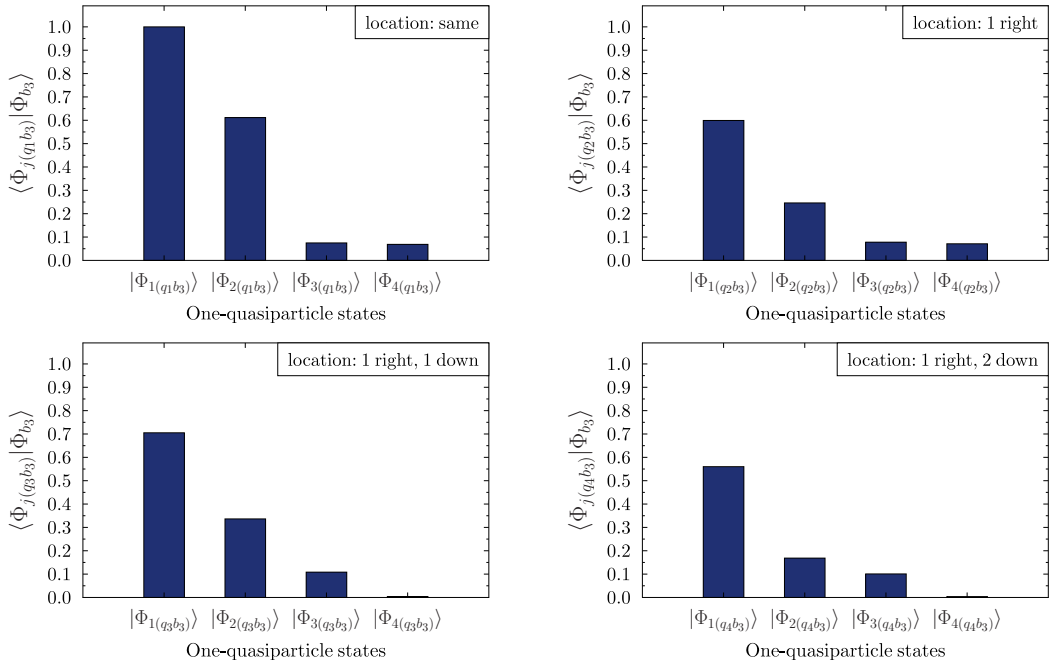

Figure 4.8: Same as Fig. 4.6 but for $|\Phi_{b_3}\rangle$ (redefining all the labels relatively to $|\Phi_{b_3}\rangle$).

deformation as $|\Phi_{b_3}\rangle$.

From this analysis, we conclude that the overlap between one-quasiparticle states is not a trivial thing. The one-quasiparticle states in our set are clearly not independent of one another, and thus it is not possible to speak of a specified one-quasiparticle state.

4.1.4 Pairing Energy

We conclude this brief SR-EDF analysis by looking at the pairing part of the energy surfaces presented in Fig. 4.3. We define the neutron (resp. proton) pairing energy as the terms of the functional which include neutron (resp. proton) abnormal densities (without LN correction), and for terms including both neutron and proton abnormal densities (see equations (1.42) and (1.43)), the energy is splitted in half into the neutron and the proton pairing energies. The pairing energy for both protons and neutrons are plotted in Fig. 4.9 for lowest states with positive parity and in Fig. 4.10 for lowest states with negative parity. We want to stress that we have filled with white the regions where not enough points could have been converged to assure a good interpolation.

We first note that for both parities the absolute value of the neutron pairing energy is globally smaller than the absolute value of the proton pairing energy. This is expected because by blocking a neutron quasiparticle, we remove two single-particle states from the calculation of the neutron pairing field. The number of single-particle states in the energy window for pairing being relatively small, the blocking thus greatly reduces the pairing for neutrons, such that it even almost disappears for a large part of the (β, γ) plane. But the pairing reappears at relatively high values of β, the minimum for neutron pairing energy being at $(1.238, 13.9°)$ for positive parity states and at $(1.548, 13.9°)$ (which is actually outside of the range in β plotted for the figure) for negative parity states. The neutron pairing energy of negative parity states is globally higher (in absolute value) than the one for positive parity states, which can be easily understood because the few negative parity single-particle states in the pairing energy window are usually farther away from the fermi energy than the positive parity single-particle states, such that blocking the

former does not affect the pairing as much as blocking the latter. From these energy surfaces we can see that the Lipkin-Nogami approach, even if it often prevents the pairing to completely collapse, is not sufficient to preserve a sizable pairing everywhere in the (β, γ) plane. The problem might come from the mediocre quality of the SLyMR0 parametrization [122]. More generally, a much more reliable treatment of pairing correlations through a variation after particle-number projection approach, as done in the MR-EDF calculations for even-even nuclei by the Madrid group [112], might be necessary.

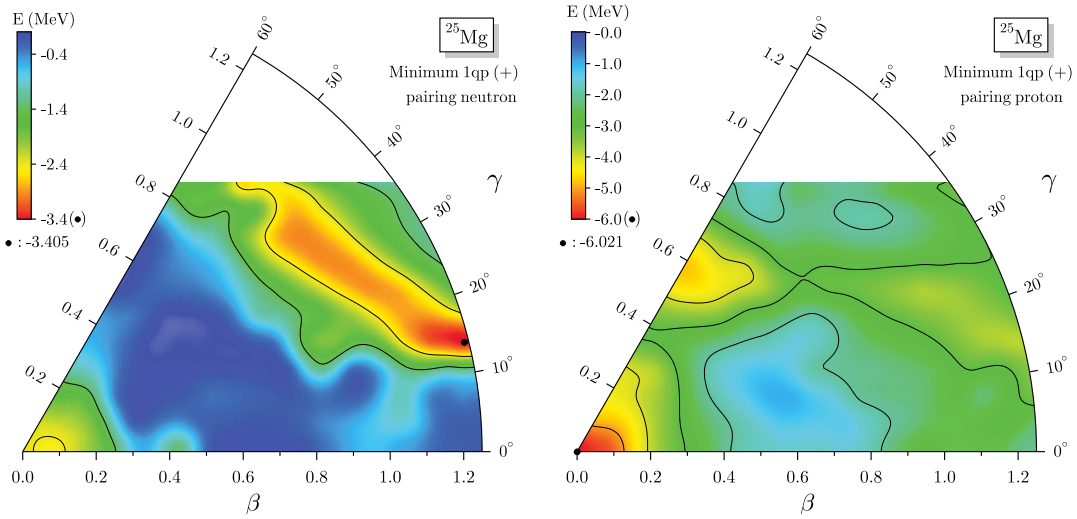

Figure 4.9: Left: Neutron pairing energy surface for the lowest one-quasiparticle states with positive parity. The black contour lines are plotted every 1 MeV from the minimum indicated by the black dot. Right: Same for protons.

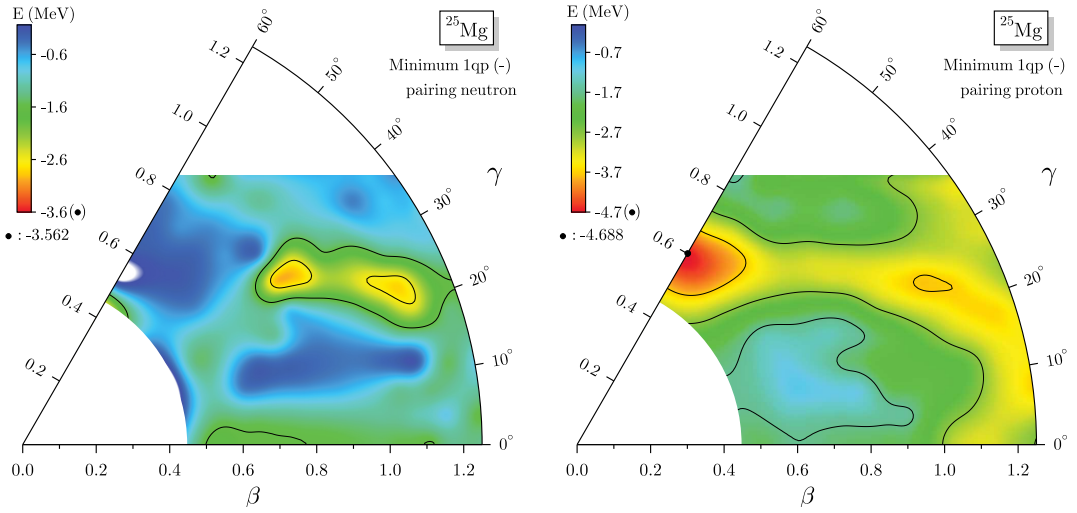

Figure 4.10: Left: Neutron pairing energy surface for the lowest one-quasiparticle states with negative parity. The black contour lines are plotted every 1 MeV from the minimum indicated by the black dot. Right: Same for protons.

4.2 Particle-Number Restoration

In the previous section, we have described how the one-quasiparticle states are constructed that are going to be used for our configuration mixing at the MR-EDF level. We also have briefly studied the global properties of these states, in particular the energy surfaces and how the states overlap. We want now to go further and to include more correlations in our states. We will proceed step by step to see how the results are affected by each of the "beyond mean-field" correlations. The first, and the simplest, step of our MR-EDF calculation is the Particle-Number Restoration for protons and neutrons.

4.2.1 Energy Surfaces

We first want to compare the energy surfaces before and after particle number projection to see the possible impact of particle-number restoration. The energy surface for the lowest projected quasiparticle states of positive (resp. negative parity is displayed in the left (resp. right) panel of Fig. 4.11, and should be compared with the non-projected surface in the left (resp. right) panel of Fig. 4.3. The surface is defined such that we plot the energy of each projected state at the deformation (β, γ) of the non-projected state it originates from. It is important to note that the PNR energy surfaces are determined considering the states that give the lowest energy at the PNR level. Those states can *a priori* be different from the states giving the lowest energy at the SR level. In our case, however, they are almost always the same. And globally we can see that the overall topography of the surfaces is not affected by the PNR. The positions of the minima are slightly changed, but the positive parity minimum $(0.515, 0°)$ remains axial and the negative parity minimum $(0.733, 5.82°)$ stays in the same region of triaxility.
In the left (resp. right) panel of Fig. 4.12 is plotted the difference in energy[1]

$$\Delta E(q) = \frac{\langle \Phi_{qa}|\hat{H}\hat{P}^N\hat{P}^Z|\Phi_{qa}\rangle}{\langle \Phi_{qa}|\hat{P}^N\hat{P}^Z|\Phi_{qa}\rangle} - \langle \Phi_{qb}|\hat{H}|\Phi_{qb}\rangle \tag{4.1}$$

at every deformation q between particle-number projected states with positive (resp. negative parity $\hat{P}^N\hat{P}^Z|\Phi_{qa}\rangle$ of Fig. 4.11 and the lowest one-quasiparticle states with same parity and same deformation $|\Phi_{qb}\rangle$ of Fig. 4.3. Note in particular that, even if they have same deformation q, $|\Phi_{qa}\rangle$ is not necessarily the same state as $|\Phi_{qb}\rangle$ (as described above). We can see that for positive (resp. negative) parity, the energy gain by the particle-number restoration in the region situated around the minimum of Fig. 4.11 is approximately constant, with a gain of roughly 1-2 MeV (resp. 2-3 MeV) downwards. This explains why, for both positive and negative parity, the topography of the projected surface displayed in Fig. 4.11 is very similar to the one of the non-projected surface displayed in Fig. 4.3. On the other hand, we can see that in other regions of the surfaces displayed in Fig. 4.12, the gain in energy can be greater than 5 MeV.[2]

4.2.2 Overlap Between Projected One-Quasiparticle States

Similarly to what has been done in section 4.1.3, we can look at the overlap between the projected one-quasiparticle states. For the sake of clarity, we will use exactly the same one-quasiparticle states with the same notations as in section 4.1.3, but where one should replace:

$$|\Phi_x\rangle \equiv \frac{\hat{P}^N\hat{P}^Z|\Phi_x\rangle}{\sqrt{\langle \Phi_x|\hat{P}^N\hat{P}^Z|\Phi_x\rangle}} \quad .$$

[1] We do not consider the LN correction to the energy of one-quasiparticle states.
[2] At some deformations that are outside the range in β plotted here, the gain can be as large as 7 MeV.

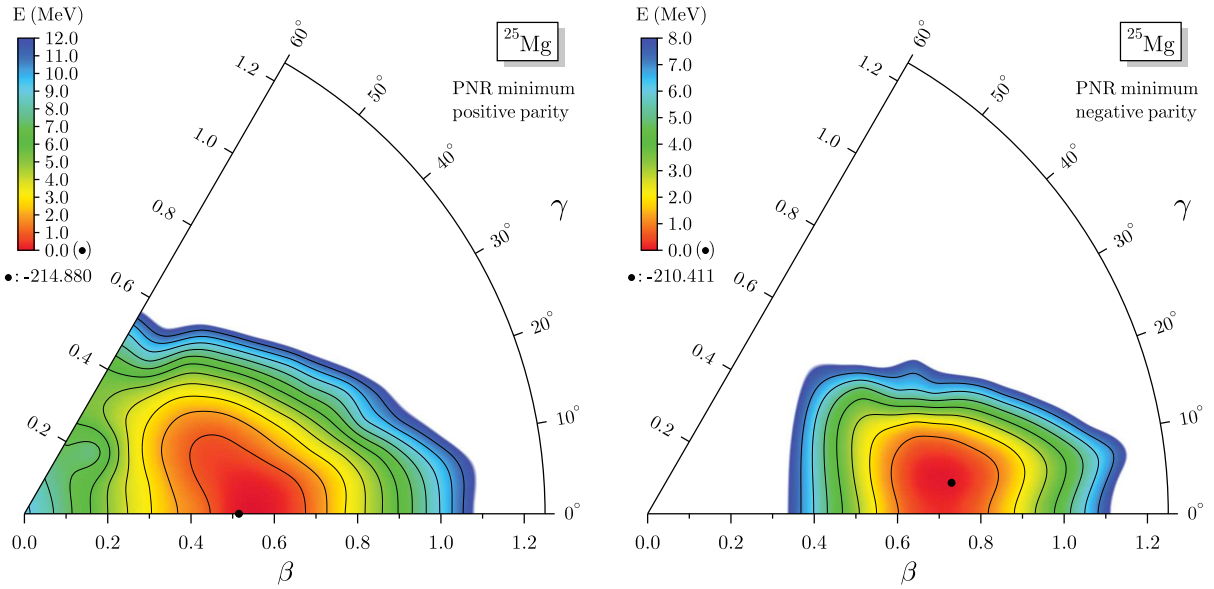

Figure 4.11: Left: PNR energy surface for the lowest one-quasiparticle states with positive parity. The black contour lines are plotted every 1 MeV from the minimum indicated by the black dot. Right: Same for negative parity.

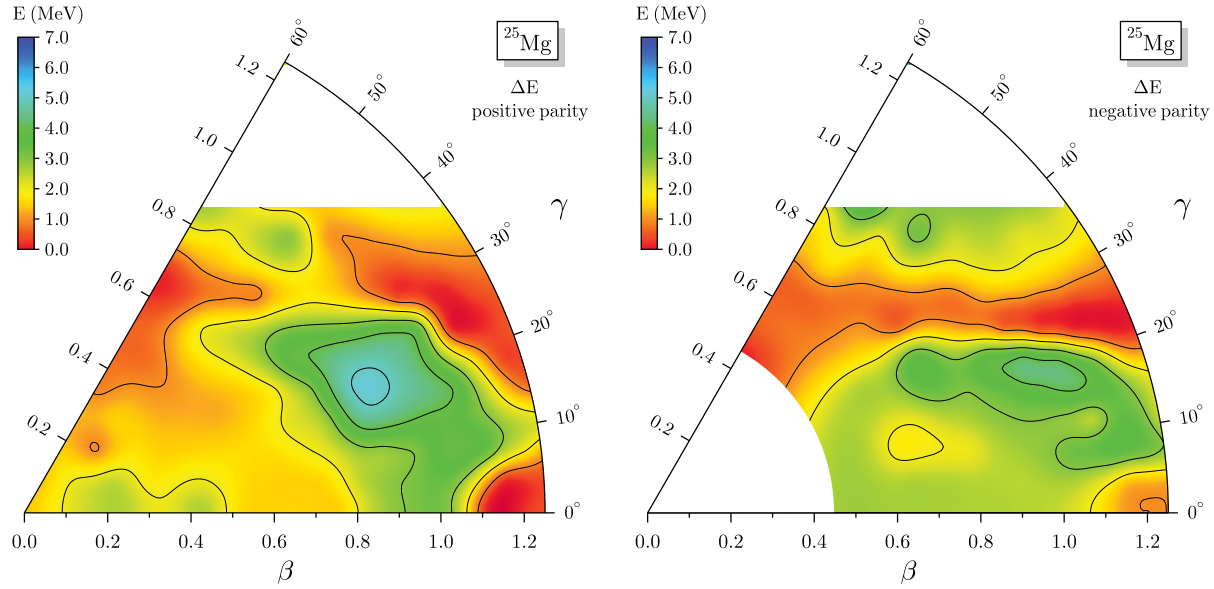

Figure 4.12: Left: Difference between the energy of the lowest projected one-quasiparticle states with positive parity and the energy of the lowest one-quasiparticle state with positive parity (at same deformation). The LN correction is not considered for the latter. The black contour lines are plotted every 1 MeV from the minimum indicated by the black dot. Right: Same for negative parity.

The results are displayed in Fig. 4.13, 4.14, and Fig. 4.15. As we can notice apart from the fact that the overlap between projected states are a little bit larger than for the corresponding non-projected one-quasiparticle states, there is no essential difference in the conclusions.

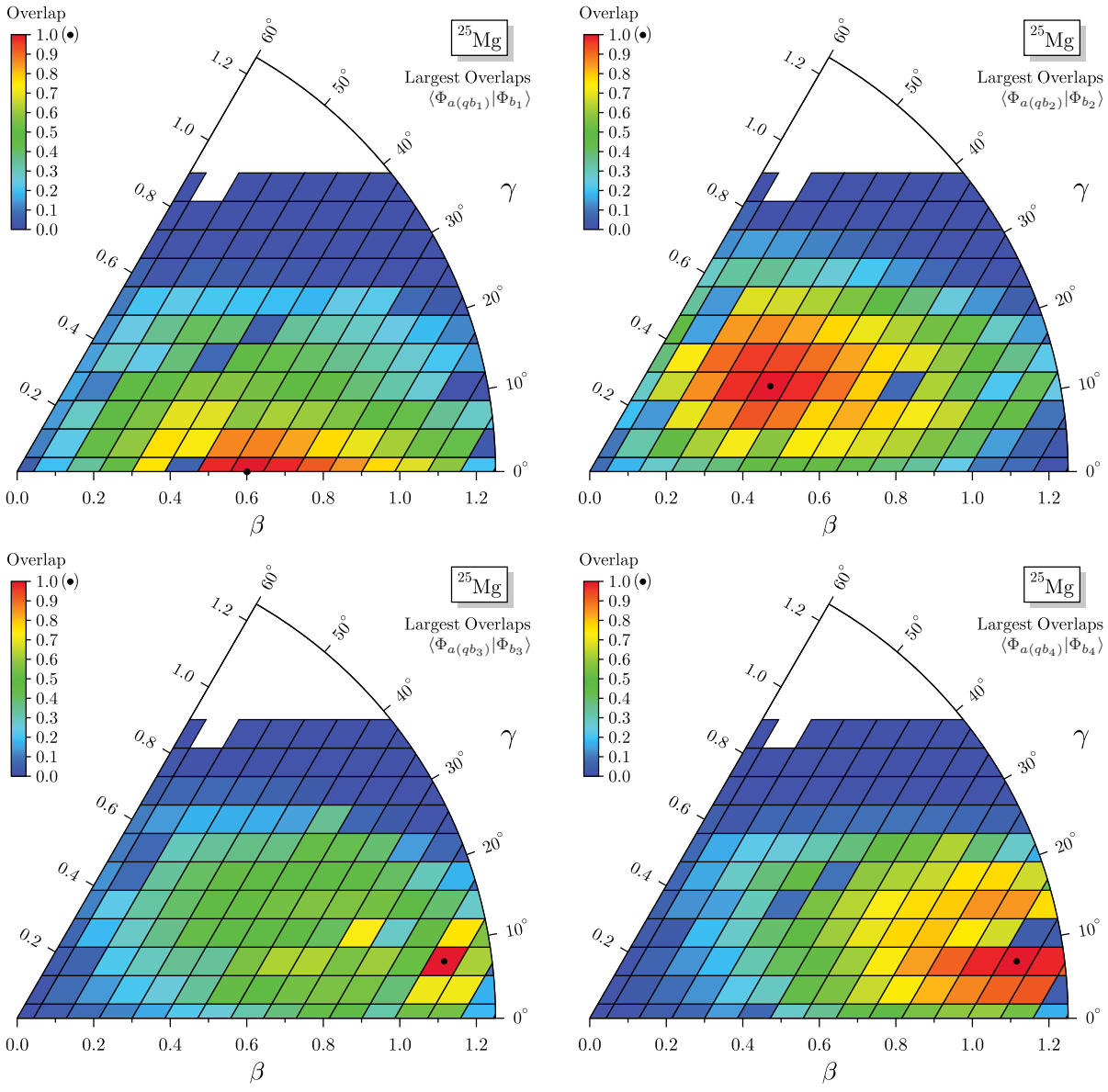

Figure 4.13: Same as Fig. 4.5 but for the normalized projected states obtained from $|\Phi_{b_i}\rangle$.

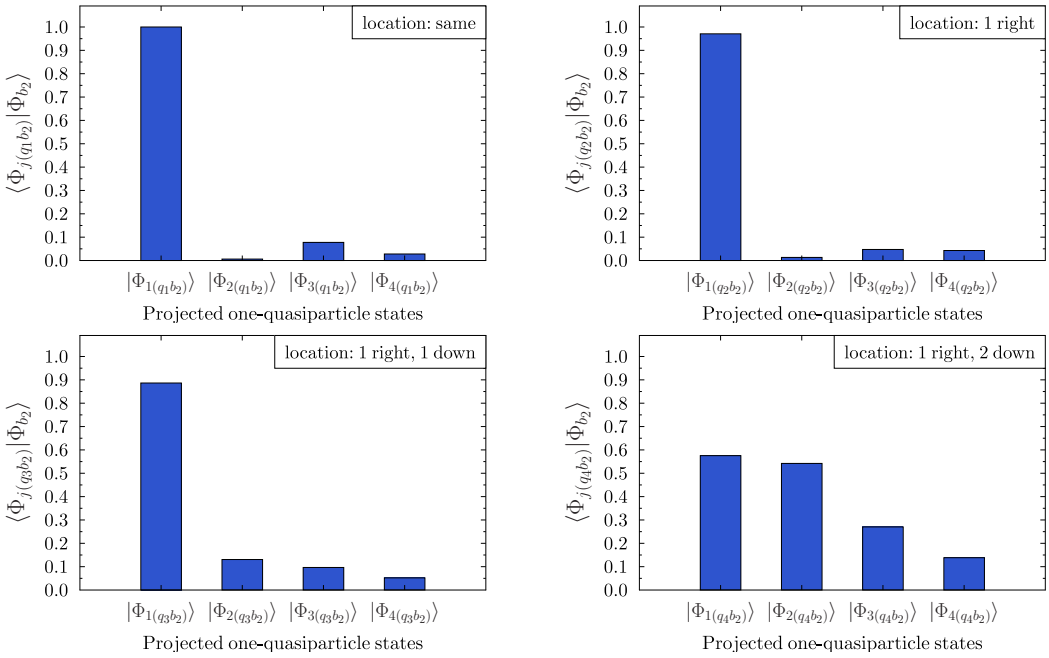

Figure 4.14: Same as Fig. 4.6 but for the normalized projected state obtained from $|\Phi_{b_2}\rangle$.

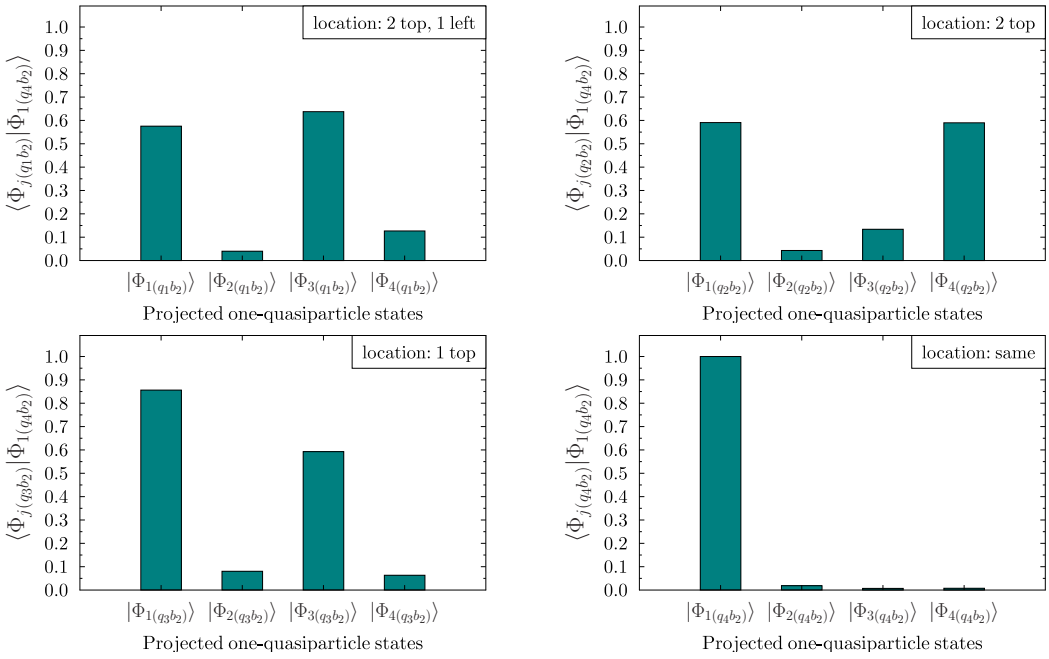

Figure 4.15: Same as Fig. 4.7 but for the normalized projected state obtained from $|\Phi_{1(q_4b_2}\rangle$.

4.2.3 N and Z Decompositions

It can be interesting to project not only on the physical component $N = 13$ and $Z = 12$, but also on other values of N and Z to study how the one-quasiparticle states are decomposed onto the different irrep basis functions of $U(1)_N \times U(1)_Z$

$$\begin{aligned} \langle \Phi_a | \hat{P}^N | \Phi_a \rangle &= \sum_{Z\tau} |c^{NZ\tau}|^2 \equiv |c^N|^2 \quad , \\ \langle \Phi_a | \hat{P}^Z | \Phi_a \rangle &= \sum_{N\tau} |c^{NZ\tau}|^2 \equiv |c^Z|^2 \quad , \end{aligned} \tag{4.2}$$

where τ labels the different irreps of $U(1)_N \times U(1)_Z$ with same value of N and Z. Working with normalized states $\langle \Phi_a | \Phi_a \rangle = 1$, we have for the weights $|c^N|^2$ and $|c^Z|^2$ the sum rules

$$\begin{aligned} \sum_N |c^N|^2 &= 1 \quad , \\ \sum_Z |c^Z|^2 &= 1 \quad , \end{aligned} \tag{4.3}$$

which can be used as a measure for the accuracy of the particle-number projection. This will be discussed in next section. In Fig. 4.16, we plot the weights of neutron and proton components for two different one-quasiparticle states, the first one (left panels) being the spherical point and the second one (right panels) being the minimum of the energy surface displayed in the right panel of Fig. 4.3. We clearly see that for the spherical point, where the pairing is (relatively) strong for both particle species, we have much wider distributions than for the minimum. Indeed, the latter is almost a pure $N = 13$ state and also has a narrow distribution for Z components, which is in agreement with the very low pairing energy of this state as seen in Fig. 4.9. But even when the pairing is very weak, we see that it does not completely disappear, thanks to Lipkin-Nogami prescription. In summary these results are in complete agreement with what we expect and with what has been observed in previous calculations [124], i.e. the stronger the pairing the larger is the symmetry breaking and the wider is the distribution in particle number.

4.2.4 Precision and Convergence of the PNR

Solving the problem numerically, the integral over $U(1)_N$ (resp. $U(1)_Z$) angles of the particle-number projection operator is in practice discretized. It thus important to look if the chosen discretization, here 9 points for neutrons and 9 points for protons, is sufficient to properly project on the desired numbers of particles.
Looking first at the sum rules plotted in top right corner of the N and Z decompositions of 4.16, we see that they are perfectly respected. It is a sign of the good precision of our discretization and it is worth noting that, because we use pure pseudo-potential based energy functional, this sum rule also applies to the total energy [23].
To continue the analysis, we give in Tab. 4.1 for the lowest one-quasiparticle with positive parity at the spherical point, the expectation value of the projected energy

$$E = \frac{\langle \Phi_a | \hat{H} \hat{P}^N \hat{P}^Z | \Phi_a \rangle}{\langle \Phi_a | \hat{P}^N \hat{P}^Z | \Phi_a \rangle} \quad ,$$

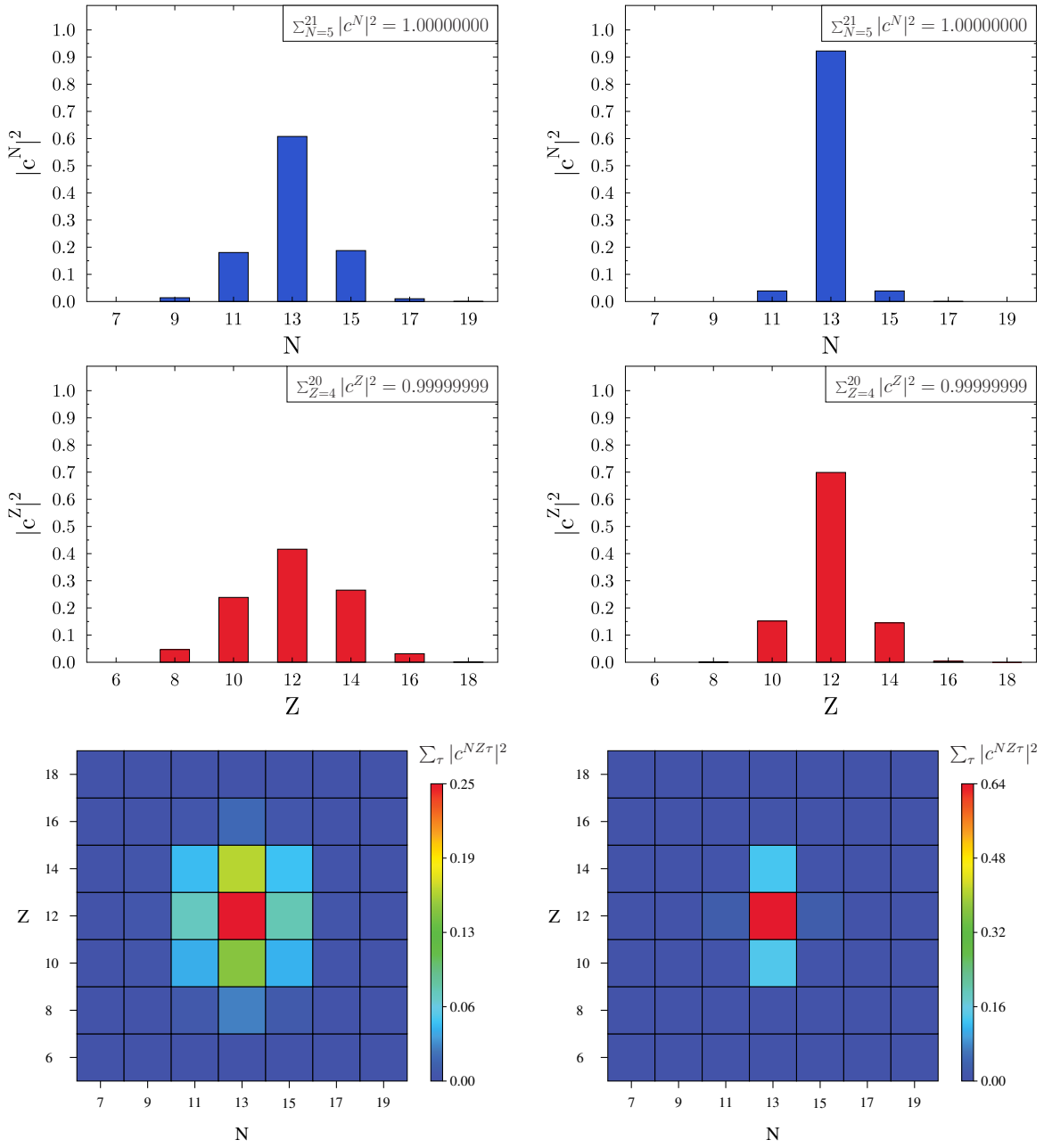

Figure 4.16: Top : Weights of neutron components for the lowest quasiparticle state with positive parity at the spherical point (left) and for the absolute minimum in the energy surface of non-projected states with positive parity (right), see Fig. 4.3. Center: Same for proton components. Bottom: Weights of the components $\langle\Phi_a|\hat{P}^N\hat{P}^Z|\Phi_a\rangle$ in the N,Z plane.

the neutron and proton numbers

$$\langle N \rangle = \frac{\langle \Phi_a | \hat{N} \hat{P}^N \hat{P}^Z | \Phi_a \rangle}{\langle \Phi_a | \hat{P}^N \hat{P}^Z | \Phi_a \rangle} \quad ,$$
$$\langle Z \rangle = \frac{\langle \Phi_a | \hat{Z} \hat{P}^N \hat{P}^Z | \Phi_a \rangle}{\langle \Phi_a | \hat{P}^N \hat{P}^Z | \Phi_a \rangle} \quad ,$$

and the neutron and proton variances

$$(\Delta N)^2 = \langle N^2 \rangle - \langle N \rangle^2 \quad ,$$
$$(\Delta Z)^2 = \langle Z^2 \rangle - \langle Z \rangle^2 \quad ,$$

for different discretization of the integrals over gauge angles. This point has been selected as an example because it exhibits (relatively) strong pairing for both neutrons and protons and thus (relatively) wide distributions over states with different number of particles, as shown in Fig. 4.16. Because of the structure of the discretized projection operator discussed in appendix B.6, we expect[3] that if the discretization is converged for this point, it will be also the case for states with much narrower N and Z distributions.

From Tab. 4.1 we see that our choice of discretization for the particle-number restoration is more than safe, the convergence of all the quantities, and in particular of the energy, being already achieved with only 5 points. And it does not seem necessary to choose a denser discretization because, as we can see, the numerical noise is dominant below 10^{-7} for the energy whatever the number of points chosen. Given all the possible sources of numerical noise in our calculations, a relative error of the order 10^{-7} on the energy is more than acceptable. Lastly, we want to stress that, like for the sum rules, a such good convergence of the projected energy is only possible because we use a functional properly derived from a Hamiltonian [23].

Discretization ($N \times Z$)	Energy (MeV)	$\langle N \rangle$	$(\Delta N)^2$	$\langle Z \rangle$	$(\Delta Z)^2$
No PNR	-204.2933590273	13.0000000000	1.864E+00	12.0000000000	3.316E+00
3×3	-205.8270246965	13.0014836799	8.900E-03	12.0190518490	1.139E-01
5×5	-205.7232309055	13.0000000000	-2.842E-14	12.0000000000	-2.842E-14
7×7	-205.7232310745	13.0000000000	2.842E-14	12.0000000000	2.842E-14
9×9	-205.7232311973	13.0000000000	-2.842E-14	12.0000000000	5.684E-14
11×11	-205.7232310556	13.0000000000	-2.842E-14	12.0000000000	2.842E-14
21×21	-205.7232311067	13.0000000000	2.842E-14	12.0000000000	-8.527E-14
31×31	-205.7232311123	13.0000000000	8.527E-14	12.0000000000	-1.137E-13
41×41	-205.7232311296	13.0000000000	2.842E-14	12.0000000000	0.000E+00
51×51	-205.7232311264	13.0000000000	2.842E-13	12.0000000000	8.527E-14
71×71	-205.7232311069	13.0000000000	-5.684E-14	12.0000000000	-8.527E-14
91×91	-205.7232311130	13.0000000000	-5.684E-14	12.0000000000	2.842E-14

Table 4.1: Precision of the Particle-Number Restorartion as a function of the number of points used in discretization of the PNR integrals for the lowest energy one-quasiparticle state at the spherical point. The red line indicates the discretization chosen elsewhere in this work. For Fomenko-type discretization (B.33), taking only one point for the discretizations for both integrals (1×1) is equivalent to no projection at all.

[3] As a matter of fact, I checked for other states with different deformation or blocked one-quasiparticle, and the precision of the PNR was found to be at least equally good for those states.

4.3 Angular-Momentum Restoration

After the inclusion of dynamical correlations related to particle-number restoration that has been discussed in the previous section, we now continue to add more correlations by projecting on particle-number **and** on angular-momentum. As explained in the section on projection 3.4, because of the structure of the group associated with the rotational invariance, this projection is much more complex and more computational ressources demanding and thus will require a little more comments.

4.3.1 Energy Surfaces

As done in the two previous sections on SR and PNR calculations, we will first look at energy surfaces in the first sextant of the (β, γ) plane. But here, contrary to the PNR where only components $N = 13$ and $Z = 12$ have a physical relevance for the study of ^{25}Mg, the states with different values for the total angular momentum J represent the ground state and excited states of the nucleus. We thus plot in Fig. 4.17 and Fig. 4.18, for positive parity and negative parity, respectively, the lowest energy surfaces for J values ranging from $J = \frac{1}{2}$ to $J = \frac{7}{2}$. It is of course possible to project also on higher values of J, but they appear in our case at higher energy and do not bring anything interesting to the analysis. Also we point out that similar rationale as for PNR energy surface has been used to determine the deformations in the AMR+PNR surfaces, i.e. the projected energies are plotted at the deformation of the one-quasiparticle states they originate from. First looking at positive parity surfaces, we see that all four surfaces present a very similar topography, but with some noticeable differences. First and foremost the minimum of the $J^\pi = \frac{5}{2}^+$ surface, which is the absolute minimum of all projected states, is located at a different location $(0.522, 25.29°)$ than the minimum of $J^\pi = \frac{1}{2}^+$ and $J^\pi = \frac{3}{2}^+$ positioned at $(0.619, 13.90°)$. The three minima are energetically very close to each other, with less than 200 keV separating one from the others. One finds first the $J^\pi = \frac{5}{2}^+$ at an energy $E_{min}\left(\frac{5}{2}^+\right) = -220.752$ MeV, and then the $J^\pi = \frac{3}{2}^+$ at $E_{min}\left(\frac{3}{2}^+\right) = -220.625$ MeV, and finally the $J^\pi = \frac{1}{2}^+$ with $E_{min}\left(\frac{1}{2}^+\right) = -220.565$ MeV. With the $\frac{3}{2}^+$ being lower than the $\frac{1}{2}^+$, the level sequence disagrees with experiment. As we will see later, this is a defect coming from the SLyMR0 parametrization. However, this will be possible to judge only after carrying out the complete MR-EDF calculation where all states are mixed together, because it is possible, from where we stand right now, that mixing different states will change the order of the levels in the excitation spectrum. Another difference is that the $J^\pi = \frac{5}{2}^+$ surface is also less rigid when going toward small β deformation. The $J^\pi = \frac{7}{2}^+$ surface is particular in the sense that, even if the minimum is located at the same point as for $J^\pi = \frac{5}{2}^+$, the surface seems to be a mix between the shape of the $J^\pi = \frac{5}{2}^+$ and $J^\pi = \frac{3}{2}^+$ surfaces. The minimum is relatively soft and the line representing $E_{min}\left(\frac{7}{2}^+\right) + 1$ MeV includes completely the region situated around the minimum of the $J^\pi = \frac{3}{2}^+$. As we will see below, this can be understood as the presence of two different $J^\pi = \frac{7}{2}^+$ states that are very close in energy, one belonging to a rotational band based on $J^\pi = \frac{5}{2}^+$ states, and the other belonging to a rotational band based on $J^\pi = \frac{3}{2}^+$ states.

All the surfaces for negative parity are rather similar to one another, with a minimum situated for all four surfaces at the deformation $(0.787, 10.89°)$, the minium for negative parity belonging to $J^\pi = \frac{3}{2}^-$ with an energy $E_{min}\left(\frac{3}{2}^-\right) = -217.733$ MeV. We can also note that the $J^\pi = \frac{3}{2}^-$ and the $J^\pi = \frac{7}{2}^-$ surfaces are almost identical, whereas the $J^\pi = \frac{1}{2}^-$ and the $J^\pi = \frac{5}{2}^-$ surfaces present the same extension towards oblate deformations.

For both parities the projection on angular-momentum completely changes the picture one ob-

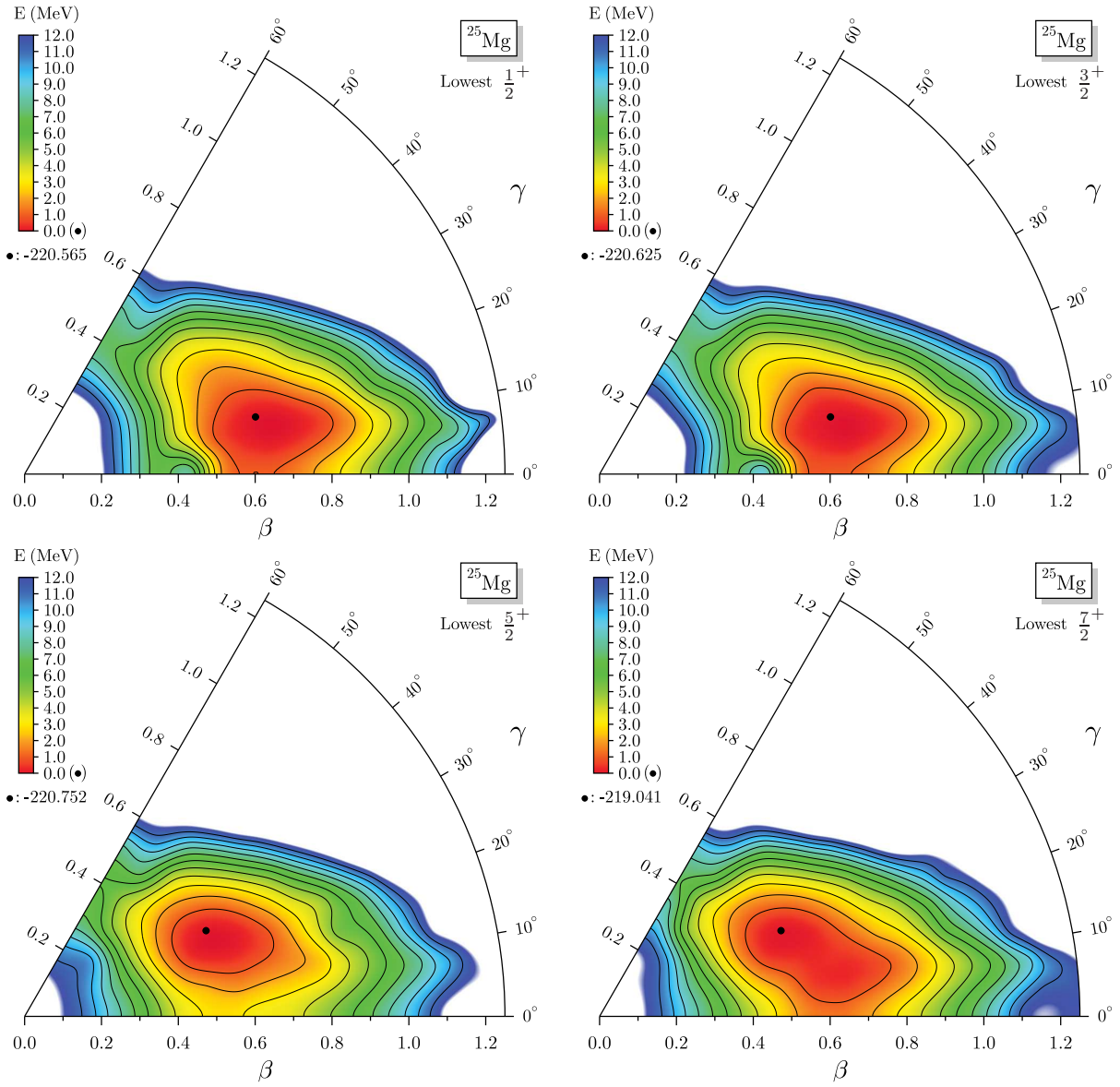

Figure 4.17: Top left: AMR+PNR energy surface for the lowest projected one-quasiparticle states with $J^\pi = \frac{1}{2}^+$. The black contour lines are plotted every 1 MeV from the minimum indicated by the black dot. Top right: Same for $J^\pi = \frac{3}{2}^+$. Bottom left: Same for $J^\pi = \frac{5}{2}^+$. Bottom right: Same for $J^\pi = \frac{7}{2}^+$.

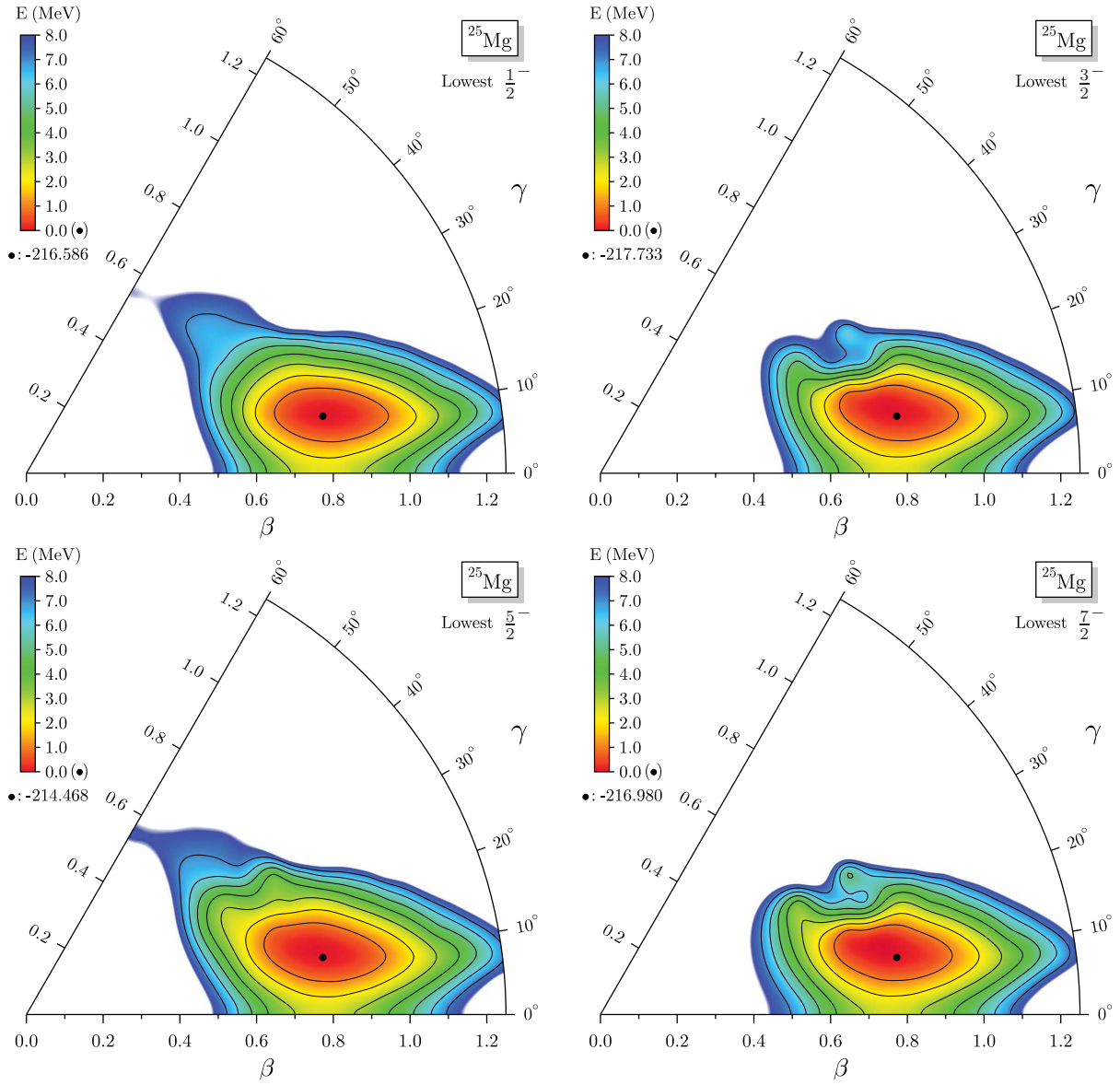

Figure 4.18: Top left: Minimum AMR+PNR energy surface for the lowest projected one-quasiparticle states with $J^\pi = \frac{1}{2}^-$. The black contour lines are plotted every 1 MeV from the minimum indicated by the black dot. Top right: Same for $J^\pi = \frac{3}{2}^-$. Bottom left: Same for $J^\pi = \frac{5}{2}^-$. Bottom right: Same for $J^\pi = \frac{7}{2}^-$.

tains for the energy surfaces. Indeed, we recall that before projection the absolute minimum is axial, but when we look at Fig. 4.3 we observe that the general shapes of the surfaces are very different before and after projection. The projected surfaces are softer, clearly favour more triaxiality, and finally present an ovoid shape around their relative minimum which is absent for non-projected surfaces. Moreover, the difference in energy between the absolute minimum of positive parity $E_{min}(\frac{5}{2}^+) = -220.752$ MeV and the minimum of negative parity $E_{min}(\frac{3}{2}^-) = -217.733$ MeV is reduced to only 3 MeV, whereas it is 4.5 MeV when only doing the PNR and even more than 5 MeV for non-projected states. The negative parity minimum having a larger deformation, it tends to gain more energy when projecting on angular-momentum. All these results clearly indicate the need for angular-momentum projection if one wants to say something conclusive about the energy surfaces of ^{25}Mg.

In the same manner as for PNR, we want to stress that all energy surfaces are constructed by using, for a given deformation and a given angular momentum, the lowest energy states at the AMR+PNR level, which is *a priori* different from projecting the SR lowest energy one-quasiparticle states of surface of Fig. 4.3 on the different J values. Such surfaces are plotted for $J^\pi = \frac{1}{2}^+$ and $J^\pi = \frac{5}{2}^+$ in Fig. 4.19 as examples. Surprisingly, we see that the surfaces are very similar to the ones obtained by looking for the minimum after projection. There are some differences, as for example the more rigid behavior of the lowest quasiparticle states projected on $J^\pi = \frac{1}{2}^+$ for deformation with $(\beta > 1, \gamma < 10°)$, or the narrower minimum for the lowest quasiparticle states projected on $J^\pi = \frac{5}{2}^+$, but overall the surfaces resemble one another. Even if not shown here, similar conclusions are obtained for other values of J with positive parity and for negative parity states. Recalling that we do PAV calculations here, it is quite reassuring that the projection of the lowest states at the SR level give almost always also the lowest states after projection. This way we can hope that the minimization done at the SR level gives us states that are indeed relevant for the configuration mixing and that the overall description of the nucleus is close to what one would obtain in a VAP approach. Of course that is more an expectation than

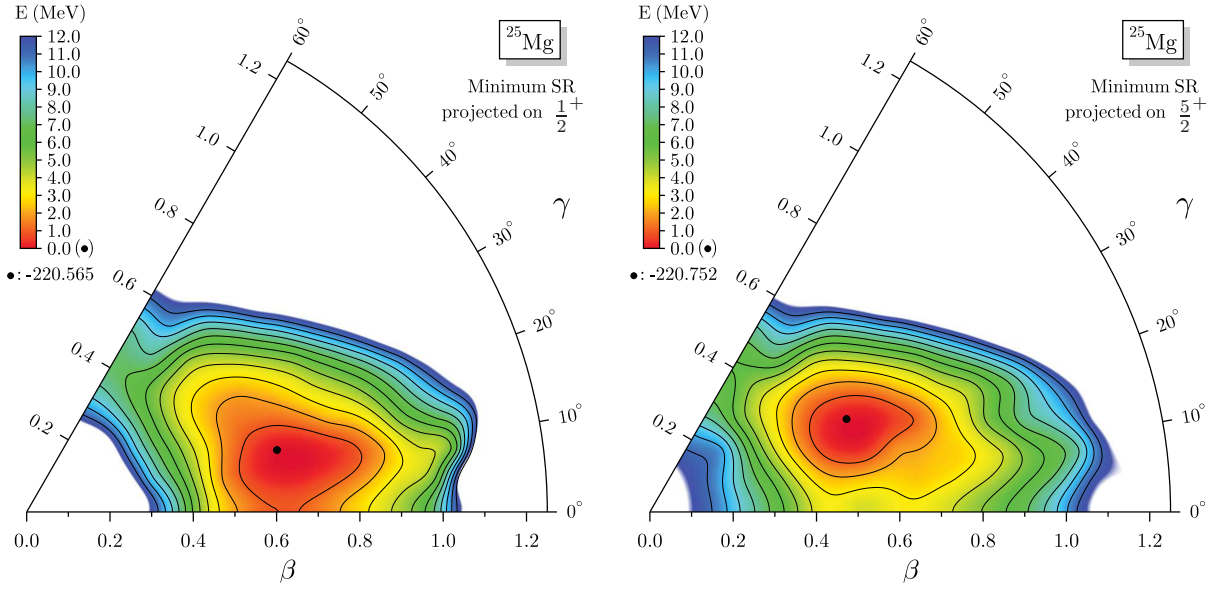

Figure 4.19: Left: AMR+PNR energy surface for $J^\pi = \frac{1}{2}^+$ built from the lowest one-quasiparticle states with positive parity at the SR level, i.e. the states used to construct Fig. 4.3. The black contour lines are plotted every 1 MeV from the minimum indicated by the black dot. Right: Same for $J^\pi = \frac{5}{2}^+$.

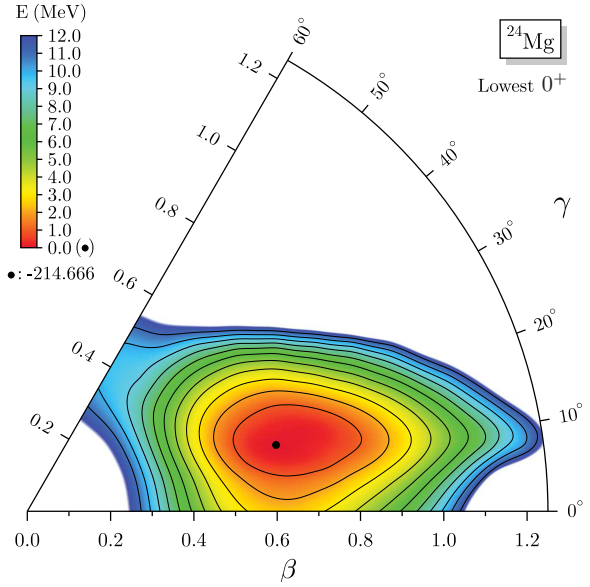

Figure 4.20: Energy surface of the $J = 0^+$ projected states of ^{24}Mg. The black contour lines are plotted every 1 MeV from the minimum indicated by the black dot.

an actual statement, and only a full VAP calculation could tell us if this is indeed the case. But the computational cost prohibits for the time-being such kind of calculation in a GCM oriented approach.

Finally one can compare positive parity and negative parity energy surfaces with the surface of the $J = 0^+$ of ^{24}Mg plotted in Fig. 4.20. The addition of one neutron does not seem to affect much the overall topography of the energy surface, ^{24}Mg presenting a triaxial minimum very close to the one one gets for $J^\pi = \frac{3}{2}^+$ in ^{25}Mg, and the surface also favouring deformation with high β and small γ deformations with the ovoid shape we mentioned before. But we should recall that for ^{25}Mg the absolute minimum is obtained for the $J^\pi = \frac{5}{2}^+$ energy surface, which is at a different deformation than the minimum of the $J^\pi = \frac{3}{2}^+$ energy surface.

4.3.2 Mixing of K-components

All the energy surfaces discussed in the previous section have been plotted using states obtained at the end of the projection on angular momentum, i.e. after mixing of the different K components[4] (see section 3.4.3). In the present section, we want to illustrate for two examples the effects of such mixing. In order to do so we display in Fig. 4.21 (resp. Fig. 4.22) the spectrum (up to -211 MeV) of the states

$$\frac{\hat{P}^J_{MK}\hat{P}^N\hat{P}^Z|\Phi_a\rangle}{\langle\Phi_a|\hat{P}^J_{KK}\hat{P}^N\hat{P}^Z|\Phi_a\rangle}$$

with different values of J and K, for the one-quasiparticle state $|\Phi_a\rangle$ that gives the minimum for $J^\pi = \frac{5}{2}^+$ (resp. $J^\pi = \frac{1}{2}^+$ and $J^\pi = \frac{3}{2}^+$) states after projection. We recall that because of the x-signature, for a given J, the component $-K$ is linked to the component K and we have only $\frac{2j+1}{2}$ independent states (see section 3.4.3). And this is why we plot here only states with positive

[4] I want here to stress that the term "K component" is a convenience of language as K is not a good quantum number nor an index labeling the basis functions of the irreps of $SU(2)$ after obtaining them from projection on angular momentum (it is M which plays this role). The term "K component" indicates from which basis function in the decomposition of the non-projected state has been obtained the state before mixing.

value of K. We can observe that in Fig. 4.21, states projected from $K^\pi = \frac{5}{2}^+$ are energetically favoured, whereas in Fig. 4.22 it is states projected from $K^\pi = \frac{1}{2}^+$.

In Fig. 4.23 and 4.24 are presented for the one-quasiparticle state that gives the minimum for $J^\pi = \frac{5}{2}^+$, the spectrum before and after K-mixing for $J^\pi = \frac{5}{2}^+$ and $J^\pi = \frac{9}{2}^+$, respectively. As we can see, in both cases the energy of the lowest state in the spectrum after mixing is only lowered by few keV or tens of keV, comparatively to the lowest state before mixing. On the other hand, the highest states after mixing are pushed up by more than 100 keV in both cases. Also, the 4^{th} state of the spectrum after mixing of Fig. 4.24 is almost 1 MeV higher than the 4^{th} state of the spectrum before mixing!
We now look at the mixing of $J^\pi = \frac{9}{2}^+$ states given by the one-quasiparticle that gives the minimum for $J^\pi = \frac{1}{2}^+$ and $J^\pi = \frac{3}{2}^+$ states, and which is displayed in Fig. 4.25. Before K-mixing there are 3 different states that are very close in energy. After the mixing we obtain 3 states that are splitted in energy, the lowest of them being 352 keV lower than the lowest state before mixing. We also notice that the 4^{th} state of the spectrum is largely affected by the mixing.

Finally, we want to stress that the mixing of the different K-components, even if this lowers by only few keV the lowest energy state in the spectrum, is always necessary!

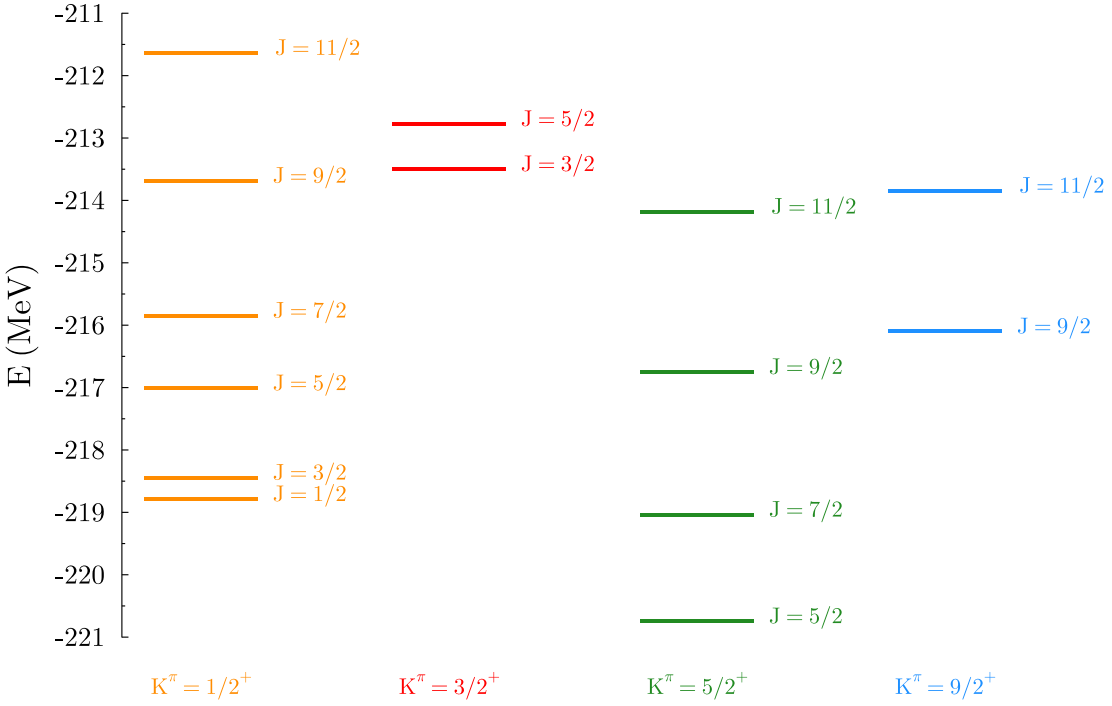

Figure 4.21: Spectrum (up to -211 MeV) of the states $\frac{\hat{P}^J_{MK}\hat{P}^N\hat{P}^Z|\Phi_a\rangle}{\langle\Phi_a|\hat{P}^J_{KK}\hat{P}^N\hat{P}^Z|\Phi_a\rangle}$, where $|\Phi_a\rangle$ is the one-quasiparticle state giving the minimum for $J^\pi = \frac{5}{2}^+$ states.

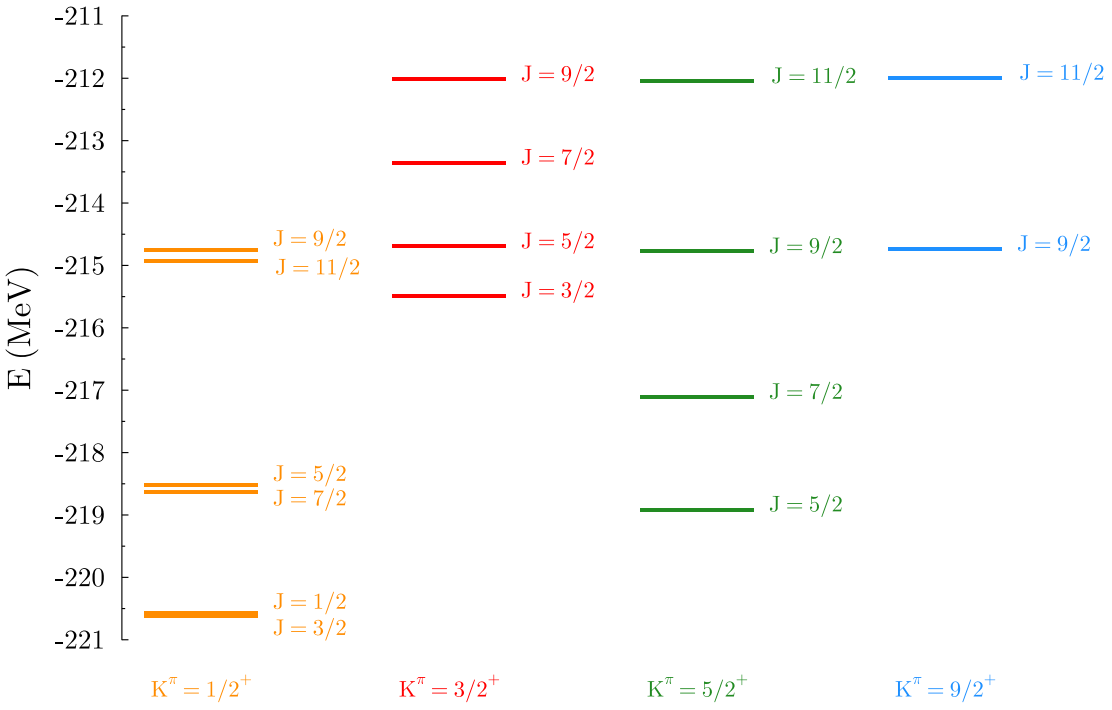

Figure 4.22: Same as Fig. 4.21 but for the one-quasiparticle state that gives the minimum for $J^{\pi} = \frac{1}{2}^{+}$ and $J^{\pi} = \frac{3}{2}^{+}$ states.

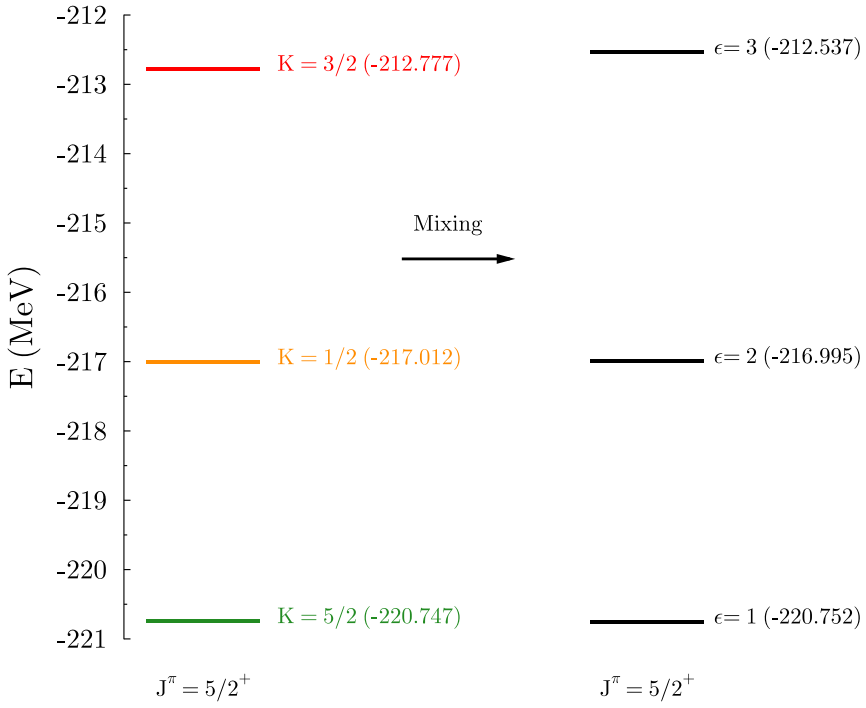

Figure 4.23: Mixing of the K components of $J^{\pi} = \frac{5}{2}^{+}$ for the one-quasiparticle state of Fig. 4.21.

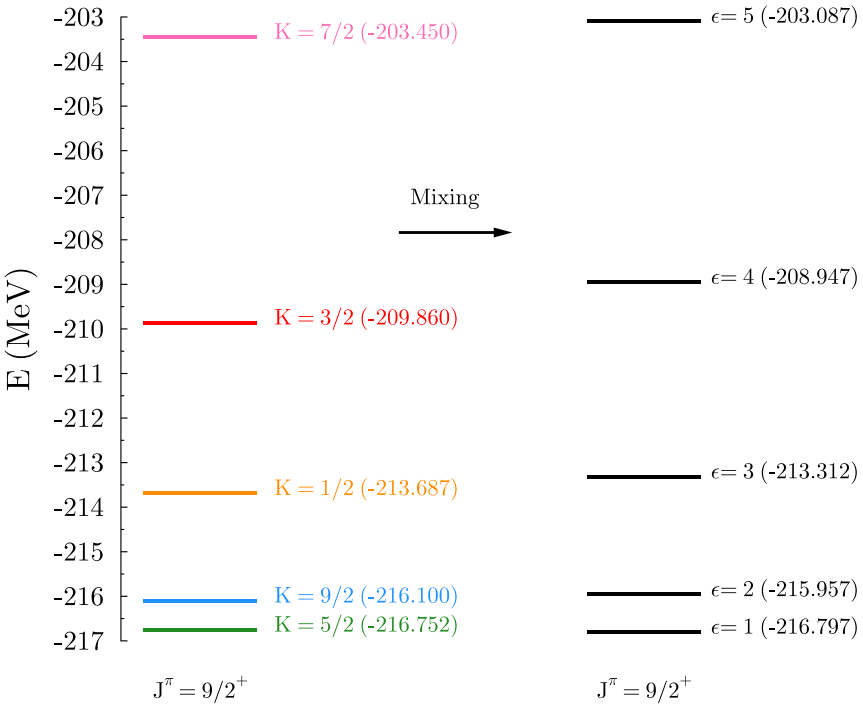

Figure 4.24: Mixing of the K components of $J^\pi = \frac{9}{2}^+$ for the one-quasiparticle state of Fig. 4.21.

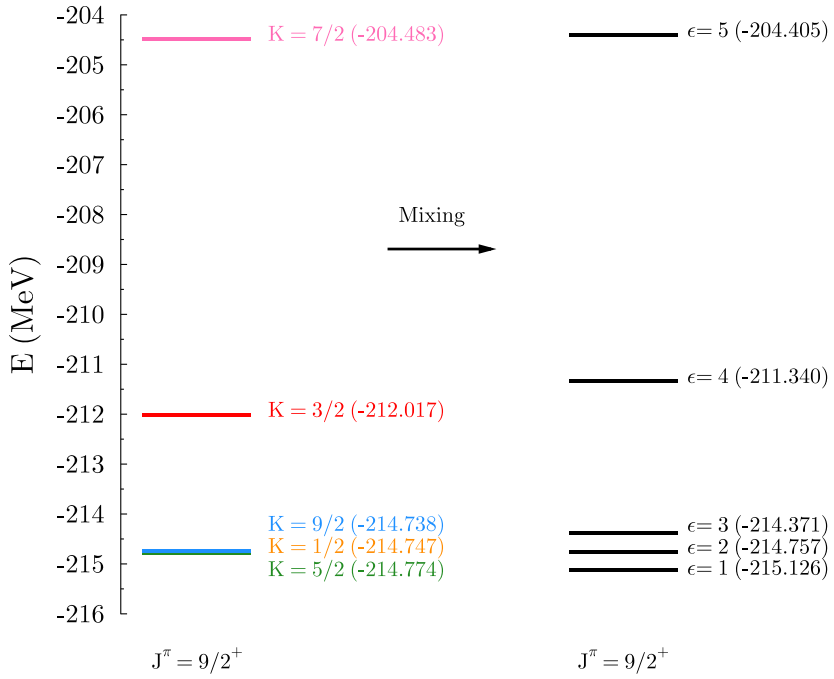

Figure 4.25: Mixing of the K components of $J^\pi = \frac{9}{2}^+$ for the one-quasiparticle state of Fig. 4.22.

4.3.3 J and K Decompositions

Equivalently to what has been done for PNR for N and Z components, we study the decomposition of the one-quasiparticle states into the $|JK\rangle$ basis functions. Given the fact that here we also project on particle-number, we define the weight of the basis function $|JK\rangle$ as

$$N^J_{KK} = \frac{\langle\Phi_a|\hat{P}^J_{KK}\hat{P}^N\hat{P}^Z|\Phi_a\rangle}{\langle\Phi_a|\hat{P}^N\hat{P}^Z|\Phi_a\rangle} = \frac{\sum_\tau |c^{JNZ\tau}_K|^2}{\sum_{JK\tau}|c^{JNZ\tau}_K|^2} \equiv |c^J_K|^2 \tag{4.4}$$

where τ labels the different irreps with same value of J, N and Z. Following the idea of [82], we define the total weight for a given J or a given K as

$$N^J = \sum_{K=-J}^{J} N^J_{KK} \tag{4.5}$$

$$N_K = \sum_J N^J_{KK} \tag{4.6}$$

which follow the sum rule

$$\sum_J N^J = \sum_K N_K = \sum_J \sum_{K=-J}^{J} |c^J_K|^2 = 1 \quad . \tag{4.7}$$

But anticipating the possible reaction of the readers, we prefer to state in advance that we will wait with the discussion of the numerical accuracy that can be achieved for the sum rule until section 4.3.4 on the numerical precision of the AMR. To examine how one-quasiparticle states are decomposed on the $|JK\rangle$ basis, we will consider a set composed of several one-quasiparticle states with different deformations that are presented and labeled in Fig. 4.26. All the considered one-quasiparticle states are of positive parity, but there is no reason to assume that negative parity states might behave differently, as the group $SU(2)_A$ associated with angular-momentum restoration has nothing to do with parity.

Sphericity

We will start by looking at the special case of spherical points for three different blocked one-quasiparticle states. It is important to understand that these points do not have an exact spherical symmetry, but are only constrained to have a spherical total mass density. For these states, all time-odd densities and currents are non-zero and do not exhibit spherical symmetry. Figure 4.27 (resp. Fig. 4.28 and Fig. 4.29) represents the decomposition of the one-quasiparticle A (resp. B and C), where a single-particle state with $j \approx 2.5$ (resp. $j \approx 0.5$ and $j \approx 1.5$) is blocked. One immediately sees that for all three one-quasiparticle states the main and almost only J component is the one with $J \approx j$. This is indeed the behavior one would expect from a state obtained by coupling a single-particle state with good j to a spherical core, but here the relation is not exact as one can see for the one-quasiparticle states A and C for which a very small, but non-zero, $J = \frac{1}{2}$ component exists. We also observe that K and $-K$ components have rigorously the exact same weight. This is, as already explained in section 3.4.3, a consequence of the $\hat{R}_x$ signature symmetry imposed on the one-quasiparticle states. For the one-quasiparticle state B that has an almost pure $J = \frac{1}{2}$, there are only two possible components with $|K| = \frac{1}{2}$. By contrast, for the one-quasiparticle state A one can also see $|K| = \frac{1}{2}$ components in addition to the dominating $|K| = \frac{5}{2}$ components, and we can see on the map of the N^J_{KK} (bottom panel of the figure) that these $|K| = \frac{1}{2}$ components do not belong only to the $J = \frac{1}{2}$ but also to the

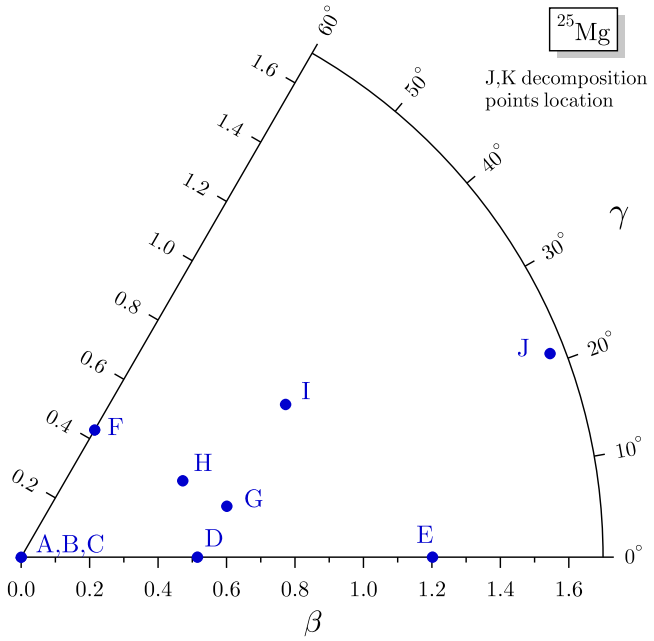

Figure 4.26: Location in the (β, γ) plane of the one-quasiparticle states used in the analysis of $|JK\rangle$ components.

$J = \frac{5}{2}$. Indeed, this one-quasiparticle state has been converged, starting from a false vacuum where we decided to block a single-particle state with $k \approx 2.5$, but nothing prevents the three different degenerated single-particle states with $j \approx 2.5$, and same conserved quantum numbers, i.e. positive parity and signature $-i$, to be arbitrarily mixed during the iterative solution of the HFB equations. In the end, we can say that at the spherical point, one-quasiparticle states present a very simple decomposition which mimics the behavior of states with good angular-momentum, with a very strong, but not pure, J component corresponding to the j of the blocked single-particle state.

Prolate Along the Quantization Axis

We now turn our attention to the quasiparticle states D and E (Fig. 4.30 and 4.31 respectively) that have been constrained to have an axial deformation of the total mass density $\rho(\vec{r})$ along the z-axis, which is also used as the quantization axis for angular momenta. With the symmetries of our codes, nothing prevents the other densities from being non-axial for these states. Nevertheless, from what can be seen in Fig. 4.30 and 4.31, alike axially symmetric states, those states have almost pure[5] $|K| = \frac{1}{2}$ and $|K| = \frac{5}{2}$ components, respectively, for the one-quasiparticle states D and E. Here the K values are dictated by the k of the blocked single-particle state, which is $k \approx 0.5$ for one-quasiparticle state D and $k \approx 2.5$ for one-quasiparticle state E. It is to be noted that prolate deformation along the x- or y-axis could result in very different K decompositions. In contrast to spherical states, the two prolate states have wide distributions of J components, but different in each case. For one-quasiparticle state D, the distribution presents significant components only up to $J = \frac{15}{2}$ and has a stagggered distribution where every other J is favoured, i.e. the components $J = \frac{3}{2}, \frac{7}{2}, \frac{11}{2}, \ldots$ are bigger[6] than the components $J = \frac{5}{2}, \frac{9}{2}, \frac{13}{2}, \ldots$ By con-

[5] It is exactly pure for axially symmetric states.

[6] This is a has nothing to do with the signature of the blocked one-quasiparticle.

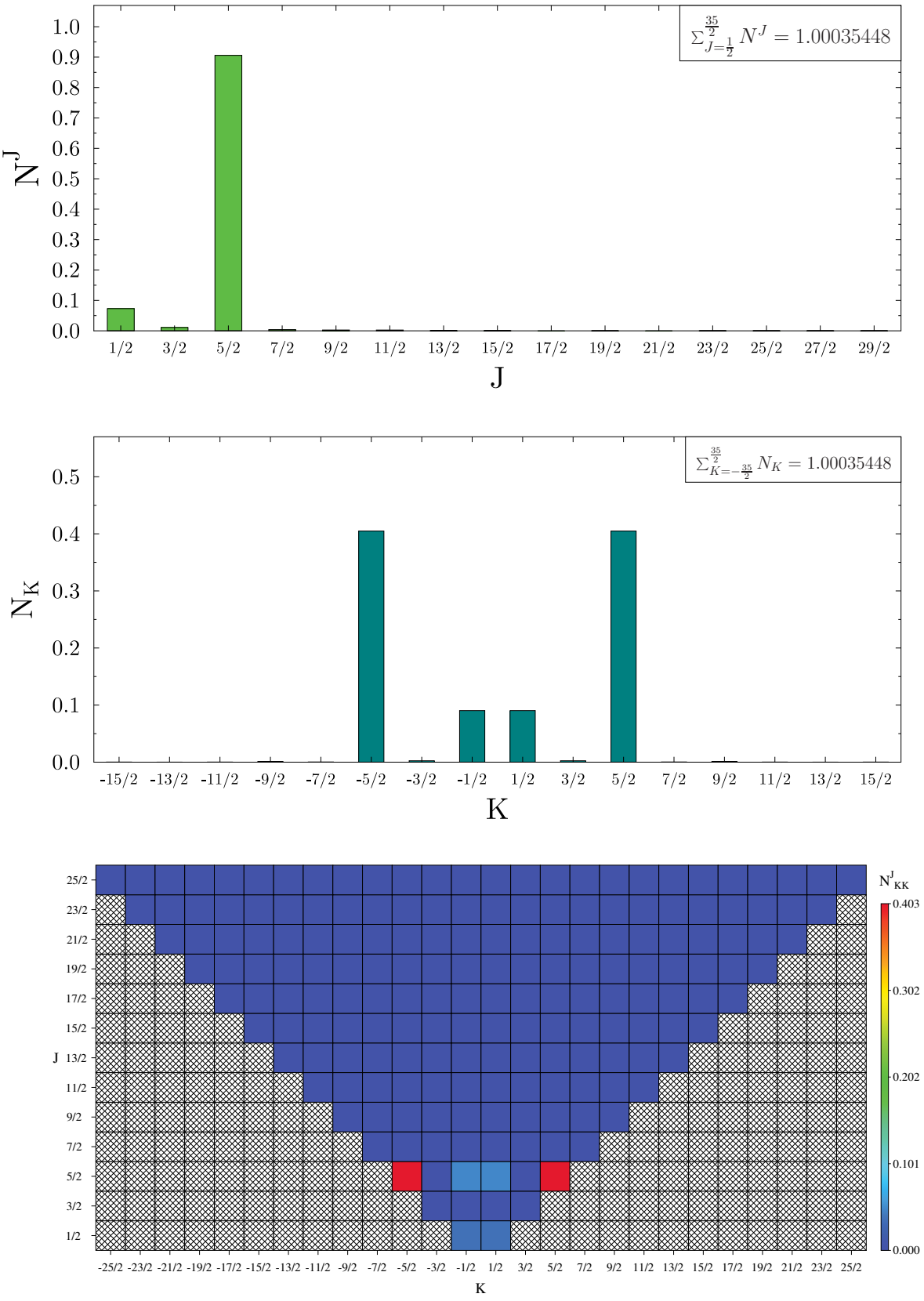

Figure 4.27: Top : Total weight N^J of J components for the one-quasiparticle state A. Center: Same for the total weight N_K of K components. Bottom: Weight N^J_{KK} of each $|JK\rangle$ component.

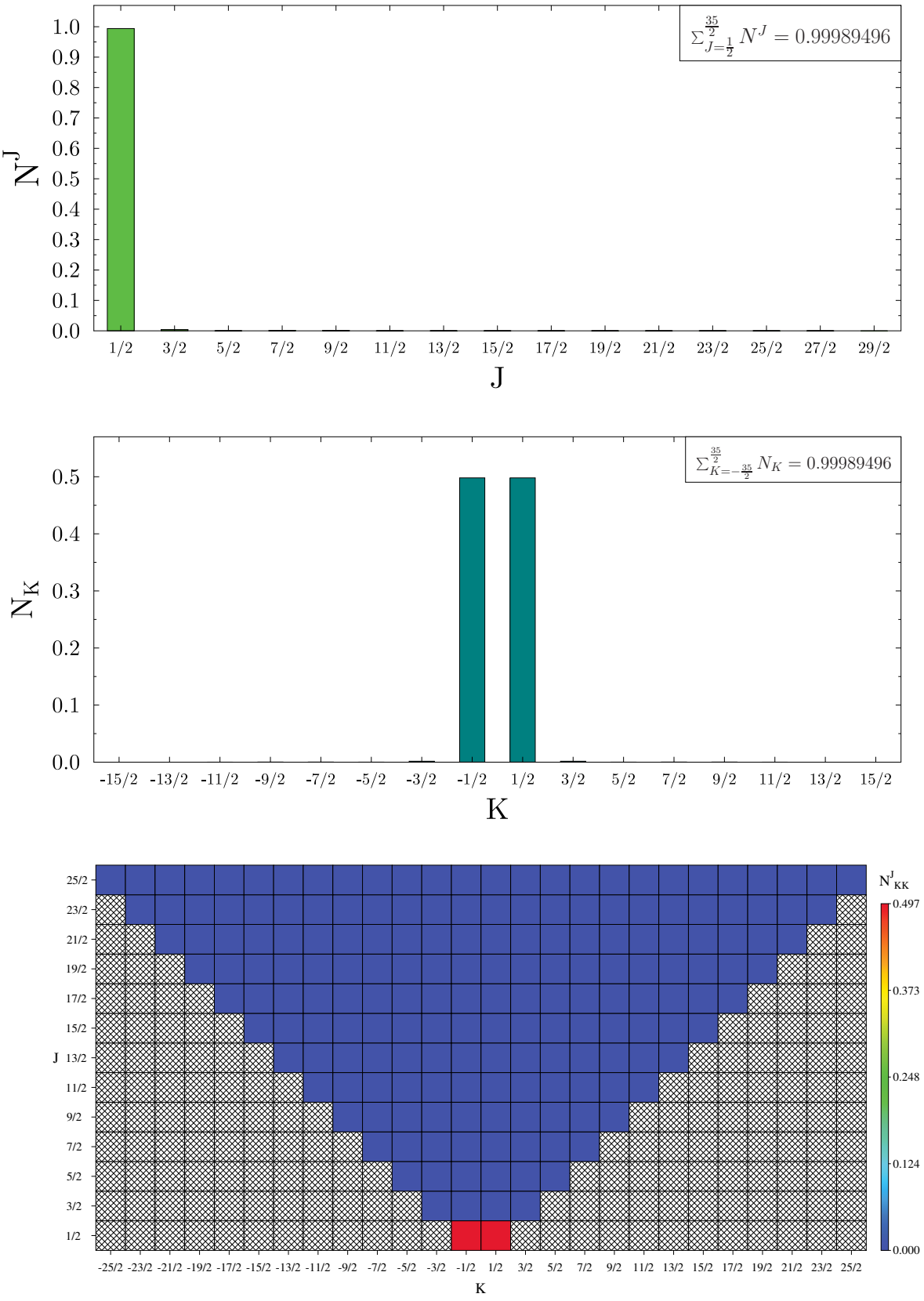

Figure 4.28: Top : Total weight N^J of J components for the one-quasiparticle state B. Center: Same for the total weight N_K of K components. Bottom: Weight N^J_{KK} of each $|JK\rangle$ component.

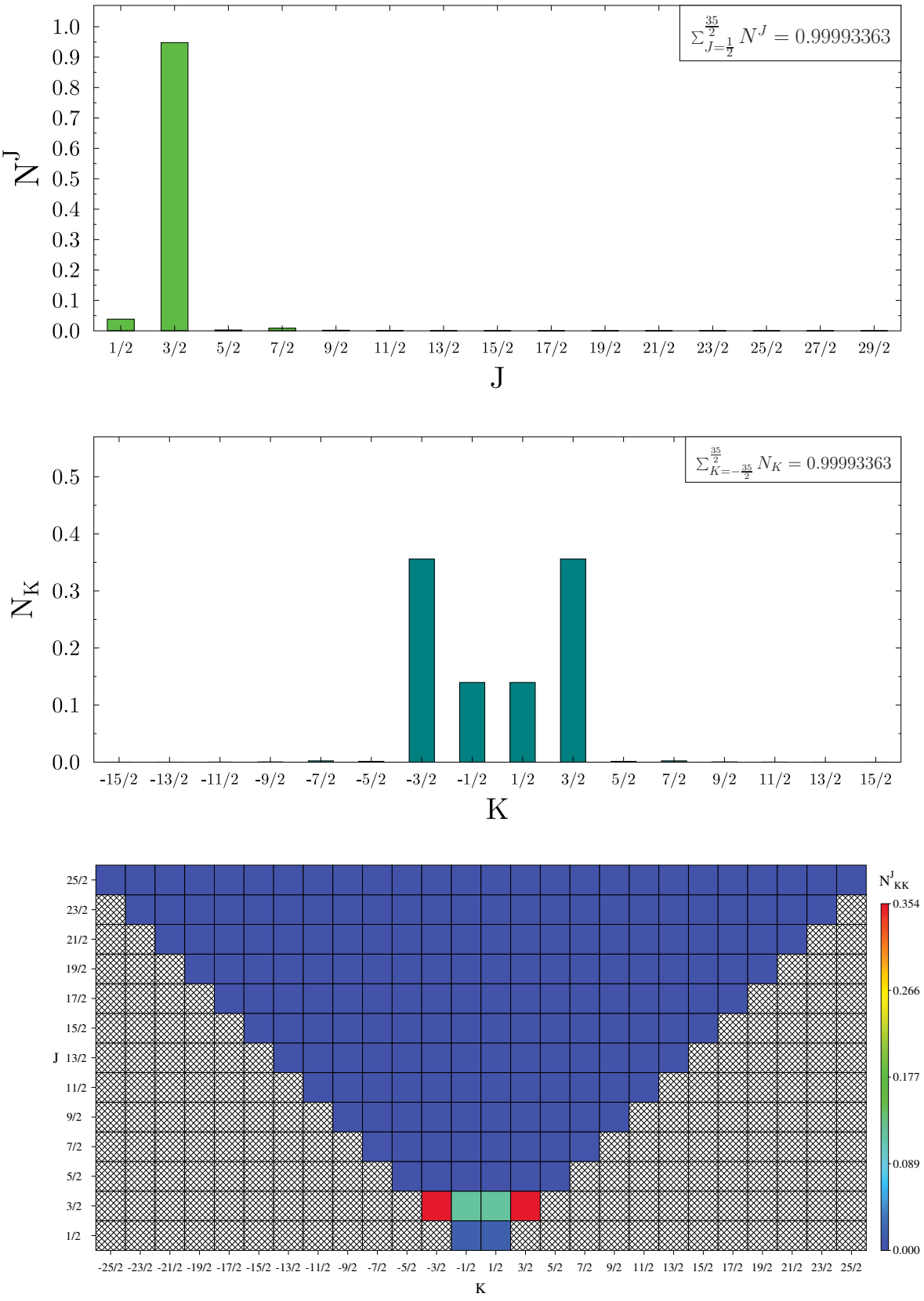

Figure 4.29: Top : Total weight N^J of J components for the one-quasiparticle state C. Center: Same for the total weight N_K of K components. Bottom: Weight N^J_{KK} of each $|JK\rangle$ component.

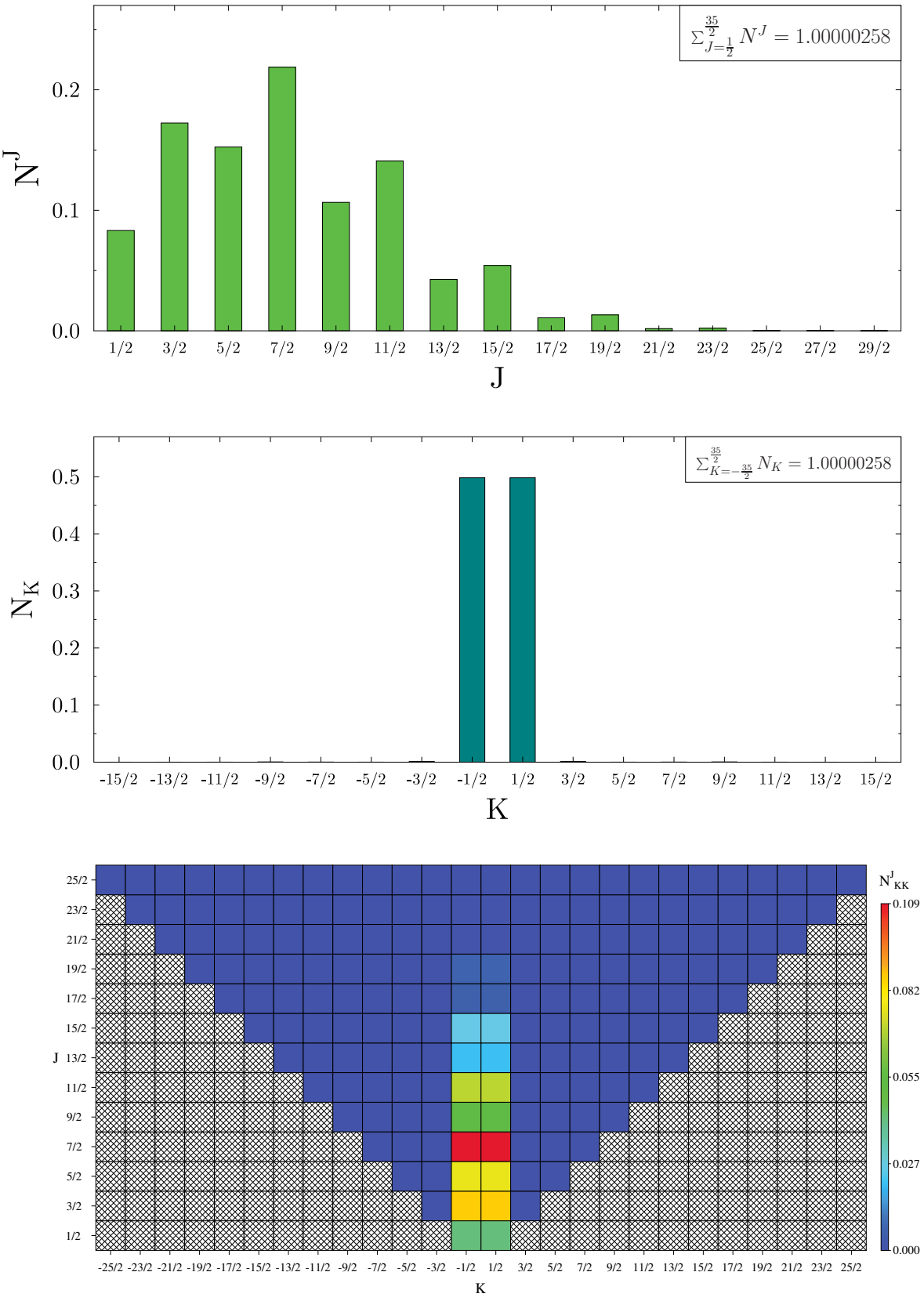

Figure 4.30: Top : Total weight N^J of J components for the one-quasiparticle state D. Center: Same for the total weight N_K of K components. Bottom: Weight N^J_{KK} of each $|JK\rangle$ component.

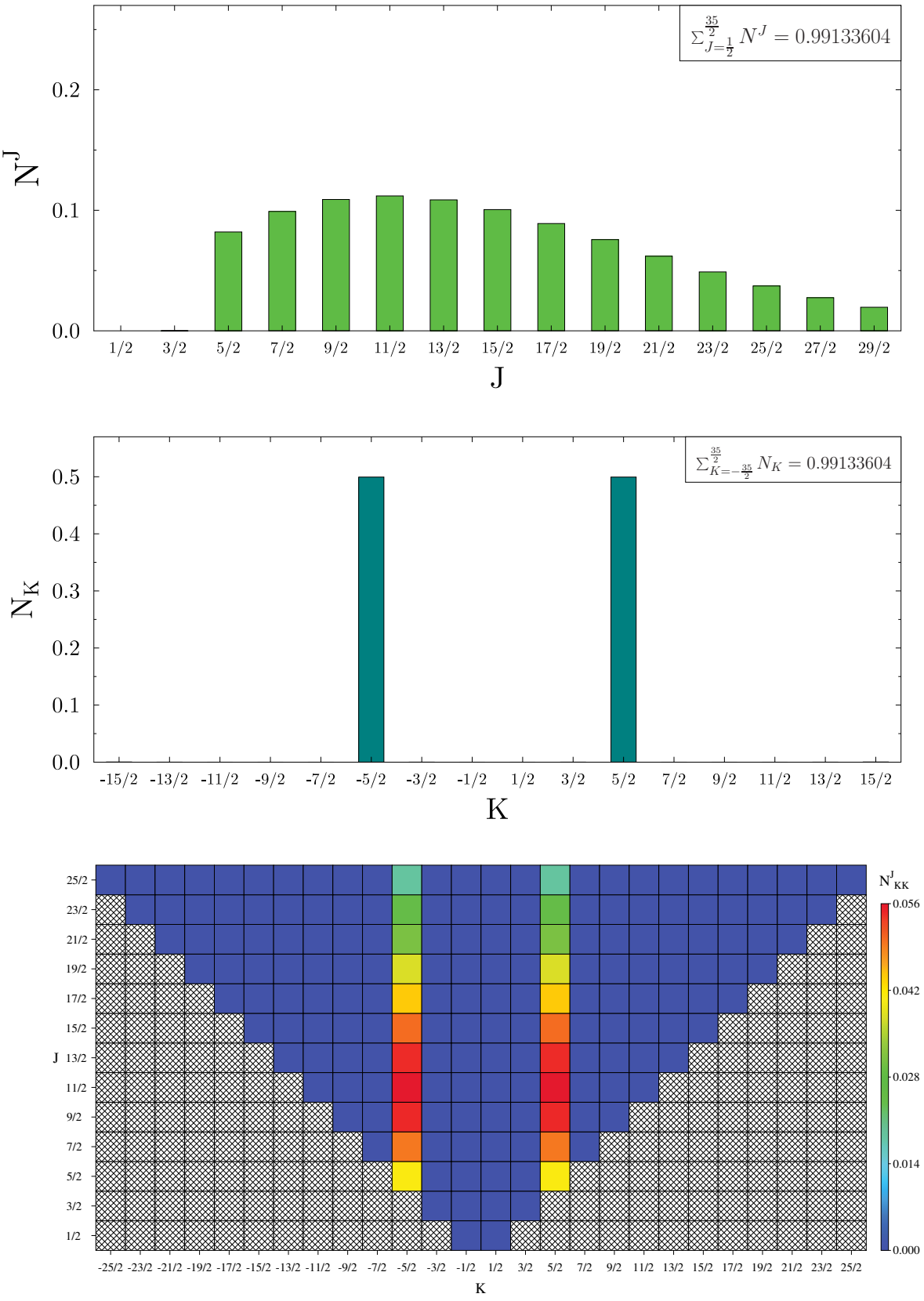

Figure 4.31: Top : Total weight N^J of J components for the one-quasiparticle state E. Center: Same for the total weight N_K of K components. Bottom: Weight N^J_{KK} of each $|JK\rangle$ component.

trast, the distribution of J components of one-quasiparticle E state is a lot wider, with a long tail continuing up to $J = \frac{29}{2}$ (and even higher) and, contrary to the previous case, this time the distribution is relatively "continuous", except for $J = \frac{1}{2}$ and $J = \frac{3}{2}$ components that are vanishing. The distribution only starts at $J = \frac{5}{2}$ because we have a (almost) pure $|K| = \frac{5}{2}$, and J cannot be smaller than $|K|$.

Oblate Deformation Perpendicular to the Quantization Axis

For the case of the one-quasiparticle state F with an oblate deformation along the y-axis one obtains Fig. 4.32. In contrast to what has been seen in the cases discussed above, here the decomposition is spread over several J and K components, and in particular it seems that for a given value of J the states prefer the components with an high value of $|K|$. As the oblate states are relatively high in energy in our case, I have decided not comment further their structure. I apologize to the reader who would like to learn more on the subject.

Triaxiality

Finally, we conclude this analysis of the decomposition of one-quasiparticle states in terms of $|JK\rangle$ basis functions by looking at the more general case of triaxial deformations (in the first sextant of the (β, γ) plane). We have selected for that four different one-quasiparticle states: the quasiparticle state G (Fig. 4.34) that corresponds to the minimum for $J^\pi = \frac{1}{2}^+$ and $J^\pi = \frac{3}{2}^+$, the quasiparticle state H (Fig. 4.33), which is the one that gives the minimum for $J^\pi = \frac{5}{2}^+$, the quasiparticle state I (Fig. 4.35), which has deformation with $\gamma = 30°$, and, finally, the quasiparticle state J (Fig. 4.36), which is the most deformed state that will be used in the GCM presented lateron. As a general comment we can say that all the triaxial points have N^J and N_K distributed over a wide range of J and K values. We can note in particular that starting from the point state G, which is the closest to axial deformation and going to states with higher value of γ like the states H and I, the weights N_K tend to be more and more spread over the possible values of K.
Moving towards greater β from H to I and finally J, it is the weights N^J which become also more and more evenly distributed, with the center of the distribution being shifted to higher values of J. This is also what one can observe for the two prolate quasiparticle states D and E, the latter being more deformed and possessing a wider N^J distribution. The net result of the two effects (greater β and γ closer to 30°) is that the components N^J_{KK} become more and more uniformly dispersed over a wider and wider range of J and K values, and hence logically the biggest component N^J_{KK} in each distribution is becoming smaller and smaller.

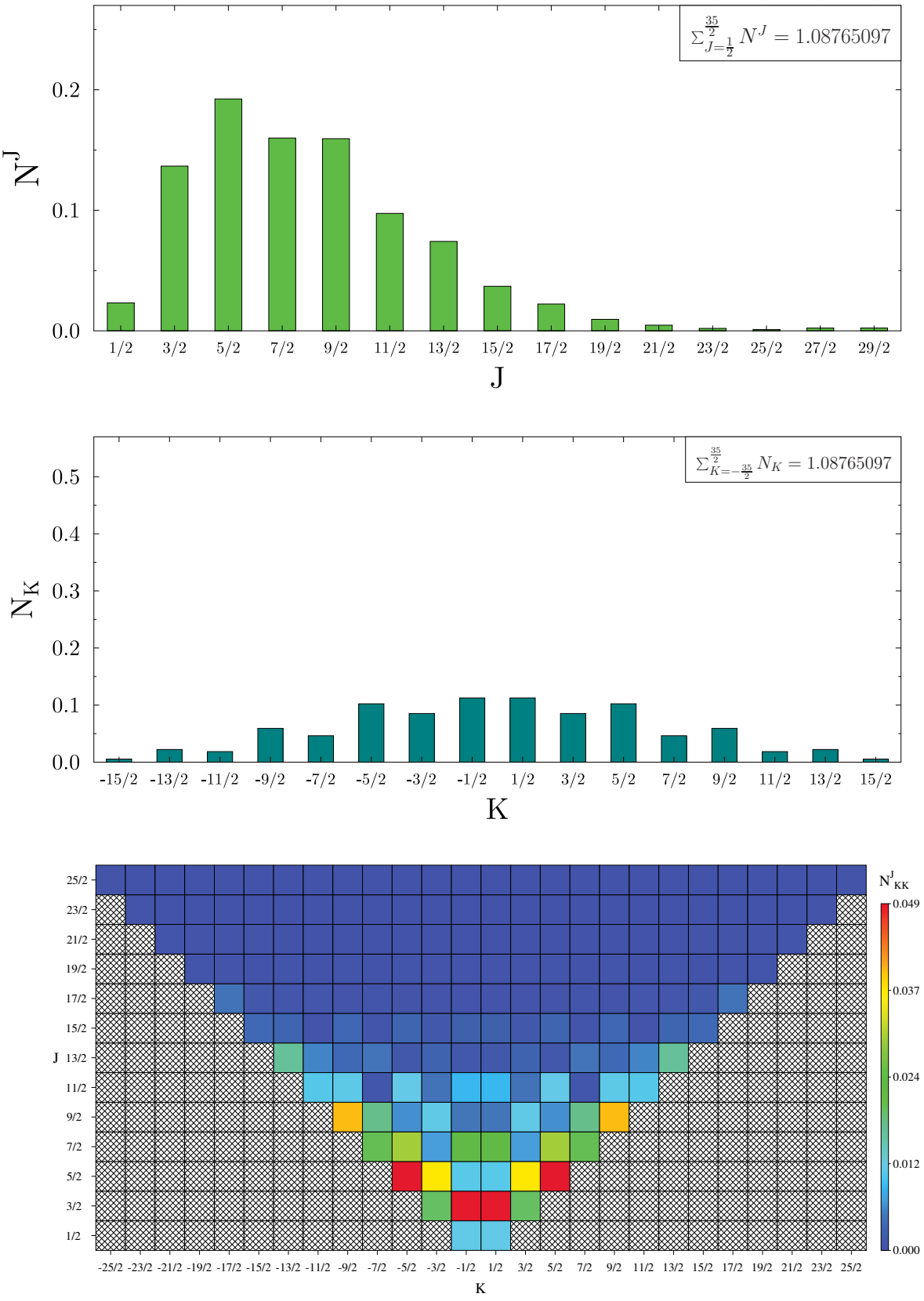

Figure 4.32: Top : Total weight N^J of J components for the one-quasiparticle state F. Center: Same for the total weight N_K of K components. Bottom: Weight N^J_{KK} of each $|JK\rangle$ component.

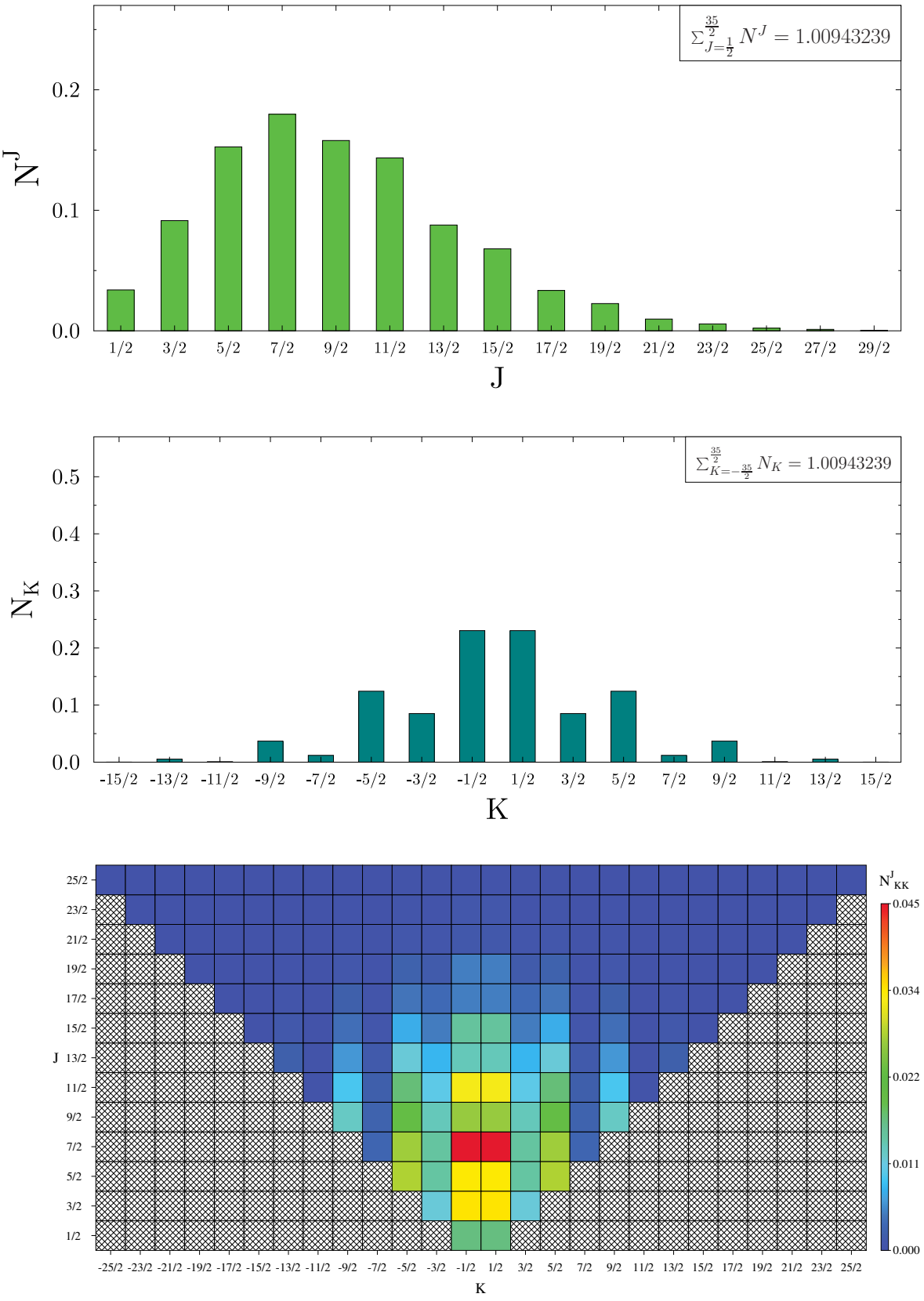

Figure 4.33: Top : Total weight N^J of J components for the one-quasiparticle state G. Center: Same for the total weight N_K of K components. Bottom: Weight N^J_{KK} of each $|JK\rangle$ component.

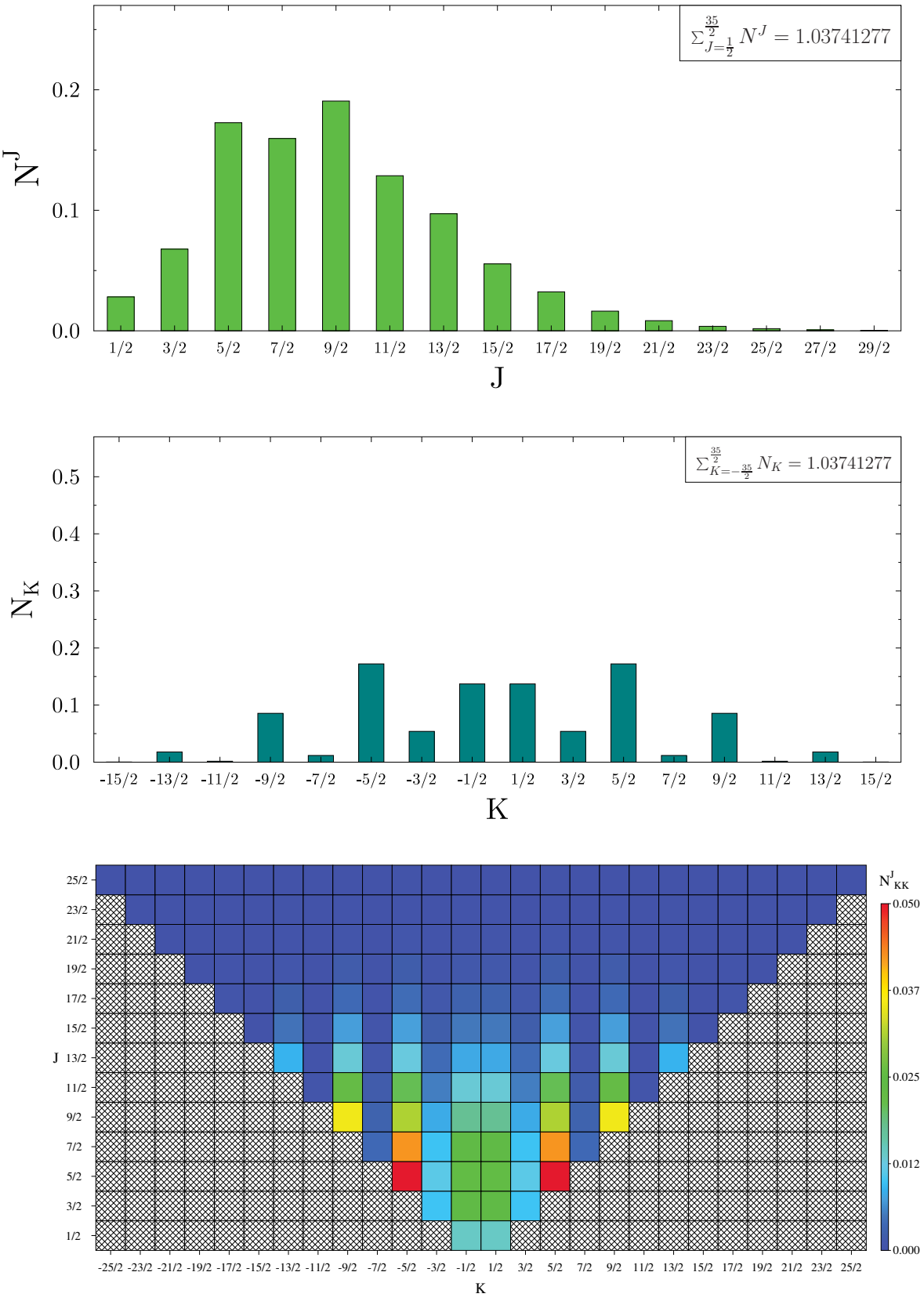

Figure 4.34: Top : Total weight N^J of J components for the one-quasiparticle state H. Center: Same for the total weight N_K of K components. Bottom: Weight N^J_{KK} of each $|JK\rangle$ component.

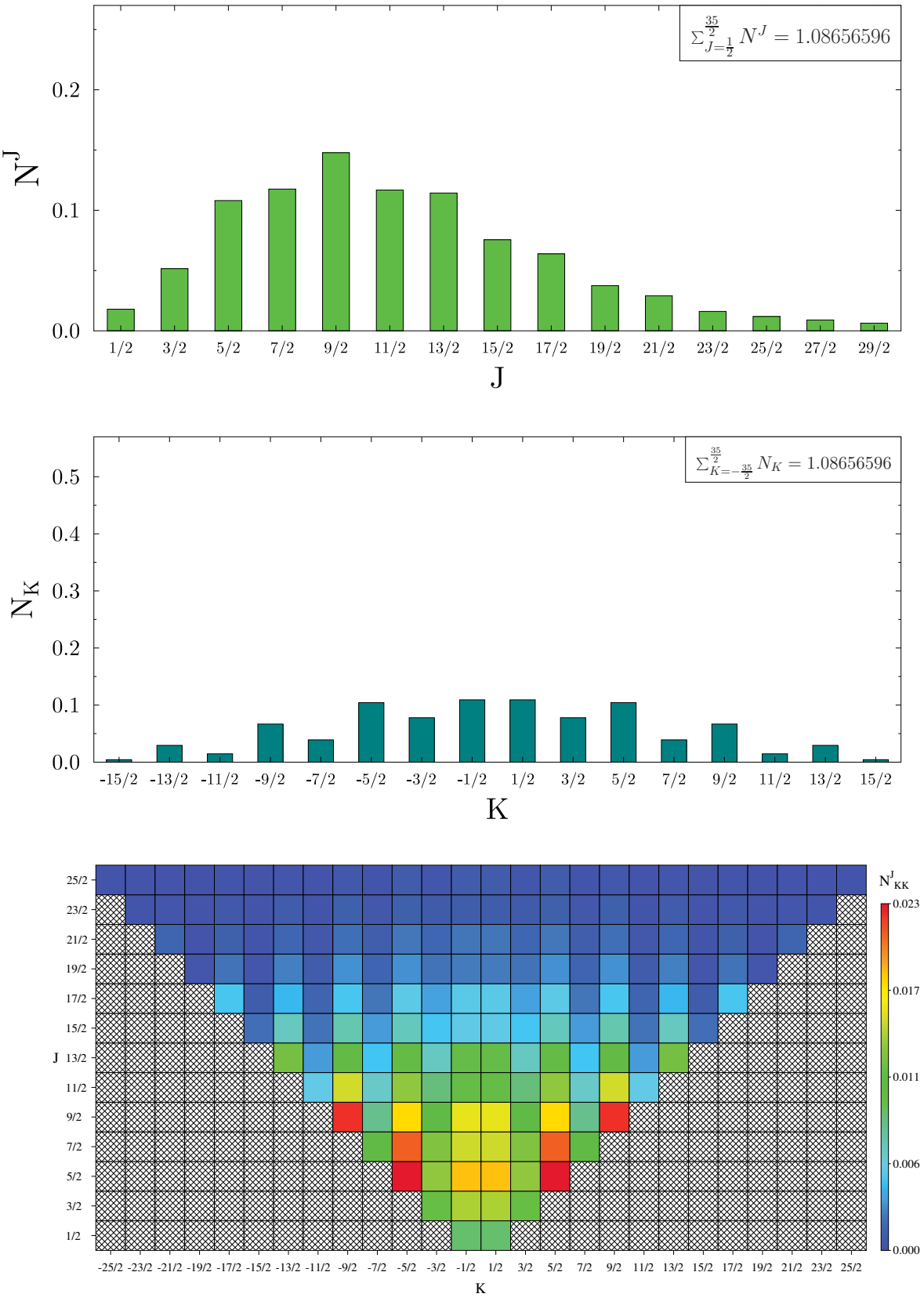

Figure 4.35: Top : Total weight N^J of J components for the one-quasiparticle state I. Center: Same for the total weight N_K of K components. Bottom: Weight N^J_{KK} of each $|JK\rangle$ component.

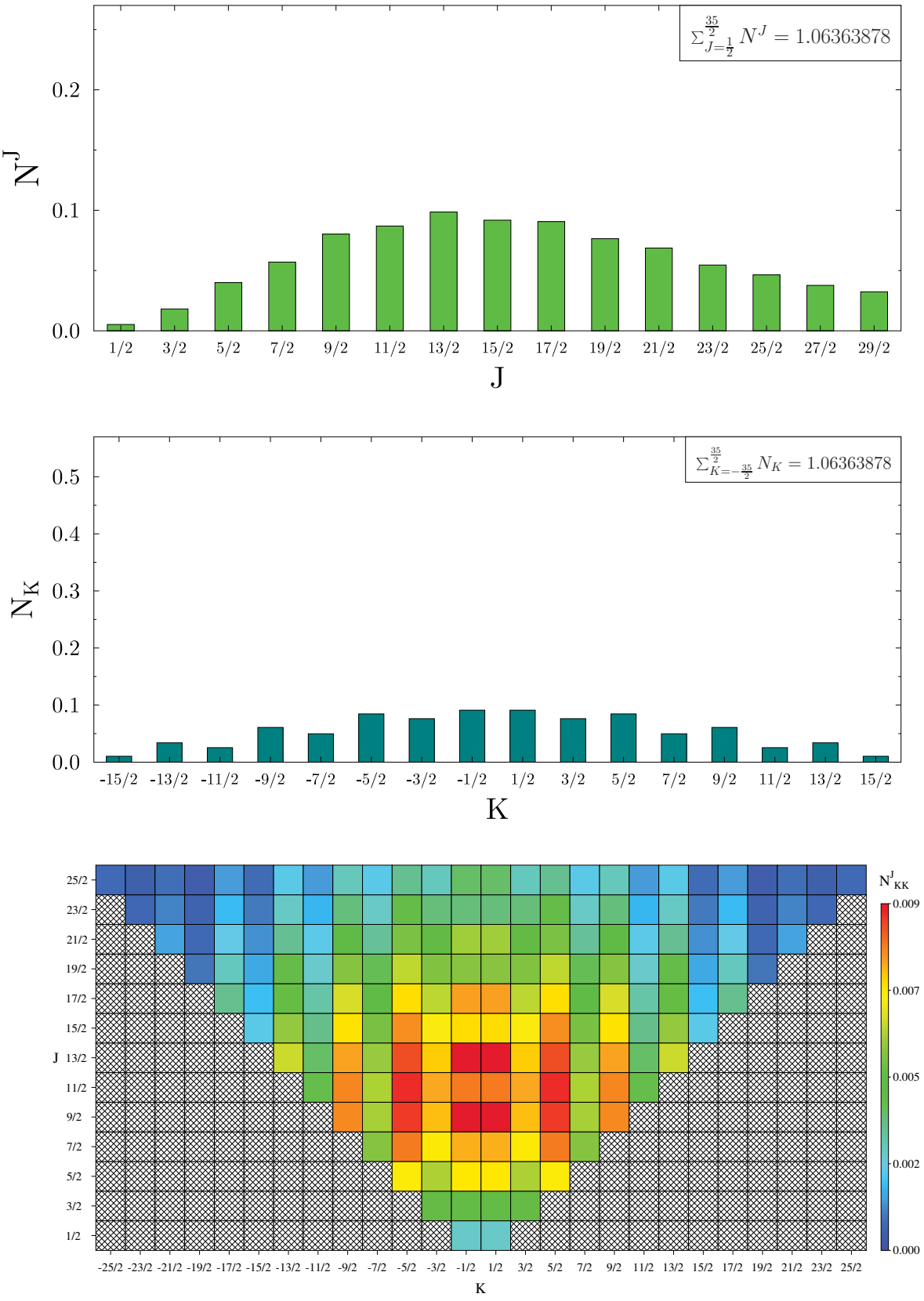

Figure 4.36: Top : Total weight N^J of J components for the one-quasiparticle state J. Center: Same for the total weight N_K of K components. Bottom: Weight N^J_{KK} of each $|JK\rangle$ component.

$n_\alpha \times n_\beta \times n_\gamma$	D	E	G	H	I	J
$16 \times 40 \times 16$	2.98251156	1.88891698	2.57350710	2.37338601	2.32498212	2.02265138
$20 \times 40 \times 20$	1.00113408	1.39650939	1.32295856	1.59261704	1.52678331	1.39559136
$24 \times 40 \times 24$	1.00000258	0.99133604	1.00943239	1.03741277	1.08656596	1.06363878
$28 \times 40 \times 28$	1.00000167	0.99097674	0.99999306	1.00015094	1.00529123	0.98364401
$32 \times 40 \times 32$	1.00000150	0.99097638	0.99997727	0.99998013	0.99946720	0.97479191

Table 4.2: Sum rule $\sum_{J=\frac{1}{2}}^{\frac{35}{2}} N^J$ for different one-quasiparticle states and different discretization of the integrals over Euler angles. The red line indicates the discretization chosen in this work.

4.3.4 AMR Precision and Convergence

The attentive reader will have noticed that the accuracy of the sum rule for the $|c_K^J|^2$, written at the top right of each N^J and N_K decomposition, is very contrasted depending of the state, and, even in the best cases, is clearly not as accurate as what we saw for the specific sum rule of PNR. Some states, like one-quasiparticle D, have an accuracy better than 10^{-5} but others, like state F, show a sum rule accuracy no better than 10^{-1}. From a general point of view states with wider J and K distributions tend to have a poorer sum rule accuracy. Because of this numerical inaccuracy in our calculations, the N^J and N_K distributions plotted above shall be taken, for small components or for components with high value of J or K, more as a guidline for the eyes than precise numbers.

Increasing the total number of points in the discretization of the integrals over Euler angles from the selected values for this work of ($n_\alpha = 24$, $n_\beta = 40$, $n_\gamma = 24$) to ($n_\alpha = 32$, $n_\beta = 40$, $n_\gamma = 32$)[7], we can observe in Tab. 4.2 an improvement in the accuracy of the sum rule for some, but not all, states. The accuracy achieved for the most deformed states remains rather unsatisfactory. Anyway, planning for a large configuration mixing of several tens of states through the GCM and due to the numerical cost of the angular-momentum projection, it was not possible to choose a discretization of ($n_\alpha = 32$, $n_\beta = 40$, $n_\gamma = 32$) points for the integrals over Euler angles.

To evaluate in more detail the accuracy achieved in AMR calculations, we display in Tab. 4.3, 4.4, 4.5, 4.6, and 4.7, the weight N_{KK}^J, the energy, and the angular momentum J_e obtained from equation $\langle J^2 \rangle = J_e(J_e+1)$, for a selected set of components and for different discretization of the integrals over Euler angles. The first thing we can notice in Tab. 4.3 is that the choice of points for the discretization of β is sufficient, as none of the quantities significantly change as we increase the number of points in the integral. For α and γ it is more contrasted, but overall the states with the largest values of N_{KK}^J seem to be also sufficiently well converged for the discretization chosen in this work. Actually, what we can notice from those tables is that it is not only the values of J and K, and thus not only the number of points in the discretization of Euler angles, which play an important role for the precision of the AMR, but also how big the component N_{KK}^J is. For example, the state with $J = \frac{13}{2}$ and $K = \frac{13}{2}$ in Tab. 4.3 or the state with $J = \frac{15}{2}$, $K = \frac{5}{2}$ in Tab. 4.5, are better converged than the state with $J = \frac{5}{2}$, $K = \frac{5}{2}$ in Tab. 4.4, even taking denser discretization for the latter than for the former. So increasing the number of points in the discretization of the integrals will help to get more precise results for small components, but it may not be enough. Another numerical parameter whose influence

[7] As we will see below, the number of points for β is already more than sufficient, this is why we did not increased it here.

	One-quasiparticle H								
	$J = 5/2 \quad K = 5/2$			$J = 13/2 \quad K = 11/2$			$J = 13/2 \quad K = 13/2$		
Discretization ($\alpha \times \beta \times \gamma$)	N^J_{KK}	Energy (MeV)	$\langle J^2 \rangle \to J_e$	N^J_{KK}	Energy (MeV)	$\langle J^2 \rangle \to J_e$	N^J_{KK}	Energy (MeV)	$\langle J^2 \rangle \to J_e$
PNR Only	-	-213.30718652	-	-	-213.30718652	-	-	-213.30718652	-
24×24×24	0.03839964	-220.74685190	2.50008452	0.00031517	-187.86638937	6.49973262	0.00680337	-206.37170853	6.50004136
24×32×24	0.03839964	-220.74685124	2.50008452	0.00031517	-187.86642113	6.49973269	0.00680337	-206.37175171	6.50004137
24×40×24	0.03839963	-220.74685217	2.50008448	0.00031517	-187.86630766	6.49972976	0.00680337	-206.37175866	6.50004146
24×48×24	0.03839964	-220.74685544	2.50008452	0.00031517	-187.86624952	6.49973268	0.00680337	-206.37170959	6.50004137
24×56×24	0.03839964	-220.74685368	2.50008452	0.00031517	-187.86613604	6.49973268	0.00680337	-206.37173016	6.50004137
16×40×16	0.03839971	-220.74647042	2.50014265	0.00033296	-186.29835678	6.80395418	0.00681558	-206.25509952	6.50636675
20×40×20	0.03839964	-220.74696740	2.50008626	0.00031520	-187.87880377	6.50120381	0.00680350	-206.37102286	6.50023740
24×40×24	0.03839963	-220.74685217	2.50008448	0.00031517	-187.86630766	6.49972976	0.00680337	-206.37175866	6.50004146
28×40×28	0.03839964	-220.74677579	2.50008411	0.00031517	-187.87949327	6.49966826	0.00680337	-206.37300996	6.50003462
32×40×32	0.03839964	-220.74681512	2.50008376	0.00031517	-187.86922801	6.49967040	0.00680337	-206.37288026	6.50003378

Table 4.3: One-quasiparticle H: Precision of the Angular-Momentum Restorartion as a function of the number of points used in discretization of the AMR integrals. The red line indicates the discretization chosen in this work.

	One-quasiparticle D								
	$J = 3/2 \quad K = 1/2$			$J = 5/2 \quad K = 1/2$			$J = 5/2 \quad K = 5/2$		
Discretization ($\alpha \times \beta \times \gamma$)	N^J_{KK}	Energy (MeV)	$\langle J^2 \rangle \to J_e$	N^J_{KK}	Energy (MeV)	$\langle J^2 \rangle \to J_e$	N^J_{KK}	Energy (MeV)	$\langle J^2 \rangle \to J_e$
PNR Only	-	-214.87949912	-	-	-214.87949912	-	-	-214.87949912	-
16×40×16	0.05547655	-218.80656650	1.50013275	0.04905819	-216.75019876	2.50004935	0.00000152	-196.01209172	2.50188417
20×40×20	0.05547654	-218.80732033	1.50012916	0.04905818	-216.75085685	2.50004858	0.00000152	-195.93578131	2.50215318
24×40×24	0.05547654	-218.80732809	1.50012531	0.04905818	-216.75099661	2.50004502	0.00000152	-195.90167169	2.50207959
28×40×28	0.05547654	-218.80705581	1.50012613	0.04905818	-216.75066873	2.50004527	0.00000152	-195.86814833	2.50200796
32×40×32	0.05547654	-218.80714428	1.50012558	0.04905818	-216.75077054	2.50004485	0.00000152	-195.84601600	2.50203080

Table 4.4: One-quasiparticle D: Precision of the Angular-Momentum Restorartion as a function of the number of points used in discretization of the AMR integrals. The red line indicates the discretization chosen in this work.

	One-quasiparticle J								
	$J = 15/2 \quad K = 5/2$			$J = 15/2 \quad K = 15/2$			$J = 25/2 \quad K = 25/2$		
Discretization ($\alpha \times \beta \times \gamma$)	N^J_{KK}	Energy (MeV)	$\langle J^2 \rangle \to J_e$	N^J_{KK}	Energy (MeV)	$\langle J^2 \rangle \to J_e$	N^J_{KK}	Energy (MeV)	$\langle J^2 \rangle \to J_e$
PNR Only	-	-179.22534237	-	-	-179.22534237	-	-	-179.22534237	-
16×40×16	0.00431931	-185.34623090	7.53097440	0.00275874	-171.10433543	8.07743074	0.00846153	-182.64225172	4.72540760
20×40×20	0.00430822	-185.50266494	7.50207884	0.00128567	-165.97077673	8.25171852	0.00195289	-165.65269974	8.45869660
24×40×24	0.00430782	-185.50980438	7.50033819	0.00113342	-167.98837923	7.59073769	0.00039507	-147.11434939	12.13028528
28×40×28	0.00430780	-185.51050504	7.50026658	0.00112600	-168.29959319	7.50364212	0.00024982	-148.13556628	12.58856466
32×40×32	0.00430781	-185.51046524	7.50026175	0.00112578	-168.31354160	7.49922389	0.00024297	-149.04018037	12.50423223

Table 4.5: One-quasiparticle J: Precision of the Angular-Momentum Restorartion as a function of the number of points used in discretization of the AMR integrals. The red line indicates the discretization chosen in this work.

	One-quasiparticle I								
	$J = 3/2 \quad K = 1/2$			$J = 5/2 \quad K = 1/2$			$J = 17/2 \quad K = 13/2$		
Discretization ($\alpha \times \beta \times \gamma$)	N^J_{KK}	Energy (MeV)	$\langle J^2 \rangle \to J_e$	N^J_{KK}	Energy (MeV)	$\langle J^2 \rangle \to J_e$	N^J_{KK}	Energy (MeV)	$\langle J^2 \rangle \to J_e$
PNR Only	-	-195.43827595	-	-	-195.43827595	-	-	-195.43827595	-
16×40×16	0.00503590	-206.23690556	1.51167980	0.00651381	-205.37484327	2.50973593	0.00153459	-184.98925340	8.57563636
20×40×20	0.00503508	-206.24876711	1.50097826	0.00651250	-205.38893537	2.50066488	0.00148695	-185.87436513	8.50806435
24×40×24	0.00503506	-206.24896562	1.50074024	0.00651247	-205.38920078	2.50044019	0.00148521	-185.93541919	8.49996264
28×40×28	0.00503506	-206.24903567	1.50073635	0.00651247	-205.38926931	2.50043585	0.00148518	-185.93926318	8.49964470
32×40×32	0.00503506	-206.24900856	1.50073545	0.00651247	-205.38923701	2.50043512	0.00148518	-185.93837761	8.49963494

Table 4.6: One-quasiparticle I: Precision of the Angular-Momentum Restorartion as a function of the number of points used in discretization of the AMR integrals. The red line indicates the discretization chosen in this work.

	One-quasiparticle G								
	$J = 7/2 \quad K = 3/2$			$J = 7/2 \quad K = 5/2$			$J = 7/2 \quad K = 7/2$		
Discretization ($\alpha \times \beta \times \gamma$)	N^J_{KK}	Energy (MeV)	$\langle J^2 \rangle \to J_e$	N^J_{KK}	Energy (MeV)	$\langle J^2 \rangle \to J_e$	N^J_{KK}	Energy (MeV)	$\langle J^2 \rangle \to J_e$
PNR Only	-	-213.21421625	-	-	-213.21421625	-	-	-213.21421625	-
16×40×16	0.01059686	-213.35294827	3.50005402	0.01959151	-217.10835611	3.50007184	0.00207752	-206.10280097	3.50049851
20×40×20	0.01059686	-213.35319466	3.50004234	0.01959150	-217.10872512	3.50006685	0.00207747	-206.10426861	3.50007238
24×40×24	0.01059686	-213.35323152	3.50004160	0.01959150	-217.10874941	3.50006543	0.00207748	-206.10343169	3.50008912
28×40×28	0.01059686	-213.35316558	3.50004101	0.01959150	-217.10860971	3.50006534	0.00207748	-206.10541633	3.50007835
32×40×32	0.01059686	-213.35323747	3.50004038	0.01959150	-217.10867303	3.50006492	0.00207748	-206.10562070	3.50007605

Table 4.7: One-quasiparticle G: Precision of the Angular-Momentum Restorartion as a function of the number of points used in discretization of the AMR integrals. The red line indicates the discretization chosen in this work.

shall be checked is the number of points, and their spacing, in the 3D cartesian mesh. Indeed, such a mesh is not particularly well suited to perform a rotation of the wave functions, as it is required in the angular momentum projection.
Also, another interesting remark we want to make is that, for a given one-quasiparticle state, states with small value of N^J_{KK} tend to have higher energy (e.g. Tab. 4.7). It is not always true (e.g. Tab. 4.6), but it is nevertheless a very strong trend in all calculations we have looked at in detail.

From this analysis, we are confident that the number of points chosen in this work for the discretization of the integrals over Euler angles is sufficient for the largest components which we expect to play the principal role in the configuration mixing. And to eliminate the imprecise components that could pollute our calculations, we add two cut-offs before K-mixing. The first one remove states with

$$|J_e - J| > 5.10^{-3} \quad ,$$

where J is the angular momentum we project the state on. The second cut-off removes states with a weight

$$N^J_{KK} < 1.10^{-5} \quad .$$

These particular values for the cut-offs have been chosen after trial and error, in order to remove the most problematic components while not removing too many components. For example, with such choice of cut-off, we will remove the state $J = \frac{5}{2}$, $K = \frac{5}{2}$ in Tab. 4.4, the states $J = \frac{15}{2}$, $K = \frac{15}{2}$ and $J = \frac{25}{2}$, $K = \frac{25}{2}$ in Tab. 4.5, but not the state $J = \frac{13}{2}$, $K = \frac{11}{2}$ in Tab. 4.3. The former is not necessarily fully well represented with our numerical parameter, but an error of few keV or tens of keV on a state with an energy more than 30 MeV higher than the minimum ($\approx$ 221 MeV) should not be too much of an issue.

Finally, to be on the safe side, we will consider only components up to $J = \frac{15}{2}$ and $K = \frac{15}{2}$ in our configuration mixing. Indeed, components with higher value of J or K have the double disadvantage that they may require a denser discretization of the integrals over Euler angles and, that their weights in the lowest energy one-quasiparticle states tend to be small. Also, in the experimental data, the first identified $J = \frac{15}{2}$ state appears at approximately 10 MeV and in this first calculation we do not aim at the complete description of such high-lying states.

4.3.5 Other Sextants of the (β, γ) Plane

Up until now, we have discussed only the results for one-quasiparticle states constructed in one sextant, with $0° \leq \gamma \leq 60°$, of the (β, γ) plane. But as discussed for example by Schunck *et al.* [129], and contrary to even-even systems with time-reversal invariance [112], for one-quasiparticle states all the sextants are not equivalent. Depending on how the nucleus is aligned to the signature axis, one obtains slightly different one-quasiparticle states (with slightly different energies) at the single-reference level. Schunck *et al.* [129] named the concept "alispin". It would certainly be interesting to study the effects of the angular momentum restoration (and the configuration mixing) for one-quasiparticle states obtained from each sextant (or at least the three of them which are not equivalent for the choice of alignment [129]), as it has been done for even-even vacua in [112]. But for numerical reasons that will become obvious in section 4.4 on configuration mixing, it was not possible to perform calculations in all the different sextants of the (β, γ) plane. Nevertheless, we have calculated for the one-quasiparticle state that gives the minimum for $J^\pi = \frac{5}{2}^+$ projected states, the projected states in all other sextants. The energy spectra (up to 5 MeV above the minimum) after K-mixing for those states are displayed in Fig. 4.37. There are some small differences between all the spectra, either because these states having different alispin, or because of numerical uncertainty when converging the one-quasiparticle

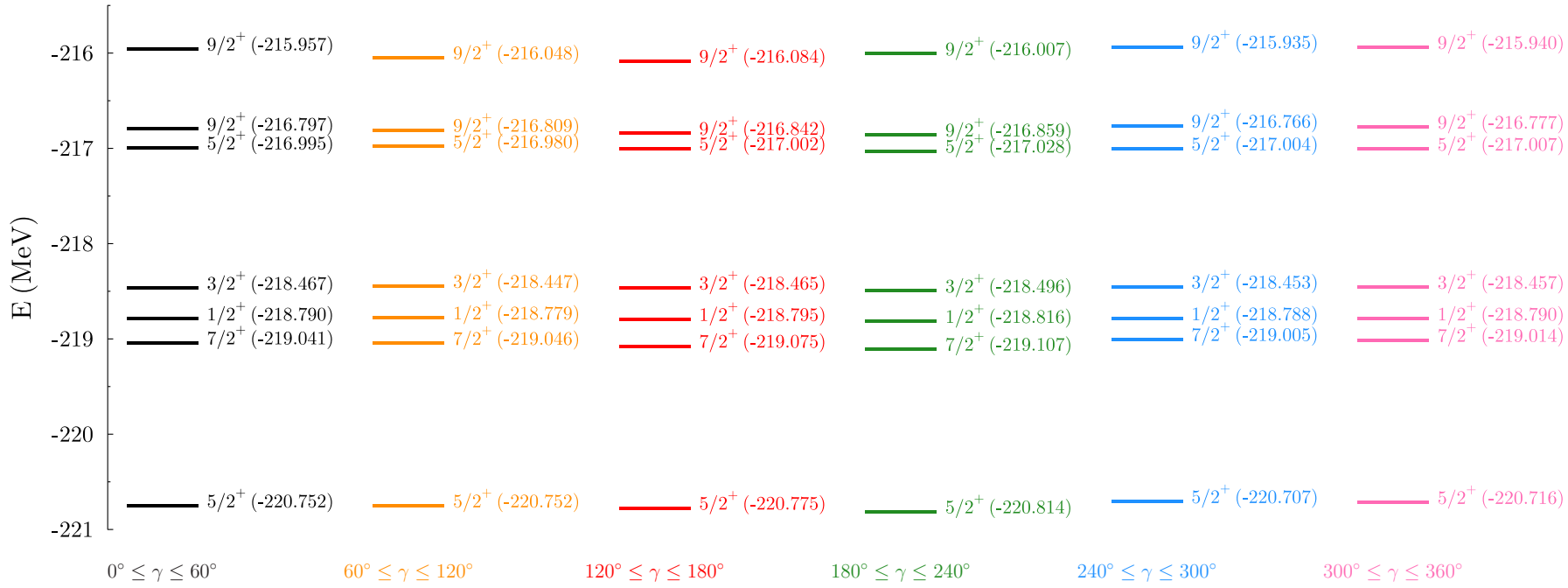

Figure 4.37: Spectra after angular momentum restoration for the "same" one-quasiparticle state, which gives the minimum for $J^\pi = \frac{5}{2}^+$ states in the sextant $0° \leq \gamma \leq 60°$, calculated in the six sextants of the (β, γ) plane.

states, or finally because of the numerical uncertainty when projecting on angular momentum, but the relative importance of each is not entirely possible. For example, the first and fourth spectra (starting from the left) are obtained from two states having same alispin, but present some differences in the energies of their levels. The same is true for the second and the third spectra. The fifth and the sixth spectra, also obtained from two states having same alispin, are in much better agreement, but we observe, nevertheless, discrepancies up to 10 keV.

We observe also some variations for other observables. As an example, we give in Tab. 4.8 the values of the spectroscopic quadrupole moment and magnetic moment (see section D.3 for their definitions) for the lowest $J^\pi = \frac{5}{2}^+$ state obtained from each of the one-quasiparticle states.

The conclusion we can draw from these calculations is that, even if there are small differences in the numbers, and which shall be investigated on further detail, the overall picture we obtain from those 6 one-quasiparticle states is globally the same. We thus hope that the limitation to only one sextant of the (β, γ) plane for our calculations will not diminish the generality of the results presented in the section on configuration mixing.

Sextant	$Q_s(\frac{5}{2}^+, \epsilon = 1)$ $(e\,\mathrm{fm}^2)$	$\mu(\frac{5}{2}^+, \epsilon = 1)$ (μ_N)
$0° \leq \gamma \leq 60°$	22.50	-0.9332
$60° \leq \gamma \leq 120°$	22.52	-0.8632
$120° \leq \gamma \leq 180°$	22.52	-0.8608
$180° \leq \gamma \leq 240°$	22.50	-0.9212
$240° \leq \gamma \leq 300°$	22.52	-0.9363
$300° \leq \gamma \leq 360°$	22.52	-0.9358

Table 4.8: Spectroscopic quadrupole moment and magnetic moment of the lowest $J^\pi = \frac{5}{2}^+$ state for the "same" one-quasiparticle state, which gives the minimum for $J^\pi = \frac{5}{2}^+$ states in the sextant $0° \leq \gamma \leq 60°$, calculated in the six sextants of the (β, γ) plane. Rows printed in the same color indicate that the projected states have been obtained from one-quasiparticle states with same alispin.

4.3.6 Cranking

Even if we are not going to include cranked calculations in our configuration mixing, we wanted to present some results on the cranking of one-quasiparticle states, similarly to what has been done in [162] for even-even nuclei, and using same notations as in section 4.3.3.

Cranking of States with Opposite Signature

For one-quasiparticle states with a signature[8] quantum number, there is an additional ambiguity, compared to the even-even case, concerning which cranked states one should look at. Indeed, from a given even-even vacuum it is possible to block one-quasiparticle states either with a

[8]For the sake of simplicity, we speak here of the states obtained after the permutation (3.1), i.e. we consider one-quasiparticle states with a x-signature. In particular it implies for cranking that the constraint on $\langle \hat{J}_z \rangle$ of section 2.4.3 is transformed as a constraint on $\langle \hat{J}_x \rangle$.

signature $+i$ or with a signature $-i$. Without cranking, the states with opposite signature are related by time-reversal, but as soon as one includes a constraint on $\hat{J}_x$, this is not the case anymore. Hence, we will look at the evolution of the distributions of J components for a pair of one-quasiparticle states with positive parity that are time-reversed without cranking, and which have dominant $K = \frac{5}{2}$ component (without cranking). We recall that in our work the constraint on $\hat{J}_x$ takes the form

$$\langle \hat{J}_x \rangle = \sqrt{J_c(J_c+1) - K_c^2} \quad ,$$

and we will start the cranking at $J_c = \frac{7}{2}$.
The distributions of J components up to a cranking of $J_c = \frac{15}{2}$ are found in Fig. 4.39 and 4.40. Without cranking we can check that the states with opposite signature present (up to numerical precision) exactly the same distributions. As we increase the value of the cranking constraint, we observe two phenomena. Firstly, the center of the distributions moves to higher values of J, as already observed for even-even nuclei [162]. Secondly, for states with signature $-i$, the components with $J = \frac{1}{2}, \frac{5}{2}, \frac{9}{2}, \frac{13}{2}, \ldots$ are favoured, whereas the components with $J = \frac{3}{2}, \frac{7}{2}, \frac{11}{2}, \frac{15}{2}, \ldots$ are hindered. For states with signature $+i$, this is the other way around.
This can be understood as follows, the constraint $\sqrt{J_c(J_c+1) - K_c^2}$ is derived in a Kamlah expansion [83, 106] as an approximation of the term

$$\frac{\langle \Phi_a | \hat{J}_x \hat{P}^{J_c} | \Phi_a \rangle}{\langle \Phi_a | \hat{P}^{J_c} | \Phi_a \rangle} \approx \sqrt{J_c(J_c+1) - K_c^2} \quad , \tag{4.8}$$

where

$$\hat{P}^{J_c} = \sum_{K',K=-J_c}^{J_c} \hat{P}^{J_c}_{K'K} \quad . \tag{4.9}$$

Applying $\hat{P}^{J_c}$ to a state $|\Phi_a\rangle$ with a signature η_a, we obtain

$$\begin{aligned}
\hat{P}^{J_c}|\Phi_a\rangle &= \sum_{K',K=-J_c}^{J_c} \hat{P}^{J_c}_{K'K} |\Phi_a\rangle \\
&= \sum_{K',K=-J_c}^{J_c} \hat{P}^{J_c}_{K'K} \left[\sum_{J''} \sum_{K''=-J}^{J} c^{J''}_{K''}(a) |J''K''\rangle \right] \\
&= \sum_{K'=-J_c}^{J_c} \left[\sum_{K=-J_c}^{J_c} c^{J_c}_{K}(a) \right] |J_c K'\rangle \\
&= \sum_{K'=-J_c}^{J_c} \left[\sum_{K\geq\frac{1}{2}}^{J_c} c^{J_c}_{K}(a) + c^{J_c}_{-K}(a) \right] |J_c K'\rangle \\
&= \sum_{K'=-J_c}^{J_c} \left[\sum_{K\geq\frac{1}{2}}^{J_c} c^{J_c}_{K}(a) \left(1 + \eta_a e^{+i\pi J_c}\right) \right] |J_c K'\rangle \quad ,
\end{aligned} \tag{4.10}$$

where we have used equation (C.4.2). Therefore, for a state with signature $\eta_a = -i$ and $J_c = \frac{3}{2}, \frac{7}{2}, \frac{11}{2}, \frac{15}{2}, \ldots$ we have $\eta_a e^{+i\pi J_c} = -1$ and $\hat{P}^{J_c}|\Phi_a\rangle$ vanishes. By contrast, for a state with signature $\eta_a = +i$, $\hat{P}^{J_c}|\Phi_a\rangle$ vanishes for $J_c = \frac{1}{2}, \frac{5}{2}, \frac{9}{2}, \frac{13}{2}, \ldots$
We can thus say that as we increase the constraint on $\langle \hat{J}_x \rangle$, we get closer and closer to the correct behavior of the constraint $\frac{\langle \Phi_a | \hat{J}_x \hat{P}^{J_c} | \Phi_a \rangle}{\langle \Phi_a | \hat{P}^{J_c} | \Phi_a \rangle}$ as it appears in the Kamlah expansion, and we

recover the property described in many text books [139, 32] that states with $J = \frac{1}{2}, \frac{5}{2}, \frac{9}{2}, \frac{13}{2}, \ldots$ are described by cranking states with signature $\eta_a = -i$, and states with $J = \frac{3}{2}, \frac{7}{2}, \frac{11}{2}, \frac{15}{2}, \ldots$ are described by cranking states with signature $\eta_a = +i$. But in our case this property turns out to be true only in the limit case of large cranking constraint $\sqrt{J_c(J_c+1) - K_c^2}$. Conversely, we could question the validity of the cranking for small value of our cranking constraint.

Another possible shortcoming of the approximated cranking constraint we are using is that we keep the value of K_c fixed. But if we look at Fig. 4.38 where is displayed the distributions of K components for different values of cranking constraint, we see that as we increase the constraint, the K distributions change. They become wider and centered around $K = \frac{1}{2}$, whereas without cranking the distribution is centered around $K = \frac{5}{2}$. Ring *et al.* [106] proposed a more suitable constraint

$$\langle \hat{J}_x \rangle = \sqrt{J_c(J_c+1) - \langle \hat{J}_z^2 \rangle}$$

that may be interesting to be investigated in the context of projection on angular momentum of cranked states.

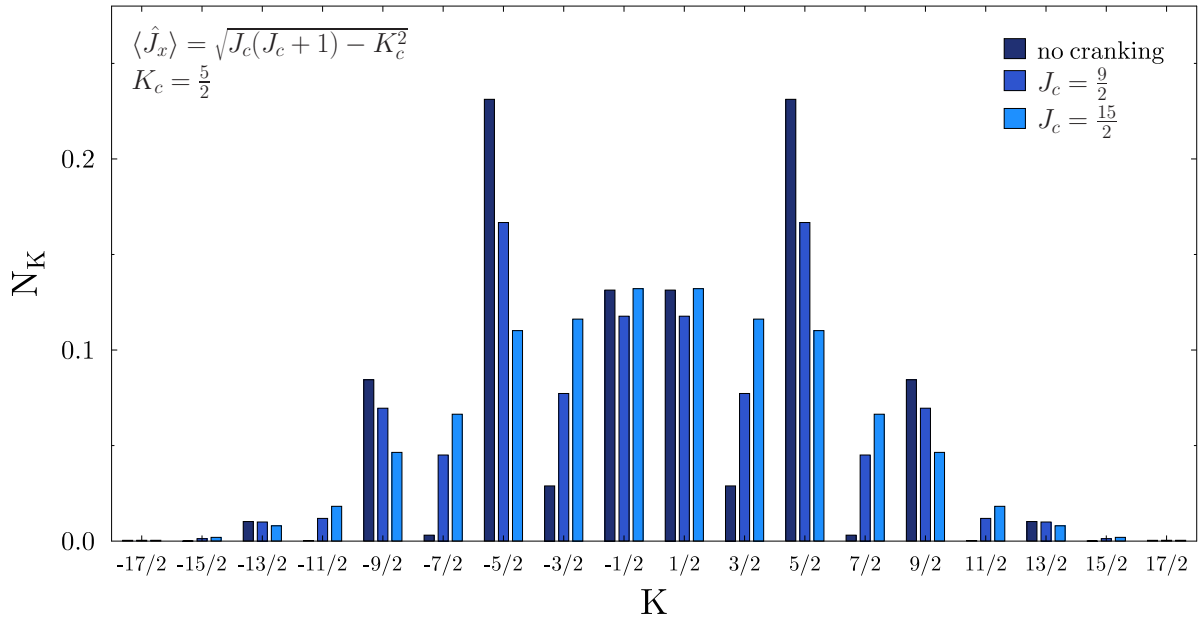

Figure 4.38: Distributions of K components for different values of the cranking constraint, and for the state with signatre $-i$.

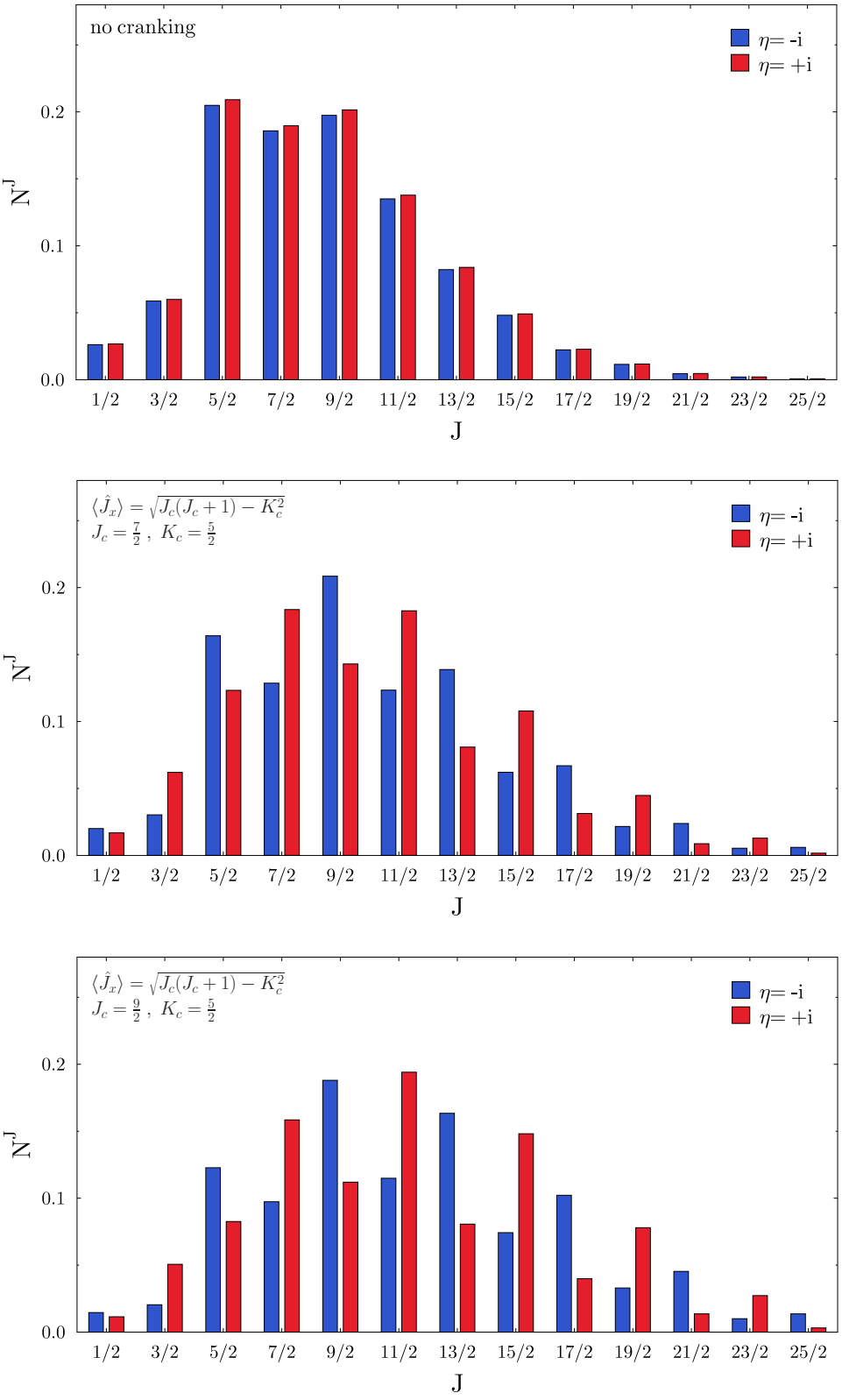

Figure 4.39: Distributions of J components for different values of the cranking constraint.

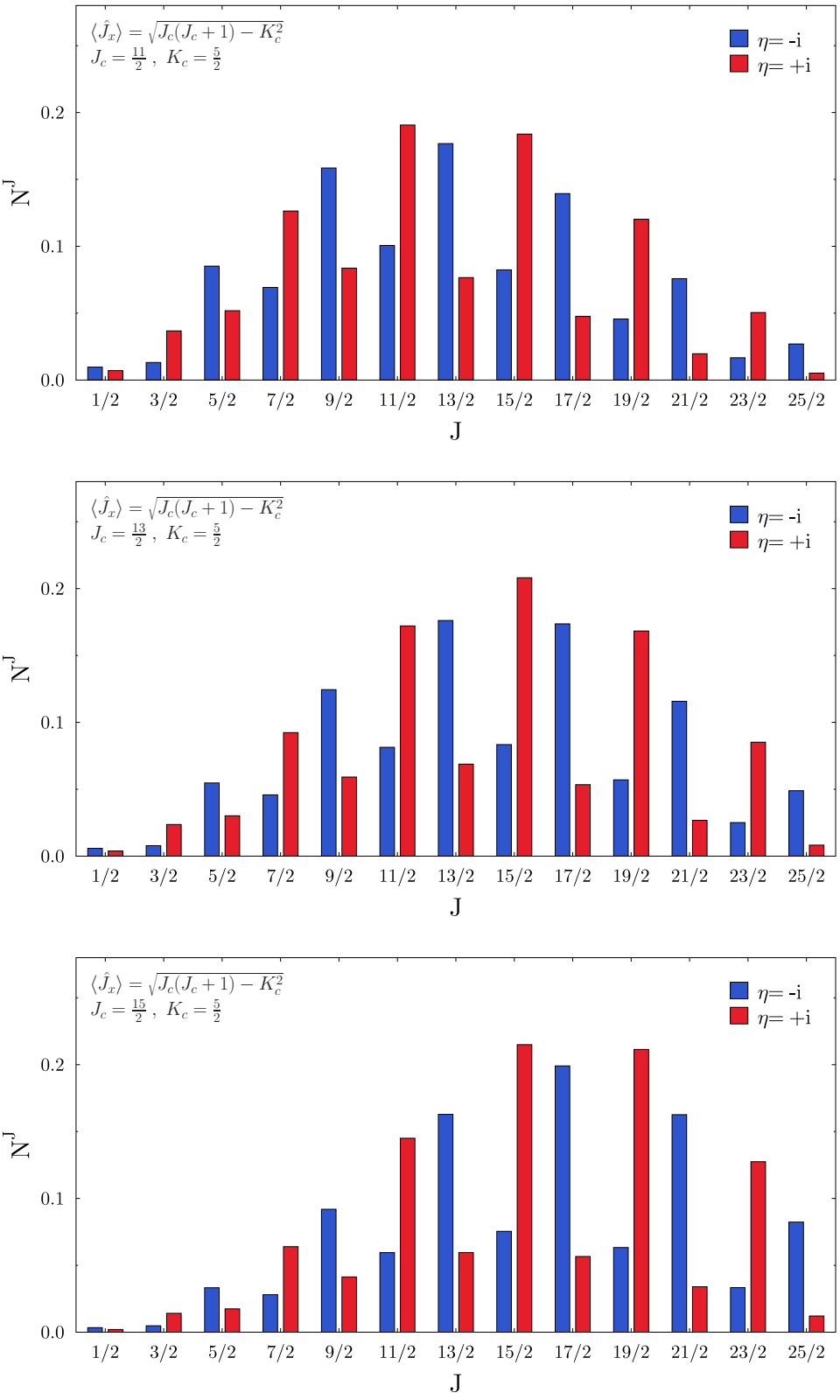

Figure 4.40: Distributions of J components for different values of the cranking constraint.

Spectra of Projected Cranked One-Quasiparticle States

To conclude this section on projection of cranked one-quasiparticle states, we display in Fig. 4.41 and Fig. 4.42 the spectra of the Yrast states up to $J = \frac{15}{2}$ obtained after angular momentum projection for the non-cranked state and for the cranked states of signature $-i$ and $+i$. In Figure 4.41 is shown the evolution of Yrast energies as a function of the value of J_c, whereas in of Fig. 4.42 is shown the spectra obtained by searching, for each J and for each signature, the projected state that has the lowest energy in the set of all projected states obtained from one-quasiparticle with different values of J_c. Firstly, we can observe that spectra of the projected cranked states are much more compressed than the spectra of the projected non-cranked state. This is in perfect agreement with what had been already observed for even-even nuclei [162, 6]. Also, we can notice that the $J = \frac{5}{2}$ is also lowered for the cranked state with signature $-i$, with the minimum being given by the state with $J_c = \frac{13}{2}$. Finally, we can remark that it is not necessarily the state with the "appropriate" signature for a given J_c, i.e. the signature which does not cancel $\hat{P}^{J_c}|\Phi_a\rangle$, which gives lowest energy state for this particular J_c. For example, the state $J = \frac{11}{2}$ is lower for cranked states with signature $-i$ than for cranked states with signature $+i$. It is thus not very clear which signature shall be chosen for a given J_c. Certainly, if we consider the projected state of lowest energy in a set of projected states obtained from cranked one-quasiparticle states with both signatures, we will always find the true projected state of lowest energy. On the other hand, with the weight of every other J component decreasing as the cranking constraint increases, we can question the numerical precision of the projected states obtained for those states with small value of N^J. One thing is sure, this problem shall deserve a more thorough study in the future.

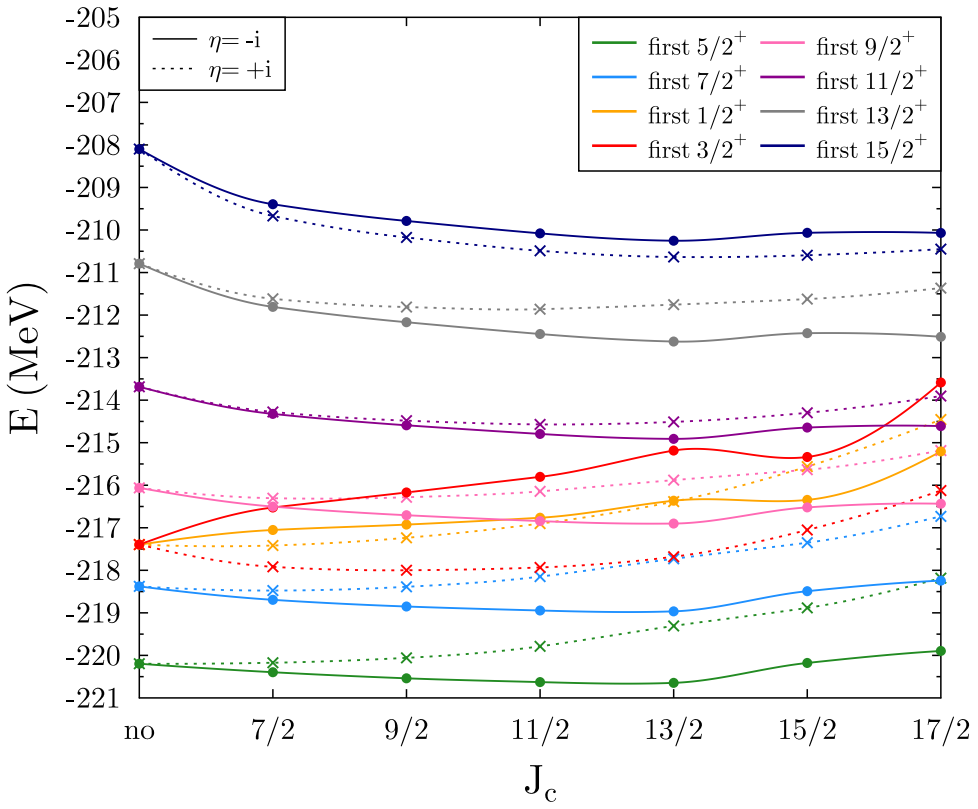

Figure 4.41: Yrast energies for different values of the cranking constraint and for both signatures.

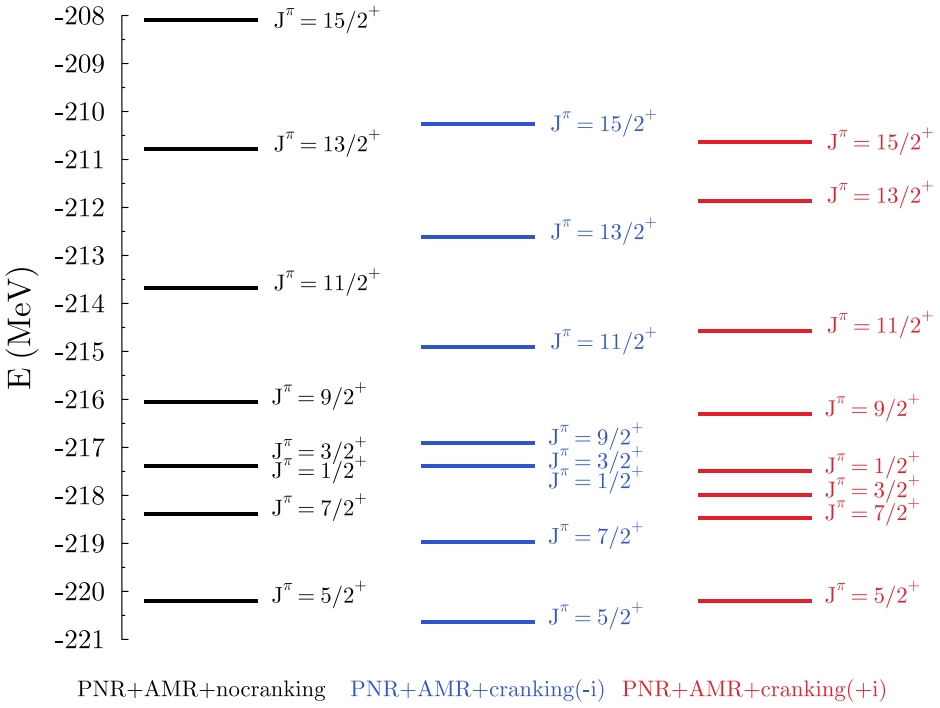

Figure 4.42: Energy spectra obtained by selecting, for each signature, the state of lowest energy of a given J in Fig. 4.41.

4.4 Configuration Mixing of Projected One-Quasiparticle States

We come now to the final step of our MR-EDF calculation that is the configuration mixing of one-quasiparticle states projected on particle number and angular momentum. As this method has, until now, never been attempted in its full-fledged version, we will give particular attention to the description of the calculation and its numerical aspects (e.g. good convergence of the GCM). We will also compare our results to experimental data, as that is, or that shall be, the ultimate test of any theoretical model. Of course, with this first calculation we do not expect full agreement with experimental data. Neither are we aiming at it. But this should at least indicate to us if we are going into the right direction and help us to determine where we still have to improve further.

4.4.1 Description of the Method

For this first GCM, out of the sets of 604 and 222 one-quasiparticle states converged of positive and negative parity, respectively, we have selected **100** one-quasiparticle states of positive parity and **60** one-quasiparticle states of negative parity. To select the one-quasiparticle states, we have followed a mesh in deformation with a step of 40 fm^2, starting from $q_1 = 0$ fm^2 and $q_2 = 0$ fm^2, and up to $q_1 = 280$ fm^2 and $q_2 = 160$ fm^2. At each deformation we have taken as many one-quasiparticle states as possible, taking in priority the one-quasiparticle states that give the lowest projected energies. But as we tried to explore simultaneously two degrees of freedom, i.e. deformation and one-quasiparticle structure, and because we were limited by the CPU time available to us, it was not possible to take into account all converged one-quasiparticle states at each deformation, even if the projected states obtained from them had lower energy than some of the projected states obtained from one-quasiparticle states selected at a different deformation.

The experimental ground state of ^{25}Mg is of positive parity, and the spectrum above it exhibits a majority of states with positive parity, as expected from a nucleus in the middle of the sd-shell. This explains why we decided to put more emphasis on those states by choosing more one-quasiparticle states with positive parity. Also, we have seen in the previous section that in our calculations projected states of positive parity are in general lower in energy than those of negative parity.
Finally, we want to stress that the precise numbers of one-quasiparticle states chosen for the GCM have been motivated only by the limitation in CPU time available to us to perform the calculation. There is nothing physical (or metaphysical) about this particular choice, and if we could have included more states in the configuration mixing, we would have done it.

Various Cut-Offs

When solving the HWG equation numerically, it is sometimes necessary to remove some states that do not meet a certain required numerical accuracy and thus could spoil our calculations. We already saw in section 4.3.4 some examples of such states. So in order to remove them, we have included in the GCM a series of cut-offs that will be described in this section. The first two of these cut-offs have already been introduced in section 4.3.4, but we recall them here. Before the K-mixing, we remove all the states

$$|JMNZP = p_i, iK\rangle = \frac{\hat{P}^J_{MK}\hat{P}^N\hat{P}^Z|\Phi_i\rangle}{\langle\Phi_i|\hat{P}^J_{KK}\hat{P}^N\hat{P}^Z|\Phi_i\rangle}$$

with a bad value of J after projection

$$|J_e - J| > 5.10^{-3} \quad ,$$

with J_e being solution of $\langle JMNZP, iK|\hat{J}^2|JMNZP, iK\rangle = J_e(J_e+1)$.
We also remove all the states that have a too small overlap

$$\langle JMNZP, iK|JMNZP, iK\rangle < 1.10^{-5} \quad .$$

During the mixing of K components, we remove all norm eigenvalues that are too small

$$\lambda(JNZP, i) < 1.10^{-5} \quad .$$

After the mixing of K components, and before the mixing of projected states coming from different one-quasiparticle states, we remove all the states

$$|JMNZP\epsilon, i\rangle = \sum_{K=-J}^{J} f_\epsilon^{JNZP}(i,K)|JMNZP, iK\rangle$$

that have a bad value of J

$$|J_g - J| > 5.10^{-3} \quad ,$$

with J_g being solution of $\langle JMNZP\epsilon, i|\hat{J}^2|JMNZP\epsilon, i\rangle = J_g(J_g+1)$.
Finally, during the final diagonalization, we remove all norm eigenstates that have too small eigenvalue

$$\lambda(JNZP) < 1.10^{-5} \quad .$$

However, it turned out that during the calculation reported here, no norm eigenstates had to be removed because of this final cut-off. For both parities, and for all values of J calculated, the

norm eigenvalues were always larger than 1.10^{-5}. Similarly, the cut-off of the norm eigenvalues during the mixing of K components was triggered only in very few cases over the thousands of norm eigenstates we had to consider in this work.
The most efficient cut-off to remove states with large numerical inaccuracy seems to be the test of their value of J after projection. And it is important to carry out the test both before and after the mixing of K-components, as some of the states $|JMNZP\epsilon, i\rangle$ might take values of J far away from what they should be.
Finally, and similarly to section 4.3.4, we stress that the values for the cut-off have been selected as to remove the states with unacceptable inaccuracy while keeping a maximum of states in the configuration mixing. We checked that the final results vary only by a little when changing (by a little) the values of the cut-offs, but a more thorough study of the cut-off dependence of the results shall be intended in future calculations.

4.4.2 Convergence of the Energy Spectrum

In this section, we want to look at the evolution of the value of the total binding energy for the lowest energy states obtained after configuration mixing (hereafter also referred to as "mixed states") as a function of the number of one-quasiparticle states included in the GCM. The goal of this analysis is to see if we reach a form of convergence for the energies of our mixed states with the number of one-quasiparticle states included in the GCM. As we will see, it may not be possible to speak of convergence in the strict mathematical sense, but we can still expect that as we increase the number of one-quasiparticle states in our GCM, the observables vary more slowly. But to look at the evolution of the results with the number of one-quasiparticle states, it is first necessary to define the order in which we add the one-quasiparticle states. For this first analysis, we have decided to add the one-quasiparticle states by order of increasing non-projected energy. In section 4.4.3 we will investigate other possibilities of order and we will see that they are not all equivalent. Figure 4.43 displays the total binding energies of all the one-quasiparticle states (ordered by increasing energy) considered in our configuration mixing.

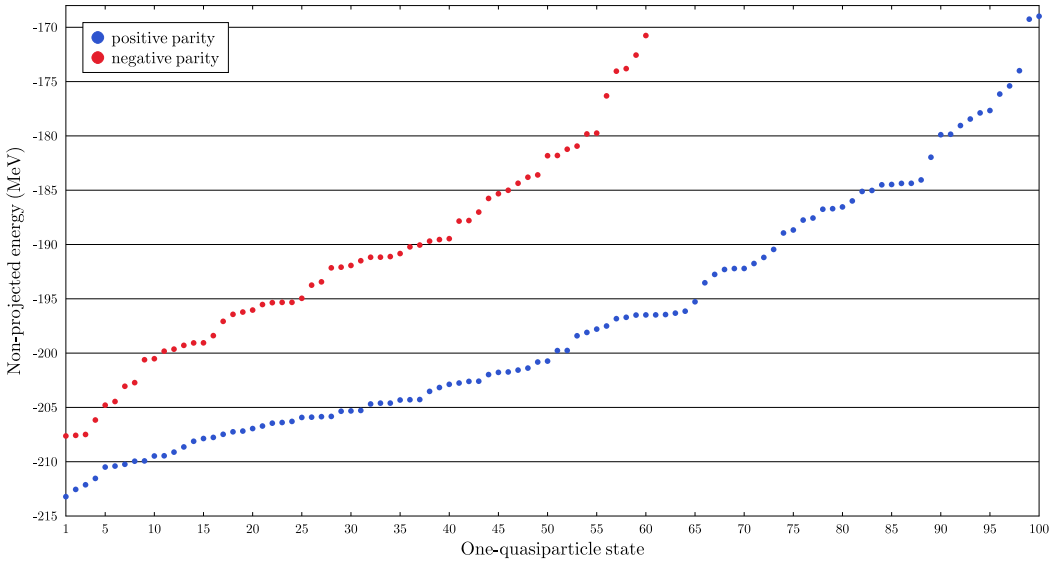

Figure 4.43: Energy of the one-quasiparticle states used for the configuration mixing.

For the three (resp. two) lowest mixed states of positive (resp. negative) parity with $\frac{1}{2} \leq J \leq \frac{7}{2}$, we plot in the top (resp. bottom) panel of Fig. 4.44 the evolution of their energy with the number of one-quasiparticle states included in the GCM. In each figure, the abscissa indicates how many one-quasiparticle states have been included in the GCM, e.g. if the abscissa is equal to twenty this means that the twenty first states of Fig. 4.43 have been included. First, we can observe that the energy of all mixed states is lowered as the number of one-quasiparticle states included in the GCM increases. This is expected because, as we include more and more one-quasiparticle states in the configuration mixing, we diagonalize the Hamiltonian in a larger and larger space. We also observe that the energy gained when adding a state tends, except for a few jumps, to become smaller and smaller when the number of one-quasiparticle states in the GCM increases. But contrary to what one could conclude from Fig. 4.44, the energies are still going a little bit downward for large numbers of one-quasiparticle states included in the configuration mixing. In order to better see that, we plot in Fig. 4.45 and Fig. 4.46, a zoom on Fig. 4.44 for positive and negative parity mixed states, respectively.

To be more precise, in Tab. 4.9 we compare, for the two mixed states of lowest energy with $\frac{1}{2}^+ \leq J^\pi \leq \frac{7}{2}^+$, the energy gained every twenty one-quasiparticle states added to the GCM. As we can see, we still gain a little bit of energy going from eighty to one hundred one-quasiparticle states. But, the gain is rather small and, it is also rather similar for all mixed states. Such that the energy spectrum is only barely modified. Similar results can be obtained for negative parity states.

# States	$1/2^+_1$	$1/2^+_2$	$3/2^+_1$	$3/2^+_2$	$5/2^+_1$	$5/2^+_2$	$7/2^+_1$	$7/2^+_2$
$1 \rightarrow 20$	2645	19636	2652	44771	4695	46697	2667	47340
$20 \rightarrow 40$	110	136	90	287	213	171	180	160
$40 \rightarrow 60$	142	186	150	155	136	143	124	138
$60 \rightarrow 80$	51	40	54	76	68	51	79	61
$80 \rightarrow 100$	11	17	9	11	12	13	11	14

Table 4.9: Gain in energy (keV) as we increase the number of one-quasiparticle states included in the GCM for different mixed states J^π_ξ. For the state $1/2^+_2$, the gain in energy in the first row is relative to a GCM with 2 states (because of the x-signature we can obtain only one $1/2^+$ projected state from each one-quasiparticle state).

From this analysis, we want to conclude that there seems to be a sort of convergence in our calculation in the sense that, as we include more and more one-quasiparticle states, of higher and higher non-projected energy, the gain in energy for the mixed seems to become smaller and smaller. In particular, the excitation spectrum we can built from these energies seems to change less and less. But we have to be cautious, as it is not fully possible to extrapolate this result to a larger set of one-quasiparticle states. In the first place, for theoretical reasons: (i) the integral (discretized here) over the deformation degree of freedom may not converge, and (ii) we use a zero-range interaction which may problematic as observed in other beyond-mean-field approches [42, 96, 123]. But even putting on the side these theoretical problems, we can see in Fig. 4.44 (it is more visible in Fig. 4.45 and Fig. 4.46) that gain in energy we obtain by adding one-quasiparticle states is not smooth at all. The addition of some one-quasiparticle states produces a big jump in the energy whereas some others barely change it. To illustrate this behaviour, we display in the top panel of Fig. 4.47 the evolution of the first $\frac{5}{2}^+$ mixed state, but adding the one-quasiparticle

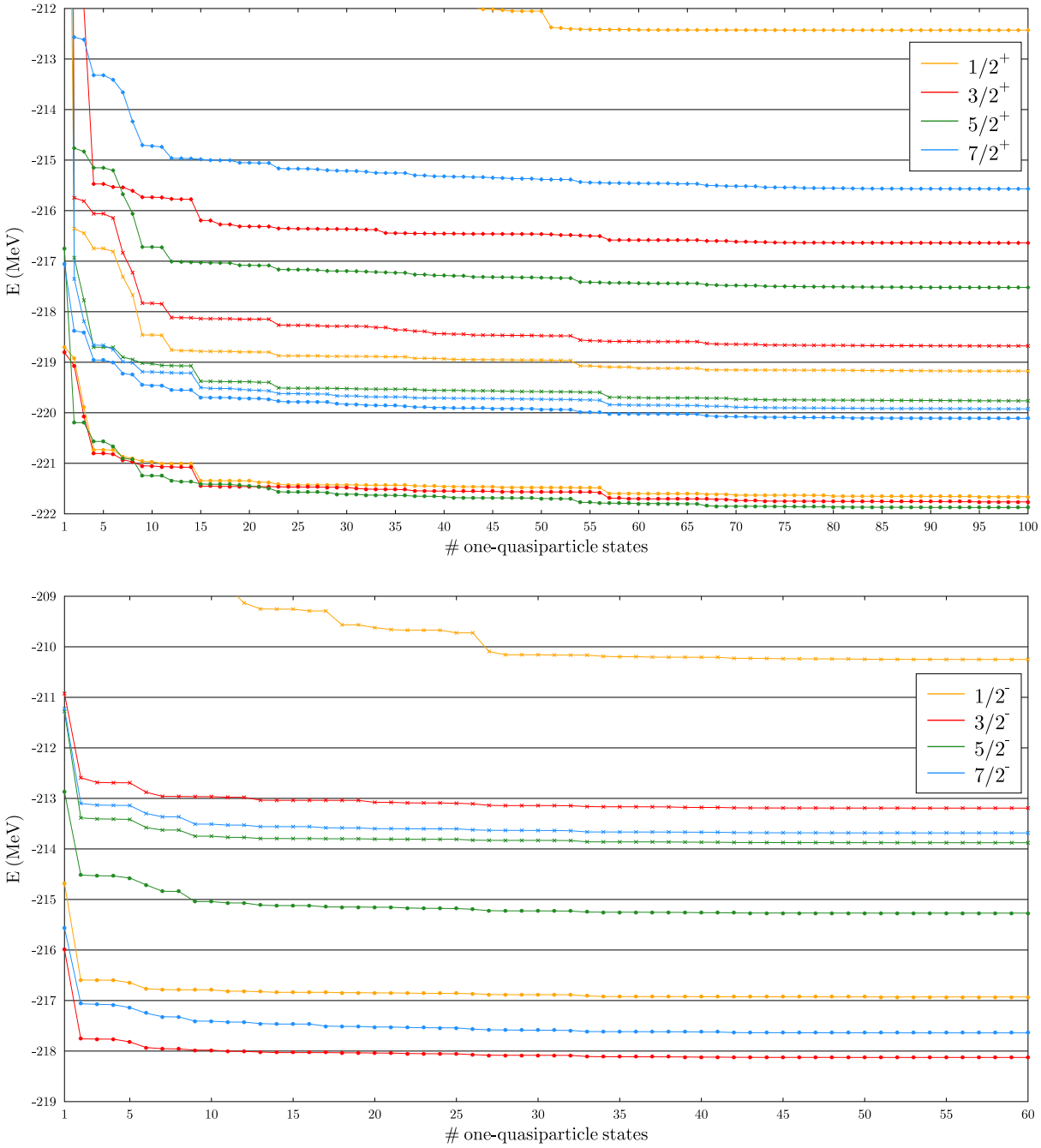

Figure 4.44: Top: Evolution of the energy for the lowest energy mixed states of positive parity. Circles, crosses, and diamonds, indicate the lowest, the second lowest, and the third lowest, state of a given J, respectively. Bottom: Same for negative parity states.

states in two different manner. The first manner (green) is identical to what has been done before. But in the second manner (red), we add the one-quasiparticle states in the reverse order, i.e. we add the one-quasiparticle states by order of decreasing non-projected energy. Of course, even if we start from a different energy in the beginning, we obtain the same energy in the end. Also, we see that some of the states that change the energy only by a little for the green curve, produce big jump for the red curve. This is not unexpected as our one-quasiparticle states are not

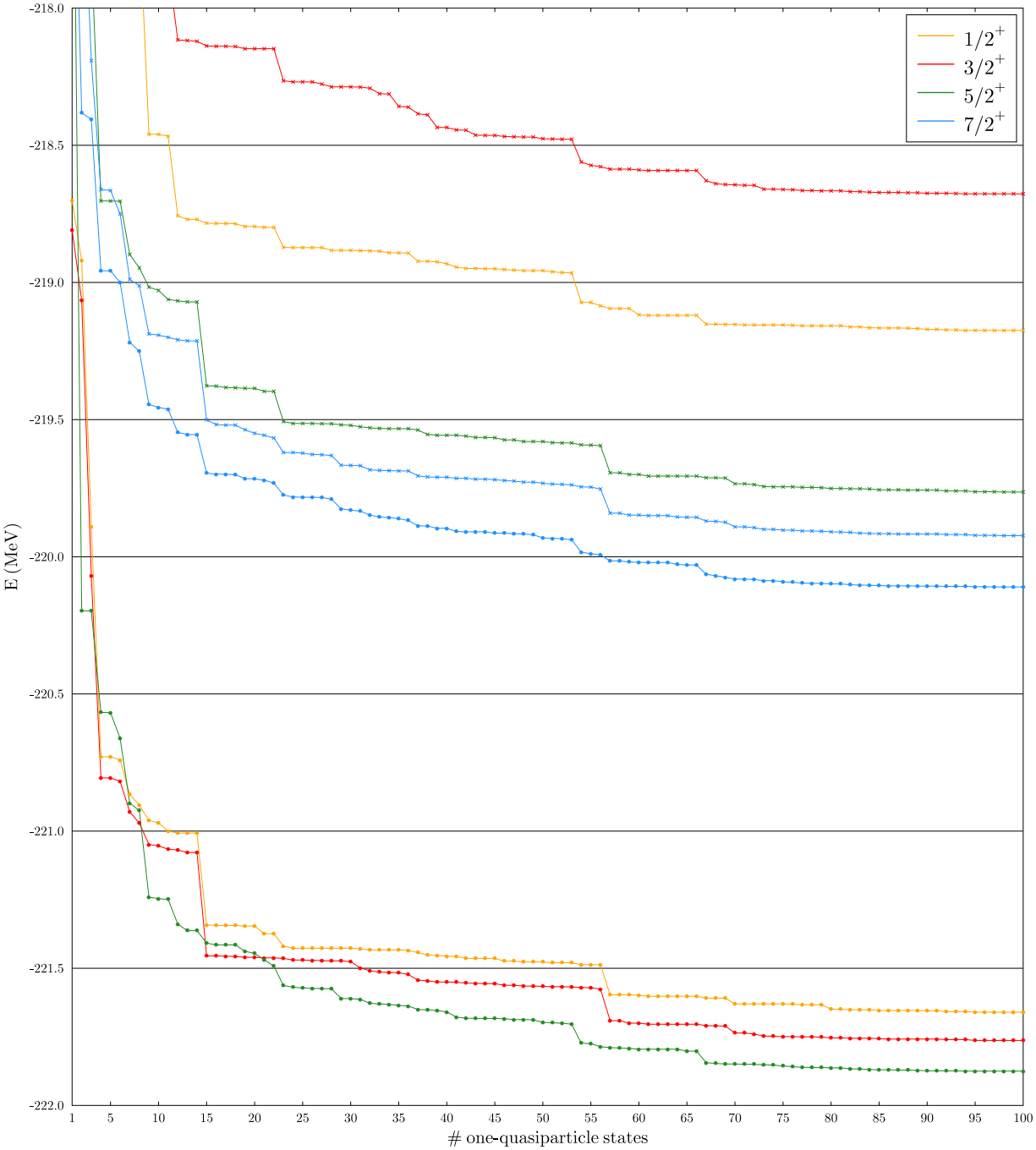

Figure 4.45: Zoom on Fig. 4.44, with also a much bigger scale.

independent one from another and thus their impact on the configuration mixing is only relative to which one-quasiparticle states we already included before them in the configuration mixing. But we can also observe that the ninety-ninth state for the red curve (which corresponds to the second state for the green curve) by itself produces a jump of 184 keV in the energy. Or to say it differently, even with a configuration mixing including ninety eight state, it was not possible to grasp all the information carried by this ninety-ninth state. This fact indicates that some one-quasiparticle states are more important than others, which is not completely surprising, but it

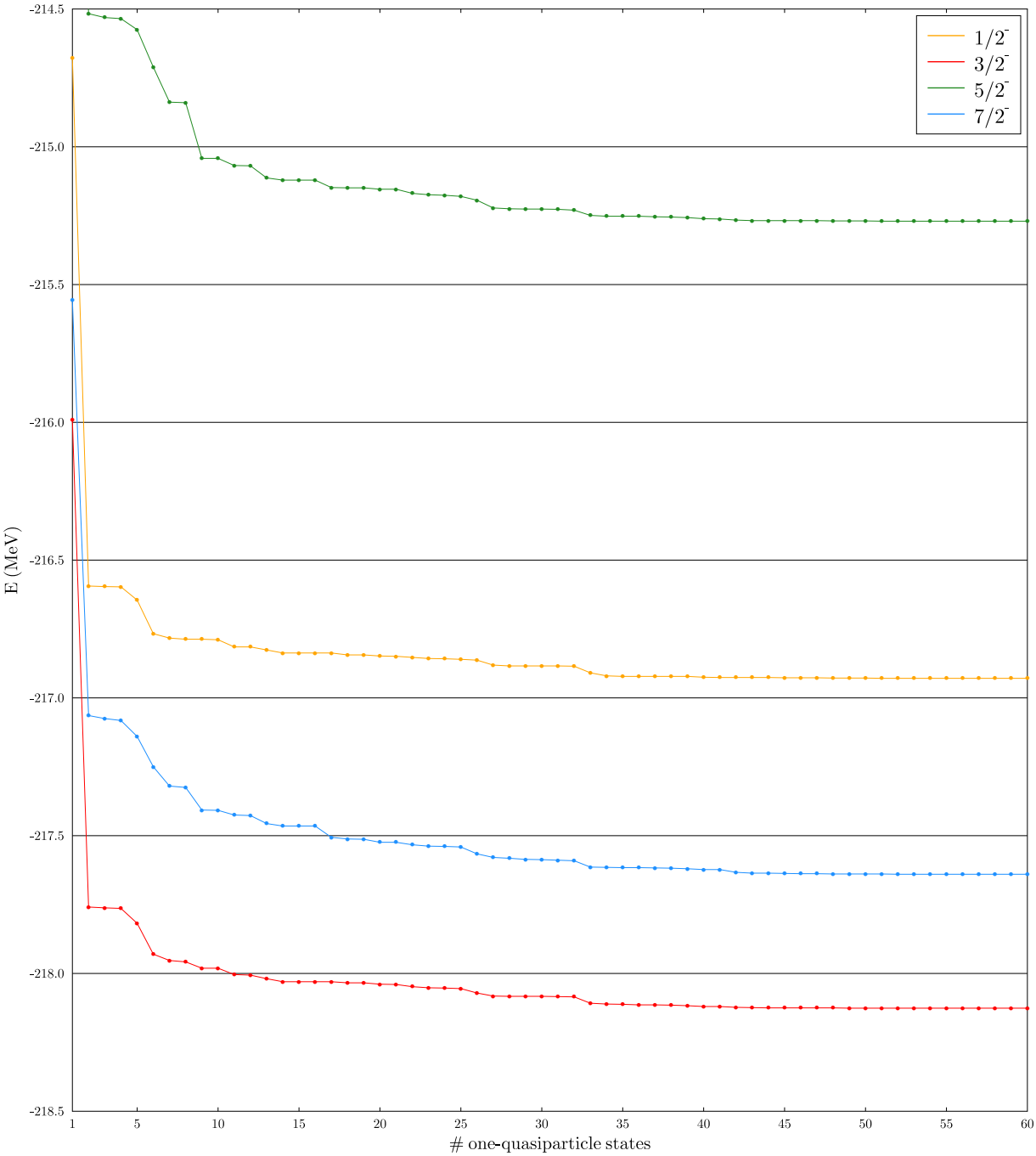

Figure 4.46: Zoom on Fig. 4.44, with also a much bigger scale.

also indicates that even with a very large number of one-quasiparticle states it is not necessarily possible to compensate for their absence in the configuration mixing. In the bottom panel of Fig. 4.47, we plotted in pink the evolution of the energy for the first $\frac{5}{2}^+$ mixed state, but removing the second state (of the green curve) from the GCM. As we can observe, both curves are very similar and give the same impression of convergence, but the pink curve is shifted by approximately 100 keV upward compared to the green one. So we cannot conclude that our GCM is fully converged, but only to the fact that, for a given discretization of deformation degrees of freedom,

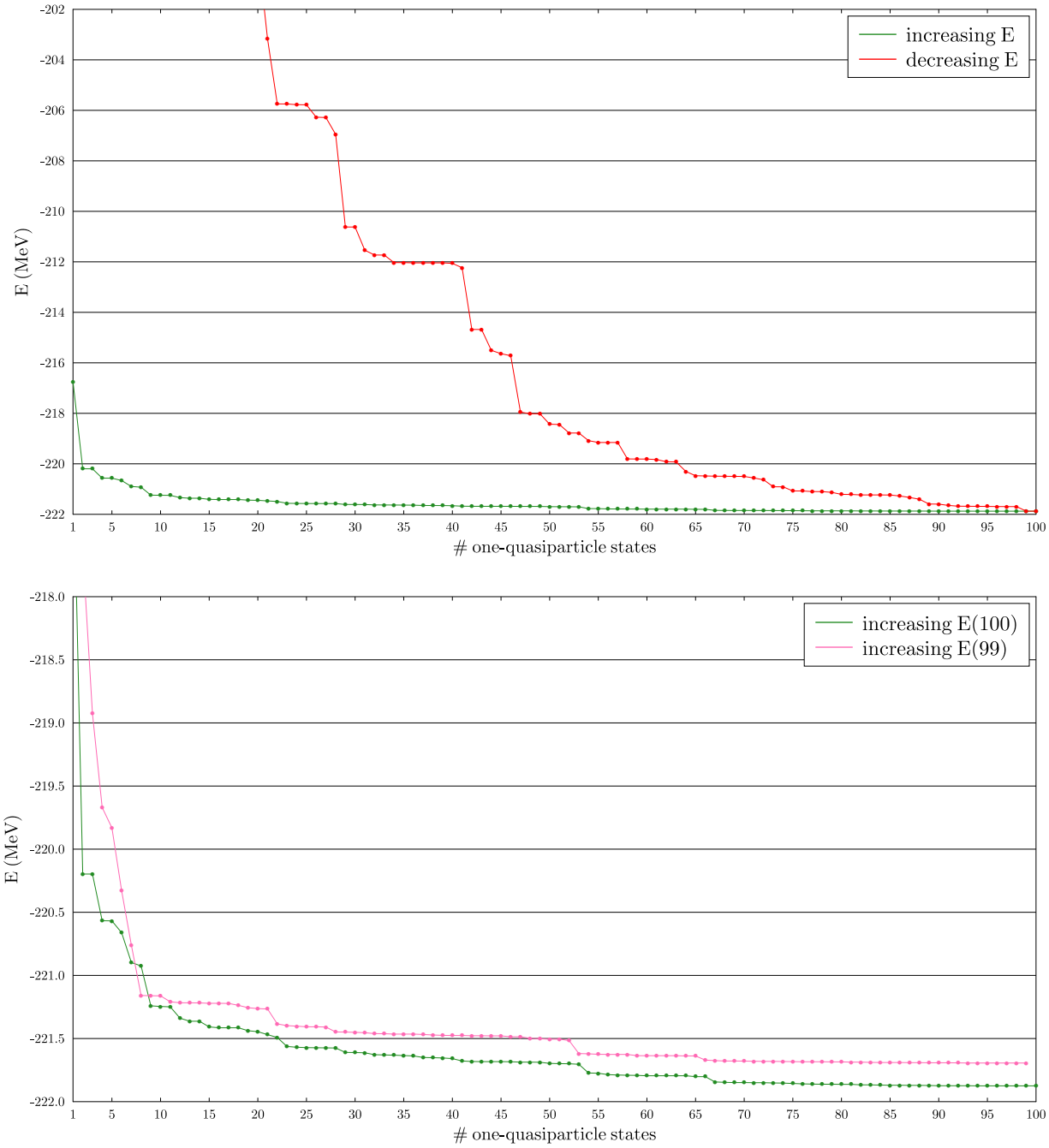

Figure 4.47: Top: Evolution of the energy for the first $\frac{5}{2}^+$ mixed state. The green (resp. red) dots represent a series of calculations where one-quasiparticle states are added by increasing (resp. deacreasing) order of their non-projected energy. Bottom: Same as in top panel, but now comparing a GCM with one hundred states and a GCM with ninety nine states (we removed the second state of the green curve).

including one-quasiparticle states of higher and higher non-projected energy brings less and less extra energy in the configuration mixing. Even if we seem very cautious here, we consider this result already as precious and encouraging for future GCMs. The problem is now: is there a way to recognize the most important one-quasiparticle states?

4.4.3 How to Select One-Quasiparticle States

In this section, we try to answer the question we asked at the end of the previous section. But we prefer to inform the reader beforehand that we do not have any definitive answer, neither that we are sure there is one. Nevertheless, we still want to look for a method that allows, for a given number of one-quasiparticle states included in the configuration mixing, for chosing the ones that will be the most likely to be important. In that order, we consider several choices for the order in which we add the one-quasiparticle states of our set to the configuration mixing. For this study we have tried 5 differents orders:

- We order the states by increasing non-projected energy, as done above. This choice will be labeled "E(Non-projected)" in the figures to follow.
- We order the states by increasing energy of their first $\frac{5}{2}^+$ projected state. This choice will be labeled "E(Projected $5/2^+$)" in the figures to follow.
  We also mention that the lowest $\frac{5}{2}^+$ projected state corresponds to the second one-quasiparticle in the list of Fig. 4.43. You can also see the spectrum of the projected states given by this one-quasiparticle state in Fig. 4.41 (non-cranked spectrum).
- We order the states by decreasing size of their non-projected overlap with the state giving the lowest non-projected energy ($\equiv$ first state of Fig. 4.43). This choice will be labeled "O(Non-projected)" in the figures to follow.
  We also mention that this state is the one giving the lowest energy at the SR level in Fig. 4.3 and that the spectrum (before K-mixing) of its K-components can be found in Fig. 4.22.
- We order the states by decreasing size of their non-projected overlap with the state giving the lowest energy $\frac{5}{2}^+$ projected state ($\equiv$ second state of Fig. 4.43). This choice will be labeled "O(Non-projected $5/2^+$)" in the figures to follow.
- At random. More exactly, we have done seven different GCMs including the states in a random order and we present the mean-value of the seven GCMs. The main purpose of this little exercice is to assure us that we do not over-interpret what we find for the choices specified above. Indeed, the human mind likes to recognize pattern in our surrounding world, even when there is none to be seen. In terms of medical sciences, you could think of this as a test versus placebo. We chose to repeat the operation seven times because we did not want to be, by chance, in a favorable (or unfavorable) case. Seven is surely a low statistics, but just as surely, it is still a better statistics than one or zero. This choice will be labeled "Random" in the figures to follow.

For the different choices of order, we plot in Figures 4.48 to 4.51 the evolution of the energies of the two lowest energy states of positive parity with $\frac{1}{2} \leq J \leq \frac{7}{2}$. Overall, the second choice, i.e. adding the one-quasiparticle states ordered by increasing energy of their first $\frac{5}{2}^+$ projected state, seems to achieve the fastest convergence *within our set*. Adding the states in function of their overlap gives very contrasted results. For some states it is the best choice possible and for others it is a pretty mediocre choice, even if better than addding the states at random. Finally, adding the states in function of their non-projected energy seems to be of an intermediate quality between the second choice (projected energies) and the third and fourth choices (overlaps).

For all the lowest mixed states of positive parity with $\frac{1}{2} \leq J \leq \frac{7}{2}$, we plot in Fig. 4.52 the evolution of their energy, but this time as a function of the number of projected states[9] (keeping

[9]For a given J, the number of projected states depends of the number of K components and of the cut-offs. This explains why there are more projected states with increasing values of J.

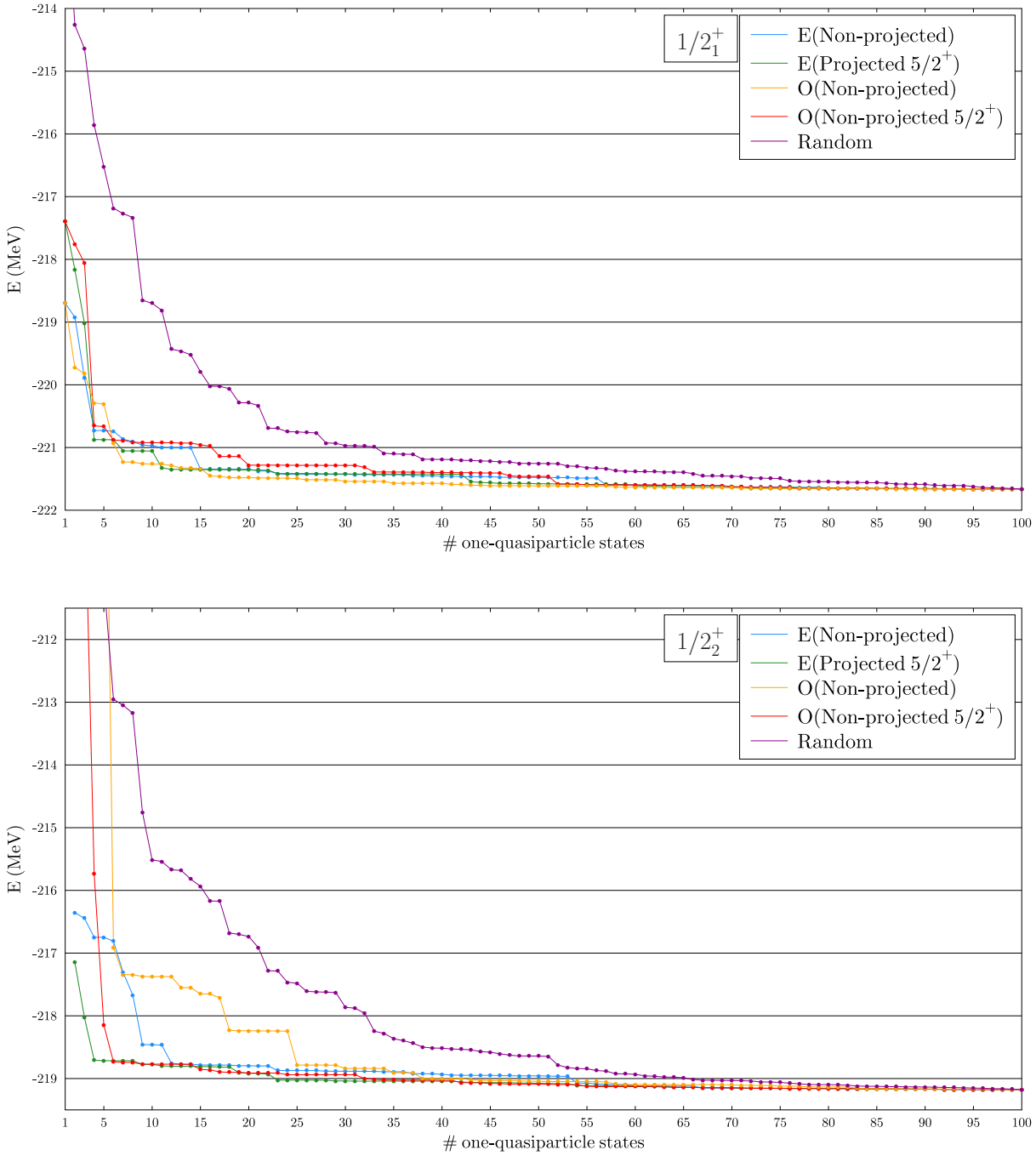

Figure 4.48: Top: Evolution of the energy for the lowest energy $J^\pi = \frac{1}{2}^+$ mixed state for different choices for the order by which the one-quasiparticle states are added to the GCM (see text). Bottom: Same for the second lowest $J^\pi = \frac{1}{2}^+$ mixed state.

the number of one-quasiparticle states included fixed to one hundred) in the configuration mixing. The projected states are added, for each J, by increasing order of their projected energy. As we can see, there seems also to be the same pattern for the projected states as for the one-quasiparticle states. Projected states with high (projected) energy tend to be less important for the configuration mixing than states with low (projected) energy. This is the reason why adding

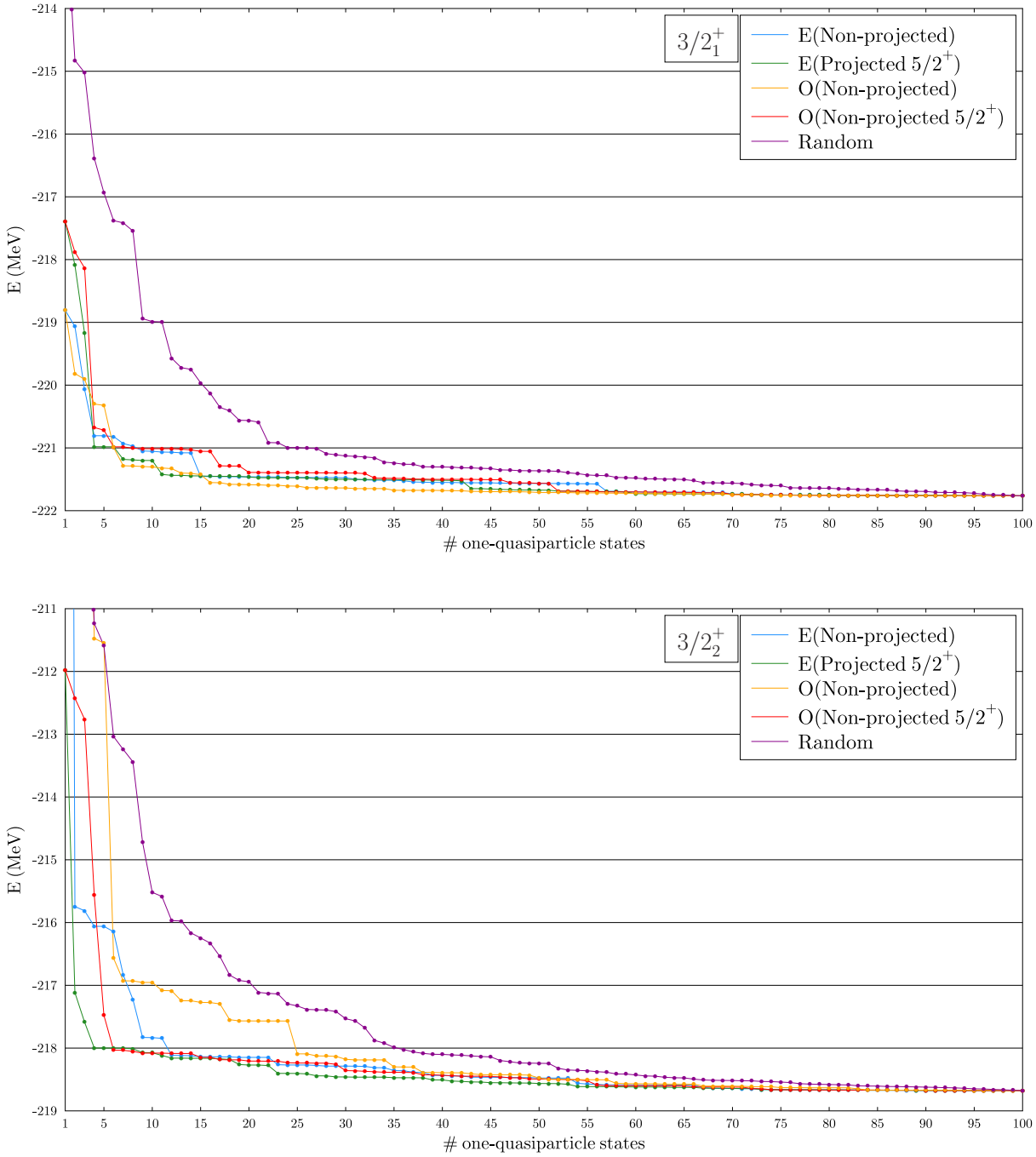

Figure 4.49: Top: Evolution of the energy for the lowest energy $J^\pi = \frac{3}{2}^+$ mixed state for different choices for the order by which the one-quasiparticle states are added to the GCM (see text). Bottom: Same for the second lowest $J^\pi = \frac{3}{2}^+$ mixed state.

the one-quasiparticle states by increasing order of their projected energy represent a good choice. This also explain why adding the states by order of increasing non-projected energy is also an appreciable choice, because even if there are differences for the non-projected energy surfaces of section 4.1 and the projected energy surfaces of section 4.3.1, one-quasiparticle states with high non-projected energy tend to have high projected energy. In particular, we already mentionned

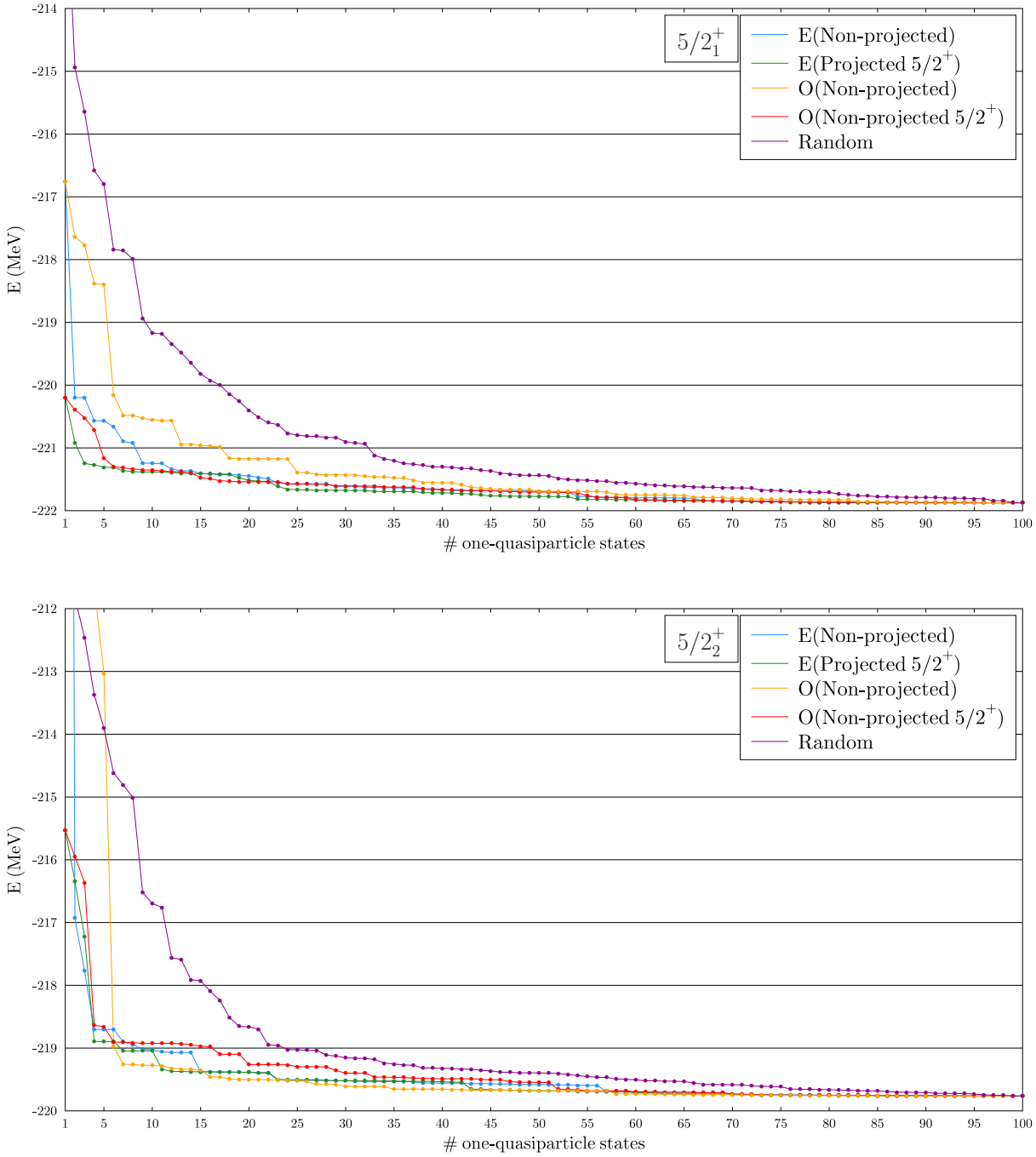

Figure 4.50: Top: Evolution of the energy for the lowest energy $J^\pi = \frac{5}{2}^+$ mixed state for different choices for the order by which the one-quasiparticle states are added to the GCM (see text). Bottom: Same for the second lowest $J^\pi = \frac{5}{2}^+$ mixed state.

that the one-quasiparticle states used to plot the lowest non-projected energy surfaces in Fig. 4.3, for most of them give also the lowest projected energy used to plot the projected energy surfaces.

From all these plots, we want to conclude that, between all the choices tested here, the most advantageous one seems to be the one where we ordered the one-quasiparticle states by increasing

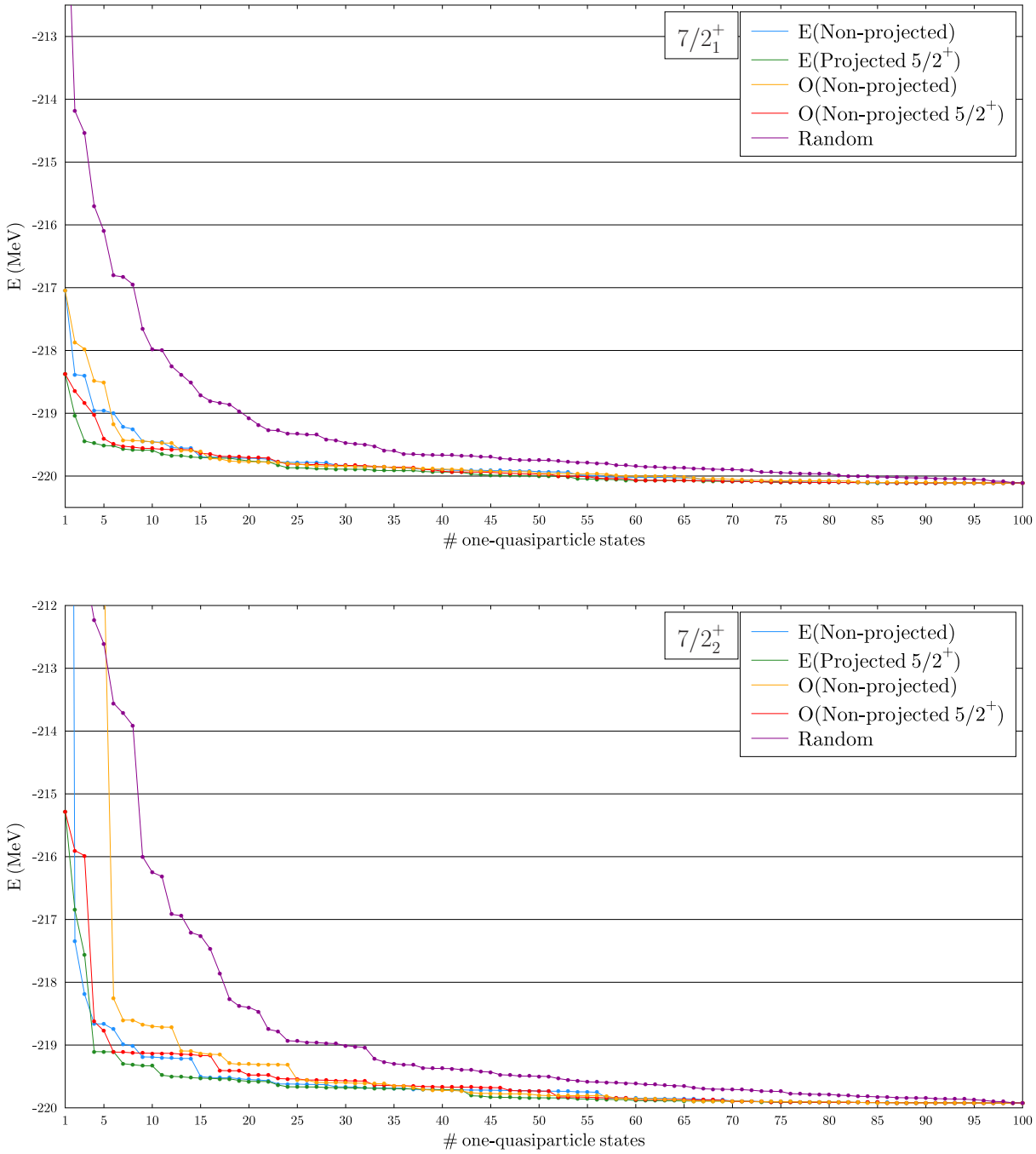

Figure 4.51: Top: Evolution of the energy for the lowest energy $J^\pi = \frac{7}{2}^+$ mixed state for different choices for the order by which the one-quasiparticle states are added to the GCM (see text). Bottom: Same for the second lowest $J^\pi = \frac{7}{2}^+$ mixed state.

energy of their first $\frac{5}{2}^+$ projected state. By the most advantageous, we mean that this choice requires a smaller number of one-quasiparticle states to get close to the final value obtained with one hundred states. So we can expect that, for a given number of one-quasiparticle states, choosing which ones to include on this criterion is more likely to give "more converged" results than for other choices. We tested here only the case where we order the states relatively to the

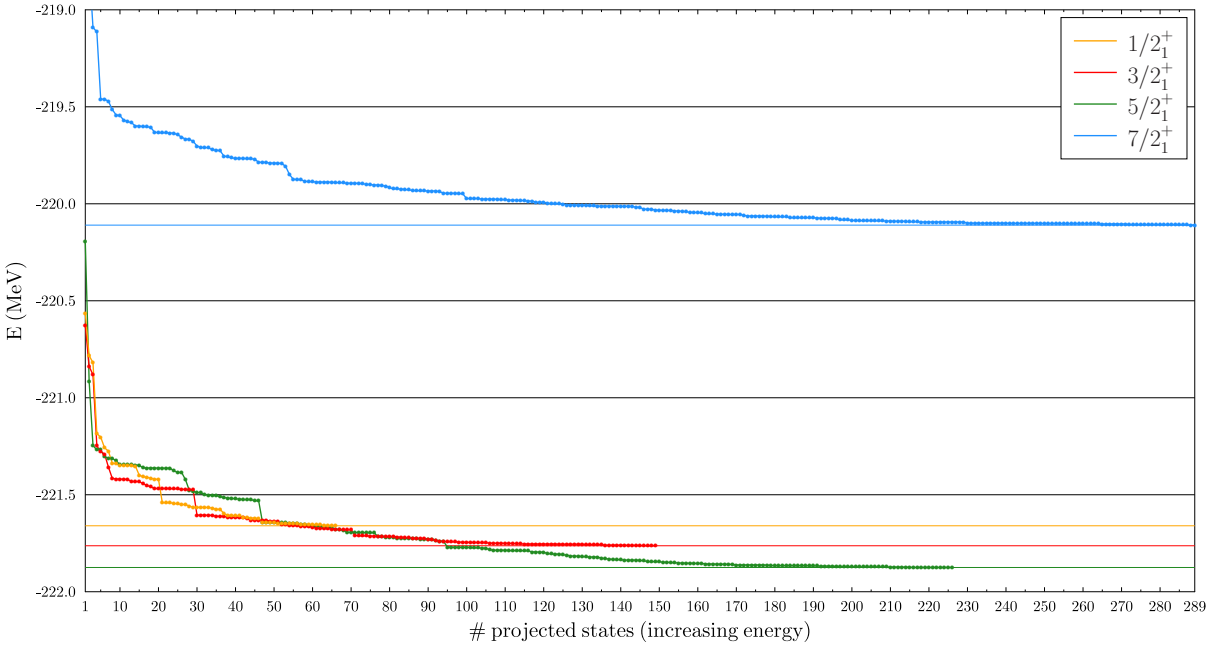

Figure 4.52: Evolution of the energy for the lowest energy mixed states up to $J^\pi = \frac{7}{2}^+$ as a function of the number of projected states in the configuration mixing. The projected states are added by increasing order of their (projected) energy. The horizontal colored lines represent the final energies when all states have been included.

lowest $\frac{5}{2}^+$ projected state because it is the projected state giving the absolute minimum before configuration mixing. It is quite surprising that it gives also good results for mixed states with other values of J. This may be related to the topographies of the projected energy surfaces shown in section 4.3.1. Indeed, in our case the minima for all the J considered here are located at relatively close deformations. Moreover, the topographies of all surfaces are very similar such that one-quasiparticle states with a relatively low energy $\frac{5}{2}^+$ projected state usually also have, for example, a low energy $\frac{3}{2}^+$ projected state (see for example Fig. 4.21). For energy surfaces with a different topograpy, for example with several distant (in deformation and/or energy) minima, it may be necessary, if one wants to describe all states related to each minimum, to take a more hybrid approach where one selects, for each minimum, a given number of one-quasiparticle states above the lowest energy projected state of this region. The disadvantage of selecting the one-quasiparticle states by the energy of their projected states is that it requires to perform the angular-momentum and particle-number projections before choosing the one-quasiparticle states to be included in the configuration mixing. But this not an unsurmontable problem, as to obtain the projected energies it is only necessary to calculate diagonal ($|\Phi_a\rangle = |\Phi_b\rangle$ in all formulas of section 3.4) projected matrix elements, which is far from being the most costly operation in our framework. Indeed, in our case we had to calculate 604 different diagonal matrix elements for positive parity states, whereas for the one-hundred states GCM, we had to calculate $\frac{100(100+1)}{2} = 5050$ matrix elements. A good alternative, which requires only single-reference calculations, may be to select the one-quasiparticle states by increasing order of their non-projected energy.

We want to stress that we analyzed above the impact of different choices for the ordering of the one-quasiparticle states *within our set*. But the one hundred one-quasiparticle states that compose the set have been selected using one of the choice presented above. We have instead used

a more hybrid approach where we tried explore equitably the deformation of degree of freedom and, for each deformation, the blocking degree of freedom, taking as many one-quasiparticle states that gives relatively low energy projected states (whatever the value of J) as possible. After the fact, this turns out not be the best choice we could have done, but there was no way to know it beforehand. Moreover, this is precisely because we took a more general approach taking a large variety of one-quasiparticle states that we can conclude that some of them are more, or less, important than others. Also, even if we have missed a few projected states of intermediate energy, we have checked that we have in our set the vast majority of the lowest energy projected states (for small values of the angular momentum and for a mesh in deformation with a step of 40 fm^2).

Finally, we mention that even if we have not looked at negative parity states with the same attention, there is no reason to expect they would behave differently. The "convergence" of their energy in Fig. 4.44 is actually better than for states of positive parity.

4.4.4 Convergence of Other Observables

Until now, we have looked only at the energies of the mixed states obtained after configuration mixing. But it is also a good idea to look at other observables to see if the conclusions drawn in previous sections about the energies also hold for them. In that order, we plot in Fig. 4.53, Fig. 4.54, and Fig. 4.55, the evolution of the electric quadrupole moment Q_s, of the magnetic moment μ, and of the reduced transition probabilities $B(E2 : J^+_{i\xi_i} \rightarrow J^+_{f\xi_f})$, respectively, for different mixed states. The definitions of these observables are found in appendix D. As we can observe, for most of the mixed states the observables vary a lot for small numbers of one-quasiparticle states in the GCM, but then they rapidly stabilize themselves around their final value. Only for the two $\frac{7}{2}^+$ mixed states of lowest energy, the observables continue to vary also for large number of states in the GCM. In particular, one can note that their electric quadrupole moment varies in opposition of one another. The same is true for their magnetic moment. If we look at Fig. 4.45, we can see that these two mixed states are very close in energy and we may have not enough (relevant) one-quasiparticle states in our GCM to completely describe these two states.

For the lowest energy $\frac{5}{2}^+$, $\frac{3}{2}^+$, and $\frac{7}{2}^+$, mixed states, we plot in Fig. 4.56, 4.57, and 4.58, respectively, the evolution of the electric quadrupole moment and magnetic moment for the different choices of order for the inclusion of additional one-quasiparticle states. For the $\frac{5}{2}^+$ and $\frac{3}{2}^+$ mixed states, the order does not seem to be very important, and even adding the states at random we rapidly get for the observables a value very close to their final one. This may be taken as an indication that these observables are less sensitive to the one-quasiparticle states in our set, which is a good thing. On the other hand, the observables for the lowest energy $\frac{7}{2}^+$ mixed state display huge variations. And we can observe that, in that case, the variations of the green, blue, and red, curves tend do diminish faster than for the other curves. So, even if there is no reason to think that the final values obtained for the full GCM with one-hundred states is a "converged" one, this may indicate that selecting the one-quasiparticle states by their energy (projected or non-projected) represents a better choice also in that case.

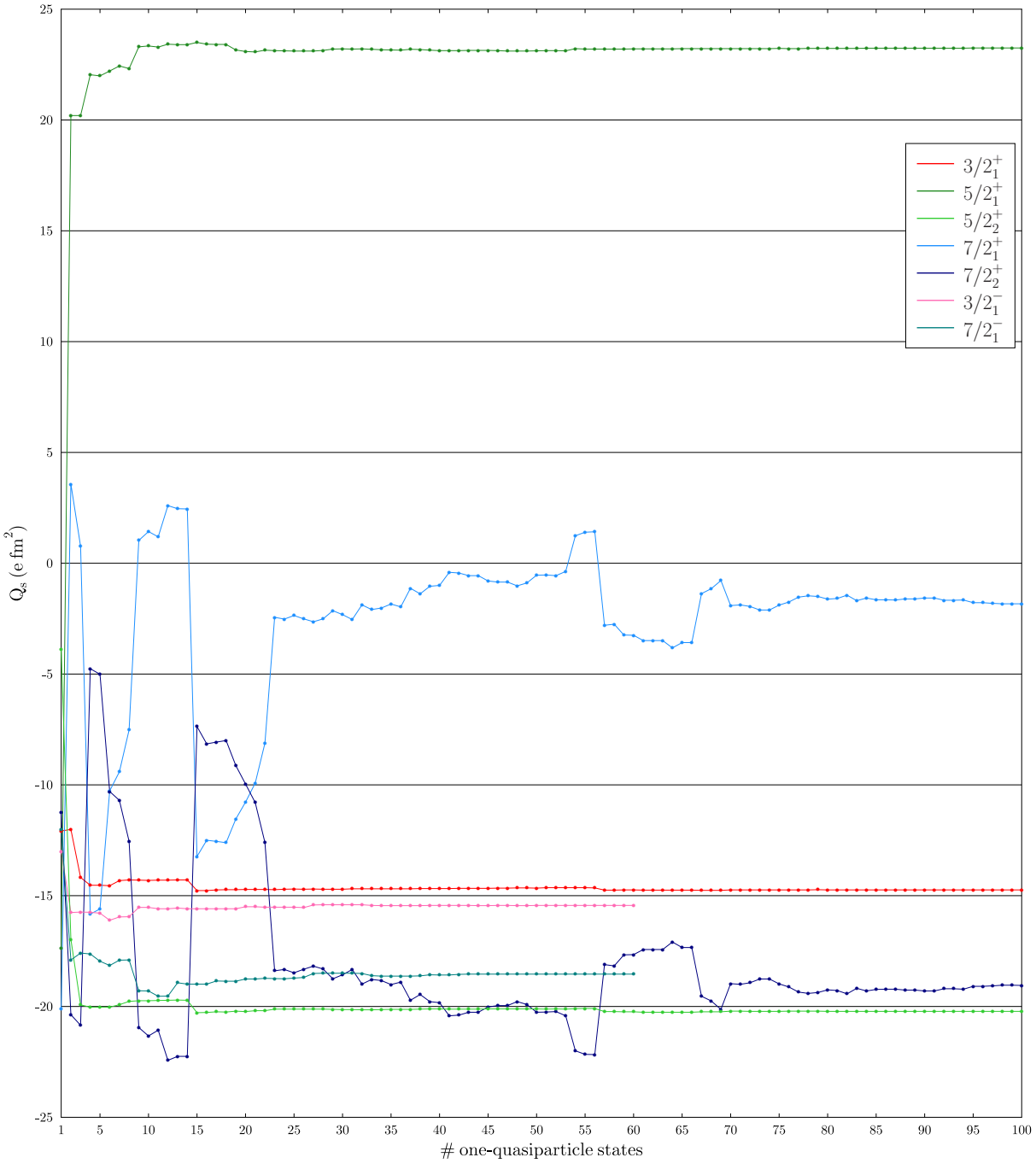

Figure 4.53: Evolution of the electric quadrupole moment Q_s as a function of the number of one-quasiparticle states included in the GCM for different mixed states as indicated.

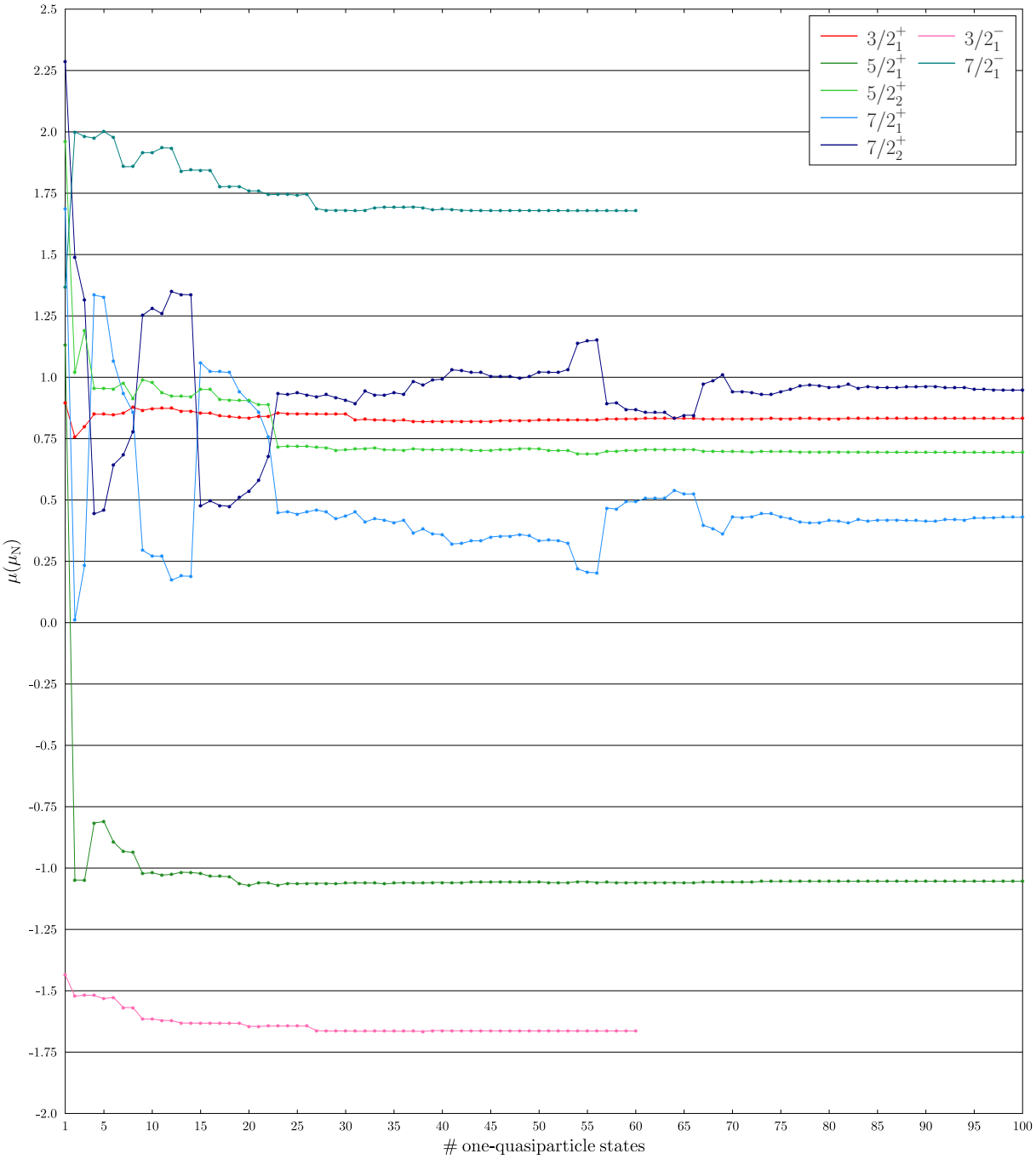

Figure 4.54: Evolution of the magnetic moment μ as a function of the number of one-quasiparticle states included in the GCM for different mixed states as indicated.

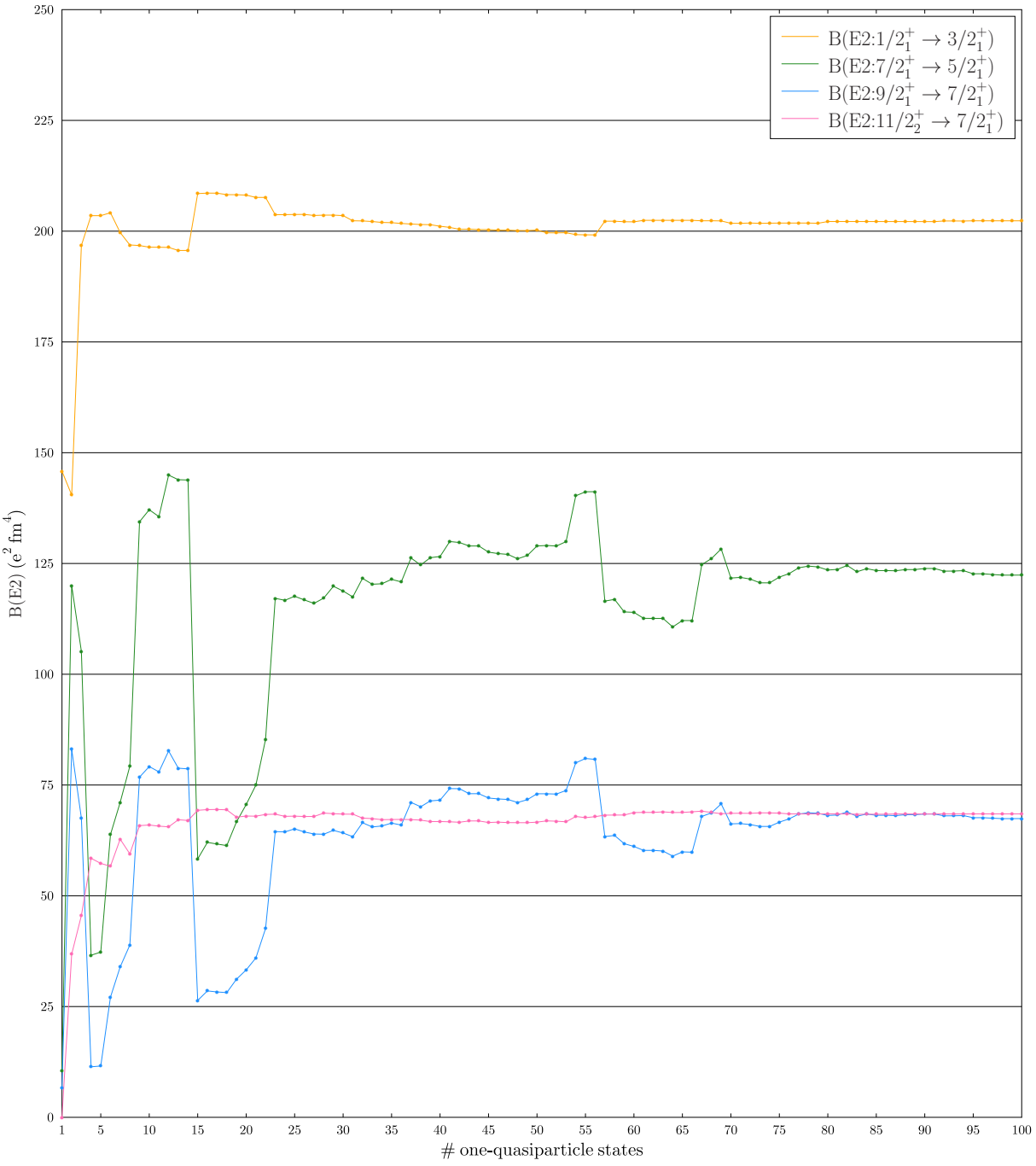

Figure 4.55: Evolution of the reduced transitions probabilties $B(E2 : J^+_{\xi_f} \rightarrow J^+_{\xi_i})$ as a function of the number of one-quasiparticle states included in the GCM for different transitions between mixed states as indicated.

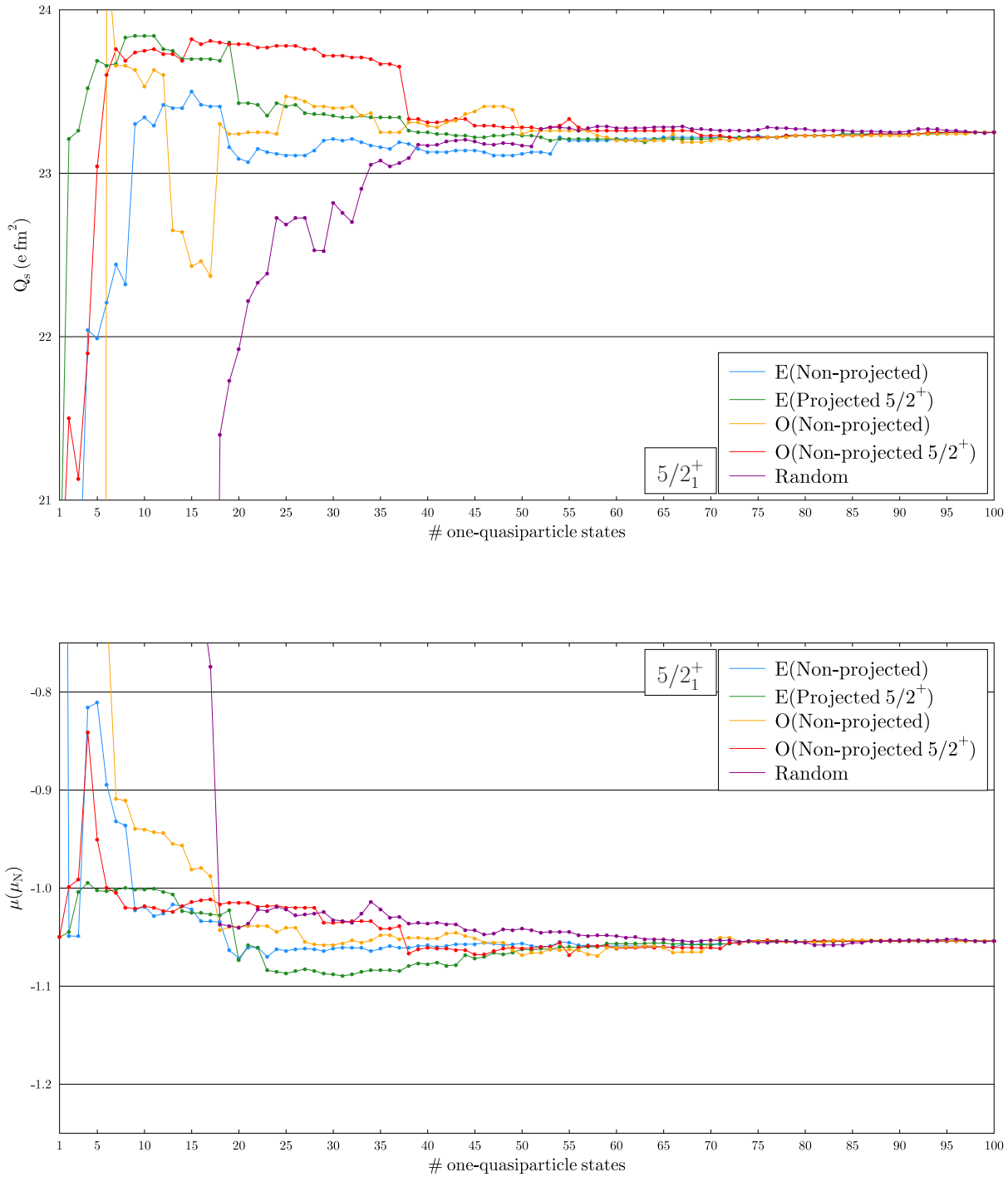

Figure 4.56: Top: Evolution of the electric quadrupole moment Q_s of the mixed state $\frac{5}{21}^+$ for different choices for the order by which the one-quasiparticle states are added to the GCM. Bottom: Same for the magnetic moment μ.

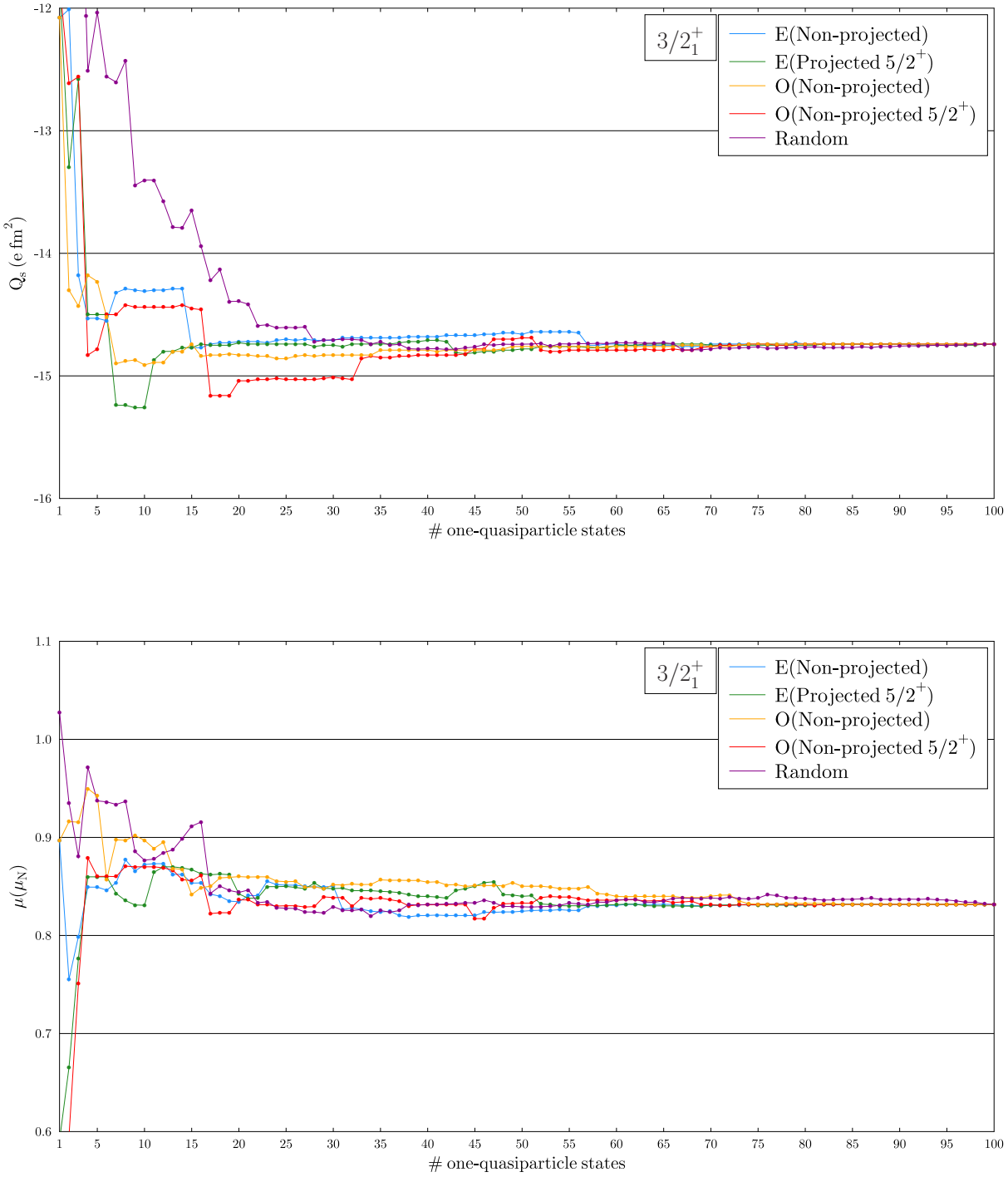

Figure 4.57: Top: Evolution of the electric quadrupole moment Q_s of the mixed state $\frac{3}{21}^+$ for different choices for the order by which the one-quasiparticle states are added to the GCM. Bottom: Same for the magnetic moment μ.

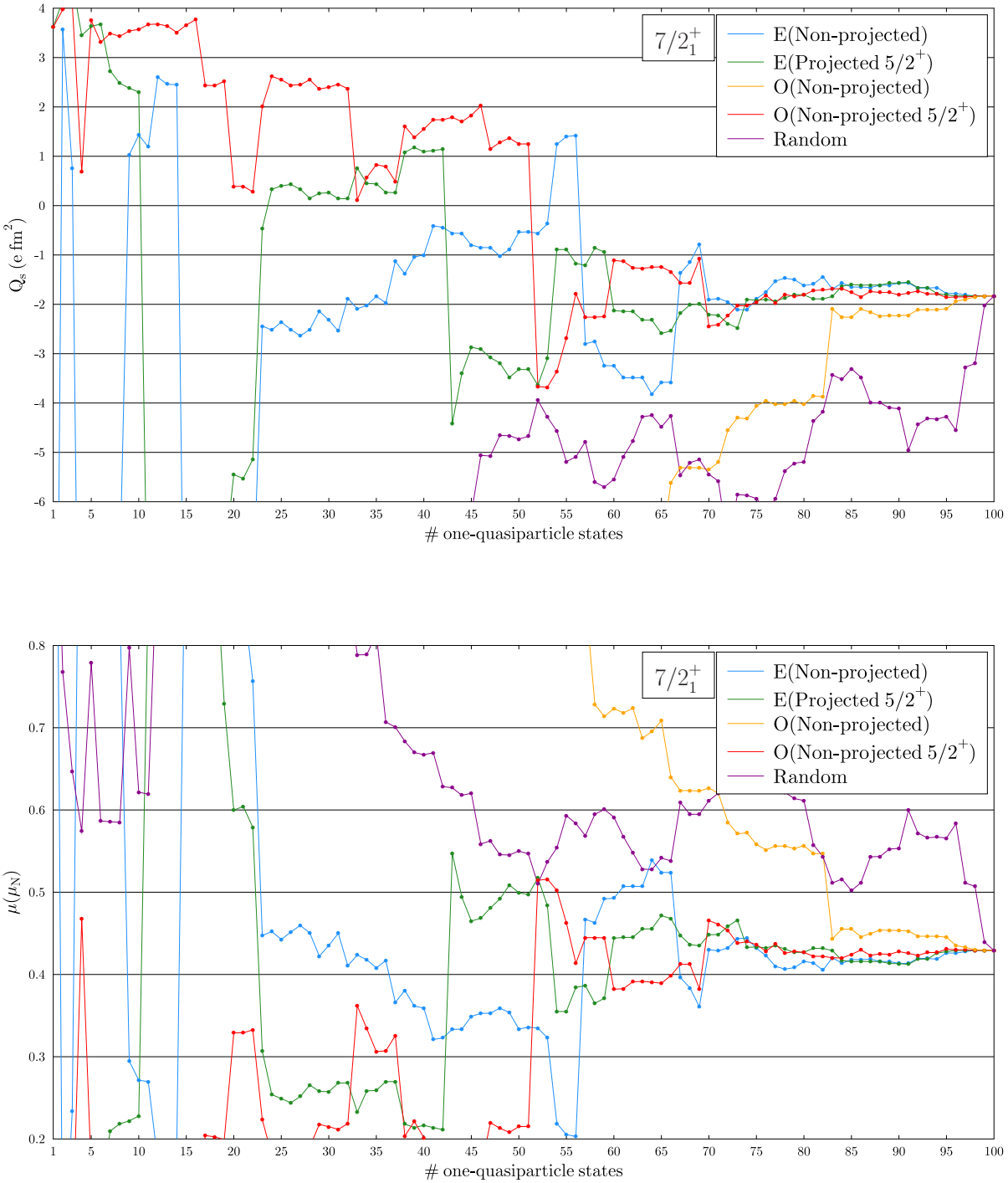

Figure 4.58: Top: Evolution of the electric quadrupole moment Q_s of the mixed state $\frac{7}{21}^+$ for different choices for the order by which the one-quasiparticle states are added to the GCM. Bottom: Same for the magnetic moment μ.

4.4.5 Norm Eigenvalues

As already stated in section 4.4.1, we found that we did not have to cut any norm eigenstates during the configuration mixing. To explain this, we have looked at the values of the norm eigenvalues as a function of the number of projected states included in the GCM. All J^π that we have looked at behave similarly and, as examples, we plot (in logarithmic scale) the results for $J^\pi = \frac{5}{2}^+$ and $J^\pi = \frac{3}{2}^-$ in Fig. 4.59, Fig. 4.60, and Fig. 4.61. We precise that, for both parities, we have included all the one-quasiparticle states (one hundred for positive parity and sixty for negative parity), and that, for each J^π, we add the projected states by order of increasing projected energy. We observe that, for both J^π, after that a certain number of projected states

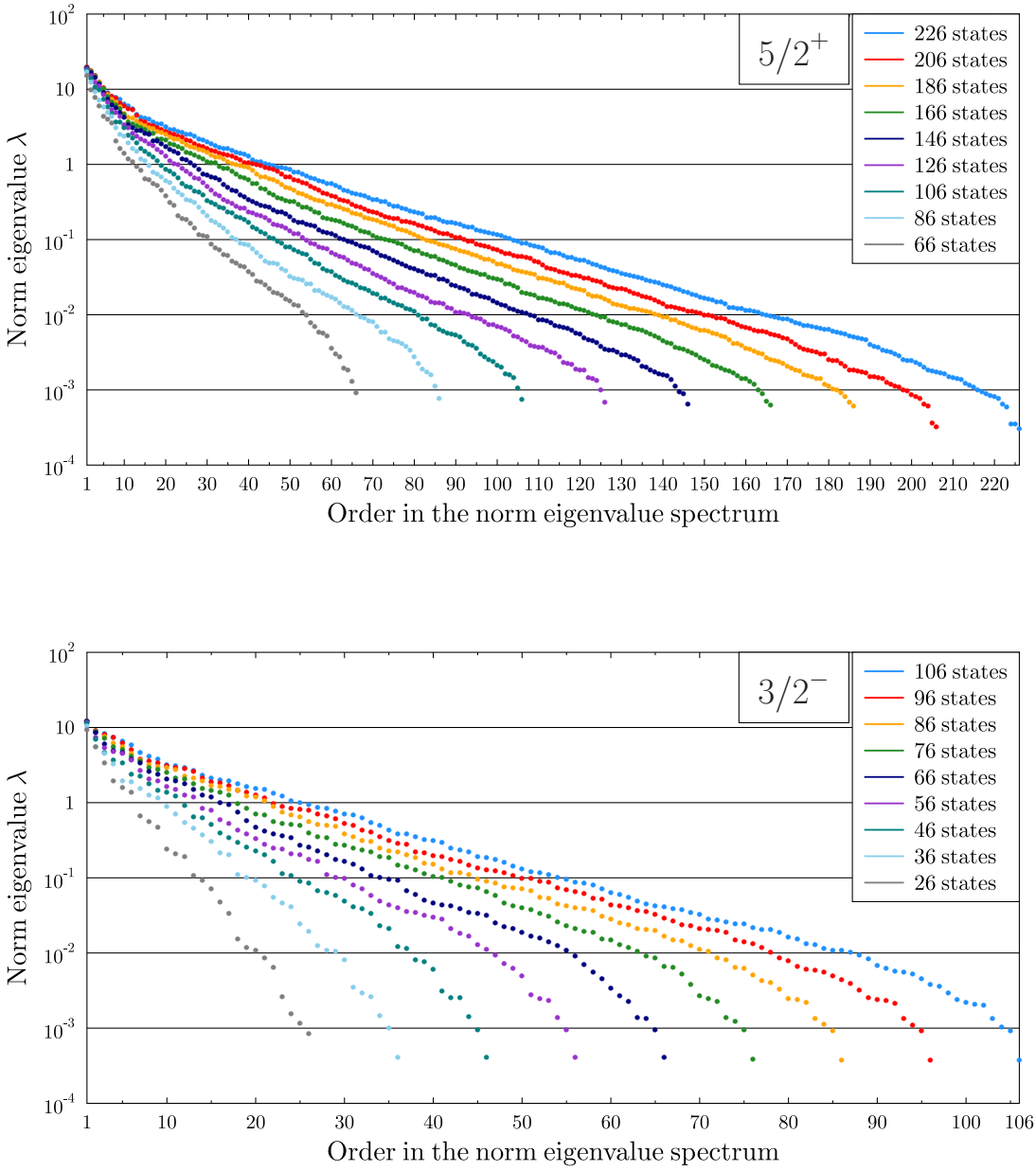

Figure 4.59: Top: Norm eigenvalues of $J^\pi = \frac{5}{2}^+$ for different numbers of projected states included in the GCM as indicated. Bottom: Same for $J^\pi = \frac{3}{2}^-$.

has been included, the biggest and smallest norm eigenvalues only vary by a little, and the latter are always bigger than 10^{-4}. Instead of pushing the extremal norm eigenvalues up or down, including more projected states seems to make more dense the "mesh" of norm eigenvalues. This is particularly visible in Fig. 4.61 where we have normalized all the abscissa of Fig. 4.59. We see that the values taken by the norm eigenvalues are very similar for all the sets of projected states considered here.

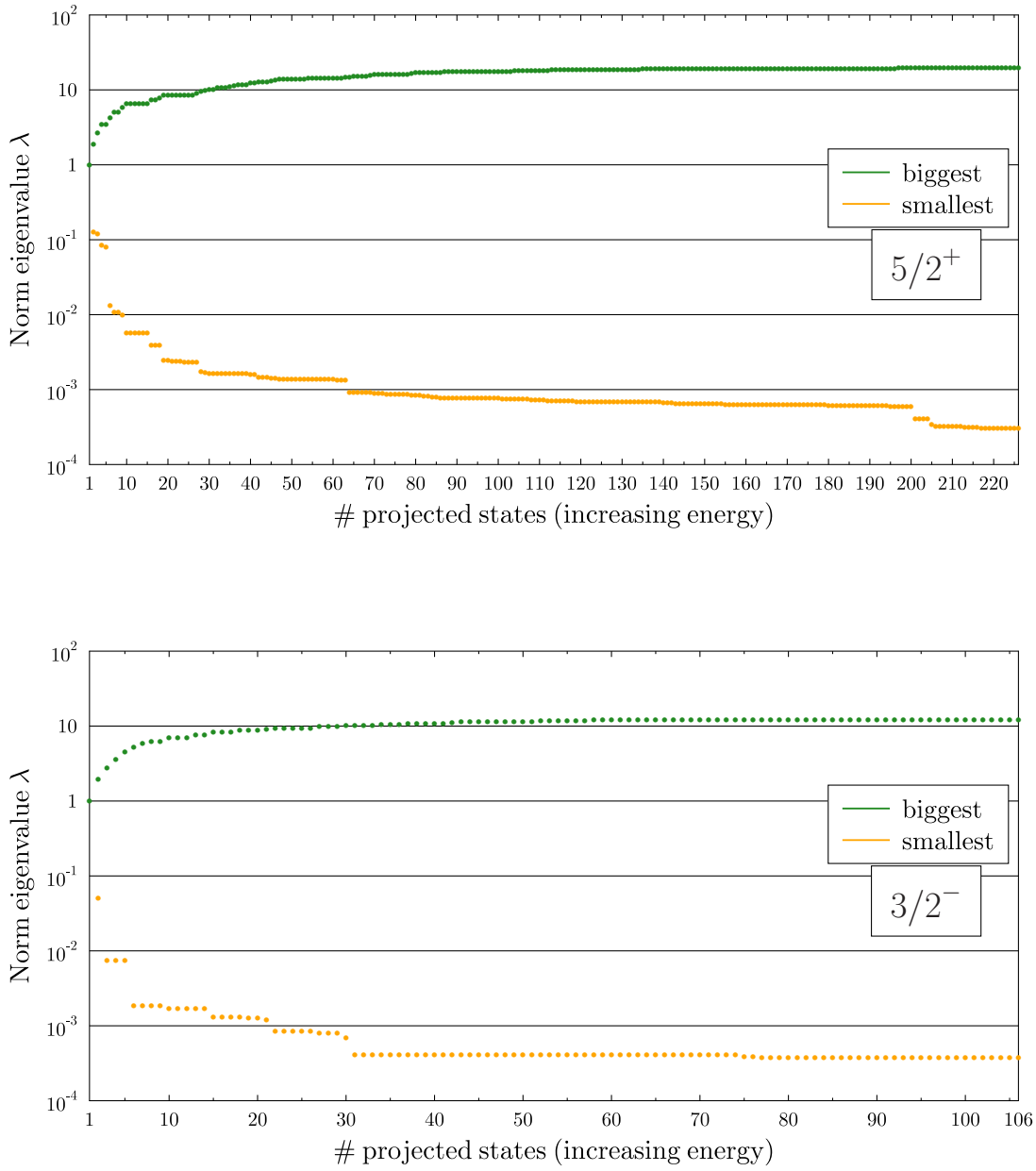

Figure 4.60: Top: Evolution of the biggest and smallest norm eigenvalues of $J^\pi = \frac{5}{2}^+$ as a function of the number of projected states in the GCM as indicated. Bottom: Same for $J^\pi = \frac{3}{2}^-$.

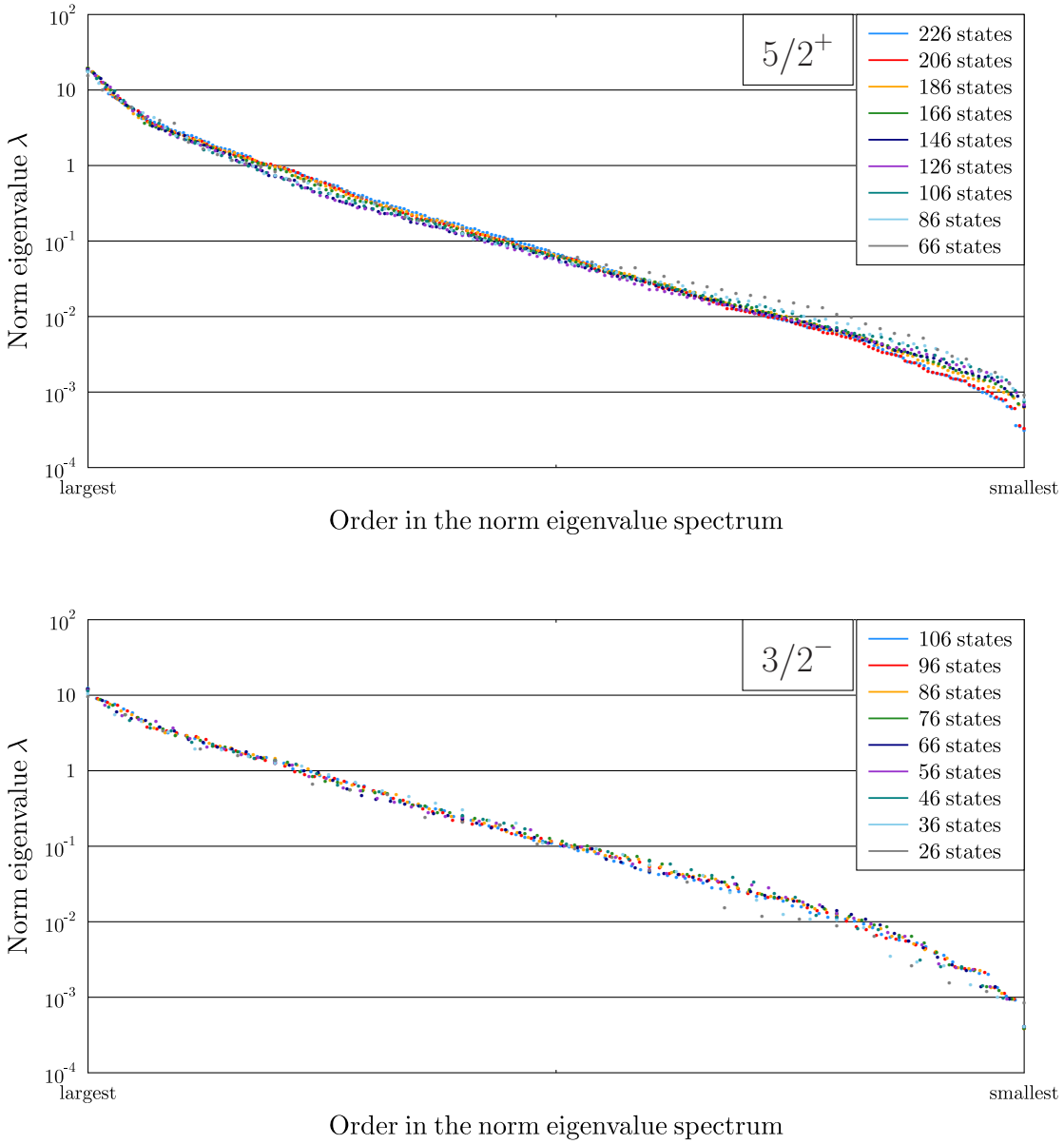

Figure 4.61: Same as Fig. 4.59 but with the abscissa normalized.

4.4.6 Precision of the Calculation

In this last technical section, we briefly investigate the numerical accuracy of the solutions of the HWG equation as a function of the number of one-quasiparticle states included in the GCM. We add here the one-quasiparticle states by order of increasing non-projected energy. Taking the lowest energy $\frac{5}{2}^+$ and the lowest energy $\frac{3}{2}^-$ mixed states as examples, we plot in Fig. 4.62 the evolution of the neutron and proton variances

$$\begin{aligned}(\Delta N)^2 &= \langle \Lambda M \xi | \hat{N}^2 | \Lambda M \xi \rangle - \langle \Lambda M \xi | \hat{N} | \Lambda M \xi \rangle^2 \ , \\ (\Delta Z)^2 &= \langle \Lambda M \xi | \hat{Z}^2 | \Lambda M \xi \rangle - \langle \Lambda M \xi | \hat{Z} | \Lambda M \xi \rangle^2 \ .\end{aligned} \tag{4.11}$$

and of the root mean square deviation of the HWG equation from 0

$$RMS(\xi,\Lambda,\Omega_I^\Lambda) = \sqrt{\frac{\sum_{\alpha=1}^{\Omega_I^\Lambda}\left(\sum_{\alpha'=1}^{\Omega_I^\Lambda}\left(\langle\Lambda M\alpha|\hat{H}|\Lambda M\alpha'\rangle - E_\xi^\Lambda(\Omega_I^\Lambda)\langle\Lambda M\alpha|\Lambda M\alpha'\rangle\right)F_\xi^\Lambda(\alpha')\right)^2}{\Omega_I^\Lambda}}, \tag{4.12}$$

where we have used the notations of section 3.5.4 for the equation (4.12). As we can see, all the quantites remain very small even when including all the one-quasiparticle states. We mention that the quantity $RMS(\xi,\Lambda,\Omega_I^\Lambda)$ is very sensitive to the removal of norm eigenvalues. Indeed, it increases rather rapidly with an increasing value of the norm eigenvalue cut-off. In our case, we did not remove any of the norm eigenvalues so it remained small. Finally, for selected J^π values, we display in Tab. 4.10 the values of J_e obtained from

$$\langle\Lambda M\xi|\hat{J}^2|\Lambda M\xi\rangle = J_e(J_e+1) \tag{4.13}$$

for the ten first eigenvalues of the Hamiltonian obtained in the final calculations including all the one-quasiparticle states (one hundred for positive parity states and sixty for the negative parity states). The inaccuracy for J_e is of the order of 10^{-3} or better. For some eigenvalues higher in energy the inaccuracy can be as big as 10^{-2}, but these states will not be considered in the final comparison to experiment. Actually, the most inaccurate used in the next section will have a deviation of 3.10^{-3} from the correct value and it is a state with $J^\pi = \frac{1}{2}$. Paradoxically, these states, which have the smallest value of J possible (for an odd-mass nucleus), tend to be the most inaccurate for J_e.

ξ	J_e				
	$J^\pi = \frac{5}{2}^+$	$J^\pi = \frac{9}{2}^+$	$J^\pi = \frac{15}{2}^+$	$J^\pi = \frac{1}{2}^-$	$J^\pi = \frac{3}{2}^-$
1	2.500	4.500	7.500	0.499	1.500
2	2.500	4.500	7.500	0.495	1.499
3	2.500	4.500	7.499	0.500	1.498
4	2.500	4.500	7.500	0.499	1.496
5	2.500	4.500	7.499	0.500	1.500
6	2.500	4.500	7.500	0.499	1.500
7	2.500	4.500	7.500	0.500	1.499
8	2.501	4.500	7.499	0.500	1.500
9	2.502	4.500	7.499	0.503	1.499
10	2.500	4.500	7.498	0.506	1.500

Table 4.10: Values of J_e, obtained from equation (4.13), for the ten lowest energy eigenstates with different values of J^π. All one hundred one-quasiparticle states of positive parity, and all sixty one-quasiparticle states of negative parity, have been taken into account in the GCM.

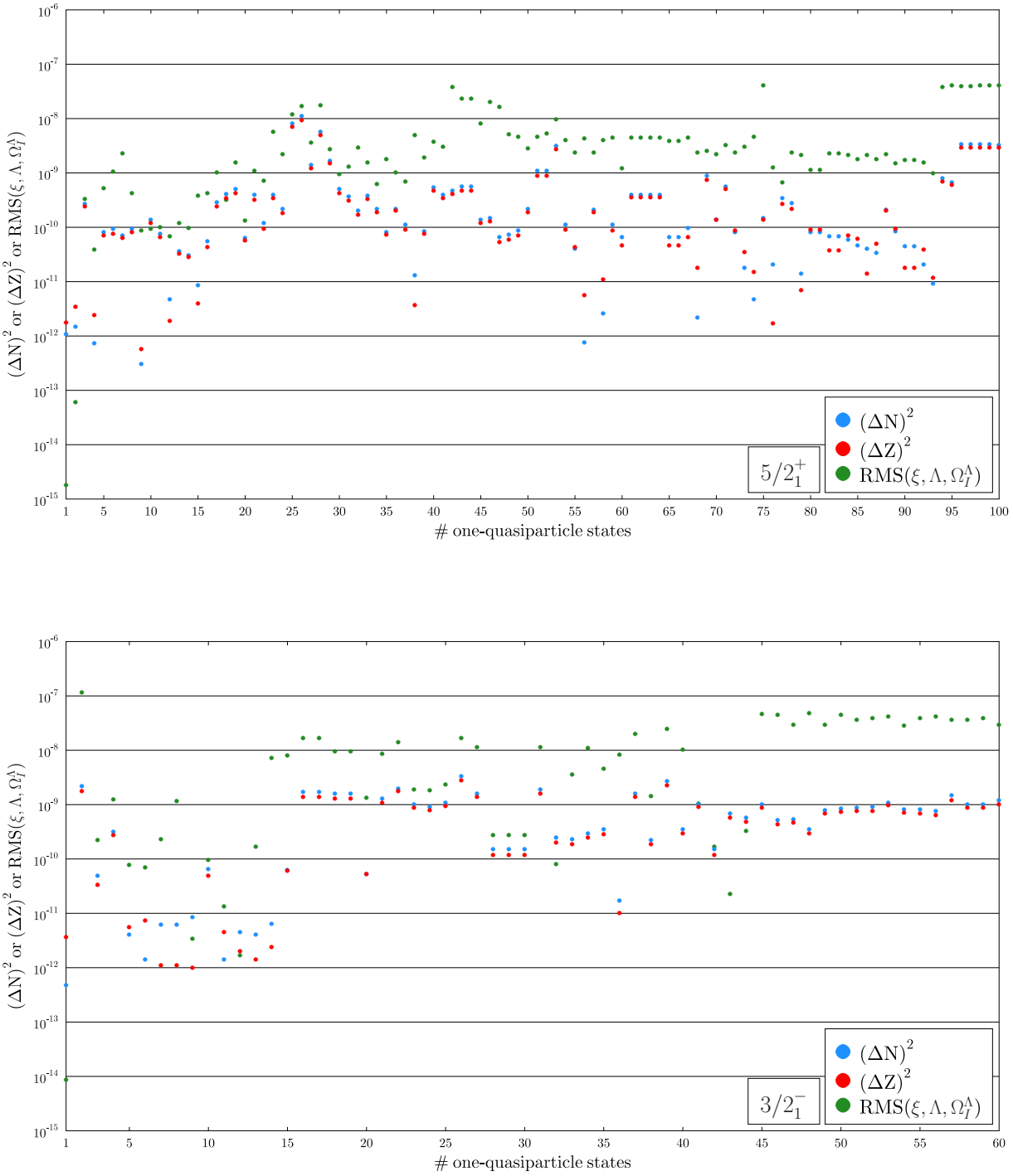

Figure 4.62: Top: Evolution of the variance of neutron number $(\Delta N)^2$, of the variance of proton number $(\Delta Z)^2$, and of root mean square deviation of the HWG equation from 0, equation (4.12), as a function of the number of one-quasiparticle states included in the GCM for the lowest energy $J^\pi = \frac{5}{2}^+$ mixed state. Bottom: Same for the lowest energy $J^\pi = \frac{3}{2}^-$ mixed state.

4.4.7 Comparison to Experiment

The ultimate analysis of our calculations consists in a direct comparison of our results to experimental data; the latter being taken, for the most of them, from [65]. We begin by looking at the properties of the ground state that are listed in Tab. 4.11. First and foremost, we note that our calculations predict the correct angular momentum and parity values: $J^\pi = \frac{5}{2}^+$ for the ground state. All the other observables (binding energy, spectroscopic moment, magnetic moment, and charge radius) are too large (in absolute value) in our calculations compared to their experimentally measured value. For example, the total binding energy is off by approximately 15 MeV. We also precise that the charge radius has been calculated using a (crude) correction for the finite size of the proton [21]

$$r_{ch}^2 = r_p^2 + 0.64 \quad , \tag{4.14}$$

where

$$r_p^2 = \frac{1}{Z}\langle \Lambda M \xi | \hat{r}_p^2 | \Lambda M \xi \rangle \tag{4.15}$$

is the square radius of the protons' intrinsic charge distribution.
In the last row of Tab. 4.11, we print the relative error

$$\frac{\mathrm{O}_{\mathrm{theory}} - \mathrm{O}_{\mathrm{experiment}}}{\mathrm{O}_{\mathrm{experiment}}} \tag{4.16}$$

for all quantities O. We see that the largest deviation from experimental data is for the magnetic moment μ which is 23 % too big. But we want to stress that we use in our calculations the bare nucleon electric charges and the bare nucleon g-factors for the computation of the electric quadrupole moments and of the magnetic moments (see appendix D). And the fact that we do not perfectly reproduce experimental data does not come as surprise given the bad properties of the SLyMR0 interaction [122]. It is nevertheless encouraging to see that, even with this rather mediocre interaction, we obtain results that are only off by ten or twenty percent. Moreover, we get in our calculations the correct sign for both the spectroscopic quadrupole moment and the magnetic moment of the ground state.

	J^π	Binding energy (MeV)	Q_s ($e\,\mathrm{fm}^2$)	μ (μ_N)	$\sqrt{\langle \hat{r}_{ch}^2 \rangle}$ (fm)
Experimental	$\frac{5}{2}^+$	-205.587	20.1(3)	$-0.85545(8)$	$3.0290(7)_{\mathrm{stat}}[31]_{\mathrm{syst}}$
MR-EDF	$\frac{5}{2}^+$	-221.875	23.25	-1.0538	3.118
Relative error (%)	-	+8	+16	+23	+3

Table 4.11: Ground-state properties of ^{25}Mg. For experimental data the values are taken from [3] for the binding energy, [65] for the electric quadrupole moment and the magnetic moment, and [161] for the charge radius. The numbers between brackets are the uncertainties (e.g. 20.1(3) = 20.1 ± 0.3).

In Figure 4.63, we display the energy spectrum of ^{25}Mg from experimental data, from our MR-EDF calculations, and from a shell-model calculation carried out in *sd*-shell model space with the USDB interation [38] and the NuShellX@MSU numerical code [39]. As we can observe, except for the first $\frac{3}{2}^+$ and the second $\frac{7}{2}^+$ states in our calculations, there is a very good agreement between all three spectra for the states below 4 MeV. As we will see below, the first $\frac{3}{2}^+$ and the second $\frac{7}{2}^+$ states belong to a rotational band that is not particularly well reproduced in our calculations. Also, and as previously noted in the section 4.3.6 on cranking, MR-EDF spectra tend to be too spread out. This is also what can see seen here, with all the excitation energies of the levels, as well as the spacing between the levels, becoming too large with an increasing excitation energy. Overall, the shell-model gives better results than our calculation, but it is important to emphasize that contrary to the USDB interaction, the SLyMR0 interaction has not been fitted to any experimental data of nuclei lying in the *sd*-shell. Besides, as the shell-model calculations have been realized on a basic desktop computer, only the *sd*-shell model space was considered and thus there is no state of negative parity in the spectrum. By contrast, the two levels of negative parity appearing below 5 MeV in the experimental spectrum are fairly well reproduced in our calculation. This is indeed an advantage of our model compared to shell model that states of both parities are treated exactly in the same way: (i) the valence space considered is composed of all occupied particle, (ii) considering enough single-particle wave functions in our three-dimensional cartesian mesh to treat states of both parities is not as numerically limiting as is the consideration of large model space in shell model calculations.

Taking now a more global perspective, we compare in Fig. 4.64 the experimental data for the rotational bands built on the lowest energy band heads with our MR-EDF calculations. For the experimental data, we follow the band assignments of [65]. For our theoretical calculations, we have determined the assignment of each state by looking how strong are the B(E2) and B(M1) values for the transitions from this state to other states (or the other way around). In Figures 4.65, 4.66, 4.67, and 4.68, each theoretical rotational band is compared to its experimental counterpart. We also give in those figures the B(E2) and B(M1) values for the intra-band transitions. Finally, in Fig. 4.69, we give for the three lowest bands of positive parity, the values of the reduced probabilities for some of the inter-band transitions. As a general comment, we can say that the overall picture is similar for experimental and theoretical results. In particular the excitation energies of the band heads of our calculations are in good agreement with the corresponding experimental values, except for the second band which will be commented below.
The first rotational band (see Fig. 4.65), based on the $J^\pi = \frac{5}{2}^+$ ground state, is probably the one which is the best described by our calculations, even if again the states are too spread out. The B(E2) and B(M1) values up to $J^\pi = \frac{11}{2}^+$, even if often quantitatively too large, are qualitatively in good agreement with experimental data.
The second rotational band (see Fig. 4.66) on the other hand, is not well described at all. There is an inversion of the $\frac{1}{2}^+$ and $\frac{3}{2}^+$ states, and also of the $\frac{5}{2}^+$ and $\frac{7}{2}^+$ states, compared to experiment. The experimental $\frac{11}{2}^+$ state has not been assigned/observed yet, but we suspect that, contrary to our calculations, it will be higher in energy than the $\frac{9}{2}^+$ state. The reduced probabilities of the transitions are, overall, not completely stupid, but if we look more specifically at the transitions between the inverted states, they are very badly described.
The third rotational band (see Fig. 4.67) has not been assigned in [65], but it has been suggested in previous works [115, 116, 80] based on results from either the Nilsson model or shell-model calculations. Similar $J^\pi = \frac{1}{2}^+$, $\frac{3}{2}^+$, and $\frac{5}{2}^+$, states are also present also in the shell-model calculations with USDB as can be seen in Fig. 4.63. No transition probability has been measured yet, only a lower bound of 7 e^2 fm^4 for the transition from the $\frac{11}{2}^+$ state to the $\frac{7}{2}^+$ state, which is

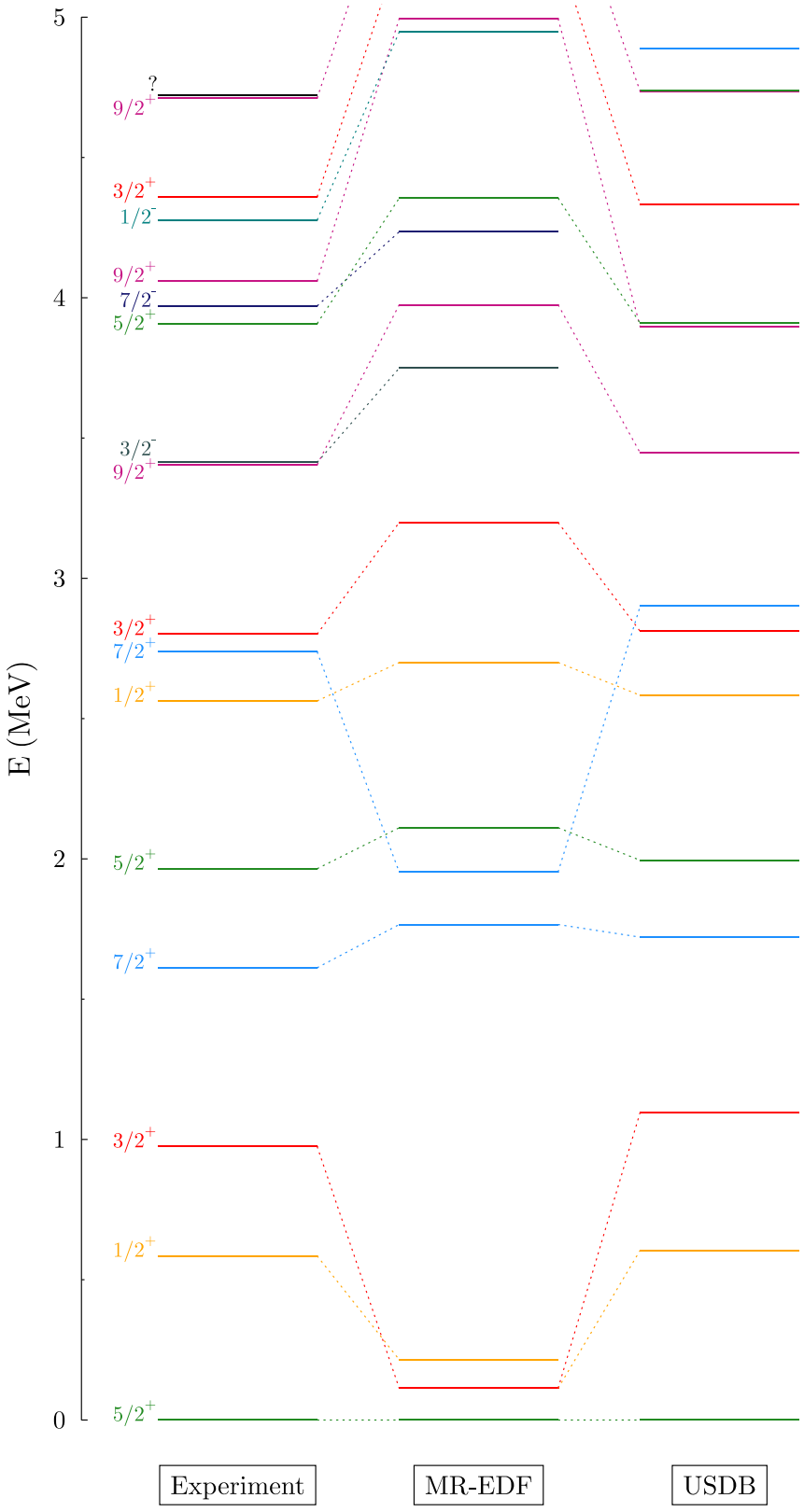

Figure 4.63: Comparison between experimental observations, MR-EDF calculations, and shell-model calculations, for the states below 5 MeV excitation energy. The experimental data are taken from [65]. The shell-model calculations have been realized in the *sd*-shell model space using the USDB interaction [38] and the NuShellX@MSU numerical code [39].

far from being helpful. A problem with the theoretical band, which will be commented lateron, is that the $\frac{7}{2}^+$ is clearly too high in energy, and thus too close to the $\frac{9}{2}^+$ state.

The fourth rotational band (see Fig. 4.68) is based on a $J^\pi = \frac{3}{2}^-$ state in both experimental and theoretical data. In the article by Firestone [65], there are two bands of negative parity as shown in Fig. 4.64, one based on a $\frac{3}{2}^-$ state, and the other one based on a $\frac{1}{2}^-$ state. In our theoretical calculations, however, these two states belong to the same rotational band, even if the E2 transitions with $\Delta J = 2$ are favoured. This is also what is obtained in the Nilsson model, with a strongly decoupled $K^\pi = \frac{1}{2}^-$ band [116, 80]. For a long time, the fourth state in the band was identified to be either a $J^\pi = \frac{11}{2}^-$ state or a $J^\pi = \frac{7}{2}^-$ state [115, 41, 80], with a preference for the former (presumably because of the picture one obtains in the Nilsson model). However, in the article by Firestone [65], the level is identified as having $J^\pi = \frac{7}{2}^-$, supposedly because there is a M1 transition to the first $\frac{7}{2}^-$ state which makes it impossible for this state to be a $\frac{11}{2}^-$ state. There is no similar $J^\pi = \frac{7}{2}^-$ state, i.e. with such B(E2) and B(M1) to the first $\frac{7}{2}^-$ state, in our calculations. As we have taken a smaller number of one-quasiparticle states for negative parity, it is possible that we missed the ones which are important for the description of this state, although we think that this is quite unlikely. Indeed, if we consider positive parity states, we can see that in the spectrum of K components of the one-quasiparticle state giving the lowest projected $\frac{5}{2}^+$ state (Fig. 4.21), we find also relatively low energy $\frac{1}{2}^+$ and $\frac{3}{2}^+$ states. Conversely, in the spectrum of K components of the one-quasiparticle state giving the lowest projected $\frac{1}{2}^+$ state (Fig. 4.22), we find also relatively a low-lying $\frac{5}{2}^+$ state. So it is unlikely to consider that in all sixty one-quasiparticle states of negative parity considered in our configuration mixing, none would have given such a $\frac{7}{2}^-$ state. Other explanations could be: (i) the bad quality of the SLyMR0 interaction (but in overall this interaction describes not so badly the other states at same energy), (ii) that this state is indeed a $\frac{11}{2}^-$ state, with an erroneous M1 assignment for the transition to the first $\frac{7}{2}^-$ and with our calculation getting the state inverted with the $\frac{5}{2}^-$ state compared to what it should be, (iii) that this state is described by three-, or higher, quasiparticle states, (iv) other explanations we have not thought of.

Finally, we look at the inter-band transitions displayed in Fig. 4.69. As we can observe, all the transitions from the second band to the first are very small in experimental data, which is also the case in our calculations except for the second $\frac{7}{2}^+$ state. The second $\frac{7}{2}^+$ state is largely connected to the first band, either with the first $\frac{5}{2}^+$ state, the first $\frac{7}{2}^+$ state, or the first $\frac{9}{2}^+$ state. This may come from a too large mixing of the $\frac{7}{2}^+$ states in each of to the two bands. This also would explain the particular behaviour of the electric quadrupole moment (Fig. 4.53), of the magnetic moment (Fig. 4.54), and of the B(E2) value (Fig. 4.55) in the analysis of convergence of these two $\frac{7}{2}^+$ states. The origin of the problem probably lies again with the SLyMR0 interaction. As we already pointed out in section 4.3.1 when discussing projected energy surfaces, the surface for the lowest $\frac{7}{2}^+$ projected states (Fig. 4.17) is particular in the sense that its minimum is very wide and cover both the region where is located the minimum of $\frac{5}{2}^+$ projected states and the region where is located the minimum of $\frac{1}{2}^+$ projected states. We expect the former region to be more important for the description of the $\frac{7}{2}^+$ based on the $\frac{5}{2}^+$ ground state and the latter to be more important for the description of the $\frac{7}{2}^+$ based on the first $\frac{1}{2}^+$ excited state (in experimental data). But in our calculation the states are too close in energy and seem to be too much mixed after the configuration mixing. This problem may also be the reason why the third $\frac{7}{2}^+$ state, shown in Fig. 4.67, is too close to the $\frac{9}{2}^+$ state in the rotational band that both states belong to. There clearly is a problem with the $\frac{7}{2}^+$ states in our calculations. It would be interesting to see

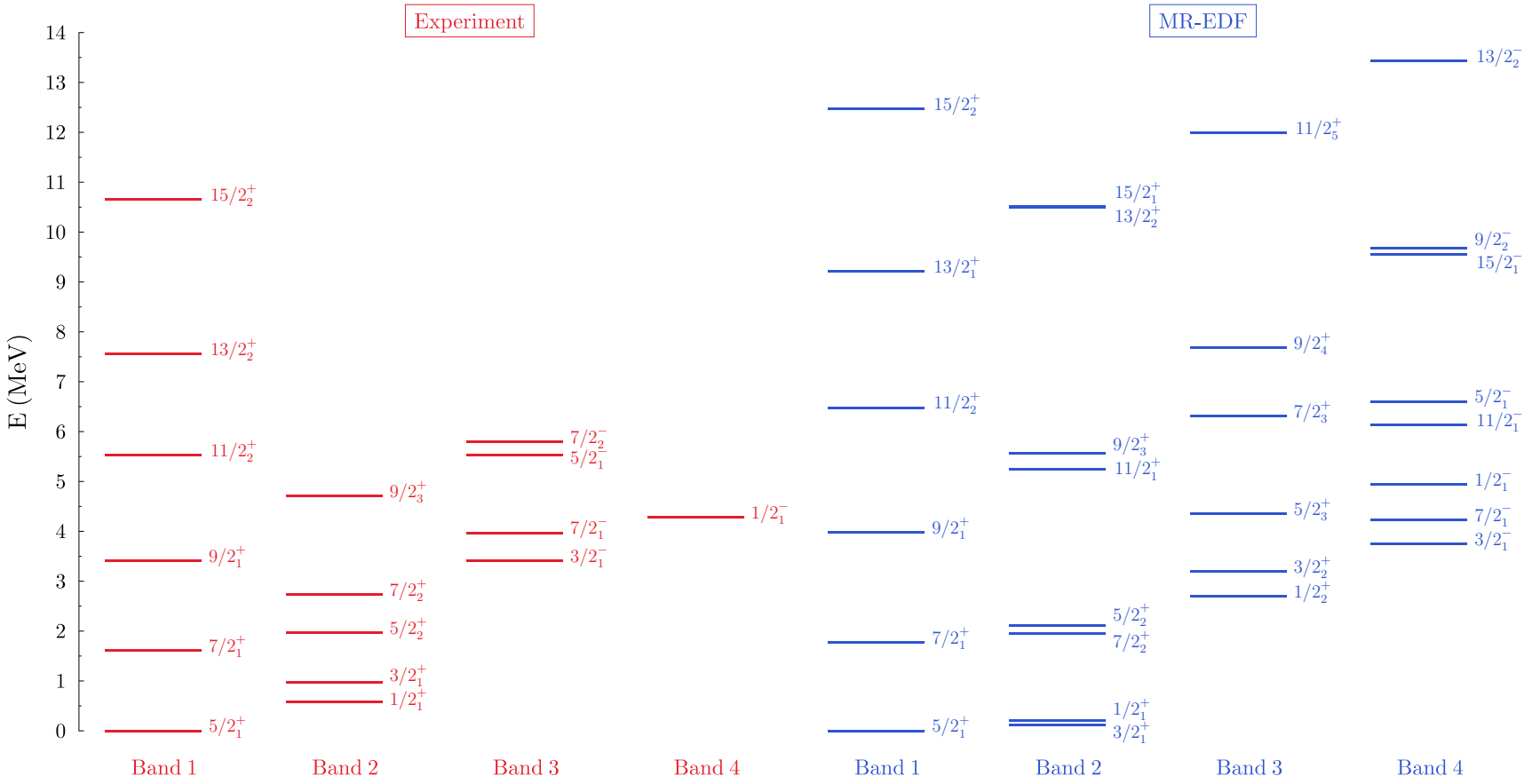

Figure 4.64: Comparison between experimental observations and theoretical calculations for the lowest rotational bands, i.e. the bands with the band heads of lowest energy. We also give the order of appearance of the states in the excitation spectrum. The experimental data (and band assignments) are taken from [65].

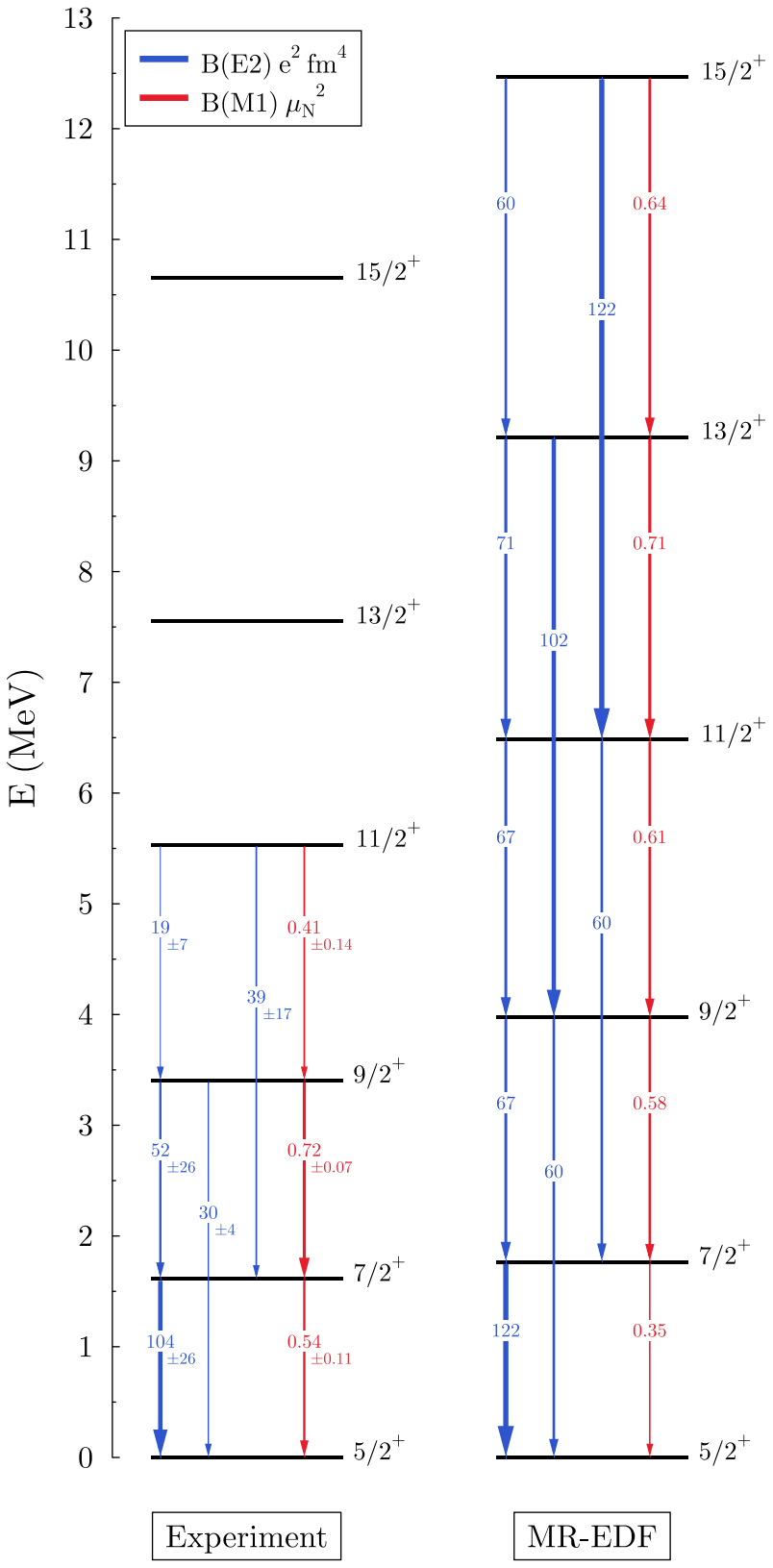

Figure 4.65: Comparison between experimental observations and theoretical calculations for the rotational band built on the $J^\pi = \frac{5}{2}^+$ ground state. The experimental data are taken from [65].

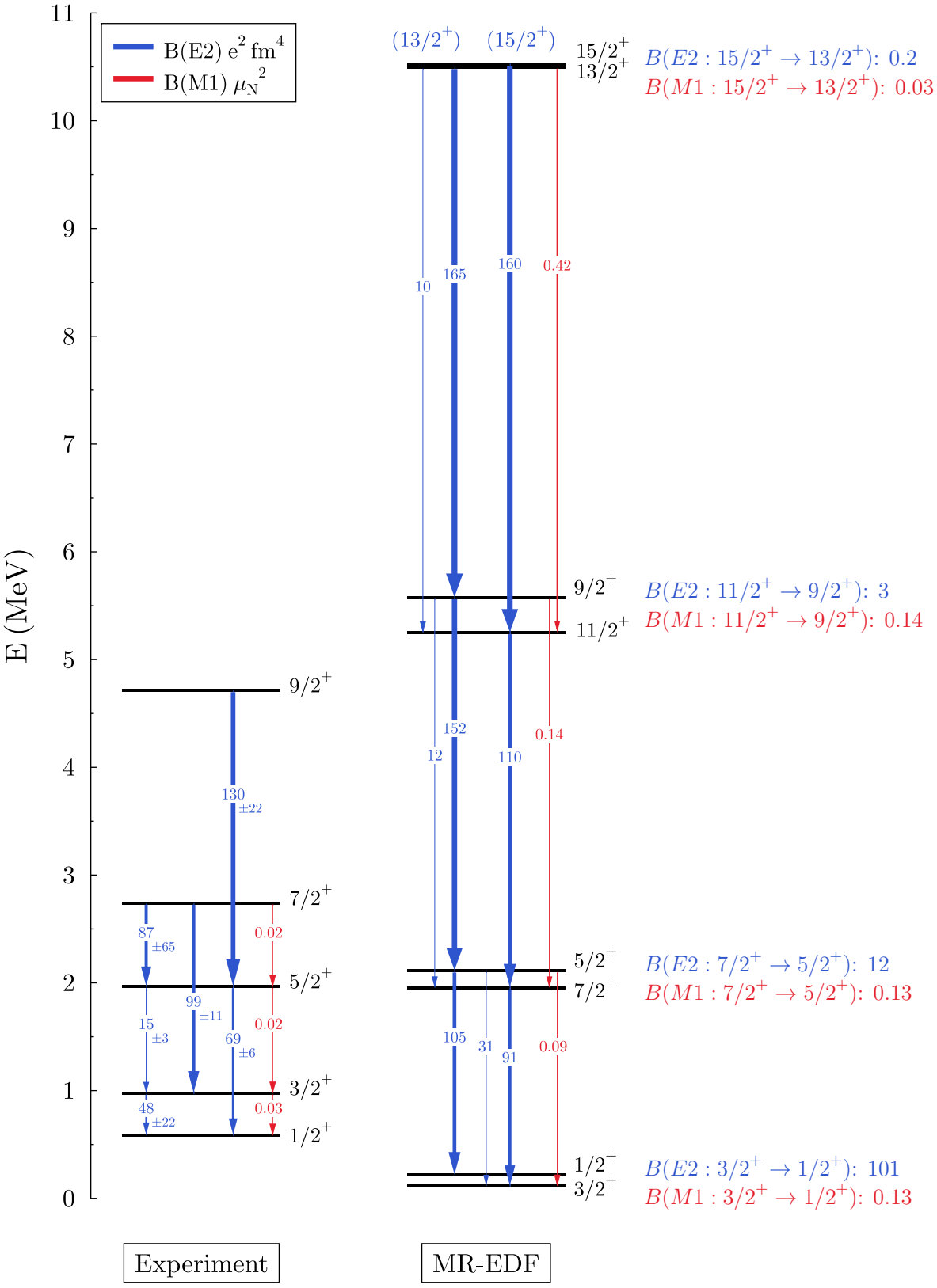

Figure 4.66: Comparison between experimental observations and theoretical calculations for the rotational band built on the first $J^\pi = \frac{1}{2}^+$ state (in experimental data). The experimental data are taken from [65].

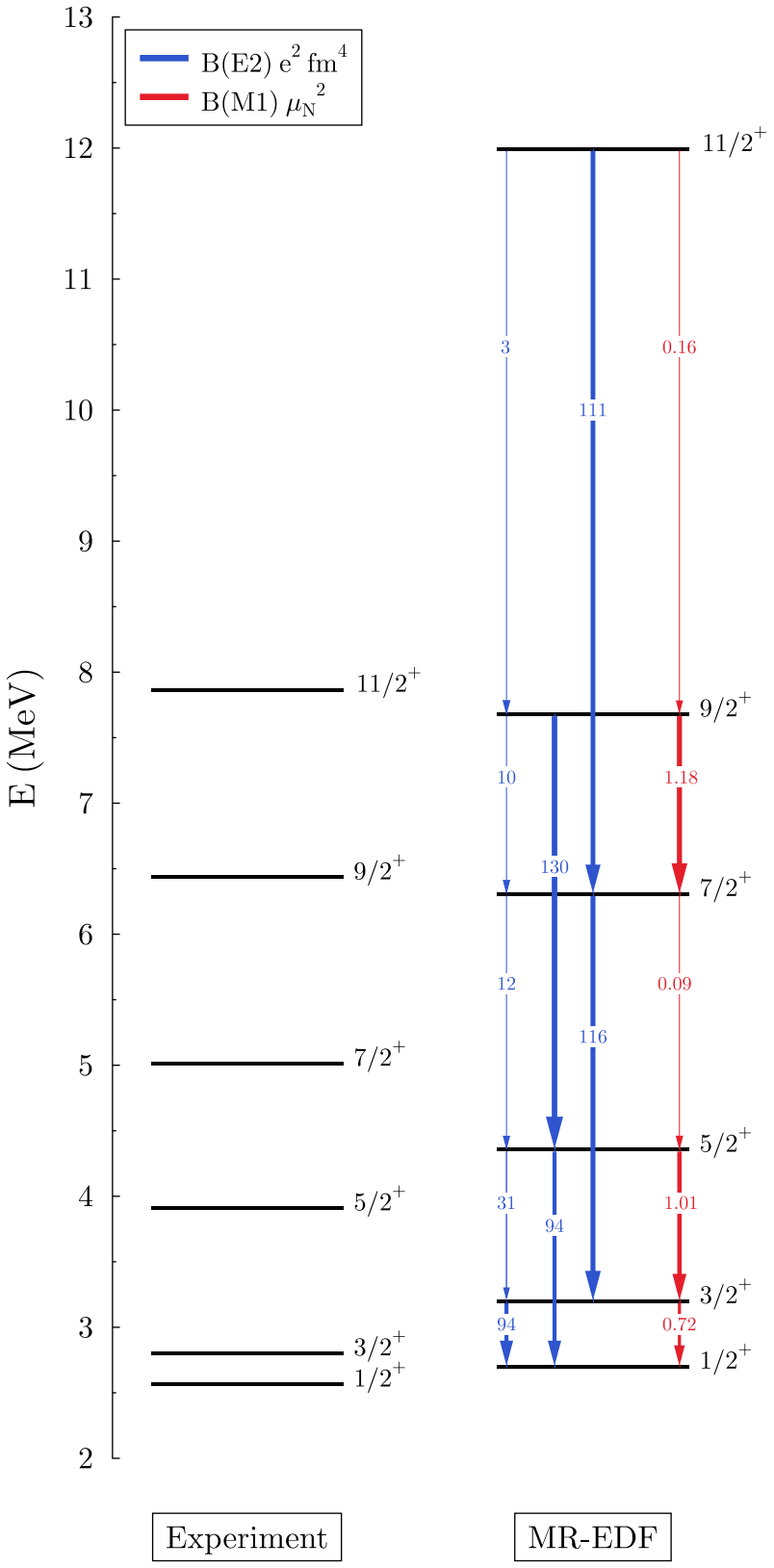

Figure 4.67: Comparison between experimental observations and theoretical calculations for the rotational band built on the second $J^\pi = \frac{1}{2}^+$ state (in theoretical calculations). The experimental data are taken from [65], but the band assignment is taken from [80].

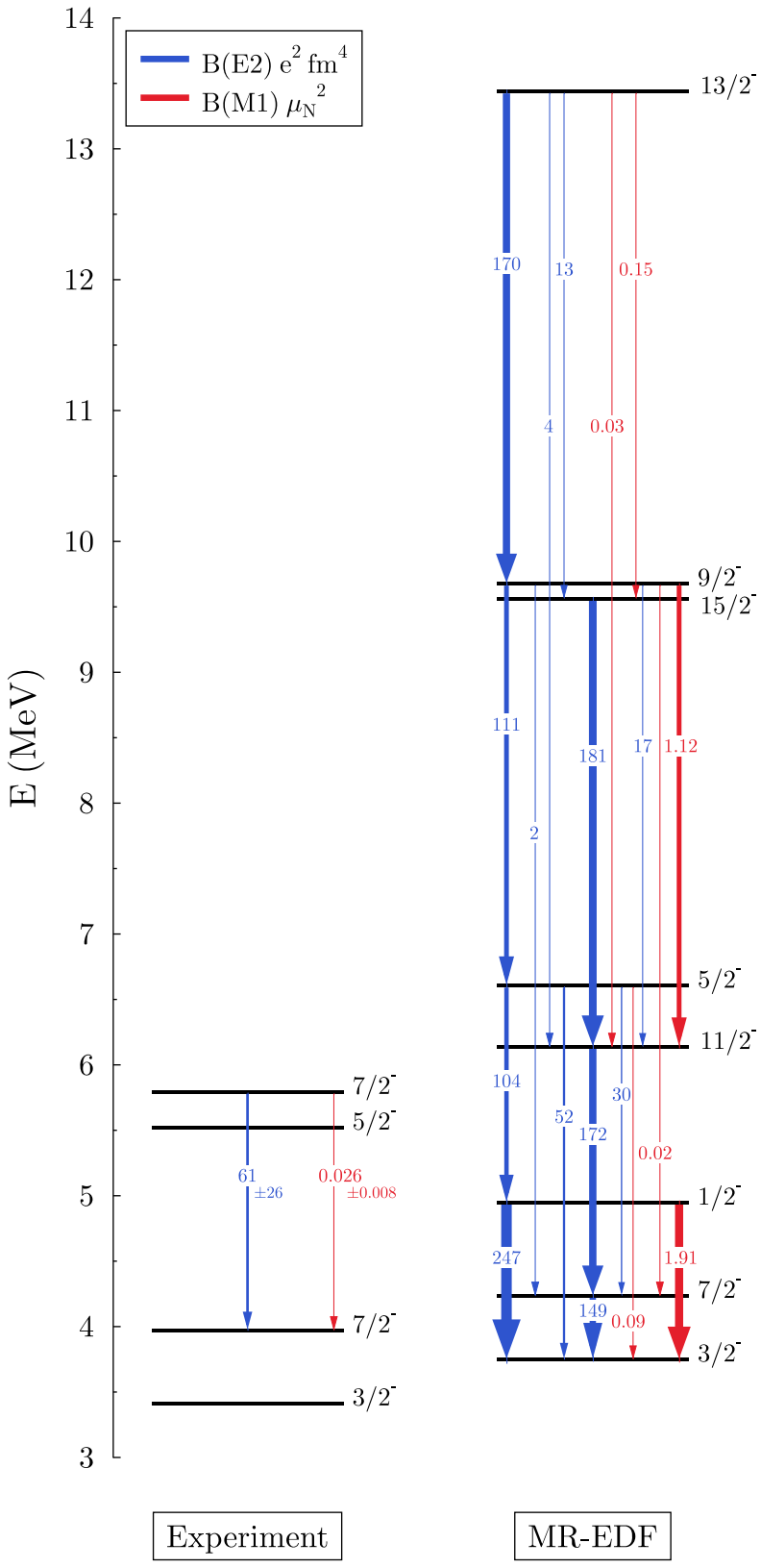

Figure 4.68: Comparison between experimental observations and theoretical calculations for the rotational band built on the first $J^\pi = \frac{3}{2}^-$ state. The experimental data are taken from [65].

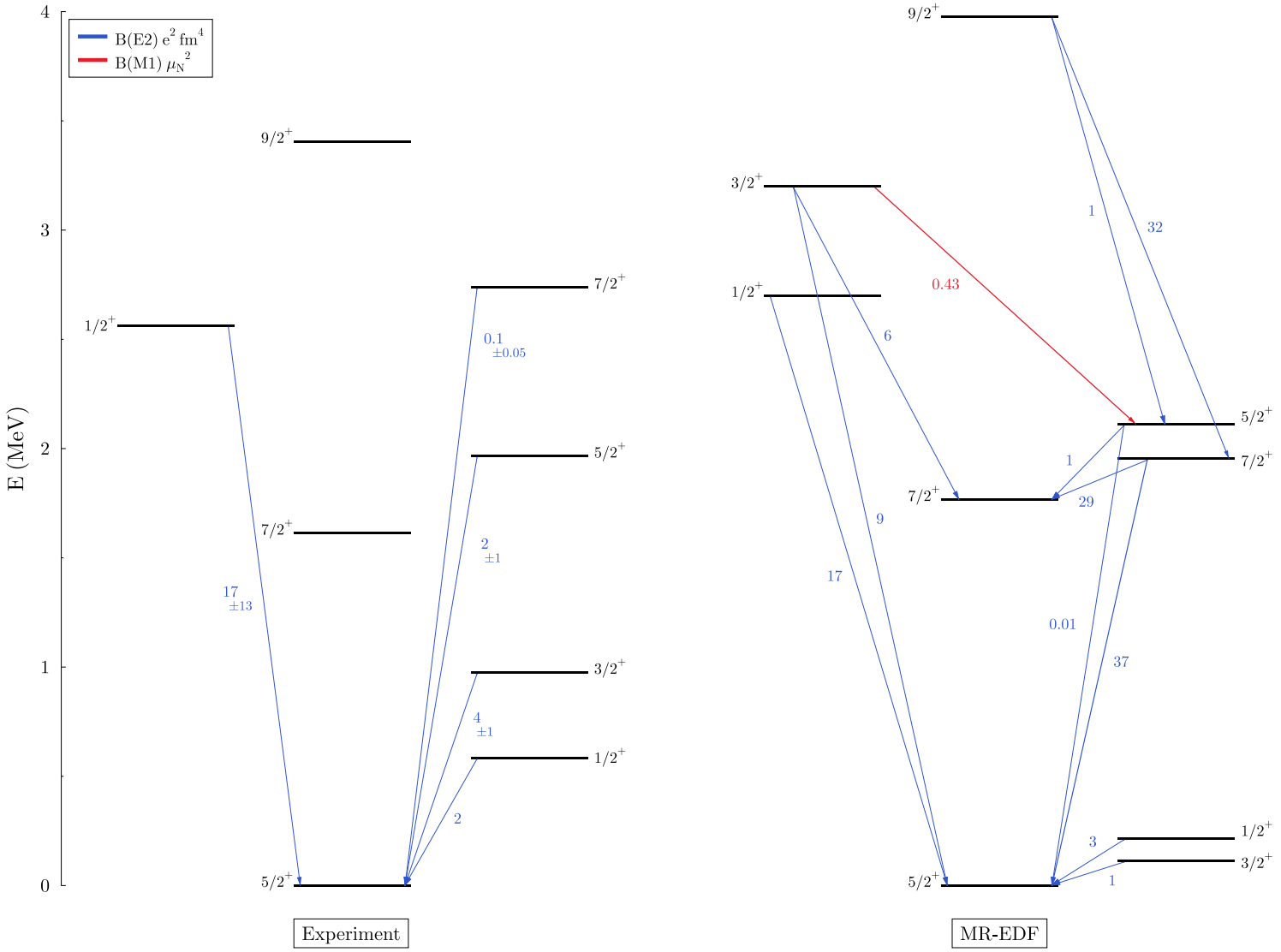

Figure 4.69: Comparison between experimental observations and theoretical calculations for the transitions between the lowest states in the different rotational bands composed of positive parity states. The experimental data are taken from [65]. For theoretical calculations, only the strongest and/or the most relevant transitions are plotted.

if adding more one-quasiparticle states (by reducing the discretized mesh in deformation used for the GCM) could help to better describe these states. But unfortunately, such study has to be postponed to future work, as the time has come to conclude our long and perilous journey.[10]

[10] So sad ☹.

Conclusion and Outlook

Nous n'avons qu'à continuer nos investigations et à attendre patiemment les solutions de la science. Elle ne peut nous conduire qu'à la vérité, et tenons pour certain que la vérité scientifique sera toujours plus belle que les créations de notre imagination et que les illusions de notre ignorance.

Claude Bernard, Le problème de la physiologie générale - Revue des Deux Mondes (1867).

In this work, we were interested in the treatment of odd-mass nuclei in multi-reference energy density functional methods. In the recent years, these methods had been successfully used to describe even-even nuclei [22, 113], and the goal of this thesis was to develop the theoretical and numerical tools to achieve the same degree of refinement in the description of odd-even nuclei.

In the first part of this work, we described the theoretical formalism of the energy density functional methods. We gave particular attention to the treatment of symmetries in our calculations, either concerning the symmetries imposed on the one-quasiparticle states at the single-reference level, or concerning the restoration of the Hamiltonian's symmetries at the multi-reference level. We tried to be as general as possible such that the given formalism can, in principle, be applied to both even- and odd-A nuclei. In particular, we gave, in the most general case, the symmetry relations of matrix elements between quasiparticles states, with the symmetries of the group $\left\{\hat{P}, \hat{R}_z, \hat{S}_y^T\right\}_g$ [50, 51], rotated over Euler angles. These relations allow for reducing by a factor of sixteen the number of rotations needed to be calculated, and thus allows for reducing by approximately the same factor the CPU-time needed for the calculation. In appendices B and C, we gave full derivations of these relations, along with other demonstrations of basic symmetry relations that are frequently used, but whose derivations are rarely, if ever, given. And I would like to put even more emphasis in this conclusion on the treatment of symmetries, as it appeared to me that there is often a lack of rigour from the "mean-field" community on this particular matter, notably on the formal aspect of it. For example, one of the things that stroke me the most when writing this thesis is the complete absence of a precise definition of projection operators in books, articles, or lectures, written by nuclear physicists; with very few notable exceptions [93, 141, 59]. Another example is the fact that I can almost count on my fingers the number of articles where is used the term: "irreducible representation". It is somewhat surprising when considering that the projection technique has been used in nuclear physics for more than fifty years [100, 90]. And it is even startling when considering that group-theoretical principles have been introduced in quantum mechanics by Hermann Weyl and Eugene Wigner back in the late 1920s, and have proved, since then, to be an extremely valuable and predictive tool at the disposal of physicists. I thus hope that by taking in this thesis a more formal approach on this matter, I may inspire other members of the community to do the same.

In the second part of this thesis, we applied our model to the nucleus ^{25}Mg. We investigated several aspects of the method such as the effects of symmetry restoration on the description

of the nucleus, the decomposition of one-quasiparticle states on the irreps' basis functions, the numerical precision reached in our calculations, and the convergence of the configuration mixing. Finally, we compared our MR-EDF calculation to the available experimental data and found a very promising agreement between the two. Actually, it is impressive that we achieve such good results using a Skyrme-type effective interaction fitted only to mass and radii of spherical nuclei [122]. And it is even more impressive when recalling that SLyMR0 is rather a poor parametrization according to our criteria. This is, therefore, really encouraging for future calculations with better parametrizations of Skyrme-type effective interactions, which at least require a three-body force with gradients [123]. There is also room for improvement in the numerical accuracy of the calculations by, for example, using a denser 3-dimensional cartesian mesh and a denser discretization of the integrals over Euler angles. Additionally, we could also consider adding even more one-quasiparticle states to the configuration mixing, and maybe envisage, in the future, the inclusion of three-quasiparticle states. On that account, we investigated in chapter 4 different objective criteria for the selection of the one-quasiparticle states to be included in the configuration mixing. The projected energy appeared to be the most robust choice, but selecting one-quasiparticle states simply on their energy at the single-reference level seemed also to be a good option, which has the advantage that it does not require to project the one-quasiparticle states beforehand.

From a general point of view, we must admit that we are already very satisfied with this first calculation. And to try to give a global perspective of the work achieved, we give here some of the key numbers that characterize its complexity:

Multi-Reference Calculation of ^{25}Mg in Numbers

- **604** one-quasiparticle states of positive parity and **222** of negative parity have been self-consistently blocked and have been projected on particle number and angular momentum.
- The configuration mixing included **100** one-quasiparticle states with positive parity and **60** one-quasiparticle states with negative parity, all projected on particle number and angular momentum. This represents a total of **5050** calculated matrix elements for positive parity and **1830** for negative parity.
- Given the discretization in gauge angles (protons and neutrons) and in Euler angles, it represents **186 624 000** rotated quasiparticle states for positive parity and **111 974 400** rotated quasiparticle states for negative parity. Because of symmetry relations 3.84 - 3.91, only **11 640 000** rotations are needed to be calculated for positive parity and only **6 998 400** for negative parity.
- For positive parity states, the calculations were carried out on the CNRS/IDRIS-GENCI[11] supercomputer **Turing**. The machine has a peak performance of **838.9** Teraflops, and is (only) ranked **45** in the last TOP500 of November 2013 [148]. For negative parity states, the calculations were carried out on the local machine **Avakas** of the MCIA (Mésocentre de Calcul Intensif Aquitain), wich has a peak performance of **38.8** Teraflops.
- The configuration mixing cost approximately **620 000** CPU hours on Turing and **66 500** CPU hours on Avakas. Avakas' processors being roughly 3 times faster than those of Turing, it would represent for both GCMs a total of approximately **820 000** equivalent CPU hours on Turing.

[11] Grants No. 2011-050707, 2012-050707 and 2013-050707.

The number of CPU hours required for this calculation may seem enormous, especially if compared to the few minutes it took me, on my personal computer, to realize the shell-model calculation used for Fig. 4.63. But this number has to be put into perspective. Firstly, even if our calculation is far more expensive than a traditional shell-model calculation, we also use far less parameters, and those parameters are not fitted to any experimental data on nuclei in this mass region. Secondly, there are approximately 345 millions CPU hours available for attribution each year on Turing, such that our calculation represent only 0.25 % of the total CPU time available on this machine. Of course, nowadays this type of supercomputer are used by many scientists, so we cannot expect to obtain all the CPU time available just for ourselves. But we do not think that, with only 0.25 % of the total CPU time available, we have reached yet the maximum number of hours we can ask for and obtain on this type of machine. Besides, we also have to consider the exponential growth of the computers' performances. Indeed, looking at the history of supercomputers, we can see that, approximately every decade, the speed of supercomputers gains a factor one thousand: in 1985 the Gigaflops barrier was broken, in 1997 the Teraflops barrier was broken, in 2008 the Petaflops barrier was broken, and, finally, the Exaflops barrier is expected to be broken around the year 2020. With such a fast evolution, there is no doubt that tomorrow's supercomputers will be able to handle pretty easily MR-EDF calculations similar to the one presented in this work. It will even be possible to envisage more complex calculations with: (i) more broken/restored symmetries, (ii) a variation after projection, or (iii) the computation of heavy systems. The lattest possibility is particularly important, as energy density funcational models are probably the microscopic approches having the best scaling with the number of nucleons, and therefore, the only ones that will allow us for performing microscopic computation of heavy nuclei for a foreseable future. While awaiting the advent of Exascale computing, there are already a lot of possibilities to exploit the capacities of our model. In particular, it would be interesting to look at the influence of correlations on the evaluation of various observables, as for examples, the energy differences $\Delta^{(3)}$ and $\Delta^{(5)}$ [57] or the one-nucleon separation energy [60]. Related to the latter example, we want to mention that we originally planned to incorporate in this thesis another application of the model on the doubly-magic plus one neutron nucleus ^{17}O. Unfortunately, due to the lack of time, it was not possible to analyze the results and to integrate them in the manuscript. However, all matrix elements for a configuration mixing including 184 one-quasiparticle states with positive parity and 94 one-quasiparticle states with negative parity have been calculated. The analyses shall be carried out during the next few months and the results published somewhere else.

So to conclude this thesis, we will simply say this: prepare yourself, MR-EDF IS COMING! MWA HA HA HA HAAAAAA!

Conclusion et perspectives

Nous n'avons qu'à continuer nos investigations et à attendre patiemment les solutions de la science. Elle ne peut nous conduire qu'à la vérité, et tenons pour certain que la vérité scientifique sera toujours plus belle que les créations de notre imagination et que les illusions de notre ignorance.

Claude Bernard, Le problème de la physiologie générale - Revue des Deux Mondes (1867).

Dans ce travail de thèse, nous nous sommes intéressés à la description théorique des noyaux impairs dans les méthodes de la fonctionnelle énergie de la densité à plusieurs états de reférénce. Au cours des dernières années, de telles méthodes ont été utilisées avec succès pour décrire la structure à basse énergie des noyaux pair-pairs [22, 113], et le but de cette thèse était de développer les outils théoriques et numériques pour atteindre le même degré de précision dans la description des noyaux impairs.

Dans la première partie de ce travail, nous avons d'abord décrit le formalisme mathématique des méthodes de la fonctionnelle énergie de la densité. En particulier, nous avons mis l'accent sur le traitement des symétries dans notre approche, que cela soit concernant les symétries de nos états de quasiparticules au niveau SR-EDF ou concernant la restauration des symétries de l'Hamiltonien au niveau MR-EDF. Nous avons aussi essayé d'être aussi général que possible de telle manière que le formalisme présenté ici peut, en principe, être appliqué tout autant aux noyaux pair-pairs qu'aux noyaux impairs. Par exemple, nous avons donné dans le cas le plus général les relations de symétries pour les éléments de matrices entre états de quasiparticules ayant les symétries du groupe $\left\{\hat{P}, \hat{R}_z, \hat{S}_y^T\right\}_g$ [50, 51] et ayant subis une rotation dans l'espace paramétrisée par les angles d'Euler. Ces relations de symétries permettent de réduire par un facteur seize le nombre de rotations à calculer, et permettent donc de réduire d'approximativement autant le temps processeur nécessaire pour le calcul. Les démonstrations de ces relations sont données dans les annexes B et C, avec aussi les démonstrations d'autres relations de symétries de bases fréquement utilisées mais rarement démontrées. Et je voudrais d'ailleurs insister encore davantage dans cette conclusion sur le traitement des symétries, car il me semble qu'il y a souvent dans la communauté « champ-moyen » un certain manque de rigueur sur les aspects formels relatifs aux groupes de symétries. Par exemple, une des choses qui m'a le plus surpris pendant la rédaction de cette thèse est la quasi-absence d'une définition précise pour les opérateurs de projection dans les ouvrages, cours, ou articles, écrits par des physiciens de la communauté en question, à quelques rares exceptions près [93, 141, 59]. Un autre exemple parlant est le simple fait que personne ne mentionne jamais le terme de « représentation irréductible ». Ceci paraît assez étonnant quand on sait que les techniques de projection ont été introduites il y a plus de cinquante ans en physique nucléaire [100, 90]. Cela paraît même plus surprenant encore quand on rappelle que les principes de la théorie des groupes ont été introduits en mécanique quantique dès les années 1920 par Hermann Weyl et Eugène Wigner, et qu'ils se sont révélés, depuis lors,

comme étant des outils extrêmement utiles et prédictifs au service des physiciens. J'espère donc qu'en utilisant dans ce travail une approche plus formelle sur ces sujets, cela incitera d'autres personnes dans la communauté à faire de même.

Dans la seconde partie de cette thèse, nous avons appliqué notre modèle au cas du noyau de ^{25}Mg et avons étudié plusieurs aspects de la méthode tels que les changements apportés par la restauration des symétries sur la description du noyau, la décomposition des états à une quasiparticule sur les fonctions de bases des irreps, la précision numérique atteinte dans nos calculs, ou la convergence du mélange de configurations. Enfin, nous avons comparé notre calcul MR-EDF aux données expérimentales disponibles pour ce noyau et avons constaté un accord plus que prometteur entre théorie et expérience. En fait il est même assez impressionnant que nous arrivions à un tel accord en ayant utilisé une interaction effective de type Skyrme dont les paramètres ont été ajustés seulement dans le but de reproduire les rayons et les masses de certains noyaux sphériques [122]. De plus, on peut aussi rappeler que la paramétrisation utilisée dans ce travail, SLyMR0, est somme toute assez médiocre. Tout ceci est donc très encourageant pour de futurs calculs utilisant une meilleure paramétrisation d'une interaction effective de type Skyrme, mais il faut préciser que cette dernière devra sûrement nécessiter la prise en compte de termes gradients dans la force à trois corps [123]. Ensuite, il devrait être aussi possible d'obtenir de meilleurs résultats en améliorant la précision numérique des calculs, c'est à dire par exemple en utilisant un pas plus fin pour notre maillage cartésien tridimensionnel de l'espace ou en utilisant une discrétisation plus fine des intégrales sur les angles d'Euler. Enfin, on pourrait aussi envisager d'inclure davantage d'états à une quasiparticule dans le mélange de configurations ou, dans un futur un peu plus lointain, d'inclure des états à trois quasiparticules. En liens à de telles considérations, nous avons étudié dans le chapitre 4 différents critères pour essayer de déterminer parmi tous les états à une quasiparticule calculés, ceux susceptibles d'être les plus importants pour le mélange de configurations. Le critère qui semble le plus fiable pour choisir les états à une quasiparticule à inclure dans le mélange est l'énergie des états projetés obtenus de ces états. Mais choisir les états à une quasiparticule directement en fonction de leur énergie non projetée représente aussi un choix convenable qui en plus à l'avantage, d'un point de vue numérique, de ne pas nécessiter la projection des états avant leur sélection.

D'une manière générale, nous devons avouer que nous sommes tout de même assez satisfaits de ce premier calcul et pour essayer de donner une vision plus globale du travail accompli, nous donnons ici quelques chiffres importants qui caractérisent ce calcul :

Calcul MR-EDF du ^{25}Mg en quelques chiffres

- **604** états à une quasiparticule de parité plus et **222** états à une une quasiparticule de parité moins ont été bloquées et projetées sur le nombre de particules et sur le moment angulaire.

- Le mélange de configurations comporte **100** états à une quasiparticule de parité plus et **60** états à une quasiparticule de parité moins, toutes projetées sur le nombre de particules et le moment angulaire. Cela représente au total **5050** éléments de matrice pour la parité plus et **1830** pour la parité moins.

- Compte tenu de la discrétisation utilisée pour les angles de jauges (protons et neutrons) et les angles d'Euler, cela réprésente **186 624 000** d'états à une quasiparticule « tournés » pour la parité plus et **111 974 400** pour la parité moins. Mais grâce aux relations de symétries 3.84 - 3.91, nous n'avons eu besoin de calculer seulement que **11 640 000** rotations pour la parité plus et seulement que **6 998 400** rotations pour la parité moins.

- Pour les états de parité plus, les calculs ont été effectués sur le supercalculateur **Turing** du CNRS/IDRIS-GENCI[12]. La performance crête de cette machine est de **838.9** Teraflops, et elle est (seulement) classée au 45$^{\textbf{ème}}$ rang du dernier TOP500 datant de novembre 2013 [148]. Pour les états de parités moins, les calculs ont été effectués sur la machine locale **Avakas** du MCIA (Mésocentre de Calcul Intensif Aquitain). Cette dernière a une performance crête de **38.8** Teraflops.

- Le mélange de configurations a demandé environ **620 000** heures CPU sur Turing et **66 500** heures CPU sur Avakas. Compte tenu que les processeurs d'Avakas sont environs 3 fois plus rapides que ceux de Turing, cela représenterait pour les deux GCMs un temps total d'environ **820 000** heures CPU si on avait seulement utilisé Turing.

On pourrait facilement se laisser impressionner par le nombre d'heures processeur demandé par un tel calcul, surtout si on le compare aux quelques minutes qu'a pris le calcul du modèle en couches utilisé pour la Fig. 4.63 sur un ordinateur de bureau standard. Mais nous pensons qu'il est important de remettre ces chiffres en perspective. Tout d'abord, même si notre calcul est d'un point de vue numérique beaucoup plus lourd qu'un calcul classique du modèle en couches, nous utilisons beaucoup moins de paramètres que dans ces derniers, et de plus ces paramètres ne sont pas ajustés à une région de masse particulière. Ensuite, il y a chaque année un total d'environ 345 millions d'heures processeur disponibles pour attribution sur le supercalculateur Turing. Notre calcul ne représente donc seulement que 0.25 % de ce nombre total d'heures disponibles. Alors certes, nous ne pouvons pas espérer obtenir l'attribution de l'intégralité du temps CPU disponible sur un tel ordinateur, qui est là pour servir à toute la communauté scientifique. Mais nous ne pensons pas non plus qu'avec seulement 0.25 % du nombre total d'heures disponibles, nous avons atteint la limite de temps processeur que l'on peut décemment demander et obtenir sur ce genre de machines. De plus, il faut considérer que la puissance de ces supercalculateurs ne cessse d'augmenter. En effet, si on regarde l'historique de ces ordinateurs, on peut constater que leur vitesse gagne un facteur mille environ tous les dix ans : la barrière du Gigaflops a été franchie en 1985, la barrière du Teraflops a été franchie en 1997, la barrière du Petaflops a été franchie en 2008, et, enfin, la barrière de l'Exaflops devrait être franchie aux alentours de l'année 2020. Avec une telle rapidité d'évolution, il ne fait aucun doute que les ordinateurs de demain permettront de réaliser facilement des calculs MR-EDF non seulement tel que celui présenté dans ce travail mais aussi d'autres bien plus sophistiqués que celui ci. On pourrait par exemple envisager des calculs avec : (i) plus de symétries brisées et restaurées, (ii) une variation après projection, ou (iii) des noyaux de masse plus élevée. Cette dernière possibilité est particulièrement intéressante car de toutes les approches microscopiques disponibles pour l'étude de la structure nucléaire, les méthodes de la fonctionnelle énergie de la densité sont sans aucun doute celles qui ont le meilleur dimensionnement avec le nombre de particules et donc, les seules qui pourront nous permettre de calculer des noyaux lourds dans un futur proche. Mais même en attendant l'arrivée des machines exaflopiques, il y a déjà au jour d'aujourd'hui énormément de possibilités pour exploiter la puissance de nos modèles. En particulier il serait intéressant de regarder l'influence des corrélations sur le calcul de différentes observables comme par exemple les différences d'énergies $\Delta^{(3)}$ et $\Delta^{(5)}$ [57] ou l'énergie de séparation d'un nucléon [60]. D'ailleurs, en lien à ce dernier exemple, nous signalons qu'il était originellement prévu d'inclure dans cette thèse un autre calcul d'application sur le noyau d'^{17}O. Malheureusemnt, à cause du manque de temps il n'a pas été possible d'analyser les résultats et de les inclure dans le manuscrit. Cela dit, tous les éléments de matrices pour un mélange de configurations comportant jusqu'à 184 états à une quasiparticule de parité plus et jusqu'à 94 états à une quasiparticule de parité moins ont

[12] Attributions No. 2011-050707, 2012-050707 and 2013-050707.

été calculés. L'analyse des résultats devrait être réalisée dans les prochains mois et les résultats publiés par la suite.

Donc pour conclure cette thèse, nous dirons simplement : préparez-vous, le MR-EDF est en marche ! MOUAH HA HA HA HAAAAAA !

Part III

Appendices

Appendix A

Some Basic Commutation Rules for Single-Particle Creation and Annihilation Operators

La filosofia è scritta in questo grandissimo libro che continuamente ci sta aperto innanzi a gli occhi (io dico l'universo), ma non si può intendere se prima non s'impara a intender la lingua, e conoscer i caratteri, ne' quali è scritto. Egli è scritto in lingua matematica, e i caratteri son triangoli, cerchi, ed altre figure geometriche, senza i quali mezi è impossibile a intenderne umanamente parola; senza questi è un aggirarsi vanamente per un oscuro laberinto.

Galileo Galilei, Il Saggiatore (1623).

Let us consider a linear and hermitean one-body operator $\hat{U}$, and an orthonormal basis of fermionic single-particle states, associated with the creation/annihilation operators $(\hat{a}^\dagger, \hat{a})$, which are eigenstates of $\hat{U}$. By definition, we have

$$\hat{U}^\dagger = \hat{U} \quad , \tag{A.1}$$

$$\hat{U}|i\rangle = u_i|i\rangle \quad , \tag{A.2}$$

$$\langle i|j\rangle = \delta_{ij} \quad , \tag{A.3}$$

$$\left\{\hat{a}_i^\dagger, \hat{a}_j\right\} = \left\{\hat{a}_i, \hat{a}_j^\dagger\right\} = \hat{\delta}_{ij} \quad , \tag{A.4}$$

$$\left\{\hat{a}_i^\dagger, \hat{a}_j^\dagger\right\} = \left\{\hat{a}_i, \hat{a}_j\right\} = 0 \quad . \tag{A.5}$$

In this basis, the only non-vanishing matrix elements of $\hat{U}$ are the diagonal ones

$$\langle i|\hat{U}|j\rangle = u_i\,\delta_{ij} \quad , \tag{A.6}$$

and the operator $\hat{U}$ can thus be written very simply in second quantization formalism as

$$\hat{U} = \sum_i u_i\,\hat{a}_i^\dagger \hat{a}_i \quad . \tag{A.7}$$

The commutation of $\hat{U}$ with an arbitrary creation operator $\hat{a}_m^\dagger$ in the basis reads

$$\begin{aligned}\hat{U}\hat{a}_m^\dagger &= \sum_i u_i\, \hat{a}_i^\dagger \hat{a}_i \hat{a}_m^\dagger \\ &= \sum_i u_i\, \hat{a}_i^\dagger \big(\delta_{mi} - \hat{a}_m^\dagger \hat{a}_i\big) \\ &= u_m\, \hat{a}_m^\dagger - \sum_i u_i\, \hat{a}_i^\dagger \hat{a}_m^\dagger \hat{a}_i \\ &= u_m\, \hat{a}_m^\dagger + \hat{a}_m^\dagger \sum_i u_i\, \hat{a}_i^\dagger \hat{a}_i \\ &= \hat{a}_m^\dagger \big(\hat{U} + u_m\big) \quad .\end{aligned} \tag{A.8}$$

Similarly, the commutation of $\hat{U}$ with the annihilation operator $\hat{a}_m$, associated to $\hat{a}_m^\dagger$, reads

$$\begin{aligned}\hat{U}\hat{a}_m &= \sum_i u_i\, \hat{a}_i^\dagger \hat{a}_i \hat{a}_m \\ &= -\sum_i u_i\, \hat{a}_i^\dagger \hat{a}_m \hat{a}_i \\ &= -\sum_i u_i\, \big(\delta_{mi} - \hat{a}_m \hat{a}_i^\dagger\big) \hat{a}_i \\ &= -u_m \hat{a}_m + \hat{a}_m \sum_i u_i\, \hat{a}_i^\dagger \hat{a}_i \\ &= \hat{a}_m \big(\hat{U} - u_m\big) \quad .\end{aligned} \tag{A.9}$$

It is straightforward to generalize these results to the case of the operator $\hat{U}$ taken to the power of k

$$\hat{U}^k\, \hat{a}_m^\dagger = \hat{a}_m^\dagger \big(\hat{U} + u_m\big)^k \quad , \tag{A.10}$$

$$\hat{U}^k\, \hat{a}_m = \hat{a}_m \big(\hat{U} - u_m\big)^k \quad . \tag{A.11}$$

Let us now define the operator $\hat{V}$ that is the exponential of the operator $-i\phi\hat{U}$, ϕ being a real number and i the imaginary unit; $\hat{V}$ reads

$$\hat{V} = e^{-i\phi\hat{U}} = \sum_{k=0}^{+\infty} \frac{(-i\phi\hat{U})^k}{k!} \quad . \tag{A.12}$$

The eigenstates of $-i\phi\hat{U}$ are also eigenstates of the newly defined linear, and unitary, operator $\hat{V}$ with eigenvalues being the exponentials of the eigenvalues of $-i\phi\hat{U}$

$$\hat{V}|i\rangle = e^{-i\phi u_i}|i\rangle \quad , \tag{A.13}$$

$$\hat{V}^\dagger \hat{V} = \hat{V}\hat{V}^\dagger = \hat{\mathbb{1}} \quad . \tag{A.14}$$

The commutation rules of $\hat{V}$ are easily determined using (A.10) and (A.11)

$$\begin{aligned}\hat{V}\hat{a}_m^\dagger &= \sum_{k=0}^{+\infty} \frac{(-i\phi\hat{U})^k}{k!} \hat{a}_m^\dagger \\ &= \hat{a}_m^\dagger \sum_{k=0}^{+\infty} \frac{\big\{-i\phi\big(\hat{U} + u_m\big)\big\}^k}{k!} \\ &= \hat{a}_m^\dagger\, e^{-i\phi\left(\hat{U}+u_m\right)} \\ &= e^{-i\phi u_m} \hat{a}_m^\dagger\, \hat{V} \quad ,\end{aligned} \tag{A.15}$$

$$\begin{aligned}\hat{V}\hat{a}_m &= \sum_{k=0}^{+\infty} \frac{(-i\phi\hat{U})^k}{k!}\hat{a}_m \\ &= \hat{a}_m \sum_{k=0}^{+\infty} \frac{\big\{-i\phi\big(\hat{U}-u_m\big)\big\}^k}{k!} \\ &= \hat{a}_m\, e^{-i\phi\left(\hat{U}-u_m\right)} \\ &= e^{+i\phi u_m}\hat{a}_m\,\hat{V} \quad .\end{aligned} \tag{A.16}$$

We can also note that, because of its exponential form, we have for the action of the operator $\hat{V}$ on the vacuum: $\hat{V}|0\rangle = |0\rangle$, whereas for the operator $\hat{U}$ we have: $\hat{U}|0\rangle = 0$. Finally, renaming $v_m = e^{-i\phi u_m}$, we can rewrite the above relations as

$$\hat{V}\hat{a}_m^\dagger = v_m\,\hat{a}_m^\dagger\hat{V} \quad , \tag{A.17}$$

$$\hat{V}\hat{a}_m = v_m^*\,\hat{a}_m\hat{V} \quad . \tag{A.18}$$

Appendix B

Particle Number

Aujourd'hui, nous ne sollicitons plus la Nature : nous lui commandons, parce que nous avons découvert quelques-uns de ses secrets et que nous en découvrons chaque jour de nouveaux. Nous lui commandons au nom de lois qu'elle ne peut récuser, parce que ce sont les siennes ; ces lois, nous ne lui demandons pas follement de les changer, nous sommes les premiers à nous y soumettre. Naturæ non imperatur nisi parendo.

Henri Poincaré, La valeur de la science (1905).

B.1 Basic Definitions

Let us consider two sets of states, one associated with the neutron single-particle states $(\hat{a}^\dagger, \hat{a})_n$, and the other one associated with the proton single-particle states $(\hat{a}^\dagger, \hat{a})_z$. When considering the full space of single-particle states, the creation/annihilation operators of one set commute with all creation/annihilation operators of the other set. We define the neutron, proton, and nucleon, number one-body operators as

$$\hat{N} = \sum_i \hat{a}^\dagger_{n,i} \hat{a}_{n,i} \quad , \tag{B.1}$$

$$\hat{Z} = \sum_i \hat{a}^\dagger_{z,i} \hat{a}_{z,i} \quad , \tag{B.2}$$

$$\hat{A} = \hat{N} + \hat{Z} \quad , \tag{B.3}$$

respectively.
The elements of the compact, and abelian, Lie group $U(1)_X$, $X \in \{N, Z\}$, are represented by the operators

$$\hat{R}_X(\phi) = e^{-i\phi\hat{X}} \quad . \tag{B.4}$$

with the properties

$$\hat{R}_X(\phi)\hat{R}_X(\phi') = \hat{R}_X(\phi + \phi') \quad , \tag{B.5}$$

$$\hat{R}_X(\phi)\hat{R}_X(\phi') = \hat{R}_X(\phi')\hat{R}_X(\phi) \quad , \tag{B.6}$$

$$\hat{R}_X(0) = \hat{\mathbb{1}} \quad . \tag{B.7}$$

The hermitean conjugate of $\hat{R}_X$ is

$$\hat{R}_X^\dagger(\phi) = e^{+i\phi\hat{X}} = \hat{R}_X(-\phi) \quad , \tag{B.8}$$

with the unitarity relation

$$\hat{R}_X(\phi)\hat{R}_X^\dagger(\phi) = \hat{\mathbb{1}} \quad . \tag{B.9}$$

The number parity operator is defined as the special case of a rotation with $\phi = \pi$

$$\hat{\Pi}_{\hat{X}} = e^{-i\pi\hat{X}} \quad . \tag{B.10}$$

The eigenstates $|X\rangle$ of the operator $\hat{X}$ with the eigenvalues X, X being a positive[1] or null integer, are basis functions for the irreducible representations D^X of $U(1)_X$

$$\hat{R}_X(\phi)|X\rangle = D^X(\phi)|X\rangle \quad , \tag{B.11}$$

with

$$D^X(\phi) = \langle X|e^{-i\phi\hat{X}}|X\rangle = e^{-i\phi X} \quad . \tag{B.12}$$

The irreps D^X have the properties

$$D^X(\phi+\pi) = (-)^X D^X(\phi) \quad , \tag{B.13}$$
$$D^X(\phi+2\pi) = D^X(\phi) \quad , \tag{B.14}$$
$$D^X(\phi)D^X(\phi') = D^X(\phi+\phi') \quad , \tag{B.15}$$
$$D^X(\phi)D^{X'}(\phi) = D^{X+X'}(\phi) \quad , \tag{B.16}$$
$$D^0(\phi) = 1 \quad , \tag{B.17}$$
$$D^X(0) = 1 \quad , \tag{B.18}$$

and follow the orthogonality relation

$$\frac{1}{2\pi}\int_0^{2\pi} d\phi\, D^{X*}(\phi)D^{X'}(\phi) = \delta_{X,X'} \quad . \tag{B.19}$$

Commutation Relations

In this work, apart from the quasiparticle creation/annihilation operators, all the operators considered commute with the particle number operator, and thus with the rotations of $U(1)_X$ and the projection operators on the number of particles.

B.2 Decomposition of a State that has Good Number Parity

Let us consider a state $|\Phi_a\rangle$ (which is not necessarily a one-quasiparticle state) that has good number parity for the particle species $(X,x) \in \{(N,n),(Z,z)\}$

$$\begin{aligned}\hat{\Pi}_{\hat{X}}|\Phi_a\rangle &= e^{-i\pi\hat{X}}|\Phi_a\rangle \\ &= \pi_{x,a}|\Phi_a\rangle \quad ,\end{aligned} \tag{B.20}$$

[1] In our framework, there is no state with a negative number of particles.

with $\pi_{x,a} = \pm 1$.
The decomposition of $|\Phi_a\rangle$ on the basis functions $|X\rangle$ of the irreducible representations of $U(1)_X$ can be written as

$$|\Phi_a\rangle = \sum_{\tau} \sum_{X} c^{X\tau}(a)|X\tau\rangle \quad , \tag{B.21}$$

where τ stands for all the other quantum numbers that label the different, but equivalent, irreps of $U(1)_X$, and with the restriction that X is a positive or null integer. For the sake of compact notations, we will omit in this section the label τ and simply write

$$|\Phi_a\rangle = \sum_{X} c^{X}(a)|X\rangle \quad . \tag{B.22}$$

Applying the number parity operator on both sides of the equation, and then projecting on a given particle number $X_0 \in \{N_0, Z_0\}$, we get

$$\begin{aligned}
& \hat{\Pi}_{\hat{X}}|\Phi_a\rangle = \hat{\Pi}_{\hat{X}} \sum_{X'} c^{X'}(a)|X'\rangle \\
\iff \quad & \pi_{x,a}|\Phi_a\rangle = \sum_{X'} (-)^{X'} c^{X'}(a)|X'\rangle \\
\iff \quad & \pi_{x,a} \sum_{X} c^{X}(a)|X\rangle = \sum_{X'} (-)^{X'} c^{X'}(a)|X'\rangle \\
\iff \quad & \langle X_0|\pi_{x,a} \sum_{X} c^{X}(a)|X\rangle = \langle X_0| \sum_{X'} (-)^{X'} c^{X'}(a)|X'\rangle \\
\iff \quad & \pi_{x,a} c^{X_0}(a) = (-)^{X_0} c^{X_0}(a) \quad .
\end{aligned} \tag{B.23}$$

As the equation has to hold for any X_0, we can deduce that for $\pi_{x,a} = 1$ there are only basis functions with even values of X_0 in the decomposition, whereas for $\pi_{x,a} = -1$ there are only basis functions with odd values of X_0 in the decomposition:

$$\pi_{x,a} = +1 \quad \iff \quad \forall\, X_0 \in \{X, c^X(a) \neq 0\},\ X_0 \text{ is even}, \tag{B.24}$$

$$\pi_{x,a} = -1 \quad \iff \quad \forall\, X_0 \in \{X, c^X(a) \neq 0\},\ X_0 \text{ is odd}. \tag{B.25}$$

We can thus write the expansion of $|\Phi_a\rangle$ on the functions $|X\rangle$ as

$$|\Phi_a\rangle = \sum_{X} \delta_{\pi_{x,a},(-)^X}\, c^{X}(a)|X\rangle \quad . \tag{B.26}$$

B.3 Properties of the Projection Operator

Let us consider the projection operator $\hat{P}^{X_0}$ that projects on the number of particles X_0. According to equation (3.21), $\hat{P}^{X_0}$ reads

$$\hat{P}^{X_0} = \frac{1}{2\pi} \int_0^{2\pi} d\phi\, e^{-i\phi(\hat{X} - X_0)} \quad . \tag{B.27}$$

The group $U(1)_X$ being abelian, all its irreps are of dimension one and we have for $\hat{P}^X$ the following properties

$$\left(\hat{P}^{X_0}\right)^2 = \hat{P}^{X_0} \quad , \tag{B.28}$$

$$\left(\hat{P}^{X_0}\right)^\dagger = \hat{P}^{X_0} \quad . \tag{B.29}$$

We also note that the projection operator $\hat{P}^{X_0}$ can be written in Dirac's bracket notation as

$$\hat{P}^{X_0} = |X_0\rangle\langle X_0| \quad . \tag{B.30}$$

B.4 Reduction of the Interval of Integration for the Projection from $[0, 2\pi]$ to $[0, \pi]$

Using the good number parity of $|\Phi_a\rangle$, and the substitution $\phi' = \phi - \pi$ (renaming ϕ' as ϕ afterwards), we can simplify the projection operator as

$$\begin{aligned}
\hat{P}^{X_0}|\Phi_a\rangle &= \frac{1}{2\pi}\int_0^{2\pi} d\phi\, e^{-i\phi(\hat{X}-X_0)}|\Phi_a\rangle \\
&= \frac{1}{2\pi}\left[\int_0^{\pi} d\phi\, e^{-i\phi(\hat{X}-X_0)} + \int_{\pi}^{2\pi} d\phi\, e^{-i\phi(\hat{X}-X_0)}\right]|\Phi_a\rangle \\
&= \frac{1}{2\pi}\left[\int_0^{\pi} d\phi\, e^{-i\phi(\hat{X}-X_0)} + \int_0^{\pi} d\phi'\, e^{-i(\phi'+\pi)(\hat{X}-X_0)}\right]|\Phi_a\rangle \\
&= \frac{1}{2\pi}\left[\int_0^{\pi} d\phi\, e^{-i\phi(\hat{X}-X_0)} + \int_0^{\pi} d\phi\, e^{-i\phi(\hat{X}-X_0)}e^{-i\pi(\hat{X}-X_0)}\right]|\Phi_a\rangle \\
&= \frac{1}{2\pi}\left[\int_0^{\pi} d\phi\, e^{-i\phi(\hat{X}-X_0)} + \int_0^{\pi} d\phi\, e^{-i\phi(\hat{X}-X_0)}\hat{\Pi}_{\hat{X}}e^{i\pi X_0}\right]|\Phi_a\rangle \\
&= \frac{1}{2\pi}\left[\int_0^{\pi} d\phi\, e^{-i\phi(\hat{X}-X_0)} + \pi_{x,a}(-)^{X_0}\int_0^{\pi} d\phi\, e^{-i\phi(\hat{X}-X_0)}\right]|\Phi_a\rangle \\
&= \delta_{\pi_{x,a},(-)^{X_0}}\,\frac{1}{\pi}\int_0^{\pi} d\phi\, e^{-i\phi(\hat{X}-X_0)}|\Phi_a\rangle \quad .
\end{aligned} \tag{B.31}$$

If we project on a number of particles X_0 that has same number parity as $|\Phi_a\rangle$: $(-)^{X_0} = \pi_{x,a}$, the interval of integration can be reduced from $[0, 2\pi]$ to $[0, \pi]$. On the other hand, and accordingly to what has been discussed above, the projection on a number of particles X_0 that has an opposite number parity as $|\Phi_a\rangle$: $(-)^{X_0} = -\pi_{x,a}$, vanishes. This result can be seen as a consequence of the property (B.13) and of the orthogonality relation (B.19) of the irreps of $U(1)_X$.

B.5 Projection in the Canonical Basis

Using the expression of a one-quasiparticle state $|\Phi_b\rangle$ in its canonical basis and using the commutation relations (A.15) and (A.16) in the case of the particle number operator: $\hat{U} = \hat{X} \in \{\hat{N}, \hat{Z}\}$ and $\hat{V} = e^{-i\phi\hat{X}}$, with all eigenvalues being equal to one: $\forall i\,,\ u_i = 1$, it is possible to obtain a simple expression for the projection of $|\Phi_b\rangle$ on the number of particles X_0 in the canonical basis

$$\begin{aligned}
\hat{P}^{X_0}|\Phi_{x,b}\rangle &= \frac{1}{\pi}\int_0^{\pi} d\phi\ e^{-i\phi(\hat{X}-X_0)}\, c_b^{\dagger}\prod_{\substack{k\geq 0\\ k\neq b}}\left(u_{x,k} + v_{x,k}c_{x,k}^{\dagger}c_{x,\bar{k}}^{\dagger}\right)|0_x\rangle \\
&= \frac{1}{\pi}\int_0^{\pi} d\phi\ e^{i\phi X_0}e^{-i\phi\hat{X}}\, c_b^{\dagger}\prod_{\substack{k\geq 0\\ k\neq b}}\left(u_{x,k} + v_{x,k}c_{x,k}^{\dagger}c_{x,\bar{k}}^{\dagger}\right)|0_x\rangle
\end{aligned}$$

$$
\begin{aligned}
&= \frac{1}{\pi}\int_0^{\pi} d\phi\; e^{i\phi X_0} e^{-i\phi\hat{X}}\, c_b^{\dagger} e^{+i\phi\hat{X}} e^{-i\phi\hat{X}} \\
&\quad \times \prod_{\substack{k\geq 0\\ k\neq b}} \left(u_{x,k} + v_{x,k} c_{x,k}^{\dagger} e^{+i\phi\hat{X}} e^{-i\phi\hat{X}} c_{x,\bar{k}}^{\dagger}\right) e^{+i\phi\hat{X}} e^{-i\phi\hat{X}} |0_x\rangle \\
&= \frac{1}{\pi}\int_0^{\pi} d\phi\; e^{i\phi X_0} e^{-i\phi\hat{X}}\, c_b^{\dagger} e^{+i\phi\hat{X}} \\
&\quad \times \prod_{\substack{k\geq 0\\ k\neq b}} \left(u_{x,k} + v_{x,k} e^{-i\phi\hat{X}} c_{x,k}^{\dagger} e^{+i\phi\hat{X}} e^{-i\phi\hat{X}} c_{x,\bar{k}}^{\dagger} e^{+i\phi\hat{X}}\right) |0_x\rangle \\
&= \frac{1}{\pi}\int_0^{\pi} d\phi\; e^{i\phi X_0}\, e^{-i\phi} c_b^{\dagger} \prod_{\substack{k\geq 0\\ k\neq b}} \left(u_{x,k} + v_{x,k} e^{-2i\phi} c_{x,k}^{\dagger} c_{x,\bar{k}}^{\dagger}\right) |0_x\rangle \quad .
\end{aligned}
\tag{B.32}
$$

Note that, as we use the reduced interval of integration $[0,\pi]$, it is assumed that $(-)^{X_0} = \pi_{x,b}$.

B.6 Fomenko's Discretization of the Projection Operator

In this work, we use Fomenko's prescription [68] for the discretization of the integral in the projection operator

$$
\hat{\mathcal{P}}^{X_0}(M_x) = \frac{1}{M_x}\sum_{m_x=1}^{M_x} e^{-i\pi\frac{m_x-1}{M_x}(\hat{X}-X_0)} \quad , \tag{B.33}
$$

where M_x is the total (odd) number of points in the discretization. For this presciption to be valid, we have to assume that the integral can be reduced from $[0,2\pi]$ to $[0,\pi]$, i.e. we act with $\hat{\mathcal{P}}^{X_0}(M_x)$ on states with number parity equal to $(-)^{X_0}$.
It is straightforward to see that if $M_x = 1$, the projection operator reduces to the identity operator

$$
\hat{\mathcal{P}}^{X_0}(1) = \hat{\mathbb{1}} \quad . \tag{B.34}
$$

Acting with $\hat{\mathcal{P}}^{X_0}(M_x)$ on a state $|\Phi_a\rangle$, with a number parity $\pi_{x,a} = (-)^{X_0}$, we get

$$
\begin{aligned}
\hat{\mathcal{P}}^{X_0}(M_x)|\Phi_a\rangle &= \hat{\mathcal{P}}^{X_0}(M_x)\sum_{X_1} \delta_{\pi_{x,a},(-)^{X_1}}\, c^{X_1}(a)\,|X_1\rangle \\
&= \sum_{X_1} \delta_{\pi_{x,a},(-)^{X_1}}\, c^{X_1}(a)\,\hat{\mathcal{P}}^{X_0}(M_x)|X_1\rangle \\
&= \sum_{X_1}\left\{\delta_{\pi_{x,a},(-)^{X_1}}\, c^{X_1}(a)\left(\frac{1}{M_x}\sum_{m_x=1}^{M_x} e^{-i\pi\frac{m_x-1}{M_x}(X_1-X_0)}\right)|X_1\rangle\right\} \quad .
\end{aligned}
\tag{B.35}
$$

The factor

$$
F = \frac{1}{M_x}\sum_{m_x=1}^{M_x} e^{-i\pi\frac{m_x-1}{M_x}(X_1-X_0)}
$$

is a geometric progression, i.e. a sum of the type

$$
\sum_{k=m}^{n} ar^k \quad , \tag{B.36}
$$

with a common ratio

$$
r = e^{-i\pi\frac{1}{M_x}(X_1-X_0)}
$$

and a scale factor

$$a = \frac{1}{M_x} \quad .$$

A geometric progression presents two cases, either the common ratio is equal to one and the progession is simply written

$$\sum_{k=m}^{n} ar^k = \sum_{k=m}^{n} a = (n-m+1)a \quad , \tag{B.37}$$

or the common ratio is different from one and we can write

$$\sum_{k=m}^{n} ar^k = a\frac{r^m - r^{n+1}}{1-r} \quad . \tag{B.38}$$

In our case we have

- for $r = 1 \Leftrightarrow X_1 = X_0 + 2lM_x$ with l being an integer, we have

  $$F = \sum_{m_x=1}^{M_x} \frac{1}{M_x} = 1$$

  and thus

  $$X_1 = X_0 + 2lM_x \, , \, l \in \mathbb{Z} \implies \hat{\mathcal{P}}^{X_0}(M_x)|X_1\rangle = |X_1\rangle \quad . \tag{B.39}$$

- for $r \neq 1 \Leftrightarrow X_1 \neq X_0 + 2lM_x$ with l being an integer, we have

  $$F = \frac{1}{M_x}\frac{1 - e^{-i\pi(X_1 - X_0)}}{1 - e^{-i\pi\frac{1}{M_x}(X_1 - X_0)}} \quad .$$

  As a consequence of the number parity of $|\Phi_a\rangle$, we always have $X_1 = X_0 + 2k$ (see equation (B.23)), with k being an integer, and thus

  $$e^{-i\pi(X_1 - X_0)} = 1 \quad .$$

  As a result we always have

  $$F = 0 \quad ,$$

  and thus

  $$X_1 \neq X_0 + 2lM_x \, , \, l \in \mathbb{Z} \implies \hat{\mathcal{P}}^{X_0}(M_x)|X_1\rangle = 0 \quad . \tag{B.40}$$

Finally the action of the projection operator reads

$$\hat{\mathcal{P}}^{X_0}(M_x)|\Phi_a\rangle = \sum_{\substack{m \in \mathbb{Z} \\ X_0 + 2mM_x \geq 0}} c^{X_1}(a)\,|X_1 = X_0 + 2mM_x\rangle \quad . \tag{B.41}$$

For a value of M_x large enough (depending on the width of the distribution of the components X_1), we get only the desired component

$$\hat{\mathcal{P}}^{X_0}(M_x)|\Phi_a\rangle = c^{X_0}(a)\,|X_0\rangle \quad . \tag{B.42}$$

Appendix C

Angular Momentum

Je vais présenter dans cette Introduction, les principes du calcul des probabilités, et les résultats généraux auxquels je suis parvenu dans cet ouvrage, en les appliquant aux questions les plus importantes de la vie, qui ne sont en effet, pour la plupart, que des problèmes de probabilité.

Pierre-Simon de Laplace, Théorie Analytique des Probabilités (1812).

As a short introduction, let me mention that this appendix has been inspired by, and constitutes an expansion of, the work done by Michael for even-even nuclei [24]. Also, elemental definitions are omitted as it is assumed that the reader has (at least) a basic knowledge of quantum mechanics[1].

C.1 Basic Definitions

Let us consider the total angular momentum $\hat{\vec{J}} = \hat{\vec{L}} + \hat{\vec{S}}$, with $\hat{\vec{L}}$ and $\hat{\vec{S}}$ being the orbital and the spin angular momentum, respectively. Its cartesian components $\hat{J}_x$, $\hat{J}_y$, and $\hat{J}_z$, in the second quantization formalism, read

$$\hat{J}_k = \sum_{t=n,z} \sum_{mn} \langle m_t | \hat{J}_k | n_t \rangle \, \hat{a}^\dagger_{t,m} \hat{a}_{t,n} \quad \text{for } k = x, y, z \quad , \tag{C.1}$$

where $\langle m_t | \hat{J}_k | n_t \rangle$ are their matrix elements in the basis of single-particle states $(\hat{a}^\dagger, \hat{a})_t$, with $t = n, z$. Note that we consider here the total nucleon angular momentum, and not the total angular momentum of each particle species.
The elements of $SU(2)_A$ are represented by the operators

$$\hat{R}(\alpha, \beta, \gamma) = e^{-i\alpha \hat{J}_z} e^{-i\beta \hat{J}_y} e^{-i\gamma \hat{J}_z} \quad , \tag{C.2}$$

parametrized here by the Euler angles (α, β, γ) [155], with obviously

$$\hat{R}(0, 0, 0) = \hat{\mathbb{1}} \quad , \tag{C.3}$$

[1] If you don't, I see two solutions: either you learn quantum mechanics (there's probably an app for that) or you go do something else. If I were you, I would opt for the latter. Unfortunately, it is too late for me, but not for you. So just go, go as far away as possible, and never look back.

and recalling that $SU(2)_A$ is *not* abelian!
The hermitean conjugate of $\hat{R}(\alpha,\beta,\gamma)$ is

$$\hat{R}^\dagger(\alpha,\beta,\gamma) = e^{+i\gamma\hat{J}_z} e^{+i\beta\hat{J}_y} e^{+i\alpha\hat{J}_z} = \hat{R}(-\gamma,-\beta,-\alpha) \quad , \tag{C.4}$$

with the unitarity relation

$$\hat{R}(\alpha,\beta,\gamma)\hat{R}^\dagger(\alpha,\beta,\gamma) = \hat{\mathbb{1}} \quad . \tag{C.5}$$

The x, y, and z, signatures are defined as the rotations by an angle π around the x, y, and z, axes, respectively,

$$\hat{R}_x = e^{-i\pi\hat{J}_x} = \hat{R}(0,\pi,\pi) \quad , \tag{C.6}$$

$$\hat{R}_y = e^{-i\pi\hat{J}_y} = \hat{R}(0,\pi,0) \quad , \tag{C.7}$$

$$\hat{R}_z = e^{-i\pi\hat{J}_z} = \hat{R}(0,0,\pi) = \hat{R}(\pi,0,0) \quad , \tag{C.8}$$

$$\tag{C.9}$$

with the relation

$$\hat{R}_l\hat{R}_m = \delta_{lm}\hat{R}_l^2 + \sum_{n=x,y,z} \epsilon_{lmn}^2 e^{-i\pi\epsilon_{lmn}\hat{J}_n} \quad , \tag{C.10}$$

where $l,m,n = x,y$, or z, and ϵ_{lmn} is the Levi-Civita tensor.

The eigenstates $|JK\rangle$ common to $\hat{J}^2 = \hat{J}_x^2 + \hat{J}_y^2 + \hat{J}_z^2$ and $\hat{J}_z$ can be used as basis functions for the irreps of $SU(2)_A$

$$\hat{R}(\alpha,\beta,\gamma)|JK\rangle = \sum_{M=-J}^{J} D^J_{MK}(\alpha,\beta,\gamma)|JM\rangle \quad , \tag{C.11}$$

with

$$D^J_{MK}(\alpha,\beta,\gamma) = \langle JM|\hat{R}(\alpha,\beta,\gamma)|JK\rangle \tag{C.12}$$

being Wigner's D functions, J being an integer or a half-integer, and $M,K \in \{-J,-J+1,\ldots,J-1,J\}$. We can express the $D^J_{MK}(\alpha,\beta,\gamma)$ in terms of (real) Wigner's d functions

$$D^J_{MK}(\alpha,\beta,\gamma) = e^{-i\alpha M} d^J_{MK}(\beta) e^{-i\gamma K} \quad , \tag{C.13}$$

with

$$d^J_{MK}(\beta) = \langle JM|\hat{R}(0,\beta,0)|JK\rangle \quad . \tag{C.14}$$

It is clearly not possible to enumerate here all the many properties of Wigner's D functions, so we give here only the relations needed lateron

$$\begin{aligned} D^J_{MK}(\alpha+2k\pi,\beta,\gamma) &= D^J_{MK}(\alpha,\beta+2k\pi,\gamma) = D^J_{MK}(\alpha,\beta,\gamma+2k\pi) \\ &= (-)^{2Jk} D^J_{MK}(\alpha,\beta,\gamma) \quad \text{for } k \text{ integer} \quad , \end{aligned} \tag{C.15}$$

$$D^J_{MK}(0,0,\pi) = D^J_{MK}(\pi,0,0) = e^{-i\pi M}\delta_{M,K} \quad , \tag{C.16}$$

$$D^J_{MK}(0,\pi,0) = (-)^{J-K}\delta_{-M,K} = (-)^{J+M}\delta_{M,-K} \quad , \tag{C.17}$$

$$D^J_{MK}(0,0,0) = \delta_{M,K} \quad . \tag{C.18}$$

Also, Wigner's D functions follow the orthogonality relation

$$\frac{2J+1}{16\pi^2}\int_0^{2\pi} d\alpha \int_0^{\pi} d\beta \, \sin(\beta) \int_0^{4\pi} d\gamma \, {D^J_{MK}}^*(\alpha,\beta,\gamma)\, D^{J'}_{M'K'}(\alpha,\beta,\gamma) = \delta_{JJ'}\delta_{MM'}\delta_{KK'} \, . \quad \text{(C.19)}$$

We refer the interested reader to the very complete book by Varshalovich *et al.* [155] for a more thorough study of Wigner's D functions.
Using the properties of the D^J_{MK}, we get for the action of $\hat{R}_i$, with $i = x, y, z$, on $|JK\rangle$

$$\begin{aligned}
\hat{R}_x|JK\rangle &= \hat{R}_y\hat{R}_z|JK\rangle \\
&= \sum_{M=-J}^{J} D^J_{MK}(0,\pi,\pi)|JM\rangle \\
&= e^{-i\pi K}\sum_{M=-J}^{J} D^J_{MK}(0,\pi,0)|JM\rangle \\
&= e^{-i\pi K}\sum_{M=-J}^{J} (-)^{J+M}\delta_{M,-K}|JM\rangle \\
&= e^{-i\pi K}(-)^{J-K}|J-K\rangle \\
&= e^{-i\pi J}|J-K\rangle \quad ,
\end{aligned} \quad \text{(C.20)}$$

$$\begin{aligned}
\hat{R}_y|JK\rangle &= \sum_{M=-J}^{J} D^J_{MK}(0,\pi,0)|JM\rangle \\
&= \sum_{M=-J}^{J} (-)^{J+M}\delta_{M,-K}|JM\rangle \\
&= (-)^{J-K}|J-K\rangle \quad ,
\end{aligned} \quad \text{(C.21)}$$

$$\begin{aligned}
\hat{R}_z|JK\rangle &= \sum_{M=-J}^{J} D^J_{MK}(0,0,\pi)|JM\rangle \\
&= e^{-i\pi K}\sum_{M=-J}^{J} \delta_{M,K}|JM\rangle \\
&= e^{-i\pi K}|JK\rangle \quad ,
\end{aligned} \quad \text{(C.22)}$$

and consequently for the action of the square of $\hat{R}_i$, with $i = x, y, z$, on $|JK\rangle$

$$\begin{aligned}
\hat{R}^2_x|JK\rangle &= \hat{R}_x\hat{R}_x|JK\rangle \\
&= \hat{R}_x e^{-i\pi J}|J-K\rangle \\
&= e^{-i2\pi J}|JK\rangle \\
&= (-)^{2J}|JK\rangle \quad ,
\end{aligned} \quad \text{(C.23)}$$

$$\begin{aligned}
\hat{R}^2_y|JK\rangle &= \hat{R}_y\hat{R}_y|JK\rangle \\
&= \hat{R}_y(-)^{J-K}|J-K\rangle \\
&= (-)^{J-K}(-)^{J+K}|JK\rangle \\
&= (-)^{2J}|JK\rangle \quad ,
\end{aligned} \quad \text{(C.24)}$$

$$\begin{aligned}\hat{R}_z^2|JK\rangle &= \hat{R}_z\hat{R}_z|JK\rangle \\ &= \hat{R}_z e^{-i\pi K}|JK\rangle \\ &= e^{-i2\pi K}|JK\rangle \\ &= (-)^{2J}|JK\rangle \quad .\end{aligned} \tag{C.25}$$

Note that no assumption has been made on the values of J and K. In particular they can be either integers or half-integers, so we have to be careful with the identification $e^{-i\pi Q} = (-)^Q$.

C.2 Commutation Relations

We give here some basic commutation relations that we will need lateron in this section. First, let us recall the commutation relation between a rotation $\hat{R}(\alpha,\beta,\gamma)$ and the irreducible tensor operators $\hat{T}^\lambda_\mu$

$$\hat{R}(\alpha,\beta,\gamma)\hat{T}^\lambda_\mu\hat{R}^\dagger(\alpha,\beta,\gamma) = \sum_{\nu=-\lambda}^{\lambda} D^\lambda_{\nu\mu}(\alpha,\beta,\gamma)\hat{T}^\lambda_\nu \quad . \tag{C.26}$$

In this work, we will consider only irreducible tensor operators such that λ and μ are integers. Now, we can deduce the commutation relations betwen the i-signatures $\hat{R}_i$, $i = x, y, z$, and the irreducible tensor operators $\hat{T}^\lambda_\mu$

$$\hat{R}_z\hat{T}^\lambda_\mu\hat{R}^\dagger_z = \sum_{\nu=-\lambda}^{\lambda} D^\lambda_{\nu\mu}(0,0,\pi)\hat{T}^\lambda_\nu = \sum_{\nu=-\lambda}^{\lambda} \delta_{\nu,\mu}(-)^\nu\hat{T}^\lambda_\nu = (-)^\mu\,\hat{T}^\lambda_\mu \quad , \tag{C.27}$$

$$\hat{R}_y\hat{T}^\lambda_\mu\hat{R}^\dagger_y = \sum_{\nu=-\lambda}^{\lambda} D^\lambda_{\nu\mu}(0,\pi,0)\hat{T}^\lambda_\nu = \sum_{\nu=-\lambda}^{\lambda} \delta_{\nu,-\mu}(-)^{\lambda+\nu}\hat{T}^\lambda_\nu = (-)^{\lambda-\mu}\,\hat{T}^\lambda_{-\mu} \quad , \tag{C.28}$$

$$\hat{R}_x\hat{T}^\lambda_\mu\hat{R}^\dagger_x = \hat{R}_y\hat{R}_z\hat{T}^\lambda_\mu\hat{R}^\dagger_z\hat{R}^\dagger_y = \hat{R}_y(-)^\mu\,\hat{T}^\lambda_\mu\hat{R}^\dagger_y = (-)^\lambda\,\hat{T}^\lambda_{-\mu} \quad . \tag{C.29}$$

From these relations, we immediately see that for k integer we have

$$\hat{R}_i^{2k}\hat{T}^\lambda_\mu\hat{R}_i^{\dagger 2k} = \hat{T}^\lambda_\mu \quad \text{for } i = x, y, z \quad . \tag{C.30}$$

Applying these relations to the case of $\hat{J}$ ($\lambda = 1$), we get

$$\hat{R}_z\hat{J}_\mu\hat{R}^\dagger_z = (-)^\mu\hat{J}_\mu \quad , \tag{C.31}$$

$$\hat{R}_y\hat{J}_\mu\hat{R}^\dagger_y = (-)^{\mu+1}\hat{J}_{-\mu} \quad , \tag{C.32}$$

$$\hat{R}_x\hat{J}_\mu\hat{R}^\dagger_x = (-)\hat{J}_{-\mu} \quad , \tag{C.33}$$

and we recall that the $\hat{J}_\mu$ commute with spherical tensor operators as

$$[\hat{J}_{\pm1},\hat{T}^\lambda_\mu] = \mp\frac{1}{\sqrt{2}}\sqrt{\lambda(\lambda+1)-\mu(\mu\pm1)}\,\hat{T}^\lambda_{\mu\pm1} \quad , \tag{C.34}$$

$$[\hat{J}_0,\hat{T}^\lambda_\mu] = \mu\,\hat{T}^\lambda_\mu \quad . \tag{C.35}$$

Using the relations between the spherical components and the cartesian components of the angular momentum

$$\hat{J}_{+1} = -\frac{1}{\sqrt{2}}(\hat{J}_x + i\hat{J}_y) \quad , \tag{C.36}$$

$$\hat{J}_0 = \hat{J}_z \quad , \tag{C.37}$$

$$\hat{J}_{-1} = \frac{1}{\sqrt{2}}(\hat{J}_x - i\hat{J}_y) \quad , \tag{C.38}$$

$$\hat{J}_x = \frac{1}{\sqrt{2}}(\hat{J}_{-1} - \hat{J}_{+1}) \quad , \tag{C.39}$$

$$\hat{J}_y = \frac{i}{\sqrt{2}}(\hat{J}_{-1} + \hat{J}_{+1}) \quad , \tag{C.40}$$

$$\hat{J}_z = \hat{J}_0 \quad , \tag{C.41}$$

we obtain the relations

$$\hat{R}_x \hat{J}_x \hat{R}_x^\dagger = +\hat{J}_x \quad , \tag{C.42}$$

$$\hat{R}_x \hat{J}_y \hat{R}_x^\dagger = -\hat{J}_y \quad , \tag{C.43}$$

$$\hat{R}_x \hat{J}_z \hat{R}_x^\dagger = -\hat{J}_z \quad , \tag{C.44}$$

$$\hat{R}_y \hat{J}_x \hat{R}_y^\dagger = -\hat{J}_x \quad , \tag{C.45}$$

$$\hat{R}_y \hat{J}_y \hat{R}_y^\dagger = +\hat{J}_y \quad , \tag{C.46}$$

$$\hat{R}_y \hat{J}_z \hat{R}_y^\dagger = -\hat{J}_z \quad , \tag{C.47}$$

$$\hat{R}_z \hat{J}_x \hat{R}_z^\dagger = -\hat{J}_x \quad , \tag{C.48}$$

$$\hat{R}_z \hat{J}_y \hat{R}_z^\dagger = -\hat{J}_y \quad , \tag{C.49}$$

$$\hat{R}_z \hat{J}_z \hat{R}_z^\dagger = +\hat{J}_z \quad , \tag{C.50}$$

that we can summarize as

$$\hat{R}_i \hat{J}_j \hat{R}_i^\dagger = (-)^{1-\delta_{ij}} \hat{J}_j \quad \text{for } i,j = x,y,z \quad . \tag{C.51}$$

Let us define the rotation around a fixed axis

$$\hat{R}_i(\omega) = e^{-i\omega \hat{J}_i} \quad \text{for } i = x,y,z \quad . \tag{C.52}$$

It is easy to see that $\hat{R}_i(\omega)$ commutes with the m-signature $\hat{R}_m$, $m = x,y,z$, as

$$\begin{aligned}
\hat{R}_m \hat{R}_i(\omega) \hat{R}_m^\dagger &= \hat{R}_m e^{-i\omega \hat{J}_i} \hat{R}_m^\dagger \\
&= \hat{R}_m \left[\sum_{k=0}^{\infty} \frac{(-i\omega \hat{J}_i)^k}{k!} \right] \hat{R}_m^\dagger \\
&= \sum_{k=0}^{\infty} \frac{\left[\hat{R}_m (-i\omega \hat{J}_i) \hat{R}_m^\dagger \right]^k}{k!} \\
&= \sum_{k=0}^{\infty} \frac{\left[-i(-)^{1-\delta_{mi}} \omega \hat{J}_m \right]^k}{k!}
\end{aligned} \tag{C.53}$$

$$
\begin{aligned}
&= e^{-i(-)^{1-\delta_{mi}}\omega \hat{J}_m} \\
&= \hat{R}_i\big((-)^{1-\delta_{mi}}\omega\big) \quad ,
\end{aligned}
$$

or, if we want to write all the relations explicitely,

$$\hat{R}_x\hat{R}_x(\omega)\hat{R}_x^\dagger = \hat{R}_x(\omega) \quad , \tag{C.54}$$
$$\hat{R}_x\hat{R}_y(\omega)\hat{R}_x^\dagger = \hat{R}_y(-\omega) \quad , \tag{C.55}$$
$$\hat{R}_x\hat{R}_z(\omega)\hat{R}_x^\dagger = \hat{R}_z(-\omega) \quad , \tag{C.56}$$

$$\hat{R}_y\hat{R}_x(\omega)\hat{R}_y^\dagger = \hat{R}_x(-\omega) \quad , \tag{C.57}$$
$$\hat{R}_y\hat{R}_y(\omega)\hat{R}_y^\dagger = \hat{R}_y(\omega) \quad , \tag{C.58}$$
$$\hat{R}_y\hat{R}_z(\omega)\hat{R}_y^\dagger = \hat{R}_z(-\omega) \quad , \tag{C.59}$$

$$\hat{R}_z\hat{R}_x(\omega)\hat{R}_z^\dagger = \hat{R}_x(-\omega) \quad , \tag{C.60}$$
$$\hat{R}_z\hat{R}_y(\omega)\hat{R}_z^\dagger = \hat{R}_y(-\omega) \quad , \tag{C.61}$$
$$\hat{R}_z\hat{R}_z(\omega)\hat{R}_z^\dagger = \hat{R}_z(\omega) \quad . \tag{C.62}$$

From these relations, we immediately see that for k integer we have

$$\hat{R}_i^{2k}\hat{R}_j(\omega)\hat{R}_i^{\dagger 2k} = \hat{R}_j(\omega) \quad \text{for } i,j = x,y,z \quad . \tag{C.63}$$

Finally, reexpressing the rotation about Euler angles $\hat{R}(\alpha,\beta,\gamma)$ as

$$\hat{R}(\alpha,\beta,\gamma) = \hat{R}_z(\alpha)\hat{R}_y(\beta)\hat{R}_z(\gamma) \quad , \tag{C.64}$$

we can derive the following relations

$$
\begin{aligned}
\hat{R}_z\hat{R}(\alpha,\beta,\gamma)\hat{R}_z^\dagger &= \hat{R}_z\hat{R}_z(\alpha)\hat{R}_y(\beta)\hat{R}_z(\gamma)\hat{R}_z^\dagger \\
&= \hat{R}_z(\alpha+\pi)\hat{R}_y(\beta)\hat{R}_z(\gamma-\pi) \\
&= \hat{R}(\pi+\alpha,\beta,\gamma-\pi) \quad ,
\end{aligned} \tag{C.65}
$$

$$
\begin{aligned}
\hat{R}_z\hat{R}(\alpha,\beta,\gamma)\hat{R}_z^\dagger &= \hat{R}_z\hat{R}_z(\alpha)\hat{R}_y(\beta)\hat{R}_z(\gamma)\hat{R}_z^\dagger \\
&= \hat{R}_z\hat{R}_z(\alpha)\hat{R}_z^\dagger\hat{R}_z\hat{R}_y(\beta)\hat{R}_z^\dagger\hat{R}_z\hat{R}_z(\gamma)\hat{R}_z^\dagger \\
&= \hat{R}_z(\alpha)\hat{R}_y(-\beta)\hat{R}_z(\gamma) \\
&= \hat{R}(\alpha,-\beta,\gamma) \quad ,
\end{aligned} \tag{C.66}
$$

$$
\begin{aligned}
\hat{R}_y\hat{R}(\alpha,\beta,\gamma)\hat{R}_y^\dagger &= \hat{R}_y\hat{R}_z(\alpha)\hat{R}_y(\beta)\hat{R}_z(\gamma)\hat{R}_y^\dagger \\
&= \hat{R}_y\hat{R}_z(\alpha)\hat{R}_y^\dagger\hat{R}_y\hat{R}_y(\beta)\hat{R}_y^\dagger\hat{R}_y\hat{R}_z(\gamma)\hat{R}_y^\dagger \\
&= \hat{R}_z(-\alpha)\hat{R}_y(\beta)\hat{R}_z(-\gamma) \\
&= \hat{R}(-\alpha,\beta,-\gamma) \quad ,
\end{aligned} \tag{C.67}
$$

$$
\begin{aligned}
\hat{R}_x\hat{R}(\alpha,\beta,\gamma)\hat{R}_x^\dagger &= \hat{R}_y\hat{R}_z\hat{R}(\alpha,\beta,\gamma)\hat{R}_z^\dagger\hat{R}_y^\dagger \\
&= \hat{R}_y\hat{R}(\alpha,-\beta,\gamma)\hat{R}_y^\dagger \\
&= \hat{R}(-\alpha,-\beta,-\gamma) \quad ,
\end{aligned} \tag{C.68}
$$

and obviously, for k integer we have

$$\hat{R}_i^{2k}\hat{R}(\alpha,\beta,\gamma)\hat{R}_i^{\dagger 2k} = \hat{R}(\alpha,\beta,\gamma) \quad \text{for } i = x,y,z \quad . \tag{C.69}$$

Two last relations that will become useful later when expressing the rotated matrix elements:

$$\begin{aligned}
\hat{R}_x\hat{R}(\alpha,\beta,\gamma) &= \hat{R}_x\hat{R}_z(\alpha)\hat{R}_y(\beta)\hat{R}_z(\gamma) \\
&= \hat{R}_x\hat{R}_z(\alpha)\hat{R}_x^\dagger\hat{R}_x\hat{R}_y(\beta)\hat{R}_z(\gamma) \\
&= \hat{R}_z(-\alpha)\hat{R}_y\hat{R}_z\hat{R}_y(\beta)\hat{R}_z(\gamma) \\
&= \hat{R}_z(-\alpha)\hat{R}_z^\dagger\hat{R}_y\hat{R}_y(\beta)\hat{R}_z(\gamma) && = \hat{R}_z(-\alpha)\hat{R}_z\hat{R}_y^\dagger\hat{R}_y(\beta)\hat{R}_z(\gamma) \\
&= \hat{R}_z(-\alpha-\pi)\hat{R}_y(\pi+\beta)\hat{R}_z(\gamma) && = \hat{R}_z(\pi-\alpha)\hat{R}_y(\beta-\pi)\hat{R}_z(\gamma) \\
&= \hat{R}(-\alpha-\pi,\pi+\beta,\gamma) && = \hat{R}(\pi-\alpha,\beta-\pi,\gamma) \quad ,
\end{aligned} \tag{C.70}$$

$$\begin{aligned}
\hat{R}(\alpha,\beta,\gamma)\hat{R}_x^\dagger &= \hat{R}_z(\alpha)\hat{R}_y(\beta)\hat{R}_z(\gamma)\hat{R}_x^\dagger \\
&= \hat{R}_z(\alpha)\hat{R}_y(\beta)\hat{R}_x^\dagger\hat{R}_x\hat{R}_z(\gamma)\hat{R}_x^\dagger \\
&= \hat{R}_z(\alpha)\hat{R}_y(\beta)\hat{R}_z^\dagger\hat{R}_y^\dagger\hat{R}_z(-\gamma) \\
&= \hat{R}_z(\alpha)\hat{R}_y(\beta)\hat{R}_y\hat{R}_z^\dagger\hat{R}_z(-\gamma) && = \hat{R}_z(\alpha)\hat{R}_y(\beta)\hat{R}_y^\dagger\hat{R}_z\hat{R}_z(-\gamma) \\
&= \hat{R}_z(\alpha)\hat{R}_y(\beta+\pi)\hat{R}_z(-\pi-\gamma) && = \hat{R}_z(\alpha)\hat{R}_y(\beta-\pi)\hat{R}_z(\pi-\gamma) \\
&= \hat{R}(\alpha,\beta+\pi,-\pi-\gamma) && = \hat{R}(\alpha,\beta-\pi,\pi-\gamma) \quad .
\end{aligned} \tag{C.71}$$

C.3 Time Reversal and Rotations

We briefly show here that the rotations commute with the time-reversal operator. We recall that the time-reversal operator anticommutes with the angular-momentum operator

$$\hat{T}\hat{J}_m\hat{T}^\dagger = -\hat{J}_m \qquad \text{for } m = x,y,z \quad , \tag{C.72}$$

$$\hat{T}\hat{J}_\mu\hat{T}^\dagger = (-)^{1+\mu}\hat{J}_{-\mu} \quad \text{for } \mu = -1,0,+1 \quad . \tag{C.73}$$

Hence, $\hat{T}$ commutes with a rotation $\hat{R}_m(\omega)$, $m = x,y,z$,

$$\begin{aligned}
\hat{T}\hat{R}_m(\omega)\hat{T}^\dagger &= \hat{T}e^{-i\omega\hat{J}_m}\hat{T}^\dagger \\
&= \hat{T}\left[\sum_{k=0}^{\infty}\frac{\left(-i\omega\hat{J}_m\right)^k}{k!}\right]\hat{T}^\dagger \\
&= \sum_{k=0}^{\infty}\frac{\left[\hat{T}(-i\omega\hat{J}_m)\hat{T}^\dagger\right]^k}{k!} \\
&= \sum_{k=0}^{\infty}\frac{\left(+i\omega(-)\hat{J}_m\right)^k}{k!} \\
&= \sum_{k=0}^{\infty}\frac{\left(-i\omega\hat{J}_m\right)^k}{k!} \\
&= \hat{R}_m(\omega) \quad ,
\end{aligned} \tag{C.74}$$

and therefore with $\hat{R}(\alpha,\beta,\gamma)$

$$\begin{aligned}\hat{T}\hat{R}(\alpha,\beta,\gamma)\hat{T}^\dagger &= \hat{T}e^{-i\alpha\hat{J}_z}e^{-i\beta\hat{J}_y}e^{-i\gamma\hat{J}_z}\hat{T}^\dagger \\ &= \hat{T}e^{-i\alpha\hat{J}_z}\hat{T}\hat{T}^\dagger e^{-i\beta\hat{J}_y}\hat{T}\hat{T}^\dagger e^{-i\gamma\hat{J}_z}\hat{T}^\dagger \\ &= e^{-i\alpha\hat{J}_z}e^{-i\beta\hat{J}_y}e^{-i\gamma\hat{J}_z} \\ &= \hat{R}(\alpha,\beta,\gamma) \quad .\end{aligned} \tag{C.75}$$

C.4 Decomposition of a State that has the Symmetries $\left\{\hat{P},\hat{R}_x,\hat{S}_y^T\right\}_g$ and Good Number Parity

Let us consider a quasiparticle state $|\Phi_a\rangle$ (which is not necessarily a one-quasiparticle state) that has $\left\{\hat{P},\hat{R}_x,\hat{S}_y^T\right\}_g$ as symmetry group, and that has good number parity. The state $|\Phi_a\rangle$ hence verifies the symmetry relations of section 3.1.
The expansion of $|\Phi_a\rangle$ on the basis functions $|JK\rangle$ reads

$$|\Phi_a\rangle = \sum_\tau \sum_J \sum_{K=-J}^{J} c_K^J(a)|JK\tau\rangle \quad , \tag{C.76}$$

where τ stands for all the other quantum numbers that label the different, but equivalent, irreps of $SU(2)_A$. For the sake of compact notations, we will omit in this section the label τ and simply write

$$|\Phi_a\rangle = \sum_J \sum_{K=-J}^{J} c_K^J(a)|JK\rangle \quad . \tag{C.77}$$

C.4.1 Integer or Half-Integer Values of J

Applying twice the x-signature operator on $|\Phi_a\rangle$ we can deduce that

$$\begin{aligned}
& & \hat{R}_x^2|\Phi_a\rangle &= \eta_a^2|\Phi_a\rangle \\
\iff & & \hat{R}_x^2\sum_{J'}\sum_{K'=-J'}^{J'} c_{K'}^{J'}(a)|J'K'\rangle &= \eta_a^2\sum_{J''}\sum_{K''=-J''}^{J''} c_{K''}^{J''}(a)|J''K''\rangle \\
\iff & & \sum_{J'}\sum_{K'=-J'}^{J'} (-)^{2J'}c_{K'}^{J'}(a)|J'K'\rangle &= \eta_a^2\sum_{J''}\sum_{K''=-J''}^{J''} c_{K''}^{J''}(a)|J''K''\rangle \\
\iff & \langle JK| & \sum_{J'}\sum_{K'=-J'}^{J'} (-)^{2J'}c_{K'}^{J'}(a)|J'K'\rangle &= \langle JK|\eta_a^2\sum_{J''}\sum_{K''=-J''}^{J''} c_{K''}^{J''}(a)|J''K''\rangle \\
\iff & & (-)^{2J}c_K^J(a) &= \eta_a^2 c_K^J(a) \\
\iff & & c_K^J(a) &= \eta_a^2(-)^{2J}c_K^J(a) \quad .
\end{aligned} \tag{C.78}$$

Equation (C.78) implies that

$$\begin{aligned}
J \text{ integer and } \eta_a^2 = -1 \quad &\Longrightarrow \quad \forall K\,,\, c_K^J(a) = 0 \quad , \\
J \text{ half-integer and } \eta_a^2 = \quad 1 \quad &\Longrightarrow \quad \forall K\,,\, c_K^J(a) = 0 \quad .
\end{aligned} \tag{C.79}$$

A state $|\Phi_a\rangle$ with $\eta_a^2 = 1$ has only components with integer values of J in its decomposition on the basis functions $|JK\rangle$. By contrast, a state $|\Phi_a\rangle$ with $\eta_a^2 = -1$ has only components with

half-integer values of J in its decomposition on the basis functions $|JK\rangle$. This is natural as the state $|\Phi_a\rangle$ has good number parity, therefore it is a superposition of states with only either an even number of fermions, which have only integer values of J, or an odd number of fermions, which have only half-integer values of J. We have: $\eta_a^2 = \pi_a$.
We can thus write the expansion of $|\Phi_a\rangle$ on the $|JK\rangle$ as

$$|\Phi_a\rangle = \sum_J \sum_{K=-J}^{J} \delta_{\pi_a,(-)^{2J}}\, c_K^J(a)|JK\rangle \quad . \tag{C.80}$$

C.4.2 Relation Between $|JK\rangle$ and $|J-K\rangle$

Acting once with the x-signature operator on $|\Phi_a\rangle$ we can deduce that

$$\begin{aligned}
&\hat{R}_x|\Phi_a\rangle = \eta_a|\Phi_a\rangle \\
\iff \quad &\hat{R}_x \sum_{J'} \sum_{K'=-J'}^{J'} c_{K'}^{J'}(a)|J'K'\rangle = \eta_a \sum_{J''} \sum_{K''=-J''}^{J''} c_{K''}^{J''}(a)|J''K''\rangle \\
\iff \quad &\sum_{J'} \sum_{K'=-J'}^{J'} e^{-i\pi J'} c_{K'}^{J'}(a)|J'-K'\rangle = \eta_a \sum_{J''} \sum_{K''=-J''}^{J''} c_{K''}^{J''}(a)|J''K''\rangle \\
\iff \quad &\langle JK| \sum_{J'} \sum_{K'=-J'}^{J'} e^{-i\pi J'} c_{K'}^{J'}(a)|J'-K'\rangle = \langle JK|\eta_a \sum_{J''} \sum_{K''=-J''}^{J''} c_{K''}^{J''}(a)|J''K''\rangle \\
\iff \quad &e^{-i\pi J} c_{-K}^J(a) = \eta_a c_K^J(a) \\
\iff \quad &c_{-K}^J(a) = \eta_a e^{+i\pi J} c_K^J(a) \quad ,
\end{aligned} \tag{C.81}$$

and thus that, for any values of J and K, $|J-K\rangle$ and $|JK\rangle$ have equal modulus of their weights

$$\forall\, J, K\,, \quad |c_{-K}^J(a)| = |c_K^J(a)| \quad . \tag{C.82}$$

Equation (C.81) also implies that for $K=0$ we have: $c_0^J(a) = \eta_a e^{+i\pi J} c_0^J(a)$, and thus that

$$\begin{aligned}
J \text{ even and } \eta_a = -1 \quad &\Longrightarrow \quad c_0^J(a) = 0 \quad , \\
J \text{ odd and } \eta_a = \ \ 1 \quad &\Longrightarrow \quad c_0^J(a) = 0 \quad .
\end{aligned} \tag{C.83}$$

In particular, there is no $J=0$ component in the decomposition of a state $|\Phi_a\rangle$ with $\eta_a = -1$.

C.4.3 Relation Between $|\Phi_a\rangle$ and $\hat{T}|\Phi_a\rangle$

Using the y-time-simplex, we can derive, from the definition of the time-reversed state, that

$$\begin{aligned}
&\hat{T}|\Phi_a\rangle = |\tilde{\Phi}_a\rangle \\
\iff \quad &\hat{T}\hat{S}_y^T|\Phi_a\rangle = |\tilde{\Phi}_a\rangle \\
\iff \quad &\hat{T}\hat{T}\hat{R}_y\hat{P}|\Phi_a\rangle = |\tilde{\Phi}_a\rangle \\
\iff \quad &\pi_a\hat{R}_y\hat{P}|\Phi_a\rangle = |\tilde{\Phi}_a\rangle \\
\iff \quad &\pi_a\hat{R}_z\hat{R}_x\hat{P}|\Phi_a\rangle = |\tilde{\Phi}_a\rangle
\end{aligned}$$

$$
\begin{aligned}
&\iff && \pi_a p_a \eta_a \hat{R}_z |\Phi_a\rangle = |\tilde{\Phi}_a\rangle && \text{(C.84)}\\
&\iff && p_a \eta_a \hat{R}_z^\dagger |\Phi_a\rangle = |\tilde{\Phi}_a\rangle &\\
&\iff && p_a \eta_a \hat{R}_z^\dagger \sum_{J'} \sum_{K'=-J'}^{J'} c_{K'}^{J'}(a) |J'K'\rangle = \sum_{J''} \sum_{K''=-J''}^{J''} c_{K''}^{J''}(\tilde{a}) |J''K''\rangle &\\
&\iff && p_a \eta_a \sum_{J'} \sum_{K'=-J'}^{J'} e^{+i\pi K'} c_{K'}^{J'}(a) \, |J'K'\rangle = \sum_{J''} \sum_{K''=-J''}^{J''} c_{K''}^{J''}(\tilde{a}) |J''K''\rangle &\\
&\iff && \langle JK| p_a \eta_a \sum_{J'} \sum_{K'=-J'}^{J'} e^{+i\pi K'} c_{K'}^{J'}(a) |J'K'\rangle = \langle JK| \sum_{J''} \sum_{K''=-J''}^{J''} c_{K''}^{J''}(\tilde{a}) |J''K''\rangle &\\
&\iff && p_a \eta_a e^{+i\pi K} c_K^J(a) = c_K^J(\tilde{a}) \quad , &
\end{aligned}
$$

and thus that, for any values of J and K, we have equal modulus for the weight of $|JK\rangle$ in the decomposition of $|\Phi_a\rangle$ and in the decomposition of $\hat{T}|\Phi_a\rangle$

$$\forall\, J, K\,, \quad |c_K^J(a)| = |c_K^J(\tilde{a})| \quad . \tag{C.85}$$

Equation (C.84) also implies that for states that are invariant under time-reversal $\left(|\tilde{\Phi}_a\rangle = |\Phi_a\rangle\right)$ we have : $p_a \eta_a e^{+i\pi K} c_K^J(a) = c_K^J(a)$, and thus that

$$
\begin{aligned}
K \text{ even} \;\text{ and }\; p_a\eta_a = -1 \quad &\Longrightarrow \quad \forall\, J\,,\, c_K^J(a) = 0 \quad ,\\
K \text{ odd} \;\text{ and }\; p_a\eta_a = \;\; 1 \quad &\Longrightarrow \quad \forall\, J\,,\, c_K^J(a) = 0 \quad .
\end{aligned}
\tag{C.86}
$$

There is no $K = \pm 1$ component in the decomposition of a time-reversal symmetric even vacuum, with $p_a = \eta_a = 1$, and combined with the fact that, for odd values of J there is no $K = 0$ component either (see equation (C.81)), we can deduce that there is no $J = 1$ component at all in its decomposition.

C.5 Properties of the Projection Operator

Let us consider the projection operator $\hat{P}^J_{MK}$ that projects on the angular momentum J with third component M and from third component K. According to equation (3.21), $\hat{P}^J_{MK}$ reads

$$\hat{P}^J_{MK} = \frac{2J+1}{16\pi^2} \int_0^{2\pi} d\alpha \int_0^{\pi} d\beta \, \sin(\beta) \int_0^{4\pi} d\gamma \, {D^J_{MK}}^*(\alpha,\beta,\gamma) \, \hat{R}(\alpha,\beta,\gamma) \quad , \tag{C.87}$$

where we have chosen to carry out the integral over $[0, 4\pi]$ on γ [155]. The Lie group $SU(2)_A$ is compact but not abelian, therefore the properties of the projection operator $\hat{P}^J_{MK}$ are a little bit more complicated than those of the projection operator on particle number

$$\hat{P}^J_{K'M'} \hat{P}^J_{MK} = \hat{P}^J_{K'K} \, \delta_{M',M} \quad , \tag{C.88}$$

$$\left(\hat{P}^J_{MK}\right)^\dagger = \hat{P}^J_{KM} \quad . \tag{C.89}$$

We also note that the projection operator $\hat{P}^J_{MK}$ can be written in Dirac's bracket notation as

$$\hat{P}^J_{MK} = |JM\rangle\langle JK| \quad . \tag{C.90}$$

C.6 Reduction of the Interval of Integration over γ from $[0, 4\pi]$ to $[0, 2\pi]$

Using the symmetries of $|\Phi_a\rangle$ and of Wigner's D functions, and the substitution $\gamma' = \gamma - 2\pi$ (renaming γ' as γ afterwards), the inverval of integration over γ can be reduced

$$
\begin{aligned}
\hat{P}^J_{MK}|\Phi_a\rangle &= \frac{2J+1}{16\pi^2}\int_0^{2\pi} d\alpha \int_0^{\pi} d\beta\, \sin(\beta) \int_0^{4\pi} d\gamma\, {D^J_{MK}}^*(\alpha,\beta,\gamma)\, \hat{R}(\alpha,\beta,\gamma)|\Phi_a\rangle \\
&= \frac{2J+1}{16\pi^2}\int_0^{2\pi} d\alpha \int_0^{\pi} d\beta\, \sin(\beta) \Bigg[\int_0^{2\pi} d\gamma\, {D^J_{MK}}^*(\alpha,\beta,\gamma)\, \hat{R}(\alpha,\beta,\gamma) \\
&\quad + \int_{2\pi}^{4\pi} d\gamma\, {D^J_{MK}}^*(\alpha,\beta,\gamma)\, \hat{R}(\alpha,\beta,\gamma) \Bigg] |\Phi_a\rangle \\
&= \frac{2J+1}{16\pi^2}\int_0^{2\pi} d\alpha \int_0^{\pi} d\beta\, \sin(\beta) \Bigg[\int_0^{2\pi} d\gamma\, {D^J_{MK}}^*(\alpha,\beta,\gamma)\, \hat{R}(\alpha,\beta,\gamma) \\
&\quad + \int_0^{2\pi} d\gamma'\, {D^J_{MK}}^*(\alpha,\beta,\gamma'+2\pi)\, \hat{R}(\alpha,\beta,\gamma'+2\pi) \Bigg] |\Phi_a\rangle \\
&= \frac{2J+1}{16\pi^2}\int_0^{2\pi} d\alpha \int_0^{\pi} d\beta\, \sin(\beta) \Bigg[\int_0^{2\pi} d\gamma\, {D^J_{MK}}^*(\alpha,\beta,\gamma)\, \hat{R}(\alpha,\beta,\gamma) \\
&\quad + \int_0^{2\pi} d\gamma\, (-)^{2J} {D^J_{MK}}^*(\alpha,\beta,\gamma)\, \hat{R}(\alpha,\beta,\gamma)\hat{R}^2_z \Bigg] |\Phi_a\rangle \\
&= \frac{2J+1}{16\pi^2}\int_0^{2\pi} d\alpha \int_0^{\pi} d\beta\, \sin(\beta) \Bigg[\int_0^{2\pi} d\gamma\, {D^J_{MK}}^*(\alpha,\beta,\gamma)\, \hat{R}(\alpha,\beta,\gamma) \\
&\quad + (-)^{2J}\,\pi_a \int_0^{2\pi} d\gamma\, \pi_a {D^J_{MK}}^*(\alpha,\beta,\gamma)\, \hat{R}(\alpha,\beta,\gamma) \Bigg] |\Phi_a\rangle \\
&= \delta_{(-)^{2J},\,\pi_a}\, \frac{2J+1}{8\pi^2}\int_0^{2\pi} d\alpha \int_0^{\pi} d\beta\, \sin(\beta) \int_0^{2\pi} d\gamma\, {D^J_{MK}}^*(\alpha,\beta,\gamma)\, \hat{R}(\alpha,\beta,\gamma)|\Phi_a\rangle \quad .
\end{aligned}
\tag{C.91}
$$

This is a simple consequence of the fact that there are either only components with integer values of J, or only components with half integer values of J, in the decomposition of $|\Phi_a\rangle$ on the basis functions $|JK\rangle$.

C.7 Symmetries of the Rotated Matrix Elements

It is possible to further reduce the complexity of the integrals in the projection operator using the symmetry relations implied by the choice of $\left\{\hat{P}, \hat{R}_x, \hat{S}^T_y\right\}_g$ as symmetry group for the quasiparticle states $|\Phi_a\rangle$ and $|\Phi_b\rangle$ (which are not necessarily one-quasiparticle states). To this end, we give here detailed derivations of the symmetries of the rotated matrix elements. An extensive use of the relations presented in C.2 and of the symmetry relations of section 3.1 is done. Also, we assume throughout all derivations that the states $|\Phi_a\rangle$ and $|\Phi_b\rangle$ have same number parity: $\pi_a = \pi_b$.

C.7.1 Rotation by $2\pi k$, $k \in \mathbb{Z}$

First a series of symmetries that consists of "translations" of α, β, or γ, by an angle $2\pi k$, k being an arbitrary integer:

$$\begin{aligned}\langle\Phi_a|\hat{R}(\alpha,\beta,\gamma)\hat{T}^\lambda_\mu|\Phi_b\rangle &= \langle\Phi_a|\big(\hat{R}^\dagger_z\hat{R}^\dagger_z\big)^k\big(\hat{R}_z\hat{R}_z\big)^k\hat{R}(\alpha,\beta,\gamma)\hat{T}^\lambda_\mu|\Phi_b\rangle \\ &= \Big[\langle\Phi_a|\big(\hat{R}^\dagger_z\hat{R}^\dagger_z\big)^k\Big]\Big[\big(\hat{R}_z\hat{R}_z\big)^k\hat{R}(\alpha,\beta,\gamma)\Big]\hat{T}^\lambda_\mu|\Phi_b\rangle \\ &= \pi_a^k\langle\Phi_a|\hat{R}(\alpha+2k\pi,\beta,\gamma)\hat{T}^\lambda_\mu|\Phi_b\rangle \quad ,\end{aligned} \tag{C.92}$$

$$\begin{aligned}\langle\Phi_a|\hat{R}(\alpha,\beta,\gamma)\hat{T}^\lambda_\mu|\Phi_b\rangle &= \langle\Phi_a|\big(\hat{R}^\dagger_y\hat{R}^\dagger_y\big)^k\big(\hat{R}_y\hat{R}_y\big)^k\hat{R}(\alpha,\beta,\gamma)\hat{T}^\lambda_\mu|\Phi_b\rangle \\ &= \Big[\langle\Phi_a|\big(\hat{R}^\dagger_y\hat{R}^\dagger_y\big)^k\Big]\Big[\big(\hat{R}_y\hat{R}_y\big)^k\hat{R}(\alpha,0,0)\hat{R}(0,\beta,\gamma)\Big]\hat{T}^\lambda_\mu|\Phi_b\rangle \\ &= \pi_a^k\langle\Phi_a|\Big[\hat{R}(\alpha,0,0)\big(\hat{R}_y\hat{R}_y\big)^k\hat{R}(0,\beta,\gamma)\Big]\hat{T}^\lambda_\mu|\Phi_b\rangle \\ &= \pi_a^k\langle\Phi_a|\hat{R}(\alpha,\beta+2k\pi,\gamma)\hat{T}^\lambda_\mu|\Phi_b\rangle \quad ,\end{aligned} \tag{C.93}$$

$$\begin{aligned}\langle\Phi_a|\hat{R}(\alpha,\beta,\gamma)\hat{T}^\lambda_\mu|\Phi_b\rangle &= \langle\Phi_a|\hat{R}(\alpha,\beta,\gamma)\Big[\big(\hat{R}_z\hat{R}_z\big)^k\hat{T}^\lambda_\mu\big(\hat{R}^\dagger_z\hat{R}^\dagger_z\big)^k\Big]|\Phi_b\rangle \\ &= \langle\Phi_a|\Big[\hat{R}(\alpha,\beta,\gamma)\big(\hat{R}_z\hat{R}_z\big)^k\Big]\hat{T}^\lambda_\mu\Big[\big(\hat{R}^\dagger_z\hat{R}^\dagger_z\big)^k|\Phi_b\rangle\Big] \\ &= \pi_a^k\langle\Phi_a|\hat{R}(\alpha,\beta,\gamma+2k\pi)\hat{T}^\lambda_\mu|\Phi_b\rangle \quad .\end{aligned} \tag{C.94}$$

C.7.2 Relations Between γ and $\gamma+\pi$

The relations between the angles γ and $\gamma+\pi$ are obtained in two steps.
First we derive that

$$\begin{aligned}\langle\Phi_a|\hat{R}(\alpha,\beta,\gamma)\hat{T}^\lambda_\mu|\tilde{\Phi}_b\rangle &= p_b\eta_b\langle\Phi_a|\hat{R}(\alpha,\beta,\gamma)\hat{T}^\lambda_\mu\big(\hat{R}^\dagger_z|\Phi_b\rangle\big) \\ &= p_b\eta_b\langle\Phi_a|\hat{R}(\alpha,\beta,\gamma)\hat{R}^\dagger_z\hat{R}_z\hat{T}^\lambda_\mu\hat{R}^\dagger_z|\Phi_b\rangle \\ &= p_b\eta_b\langle\Phi_a|\big(\hat{R}(\alpha,\beta,\gamma)\hat{R}^\dagger_z\big)\big(\hat{R}_z\hat{T}^\lambda_\mu\hat{R}^\dagger_z\big)|\Phi_b\rangle \\ &= (-)^\mu p_b\eta_b\langle\Phi_a|\hat{R}(\alpha,\beta,\gamma-\pi)\hat{T}^\lambda_\mu|\Phi_b\rangle \\ &= (-)^\mu\pi_a p_b\eta_b\langle\Phi_a|\hat{R}(\alpha,\beta,\pi+\gamma)\hat{T}^\lambda_\mu|\Phi_b\rangle \quad .\end{aligned} \tag{C.95}$$

Then, noticing [95] that for any linear operator $\hat{A}$ we can express $\langle\Phi_a|\hat{A}|\Phi_b\rangle$ as

$$\begin{aligned}\langle\Phi_a|\hat{A}|\Phi_b\rangle &= \big(\langle\Phi_a|\hat{T}^\dagger\hat{T}\big)\hat{A}\big(\hat{T}^\dagger\hat{T}|\Phi_b\rangle\big) \\ &= \big(\langle\tilde{\Phi}_a|\hat{T}\big)\hat{A}\big(\hat{T}^\dagger|\tilde{\Phi}_b\rangle\big) \\ &= \langle\tilde{\Phi}_a|\big(\hat{T}\hat{A}\hat{T}^\dagger\big)|\tilde{\Phi}_b\rangle^* \\ &= \langle\tilde{\Phi}_a|\hat{\tilde{A}}|\tilde{\Phi}_b\rangle^* \quad ,\end{aligned} \tag{C.96}$$

where $\hat{\tilde{A}} = \hat{T}\hat{A}\hat{T}^\dagger$, we can derive that

$$\langle\Phi_a|\hat{R}(\alpha,\beta,\gamma)\hat{T}^\lambda_\mu|\tilde{\Phi}_b\rangle = \pi_a\langle\tilde{\Phi}_a|\hat{R}(\alpha,\beta,\gamma)\hat{\tilde{T}}^\lambda_\mu|\Phi_b\rangle^* \quad , \tag{C.97}$$

where we have used that $|\hat{\tilde{\Phi}}_b\rangle = \hat{T}|\tilde{\Phi}_b\rangle = \pi_a|\Phi_b\rangle$ and the notation $\hat{\tilde{T}}^\lambda_\mu = \hat{T}\hat{T}^\lambda_\mu\hat{T}^\dagger$.
Combining equations (C.95) and (C.97), we obtain the relation

$$\begin{aligned}\langle\tilde{\Phi}_a|\hat{R}(\alpha,\beta,\gamma)\hat{\tilde{T}}^\lambda_\mu|\Phi_b\rangle &= \pi_a\langle\Phi_a|\hat{R}(\alpha,\beta,\gamma)\hat{T}^\lambda_\mu|\tilde{\Phi}_b\rangle^* \\ &= (-)^\mu p_b\eta_b^*\langle\Phi_a|\hat{R}(\alpha,\beta,\pi+\gamma)\hat{T}^\lambda_\mu|\Phi_b\rangle^* \quad .\end{aligned} \tag{C.98}$$

C.7.3 Direct Relations

Using only symmetry relations of sections 3.1 and C.2, we can derive a series of three direct relations:

$$\begin{aligned}
\langle\Phi_a|\hat{R}(\alpha,\beta,\gamma)\hat{T}^\lambda_\mu|\Phi_b\rangle &= \langle\Phi_a|\hat{R}^\dagger_x\hat{R}^\dagger_x\hat{R}_x\hat{R}_x\hat{R}(\alpha,\beta,\gamma)\hat{R}^\dagger_x\hat{R}_x\hat{T}^\lambda_\mu\hat{R}^\dagger_x\hat{R}_x|\Phi_b\rangle \\
&= \big(\langle\Phi_a|\hat{R}^\dagger_x\hat{R}^\dagger_x\big)\hat{R}_x\big(\hat{R}_x\hat{R}(\alpha,\beta,\gamma)\hat{R}^\dagger_x\big)\big(\hat{R}_x\hat{T}^\lambda_\mu\hat{R}^\dagger_x\big)\big(\hat{R}_x|\Phi_b\rangle\big) \\
&= (-)^\lambda\pi_a\eta_b\langle\Phi_a|\big(\hat{R}_x\hat{R}(-\alpha,-\beta,-\gamma)\big)\hat{T}^\lambda_{-\mu}|\Phi_b\rangle \\
&= (-)^\lambda\pi_a\eta_b\langle\Phi_a|\hat{R}(\alpha-\pi,\pi-\beta,-\gamma)\hat{T}^\lambda_{-\mu}|\Phi_b\rangle \\
&= (-)^\lambda\pi_a\eta_b\langle\Phi_a|\hat{R}(\pi+\alpha,\pi-\beta,2\pi-\gamma)\hat{T}^\lambda_{-\mu}|\Phi_b\rangle \quad ,
\end{aligned} \tag{C.99}$$

$$\begin{aligned}
\langle\Phi_a|\hat{R}(\alpha,\beta,\gamma)\hat{T}^\lambda_\mu|\Phi_b\rangle &= \langle\Phi_a|\hat{R}^\dagger_x\hat{R}_x\hat{R}(\alpha,\beta,\gamma)\hat{R}^\dagger_x\hat{R}^\dagger_x\hat{R}_x\hat{R}_x\hat{T}^\lambda_\mu|\Phi_b\rangle \\
&= \big(\langle\Phi_a|\hat{R}^\dagger_x\big)\big(\hat{R}_x\hat{R}(\alpha,\beta,\gamma)\hat{R}^\dagger_x\big)\hat{R}^\dagger_x\big(\hat{R}_x\hat{R}_x\hat{T}^\lambda_\mu\big)|\Phi_b\rangle \\
&= \eta^*_a\langle\Phi_a|\big(\hat{R}(-\alpha,-\beta,-\gamma)\hat{R}^\dagger_x\big)\big(\hat{T}^\lambda_\mu\hat{R}_x\hat{R}_x\big)|\Phi_b\rangle \\
&= \pi_a\eta^*_a\langle\Phi_a|\big(\hat{R}(-\alpha,-\beta,-\gamma)\hat{R}^\dagger_x\big)\hat{T}^\lambda_\mu|\Phi_b\rangle \\
&= \pi_a\eta^*_a\langle\Phi_a|\hat{R}(-\alpha,-\pi-\beta,\pi+\gamma)\hat{T}^\lambda_\mu|\Phi_b\rangle \\
&= \pi_a\eta^*_a\langle\Phi_a|\hat{R}(2\pi-\alpha,\pi-\beta,\pi+\gamma)\hat{T}^\lambda_\mu|\Phi_b\rangle \quad ,
\end{aligned} \tag{C.100}$$

$$\begin{aligned}
\langle\Phi_a|\hat{R}(\alpha,\beta,\gamma)\hat{T}^\lambda_\mu|\Phi_b\rangle &= \big(\langle\tilde{\Phi}_a|\hat{T}\big)\big(\hat{R}(\alpha,\beta,\gamma)\hat{T}^\dagger\hat{T}\hat{T}^\lambda_\mu\hat{T}^\dagger|\tilde{\Phi}_b\rangle\big) \\
&= \Big[\langle\tilde{\Phi}_a|\big(\hat{T}\hat{R}(\alpha,\beta,\gamma)\hat{T}^\dagger\hat{T}\hat{T}^\lambda_\mu\hat{T}^\dagger|\tilde{\Phi}_b\rangle\big)\Big]^* \\
&= \langle\tilde{\Phi}_a|\big(\hat{T}\hat{R}(\alpha,\beta,\gamma)\hat{T}^\dagger\hat{T}\hat{T}^\lambda_\mu\hat{T}^\dagger\big)|\tilde{\Phi}_b\rangle^* \\
&= \langle\tilde{\Phi}_a|\big(\hat{T}\hat{R}(\alpha,\beta,\gamma)\hat{T}^\dagger\big)\big(\hat{T}\hat{T}^\lambda_\mu\hat{T}^\dagger\big)|\tilde{\Phi}_b\rangle^* \\
&= \langle\tilde{\Phi}_a|\hat{R}(\alpha,\beta,\gamma)\hat{\tilde{T}}^\lambda_\mu|\tilde{\Phi}_b\rangle^* \\
&= \langle\tilde{\Phi}_a|\hat{R}^\dagger_z\hat{R}_z\hat{R}(\alpha,\beta,\gamma)\hat{R}^\dagger_z\hat{R}_z\hat{\tilde{T}}^\lambda_\mu\hat{R}^\dagger_z\hat{R}_z|\tilde{\Phi}_b\rangle^* \\
&= \Big[\big(\langle\tilde{\Phi}_a|\hat{R}^\dagger_z\big)\big(\hat{R}_z\hat{R}(\alpha,\beta,\gamma)\hat{R}^\dagger_z\big)\big(\hat{R}_z\hat{\tilde{T}}^\lambda_\mu\hat{R}^\dagger_z\big)\big(\hat{R}_z|\tilde{\Phi}_b\rangle\big)\Big]^* \\
&= (-)^\mu p_a p_b\eta_a\eta^*_b\langle\Phi_a|\hat{R}(\pi+\alpha,\beta,\gamma-\pi)\hat{\tilde{T}}^\lambda_\mu|\Phi_b\rangle^* \\
&= (-)^\mu\pi_a p_a p_b\eta_a\eta^*_b\langle\Phi_a|\hat{R}(\pi+\alpha,\beta,\pi+\gamma)\hat{\tilde{T}}^\lambda_\mu|\Phi_b\rangle^* \quad .
\end{aligned} \tag{C.101}$$

C.7.4 Combined Relations

Combining the direct relations we can obtained an additional series of relations. Using successively (C.99) and (C.100), we get

$$\begin{aligned}
\langle\Phi_a|\hat{R}(\alpha,\beta,\gamma)\hat{T}^\lambda_\mu|\Phi_b\rangle &= (-)^\lambda\pi_a\eta_b\langle\Phi_a|\hat{R}(\pi+\alpha,\pi-\beta,2\pi-\gamma)\hat{T}^\lambda_{-\mu}|\Phi_b\rangle \\
&= (-)^\lambda\eta^*_a\eta_b\langle\Phi_a|\hat{R}(\pi-\alpha,\beta,3\pi-\gamma)\hat{T}^\lambda_{-\mu}|\Phi_b\rangle \\
&= (-)^\lambda\pi_a\eta^*_a\eta_b\langle\Phi_a|\hat{R}(\pi-\alpha,\beta,\pi-\gamma)\hat{T}^\lambda_{-\mu}|\Phi_b\rangle \quad .
\end{aligned} \tag{C.102}$$

Using successively (C.99) and (C.101), we get

$$\begin{aligned}
\langle\Phi_a|\hat{R}(\alpha,\beta,\gamma)\hat{T}^\lambda_\mu|\Phi_b\rangle &= (-)^\lambda\pi_a\eta_b\langle\Phi_a|\hat{R}(\pi+\alpha,\pi-\beta,2\pi-\gamma)\hat{T}^\lambda_{-\mu}|\Phi_b\rangle \\
&= (-)^{\lambda+\mu}p_a p_b\eta_a\langle\Phi_a|\hat{R}(2\pi+\alpha,\pi-\beta,3\pi-\gamma)\hat{\tilde{T}}^\lambda_{-\mu}|\Phi_b\rangle^* \\
&= (-)^{\lambda+\mu}p_a p_b\eta_a\langle\Phi_a|\hat{R}(\alpha,\pi-\beta,\pi-\gamma)\hat{\tilde{T}}^\lambda_{-\mu}|\Phi_b\rangle^* \quad .
\end{aligned} \tag{C.103}$$

Using successively (C.100) and (C.101), we get

$$\begin{aligned}\langle\Phi_a|\hat{R}(\alpha,\beta,\gamma)\hat{T}^\lambda_\mu|\Phi_b\rangle &= \pi_a\eta_a^*\langle\Phi_a|\hat{R}(2\pi-\alpha,\pi-\beta,\pi+\gamma)\hat{T}^\lambda_\mu|\Phi_b\rangle \\ &= (-)^\mu p_a p_b \eta_b^* \langle\Phi_a|\hat{R}(3\pi-\alpha,\pi-\beta,2\pi+\gamma)\hat{\tilde{T}}^\lambda_\mu|\Phi_b\rangle^* \\ &= (-)^\mu p_a p_b \eta_b^* \langle\Phi_a|\hat{R}(\pi-\alpha,\pi-\beta,\gamma)\hat{\tilde{T}}^\lambda_\mu|\Phi_b\rangle^* \quad .\end{aligned} \tag{C.104}$$

Using successively (C.102) and (C.101), we get

$$\begin{aligned}\langle\Phi_a|\hat{R}(\alpha,\beta,\gamma)\hat{T}^\lambda_\mu|\Phi_b\rangle &= (-)^\lambda\pi_a\eta_a^*\eta_b\langle\Phi_a|\hat{R}(\pi-\alpha,\beta,\pi-\gamma)\hat{T}^\lambda_{-\mu}|\Phi_b\rangle \\ &= (-)^{\lambda+\mu} p_a p_b \langle\Phi_a|\hat{R}(2\pi-\alpha,\beta,2\pi-\gamma)\hat{\tilde{T}}^\lambda_{-\mu}|\Phi_b\rangle^* \quad .\end{aligned} \tag{C.105}$$

C.7.5 Final Relations and Expression of the Integral over the Euler Angles

Taking all the relations derived above, we can construct for the rotated matrix elements of spherical tensor operators the following set of symmetries

$$\langle\Phi_a|\hat{R}(\pi-\alpha,\beta,\pi-\gamma)\hat{T}^\lambda_\mu|\Phi_b\rangle = (-)^\lambda\pi_a\eta_a\eta_b^* \quad \langle\Phi_a|\hat{R}(\alpha,\beta,\gamma)\hat{T}^\lambda_{-\mu}|\Phi_b\rangle \quad , \tag{C.106}$$

$$\langle\Phi_a|\hat{R}(\pi+\alpha,\pi-\beta,2\pi-\gamma)\hat{T}^\lambda_\mu|\Phi_b\rangle = (-)^\lambda\pi_a\eta_b^* \quad \langle\Phi_a|\hat{R}(\alpha,\beta,\gamma)\hat{T}^\lambda_{-\mu}|\Phi_b\rangle \quad , \tag{C.107}$$

$$\langle\Phi_a|\hat{R}(2\pi-\alpha,\pi-\beta,\pi+\gamma)\hat{T}^\lambda_\mu|\Phi_b\rangle = \pi_a\eta_a \quad \langle\Phi_a|\hat{R}(\alpha,\beta,\gamma)\hat{T}^\lambda_\mu|\Phi_b\rangle \quad , \tag{C.108}$$

$$\langle\Phi_a|\hat{R}(\alpha,\pi-\beta,\pi-\gamma)\hat{T}^\lambda_\mu|\Phi_b\rangle = (-)^{\lambda+\mu}p_a p_b\eta_a \quad \langle\Phi_a|\hat{R}(\alpha,\beta,\gamma)\hat{\tilde{T}}^\lambda_{-\mu}|\Phi_b\rangle^* \quad , \tag{C.109}$$

$$\langle\Phi_a|\hat{R}(\pi-\alpha,\pi-\beta,\gamma)\hat{T}^\lambda_\mu|\Phi_b\rangle = (-)^\mu p_a p_b\eta_b^* \quad \langle\Phi_a|\hat{R}(\alpha,\beta,\gamma)\hat{\tilde{T}}^\lambda_\mu|\Phi_b\rangle^* \quad , \tag{C.110}$$

$$\langle\Phi_a|\hat{R}(\pi+\alpha,\beta,\pi+\gamma)\hat{T}^\lambda_\mu|\Phi_b\rangle = (-)^\mu\pi_a p_a p_b\eta_a\eta_b^* \quad \langle\Phi_a|\hat{R}(\alpha,\beta,\gamma)\hat{\tilde{T}}^\lambda_\mu|\Phi_b\rangle^* \quad , \tag{C.111}$$

$$\langle\Phi_a|\hat{R}(2\pi-\alpha,\beta,2\pi-\gamma)\hat{T}^\lambda_\mu|\Phi_b\rangle = (-)^{\lambda+\mu}p_a p_b \quad \langle\Phi_a|\hat{R}(\alpha,\beta,\gamma)\hat{\tilde{T}}^\lambda_{-\mu}|\Phi_b\rangle^* \quad , \tag{C.112}$$

$$\langle\Phi_a|\hat{R}(\alpha,\beta,\pi+\gamma)\hat{T}^\lambda_\mu|\Phi_b\rangle = (-)^\mu p_b\eta_b^* \quad \langle\tilde{\Phi}_a|\hat{R}(\alpha,\beta,\gamma)\hat{\tilde{T}}^\lambda_\mu|\Phi_b\rangle^* \quad . \tag{C.113}$$

Finally, noticing also that, because of equations (C.15) and (3.9), the function $D^J_{MK}(\alpha,\beta,\gamma)\langle\Phi_a|\hat{R}(\alpha,\beta,\gamma)\hat{T}^\lambda_\mu|\Phi_b\rangle$ is 2π periodic in α, β, and γ

$$\begin{aligned}&D^J_{MK}(\alpha+2k\pi,\beta,\gamma)\langle\Phi_a|\hat{R}(\alpha+2k\pi,\beta,\gamma)\hat{T}^\lambda_\mu|\Phi_b\rangle \\ &= D^J_{MK}(\alpha,\beta+2k\pi,\gamma)\langle\Phi_a|\hat{R}(\alpha,\beta+2k\pi,\gamma)\hat{T}^\lambda_\mu|\Phi_b\rangle \\ &= D^J_{MK}(\alpha,\beta,\gamma+2k\pi)\langle\Phi_a|\hat{R}(\alpha,\beta,\gamma+2k\pi)\hat{T}^\lambda_\mu|\Phi_b\rangle \\ &= (-)^{2Jk}\pi_a^k\, D^J_{MK}(\alpha,\beta,\gamma)\langle\Phi_a|\hat{R}(\alpha,\beta,\gamma)\hat{T}^\lambda_\mu|\Phi_b\rangle \\ &= D^J_{MK}(\alpha,\beta,\gamma)\langle\Phi_a|\hat{R}(\alpha,\beta,\gamma)\hat{T}^\lambda_\mu|\Phi_b\rangle \quad ,\end{aligned} \tag{C.114}$$

where k is an integer, it is possible to reexpress the integral over the Euler angles with the help of the above symmetry relations.
Using equation (C.106), the substitutions $\alpha' = \pi-\alpha$ (renaming α' as α afterwards) and $\gamma' = \pi-\gamma$ (renaming γ' as γ afterwards), and the periodicity equation (C.114), we get

$$\begin{aligned}&\int_{\frac{\pi}{2}}^{\pi} d\alpha \int_0^{\frac{\pi}{2}} d\beta\, \sin(\beta) \int_0^{2\pi} d\gamma\, {D^J_{MK}}^*(\alpha,\beta,\gamma)\,\langle\Phi_a|\hat{R}(\alpha,\beta,\gamma)\hat{T}^\lambda_\mu|\Phi_b\rangle \\ &= \int_0^{\frac{\pi}{2}} d\alpha' \int_0^{\frac{\pi}{2}} d\beta\, \sin(\beta) \int_{-\pi}^{\pi} d\gamma'\, {D^J_{MK}}^*(\pi-\alpha',\beta,\pi-\gamma')\,\langle\Phi_a|\hat{R}(\pi-\alpha',\beta,\pi-\gamma')\hat{T}^\lambda_\mu|\Phi_b\rangle\end{aligned}$$

$$
\begin{aligned}
&= \int_0^{\frac{\pi}{2}} d\alpha \int_0^{\frac{\pi}{2}} d\beta \, \sin(\beta) \int_0^{2\pi} d\gamma \, {D^J_{MK}}^* (\pi-\alpha, \beta, \pi-\gamma) \, \langle \Phi_a | \hat{R}(\pi-\alpha, \beta, \pi-\gamma) \hat{T}^\lambda_\mu | \Phi_b \rangle \\
&= \int_0^{\frac{\pi}{2}} d\alpha \int_0^{\frac{\pi}{2}} d\beta \, \sin(\beta) \int_0^{2\pi} d\gamma \, \left[(-)^\lambda \pi_a \eta_a \eta_b^* \right] {D^J_{MK}}^* (\pi-\alpha, \beta, \pi-\gamma) \, \langle \Phi_a | \hat{R}(\alpha, \beta, \gamma) \hat{T}^\lambda_{-\mu} | \Phi_b \rangle \quad .
\end{aligned}
\tag{C.115}
$$

Using equation (C.107), the substitutions $\alpha' = \alpha - \pi$ (renaming α' as α afterwards), $\beta' = \pi - \beta$ (renaming β' as β afterwards), and $\gamma' = 2\pi - \gamma$ (renaming γ' as γ afterwards), we get

$$
\begin{aligned}
&\int_\pi^{\frac{3\pi}{2}} d\alpha \int_{\frac{\pi}{2}}^{\pi} d\beta \, \sin(\beta) \int_0^{2\pi} d\gamma \, {D^J_{MK}}^* (\alpha, \beta, \gamma) \, \langle \Phi_a | \hat{R}(\alpha, \beta, \gamma) \hat{T}^\lambda_\mu | \Phi_b \rangle \\
&= \int_0^{\frac{\pi}{2}} d\alpha' \int_0^{\frac{\pi}{2}} d\beta' \, \sin(\beta') \int_0^{2\pi} d\gamma' \, {D^J_{MK}}^* (\pi+\alpha', \pi-\beta', 2\pi-\gamma') \, \langle \Phi_a | \hat{R}(\pi+\alpha', \pi-\beta', 2\pi-\gamma') \hat{T}^\lambda_\mu | \Phi_b \rangle \\
&= \int_0^{\frac{\pi}{2}} d\alpha \int_0^{\frac{\pi}{2}} d\beta \, \sin(\beta) \int_0^{2\pi} d\gamma \, \left[(-)^\lambda \pi_a \eta_b^* \right] {D^J_{MK}}^* (\pi+\alpha, \pi-\beta, 2\pi-\gamma) \, \langle \Phi_a | \hat{R}(\alpha, \beta, \gamma) \hat{T}^\lambda_{-\mu} | \Phi_b \rangle \quad .
\end{aligned}
\tag{C.116}
$$

Using equation (C.108), the substitutions $\alpha' = 2\pi - \alpha$ (renaming α' as α afterwards), $\beta' = \pi - \beta$ (renaming β' as β afterwards), and $\gamma' = \gamma - \pi$ (renaming γ' as γ afterwards), and the periodicity equation (C.114), we get

$$
\begin{aligned}
&\int_{\frac{3\pi}{2}}^{2\pi} d\alpha \int_{\frac{\pi}{2}}^{\pi} d\beta \, \sin(\beta) \int_0^{2\pi} d\gamma \, {D^J_{MK}}^* (\alpha, \beta, \gamma) \, \langle \Phi_a | \hat{R}(\alpha, \beta, \gamma) \hat{T}^\lambda_\mu | \Phi_b \rangle \\
&= \int_0^{\frac{\pi}{2}} d\alpha' \int_0^{\frac{\pi}{2}} d\beta' \, \sin(\beta') \int_{-\pi}^{\pi} d\gamma' \, {D^J_{MK}}^* (2\pi-\alpha', \pi-\beta', \pi+\gamma') \, \langle \Phi_a | \hat{R}(2\pi-\alpha', \pi-\beta', \pi+\gamma') \hat{T}^\lambda_\mu | \Phi_b \rangle \\
&= \int_0^{\frac{\pi}{2}} d\alpha \int_0^{\frac{\pi}{2}} d\beta \, \sin(\beta) \int_0^{2\pi} d\gamma \, {D^J_{MK}}^* (2\pi-\alpha, \pi-\beta, \pi+\gamma) \, \langle \Phi_a | \hat{R}(2\pi-\alpha, \pi-\beta, \pi+\gamma) \hat{T}^\lambda_\mu | \Phi_b \rangle \\
&= \int_0^{\frac{\pi}{2}} d\alpha \int_0^{\frac{\pi}{2}} d\beta \, \sin(\beta) \int_0^{2\pi} d\gamma \, \left[\pi_a \eta_a \right] {D^J_{MK}}^* (2\pi-\alpha, \pi-\beta, \pi+\gamma) \, \langle \Phi_a | \hat{R}(\alpha, \beta, \gamma) \hat{T}^\lambda_\mu | \Phi_b \rangle \quad .
\end{aligned}
\tag{C.117}
$$

Using equation (C.109), the substitutions $\beta' = \pi - \beta$ (renaming β' as β afterwards) and $\gamma' = \pi - \gamma$ (renaming γ' as γ afterwards), and the periodicity equation (C.114), we get

$$
\begin{aligned}
&\int_0^{\frac{\pi}{2}} d\alpha \int_{\frac{\pi}{2}}^{\pi} d\beta \, \sin(\beta) \int_0^{2\pi} d\gamma \, {D^J_{MK}}^* (\alpha, \beta, \gamma) \, \langle \Phi_a | \hat{R}(\alpha, \beta, \gamma) \hat{T}^\lambda_\mu | \Phi_b \rangle \\
&= \int_0^{\frac{\pi}{2}} d\alpha \int_0^{\frac{\pi}{2}} d\beta' \, \sin(\beta') \int_{-\pi}^{\pi} d\gamma' \, {D^J_{MK}}^* (\alpha, \pi-\beta', \pi-\gamma') \, \langle \Phi_a | \hat{R}(\alpha, \pi-\beta', \pi-\gamma') \hat{T}^\lambda_\mu | \Phi_b \rangle
\end{aligned}
$$

$$
\begin{aligned}
&= \int_0^{\frac{\pi}{2}} d\alpha \int_0^{\frac{\pi}{2}} d\beta \, \sin(\beta) \int_0^{2\pi} d\gamma \, {D^J_{MK}}^* (\alpha, \pi-\beta, \pi-\gamma) \, \langle \Phi_a | \hat{R}(\alpha, \pi-\beta, \pi-\gamma) \hat{T}^\lambda_\mu | \Phi_b \rangle \\
&= \int_0^{\frac{\pi}{2}} d\alpha \int_0^{\frac{\pi}{2}} d\beta \, \sin(\beta) \int_0^{2\pi} d\gamma \, \left[(-)^{\lambda+\mu} p_a p_b \eta_a \right] {D^J_{MK}}^* (\alpha, \pi-\beta, \pi-\gamma) \, \langle \Phi_a | \hat{R}(\alpha, \beta, \gamma) \hat{\tilde{T}}^\lambda_{-\mu} | \Phi_b \rangle^* \quad .
\end{aligned}
\tag{C.118}
$$

Using equation (C.110), the substitutions $\alpha' = \pi - \alpha$ (renaming α' as α afterwards) and $\beta' = \pi - \beta$ (renaming β' as β afterwards), we get

$$
\begin{aligned}
&\int_{\frac{\pi}{2}}^{\pi} d\alpha \int_{\frac{\pi}{2}}^{\pi} d\beta \, \sin(\beta) \int_0^{2\pi} d\gamma \, {D^J_{MK}}^* (\alpha, \beta, \gamma) \, \langle \Phi_a | \hat{R}(\alpha, \beta, \gamma) \hat{T}^\lambda_\mu | \Phi_b \rangle \\
&= \int_0^{\frac{\pi}{2}} d\alpha' \int_0^{\frac{\pi}{2}} d\beta' \, \sin(\beta') \int_0^{2\pi} d\gamma \, {D^J_{MK}}^* (\pi-\alpha', \pi-\beta', \gamma) \, \langle \Phi_a | \hat{R}(\pi-\alpha', \pi-\beta', \gamma) \hat{T}^\lambda_\mu | \Phi_b \rangle \\
&= \int_0^{\frac{\pi}{2}} d\alpha \int_0^{\frac{\pi}{2}} d\beta \, \sin(\beta) \int_0^{2\pi} d\gamma \, \left[(-)^{\mu} p_a p_b \eta_b^* \right] {D^J_{MK}}^* (\pi-\alpha, \pi-\beta, \gamma) \, \langle \Phi_a | \hat{R}(\alpha, \beta, \gamma) \hat{\tilde{T}}^\lambda_{\mu} | \Phi_b \rangle^* \quad .
\end{aligned}
\tag{C.119}
$$

Using equation (C.111), the substitutions $\alpha' = \alpha - \pi$ (renaming α' as α afterwards) and $\gamma' = \gamma - \pi$ (renaming γ' as γ afterwards), and the periodicity equation (C.114), we get

$$
\begin{aligned}
&\int_{\pi}^{\frac{3\pi}{2}} d\alpha \int_0^{\frac{\pi}{2}} d\beta \, \sin(\beta) \int_0^{2\pi} d\gamma \, {D^J_{MK}}^* (\alpha, \beta, \gamma) \, \langle \Phi_a | \hat{R}(\alpha, \beta, \gamma) \hat{T}^\lambda_\mu | \Phi_b \rangle \\
&= \int_0^{\frac{\pi}{2}} d\alpha' \int_0^{\frac{\pi}{2}} d\beta \, \sin(\beta) \int_{-\pi}^{\pi} d\gamma' \, {D^J_{MK}}^* (\pi+\alpha', \beta, \pi+\gamma') \, \langle \Phi_a | \hat{R}(\pi+\alpha', \beta, \pi+\gamma') \hat{T}^\lambda_\mu | \Phi_b \rangle \\
&= \int_0^{\frac{\pi}{2}} d\alpha \int_0^{\frac{\pi}{2}} d\beta \, \sin(\beta) \int_0^{2\pi} d\gamma \, {D^J_{MK}}^* (\pi+\alpha, \beta, \pi+\gamma) \, \langle \Phi_a | \hat{R}(\pi+\alpha, \beta, \pi+\gamma) \hat{T}^\lambda_\mu | \Phi_b \rangle \\
&= \int_0^{\frac{\pi}{2}} d\alpha \int_0^{\frac{\pi}{2}} d\beta \, \sin(\beta) \int_0^{2\pi} d\gamma \, \left[(-)^{\mu} \pi_a p_a p_b \eta_a \eta_b^* \right] {D^J_{MK}}^* (\pi+\alpha, \beta, \pi+\gamma) \, \langle \Phi_a | \hat{R}(\alpha, \beta, \gamma) \hat{\tilde{T}}^\lambda_{\mu} | \Phi_b \rangle^* \quad .
\end{aligned}
\tag{C.120}
$$

Using equation (C.112), the substitutions $\alpha' = 2\pi - \alpha$ (renaming α' as α afterwards) and $\gamma' = 2\pi - \gamma$ (renaming γ' as γ afterwards), we get

$$
\begin{aligned}
&\int_{\frac{3\pi}{2}}^{2\pi} d\alpha \int_0^{\frac{\pi}{2}} d\beta \, \sin(\beta) \int_0^{2\pi} d\gamma \, {D^J_{MK}}^* (\alpha, \beta, \gamma) \, \langle \Phi_a | \hat{R}(\alpha, \beta, \gamma) \hat{T}^\lambda_\mu | \Phi_b \rangle \\
&= \int_0^{\frac{\pi}{2}} d\alpha' \int_0^{\frac{\pi}{2}} d\beta \, \sin(\beta) \int_0^{2\pi} d\gamma' \, {D^J_{MK}}^* (2\pi-\alpha', \beta, 2\pi-\gamma') \, \langle \Phi_a | \hat{R}(2\pi-\alpha', \beta, 2\pi-\gamma') \hat{T}^\lambda_\mu | \Phi_b \rangle \\
&= \int_0^{\frac{\pi}{2}} d\alpha \int_0^{\frac{\pi}{2}} d\beta \, \sin(\beta) \int_0^{2\pi} d\gamma \, \left[(-)^{\lambda+\mu} p_a p_b \right] {D^J_{MK}}^* (2\pi-\alpha, \beta, 2\pi-\gamma) \, \langle \Phi_a | \hat{R}(\alpha, \beta, \gamma) \hat{\tilde{T}}^\lambda_{-\mu} | \Phi_b \rangle^* \quad .
\end{aligned}
\tag{C.121}
$$

Combining all of the above equations we get

$$
\begin{aligned}
&\int_0^{2\pi} d\alpha \int_0^{\pi} d\beta \, \sin(\beta) \int_0^{2\pi} d\gamma \, D^{J}_{MK}{}^{*}(\alpha,\beta,\gamma) \, \langle \Phi_a | \hat{R}(\alpha,\beta,\gamma) \hat{T}^{\lambda}_{\mu} | \Phi_b \rangle \\
&= \int_0^{\frac{\pi}{2}} d\alpha \int_0^{\frac{\pi}{2}} d\beta \, \sin(\beta) \int_0^{2\pi} d\gamma \left\{ \left[D^{J}_{MK}{}^{*}(\alpha,\beta,\gamma) + \pi_a \eta_a D^{J}_{MK}{}^{*}(2\pi-\alpha,\pi-\beta,\pi+\gamma) \right] \langle \Phi_a | \hat{R}(\alpha,\beta,\gamma) \hat{T}^{\lambda}_{\mu} | \Phi_b \rangle \right. \\
&+ (-)^{\lambda} \left[\pi_a \eta_a \eta_b^{*} D^{J}_{MK}{}^{*}(\pi-\alpha,\beta,\pi-\gamma) + \pi_a \eta_b^{*} D^{J}_{MK}{}^{*}(\pi+\alpha,\pi-\beta,2\pi-\gamma) \right] \langle \Phi_a | \hat{R}(\alpha,\beta,\gamma) \hat{T}^{\lambda}_{-\mu} | \Phi_b \rangle \\
&+ (-)^{\mu} \left[p_a p_b \eta_b^{*} D^{J}_{MK}{}^{*}(\pi-\alpha,\pi-\beta,\gamma) + \pi_a p_a p_b \eta_a \eta_b^{*} D^{J}_{MK}{}^{*}(\pi+\alpha,\beta,\pi+\gamma) \right] \langle \Phi_a | \hat{R}(\alpha,\beta,\gamma) \hat{\tilde{T}}^{\lambda}_{\mu} | \Phi_b \rangle^{*} \\
&\left. + (-)^{\lambda+\mu} \left[p_a p_b \eta_a D^{J}_{MK}{}^{*}(\alpha,\pi-\beta,\pi-\gamma) + p_a p_b D^{J}_{MK}{}^{*}(2\pi-\alpha,\beta,2\pi-\gamma) \right] \langle \Phi_a | \hat{R}(\alpha,\beta,\gamma) \hat{\tilde{T}}^{\lambda}_{-\mu} | \Phi_b \rangle^{*} \right\} \quad .
\end{aligned}
\tag{C.122}
$$

Using equation (C.113) and the substitution $\gamma' = \gamma - \pi$ (renaming γ' as γ afterwards), we get

$$
\begin{aligned}
&\int_0^{\frac{\pi}{2}} d\alpha \int_0^{\frac{\pi}{2}} d\beta \, \sin(\beta) \int_{\pi}^{2\pi} d\gamma \, D^{J}_{MK}{}^{*}(f_a(\alpha), f_b(\beta), f_g(\gamma)) \, \langle \Phi_a | \hat{R}(\alpha,\beta,\gamma) \hat{T}^{\lambda}_{\mu} | \Phi_b \rangle \\
&= \int_0^{\frac{\pi}{2}} d\alpha \int_0^{\frac{\pi}{2}} d\beta \, \sin(\beta) \int_0^{\pi} d\gamma' \, D^{J}_{MK}{}^{*}(f_a(\alpha), f_b(\beta), f_g(\gamma'+\pi)) \, \langle \Phi_a | \hat{R}(\alpha,\beta,\gamma'+\pi) \hat{T}^{\lambda}_{\mu} | \Phi_b \rangle \\
&= \int_0^{\frac{\pi}{2}} d\alpha \int_0^{\frac{\pi}{2}} d\beta \, \sin(\beta) \int_0^{\pi} d\gamma \left[(-)^{\mu} p_b \eta_b^{*} \right] D^{J}_{MK}{}^{*}(f_a(\alpha), f_b(\beta), f_g(\gamma+\pi)) \, \langle \tilde{\Phi}_a | \hat{R}(\alpha,\beta,\gamma) \hat{\tilde{T}}^{\lambda}_{\mu} | \Phi_b \rangle^{*} \, ,
\end{aligned}
\tag{C.123}
$$

where f_a, f_b, and f_g, are functions of α, β, and γ, respectively.
Finally, combining equations (C.122) and (C.123), we get the final expression

$$
\begin{aligned}
&\int_0^{2\pi} d\alpha \int_0^{\pi} d\beta \, \sin(\beta) \int_0^{2\pi} d\gamma \, D^{J}_{MK}{}^{*}(\alpha,\beta,\gamma) \, \langle \Phi_a | \hat{R}(\alpha,\beta,\gamma) \hat{T}^{\lambda}_{\mu} | \Phi_b \rangle \\
&= \int_0^{\frac{\pi}{2}} d\alpha \int_0^{\frac{\pi}{2}} d\beta \, \sin(\beta) \int_0^{\pi} d\gamma \left[\left\{ \left[D^{J}_{MK}{}^{*}(\alpha,\beta,\gamma) + \pi_a \eta_a D^{J}_{MK}{}^{*}(2\pi-\alpha,\pi-\beta,\pi+\gamma) \right] \langle \Phi_a | \hat{R}(\alpha,\beta,\gamma) \hat{T}^{\lambda}_{\mu} | \Phi_b \rangle \right. \right. \\
&+ (-)^{\lambda} \left[\pi_a \eta_a \eta_b^{*} D^{J}_{MK}{}^{*}(\pi-\alpha,\beta,\pi-\gamma) + \pi_a \eta_b^{*} D^{J}_{MK}{}^{*}(\pi+\alpha,\pi-\beta,2\pi-\gamma) \right] \langle \Phi_a | \hat{R}(\alpha,\beta,\gamma) \hat{T}^{\lambda}_{-\mu} | \Phi_b \rangle \\
&+ (-)^{\mu} \left[p_a p_b \eta_b^{*} D^{J}_{MK}{}^{*}(\pi-\alpha,\pi-\beta,\gamma) + \pi_a p_a p_b \eta_a \eta_b^{*} D^{J}_{MK}{}^{*}(\pi+\alpha,\beta,\pi+\gamma) \right] \langle \Phi_a | \hat{R}(\alpha,\beta,\gamma) \hat{\tilde{T}}^{\lambda}_{\mu} | \Phi_b \rangle^{*} \\
&\left. + (-)^{\lambda+\mu} \left[p_a p_b \eta_a D^{J}_{MK}{}^{*}(\alpha,\pi-\beta,\pi-\gamma) + p_a p_b D^{J}_{MK}{}^{*}(2\pi-\alpha,\beta,2\pi-\gamma) \right] \langle \Phi_a | \hat{R}(\alpha,\beta,\gamma) \hat{\tilde{T}}^{\lambda}_{-\mu} | \Phi_b \rangle^{*} \right\} \\
&+ (-)^{\mu} p_b \eta_b^{*} \left\{ \left[D^{J}_{MK}{}^{*}(\alpha,\beta,\pi+\gamma) + \pi_a \eta_a D^{J}_{MK}{}^{*}(2\pi-\alpha,\pi-\beta,2\pi+\gamma) \right] \langle \tilde{\Phi}_a | \hat{R}(\alpha,\beta,\gamma) \hat{\tilde{T}}^{\lambda}_{\mu} | \Phi_b \rangle^{*} \right. \\
&+ (-)^{\lambda} \left[\pi_a \eta_a \eta_b^{*} D^{J}_{MK}{}^{*}(\pi-\alpha,\beta,-\gamma) + \pi_a \eta_b^{*} D^{J}_{MK}{}^{*}(\pi+\alpha,\pi-\beta,\pi-\gamma) \right] \langle \tilde{\Phi}_a | \hat{R}(\alpha,\beta,\gamma) \hat{\tilde{T}}^{\lambda}_{-\mu} | \Phi_b \rangle^{*} \Big\} \\
&+ (-)^{\mu} p_b \eta_b \left\{ (-)^{\mu} \left[p_a p_b \eta_b^{*} D^{J}_{MK}{}^{*}(\pi-\alpha,\pi-\beta,\pi+\gamma) + \pi_a p_a p_b \eta_a \eta_b^{*} D^{J}_{MK}{}^{*}(\pi+\alpha,\beta,2\pi+\gamma) \right] \langle \tilde{\Phi}_a | \hat{R}(\alpha,\beta,\gamma) \hat{T}^{\lambda}_{\mu} | \Phi_b \rangle \right. \\
&\left. \left. + (-)^{\lambda+\mu} \left[p_a p_b \eta_a D^{J}_{MK}{}^{*}(\alpha,\pi-\beta,-\gamma) + p_a p_b D^{J}_{MK}{}^{*}(2\pi-\alpha,\beta,\pi-\gamma) \right] \langle \tilde{\Phi}_a | \hat{R}(\alpha,\beta,\gamma) \hat{T}^{\lambda}_{-\mu} | \Phi_b \rangle \right\} \right] \quad .
\end{aligned}
\tag{C.124}
$$

C.8 Discretization of the Projection Operator

Calculating the projection on the angular momentum numerically, we have to discretize the integrals over the Euler angles (α, β, γ). Let us rewrite the projection operator as

$$\hat{P}^{J_0}_{M_0K_0} = \hat{P}^{a}_{M_0} \hat{P}^{b\,J_0}_{M_0K_0} \hat{P}^{g}_{K_0} \quad , \tag{C.125}$$

where

$$\hat{P}^{a}_{M_0} = \frac{1}{2\pi} \int_0^{2\pi} d\alpha\, e^{+i\alpha M_0} \hat{R}_z(\alpha) \quad , \tag{C.126}$$

$$\hat{P}^{b\,J_0}_{M_0K_0} = \frac{2J_0+1}{2} \int_0^{\pi} d\beta \sin(\beta)\, d^{J_0}_{M_0K_0}(\beta) \hat{R}_y(\beta) \quad , \tag{C.127}$$

$$\hat{P}^{g}_{K_0} = \frac{1}{2\pi} \int_0^{2\pi} d\gamma\, e^{+i\gamma K_0} \hat{R}_z(\gamma) \quad . \tag{C.128}$$

As we have reduced the integral over γ from $[0, 4\pi]$ to $[0, 2\pi]$, we assume that we apply the discretized projection operator on a state that has a number parity equal to $(-)^{2J}$.

First looking at the integral over γ, we use a discretization very similar to Fomenko's for particle number projection

$$\hat{\mathcal{P}}^{g}_{K_0}(M_g) = \frac{1}{M_g} \sum_{m_g=1}^{M_g} e^{-i2\pi \frac{m_g - \frac{1}{2}}{M_g} (\hat{J}_z - K_0)} \quad , \tag{C.129}$$

where M_g is the total (even) number of points in the discretization. One difference, though, is that the first discretization point is not at $\gamma = 0$, like for Fomenko's discretization, but at $\gamma = \frac{\pi}{M_g}$. Acting with $\hat{\mathcal{P}}^{g}_{K_0}(M_g)$ on a state $|\Phi_a\rangle$, we get

$$\begin{aligned}
\hat{\mathcal{P}}^{g}_{K_0}(M_g)|\Phi_a\rangle &= \hat{\mathcal{P}}^{g}_{K_0}(M_g) \sum_{J_1} \sum_{K_1=-J_1}^{J_1} c^{J_1}_{K_1}(a)|J_1K_1\rangle \\
&= \sum_{J_1} \sum_{K_1=-J_1}^{J_1} c^{J_1}_{K_1}(a) \hat{\mathcal{P}}^{g}_{K_0}(M_g)|J_1K_1\rangle \\
&= \sum_{J_1} \sum_{K_1=-J_1}^{J_1} \left\{ c^{J_1}_{K_1}(a) \left(\frac{1}{M_g} \sum_{m_g=1}^{M_g} e^{-i2\pi \frac{m_g - \frac{1}{2}}{M_g} (K_1 - K_0)} \right) |J_1K_1\rangle \right\} \quad .
\end{aligned} \tag{C.130}$$

The factor

$$F = \frac{1}{M_g} \sum_{m_g=1}^{M_g} e^{-i2\pi \frac{m_g - \frac{1}{2}}{M_g} (K_1 - K_0)}$$

is a geometric progression (see section B.6) of common ratio

$$r = e^{-i2\pi \frac{1}{M_g} (K_1 - K_0)}$$

and scale factor

$$a = \frac{e^{-i\pi \frac{1}{M_g} (K_1 - K_0)}}{M_g} \quad .$$

In our case we have:

- for $r = 1 \Leftrightarrow K_1 = K_0 + lM_g$ with l being an integer, we have

$$F = \sum_{m_g=1}^{M_g} \frac{(-1)^l}{M_g} = (-1)^l \quad ,$$

and thus

$$K_1 = K_0 + lM_g \, , \, l \in \mathbb{Z} \implies \hat{\mathcal{P}}^g_{K_0}(M_g)|J_1K_1\rangle = (-)^l|J_1K_1\rangle \quad . \tag{C.131}$$

- for $r \neq 1 \Leftrightarrow K_1 \neq K_0 + lM_g$ with l being an integer, we have

$$\begin{aligned} F &= \frac{1}{M_g} \frac{e^{-i\frac{\pi}{M_g}(K_1-K_0)} - e^{-i\frac{2\pi}{M_g}(M_g+\frac{1}{2})(K_1-K_0)}}{1 - e^{-i\frac{2\pi}{M_g}(K_1-K_0)}} \\ &= \frac{e^{-i\frac{\pi}{M_g}(K_1-K_0)}}{M_g} \frac{1 - e^{-i2\pi(K_1-K_0)}}{1 - e^{-i\frac{2\pi}{M_g}(K_1-K_0)}} \quad . \end{aligned}$$

As a consequence of (C.78), we always have $K_1 = K_0 + k$ with k integer, and thus

$$e^{-i2\pi(K_1-K_0)} = 1 \quad .$$

As a result we always have

$$F = 0$$

and thus

$$K_1 \neq K_0 + lM_g \, , \, l \in \mathbb{Z} \implies \hat{\mathcal{P}}^g_{K_0}(M_g)|J_1K_1\rangle = 0 \quad . \tag{C.132}$$

Finally the action of the projection operator reads

$$\hat{\mathcal{P}}^g_{K_0}(M_g)|\Phi_a\rangle = \sum_{J_1} \sum_{\substack{l\in\mathbb{Z} \\ -J_1 \leq K_0+lM_g \leq J_1}} (-)^l \, c^{J_1}_{K_1}(a)|J_1K_1 = K_0 + lM_g\rangle \quad . \tag{C.133}$$

But let us consider the case where M_g is large enough as for the discretized projection operator to select only the desired K_0 component

$$\hat{\mathcal{P}}^g_{K_0}(M_g)|\Phi_a\rangle = \sum_{J_1 \geq K_0} c^{J_1}_{K_0}(a)|J_1K_0\rangle \, . \tag{C.134}$$

For the integration over β, using the variable substitution $u = \cos(\beta)$, we can rewrite $\hat{P}^{b\,J_0}_{M_0K_0}$ and then use a M_b-points Gauss-Legendre quadrature rule to approximate the integral

$$\begin{aligned} \hat{P}^{b\,J_0}_{M_0K_0} &= \frac{2J_0+1}{2} \int_0^\pi d\beta \sin(\beta) \, d^{J_0}_{M_0K_0}(\beta) \hat{R}_y(\beta) \\ &= \frac{2J_0+1}{2} \int_{-1}^1 du \, d^{J_0}_{M_0K_0}(\arccos(u)) \, \hat{R}_y(\arccos(u)) \\ &\approx \frac{2J_0+1}{2} \sum_{i=1}^{M_b} \omega_i \, d^{J_0}_{M_0K_0}(\beta_i) \, \hat{R}_y(\beta_i) = \hat{\mathcal{P}}^{b\,J_0}_{M_0K_0}(M_b) \quad , \end{aligned} \tag{C.135}$$

where $\beta_i = \arccos(x_i)$, x_i is the i^{th} root of the Legendre polynom of degree M_b, noted L_{M_b}, and ω_i is the weight defined by

$$\omega_i = \frac{2}{(1-x_i^2)[L'_{M_b}(x_i)]^2} \quad . \tag{C.136}$$

Acting with $\hat{\mathcal{P}}^{b\,J_0}_{M_0K_0}(M_b)$ on a state $\hat{\mathcal{P}}^{g}_{K_0}(M_g)|\Phi_a\rangle$, we get

$$\begin{aligned}
&\hat{\mathcal{P}}^{b\,J_0}_{M_0K_0}(M_b)\hat{\mathcal{P}}^{g}_{K_0}(M_g)|\Phi_a\rangle \\
&= \hat{\mathcal{P}}^{b\,J_0}_{M_0K_0}(M_b)\sum_{J_1\geq K_0} c^{J_1}_{K_0}(a)|J_1K_0\rangle \\
&= \sum_{J_1\geq K_0} c^{J_1}_{K_0}(a)\hat{\mathcal{P}}^{b\,J_0}_{M_0K_0}(M_b)|J_1K_0\rangle \\
&= \frac{2J_0+1}{2}\sum_{J_1\geq K_0}\sum_{M_1=-J_1}^{J_1}\left\{c^{J_1}_{K_0}(a)\Big(\sum_{i=1}^{M_b}\omega_i\, d^{J_0}_{M_0K_0}(\beta_i)\, d^{J_1}_{M_1K_0}(\beta_i)\Big)|J_1M_1\rangle\right\} \quad ,
\end{aligned} \tag{C.137}$$

recalling that

$$\hat{R}_y(\beta_i)|J_1K_0\rangle = \sum_{M_1=-J_1}^{J_1} d^{J_1}_{M_1K_0}(\beta_i)|J_1M_1\rangle \quad . \tag{C.138}$$

Finally, discretizing the integral over α similarly to what has been done for γ

$$\hat{\mathcal{P}}^{a}_{M_0}(M_a) = \frac{1}{M_a}\sum_{m_a=1}^{M_a} e^{-i2\pi\frac{m_a-\frac{1}{2}}{M_a}(\hat{J}_z-M_0)} \quad , \tag{C.139}$$

we obtain

$$\begin{aligned}
&\hat{\mathcal{P}}^{a}_{M_0}(M_a)\hat{\mathcal{P}}^{b\,J_0}_{M_0K_0}(M_b)\hat{\mathcal{P}}^{g}_{K_0}(M_g)|\Phi_a\rangle \\
&= \hat{\mathcal{P}}^{a}_{M_0}(M_a)\frac{2J_0+1}{2}\sum_{J_1\geq K_0}\sum_{M_1=-J_1}^{J_1}\left\{c^{J_1}_{K_0}(a)\Big(\sum_{i=1}^{M_b}\omega_i\, d^{J_0}_{M_0K_0}(\beta_i)\, d^{J_1}_{M_1K_0}(\beta_i)\Big)|J_1M_1\rangle\right\} \\
&= \frac{2J_0+1}{2}\sum_{J_1\geq K_0}\sum_{M_1=-J_1}^{J_1}\left\{c^{J_1}_{K_0}(a)\Big(\sum_{i=1}^{M_b}\omega_i\, d^{J_0}_{M_0K_0}(\beta_i)\, d^{J_1}_{M_1K_0}(\beta_i)\Big)\hat{\mathcal{P}}^{a}_{M_0}(M_a)|J_1M_1\rangle\right\} \quad .
\end{aligned} \tag{C.140}$$

Using for $\hat{\mathcal{P}}^{a}_{M_0}(M_a)$ the same rationale as for $\hat{\mathcal{P}}^{g}_{K_0}(M_g)$, the two operators having the same structure, we obtain, for M_a large enough, that for each J_1 with $c^{J_1}_{K_0}(a)\neq 0$

$$\hat{\mathcal{P}}^{a}_{M_0}(M_a)|J_1M_1\rangle = \delta_{M_0,M_1}|J_1M_1\rangle \quad , \tag{C.141}$$

and thus

$$\begin{aligned}
&\hat{\mathcal{P}}^{a}_{M_0}(M_a)\hat{\mathcal{P}}^{b\,J_0}_{M_0K_0}(M_b)\hat{\mathcal{P}}^{g}_{K_0}(M_g)|\Phi_a\rangle \\
&= \frac{2J_0+1}{2}\sum_{J_1\geq K_0}\sum_{M_1=-J_1}^{J_1}\left\{c^{J_1}_{K_0}(a)\Big(\sum_{i=1}^{M_b}\omega_i\, d^{J_0}_{M_0K_0}(\beta_i)\, d^{J_1}_{M_1K_0}(\beta_i)\Big)\delta_{M_0,M_1}|J_1M_1\rangle\right\} \\
&= \frac{2J_0+1}{2}\sum_{J_1\geq K_0}\left\{c^{J_1}_{K_0}(a)\Big(\sum_{i=1}^{M_b}\omega_i\, d^{J_0}_{M_0K_0}(\beta_i)\, d^{J_1}_{M_1K_0}(\beta_i)\Big)|J_1M_0\rangle\right\} \quad .
\end{aligned} \tag{C.142}$$

Then considering the number of point M_b, in the discretization of the integral over β, large

enough we have

$$\begin{aligned}\sum_{i=1}^{M_b} \omega_i \; d^{J_0}_{M_0K_0}(\beta_i)\, d^{J_1}_{M_0K_0}(\beta_i) &\approx \int_{-1}^{1} du\, d^{J_0}_{M_0K_0}(\arccos(u))\, d^{J_1}_{M_0K_0}(\arccos(u)) \\ &\approx \int_0^{\pi} d\beta\, \sin(\beta)\, d^{J_0}_{M_0K_0}(\beta)\, d^{J_1}_{M_0K_0}(\beta) \\ &\approx \delta_{J_0,J_1}\, \frac{2}{2J_0+1} \quad .\end{aligned} \tag{C.143}$$

We thus obtain as final result that for M_a, M_b, and M_g, large enough we have

$$\begin{aligned}\hat{\mathcal{P}}^{J_0}_{M_0K_0}(M_a,M_b,M_g)|\Phi_a\rangle &= \hat{\mathcal{P}}^{a}_{M_0}(M_a)\hat{\mathcal{P}}^{b\,J_0}_{M_0K_0}(M_b)\hat{\mathcal{P}}^{g}_{K_0}(M_g)|\Phi_a\rangle \\ &= \frac{2J_0+1}{2}\sum_{J_1\geq K_0}\left\{c^{J_0}_{K_0}\left(\sum_i^{M_b}\omega_i\, {d^{J_0}_{M_0K_0}}^{*}(\beta_i)\, d^{J_1}_{M_0K_0}(\beta_i)\right)|J_1M_0\rangle\right\} \\ &= \frac{2J_0+1}{2}\sum_{J_1\geq K_0}\left\{\delta_{J_0,J_1}\frac{2}{2J_0+1}\, c^{J_0}_{K_0}(a)|J_1M_0\rangle\right\} \\ &= c^{J_0}_{K_0}(a)|J_0M_0\rangle \quad .\end{aligned} \tag{C.144}$$

Finally, we stress that to use the symmetries of the rotated matrix elements (C.106 - C.113), we need to have M_a, M_b, and M_g, of the form

$$\begin{aligned} M_a &= 4i \\ M_b &= 2j \qquad i,j,k \in \mathbb{N} \quad , \\ M_g &= 2k \end{aligned} \tag{C.145}$$

because we reduced by a factor of 4, 2, and 2, the intervals on which we carry the rotations over α, β, and γ, respectively. This also explains why the first point of the discretization is not located at 0° for α and γ. We also use the same number of points for the integral over α and γ: $M_a = M_g$, as there is no reason to do otherwise and, as we have in that case a symmetric form for the discretized projection operator.

C.9 Symmetries of the Projected Overlap

We give here some symmetries for the projected overlap, but that can also be applied to any operator which commutes with the projection operator (e.g. Hamiltonian). We define the projected overlap $N^J_{KK'}(a,b)$ as

$$\begin{aligned}N^J_{KK'}(a,b) &= \langle\Phi_a|\hat{P}^J_{KK'}|\Phi_b\rangle \\ &= \sum_{J_1}\sum_{J_2}\sum_{K_1=-J_1}^{J_1}\sum_{K_2=-J_2}^{J_2} {c^{J_1}_{K_1}}^{*}(a)\, c^{J_2}_{K_2}(b)\langle J_1K_1|\hat{P}^J_{KK'}|J_2K_2\rangle \\ &= \sum_{J_1}\sum_{J_2}\sum_{K_1=-J_1}^{J_1}\sum_{K_2=-J_2}^{J_2} {c^{J_1}_{K_1}}^{*}(a)\, c^{J_2}_{K_2}(b)\langle J_1K_1|JK\rangle\langle JK'|J_2K_2\rangle \\ &= \sum_{J_1}\sum_{J_2}\sum_{K_1=-J_1}^{J_1}\sum_{K_2=-J_2}^{J_2} {c^{J_1}_{K_1}}^{*}(a)\, c^{J_2}_{K_2}(b)\,\delta_{J_1,J}\,\delta_{J_2,J}\,\delta_{K_1,K}\,\delta_{K_2,K'} \\ &= {c^{J}_{K}}^{*}(a)\, c^{J}_{K'}(b) \quad .\end{aligned} \tag{C.146}$$

It is straightforward to see that

$$\begin{aligned} N^{J}_{KK'}{}^{*}(a,b) &= \langle\Phi_a|\hat{P}^{J}_{KK'}|\Phi_b\rangle^{*} \\ &= \langle\Phi_b|\hat{P}^{J}_{KK'}{}^{\dagger}|\Phi_a\rangle \\ &= \langle\Phi_b|\hat{P}^{J}_{K'K}|\Phi_a\rangle \\ &= N^{J}_{K'K}(b,a) \quad . \end{aligned} \tag{C.147}$$

Using the x-signature operator, we can derive that

$$\begin{aligned} N^{J}_{KK'}(a,b) &= \langle\Phi_a|\hat{P}^{J}_{KK'}|\Phi_b\rangle \\ &= \langle\Phi_a|\hat{R}^{\dagger}_{x}\hat{R}_{x}\hat{P}^{J}_{KK'}|\Phi_b\rangle \\ &= \langle\Phi_a|\hat{R}^{\dagger}_{x}\hat{R}_{x}|K\rangle\langle K'|\Phi_b\rangle \\ &= \left[\left(\langle\Phi_a|\hat{R}^{\dagger}_{x}\right)\left(\hat{R}_{x}|K\rangle\right)\right]\langle K'|\Phi_b\rangle \\ &= \eta^{*}_{a}e^{-i\pi J}\langle\Phi_a|-K\rangle\langle K'|\Phi_b\rangle \\ &= \eta^{*}_{a}e^{-i\pi J}\langle\Phi_a|\hat{P}^{J}_{-KK'}|\Phi_b\rangle \\ &= \eta^{*}_{a}e^{-i\pi J}N^{J}_{-KK'}(a,b) \quad , \end{aligned} \tag{C.148}$$

which could also have been obtained using equation (C.81)

$$\begin{aligned} N^{J}_{KK'}(a,b) &= c^{J}_{K}{}^{*}(a)\, c^{J}_{K'}(b) \\ &= \left[\eta^{*}_{a}e^{-i\pi J}c^{J}_{-K}(a)\right]^{*} c^{J}_{K'}(b) \\ &= \eta_{a}e^{+i\pi J}N^{J}_{-KK'}(a,b) \\ &= \eta^{*}_{a}e^{-i\pi J}N^{J}_{-KK'}(a,b) \quad , \end{aligned} \tag{C.149}$$

where we have used the little trick: $\eta_a e^{+i\pi J} = \eta^{*}_{a}e^{-i\pi J}$.

Using the previous equation and equation (C.147), we can derive that

$$\begin{aligned} N^{J}_{KK'}(a,b) &= N^{J}_{K'K}(b,a)^{*} \\ &= \left[\eta^{*}_{b}e^{-i\pi J}N^{J}_{-K'K}(b,a)\right]^{*} \\ &= \eta_{b}e^{+i\pi J}N^{J}_{K-K'}(a,b) \quad . \end{aligned} \tag{C.150}$$

Combining equations (C.149) and (C.150), we get that

$$\begin{aligned} N^{J}_{KK'}(a,b) &= \eta^{*}_{a}e^{-i\pi J}N^{J}_{-KK'}(a,b) \\ &= \eta^{*}_{a}e^{-i\pi J}\left[\eta_{b}e^{+i\pi J}N^{J}_{-K-K'}(a,b)\right] \\ &= \eta^{*}_{a}\eta_{b}N^{J}_{-K-K'}(a,b) \quad . \end{aligned} \tag{C.151}$$

All the above relations can be summarized as

$$\begin{aligned} N^{J}_{KK'}(a,b) &= \eta_{b}e^{i\pi J} \quad N^{J}_{K-K'}(a,b) \\ &= \eta^{*}_{a}e^{-i\pi J}\, N^{J}_{-KK'}(a,b) \\ &= \eta^{*}_{a}\eta_{b} \quad\quad N^{J}_{-K-K'}(a,b) \quad . \end{aligned} \tag{C.152}$$

Finally, we give two further relations linking the projected overlap of two states with the projected overlap of their time reversed states.
Using (C.84), we derive that

$$\begin{aligned} N^J_{KK'}(\tilde{a},b) &= \langle\tilde{\Phi}_a|\hat{P}^J_{KK'}|\Phi_a\rangle \\ &= c^{J\,*}_K(\tilde{a})\, c^J_{K'}(a) \\ &= \left[p_a\eta_a e^{+i\pi K} c^J_K(a)\right]^* c^J_{K'}(b) \\ &= p_a\eta^*_a e^{-i\pi K} c^{J\,*}_K(a)\, c^J_{K'}(b) \\ &= p_a\eta^*_a e^{-i\pi K} N^J_{KK'}(a,b) \quad . \end{aligned} \tag{C.153}$$

Using the previous equation and equation (C.147), we deduce that

$$N^J_{KK'}(a,\tilde{b}) = p_b\eta_b e^{+i\pi K'} N^J_{KK'}(a,b) \quad . \tag{C.154}$$

Combing both equation, we finally get

$$N^J_{KK'}(\tilde{a},\tilde{b}) = p_a p_b \eta^*_a\eta_b (-)^{K-K'} N^J_{KK'}(a,b) \quad . \tag{C.155}$$

C.9.1 Enami's Transformation - Change of Basis

Let us consider us the normalized projected states

$$|JM,aK\rangle = \frac{\hat{P}^J_{MK}}{\sqrt{N^J_{KK}(a,a)}}|\Phi_a\rangle \quad . \tag{C.156}$$

and the resulting normalized overlaps

$$\begin{aligned} \bar{N}^J_{KK'}(a,a) &= \langle JM,aK|JM,aK'\rangle \\ &= \frac{N^J_{KK'}(a,a)}{\sqrt{N^J_{KK}(a,a)N^J_{K'K'}(a,a)}} \quad . \end{aligned} \tag{C.157}$$

Using equation (C.152), we can deduce for the normalized overlaps the following symmetries

$$\begin{aligned} \bar{N}^J_{KK'}(a,a) &= \eta_a e^{i\pi J} \quad \bar{N}^J_{K-K'}(a,a) \\ &= \eta^*_a e^{-i\pi J}\, \bar{N}^J_{-KK'}(a,a) \\ &= \qquad\quad \bar{N}^J_{-K-K'}(a,a) \quad . \end{aligned} \tag{C.158}$$

When trying to diagonalize the matrix of the normalized overlap

$$\bar{N}^J(a,a) = \begin{pmatrix} \bar{N}^J_{-J-J}(a,a) & \cdots & \bar{N}^J_{-JJ}(a,a) \\ \vdots & \ddots & \vdots \\ \bar{N}^J_{J-J}(a,a) & \cdots & \bar{N}^J_{JJ}(a,a) \end{pmatrix} \quad , \tag{C.159}$$

these symmetries give rise to null eigenvalues which are problematic from a computational point of view. The problem can be avoided by an adequate change of basis, in a generalization of what has been done by Enami *et al.* [64],

$$|JM;ak\rangle = \sum_{K=-J}^{J} W^J_{\eta_a}(K,k)|JM,aK\rangle \quad , \tag{C.160}$$

where we use k to label the states in the new basis and K to label the states in the old basis. The transformation matrix $W^J_{\eta_a}$ is taken unitary

$$W^J_{\eta_a} W^{J\dagger}_{\eta_a} = W^{J\dagger}_{\eta_a} W^J_{\eta_a} = \mathbb{1} \quad . \tag{C.161}$$

and takes, for half-integer values of J, the form

$$W^J_{\eta_a} = \begin{pmatrix} \frac{1}{\sqrt{2}} & 0 & \cdots & 0 & 0 & \cdots & 0 & \frac{\eta_a e^{+i\pi J}}{\sqrt{2}} \\ 0 & \ddots & \ddots & \vdots & \vdots & \iddots & \iddots & 0 \\ \vdots & \ddots & \ddots & 0 & 0 & \iddots & \iddots & \vdots \\ 0 & \cdots & 0 & \frac{1}{\sqrt{2}} & \frac{\eta_a e^{+i\pi J}}{\sqrt{2}} & 0 & \cdots & 0 \\ 0 & \cdots & 0 & \frac{\eta_a e^{-i\pi J}}{\sqrt{2}} & \frac{1}{\sqrt{2}} & 0 & \cdots & 0 \\ \vdots & \iddots & \iddots & 0 & 0 & \ddots & \ddots & \vdots \\ 0 & \iddots & \iddots & \vdots & \vdots & \ddots & \ddots & 0 \\ \frac{\eta_a e^{-i\pi J}}{\sqrt{2}} & 0 & \cdots & 0 & 0 & \cdots & 0 & \frac{1}{\sqrt{2}} \end{pmatrix} \quad , \tag{C.162}$$

whereas for integer values of J, it takes the form

$$W^J_{\eta_a} = \begin{pmatrix} \frac{1}{\sqrt{2}} & 0 & \cdots & 0 & \cdots & 0 & \frac{\eta_a (-)^J}{\sqrt{2}} \\ 0 & \ddots & \ddots & \vdots & \iddots & \iddots & 0 \\ \vdots & \ddots & \frac{1}{\sqrt{2}} & 0 & \frac{\eta_a (-)^J}{\sqrt{2}} & \iddots & \vdots \\ 0 & \cdots & 0 & 1 & 0 & \cdots & 0 \\ \vdots & \iddots & -\frac{\eta_a (-)^J}{\sqrt{2}} & 0 & \frac{1}{\sqrt{2}} & \ddots & \vdots \\ 0 & \iddots & \iddots & \vdots & \ddots & \ddots & 0 \\ -\frac{\eta_a (-)^J}{\sqrt{2}} & 0 & \cdots & 0 & \cdots & 0 & \frac{1}{\sqrt{2}} \end{pmatrix} \quad . \tag{C.163}$$

In the new basis, the projected overlap matrix

$$\tilde{N}^J(a,a) = W^{J\dagger}_{\eta_a} \bar{N}^J(a,a) W^J_{\eta_a} \tag{C.164}$$

has, for half-integer values of J, the structure

$$\tilde{N}^J(a,a) = \begin{pmatrix} 0 & \cdots & 0 & 0 & \cdots & 0 \\ \vdots & \ddots & \vdots & \vdots & \iddots & \vdots \\ 0 & \cdots & 0 & 0 & \cdots & 0 \\ 0 & \cdots & 0 & 2\bar{N}^J_{\frac{1}{2}\frac{1}{2}}(a,a) & \cdots & 2\bar{N}^J_{\frac{1}{2}J}(a,a) \\ \vdots & \iddots & \vdots & \vdots & \ddots & \vdots \\ 0 & \cdots & 0 & 2\bar{N}^J_{J\frac{1}{2}}(a,a) & \cdots & 2\bar{N}^J_{JJ}(a,a) \end{pmatrix} \quad , \tag{C.165}$$

whereas for integer values of J, it takes the structure

$$\tilde{N}^J(a,a) = \begin{pmatrix} 0 & \cdots & 0 & 0 & 0 & \cdots & 0 \\ \vdots & \ddots & \vdots & \vdots & \vdots & \iddots & \vdots \\ 0 & \cdots & 0 & 0 & 0 & \cdots & 0 \\ 0 & \cdots & 0 & \bar{N}^J_{00}(a,a) & \sqrt{2}\bar{N}^J_{01}(a,a) & \cdots & \sqrt{2}\bar{N}^J_{0J}(a,a) \\ 0 & \cdots & 0 & \sqrt{2}\bar{N}^J_{10}(a,a) & 2\bar{N}^J_{11}(a,a) & \cdots & 2\bar{N}^J_{1J}(a,a) \\ \vdots & \iddots & \vdots & \vdots & \vdots & \ddots & \vdots \\ 0 & \cdots & 0 & \sqrt{2}\bar{N}^J_{J0}(a,a) & 2\bar{N}^J_{J1}(a,a) & \cdots & 2\bar{N}^J_{JJ}(a,a) \end{pmatrix} \quad . \tag{C.166}$$

In the new basis we have to take into consideration only the states with $k \geq 0$. Finally, we mention that by changing the diagonal on which are the $\frac{-1}{\sqrt{2}}$, it is also possible to move the non-zero block in the top left panel of the matrix, like what is done in [64].

C.10 Wigner-Eckart Theorem

The Wigner-Eckart theorem states that any matrix element $\langle J_f M_f|\hat{T}^\lambda_\mu|J_i M_i\rangle$ can be written as the product of a Clebsch-Gordan coefficient $(J_i M_i \lambda\mu|J_f M_f)_{SU(2)}$ times a reduced matrix element $\langle J_f||\hat{T}^\lambda||J_i\rangle$ whose value is independent on the values of M_i, μ, and M_f. The Wigner-Eckart Theorem reads[2]

$$\langle J_f M_f|\hat{T}^\lambda_\mu|J_i M_i\rangle = \frac{(J_i M_i \lambda\mu|J_f M_f)}{\sqrt{2J_f+1}}\langle J_f||\hat{T}^\lambda||J_i\rangle \quad , \tag{C.167}$$

where, compared to the expression used in chapter 3, we have added the normalization factor $\frac{1}{\sqrt{2J_f+1}}$, and where $(J_i M_i \lambda\mu|J_f M_f) \equiv (J_i M_i \lambda\mu|J_f M_f)_{SU(2)}$. The Clebsch-Gordan coefficients of $SU(2)_A$ are real

$$(J_f M_f|J_i M_i \lambda\mu) = (J_i M_i \lambda\mu|J_f M_f)^* = (J_i M_i \lambda\mu|J_f M_f) \quad , \tag{C.168}$$

they are identically zero if the following conditions are not satisfied

$$J_f \in \{|J_i-\lambda|\,,\,|J_i-\lambda|+1\,,\,\ldots\,,\,J_i+\lambda-1\,,\,J_i+\lambda\} \quad , \tag{C.169}$$

$$M_f = M_i + \mu \quad , \tag{C.170}$$

and they follow the orthogonality relations

$$\begin{aligned} \sum_{M_i=-J_i}^{J_i}\sum_{\mu=-\lambda}^{\lambda}(J_i M_i \lambda\mu|J_f M_f)(J_i M_i \lambda\mu|J'_f M'_f) &= \delta_{J_f,J'_f}\,\delta_{M_f,M'_f} \\ \sum_{J_f=|J_i-\lambda|}^{J_i+\lambda}\sum_{M_f=-J_f}^{J_f}(J_i M_i \lambda\mu|J_f M_f)(J_i M'_i \lambda\mu'|J_f M_f) &= \delta_{M_i,M'_i}\,\delta_{\mu,\mu'} \quad . \end{aligned} \tag{C.171}$$

Using these orthogonality relations we can give an inverted expression of the Wigner-Eckart theorem

$$\langle J_f||\hat{T}^\lambda||J_i\rangle = \frac{1}{\sqrt{2J_f+1}}\sum_{M_f=-J_f}^{J_f}\sum_{M_i=-J_i}^{J_i}\sum_{\mu=-\lambda}^{\lambda}(J_i M_i \lambda\mu|J_f M_f)\langle J_f M_f|\hat{T}^\lambda_\mu|J_i M_i\rangle \quad . \tag{C.172}$$

[2] We consider here only integer values of λ, so we have dropped the phase $(-)^{2\lambda}$ present in the definition of [155] .

Also, taking the square modulus of equation (C.167), summing over all angular components M_i, μ, M_f, and using again the orthogonality relations of the Clebsch-Gordan, we can also deduce that

$$\sum_{M_f=-J_f}^{J_f}\sum_{M_i=-J_i}^{J_i}\sum_{\mu=-\lambda}^{\lambda}|\langle J_fM_f|\hat{T}^\lambda_\mu|J_iM_i\rangle|^2=|\langle J_f||\hat{T}^\lambda||J_i\rangle|^2 \quad . \tag{C.173}$$

C.10.1 Symmetries of the Reduced Matrix Elements

Assuming that we have $\hat{T}^{\lambda\dagger}_\mu=(-)^\mu\,\hat{T}^\lambda_{-\mu}$, we can derive the following symmetry relations between $\langle J_f||\hat{T}^\lambda||J_i\rangle$ and $\langle J_i||\hat{T}^\lambda||J_f\rangle$

$$\begin{aligned}
\langle J_fM_f|\hat{T}^\lambda_\mu|J_iM_i\rangle &= \langle J_iM_i|\hat{T}^{\lambda\dagger}_\mu|J_fM_f\rangle^*\\
\langle J_fM_f|\hat{T}^\lambda_\mu|J_iM_i\rangle &= (-)^\mu\langle J_iM_i|\hat{T}^\lambda_{-\mu}|J_fM_f\rangle^*\\
\frac{(J_iM_i\lambda\mu|J_fM_f)}{\sqrt{2J_f+1}}\langle J_f||\hat{T}^\lambda||J_i\rangle &= (-)^\mu\frac{(J_fM_f\lambda\,-\mu|J_iM_i)}{\sqrt{2J_i+1}}\langle J_i||\hat{T}^\lambda||J_f\rangle^*\\
(J_iM_i\lambda\mu|J_fM_f)\langle J_f||\hat{T}^\lambda||J_i\rangle &= (-)^{J_f-J_i}(J_iM_i\lambda\mu|J_fM_f)\langle J_i||\hat{T}^\lambda||J_f\rangle^*\\
\langle J_f||\hat{T}^\lambda||J_i\rangle &= (-)^{J_f-J_i}\langle J_i||\hat{T}^\lambda||J_f\rangle^* \quad ,
\end{aligned} \tag{C.174}$$

where we have used the symmetry properties of the Clebsch-Gordan coefficients [155]

$$\begin{aligned}
(J_fM_f\lambda-\mu|J_iM_i) &= (-)^{J_f+\lambda-J_i}(J_f\,-M_f\lambda\mu|J_i\,-M_i)\\
&= (-)^{J_f+\lambda-J_i}\left[(-)^{\lambda+\mu}\frac{\sqrt{2J_i+1}}{\sqrt{2J_f+1}}(J_iM_i\lambda\mu|J_fM_f)\right]\\
&= (-)^{J_f+\mu-J_i}\frac{\sqrt{2J_i+1}}{\sqrt{2J_f+1}}(J_iM_i\lambda\mu|J_fM_f) \quad ,
\end{aligned} \tag{C.175}$$

and the fact that μ is an integer: $(-)^{2\mu}=1$, and where we have assumed that the Clebsch-Gordan coefficient $(J_iM_i\lambda\mu|J_fM_f)$ is non-zero.

C.10.2 We Need to Project Only One State

We show here that you only need to use only one projection operator to compute the reduced matrix elements between two *a priori* different states $|\Phi_a\rangle$ and $|\Phi_b\rangle$. First let us expand $\langle\Phi_a|\hat{T}^\lambda_\mu P^{J_i}_{M_iK_i}|\Phi_b\rangle$ as

$$\begin{aligned}
\langle\Phi_a|\hat{T}^\lambda_\mu P^{J_i}_{M_iK_i}|\Phi_b\rangle &= \sum_J\sum_{J'}\sum_{M=-J}^{J}\sum_{M'=-J'}^{J'}c^J_M{}^*(a)c^{J'}_{M'}(b)\langle JM|\hat{T}^\lambda_\mu|J_iM_i\rangle\langle J_iK_i|J'M'\rangle\\
&= \sum_J\sum_{J'}\sum_{M=-J}^{J}\sum_{M'=-J'}^{J'}c^J_M{}^*(a)c^{J'}_{M'}(b)\langle JM|\hat{T}^\lambda_\mu|J_iM_i\rangle\delta_{J_i,J'}\delta_{K_i,M'}\\
&= \sum_J\sum_{M=-J}^{J}c^J_M{}^*(a)c^{J_i}_{K_i}(b)\langle JM|\hat{T}^\lambda_\mu|J_iM_i\rangle\\
&= \sum_{J=|J_i-\lambda|}^{J_i+\lambda}\sum_{M=-J}^{J}c^J_M{}^*(a)c^{J_i}_{K_i}(b)\frac{(J_iM_i\lambda\mu|JM)}{\sqrt{2J+1}}\langle J||\hat{T}^\lambda||J_i\rangle \quad ,
\end{aligned} \tag{C.176}$$

then multiplying each side of the equation by $(J_i M_i \lambda\mu | J_f K_f)$ and summing over μ and K_i, we obtain

$$\begin{aligned}
&\sum_{M_i=-J_i}^{J_i} \sum_{\mu=-\lambda}^{\lambda} (J_i M_i \lambda\mu | J_f K_f) \langle \Phi_a | \hat{T}^\lambda_\mu P^{J_i}_{M_i K_i} | \Phi_b \rangle \\
&= \sum_{J=|J_i-\lambda|}^{J_i+\lambda} \sum_{M=-J}^{J} \sum_{M_i=-J_i}^{J_i} \sum_{\mu=-\lambda}^{\lambda} {c^J_M}^*(a) c^{J_i}_{K_i}(b) (J_i M_i \lambda\mu | J_f K_f) \frac{(J_i M_i \lambda\mu | JM)}{\sqrt{2J+1}} \langle J || \hat{T}^\lambda || J_i \rangle \\
&= \sum_{J=|J_i-\lambda|}^{J_i+\lambda} \sum_{M=-J}^{J} {c^J_M}^*(a) c^{J_i}_{K_i}(b) \frac{\delta_{J,J_f}\, \delta_{M,K_f}}{\sqrt{2J+1}} \langle J || \hat{T}^\lambda || J_i \rangle \\
&= \frac{{c^{J_f}_{K_f}}^*(a) c^{J_i}_{K_i}(b)}{\sqrt{2J_f+1}} \langle J_f || \hat{T}^\lambda || J_i \rangle \quad .
\end{aligned} \tag{C.177}$$

It is interesting to note that it is the Clebsch-Gordan coefficient by which we multiply the equation that selects, through the orthogonality relations, which angular momentum J_f and which component K_f we obtain from the bra. On the other hand, when the ket and the bra are both projected, they select the Clebsch-Gordan coefficient which is factor of the reduced matrix element.
Finally, let us define the normalized reduced matrix element

$$\begin{aligned}
\langle J_f, aK_f || \hat{T}^\lambda || J_i, bK_i \rangle &= \frac{{c^{J_f}_{K_f}}^*(a) c^{J_i}_{K_i}(b)}{\sqrt{\langle \Phi_a | P^{J_f}_{K_f K_f} | \Phi_a \rangle \langle \Phi_b | P^{J_i}_{K_i K_i} | \Phi_b \rangle}} \langle J_f || \hat{T}^\lambda || J_i \rangle \\
&= \left(\sqrt{2J_f+1}\right) \sum_{M_i=-J_i}^{J_i} \sum_{\mu=-\lambda}^{\lambda} (J_i M_i \lambda\mu | J_f K_f) \\
&\quad \times \frac{\langle \Phi_a | \hat{T}^\lambda_\mu P^{J_i}_{M_i K_i} | \Phi_b \rangle}{\sqrt{\langle \Phi_a | P^{J_f}_{K_f K_f} | \Phi_a \rangle \langle \Phi_b | P^{J_i}_{K_i K_i} | \Phi_b \rangle}} \quad .
\end{aligned} \tag{C.178}$$

Note that if $J_f = J_i$, the above normalized reduced matrix elements have the same symmetries as the projected overlap, and that if $\hat{T}^{\lambda\dagger}_\mu = (-)^\mu \hat{T}^\lambda_{-\mu}$, they have also the symmetry

$$\langle J_f, aK_f || \hat{T}^\lambda || J_i, bK_i \rangle = (-)^{J_f - J_i} \langle J_i, bK_i || \hat{T}^\lambda || J_f, aK_f \rangle^* \quad . \tag{C.179}$$

Appendix D

Electromagnetic Observables

Par hasard, direz-vous peut-être, mais souvenez-vous que dans les champs de l'observation, le hasard ne favorise que les esprits préparés.

Louis Pasteur, Discours lors de l'inauguration de l'Université de Lille (1854).

D.1 Electromagnetic Transitions

In nuclear physics, the electric transition operator $\mathcal{M}(E,\lambda\mu)$ and the magnetic transition operator $\mathcal{M}(M,\lambda\mu)$ can be approximed [107] by the electric multipole operator

$$\mathcal{M}(E,\lambda\mu) \approx \hat{E}^{\lambda}_{\mu} = \sum_{i=1}^{A} \hat{e}_i \, r_i^{\lambda} \, Y^{\lambda}_{\mu}(\theta_i,\phi_i) \tag{D.1}$$

and the magnetic multipole operator

$$\mathcal{M}(M,\lambda\mu) \approx \hat{M}^{\lambda}_{\mu} = \mu_N \sum_{i=1}^{A} \left(\frac{2}{\lambda+1} \, g_l^i \, \hat{\vec{l}}_i + g_s^i \, \hat{\vec{s}}_i \right) \cdot \vec{\nabla}_i \left[r_i^{\lambda} \, Y^{\lambda}_{\mu}(\theta_i,\phi_i) \right] \quad , \tag{D.2}$$

respectively, where $\hat{\vec{l}}_i$ is the orbital angular momentum operator of the i^{th} particle, $\hat{\vec{s}}_i$ is the spin angular momentum operator of the i^{th} particle, $\hat{e}(i)$ is an operator which takes the value

$$\hat{e}_i = \begin{cases} e\hat{\mathbb{1}} & \text{if the } i^{\text{th}} \text{ particle is a proton} \\ 0 & \text{if the } i^{\text{th}} \text{ particle is a neutron} \end{cases} \quad , \tag{D.3}$$

with e being the electric charge of a proton, g_l^i is the orbital g-factor

$$g_l^i = \begin{cases} 1 & \text{if the } i^{\text{th}} \text{ particle is a proton} \\ 0 & \text{if the } i^{\text{th}} \text{ particle is a neutron} \end{cases} \quad , \tag{D.4}$$

g_s^i is the spin g-factor

$$g_s^i = \begin{cases} 5.586 & \text{if the } i^{\text{th}} \text{ particle is a proton} \\ -3.826 & \text{if the } i^{\text{th}} \text{ particle is a neutron} \end{cases} \quad , \tag{D.5}$$

and, finally, where

$$\mu_N = \frac{e\hbar}{2m_p c} \tag{D.6}$$

is the nuclear magneton with e still being the electric charge of a proton, m_p being the mass of a proton, and c is the speed of light in the vacuum.
The electric multipole operator has the commutation relations

$$\hat{R}(\alpha,\beta,\gamma)\hat{E}^\lambda_\mu\hat{R}^\dagger(\alpha,\beta,\gamma) = \sum_{\nu=-\lambda}^{\lambda} D^\lambda_{\nu\mu}(\alpha,\beta,\gamma)\hat{E}^\lambda_\nu \quad , \tag{D.7}$$

$$\hat{N}\hat{E}^\lambda_\mu\hat{N}^\dagger = \hat{E}^\lambda_\mu \quad , \tag{D.8}$$

$$\hat{Z}\hat{E}^\lambda_\mu\hat{Z}^\dagger = \hat{E}^\lambda_\mu \quad , \tag{D.9}$$

$$\hat{P}\hat{E}^\lambda_\mu\hat{P}^\dagger = (-)^\lambda\hat{E}^\lambda_\mu \quad , \tag{D.10}$$

so it is an irreducible tensor operator that transforms accordingly to the irrep

$$\Lambda_{E\lambda} \equiv (\lambda, 0, 0, (-)^\lambda)$$

of the group G defined by (3.117).
Similarly, the magnetic multipole operator has the commutation relations

$$\hat{R}(\alpha,\beta,\gamma)\hat{M}^\lambda_\mu\hat{R}^\dagger(\alpha,\beta,\gamma) = \sum_{\nu=-\lambda}^{\lambda} D^\lambda_{\nu\mu}(\alpha,\beta,\gamma)\hat{M}^\lambda_\nu \quad , \tag{D.11}$$

$$\hat{N}\hat{M}^\lambda_\mu\hat{N}^\dagger = \hat{M}^\lambda_\mu \quad , \tag{D.12}$$

$$\hat{Z}\hat{M}^\lambda_\mu\hat{Z}^\dagger = \hat{M}^\lambda_\mu \quad , \tag{D.13}$$

$$\hat{P}\hat{M}^\lambda_\mu\hat{P}^\dagger = (-)^{\lambda+1}\hat{M}^\lambda_\mu \quad , \tag{D.14}$$

so it is an irreducible tensor operator that transforms accordingly to the irrep

$$\Lambda_{M\lambda} \equiv (\lambda, 0, 0, (-)^{\lambda+1})$$

of the group G.
We also give the commutation relations of $\hat{E}^\lambda_\mu$ and $\hat{M}^\lambda_\mu$ with the time-reversal operator

$$\hat{T}\hat{E}^\lambda_\mu\hat{T}^\dagger = \hat{E}^{\lambda*}_\mu = (-)^\mu\hat{E}^\lambda_{-\mu} \quad , \tag{D.15}$$

$$\hat{T}\hat{M}^\lambda_\mu\hat{T}^\dagger = -\hat{M}^{\lambda*}_\mu = (-)^{\mu+1}\hat{M}^\lambda_{-\mu} \quad . \tag{D.16}$$

D.2 Reduced Transition Probabilities

Let us consider two states, $|\Lambda_i M_i \xi_i\rangle$ and $|\Lambda_f M_f \xi_f\rangle$, with $\Lambda_i \equiv (J_i, N_i, Z_i, P_i)$ and $\Lambda_f \equiv (J_f, N_f, Z_f, P_f)$, respectively. We define [107, 137] the reduced transition probabilities between these two states as the sum over all possible initial and final magnetic substates of the square of transition matrix elements, averaged by the number of initial magnetic substates

$$B(\hat{T}\lambda, \Lambda_i\xi_i \to \Lambda_f\xi_f) = \frac{1}{2J_i+1}\sum_{M_f=-J_f}^{J_f}\sum_{M_i=-J_i}^{J_i}\sum_{\mu=-\lambda}^{\lambda}|\langle\Lambda_f M_f\xi_f|\hat{T}^\lambda_\mu|\Lambda_i M_i\xi_i\rangle|^2 \, , \tag{D.17}$$

with the selection rules (3.121)

$$\begin{aligned} J_f &\in \{|J_i-\lambda|, |J_i-\lambda|+1\,, \ldots\,, J_i+\lambda-1, J_i+\lambda\} \quad , \\ N_f &= N_i \quad , \\ Z_f &= Z_i \quad , \\ P_f &= P_i\, P_{\Lambda_{T\lambda}} \quad , \end{aligned} \tag{D.18}$$

where for $\hat{T}^\lambda_\mu = \hat{E}^\lambda_\mu$ we have $P_{\Lambda_{E\lambda}} = (-)^\lambda$, and for $\hat{T}^\lambda_\mu = \hat{M}^\lambda_\mu$ we have $P_{\Lambda_{M\lambda}} = (-)^{\lambda+1}$.
From equation (C.173) we see that the reduced transition probabilities can also be written as

$$B(\hat{T}\lambda, \Lambda_i\xi_i \to \Lambda_f\xi_f) = \frac{1}{2J_i+1}|\langle\Lambda_f\xi_f||\hat{T}^\lambda||\Lambda_i\xi_i\rangle|^2 \quad . \tag{D.19}$$

As we have $\hat{T}^{\lambda\dagger}_\mu = (-)^\mu\, \hat{T}^\lambda_{-\mu}$, we can use the symmetry of equation (C.174) to obtain the relation

$$B(\hat{T}\lambda, \Lambda_f\xi_f \to \Lambda_i\xi_i) = \frac{2J_i+1}{2J_f+1}\, B(\hat{T}\lambda, \Lambda_i\xi_i \to \Lambda_f\xi_f) \quad . \tag{D.20}$$

Finally, we adopt for the reduced matrix elements, the units [107, 137]

$$\begin{aligned} B(E\lambda) &: e^2\,\mathrm{fm}^{2\lambda} \quad , \\ B(M\lambda) &: \mu_N^2\,\mathrm{fm}^{2\lambda-2} \quad . \end{aligned} \tag{D.21}$$

D.3 Static Moments

Other observables in nuclear physics experiments are the magnetic dipole moment

$$\mu(\Lambda_i\xi_i) = \sqrt{\frac{4\pi}{3}}\langle\Lambda_i J_i\xi_i|\hat{M}^1_0|\Lambda_i J_i\xi_i\rangle \tag{D.22}$$

and the electric quadrupole moment (often called spectroscopic quadrupole moment)

$$Q_s(\Lambda_i\xi_i) = \sqrt{\frac{16\pi}{5}}\langle\Lambda_i J_i\xi_i|\hat{E}^2_0|\Lambda_i J_i\xi_i\rangle \quad , \tag{D.23}$$

and which are chosen to be defined for the states $|\Lambda_i M_i = J_i\xi_i\rangle$ [107, 137]. Indeed, because of Wigner-Eckart theorem, the difference between all the possible values of M_i comes only from the Clebsch-Gordan coefficient multiplying the reduced matrix element, and thus calculating the static multipole moments for more than one value of M_i is useless (they do not contain more information).
The magnetic dipole moment and the electric quadrupole moment have the units

$$\begin{aligned} \mu &: \mu_N \quad , \\ Q_s &: e\,\mathrm{fm}^2 \quad . \end{aligned} \tag{D.24}$$

D.4 Expressions of the $\hat{Q}^\lambda_\mu$ up to $\lambda = 3$

Defining the multipole

$$Q^\lambda_\mu = r^\lambda\, Y^\lambda_\mu(\theta,\phi) \quad ,$$

we give the expression for all the Q_μ^λ up to $\lambda = 3$

$$Q_{-1}^1 = \frac{1}{2}\sqrt{\frac{3}{2\pi}}\, r \sin\theta\, e^{-i\phi} = \frac{1}{2}\sqrt{\frac{3}{2\pi}}(x - iy) \tag{D.25}$$

$$Q_0^1 = \frac{1}{2}\sqrt{\frac{3}{\pi}}\, r \cos\theta = \frac{1}{2}\sqrt{\frac{3}{\pi}} z \tag{D.26}$$

$$Q_{+1}^1 = -\frac{1}{2}\sqrt{\frac{3}{2\pi}}\, r \sin\theta\, e^{+i\phi} = -\frac{1}{2}\sqrt{\frac{3}{2\pi}}(x + iy) \tag{D.27}$$

$$Q_{-2}^2 = \frac{1}{4}\sqrt{\frac{15}{2\pi}}\, r^2 \sin^2\theta\, e^{-2i\phi} = \frac{1}{4}\sqrt{\frac{15}{2\pi}}(x - iy)^2 \tag{D.28}$$

$$Q_{-1}^2 = \frac{1}{2}\sqrt{\frac{15}{2\pi}}\, r^2 \sin\theta\cos\theta\, e^{-i\phi} = \frac{1}{2}\sqrt{\frac{15}{2\pi}}(x - iy) z \tag{D.29}$$

$$Q_0^2 = \frac{1}{4}\sqrt{\frac{5}{\pi}}\, r^2(3\cos^2\theta - 1) = \frac{1}{4}\sqrt{\frac{5}{\pi}}(2z^2 - x^2 - y^2) \tag{D.30}$$

$$Q_{+1}^2 = -\frac{1}{2}\sqrt{\frac{15}{2\pi}}\, r^2 \sin\theta\cos\theta\, e^{+i\phi} = -\frac{1}{2}\sqrt{\frac{15}{2\pi}}(x + iy) z \tag{D.31}$$

$$Q_{+2}^2 = \frac{1}{4}\sqrt{\frac{15}{2\pi}}\, r^2 \sin^2\theta\, e^{+2i\phi} = \frac{1}{4}\sqrt{\frac{15}{2\pi}}(x + iy)^2 \tag{D.32}$$

$$Q_{-3}^3 = \frac{1}{8}\sqrt{\frac{35}{\pi}}\, r^3 \sin^3\theta\, e^{-3i\phi} = \frac{1}{8}\sqrt{\frac{35}{\pi}}(x - iy)^3 \tag{D.33}$$

$$Q_{-2}^3 = \frac{1}{4}\sqrt{\frac{105}{2\pi}}\, r^3 \sin^2\theta\cos\theta\, e^{-2i\phi} = \frac{1}{4}\sqrt{\frac{105}{2\pi}}(x - iy)^2 z \tag{D.34}$$

$$Q_{-1}^3 = \frac{1}{8}\sqrt{\frac{21}{\pi}}\, r^3 \sin\theta(5\cos^2\theta - 1)\, e^{-i\phi} = \frac{1}{8}\sqrt{\frac{21}{\pi}}(x - iy)(4z^2 - x^2 - y^2) \tag{D.35}$$

$$Q_0^3 = \frac{1}{4}\sqrt{\frac{7}{\pi}}\, r^3(5\cos^3\theta - 3\cos\theta) = \frac{1}{4}\sqrt{\frac{7}{\pi}}(2z^2 - 3x^2 - 3y^2) z \tag{D.36}$$

$$Q_{+1}^3 = -\frac{1}{8}\sqrt{\frac{21}{\pi}}\, r^3 \sin\theta(5\cos^2\theta - 1)\, e^{+i\phi} = -\frac{1}{8}\sqrt{\frac{21}{\pi}}(x + iy)(4z^2 - x^2 - y^2) \tag{D.37}$$

$$Q_{+2}^3 = \frac{1}{4}\sqrt{\frac{105}{2\pi}}\, r^3 \sin^2\theta\cos\theta\, e^{+2i\phi} = \frac{1}{4}\sqrt{\frac{105}{2\pi}}(x + iy)^2 z \tag{D.38}$$

$$Q_{+3}^3 = -\frac{1}{8}\sqrt{\frac{35}{\pi}}\, r^3 \sin^3\theta\, e^{+3i\phi} = -\frac{1}{8}\sqrt{\frac{35}{\pi}}(x + iy)^3 \tag{D.39}$$

Appendix E

Just a Last Thing About the GCM

Bernard of Chartres used to compare us to (puny) dwarfs perched on the shoulders of giants. He pointed out that we see more and farther than our predecessors, not because we have keener vision or greater height, but because we are lifted up and borne aloft on their gigantic stature. I readily agree with the foregoing.

John of Salisbury, The Metalogicon (1159).

Let us consider the set of state of Ω_I quasiparticle states $|\Phi_i\rangle$ from which we want to construct a set of $\Omega_I^\Lambda \leq (2J+1)\Omega_I$ projected states

$$|\Lambda M \xi\rangle \equiv |JMNZP\xi\rangle = \sum_{i=1}^{\Omega_I} \sum_{K=-J}^{J} f_\xi^\Lambda(i,K)|JMNZP,iK\rangle \tag{E.1}$$

where

$$|JMNZP = p_i, iK\rangle = \frac{\hat{P}^J_{MK}\hat{P}^N\hat{P}^Z|\Phi_i\rangle}{\sqrt{\langle\Phi_i|\hat{P}^J_{KK}\hat{P}^N\hat{P}^Z|\Phi_i\rangle}} \quad ,$$

and where $\xi \in \{1,\ldots,\Omega^\Lambda\}$. The states $|\Lambda M\xi\rangle$ have good angular momentum J, good number of neutrons N and protons Z, and also good parity P (the states $|\Phi_i\rangle$ having also good parity with $p_i = P$). The overlap and the Hamiltonian matrix elements of the state $|\Lambda M\xi\rangle$ read

$$\langle\Lambda M\xi|\Lambda M\xi\rangle = \sum_{i,i'=1}^{\Omega_I} \sum_{K,K'=-J}^{J} f_\xi^{\Lambda *}(i,K)\bar{N}^\Lambda_{KK'}(i,i')f_\xi^\Lambda(i',K') \quad , \tag{E.2}$$

$$\langle\Lambda M\xi|\hat{H}|\Lambda M\xi\rangle = \sum_{i,i'=1}^{\Omega_I} \sum_{K,K'=-J}^{J} f_\xi^{\Lambda *}(i,K)\bar{H}^\Lambda_{KK'}(i,i')f_\xi^\Lambda(i',K') \quad , \tag{E.3}$$

where

$$\bar{N}^\Lambda_{KK'}(i,i') = \langle JMNZP,iK|JMNZP,i'K'\rangle \quad , \tag{E.4}$$

$$\bar{H}^\Lambda_{KK'}(i,i') = \langle JMNZP,iK|\hat{H}|JMNZP,i'K'\rangle \quad . \tag{E.5}$$

The energy E_ξ^Λ of $|\Lambda M\xi\rangle$ reads

$$E_\xi^\Lambda = \frac{\langle\Lambda M\xi|\hat{H}|\Lambda M\xi\rangle}{\langle\Lambda M\xi|\Lambda M\xi\rangle} \tag{E.6}$$

Varying the energy E^{Λ}_{ξ} over the parameter $f^{\Lambda *}_{\xi}(i,K)$, we obtain the equation

$$\begin{aligned}
\frac{\delta E^{\Lambda}_{\xi}}{\delta f^{\Lambda *}_{\xi}(i,K)} &= \frac{\delta}{\delta f^{\Lambda *}_{\xi}(i,K)} \frac{\langle \Lambda M\xi|\hat{H}|\Lambda M\xi\rangle}{\langle \Lambda M\xi|\Lambda M\xi\rangle} && = 0 \\
&= \frac{\left(\frac{\delta\langle \Lambda M\xi|\hat{H}|\Lambda M\xi\rangle}{\delta f^{\Lambda *}_{\xi}(i,K)}\right)\langle \Lambda M\xi|\Lambda M\xi\rangle - \langle \Lambda M\xi|\hat{H}|\Lambda M\xi\rangle\left(\frac{\langle \Lambda M\xi|\Lambda M\xi\rangle}{\delta f^{\Lambda *}_{\xi}(i,K)}\right)}{\langle \Lambda M\xi|\Lambda M\xi\rangle^2} && = 0 \\
&= \frac{\left(\frac{\delta\langle \Lambda M\xi|\hat{H}|\Lambda M\xi\rangle}{\delta f^{\Lambda *}_{\xi}(i,K)}\right) - E^{\Lambda}_{\xi}\left(\frac{\langle \Lambda M\xi|\Lambda M\xi\rangle}{\delta f^{\Lambda *}_{\xi}(i,K)}\right)}{\langle \Lambda M\xi|\Lambda M\xi\rangle} && = 0 \\
&= \left(\frac{\delta\langle \Lambda M\xi|\hat{H}^{nuc}|\Lambda M\xi\rangle}{\delta f^{\Lambda *}_{\xi}(i,K)}\right) - E^{\Lambda}_{\xi}\left(\frac{\langle \Lambda M\xi|\Lambda M\xi\rangle}{\delta f^{\Lambda *}_{\xi}(i,K)}\right) && = 0 \\
&= \sum_{i'=1}^{\Omega_I}\sum_{K'=-J}^{J}\left[\bar{H}^{\Lambda}_{KK'}(i,i') - E^{\Lambda}_{\xi}\bar{N}^{\Lambda}_{KK'}(i,i')\right] f^{\Lambda}_{\xi}(i',K') && = 0\,. \qquad \text{(E.7)}
\end{aligned}$$

The HWG equation (E.7) is a different representation of the HWG equation (3.136) presented in chapter 3, where we have chosen to carry out the summation over the states $|JMNZP,iK\rangle$ instead of the states $|JM\epsilon,i\rangle$ obtained after the mixing of the different K components for each $|\Phi_i\rangle$ in Ω_I. If the two representations are mathematically equivalent, equation (3.136) is safer from a numerical point of view, as solving the HWG equation step-by-step allows for better controlling and removing states of bad numerical quality or redundant states that gives zero eigenvalues.

Without Cranking, Only One Signature Is Needed

Using the equation (C.84) we can derive that

$$\begin{aligned}
|\Lambda M\xi\rangle &= \sum_{i=1}^{\Omega_I}\sum_{K=-J}^{J} f^{\Lambda}_{\xi}(i,K)|JMNZP,iK\rangle \\
&= \sum_{i=1}^{\Omega_I}\sum_{K=-J}^{J} p_i\eta^*_i e^{-i\pi K} f^{\Lambda}_{\xi}(i,K)|JMNZP,\tilde{i}K\rangle \qquad \text{(E.8)} \\
&= \sum_{i=1}^{\Omega_I}\sum_{K=-J}^{J} \tilde{f}^{\Lambda}_{\xi}(i,K)|JMNZP,\tilde{i}K\rangle \quad ,
\end{aligned}$$

where

$$\begin{aligned}
|\tilde{\Phi}_i\rangle &= \hat{T}|\Phi_i\rangle \quad , \\
|JMNZP,\tilde{i}K\rangle &= \frac{\hat{P}^J_{MK}\hat{P}^N\hat{P}^Z|\tilde{\Phi}_i\rangle}{\sqrt{\langle\tilde{\Phi}_i|\hat{P}^J_{KK}\hat{P}^N\hat{P}^Z|\tilde{\Phi}_i\rangle}} \quad , \\
\tilde{f}^{\Lambda}_{\xi}(i,K) &= p_i\eta^*_i e^{-i\pi K} f^{\Lambda}_{\xi}(i,K) \quad .
\end{aligned}$$

Considering a set of states $|\Phi_i\rangle$, all having same signature and parity, we can derive, using equations (E.7), (E.8), and (C.155), that we obtain for the set of time reversed states $|\tilde{\Phi}_i\rangle$ the

same HWG equation (with same energies E^{Λ}_{ξ})

$$\begin{aligned}
&\sum_{i'=1}^{\Omega_I}\sum_{K'=-J}^{J}\left[H^{\Lambda}_{KK'}(i,i')-E^{\Lambda}_{\xi}N^{\Lambda}_{KK'}(i,i')\right]f^{\Lambda}_{\xi}(i',K')=0\\
&\sum_{i'=1}^{\Omega_I}\sum_{K'=-J}^{J}\left[H^{\Lambda}_{KK'}(i,i')-E^{\Lambda}_{\xi}N^{\Lambda}_{KK'}(i,i')\right]\left(p_{i'}\eta_{i'}e^{+i\pi K'}\tilde{f}^{\Lambda}_{\xi}(i',K')\right)=0\\
p_i\eta^*_i e^{-i\pi K}&\sum_{i'}\sum_{K'=-J}^{J}p_{i'}\eta_{i'}e^{+i\pi K'}\left[H^{\Lambda}_{KK'}(i,i')-E^{\Lambda}_{\xi}N^{\Lambda}_{KK'}(i,i')\right]\tilde{f}^{\Lambda}_{\xi}(i',K')=0\\
&\sum_{i'=1}^{\Omega_I}\sum_{K'=-J}^{J}p_ip_{i'}\eta^*_i\eta_{i'}(-)^{K-K'}\left[H^{\Lambda}_{KK'}(i,i')-E^{\Lambda}_{\xi}N^{\Lambda}_{KK'}(i,i')\right]\tilde{f}^{\Lambda}_{\xi}(i',K')=0\\
&\sum_{i'=1}^{\Omega_I}\sum_{K'=-J}^{J}\left[H^{\Lambda}_{KK'}(\tilde{i},\tilde{i}')-E^{\Lambda}_{\xi}N^{\Lambda}_{KK'}(\tilde{i},\tilde{i}')\right]\tilde{f}^{\Lambda}_{\xi}(i',K')=0\quad ,
\end{aligned}\tag{E.9}$$

When realizing calculations without cranking, starting from an even vacuum it possible to create the one-quasiparticle states $|\Phi_i\rangle$ and $|\tilde{\Phi}_i\rangle$ by blocking the two quasiparticles that are conjugate partners, and which have opposite signature (and thus are orthogonal). But a set composed of states $|\Phi_i\rangle$ (of a given signature) and a set composed of their time-reversed states $|\tilde{\Phi}_i\rangle$ (of the opposite signature), will give same results.

A More Formal Demonstration

As said above, the two one-quasiparticle states $|\Phi_i\rangle$ and $|\tilde{\Phi}_i\rangle$ represent the two choices for blocking one-quasiparticle configurations with opposite signatures and same parity. Considering for the sake of clarity only the projection on angular momentum, we can thus rewrite equation (C.155) as

$$N^{J}_{KK'}(\tilde{i},\tilde{i})=(-)^{K-K'}N^{J}_{KK'}(i,i)\quad .\tag{E.10}$$

We call $\tilde{N}$ and N the matrices whose elements are $N^{J}_{KK'}(\tilde{i},\tilde{i})$ and $N^{J}_{KK'}(i,i)$, respectively, for different values of K and K'. The two matrices are related by a similarity transformation

$$\tilde{N}=SNS^{-1}\tag{E.11}$$

where S is a diagonal matrix of the form

$$S_{ij}=\pm(-)^{i}\delta_{ij}\quad .\tag{E.12}$$

The $\pm$ sign is here to stress that we are free to choose a global sign for the transformation.[1] Besides, we have $S^{-1}=S$ and $\det(S)^2=1$. Because $\hat{H}$ is rotational invariant, we have also

$$\tilde{H}=SHS\quad ,\tag{E.13}$$

where $\tilde{H}$ and H are matrices built along the same lines as $\tilde{N}$ and N. Calling e and f the generalized eigenvalues and generalized eigenvectors of the equation

$$Hf=eNf\quad ,\tag{E.14}$$

[1] Actually, we could multiply S by any number but then we would lose the property: $S^{-1}=S$.

the e are the solution of

$$\det(H - eN) = 0 \quad . \tag{E.15}$$

But we also have

$$\begin{aligned} \det(H - eN) &= \det(S\tilde{H}S - eS\tilde{N}S) \\ &= \det(S[\tilde{H} - e\tilde{N}]S) \\ &= \det(S)\det(\tilde{H} - e\tilde{N})\det(S) \\ &= \det(\tilde{H} - e\tilde{N}) \quad , \end{aligned} \tag{E.16}$$

and therefore the generalized eigenvalue problem

$$\tilde{H}\tilde{f} = \tilde{e}\tilde{N}\tilde{f} \quad , \tag{E.17}$$

spanned by $\tilde{H}$ and $\tilde{N}$ has the same eigenvalues as (E.14): $e = \tilde{e}$. Moreover, if f is an eigenvector of (E.14) associated with the eigenvalue e, then $\tilde{f} = Sf$ is an eigenvector of (E.17) with the same eigenvalue

$$\begin{aligned} Hf &= eNf \\ SHSSf &= eSNSSf \\ \tilde{H}Sf &= e\tilde{N}Sf \quad . \end{aligned} \tag{E.18}$$

Looking back at equations (E.8) and (E.9), we now see that in fact we used a transformation of the form (E.12)

$$S_{KK'} = p_i \eta_i^* e^{-i\pi K} \delta_{K,K'} \quad , \tag{E.19}$$

where p_i and η_i are the parity and the signature of the state $|\Phi_i\rangle$, respectively.

Finally, we consider for a given J two projected states ϵ, one built from $|\Phi_i\rangle$ and the other from $|\tilde{\Phi}_i\rangle$, normalized to one

$$f_\epsilon^\dagger N f_\epsilon = 1 \quad , \tag{E.20}$$

$$f_\epsilon^\dagger S^\dagger \tilde{N} S f_\epsilon = 1 \quad . \tag{E.21}$$

Noting $\bar{N}$ the matrix whose elements are $N^J_{KK'}(i,\tilde{i})$, and using equation (C.154), we see that the overlap between these two projected states is equal to one

$$\begin{aligned} f_\epsilon^\dagger \bar{N} S f_\epsilon &= \sum_{K,K'=-J}^{J} f_\epsilon^{J\,*}(i,K)\, N^J_{KK'}(i,\tilde{i})\, p_i \eta_i^* e^{-i\pi K'} f_\epsilon^J(i,K') \\ &= \sum_{K,K'=-J}^{J} f_\epsilon^{J\,*}(i,K)\, N^J_{KK'}(i,i)\, f_\epsilon^J(i,K') \\ &= 1 \quad . \end{aligned} \tag{E.22}$$

We are thus in the equality case of the Cauchy-Schwartz inequality and consequently the states are linearly dependent. They are even identical thanks to the choice made for the transformation.

Bibliography

[1] M. Anguiano, J. L. Egido, and L. M. Robledo, *Particle number projection with effective forces*, Nucl. Phys. A **696** 467 (2001).

[2] M. Anguiano, J. L. Egido, and L. M. Robledo, *Coulomb exchange and pairing contributions in nuclear Hartree-Fock-Bogoliubov calculations with the Gogny force*, Nucl. Phys. A **683** 227 (2001).

[3] G. Audi, A.H. Wapstrab, and C. Thibault, *The AME2003 atomic mass evaluation*, Nucl. Phys. A **729** 337 (2003).

[4] B. Avez, *Private Communications.*

[5] B. Avez and M. Bender, *Evaluation of overlaps between arbitrary fermionic quasiparticle vacua*, Phys. Rev. C **85** 034325 (2012).

[6] B. Avez, B. Bally, M. Bender, and P.-H. Heenen, in prepration.

[7] R. Balian and E. Brézin, *Nonunitarity Bogoliubov Transformations and Extension of Wick's Theorem*, Il Nuovo Cimento **LXIV B** 37 (1969).

[8] B. Banerjee, P. Ring, and H. J. Mang, *On the character of the Hartree-Fock-Bogoliubov solutions in a rotating frame*, Nucl. Phys. A **221** 564 (1974).

[9] J. Bardeen, L. N. Cooper, and J. R. Schrieffer, *Theory of Superconductivity*, Phys. Rev. Lett. **108** 1175 (1957).

[10] V. Bargmann, *Note on Wigner's Theorem on Symmetry Operations*, J. of Math. Phys. **5** 862 (1964).

[11] D. Baye and P.-H. Heenen, *Angular momentum projection on a mesh of cranked Hartree-Fock wave functions*, Phys. Rev. C **29** 1056 (1984).

[12] B.F. Bayman, *A derivation of the pairing-correlation method*, Nucl. Phys. A **15** 33 (1960).

[13] R. Beck, H. J. Mang, and P. Ring, *Symmetry-Conserving Hartree-Fock-Bogolyubov-Theory and its Application to Collective Nuclear Rotation*, Z. Physik **231** 26 (1970).

[14] M. Beiner, and R. J. Lombard, *The energy densiiy formalism and the shell structure effects*, Ann. Phys. **86** 262 (1974).

[15] M. Beiner, H. Flocard, N. V. Giai, and P. Quentin, *Nuclear ground-state properties and self-consistent calculations with the Skyrme interaction: (I). Spherical description*, Nucl. Phys. A **238** 29 (1975).

[16] S. T. Belyaev, Mat.-Fys. Medd. K. Dan. Vidensk. Selsk **31** 1 (1959).

[17] M. Bender, K. Rutz, P.-G. Reinhard and J. A. Maruhn, *Consequences of the center–of–mass correction in nuclear mean–field models*, Eur. Phys. J. A **7** 467 (2000).

[18] M. Bender, K. Rutz, P.-G. Reinhard, and J. A. Maruhn, *Pairing gaps from nuclear mean-field models*, Eur. Phys. J. A **8** 59 (2000).

[19] M. Bender, P.-H. Heenen, and P.-G. Reinhard, *Self-consistent mean-field models for nuclear structure*, Rev. Mod. Phys. **75** 121 (2003).

[20] M. Bender, K. Bennaceur, T. Duguet, and P.-H. Heenen, *Contrained HFB and pairing vibrations*, unpublished notes (2005).

[21] M. Bender, G. F. Bertsch, and P.-H. Heenen, *Global study of quadrupole correlation effects*, Phys. Rev. C **73** 034322 (2006).

[22] M. Bender and P.-H. Heenen, *Configuration mixing of angular-momentum and particle-number projected triaxial Hartree-Fock-Bogoliubov states using the Skyrme energy density functional*, Phys. Rev. C **78** 024309 (2008).

[23] M. Bender, T. Duguet, and D. Lacroix, *Particle-number restoration within the energy density functional formalism*, Phys. Rev. C **79** 044319 (2009).

[24] M. Bender, *Unpublished notes* (2001-2013).

[25] M. Bender, B. Avez, B. Bally, T. Duguet, P.-H. Heenen, and D. Lacroix, *in preparation.*

[26] J.F. Berger, M. Girod, and D. Gogny, *Time-dependent quantum collective dynamics applied to nuclear fission*, Comp. Phys. Comm. **63** 365 (1991).

[27] G. Bertsch, J. Dobaczewski, W. Nazarewicz, and J. Pei, *Hartree-Fock-Bogoliubov theory of polarized Fermi systems*, Phys. Rev. A **79** 043602 (2009).

[28] G. F. Bertsch and L. M. Robledo, *Symmetry Restoration in Hartree-Fock-Bogoliubov Based Theories*, Phys. Rev. Lett. **108** 042505 (2012).

[29] H. A. Bethe, *Theory of Nuclear Matter*, Annu. Rev. Nucl. Sci. **21** 93 (1971).

[30] J. S. Blair and I. M. Naqib, *Inelastic Scattering of 42-MeV Alpha Particles by* ^{25}Mg, Phys. Rev. C **1** 569 (1970).

[31] J.-P. Blaizot, D. Gogny, and B. Grammaticos, *Nuclear compressibility and monopole resonances*, Nucl. Phys. A **265** 315 (1976).

[32] A. Bohr and B. R. Mottelson, *Nuclear structure, volume I and II*, World Scientific Publishing (1998).

[33] J.-P. Blaizot and J.-C. Tolénado, *Symétries & Physique Microscopique*, Ellipses, Ecole Polytechnique (1997).

[34] J.-P. Blaizot and G. Ripka, *Quantum Theory of Finite Systems*, MIT Press (1986).

[35] C. Bloch and A. Messiah, *The canonical form of an antisymmetric tensor and its application to the theory of superconductivity*, Nucl. Phys. A **39** 95 (1962).

[36] P. Bonche, H. Flocard, and P.-H. Heenen, *Self-consistent calculation of nuclear rotations: The complete yrast line of* ^{24}Mg, Nucl. Phys. A **467** 115 (1987).

[37] D. M. Brink and E. Boeker, *Effective interaction for Hartree-Fock calculations*, Nucl. Phys. A **99** 1 (1967).

[38] B. A. Brown and W. A. Richter, *New "USD" Hamiltonians for the sd shell*, Phys. Rev. C **74** 034315 (2006).

[39] B. A. Brown and W.D.M.Rae, *NuShellX@MSU*, http://www.nscl.msu.edu/ brown/resources/resources.html

[40] A. Bulgac and Y. Yu, *Renormalization of the Hartree-Fock-Bogoliubov Equations in the Case of a Zero Range Pairing Interaction*, Phys. Rev. Lett. **88** 042504 (2002).

[41] P. A. Butler *et al.*, *Electromagnetic and angular momentum properties of states in* ^{25}Mg *below 6.05 MeV in excitation*, J. Phys. G **1** 665 (1975).

[42] B. G. Carlsson, J. Toivanen, and U. von Barth, *Fluctuating parts of nuclear ground-state correlation energies*, Phys. Rev. C **87** 054303 (2013).

[43] E. Chabanat, P. Bonche, P. Haensel, J. Meyer, and R. Schaeffer, *A Skyrme parametrization from subnuclear to neutron star densities Part II. Nuclei far from stabilities*, Nucl. Phys. A **635** 231 (1998). Erratum: Nucl. Phys. A **643** 441 (1998).

[44] B. E. Chi and J. P. Davidson, *Asymmetric Core Collective Model for Odd-A Nuclei with Applications to the 2s-1d Shell*, Phys. Rev. **131** 366 (1963).

[45] B. J. Cole, A. Watt, and R. R. Whitehead, *Rotational band shifts in* ^{25}Mg *and* ^{26}Al, Phys. Lett. B **49** 133 (1974).

[46] B. J. Cole, *Large-basis shell-model calculations for* ^{25}Mg, J. Phys. G **2** 541 (1976).

[47] J. Dechargé and D. Gogny, *Hartree-Fock-Bogolyubov calculations with the D1 effective interaction on spherical nuclei*, Phys. Rev. C **21** 1568 (1980).

[48] K. Dietrich, H. J. Mang, and J. H. Pradal, *Conservation Particle Number in the Nuclear Pairing Model*, Phys. Rev. **135** B22 (1964).

[49] J. Dobaczewski, H. Flocard, and J. Treiner, *Hartree-Fock-Bogolyubov description of nuclei near the neutron-drip line*, Nucl. Phys. A **422** 103 (1984).

[50] J. Dobaczewski, J. Dudek, S. G. Rohoziński, and T. R. Werner, *Point symmetries in the Hartree-Fock approach. I. Densities, shapes, and currents*, Phys. Rev. C **62** 014310 (2000).

[51] J. Dobaczewski, J. Dudek, S. G. Rohoziński, and T. R. Werner, *Point symmetries in the Hartree-Fock approach. II. Symmetry-breaking schemes*, Phys. Rev. C **62** 014311 (2000).

[52] J. Dobaczewski, M. V. Stoitsov, W. Nazarewicz, and P.-G. Reinhard, *Particle-number projection and the density functional theory*, Phys. Rev. C **76** 054315 (2007).

[53] F. Dönau, *Canonical form of transition matrix elements*, Phys. Rev. C **58** 872 (1998).

[54] J. P. Draayer, *Structure calculations for* ^{25}Mg-^{28}Al, Nucl. Phys. A **216** 457 (1973).

[55] G. W. F. Drake, *Handbook of Atomic, Molecular, and Optical Physics*, Springer (2006).

[56] T. Duguet, P. Bonche, P.-H. Heenen, and J. Meyer, *Pairing correlations. I. Description of odd nuclei in mean-field theories*, Phys. Rev. C **65** 014310 (2001).

[57] T. Duguet, P. Bonche, P.-H. Heenen, and J. Meyer, *Pairing correlations. II. Microscopic analysis of odd-even mass staggering in nuclei*, Phys. Rev. C **65** 014311 (2001).

[58] T. Duguet, M. Bender, K. Bennaceur, D. Lacroix, and T. Lesinski, *Particle-number restoration within the energy density functional formalism: Nonviability of terms depending on noninteger powers of the density matrices*, Phys. Rev. C **79** 044320 (2009).

[59] T. Duguet and J. Sadoudi, *Breaking and restoring symmetries within the nuclear energy density functional method*, J. of Phys. G **37** 064009 (2010).

[60] T. Duguet and G. Hagen, *Ab initio approach to effective single-particle energies in doubly closed shell nuclei*, Phys. Rev. C **85** 034330 (2012).

[61] T. Duguet, *The nuclear energy density functional formalism*, arXiv:1309.0440.

[62] J. L. Egido, H.-J. Mang, and P. Ring, *Selfconsistent treatment of excited rotational bands in deformed nuclei*, Nucl. Phys. A **334** 1 (1980).

[63] J. L. Egido and P. Ring, *Symmetry conserving Hartree-Fock-Bogoliubov theory: (I). On the solution of variational equations*, Nucl. Phys. A **383** 189 (1982).

[64] K. Enami, K. Tanabe, and N. Yoshinaga, *Microscopic description of high-spin states: Quantum-number projections of the cranked Hartree-Fock-Bogoliubov self-consistent solution*, Phys. Rev. C **59** 135 (1999).

[65] R. B. Firestone, *Nuclear Data Sheets for* $A = 25$, Nuclear Data Sheets **110** 1691 (2009).

[66] H. Flocard and D. Vautherin, *Generator coordinate calculations of monopole and quadrupole vibrations with Skyrme's interaction*, Phys. Lett. B **55** 259 (1975).

[67] H. Flocard and D. Vautherin, *Generator coordinate calculations of giant resonances with the Skyrme interaction*, Nucl. Phys. A **264** 197 (1976).

[68] V. N. Fomenko, *Projection in the occupation-number space and the canonical transformation*, J. Phys. **A3** 8 (1970).

[69] Y. Fujita *et al.*, *Evidence for the Existence of the [202]3/2 Deformed Band in Mirror Nuclei* ^{25}*Mg and* ^{25}*Al*, Phys. Rev. Lett. **92** 062502 (2004).

[70] R. Gilmore, *Lie Groups, Lie Algebras, and Some of Their Applications*, Dover Publications Inc. (2005).

[71] A. L. Goodman, *Approximate Angular Momentum Projection from Cranked Intrinsic States*, Phys. Rev. Lett. **42** 357 (1979).

[72] W. Greiner and B. Müller, *Mécanique Quantique: Symétries*, Springer Verlag, New York, Heidelberg, Berlin (1999).

[73] J. J. Griffin and J. A. Wheeler, *ollective Motions in Nuclei by the Method of Generator Coordinates*, Phys. Rev. **108** 311 (1957).

[74] D. R. Inglis, *Particle Derivation of Nuclear Rotation Properties Associated with a Surface Wave*, Phys. Rev. **96** 1059 (1954).

[75] M. Hamermesh, *Group Theory and its applications to Physical problems*, Dover Publications Inc., New York (1962).

[76] H.-W. Hammer, A. Nogga, and A. Schwenk, *Colloquium: Three-body forces: From cold atoms to nuclei*, Rev. Mod. Phys. **85** 197 (2013).

[77] K. Hebeler, T. Duguet, T. Lesinski, and A. Schwenk, *Non-empirical pairing energy functional in nuclear matter and finite nuclei*, Phys. Rev. C **80** 044321 (2009).

[78] D. M. Headly *et al.*, *Gamma decay of high spin states in* ^{25}*Mg above 6.1 MeV*, Phys. Rev. C **38** 1698 (1988).

[79] P.-H. Heenen, P. Bonche, J. Dobaczewski, and H. Flocard, *Generator-coordinate method for triaxial quadrupole dynamics in Sr isotopes (II). Results for particle-number-projected states*, Nucl. Phys. A **561** 367 (1993).

[80] F. Heidinger *et al.*, *The structure of* ^{25}*Mg*, Z. Phys. A **338** 23 (1991).

[81] D. L. Hill and J. A. Wheeler, *Nuclear Constitution and the Interpretation of Fission Phenomena*, Phys. Rev. **89** 1102 (1953).

[82] S. Islam, H. J. Mang, and P. Ring, *An approximate projection technique for the calculation of electromagnetic properties of deformed nuclei*, Nucl. Phys. A **326** 161 (1979).

[83] A. Kamlah, *An Approximation for Rotation-Projected Expectation Values of the Energy for Deformed Nuclei and a Derivation of the Cranking Variational Equation*, Zeitschrift für Physik **216** 52 (1968).

[84] M. Kimura, *Intruder features of* ^{31}*Mg and the coexistence of many-particle and many-hole states*, Phys. Rev. C **75** 041302(R) (2007).

[85] M. Kimura, Y. Taniguchi, Y. Kanada-En'yo, H. Horiuchi, and K. Ikeda, *Prolate, oblate, and triaxial shape coexistence, and the lost magicity of* $N = 28$ *in* ^{43}*S*, Phys. Rev. C **87** 011301(R) (2013).

[86] S. Krewald, K. W. Schmid, and A. Faessler, *The Influence of Correlations on the Odd-Mass Nuclei* ^{21}*Ne and* ^{25}*Mg*, Z. Physik **269** 125 (1974).

[87] D. Lacroix, T. Duguet, and M. Bender, *Configuration mixing within the energy density functional formalism: Removing spurious contributions from nondiagonal energy kernels*, Phys. Rev. C **79** 044318 (2009).

[88] J. Le Bloas, M.-H. Koh, P. Quentin, L. Bonneau, and J. I. A. Ithnin, *Exact coulomb exchange calculations in the Skyrme-Hartree-Fock-BCS framework and tests of the Slater approximation*, Phys. Rev. C **84** 014310 (2011).

[89] H. J. Lipkin, *Collective Motion in Many-Particle Systems*, Ann. of Phys. **9** 272 (1960).

[90] P.-O. Löwdin, *The Normal Constants of Motion in Quantum Mechanics Treated by Projection Technique*, Rev. Mod. Phys. **34** 520 (1962).

[91] P.-O. Löwdin, *Group Algebra, Convolution Algebra, and Applications to Quantum Mechanics*, Rev. Mod. Phys. **39** 259 (1967).

[92] P. Lykos and G. W. Pratt, *Discussion on The Hartree-Fock Approximation*, Rev. Mod. Phys. **35** 496 (1963).

[93] N. MacDonald, *Projection Operators in Nuclear Structure Calculations*, Advances in Phys. **19** 371 (1970).

[94] R. McWeeny, *Symmetry, An Introduction to Group Theory and Its Applications*, Dover Publications Inc. (2002).

[95] A. Messiah, *Mécanique Quantique Vol. 1 et 2*, Dunod, Paris (1995).

[96] K. Moghrabi, M. Grasso, X. Roca-Maza, and G. Colò, *Second-order equation of state with the full Skyrme interaction: Toward new effective interactions for beyond-mean-field models*, Phys. Rev. C **85** 044323 (2012).

[97] S. A. Moszkowski, *Nuclear Surface Properties with a Simple Effective Interaction*, Phys. Rev. C **9** 402 (1970).

[98] T. Nikšić, D. Vretenar, and P. Ring, *Beyond the relativistic mean-field approximation. II. Configuration mixing of mean-field wave functions projected on angular momentum and particle number*, Phys. Rev. C **74** 064309 (2006).

[99] B. Parker, *Scene in the car where Uncle Ben gives a very valuable life lesson to Peter*, Spider-man the movie **1** (2002).

[100] R. E. Peierls and J. Yoccoz, *The Collective Model of Nuclear Motion*, Proc. Phys. Soc. London A **70** 381 (1957).

[101] J. P. Perdew and A. Zunger, *Self-interaction correction to density-functional approximations for many-electron systems*, Phys. Rev. B **23** 5048 (1981).

[102] E. Perlińska, S. G. Rohoziński, J. Dobaczewski, and W. Nazarewicz, *Local density approximation for proton-neutron pairing correlations: Formalism*, Phys. Rev. C **69** 014316 (2004).

[103] P. Quentin, N. Redon, J. Meyer, and M. Meyer, *A new approach to approximate symmetry restoration with density dependent forces: The superdeformed band in* ^{192}Hg, Phys. Rev. C **41** 341 (1990).

[104] P.-G. Reinhard, W. Nazarewicz, M. Bender, and J. A. Maruhn, *Lipkin-Nogami pairing scheme in self-consistent nuclear structure calculations*, Phys. Rev. C **53** 2776 (1996).

[105] P. Ring, R. Beck, and H. J. Mang, *On the Application of the Hartree-Fock-Bogolyubov-Equations to a Microscopic Theory of Nuclear Rotation*, Z. Physik **231** 10 (1970).

[106] P. Ring, H. J. Mang, and R. Banerjee, *Theoretical investigation of rotational bands in odd-mass nuclei*, Nucl. Phys. A **225** 141 (1974).

[107] P. Ring and P. Schuck, *The Nuclear Many-Body Problem*, Springer Verlag, New York, Heidelberg, Berlin (1980).

[108] L. M. Robledo, *Particle number restoration: its implementation and impact in nuclear structure calculations*, Int. J. Mod. Phys. E **16** 337 (2007).

[109] L. M. Robledo, *Sign of the overlap of Hartree-Fock-Bogoliubov wave functions*, Phys. Rev. C **79** 021302(R) (2009).

[110] L. M. Robledo, *Technical aspects of the evaluation of the overlap of Hartree-Fock-Bogoliubov wave functions*, Phys. Rev. C **84** 014307 (2011).

[111] R. Rodriguez-Guzman and K. W. Schmid, *Spherical Hartree-Fock calculations with linear-momentum projection before the variation*, Eur. Phys. J. A **19** 45 (2004).

[112] T. R. Rodriguez and J. L. Egido, *Triaxial angular momentum projection and configuration mixing calculations with the Gogny force*, Phys. Rev. C **81** 064323 (2010).

[113] T. R. Rodriguez and J. L. Egido, *Configuration mixing description of the nucleus* ^{44}S, Phys. Rev. C **84** 051307(R) (2011).

[114] S. G. Rohoziński, J. Dobaczewski, and W. Nazarewicz, *Self-consistent symmetries in the proton-neutron Hartree-Fock-Bogoliubov approach*, Phys. Rev. C **81** 014313 (2010).

[115] H. Röpke, V. Glattes, H. J. Brundiers, and G. Hammel, *The γ-Decay of* ^{25}Mg, Z. Physik **260** 67 (1973).

[116] H. Röpke, G. Hammel, W. Brendler, P. Betz, and V. Glattes, *New Aspects of the Rotational Model in* ^{25}Mg, Z. Physik **266** 55 (1974).

[117] H. Röpke, *Alignment of individual-particle angular momenta along the deformation axis in light nuclei*, Nucl. Phys. A **674** 95 (2000).

[118] V. Rotival, *Non-empirical energy functionals for nuclear structure*, CEA Irfu Thesis (2009). http://tel.archives-ouvertes.fr/tel-00409482

[119] D. J. Rowe, *Nuclear Collective Motion*, World Scientific Publishing (1970).

[120] D. J. Rowe and J. L. Wood, *Fundamentals of Nuclear Models*, World Scientific Publishing (2010).

[121] J. Sadoudi, *Constraints on the nuclear energy density functional and new possible analytical forms*, CEA Irfu Thesis (2001).
http://tel.archives-ouvertes.fr/tel-00653740

[122] J. Sadoudi, M. Bender, K. Bennaceur, D. Davesne, R. Jodon, and T. Duguet, *Skyrme pseudo-potential-based EDF parametrization for spuriousity-free MR EDF calculations*, Physica Scripta **T154** 014013 (2013).

[123] J. Sadoudi, T. Duguet, J. Meyer, and M. Bender, *Skyrme functional from a three-body pseudo-potential of second-order in gradients. Formalism for central terms.*, Phys. Rev. C **88** 064326 (2013).

[124] M. Samyn, S. Goriely, M. Bender, and J. M. Pearson, *Further explorations of Skyrme-Hartree-Fock-Bogoliubov mass formulas. III. Role of particle-number projection*, Phys. Rev. C **70** 044309 (2004).

[125] W. Satuła, and R. A. Wyss, *Mean-field description of high-spin states*, Rep. Prog. Phys. **68** 131 (2005).

[126] W. Satuła, J. Dobaczewski, W. Nazarewicz, and M. Rafalski, *Isospin-symmetry restoration within the nuclear density functional theory: Formalism and applications*, Phys. Rev. C **81** 054310 (2010).

[127] W. Satuła, J. Dobaczewski, W. Nazarewicz, and T. R. Werner, *Isospin-breaking corrections to superallowed Fermi β decay in isospin- and angular-momentum-projected nuclear density functional theory*, Phys. Rev. C **86** 054316 (2012).

[128] P. Schuck, *Traitement dynamique des symétries : brisure et restauration*, Ecole Joliot-Curie de physique nucléaire : symétries et physique nucléaire (1986).

[129] N. Schunck, J. Dobaczewski, J. McDonnell, J. Moré, W. Nazarewicz, J. Sarich, and M. V. Stoitsov, *One-quasiparticle states in the nuclear energy density functional theory*, Phys. Rev. C **81** 024316 (2010).

[130] C. Simenel, *Particle Transfer Reactions with the Time-Dependent Hartree-Fock Theory Using a Particle Number Projection Technique*, Phys. Rev. Lett. **105**, 192701 (2010).

[131] J. Skalski, *Self-consistent calculations of the exact Coulomb exchange effects in spherical nuclei*, Phys. Rev. C **63** 024312 (2001).

[132] T. H. R. Skyrme, *The nuclear surface*, Philos. Mag. **1** 1043 (1956).

[133] T. H. R. Skyrme, *The effective nuclear potential*, Nucl. Phys. A **9** 615 (1959).

[134] J. C. Slater, *A Simplification of the Hartree-Fock Method*, Phys. Rev. **81** 385 (1951).

[135] M. Stoitsov, M. Kortelainen, S. K. Bogner, T. Duguet, R. J. Furnstahl, B. Gebremariam, and N. Schunck, *Microscopically based energy density functionals for nuclei using the density matrix expansion: Implementation and pre-optimization*, Phys. Rev. C **82** 054307 (2011).

[136] S. Stringari and D. M. Brink, *Constraints on effective interactions imposed by antisymmetry and charge independence*, Nucl. Phys. A **304** 307 (1978).

[137] J. Suhonen, *From Nucleons to Nucleus*, Springer (2007).

[138] N. A. Smirnova, *Lecture notes.*

[139] Zdzisław Szymański, *Fast nuclear rotations*, Oxford University Press (1983).

[140] N. Tajima, H. Flocard, P. Bonche, J. Dobaczewski, and P.-H. Heenen, *Generator coordinate kernels between zero- and two-quasiparticle BCS states*, Nucl. Phys. A **542** 355 (1992).

[141] K. Tanabe and H. Nakada, *Quantum number projection at finite temperature via thermofield dynamics*, Phys. Rev. C **71** 024314 (2005).

[142] M. Tinkham, *Group Theory and Quantum Mechanics*, Dover Publications (1992).

[143] C. Titin-Schnaider, and P. Quentin, *Coulomb exchange contribution in nuclear Hartree-Fock calculations*, Phys. Lett. B **49** 397 (1974).

[144] D. J. Thouless and J. G. Valatin, *Time-dependent Hartree-Fock equations and rotational states of nuclei*, Nucl. Phys. **31** 211 (1961).

[145] J. R. R. Tolkien, *The Fellowship of the Ring*, Allen & Unwin (1954).

[146] J. R. R. Tolkien, *The Two Towers*, Allen & Unwin (1954).

[147] J. R. R. Tolkien, *The Return of the King*, Allen & Unwin (1955).

[148] TOP500, http://www.top500.org .

[149] P. Van Isacker and K. Heyde, *Exactly solvable models of nuclei*, Scholarpedia (2014).

[150] A. Valor, J. L. Egido, and L. M. Robledo, *Approximate particle number projection for finite range density dependent forces*, Phys. Rev. C **53** 172 (1996).

[151] A. Valor, J. L. Egido, and L. M. Robledo, *A new approach to approximate symmetry restoration with density dependent forces: The superdeformed band in* ^{192}Hg, Phys. Lett. B **392** 249 (1997).

[152] A. Valor, J. L. Egido, and L. M. Robledo, *Approximate particle number projection with density dependent forces: superdeformed bands in the A = 150 and A = 190 regions*, Nucl. Phys. A **665** 46 (2000).

[153] A. Valor, J. L. Egido, and L. M. Robledo, *Implementation of a variational approach to approximate particle number projection with effectives forces*, Nucl. Phys. A **671** 189 (2000).

[154] A. Valor, P.H. Heenen, and P. Bonche, *Configuration mixing of mean field wave functions projected on angular momentum and particle number: Application to Mg-24*, Nucl. Phys. A **671** 145 (2000).

[155] D.A. Varshalovich, A.N. Moskalev, and V.K. Khersonskii, *Quantum Theory of Angular Momentum*, World Scientific Publishing (1988).

[156] D. Vautherin and D. M. Brink, *Hartree-Fock Calculations with Skyrme's Interaction. I. Spherical Nuclei*, Phys. Rev. C **5** 626 (1972).

[157] D. Vautherin, *Hartree-Fock Calculations with Skyrme's Interaction. II. Axially Deformed Nuclei*, Phys. Rev. C **7** 296 (1973).

[158] E. Wigner, *Group Theory and its Applications to the Quantum Mechanics of Atomic Spectra*, Academic Press Inc., New York (1959).

[159] J. M. Yao, J. Meng, P. Ring, and D. Vretenar, *Configuration mixing of angular-momentum-projected triaxial relativistic mean-field wave functions*, Phys. Rev. C **81** 044311 (2010).

[160] J. Yoccoz, *On the Moments of Inertia of Nuclei*, Proc. Phys. Soc. London A **70** 388 (1957).

[161] D. T. Yordanov *et al.*, *Nuclear Charge Radii of* $^{21-32}Mg$, Phys. Rev. Lett. **108** 042504 (2012).

[162] H. Zduńczuk, W. Satuła, J. Dobaczewski, and M. Kosmulski, *Angular momentum projection of cranked Hartree-Fock states: Application to terminating bands in A∼44 nuclei*, Phys. Rev. C **76** 044304 (2007).

[163] B. Zumino, *Normal Forms of Complex Matrices*, J. Math. Phys. **3** 1055 (1962).

Titre : Description des noyaux impairs à l'aide d'une méthode de fonctionnelle énergie de la densité à plusieurs états de référence.

Résumé : Dans ce manuscrit de thèse, nous nous intéressons à la description des noyaux atomiques composés d'un nombre impair de nucléons dans la méthode dite de la fonctionnelle énergie de la densité (EDF). Plus précisément, nous présentons et appliquons dans le cas de ces noyaux, des extensions à cette méthode : (i) la projection sur les bons nombres quantiques, (ii) le mélange de configurations à travers la méthode des coordonnées génératrices (GCM), qui permettent de prendre en compte dans nos calculs des corrélations de type « au-delà du champ moyen » entre les nucléons constituant le noyau. De telles extensions n'avaient jusqu'alors été employées, dans leurs versions les plus générales, qu'aux noyaux ayant à la fois un nombre pair de neutrons et de protons, et nous nous proposons donc de démontrer leurs applicabilités également dans le cas des noyaux impairs. Dans la première partie de ce travail, nous présentons le formalisme mathématique de la méthode EDF, en mettant tout particulièrement l'accent sur le traitement des symétries dans cette approche. Dans la seconde partie du manuscrit, nous appliquons notre modèle au cas du noyau de ^{25}Mg et analysons les résultats sous différents angles (ex : précision numérique des résultats, convergence du mélange de configurations, comparaison avec les données expérimentales connues). Les premiers résultats obtenus dans ce travail de thèse sont encourageants et démontrent l'intérêt de notre approche pour les calculs théoriques de structure nucléaire.

Mot-clefs : noyaux impairs, fonctionnelle énergie de la densité, projection, restauration de symétrie, mélange de configurations, méthode des coordonnées génératrices, structure nucléaire, spectroscopie nucléaire.

Title: Description of Odd-Mass Nuclei by Multi-Reference Energy Density Functional Methods.

Abstract: In this work, we are interested in the treatment of odd-mass atomic nuclei in energy density functional (EDF) models. More precisely, the goal of this thesis is to develop and to apply to odd-mass nuclei, the theoretical extensions of the EDF method that are: (i) the projection tehnique, and (ii) the configuration mixing by the generator coordinate method (GCM). These two extensions are part of the so-called multi-reference energy density functional (MR-EDF) formalism and allow for taking into account, within an EDF context, the "beyond-mean-field" correlations between the nucleons forming the nucleus. Until now, the MR-EDF formalism has been applied, in its full-fledged version, only to the calculation of even-even nuclei. In this thesis, we want to demonstrate the applicability of such a model also for the description of odd-mass nuclei. In the first part of this thesis, we describe the theoretical formalism of the EDF models, giving particular attention to the treatment of symmetries within our approach. In the second part of the manuscript, we apply our model to the nucleus ^{25}Mg and investigate different aspects of the method (e.g. numerical accuracy, convergence of the configuration mixing, comparison to known experimental data). The results obtained in this work are encouraging and demonstrate the potential of our approach for theoretical nuclear structure calculations.

Keywords: odd-mass nuclei, energy density functional, projection, symmetry restoration, configuration mixing, generator coordinate method, nuclear structure, nuclear spectroscopy.

Thèse préparée au Centre d'Études Nucléaires de Bordeaux Gradignan, Unité Mixte de Recherche 5797 du CNRS/IN2P3 et de l'Université de Bordeaux.
CENBG, Chemin du Solarium, Le Haut Vigneau, CS 10120, F-33175 GRADIGNAN Cedex.